Department of Petroleum Engineering

Subsurface Re-injection of Carbon Dioxide for Greenhouse Gas Control: Influence of Formation Heterogeneity on Reservoir Performance

Matthew Alexander Flett

This thesis is presented for the Degree of
Doctor of Petroleum Engineering
of
Curtin University of Technology

July 2008

Declaration

To the best of my knowledge and belief this thesis contains no material previously published by any other person except where due acknowledgment has been made.

This thesis contains no material which has been accepted for the award of any other degree or diploma in any university.

Signature: …….

Date: ……...

Abstract

Subsurface Re-injection of Carbon Dioxide for Greenhouse Gas Control: Influence of Formation Heterogeneity on Reservoir Performance

The injection of carbon dioxide (CO_2) into saline formations for the purpose of limiting greenhouse gas emissions has been proposed as an alternative to the atmospheric venting of carbon dioxide. In the evaluation process for selecting a potential target saline formation for the disposal of carbon dioxide, flow characterisation of the disposed plume should be undertaken by reservoir simulation of the target formation. The movement of injected carbon dioxide in the saline formation is influenced by many factors including the physics of carbon dioxide at deep formation depths and pressure, physical interactions with formation rock and pore water and variations in the rock flow pathways through changes in formation heterogeneity. This thesis investigates the roles of physical interactions on the disposal of carbon dioxide and the ability to contain the injected gas through evaluation of trapping mechanisms such as dissolution of CO_2 in formation water and residual gas trapping through the process of gas-water relative permeability hysteresis. Variable formation heterogeneity is evaluated for its impact on the migration of injected CO_2 plume movement and the role of formation heterogeneity in impeding or accelerating the immobilisation of injected carbon dioxide.

Multiple reservoir simulation studies were conducted to evaluate, initially, the role of different trapping mechanisms in immobilising the movement of injected carbon dioxide and subsequently, the role of variations in formation rock in the migration and trapping of and injected plume of carbon dioxide.

The major simulation study shows that the selection process for identifying appropriate saline formations should not only consider their size and permeability but should also consider their degree of heterogeneity endemic to the formation. A set of reservoir performance metrics were developed for the CO_2 disposal projects. The metrics were applied to compare plume migration of injected CO_2 (both vertically and laterally) and containment (through dissolution and residual phase trapping) in

these studies. The findings demonstrate how formation heterogeneity has a significant impact on the subsurface behaviour of the carbon dioxide. Formation dip influences the rate of migration, with low formation dipping reservoirs having slower rates of vertical migration. Increasing the tortuousity of the migration flow path by either increasing the shale (non-reservoir) content or lengthening the shale baffles in the formation (corresponding to a gradual decrease in reservoir quality), can progressively inhibit the vertical flow of the plume whilst promoting its lateral flow. The increase in the tortuosity of the CO_2 migration pathway delays the migration of CO_2 and increases the residence time for the CO_2 in the formation. Thus, formation heterogeneity impedes the onset of residual gas trapping through hysteresis effects. Ultimately less carbon dioxide is likely to collect under the seal in heterogeneous formations due to increased reservoir contact and long residence times, thereby reducing the risk of seepage to overlying formations. Given sufficient permeability for economic injection of CO_2, then low to mid net-to-gross heterogeneous saline formations with low formation dip and lengthy intra-bedded shales are desirable for selection for the geological disposal of CO_2. Detailed reservoir characterisation of any potential geological disposal saline formations is required in order to accurately predict the range of outcomes in the long term flow characterisation of injected CO_2 into those formations.

Acknowledgements

This body of research has been the product of several years of work and during that period of time many people have assisted me in my research studies.

Firstly, I would to acknowledge and thank my supervisor, Dr. Geoff Weir, formerly at the Department of Petroleum Engineering at Curtin University for his guidance and advice of my research studies, career advice, and diligence with my manuscript preparation and also for his sense of humour.

Secondly, I thank Associate Professor Jorge Sampaio for becoming my supervisor at the final stage of my thesis write-up and helping me with the final hurdles of my doctoral studies.

Additionally, I would to like to thank the host of informal supervisors at Chevron Australia that I have had while working as the reservoir simulation development engineer for CO_2 disposal project as part of the Gorgon project. These people include Dr. Randal Gurton, Dr. Ian Taggart, Dr. Seb Leigh and Mr. Bill Robinson.

- I would to thank Randy for his tireless support of my research studies, in advising my studies and the papers that grew out of them, showing me the 'ropes' with CHEARS, his strong sense of humour and being such a great person to learn from.
- Thanks to Ian for being the person responsible for creating my position at Chevron and giving me the role as a development engineer with the Gorgon Subsurface Team and the freedom to pursue research in such a dynamic field of geological CO_2 disposal.
- I give my thanks to my team leaders over the past five years, Seb Leigh and Bill Robinson, thank you for your support for my research activities.
- Thanks to Chevron Australia as a whole for supporting my research directly by sending me to participate and represent the company at important international conferences on the geological disposal of CO_2 and also indirectly by the use of the company's facilities and technology such as CHEARS for my research.

- I also appreciate the contribution of several of my team members in the Gorgon subsurface team over the last five years – for the great working environment, advice and friendship: Roger Bartlett, Graeme Beacher, Thuy Bradley, Aaron Burt, Jeroen Brantjes, Daniel Chia, Chris Dauth, Brian Green, Louisa Jack, Fiona Koelmeyer, Bob Lawrence, Dr. Jason McKenna, Craig Richards, Dr. Rob Root, Leigh Scooby-Smith, Terrell Tankersley and Francis Thompson.

I also thank Dr. Jonathon Ennis-King at CSIRO Petroleum for many email exchanges and conference discussions regarding the numerical simulation of CO_2 disposal and for aiding myself with some very handy algorithms for CO_2 physical properties.

I thank the long standing support of family throughout my doctoral studies including;

- my parents, Assoc. Prof. Peter Flett and Mrs. Louise Flett,
- my grandparents, Dr. John Flett AM and Mrs. Hilda Flett
- my brothers; Simon, Scott and Andrew,
- and my father and mother in law, Dr. Ian Halkett and Mrs. Sandy Halkett.

Finally, I give my thanks to my wife, Georgia Halkett, for her very long term support, love, encouragement and advice for my doctoral studies. It has been a long and worthwhile journey so far and I look forward to taking a new path with you.

About the Author

Matthew Flett was born in 1978, in Adelaide, South Australia. He attended the Collegiate School of Saint Peter in Adelaide, matriculating in 1996. Following school he attended the University of Adelaide from 1997 to 2001, obtaining a Bachelor of Engineering in Chemical Engineering with upper second class honours and a Bachelor of Science with majors in applied mathematics and chemistry. Throughout undergraduate studies Matthew gained work experience at a wide variety of university research centres and resource company operations including; the Australian Wine Research Institute (University of Adelaide), Daelim Industrial company (Yosu, South Korea), the Ian Wark Research Institute (University of South Australia) and Comalco Bellbay Ltd, Tasmania.

In 2002 at the conclusion of undergraduate studies, Matthew moved to Perth, Western Australia and enrolled at Curtin University for the Professional Doctorate degree of Doctor of Petroleum Engineering. In 2003, at the conclusion of the one year coursework period of the course, Matthew began the research period of the doctorate and converted to part time status. Since 2003 Matthew has been employed by Chevron Australia as development reservoir engineer for CO_2 disposal as part of the world class Gorgon Project. Since 2003, Matthew has combined the practical aspects of his role as professional engineer developing a CO_2 disposal project with those of his research interests as a research student in the field of reservoir simulation and CO_2 disposal.

Matthew married Dr. Georgia Halkett, PhD in 2005. They currently live in Perth, Western Australia.

Nomenclature

C	Land's trapping constant
k	Permeability
k_v	Vertical permeability
k_h	Horizontal permeability
k_{rw}	Relative permeability of water
k_{rg}	Relative permeability of gas
S_w	Water saturation
S_{wir}	Irreducible water saturation
S_g	Gas saturation
S_{gc}	Critical gas saturation
S_g^*	Normalised gas saturation
S_{gr}^*	Normalised residual gas saturation
S_{gi}^*	Normalised initial gas saturation
S_{gf}^*	Normalised free gas saturation
S_{grM}	Maximum residual gas saturation
S_{gt}^*	Normalised trapped gas saturation
S_w^*	Normalised water saturation
λ	Pore size distribution index
ϕ	Porosity
ppm	Parts per million
ºC	Degrees Celsius
ºF	Degrees Fahrenheit
K	Degrees Kelvin
m	Metres
ft	Feet
km	Kilometres
MMscf/d	Million standard cubic feet per day
MTPA	Million tonne per annum
psia	Pounds per square inch atmospheric
MPa	Mega pascals

Table of Contents

List of Figures

List of Tables

1. Introduction

1.1 Background

The emission of greenhouse gases such as carbon dioxide (CO_2) into the atmosphere has been associated with alterations in the Earth's climate (Houghton 2001). The injection of CO_2 into subsurface saline formations for the purpose of greenhouse gas emission control has been proposed as means of responsibly reducing anthropogenic CO_2 emissions (Koide et al. 1993; Hendriks and Blok 1995; Hitchon 1996; Cook et al. 2000).

1.1.1 Industry Projects

In the petroleum industry there are now several natural gas production projects operating that dispose of associated reservoir CO_2 into subsurface formations for greenhouse gas emission avoidance, including projects at Sleipner in the North Sea (Korbol and Kaddour 1995; Baklid et al. 1996) and In Salah in Algeria (Davis et al. 2001; Wright 2007). Notable future natural gas production projects that plan to dispose produced reservoir CO_2 in the subsurface include the Gorgon LNG Project in North-Western Australia (Chevron 2006) and Snohvit LNG Project in Norway (Engebretsen et al. 2002). Natural gas subsurface developments with reservoir CO_2 are natural candidates for CO_2 disposal as CO_2 and other acid gases must be removed from reservoir gas prior to liquefaction process of LNG manufacturing or to meet quality standards required for domestic gas sales. There have also been some small scale disposal projects such as the Frio Brine project, recently conducted in Texas, that act as pilot projects to demonstrate to government and stakeholders the effectiveness of current technology with regards to the safe injection of CO_2 into saline formations (Hovorka et al. 2004). The Sleipner Vest gas project in Norway has been injecting CO_2 into the Utsira Sand saline formation for nearly a decade, while supplying Europe domestic market with natural gas (Korbol and Kaddour 1995; Baklid et al. 1996).

1.1.2 Site Selection for Reservoir Disposal of Carbon Dioxide

Recent studies are helping to develop selection criteria for potential geological storage sites to be used to sequester CO_2 from industrial sources. The research

carried out by the Australian GEODISC consortium in determining ESSCI (Environmentally Sustainable Sites for CO_2 Injection) locations is an example of this type of study (Bradshaw et al. 2002). Bachu (2000; 2002) working for the Alberta Research Council in Canada, has developed a set of selection criteria for formations for CO_2 disposal and a general road map for site selection activities for industry and government.

The selection of a potential geological target for the sequestration of CO_2 must meet strict technical criteria to ensure, as far as reasonably possible, the success of the proposed project. These criteria must address the issues of adequate containment, capacity, injectivity, and reservoir surveillance. The basis for demonstrating sufficient containment for injected CO_2 in a selected formation has usually focused on the presence of a geological seal and trap capable of holding a column of CO_2 (Bradshaw et al. 2002). However, the containment of CO_2 in a saline formation may be achieved through three additional permanent storage mechanisms without relying entirely on an overlying seal: dissolution, residual gas trapping and mineralization.

1.1.3 Containment through Permanent Storage Mechanisms

Firstly, containment may occur through the dissolution of CO_2 in the formation water. The solubility of CO_2 in water is dependent on the salinity, pressure and temperature of the formation water (Enick and Klara 1990; Chang et al. 1998). As CO_2 is injected into the formation it contacts virgin formation water and mass transfer occurs, with CO_2 dissolving into the water until an equilibrium state is reached. At any given time the system will contain a mixture of virgin water, a plume of injected CO_2 and water that has a proportion of CO_2 dissolved in it. The literature is well developed with regards to the solubility of CO_2 in hydrocarbons and water contained in subsurface formations (such as Enick and Klara (1990)). Ennis-King and Paterson (2003) and Lindeberg and Wessel-Berg (1997) have investigated the mass transfer at the interface of a plume of CO_2 and the formation water as it migrates upwards. Under typical reservoir conditions water that has CO_2 dissolved in it is denser than virgin formation water. This contrast in density ultimately leads to instabilities in the water column, which create convection currents. These currents bring water with a relatively lower saturation of dissolved CO_2 into contact with the plume, promoting further dissolution. As a method of increasing storage this

convection mechanism is far more efficient in transporting CO_2 than diffusion but, nevertheless, is still an effect that only manifests itself over long periods of time.

A second method of containment is through the CO_2 being trapped as a residual phase. Residual trapping occurs as water is imbibed behind a migrating CO_2 plume with the trapping caused by a process known as the gas-water relative permeability hysteresis (Flett et al. 2004). As CO_2 is injected into the saline formation, a drainage process occurs as water (the formation wetting phase) recedes from the advancing non-wetting CO_2. After injection ceases, movement is driven by the buoyancy/density contrast between the lighter CO_2 plume and the denser aquifer water. As the CO_2 plume migrates upwards after injection ceases, water imbibes behind the plume. This process traps, through the action of capillary forces, CO_2 in the form of bubbles in pore throats, thereby developing an immobile residual phase. Several reservoir simulation studies have outlined that residual phase gas trapping could be significant in storing CO_2 in saline formations (Flett et al. 2004; Kumar et al. 2004). It should be noted that this storage mechanism is a post injection process whereas dissolution takes place both during and after injection. A full explanation of gas-water relative permeability hysteresis will be given in the second chapter.

A third storage mechanism is mineralisation. This mechanism can permanently store injected CO_2 as part of the formation matrix. The process of CO_2 dissolving in formation water can lead to the formation of carbonic acid, which can then react with susceptible minerals in the formation rock. This will result in certain minerals being dissolved and others being precipitated. The mineralisation process is slow and complex, and the details of the reaction dynamics are generally not well understood. Depending on the particular rocks and fluids, it is estimated that the mineralisation process may take anything from tens to thousands of years to reach equilibrium (Bachu et al. 1994; Preuss et al. 2003).

Any injected CO_2 not trapped by these storage mechanisms is, by definition, mobile in the formation and, as previously stated, will migrate upwards from the injection zone due to its buoyant nature. The expansion of the plume, particularly in the lateral direction, will be driven by the pressure from the injection well and the value of the horizontal permeability, which is invariably higher than the vertical permeability.

After injection ceases, the progress of the plume towards the top seal can be hindered by shales, if present, in heterogeneous formations, thereby increasing the residence time and allowing further entrapment to take place through the mechanisms discussed above. Ultimately any mobile gas that eventually reaches the seal must be contained to ensure successful disposal.

1.2 Objectives of this Thesis

The specific objectives of this thesis are:

1. To evaluate the role of various trapping mechanisms for CO_2 in the subsurface and how they relate to each other (Study A).
2. To evaluate the impact of formation heterogeneity on the success of a carbon dioxide geological disposal project, specifically on containment of the injected fluid (Study B).
3. To determine favourable reservoir characteristics of a formation for a successful disposal of CO_2 (Major Study).

1.3 Outline of this Thesis

This thesis is organised into seven chapters. The first chapter provides background information into the motivation for this thesis, the objectives and outline of this thesis. The second chapter provides an overview and considerations of the physics related to CO_2 disposal into saline formations. Various trapping mechanisms that can hold injected CO_2 in saline formations are explained. A literature review is included of reservoir simulation studies evaluating CO_2 geological disposal into saline formations. The third chapter outlines the research process used in this thesis. The setup of the reservoir simulation package for these CO_2 simulation studies is also explained. The fourth, fifth and sixth chapters of this thesis present sequentially the methodology, results and analysis of the three studies reported in this thesis (Study A, Study B and the Major Study). The final chapter summarises the main results and conclusions and suggests further topics of research in this area.

A set of Appendices containing published peer-reviewed papers (A), conference papers (B), raw data and results (C), supplementary figures (D) and copyright permissions (E) are included at the end of this thesis.

1.4 Significance

This thesis provides insight into desirable characteristics to be considered in selecting formations for the geological disposal of CO_2. The subsurface development of disposal of CO_2 into geological formations is dissimilar from petroleum developments in that high reservoir quality formations with high net-to-gross ratios are not desirable due to containment concerns. Given sufficient permeability for economic injection of CO_2, low net-to-gross heterogeneous formations are desirable for injection of CO_2, as these formations by their inherent tortuous migration pathways can increase the residence time of an injected plume and increase reservoir contact between the migrating plume and the formation. The increased reservoir contact allows the secondary trapping mechanisms of dissolution and gas-water relative permeability hysteresis to reduce the size of the migrating plume and reduce the reliance on a geological seal for containment.

2. Literature Review

2.1 Physics of CO_2 Disposal in the Subsurface

Understanding the physical properties of CO_2 are an important consideration for the evaluation and design of a potential carbon dioxide geological disposal project. To avoid the adverse effects from two phase flow in pipelines and wellbores (e.g water hammer effect, slug type flow in pipelines), geological disposal injection would be conducted above supercritical conditions (Preuss and Garcia 2002; Garcia 2003). The critical point for CO_2 is at P_c = 7.382 MPa, T_c = 31.04ºC (Perry and Green 1997). In oilfield units the critical points is at 1070.9 psia and 87.9° F. A phase diagram showing the physical states of carbon dioxide is shown in Figure 2-1 (Jacobs 2005).

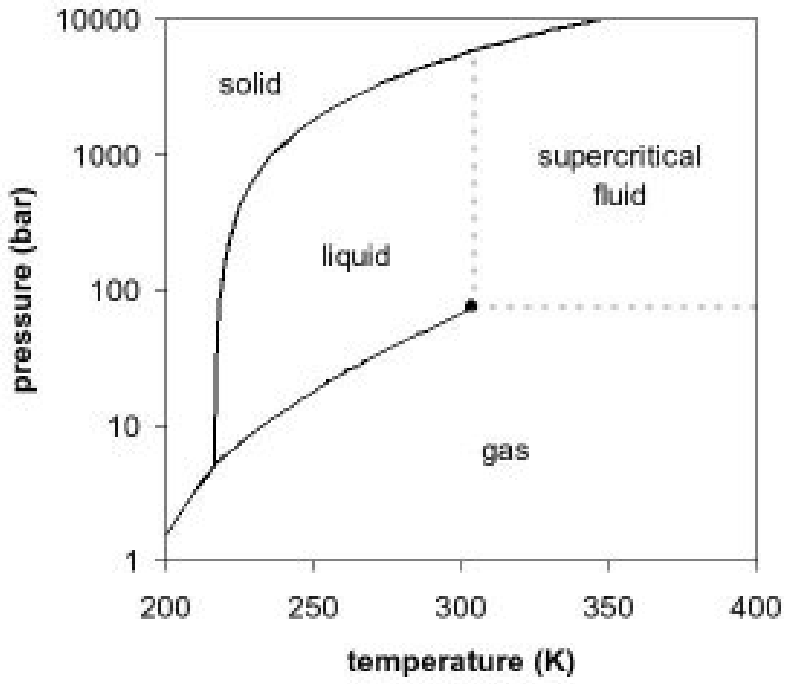

Figure 2-1: Phase diagram for pure CO_2

Thus, under normal hydrostatic and geothermal gradient conditions, supercritical conditions exist for carbon dioxide in the subsurface from the depth of 800 m or 2500 ft subsea. In essence, a depth of at least 800 m subsea is the first criteria for a target saline formation to be selected for geological disposal of carbon dioxide, as

outlined by Cook et al. (2000) and Holloway and van der Straaten (1995). As an example, at the Sleipner Vest project in the North Sea, injection occurs at 800 m subsea, thus CO_2 is injected as a single phase state into the Utsira Formation (Korbol and Kaddour 1995; Baklid et al. 1996). Another reason for this criterion is for the benefits of the disposed fluid being in a supercritical state. Fluids in the supercritical state are unique in their fluid properties, in that they tend to have a liquid like density but a gas like viscosity. The high density of supercritical CO_2 is a major benefit for geological disposal, as subsurface volumes of injected CO_2 are a fraction of surface volumes of CO_2 at standard atmospheric conditions.

The physical properties of carbon dioxide have been the subject of considerable research with many correlations for various physical traits. Garcia (2003) documented the slight differences between several correlations for density including those of Vargaftik et al. (1996), Span & Wagner (1996), Angus et al. (1976) and Altunin (1975). There were very good agreement between the various correlation outputs over a wide range of temperatures and pressures, with errors being less than 1% over the range of interest (100 – 400 bar, 0 – 150 ºC). Garcia also evaluated viscosity correlations of Vargaftik et al. (1996) and Fenghour et al. (1998) with those of Altunin (1975). The comparison showed that fairly good agreement exists over most of the pressure and temperature range, with the error being less than two percent. However, the good agreement between correlations for the Vargaftik et al. (1996) and Altunin (1975) correlations breaks down for pressures lower than 130 bar and temperatures between 40-80ºC.

The Span and Wagner Equation of State (EOS) (1996) is comprehensive in describing the range of PVT (Pressure, Volume, Temperature) properties for pure CO_2, across a wide range of pressures (0 to 800 MPa) and temperatures (triple point of CO_2 to 1100 K), wider than the range seen in most subsurface reservoirs. The physical properties of CO_2 used in reservoir simulation in this research study were based on the Span and Wagner (1996) EOS. Viscosity is derived from correlations of Vesovic et al. (1990) and Fenghour et al. (1998). The study by Garcia (2003) shows that both of these viscosity algorithms are very accurate for this purpose. The Span and Wagner EOS and the viscosity correlations were selected mainly due its

comprehensive nature and partly due to a range of algorithms kindly provided by J. Ennis-King of CSIRO Petroleum (private communication, 2003).

2.2 Trapping Mechanisms for Injected CO_2 in Saline Formations

Several trapping mechanisms for sequestering CO_2 in saline formations have been described in literature: geological seal; hydrodynamic trapping; solubility; mineralisation; and gas-water relative permeability hysteresis.

2.2.1 Geological Seal

This is a primary factor in choosing a target formation for CO_2 sequestration (Hitchon 1996; Cook et al. 2000). A geological seal of some form provides a vertical flow barrier to prevent buoyant CO_2 from leaving the formation. However, in regional saline formations, an effective geological seal is hard to demonstrate without the presence of either trapped hydrocarbons, marked salinity changes and pressure offset demonstrating containment between the sealed formation and overlying formations.

2.2.2 Hydrodynamic Trapping

CO_2 injected into a deep saline formation will exist in both dissolved and immiscible states. Bachu et al. (1994) describe that injected CO_2 will migrate slowly under the influence hydrodynamic flow of the aquifer (of the order of 1 to 10 cm/year). If CO_2 is injected in to a regionally extensive saline formation, with an overlying effective seal, mobile CO_2 can be retained in the formation for potentially many thousands of years, moving with natural flow of the formation (Bachu et al. 1994; Law and Bachu 1996; Cook et al. 2000).

2.2.3 Solubility

CO_2 solubility in water is dependent on salinity, pressure and temperature (Chang et al. 1998). As CO_2 is injected into the formation, the CO_2 contacts the formation water and mass transfer occurs, with CO_2 dissolving into water until equilibrium is reached. Injected CO_2 will displace CO_2 saturated water during injection and hence further dissolution occurs as CO_2 continues to contact virgin formation water. The literature provides a well developed understanding of CO_2 solubility and the long time scales required for further dissolution and mixing (Mansoori 1982; Enick and

Klara 1990; Lindeberg and Wessel-Berg 1997; Ennis-King and Paterson 2003; Spiteri et al. 2005). Post injection, supercritical phase CO_2 migrates vertically to the top of the formation, below a vertical flow barrier. The formation water interface between the CO_2 column and the formation water will become saturated with CO_2. Since CO_2-saturated water is denser than virgin formation water, convection currents under the CO_2 column will occur, which over extensive periods of time (thousands of year) will aid in the further dissolution of contained CO_2 plume (Weir et al. 1995; Ennis-King and Paterson 2003; Garcia 2003).

2.2.4 Mineralisation

When CO_2 dissolves into water, carbonic acid forms in the saturated water, which in turn reacts with various minerals in the rock matrix. The CO_2 rich water dissolves certain minerals in the formation susceptible to reaction and precipitates out other minerals. This process is a method of permanently sequestering the CO_2 injected into the formation, as once geochemical equilibrium is reached, it is unlikely that mineralised CO_2 will be able to leak into the atmosphere. The mineralisation process can take tens to thousands of years due to slow and relatively unknown reaction dynamics in the formation (Law and Bachu 1996; Cook et al. 2000; Preuss et al. 2003).

2.2.5 Gas-Water Relative Permeability Hysteresis

Sequestration by gas-water relative permeability hysteresis is mainly a post-injection process. As CO_2 is injected in the formation, the injection of the plume is dominated by drainage relative permeability as water, the wetting phase of the formation, drains away from the advancing non-wetting phase of the injected CO_2. Post injection, the major force acting on injected CO_2 is gravity as the pressure force driving the lateral expansion of the CO_2 plume away from the injection well has ceased. CO_2 at most typical reservoir depths is less dense than the formation water, thus the CO_2 will rise in the formation, generally migrating up-dip. Two relative permeability states are present in the migrating plume. At the head or top of the plume, drainage relative permeability is present as water drains away from the rising CO_2. At the tail of the plume, imbibition relative permeability is prevalent as water imbibes behind the migrating plume. In the imbibition process some CO_2 is trapped in the pore space as a residual immobile phase, effectively sequestering the CO_2 in the rock until the

immobile gas dissolves over geological time. The model and ranges employed to determine trapped gas saturations will discussed be later.

This phenomenon is a recent development in this field of CO_2 disposal. Many authors do not refer to this mechanism in their explanations of trapping mechanisms of carbon dioxide in saline formations (e.g Koide et al. (1995), Hitchon (1996), Gunter et al. (1993)). The implications of variable residual saturations were understood over time with further developments in the field of reservoir simulation of CO_2 disposal and understanding of CO_2 displacement processes (Flett et al. 2004; Kumar et al. 2004; Spiteri 2005; Spiteri et al. 2005; Spiteri and Juanes 2006).

There is significant experience evident in petroleum literature regarding the effect of gas-water relative permeability hysteresis generating trapped residual gas saturations in both gas field development and, more CO_2 specific, with WAG (Water-Alternate-Gas) Enhanced Oil Recovery projects (Agarwal et al. 1965; Land 1968; Keelan and Pugh 1975; Firoozabadi et al. 1987; Wegener and Harpole 1996; Kralik et al. 2000; Hamon et al. 2001; Suzanne et al. 2003). The theory behind gas-water relative permeability hysteresis is explained in section 2.3.

2.3 Theory of Gas-Water Relative Permeability Hysteresis

2.3.1 Land's Theory

Land (1968) found the following empirically derived simple relationship between the trapped gas saturation and the initial gas saturation (prior to the imbibition cycle), known as Land's Equation:

$$C = \frac{1}{S^*_{gt}} - \frac{1}{S^*_{gi}} \tag{2.1}$$

C is Land's trapping constant, a characteristic of the formation. The superscript (*) refers to normalized saturations; that is saturation space that does not contain irreducible water. The normalization is as follows:

$$S^*_w = \frac{S_w - S_{wir}}{1 - S_{wir}} \tag{2.2}$$

$$S_g^* = \frac{S_g}{1 - S_{wir}} \tag{2.3}$$

Variation in the amount of gas trapped by this process is controlled by Land's constant, and also the maximum gas saturation of the migrating plume in the pore space (Land 1968). The higher the maximum gas saturation filling the pore space, the higher the residual saturation of gas post imbibition. The significance of Land's empirical relationship is that it rationalizes values of trapped gas saturations in pore space to initial gas saturations and characteristics of the rock. As the theory is derived from real data sets, it has been readily applied in many field situations, including heterogeneous formations. For example, assuming a nominal formation porosity of 0.25, trapped gas saturations vary from 0.20 to 0.40 based on practical oilfield studies (Kralik et al. 2000). Hamon et al. (2001) concluded that in various heterogeneous sandstone reservoirs, the range of trapped gas saturations can be very wide, from 0.05 up to 0.85. There are many sources of variation for the level of trapped gas; these include microporosity, clay content maximum gas saturation. Thus Land's constant can typically be in the range of 1 to 6, representing a conservative range of reasonable trapped gas saturations from 0.05 to 0.30 and higher. Recent studies of CO_2 relative permeability from Bennion and Bachu (2006) do not change this reasoning for setting a wide range in Land's constant. Bennion and Bachu (2005) found some residual gas saturations for some Albertan formations in the region of 0.5 for CO_2, with slightly lower values for H_2S, due to differences in interfacial tension between CO_2-water and H_2S-water systems for 20md core plug samples. With variable formation permeability and other rock properties, it would be prudent to have a sufficient range in residual gas saturation outcomes. For subsurface development, special core analysis (SCAL) experimental work like the Bennion and Bachu (2006) relative permeability laboratory work should be considered as an essential part of reservoir description.

Following Land's work, a modified Brooks-Corey equation can be used for gas phase hysteresis (use of this equation and deriviation explained in the next section 2.3.2) (Brooks and Corey 1966). Once S_{gt}^* is defined, the free gas saturation S_{gf}^* can be used to calculate imbibition gas relative permeability as:

$$S_g^* = S_{gt}^* + S_{gf}^* \tag{2.4}$$

2.3.2 Drainage and Imbibition Relative Permeability Curves

The shape of the types of gas liquid relative permeability curves used in this study are similar to those that are commonly used in oilfield reservoir simulation. The intention of this research is to study the impact of a range of relative permeability relationships, rather than relying on a hypothetical reference case. In all cases CO_2 was modeled as a non-wetting fluid similar to a gas.

Drainage relative permeability curves can be estimated by the well known Brooks-Corey equations for a two phase system (Brooks and Corey 1966; Honarpour et al. 1986).

$$k_{rw}\big|_{dr} = (S_w^*)^{\frac{2+3\lambda}{\lambda}} \tag{2.5}$$

$$k_{rg}\big|_{dr} = (1 - S_w^*)^2 (1 - (S_w^*)^{\frac{2+\lambda}{\lambda}}) \tag{2.6}$$

These equations can be rewritten in terms of S_g^*, since for saline formations:

$$S_g^* + S_w^* = 1 \tag{2.7}$$

Under drainage conditions Equation 2.6 can be rewritten as:

$$k_{rg}\big|_{dr} = (S_g^*)^2 (1 - (1 - S_g^*)^{\frac{2+\lambda}{\lambda}}) \tag{2.8}$$

The parameter λ is the pore size distribution index, and typically ranges from 0.5 for a wide range of pore sizes to 5 for a uniform pore size rock. For this study, a common value employed for λ was 2. For this value of λ, the Brooks-Corey

equations reduce to the standard Corey Equations for gas and water (Honarpour et al. 1986) in Equations 2.9 and 2.10.

$$k_{rw}\big|_{dr} = (S_w^*)^4 \tag{2.9}$$

$$k_{rg}\big|_{dr} = (1 - S_w^*)^2 (1 - (S_w^*)^2) \tag{2.10}$$

Thus the standard Corey type exponents used to describe the reference drainage relative permeability curves in the following reservoir simulation studies were 2 for gas flow and 4 for wetting phase flow. Sensitivities on these exponents were included in the two initial simulation studies of this thesis, Study A and B. Variations were segregated flow curves (gas exponent 1.5, water exponent 1.5) and tight rock curves (gas exponent 2, water exponent 6) to capture a range of outcomes with relative permeability uncertainty (Private communication, Gurton 2003).

Following on from Standing (1975) we can then deduce expressions for imbibition gas relative permeability curves from Equation 2.8 using the relation for free gas saturation instead of normalized gas saturation.

$$k_{rg}\big|_{imb} = (S_{gf}^*)^2 (1 - (1 - S_{gf}^*)^{\frac{2+\lambda}{\lambda}}) \tag{2.11}$$

To effectively use Equation 2.11, the amount of free gas saturation needs to be known from the total gas saturation, through Equation 2.4.

Now at any total gas saturation value, the trapped gas saturation value is equal to the residual gas saturation when $k_{rg}|_{imb} = 0$ minus the amount of free gas saturation that is trapped during the change from S_g^* to S_{gr}^*. This can be expressed as a rearrangement of Equation 2.1:

$$S_{gt}^* = S_{gr}^* - \frac{S_{gf}^*}{CS_{gf}^* + 1} \tag{2.12}$$

Now, S^*_{gt} can be eliminated using both Equations 2.4 and 2.12, via a quadratic function, from which one can solve for S^*_{gf} :

$$S^*_{gf} = \frac{1}{2}\left[\left(S^*_g - S^*_{gr}\right) + \sqrt{\left(S^*_g - S^*_{gr}\right)^2 + \frac{4}{C}\left(S^*_g - S^*_{gr}\right)}\right] \tag{2.13}$$

A final relationship is required to solve for S^*_{gr} for use in Equation 2.13, which is provided by a re-arrangement of Equation 2.1, using initial gas saturation, S^*_{gi} :

$$S^*_{gr} = \frac{S^*_{gi}}{\left(CS^*_{gi} + 1\right)} \tag{2.14}$$

Equations 2.13 and 2.14 can then be used through Equation 2.11 to find imbibition relative permeability values at any given gas saturation value. Imbibition relative permeability is dependent on the saturation history as well as actual gas saturation value.

For practical use in reservoir simulation, the simulator sets out a number of scanning curves for relative permeability for various maximum gas saturations that may be achieved in a model cell. An example of various scanning curves is shown in Figure 2-2.

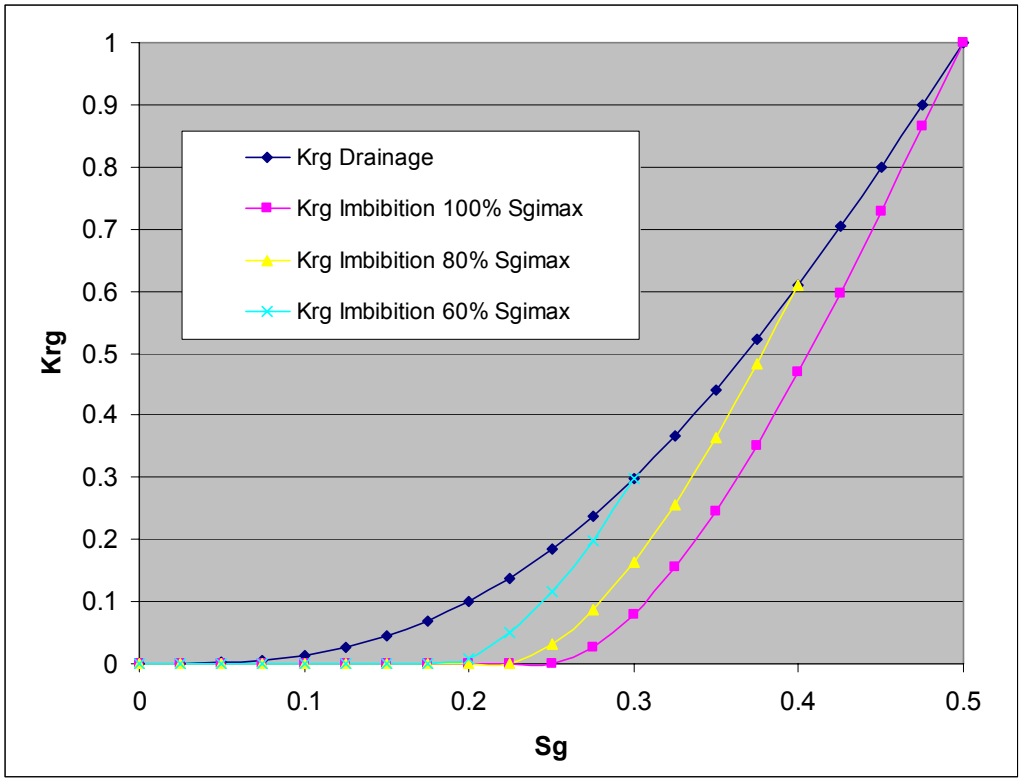

Figure 2-2: Drainage and various imbibition gas relative permeability curves

2.3.3 Other Models for Imbibition Gas Relative Curves

Several other models exist in the petroleum literature for modeling gas imbibition relative permeability and trapped gas saturations. Several are variations or developments of Land's model, such as Jerauld (1997) and also Killough's model (1976). Spiteri and colleagues (2005; 2006) has evaluated several models for gas-water relative permeability hysteresis in the development of a new trapping model for oil-wet and mix-wetness reservoirs for application for CO_2 disposal and Enhanced Oil Recovery. Spiteri's studies show that Land's theory works well in water wet systems, accurately matching experimental data for trapped saturations. Thus using Land's theory for gas-water relative permeability hysteresis for water wet systems, such as would exist in saline formations used for CO_2 disposal, is both practical and acceptable.

2.3.4 Three Phase Relative Permeability

For this thesis, it assumed that the saline formations modeled in the reservoir simulations are completely water wet and devoid of oil prior to injection of carbon dioxide. The inclusion of oil in the formation, even as a small fraction, such as a residual oil column being present would impact the relative permeability characteristics in the formation. Both drainage and imbibition of the CO_2 phase would react differently – and this would need to be taken into account when simulating these formations. Fortunately there is considerable and broad experience in petroleum literature with this phenomenon due to the long standing experience with CO_2 flooding in oil fields as secondary and tertiary methods of Enhanced Oil Recovery (EOR) projects. For example, the work of Chang et al. (1994), Deo and Deans (1990), Wegerner and Harpole (1996), Standing (1975), Honarpour et al. (1986) and Prieditis et al. (1996). The use of an alternative trapping model to that of Land's theory would need to be considered for the three phase relative permeability considerations taking into account the pore-network modeling of Spiteri (2005) showing that Land's theory does not accurately work in mixed and oil wet rocks.

2.4 Reservoir Simulations of Geological Disposal of CO_2

Over the past decade several studies have investigated the reservoir performance of CO_2 sequestration in saline formations using numerical reservoir simulations. Initially these studies have generally used simple and idealized reservoir models of the formations to gain a fundamental understanding of the various CO_2 storage processes (e.g Weir et al. (1995), van der Meer (1995)). Where studies have sought to capture aspects of formation heterogeneity, the reservoir models were based on limited data and have not used full-scale detailed geological models to capture specific aspects of the heterogeneity (as described by Ennis-King and Paterson (2002)). However, as research has matured, further evolutionary developments have been made evaluating formation heterogeneity impacts on CO_2 disposal through reservoir simulation. The follow literature review evaluates the chronological development of reservoir simulation of geological disposal of CO_2.

Weir at al. (1995) presented some computer models to evaluate CO_2 storage in deep aquifers with a focus on phase behaviour in the subsurface and timescales for the

return of injected CO_2 to the surface. The idealised mathematical model employed in this study indicated that CO_2 storage in geological disposal is a viable alternative to atmospheric venting and in need of further investigation.

van der Meer (1995; 1996) employed 2D reservoir simulation models to investigate the displacement processes of CO_2 injection in saline formations and to compare the capabilities of various reservoir simulators. The study found that heterogeneity in a formation has a larger effect on movement of the injected CO_2 than any displacement caused by viscous fingering. The simulators yielded similar results for the 2D modelling of disposal into the Lower Mannville aquifer in the Wabamun Lake Area of Alberta, Canada. The effect of numerical dispersion on the dissolution of CO_2 in large simulation model blocks was noted as a topic for further study.

Law and Bachu (1996) also investigated the Lower Mannville aquifer and compared the performance of homogeneous and heterogeneous aquifers using a 2D radial simulation model.

Baklid et al. (1996) and Korbol and Kaddour (1995) have also made simulation studies of CO_2 disposal into a saline aquifer. Both of these studies were based on the Sleipner project in the North Sea and attempted to predict the potential movement of the injected plume. A black oil model was used, comprising 28 by 27 by 7 layers, with an areal cell size of 250m by 250m. The lateral extent of the injected plume that developed was 3km, and it was noted that containment of CO_2 could be enhanced by injecting at the base of a formation to allow maximum reservoir contact time for dissolution to occur. The model predicts that up to 18% of the injected CO_2 may ultimately be dissolved.

Lindeberg (1997) also examined the containment of CO_2 injected into saline formations. In this study the performance of a radial 2D homogeneous model was compared with a layered heterogeneous 2D radial model, with properties typical of the Norwegian sector of the North Sea. The bulk of injected CO_2 remained in the target formation but there was a small amount of “leakage”. This containment risk was reduced through the feature of the model’s layered heterogeneity, which inhibited vertical migration.

Brinks and Fanchi (2001) simulated CO_2 disposal in a synthetic dome structured model of an aquifer for monitoring implications for seismic surveys. The study suggests that seismic monitoring could be a feasible and very useful modeling tool, and that reservoir simulation could be a very effective tool in predicting future seismic acquisition and expected seismic response.

Pruess et al. (2002) in collaboration with several international research teams compared the outcomes of various academic and common industry reservoir simulation codes for identical reservoir simulation problems. This study follows on from the successful comparative study conducted by the Society of Petroleum Engineers to give confidence in the range of petroleum reservoir simulation products available (e.g. Firoozabadi and Thomas (1989)). The objectives of the study were to determine if the fundamental physical and chemical processes were represented in reservoir simulation packages properly, with valid mathematical models and if the available reservoir simulators reliably and accurately model practical examples of geological disposal. Pruess et al. set up nine separate comparative problems to be tested by the collaborators' simulation codes, including: diffusion and mixing of CO_2 and CH_4, mineral trapping, various tests of displacement of CO_2 in saline and multi-component oil formations. Simulation packages that were examined included multiple adapted versions of the TOUGH2 simulator code (Battistelli et al. 1997), GEM from the Computer Modeling Group (Nghiem 2002; Nghiem et al. 2004) and ECLIPSE300 from Schlumberger. The outcome of the study showed there was in general fair to good agreement for the idealized scenarios tested in the study across several simulators, however care must be taken with specification of fluid properties. Despite the fluid properties issue, it was noted that realistic and further complexity in reservoir modeling is necessary and would likely have a greater impact on simulation outcomes.

A broad discussion of engineering considerations required for a geological disposal project was developed by Ennis-King and Paterson (2002). Previous simulation studies were described as generic in nature or scoping studies of certain real formations while examining general questions regarding CO_2 disposal. The paper discusses the energy cost required to compress CO_2 to supercritical conditions for

movement of the fluid (congruous with Garcia (2003)) and for injection, avoiding two phase flow and maintaining a dense fluid in movement. Care should be taken that energy cost of compression is not so significant as the emissions due to power the compressor trains may emit more CO_2 than the amount of CO_2 in the compressed stream, meaning that there is less net CO_2 emitted to the atmosphere. The question then was put for comparison, that was it better to concentrate the CO_2 in flue gas from a power plant (a process largely known as carbon capture) or simply inject all flue gases? In favour of relatively pure CO_2 injection is smaller injection, handling facilities and denser fluid phases, while flue gas injection would require no carbon capture processes. Fluid properties of injected CO_2 were compared to water in saline formations, where the mobility of CO_2 was shown to be much greater than water at supercritical subsurface conditions. The phenomena of viscous fingering may occur in homogeneous formations due to the mobility contrast, but formation heterogeneity and buoyancy effects are expected to have greater impact on CO_2 movement. The merits and limitations of using Buckley-Leverett theory for describing the radial distribution of CO_2 saturations about an injector were outlined with the development of terms to take into account gravity and dissolution effects. However, the best measure to take account of fluid saturation distribution is through numerical simulation. The development of a simulation model based on previous studies of the Petrel sub-basin in Northwest Australia (from Rigg et al. (2001)) was outlined. The simulation model was relatively homogeneous, set up with three zones of set formation properties. There was no lateral variation in properties due to formation heterogeneity. Several relative permeability curves were used, but assumed to be the same for drainage and imbibition thus not capturing relative permeability hysteresis in action in these studies. Varying ranges of residual gas saturation were used, but it was not clear if the residual gas saturation was also the same value as the critical gas saturation, S_{gc}, (as the same relative permeability curve was used for drainage and imbibition) which in some cases would have been a very large value, being 0.207 for one case of relative permeability curves. Numerical simulations of CO_2 injection for 30 years in a 2D radial model (used as the formation is relatively flat) compared favourably with analytical calculations of the saturation distribution of injected CO_2 using Buckley-Leverett theory. Fine grids are suggested for capturing dissolution processes more accurately and the study showed that care must be taken when selecting relative permeability curves. Post-injection processes were discussed

including various mechanisms of dissolution, which include contact by the plume during migration, hydrodynamic dispersion of the plume due to natural fluid movement, diffusion and convective mixing. The use of convective mixing is particularly important due to it being faster than diffusion processes in dissolving a stationary/trapped column of CO_2. Residual trapping was considered important but more understanding is required to gauge the impact of dissolution and residual trapping processes acting together. Mineral trapping processes were considered to be long term processes, and in the likely event of disposal in clean high permeable sands with generally low reactive compounds in the formation matrix, unlikely to have measurable effect on the success or failure of a disposal project.

Ennis-King and Paterson (2003), in a following study took a detailed evaluation of convective mixing of CO_2 dissolution in saline formations. Linking mathematical theory and numerical simulation, convective mixing was shown to be an effective means of dissolving CO_2 into formation waters and in partnering residual phase trapping, possibly removing the need for a completely demonstrated seal/structural trap being present in a selected formation for geological disposal of CO_2. Challenges remain in effectively modelling convective mixing in coarse scale models.

Convection currents caused by density contrasts in CO_2 saturated water were also developed in simulations studies by Nghiem et al. (2004) and Garcia (2003). Nghiem et al. (2004) developed a specific simulation package to take account of geochemical reaction that may occur during CO_2 contact with the reservoir and were able to track reactions within convections pathways in a simulation of disposal of CO_2 into an aquifer. Results in the paper demonstrate the capabilities of the CMG greenhouse gas disposal simulator package, with the demonstration of mineral trapping in the results of reservoir simulation studies and that the fundamental physics of the simulator are correct in regard to CO_2 disposal into a homogeneous aquifer.

Garcia (2003) builds on the work of Ennis-King and Paterson (2003) and demonstrates in a test study that demonstrates convective mixing of saturated CO_2 brine with fresh brine is a more effective means of enhancing dissolution than diffusion processes.

Pruess et al. (2003) and Xu et al. (2004) have used numerical models to investigate geo-chemical trapping of CO_2 in saline formations. They confirmed that the effectiveness of this trapping mechanism depends on the rock type in the target formation, the individual rock reaction dynamics and the surface area available for reaction. Pruess et al. (2003) also demonstrated that, as one would expect, the degree of upward movement as compared to lateral migration depended on the ratio of vertical to horizontal permeability. When the ratio was high enough (i.e. a relatively large vertical permeability) the CO_2 would spread along the top of the formation, by-passing water lower in the formation structure.

Recent further reservoir simulation studies addressed the issue of heterogeneity on the effectiveness of geological sequestration in full-scale 3D models of saline formations.

Characterisation of faults and the impact of fault derived heterogeneity was evaluated by Pasala et al. (2003) in a reservoir simulation study investigating both CO_2 disposal in saline formations and EOR scenarios. As can be expected, barriers and compartmentalization caused by faults restricted flow of CO_2 while fracturing caused fault action and was found to enhance CO_2 movement. The requirement of reservoir characterization by geologists, particularly through the identification and quantification of high and low permeability zones by fault action in sandstone formations was discussed.

Simulation of reservoir leakage through a fault was considered by Pruess and Garcia (2002) as a test scenario of the their study of fluid dynamics in CO_2 disposal in aquifer and the numerical simulation formation they had developed. It was found that grid effects, such as the size of grid cells, had a greater impact on simulated pressure than fluid saturations. The experience of simulating a fault leak, which can be self-perpetuating if it occurs, suggests if CO_2 can leak through a fault, then multiple geological barriers to vertical movement may be required for successful containment of injected CO_2.

Hovorka et al. (2004) outlined the details of the Frio Brine Pilot in Texas and the supporting research program for this publicly funded program. The simulation model

of the injection site predicted that heterogeneities in the formation would be more significant in controlling migration and overall reservoir contact of injected CO_2 plume than any viscous fingering displacement that might occur. As expected, the model demonstrated that the rate of migration of the plume into the formation is dependent on the rock permeability. In a following publication, Hovorka et al. (2004) elaborate on the effect of formation heterogeneity on the subsurface movement of injected CO_2 as part of modeling the Frio Brine Pilot. Discontinuities in reservoir rock caused by low permeability layers, result in more efficient sequestration than a homogenous model as the heterogeneity causes more reservoir coverage by the injected plume. While the inclusion of low permeability rock in reservoir models would appear to reduce the net available reservoir for injection of CO_2 and in agreement with Pruess and Garcia (2002), it was found that inclusion of multiple low permeability layers increases the 'sequestration capacity' of the injection formation by creating longer flow paths for the migrating CO_2 and increasing the interaction between the plume and the reservoir (and the associated trapping mechanisms that can trap CO_2). Geological heterogeneity in this study was seen to increase the residence time of injected CO_2 in a formation and thus provide a disposal project with more confidence that the CO_2 will be securely stored. The paper discussed the need for reasonable reservoir characterisation of a formation target, with implications for containment as part of the characterization study. Structural traps, intrabed shales and faults have to be assessed for leakage potential during subsurface evaluation. Additional investigation is required to evaluate the effectiveness of geological disposal in heterogeneous settings.

Doughty and Pruess (2004), investigated the impact of grid resolution and grid orientation, and the role played by relative permeability in the modelling of a heterogeneous formation. Several reservoir models were developed (including one based on the Frio formation) with both fine and coarse grids. The study showed that heterogeneity in the reservoir models assisted the distribution of CO_2 through the models with, as one might expect, the finer scale models capturing the effect of reservoir heterogeneity in more detail. The study confirms that the details of the relative permeability curves and, in particular, the ranges picked to determine the residual phase gas saturations, are important when attempting to model migration

and trapping processes meaningfully. Their relative importance with regards to the effects of model heterogeneity was not expanded upon.

Kumar et al. (2004), conducted a study that investigated the effects of mineralisation over very long timeframes, together with the influence of dissolution and residual phase trapping, on CO_2 disposal in a saline formation. This work suggests that residual gas phase trapping is the dominant factor in containment. In this study, the mechanism of mineralisation does not play a significant role in storing CO_2, due to the long time scales required for the slow reaction kinetics of this mechanism (even though long time scale simulation were run). Simulations show that as the amount of residual gas saturation that was set via Land's equation controlled the amount of free mobile CO_2 in the formation. Forty to eight percent of the CO_2 injected in the set of simulation models was trapped by residual phase trapping. Dissolution trapped twenty to forty percent of the injected CO_2.

The physical process undergone by injected CO_2 during leakage from a geological formation was evaluated by Pruess (2004) using numerical simulation. The movement of CO_2 through various physical states from supercritical conditions during injection, through to sub-critical conditions where liquid and gaseous CO_2 may be present was modelled. It was found that strong cooling effects occur when liquid CO_2 rises in geological formations where it begins to boil off and form a gaseous CO_2 (due to the reduced pressure and temperature conditions shallower in formations). Thus a leak of CO_2 can form a three phase zone where aqueous, gaseous and liquid CO_2 are present, which enlarges over time due to feeding of the leak by further CO_2 seepage and the cooling effect of the boil-off process in the formation creating the conditions for further gaseous CO_2 to be present. CO_2 fluid mobilities are reduced in the multiphase zone due to multiple phase or relative permeability effects, which can reduce upwards vertical movement of CO_2 and promote lateral dispersion of the leaking plume. Temperatures in the formation may be reduced to conditions where there is a possibility that ice and CO_2 hydrate forms.

Some recent studies have evaluated the effectiveness of the various CO_2 trapping mechanisms, particularly dissolution and relative permeability hysteresis. Mo et al. (2005) modeled several scenarios of geological storage in a blackoil formulation

reservoir simulator to evaluate the distribution of migrating CO_2 in an aquifer with regard to critical gas saturation during injection and residual saturations as the plume migrates. It was found that water imbibition largely occurs post injection, as this is the period when gravity segregation of the injected fluid is the dominant force in action. This finding is in good agreement with several other studies such as Spiteri et al. (2005), Flett et al. (2004) and Kumar et al. (2004). Several reservoir parameters where varied as part of the reservoir simulation study, including factors such as permeability, vertical to horizontal permeability (k_v/k_h), relative permeability and capillary pressure. This study suggests that residual gas saturation is the most important parameter in low k_v/k_h environments. However the method in which the simulation model was used in the study was not discussed, thus inhibiting general comparisons with other simulation studies evaluating CO_2 injection in heterogeneous formations.

Spiteri et al. (2005) and Juanes et al. (Juanes et al. 2006) used a reservoir simulation study to apply a new model for relative permeability hysteresis which accounts for variations in formation wetness. Using a publicly available coarse scale simulation model, the PUNQ-S3 (Floris et al. 2001; Imperial College 2008), residual trapping due to the action of relative permeability hysteresis was evaluated for the purposes of long term storage of CO_2. Residual trapping accounted for the immobilization of a large fraction of the CO_2 injected in the model. High injection rates increase the storage of CO_2 due to the larger lateral movement of CO_2 from injection pressure creating greater reservoir contact. Plans to accelerate the process of dissolution and residual trapping by injecting slugs of water post injection are suggested. The acceleration of trapping via water injection have also been made by Kumar et al. (2004) and Leonenko et al. (2006). The coarse size of grid blocks used in the simulation model and the resulting numerical dispersion may overestimate the sweep and residual trapping. The focus of further simulation studies is to use models that accurately account migration pathways and fluid flow in real formations.

2.5 Conclusion and basis for this thesis

Multiple studies have used reservoir simulation to evaluate the fundamental processes and the possible relative contribution of these various mechanisms in

storing CO_2 in saline formations. These studies have investigated trapping mechanisms including dissolution, convection of CO_2 saturated water, mineralization, residual trapping and trapping via geological traps. Reservoir simulation models employed in these studies have been generic or in the case of scoping studies of real geological formations, mainly homogeneous based on sparse input data. Integration of full reservoir characterization in reservoir simulation models, with the interaction of formation heterogeneity on the injected plume movement, has not been investigated in detail in the literature to date.

This thesis evaluates the role of formation heterogeneity and reservoir characterization on the migration and containment by trapping mechanism of injected CO_2 plume in a saline formation. The role of various trapping mechanisms for CO_2 in the subsurface and how they relate to each other will be evaluated. The impact of formation heterogeneity on the success of a carbon dioxide geological disposal project, specifically on containment of the injected fluid will be investigated. Favourable reservoir characteristics of a formation for a successful disposal of CO_2 will be determined.

3. Methods

Studies conducted as part of this research project include two enabling reservoir simulation studies that subsequently lead to the major study. The first enabling study, Study A, investigated the competing roles of various trapping mechanisms in the disposal of carbon dioxide. The second study, Study B, evaluated the impact of aspects of formation heterogeneity on the reservoir performance of injected CO_2 in a saline formation for both the migration and trapping of injected CO_2. Study A and Study B are described in detail in Chapters 4 and 5 respectively.

The findings of the two enabling studies framed the development of the major study of this thesis to investigate the key subsurface uncertainties that impact the potential reservoir performance of a geological disposal project in a saline formation. This major study comprised a detailed reservoir simulation study to evaluate the effects of formation heterogeneity via net-to-gross variability, shale length variation and changes in formation dip on the reservoir performance of a CO_2 disposal project. The major study is described in Chapter 6.

The methodology of the thesis is shown in Figure 3.1.

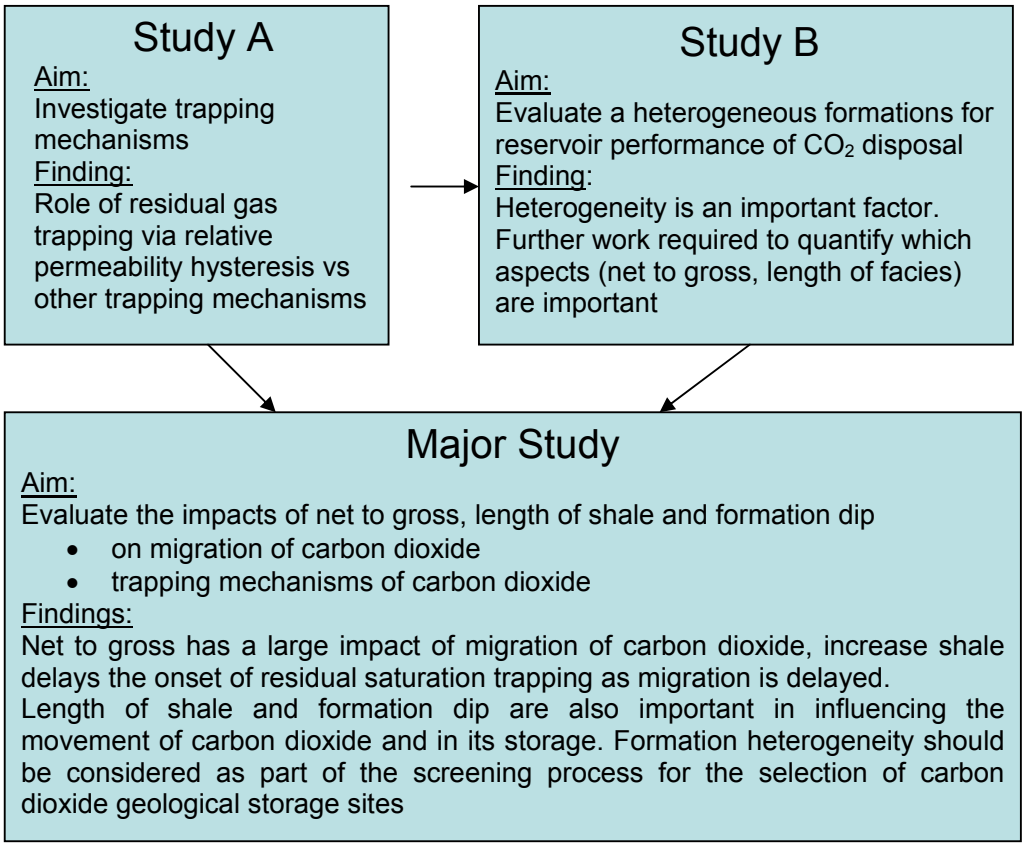

Figure 3-1: Structure of research study

The results of these studies are described in several papers. The findings of Study A were published in the conference presentation and proceedings of the 2004 SPE Asia Pacific oil and gas conference (Flett et al. 2004). Study B findings were published as a conference presentation and peer reviewed paper at the 7th International conference on Greenhouse Gas Control Technologies (Flett et al. 2004). The wide ranging findings of the Major study have been published in the Journal of Petroleum Science and Engineering (Flett et al. 2007) and also at the 8th International conference of Greenhouse Gas Control Technologies (Flett et al. 2006). The peer reviewed articles are shown in Appendix A of this thesis, while the conference papers are shown in Appendix B.

3.1 Reservoir Simulation Package and Formulation

Chevron Hydrocarbon Extended Applications Reservoir Simulator (CHEARS), a proprietary finite difference reservoir simulator, was used in its black oil formulation mode for all reservoir simulated studies in this thesis. Reservoir studies by Mo and Akervoll (Mo et al. 2005) demonstrated in their investigation of long term storage of carbon dioxide in saline formations that black oil simulation can be a flexible and appropriate method for simulating geological disposal.

In this particular type of black oil formulation, the injected CO_2 is treated as the gaseous phase and the formation water as the aqueous phase. The oleic phase is not required in these simulation studies as all formations modelled were aquifers with no hydrocarbons present. The technical scope of the simulation software meant that geochemical (i.e. mineralization) and geomechanical (i.e. rock failure) effects could not be considered in this research study. The omissions of geochemical reactions is satisfactory as the work of Pruess et al. (2003) shows that these can normally occur over the order of hundreds of years depending on formation rock, and is potentially limited to securing up to a maximum of 10% of injected carbon dioxide. As such, security of storage must be provided by other trapping mechanisms. Geomechanical effects were considered to be out of scope for this particular study, however the impact of these effects must be considered for the total evaluation of any CO_2 disposal project.

As noted previously, the Span and Wagner Equation of State (EOS) (Span and Wagner 1996) was used to model the pressure, volume and temperature (PVT) behaviour for all reservoir simulation in this thesis. Viscosity correlations employed in this study were after Vesovic et al. (1990) and Fenghour et al. (1998) implemented through an algorithm kindly provided by J. Ennis-King of CSIRO Petroleum (personal communication, 2003).

3.1.1 Integration of Dissolution Trapping and Gas-Water Relative Permeability Hysteresis with the Reservoir Simulator

Gas-water relative permeability hysteresis was enabled in CHEARS following Standing's application of Land's theory (Land 1968; Standing 1975) discussed in Chapter 2. In practical terms, gas-water relative permeability hysteresis is applied in

a reservoir simulation model, on a model cell basis, in the following manner: Gas (that is CO_2) enters the model cell from an adjoining cell under drainage relative permeability conditions; for each gas saturation or S_{gi} (initial gas saturation) the reservoir simulator determines the S_{gt} (trapped gas saturation) for the maximum S_{gi} attained in the cell and a set of imbibition relative permeability curves is calculated to be applied when gas saturation decreases from the S_{gi} in that cell. Thus in a full field reservoir simulation model, multiple imbibition relative permeability curves are in use, each curve scaled to the maximum gas saturation obtained in each cell containing gas. As in Land's theory, (Land 1968) trapped gas saturation in a model cell is dependent on the saturation history of the cell, its value being scaled to the maximum initial gas saturation attained in the cell during CO_2 injection and migration. Through this application of gas-water relative permeability hysteresis in a reservoir simulation tool, a trapping mechanism for injected CO_2 in formations can be evaluated.

The mechanism of dissolution of the CO_2 into the formation water was modelled using the correlations derived by Chang et al. (1998). Numerical dispersion effects on dissolution, as described by van der Meer (1995; 1996), were taken into account when specifying the dissolution rates. That is, large upscaled reservoir simulation grid cells will absorb more CO_2 into the aqueous phase faster than smaller 'fine scale' grid cells due to the larger grid cells areally dispersing the aqueous CO_2 at a greater rate than a fine scale model. In essence, large cells can overestimate the rate and extent CO_2 dissolution during reservoir simulation and the dissolution tables that are used as input for reservoir simulation are required to be tuned to reduce the effect of numerical dispersion. Both Juanes et al. (2006) and Mo et al. (2005) have investigated the potential impact of grid size effects on imbibition trapping, movement of injected carbon dioxide and dissolution. Juanes et al. (2006) stress that high resolution models are desirable to enhance the capture of the sweep of the migrating plume; however, Mo et al. (2005) state that the fundamental mechanisms were maintained in fairly coarse grid blocks. This dichotomy in opinion can be resolved by accounting for fine scale effects in coarse grid blocks, by using flow based upscaling techniques such as Durlofsky et al. (1996) (as used in the major simulation study in Chapter 6) which preserve fine scale flow effects in upscaled

models and tuning physical processes such as dissolution in the coarse model back to those observed in a fine scale model.

The tuning process for dissolution was derived by Gurton (personal communication, 2003) and is a short process conducted on twin sector models; the first sector model derived from the fine scale model and the second model being the coarse model derived from the fine scale model after the upscaling process. Sectors from the same section of the fine and coarse scale model where taken and a single injection well placed in the same location in each sector model. The same rate and cumulative amount of CO_2 was injected into both models and the amount of CO_2 dissolved in each model was compared. A factor of 0.4 was need to be applied to the Chang et al. (1998) correlation in order to counter the impact of numerical dispersion.

3.2 Design of Experiments methodology with Monte Carlo simulations

Studies A and B use a methodology called Design of Experiments (DOE) or Experimental Design (NIST/SEMATECH. 2004). DOE allows systematic multi-variable analysis with a suite of simultaneous experiments. In the case of Studies A and B in this thesis, an organized set of reservoir simulation runs were used as the simultaneous experiments. DOE is statistically rigorous and can formulate a ranking of parameters that affect a certain reservoir outcome in order of the size of the impact that parameter has on the outcome. From the ranking of parameters, a proxy variable equation can be developed to model the responses observed in the outcomes of the DOE results using a least squares fit method. There are many generic software packages that can accomplish the building of the proxy variable equation including Microsoft Excel, however this thesis used a proprietary tool developed by Chevron. The proxy equation can be used to generate a range of probabilistic outcomes, by using Monte Carlo simulation tools such as Crystal Ball^{TM} from Oracle. The generation of probabilistic outcomes is possible through running Monte Carlo simulations of varying the inputs variables of the proxy equations by a reasonable range and measuring the output of the equation. From running many thousands of such simulations, an estimate of the probabilistic range of results is created. The chapters of Study A and B further develop the application of DOE methodology.

3.3 Assumptions

For all models in the following studies in this thesis, the following assumptions have been made:

- All formations are saline formations with no hydrocarbon columns or residual saturations present. Two phase relative permeability only exists in the models.
- Geochemical effects not modelled.
- Geomechanical effects such as fracturing of wells are not modelled.
- The injected fluid in all simulations is pure CO_2.
- The models employed in all studies are generic in nature with model properties typical of generic shallow marine sand, not representing a particular formation or location.

4. Study A

The objective of Study A is to investigate the relative effects of various trapping mechanisms for a generic carbon dioxide geological storage project and the impact of some common reservoir uncertainty parameters on the trapping mechanisms.

4.1 Reservoir Simulation Model

A conceptual reservoir simulation model of a saline formation was constructed in the form of a rectangular tank. The model was populated with petrophysical properties consistent with a fine-grained, lower shore face shallow marine depositional environment. The basic rock properties selected for the formation are summarised in Table 4-1.

Table 4-1: Study A simulation model summary

Depositional setting	Lower Shoreface Shallow Marine
Average horizontal permeability	14.6 md mean, 0.482 log normal std. deviation
Average vertical permeability	3.2 md mean, 8.8 std. deviation
Average porosity	0.147 mean, 0.08 std. deviation
Temperature	200° F / 93.3° C
Solubility range	~ 100 scf/bbl varying with reservoir conditions, based on Chang, Coats and Nolen (1998) correlation.
Average initial pressure	3000 psia
CO_2 PVT correlation	Span & Wagner CO_2 Equation of State (Span and Wagner 1996)
Salinity	30000 ppm
Typical grid block size	400m by 400m by 5 m
Model dimensions	66 by 51 by 49
Model lengths	26.4 km by 20.4 km by 240 m
Rate of injection	25 MMscf/d (0.48 MTPA CO_2)
Injection period	50 years

The porosity distribution in the model ranges from 0 to 0.35, with a mean porosity of the formation of 0.147 and a standard deviation of 0.08. Porosity was distributed in the model using the geostatistical or stochastic process of Sequential Gaussian Simulation (SGS). SGS is a common geostatistical technique used in many commercial earth modeling packages. SGS is a method where the given rock property is randomly populated according to a specified distribution (Olea 1999). The distribution used in this study was based on lower shore face formation values (personal communication, Gurton 2004). Permeability was distributed using a generic porosity-permeability cloud transform based on lower shore face formation values (personal communication, Gurton 2004). Figures 4-1 to 4-3 show histograms describing reservoir property ranges for Study A.

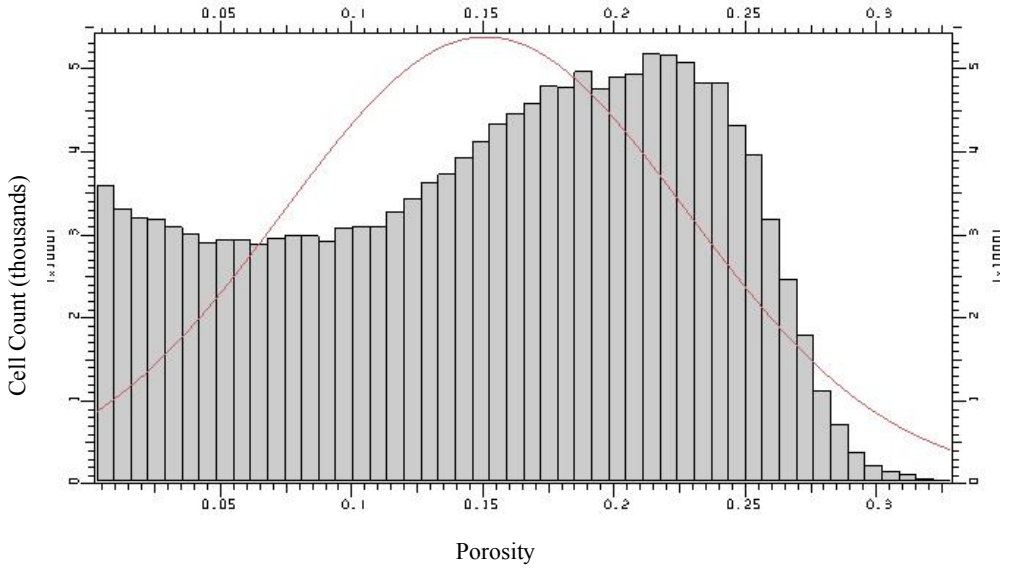

Figure 4-1: **Histogram of porosity in the Study A model**

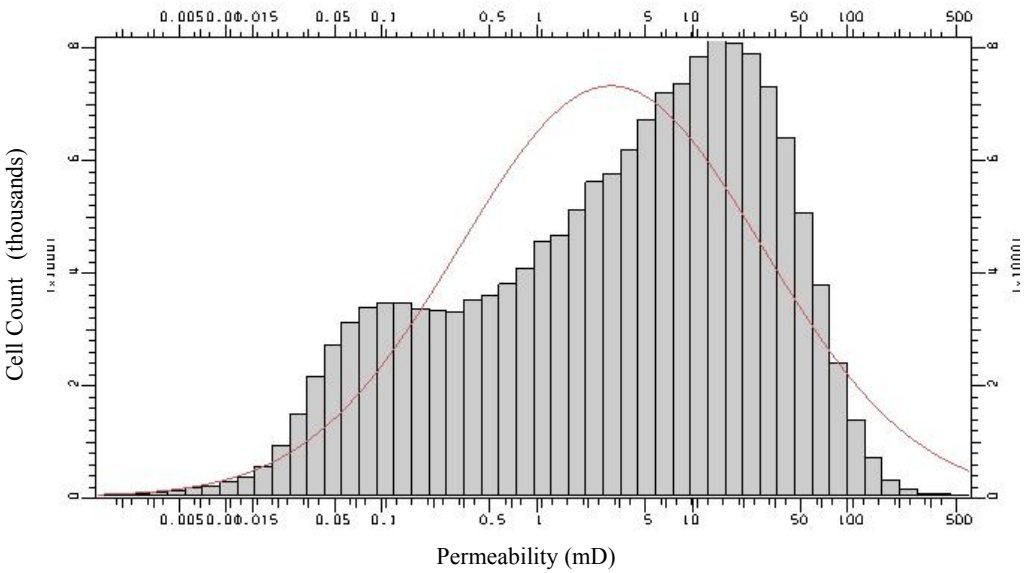

Figure 4-2: **Histogram of permeability in the Study A model**

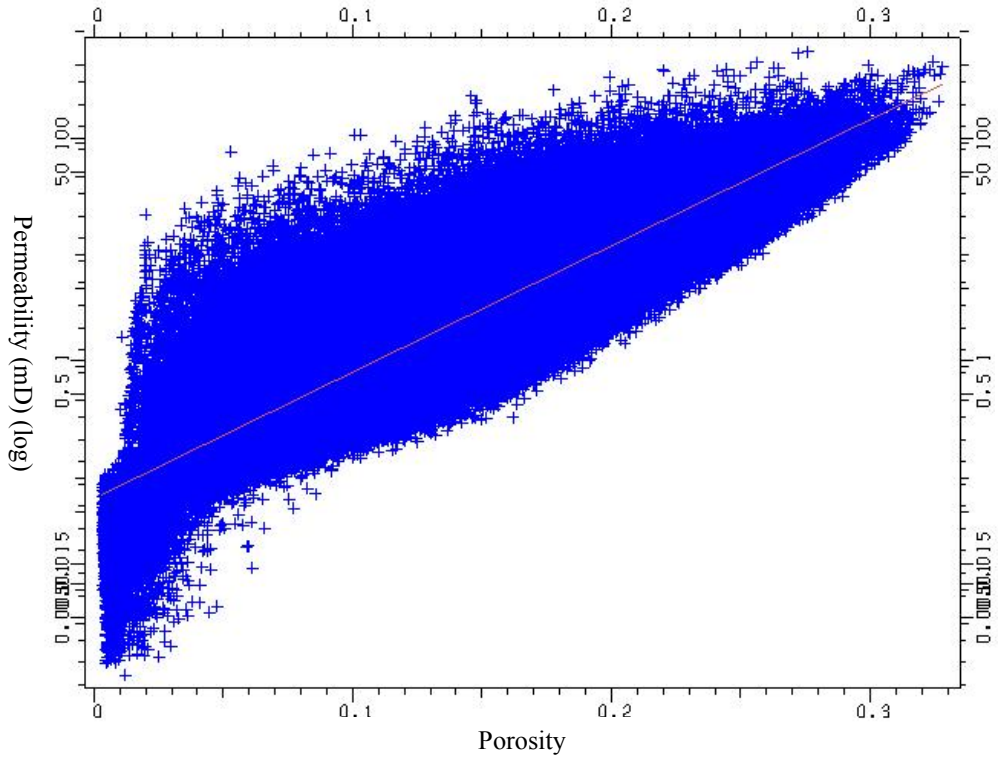

Figure 4-3: **Porosity – Permeability crossplot for the Study A model**

Figure 4-4 shows a cross-sectional slice of the model, showing some porosity trends in the model. The permeability in the model ranges from 0 to 630 md, with a mean permeability of 14.6 md and a standard deviation of 0.482 (log normal standard

deviation). The model was constructed in the form of a tank with a reservoir thickness of 240m. The formation has constant dip of two degrees from the horizontal. The formation was simulated as a totally water filled aquifer with a water salinity of 30000 ppm, reservoir pressure of 3000 psia / 20.68 MPa and a formation temperature of 200º F, consistent with a normally pressured formation at a subsea depth of approximately 2000m or 7000ft.

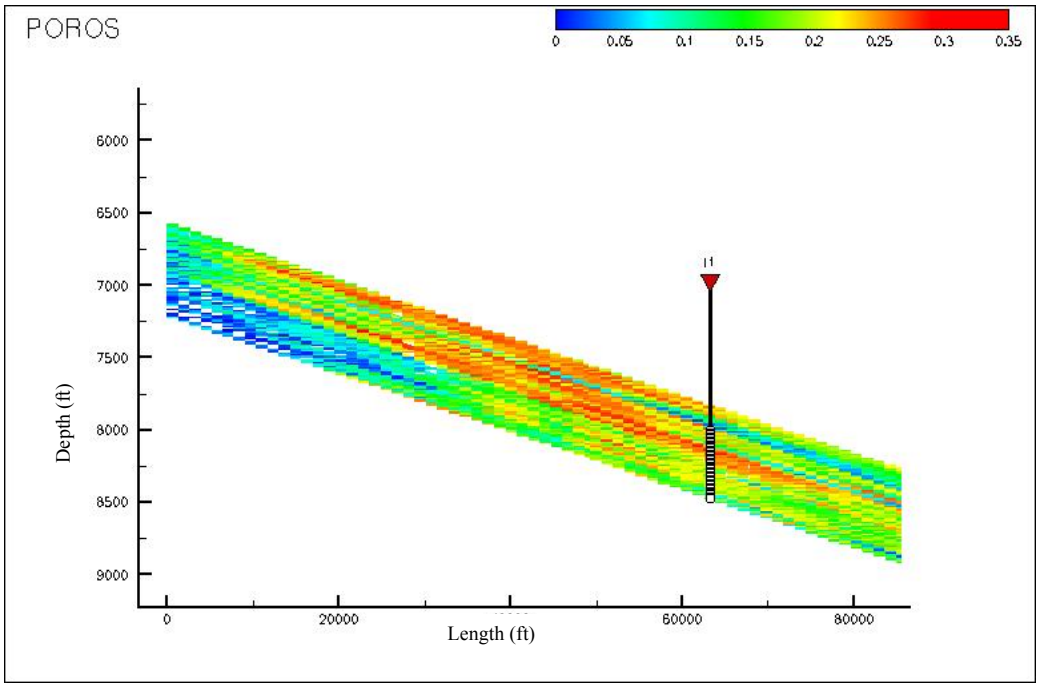

Figure 4-4: Porosity cross section of the conceptual simulation model.

This image is copyright of Society of Petroleum Engineers (2004). Published in SPE Paper 88485, proceedings of 2004 SPE Asia Pacific Oil and Gas Conference and Exhibition, Perth, Australia.

The simulation model has a single injection well situated near the down dip end of the model. A simulation was performed for the base case (or mid point) model which involved injecting 25 MMscf/d into the formation for 50 years and then shutting in the injector and monitoring the CO_2 plume movement for an additional 950 years. The mid point model parameters are shown in Table 4-2.

Plackett-Burman design, a current best practice in the petroleum industry, is a method of conducting multivariable analysis (Plackett and Burman 1946). Plackett Burman design was selected for Study A as an initial methodology for this thesis. Plackett Burman design is a simple form of Design of Experiments (DOE)

methodology (Plackett and Burman 1946; NIST/SEMATECH. 2004). This methodology allows multi-variable analysis with a suite of simultaneous experimental runs or in this case several reservoir simulation runs. This technique is statistically rigorous and can formulate a ranking of parameters that affect a certain reservoir outcome. Plackett-Burman designs assume a linear response from variable changes. If the linear response to variable changes is observed then the responses of the experimental runs can be used to generate a range of probabilistic outcomes for reservoir performance as well as saving time and effort of a more complex Design of Experiment method. The generation of probabilistic outcomes is possible through measuring the responses of the organized multiple combinations of high and low side outcomes for each parameter in the experimental design matrix. It is recognized that a higher order experimental design, consisting of many more simulation runs could be used to create an improved reservoir model response proxy and as such was considered in a subsequent Study B.

Hence a Plackett-Burman Design of Experiments study was employed to investigate the impact of the following reservoir model parameters: permeability, vertical permeability, Land's constant, relative permeability curves and irreducible water saturation (S_{wir}). For each parameter a reasonable low side and high side value was chosen to capture the range of uncertainty in the parameter. See Table 4-2 for parametric ranges.

Table 4-2: Parametric ranges for design of experiment simulation study

Parameter	Low side	Mid point	High side
Permeability Multiplier	0.5	As modelled	5
Vertical Permeability Multiplier	0.1	As modelled	10
Land's Constant	6	3	1
Relative permeability Curves	Segregated flow: Corey exponents (ngas 1.5, nwater 1.5)	Rock curves Corey exponents (ngas 2, nwater 4)	Tight rock curves Corey exponents (ngas 2, nwater 6)
Irreducible water saturation	0.6	0.5	0.4
Solubility	- 30% mid point	As calculated from Chang, Coats and Nolen (1998).	+ 30 % mid point

A Plackett-Burman matrix was created for a suite of thirteen simulation runs which included a single mid point run. The matrix is shown in Table 4-3. The matrix allows the combination of high and low values of parameters in multiple permutations, capturing the range of model outcomes. Each simulation run used the same single well design as in the midpoint model, namely injecting 25 MMscf/d CO_2 into the model for 50 years and monitoring the CO_2 plume migration after the injection well was shutin for an additional 950 years, for a total simulation time of 1000 years.

Table 4-3: **Plackett-Burman experimental design matrix used in Study A**

Simulation Run	Permeability	Vertical Permebility	Land's Constant	Relative Permeability	Irreducible Water Saturation	Solubility
1	High	Low	High	Low	Low	Low
2	High	High	Low	High	Low	Low
3	Low	High	High	Low	High	Low
4	High	Low	High	High	Low	High
5	High	High	Low	High	High	Low
6	High	High	High	Low	High	High
7	Low	High	High	High	Low	High
8	Low	Low	High	High	High	Low
9	Low	Low	Low	Low	High	High
10	High	Low	Low	Low	High	High
11	Low	High	Low	Low	Low	High
12	Low	Low	Low	Low	Low	Low
Mid point	Mid	Mid	Mid	Mid	Mid	Mid

4.2 Study A Metrics

The geological disposal of CO_2 is a new style of subsurface development compared to traditional subsurface developments in the petroleum field. Accordingly, new metrics need to be used in order to evaluate a geological disposal project compared to standard metrics used in normal petroleum reservoir simulation studies, such as cumulative oil production and net present value. Geological disposal projects are not likely to give a return on capital employed unless some type of CO_2 emission tax can be avoided, as no valuable commodity is produced. Thus to evaluate the performance of storage project, subsurface metrics will need to be employed until an agreed fiscal regime has been established.

Thus, some basic subsurface metrics for geological disposal projects were developed. The metrics are: degree of lateral plume migration away from an injection well; reservoir pressure response to CO_2 plume injection; and the volumes of trapped and mobile CO_2. Lateral migration of CO_2 away from injection wells needs to be monitored to identify the location of CO_2 as it permeates the formation. Vertical migration of CO_2 plume needs to be monitored; to quantify the any amount of CO_2

that could possibly leak from the formation through various means such as existing well-bores, leaky faults, or poor top seal. Pressure rise should be monitored, as over pressuring the formation can have geo-mechanical implications such as fracturing the formation or reactivating faults.

In terms of the long term storage fate of CO_2, various metrics can be derived. The amount of CO_2 dissolved in the formation can be estimated from simulation with calibrated CO_2 dissolution models (in reservoir simulation) such as the Chang, Coats and Nolen (1998) model. The migrating plume will also leave a residual phase behind the plume. The size of the residual phase trail can be determined by reservoir simulation using appropriate imbibition relative permeability curves described previously in Chapter 2. The fraction of potentially mobile CO_2, that is the CO_2 that can potentially breach the injected formation, can be found by subtracting the fraction of dissolved CO_2 and the fraction of residually trapped CO_2 away from unity.

4.3 Results

Model results were evaluated using the metrics outlined previously section 4.2. The results for Study A are summarised in Tables C-1, C-2 and C-3 in Appendix C. Visualisation of gas saturation cross-section at 1000 years in the midpoint model is shown in Figure 4-5. Visualisation of the top layer of the simulation model at 1000 years for the midpoint simulation run for the Plackett-Burman design is shown as Figure 4-6. Figures showing the top layer of the model for the rest of the experimental design run are shown as Figures in Appendix D. A 1000 years was selected as an appropriate time for simulation model for CO_2 disposal as an engineering judgment into allowing sufficient time for the long term trapping mechanisms to have an effect and also to allow for sufficient post injection migration of the injected CO_2 plume. Impact on distance and shape of the migrating plume due to the different combination of parameters is evident in these images.

A statistical ranking of parameters for each metric selected for the study (i.e. migration distance, pressure rise in the formation, fraction of injected plume trapped, dissolved and mobile) was calculated from the results in Tables C-1, C-2 and C-3 in

Appendix C. A test of statistical significance was set at a 95% confidence limit to determine which parameters have clearly defined effects on certain results. Tables 4-4, 4-5 and 4-6 summarises the ranking of parameters for each metric in order of significance and show if a certain parameter was statistically significant above the 95% confidence limit. From the model response a normalized response surface polynomial was calculated, for each metric. The response polynomial proxy was used as a basis for Monte Carlo simulations for each metric. For the Monte Carlo simulations, permeability and vertical permeability were modeled with log-normal distribution; the other parameters were modeled with a normal distribution of uncertainty about the midpoint value. See Table 4-7 for the Monte Carlo simulation generated p10-p50-p90 range of results for each metric.

Table 4-4: **Ranking of factors in order of significance for CO_2 plume migration and pressure rise at the model seal**

Factor	Migration 50 years	Migration 100 years	Migration 1000 years	Pressure Rise 50 years	Pressure Rise 100 years	Pressure Rise 1000 years
Permeability	**X** 1	**X** 1	**X** 1	**X** 1	**X** 2	**X** 3
Vertical Permeability	3	2	**X** 2	**X** 2	**X** 3	**X** 2
Land's Constant	5	5	3	3	5	**X** 4
Relative Permeability	7	7	4	4	**X** 4	6
Irreducible Water Saturation	6	6	6	5	6	7
Solubility	2	3	5	7	**X** 1	**X** 1
Non-linear effects	4	4	7	6	7	5

X denotes a statistically significant factor with a 95% confidence limit.

In Table 4-4, permeability is the significant factor controlling migration of the plume and a contributing factor to the degree of pressure rise in the formation. In later time, the degree of dissolution is important in effecting pressure.

Table 4-5: Ranking of factors in order of significance for fraction of CO_2 dissolved and trapped as a residual phase for the experimental design study

Factor	Fraction CO_2 dissolved 50 years	Fraction CO_2 dissolved 100 years	Fraction CO_2 dissolved 1000 years	Fraction CO_2 trapped 50 years	Fraction CO_2 trapped 100 years	Fraction CO_2 trapped 1000 years
Permeability	5	6	6	5	**X** 2	6
Vertical Permeability	3	2	3	3	4	4
Land's Constant	7	7	2	7	**X** 1	**X** 1
Relative Permeability	4	4	7	4	5	5
Irreducible Water Saturation	**X** 2	3	4	2	3	7
Solubility	**X** 1	**X** 1	**X** 1	**X** 1	7	**X** 2
Non-linear effects	6	5	5	6	6	**X** 3

X denotes a statistically significant factor with a 95% confidence limit.

In Table 4-5, solubility is a significant factor over the various time scales considered in determining the fraction of CO_2 dissolved and residually trapped. In later time, not surprisingly, the range of Land's constant is the most significant factor in determining the amount of residually trapped gas. Non-linear effects are significant in fraction of CO_2 residually trapped at 1000 years.

Table 4-6: **Ranking of factors in order of significance for fraction of CO_2 mobile for the experimental design study**

Factor	Fraction CO_2 mobile 50 years	Fraction CO_2 mobile 100 years	Fraction CO_2 mobile 1000 years
Permeability	5	4	5
Vertical Permeability	**X** 3	6	3
Land's Constant	7	**X** 2	**X** 1
Relative Permeability	4	7	7
Irreducible Water Saturation	**X** 2	**X** 3	6
Solubility	**X** 1	**X** 1	**X** 2
Non-linear effects	6	5	4

X denotes a statistically significant factor at a 95% confidence limit.

In Table 4-6, Solubility is the most significant factor over most time scale is controlling the amount of injected CO_2 that is mobile. In later time, Land's constant is more significant, suggest that residual gas trapping is more significant at later time. It should be noted that the major factors affecting the fraction of gas residually trapped, dissolved and remaining mobile are the uncertainty in the dissolution and residual trapping, not other reservoir parameters such as permeability and irreducible water saturation.

Table 4-7 shows the p10-p50-p90 range of results from Monte Carlo simulation of the Plackett Burman design response surface. Each result was derived by ten thousand Monte Carlo simulations of the relevant proxy polynomial for the metric being evaluated.

Table 4-7: **Monte Carlo simulation outcomes for Study A**

Metric	P10	P50	P90	Midpoint
Migration Distance 50 years (km)	2.20	3.63	5.06	2.79
Migration Distance 100 years (km)	2.20	4.93	7.66	2.79
Migration Distance 1000 years (km)	3.92	11.03	18.13	9.93
Pressure Rise 50 years (MPa)	0.805	1.594	2.383	1.642
Pressure Rise 100 years (MPa)	0.771	0.88	0.988	0.886
Pressure Rise 1000 years (MPa)	0.626	0.778	0.93	0.764
Fraction Dissolved 50 years	0.047	0.198	0.349	0.165
Fraction Dissolved 100 years	0.063	0.239	0.415	0.199
Fraction Dissolved 1000 years	0.094	0.330	0.566	0.274
Fraction Residually Trapped 50 years	0.003	0.009	0.015	0.007
Fraction Residually Trapped 100 years	0.011	0.129	0.247	0.109
Fraction Residually Trapped 1000 years	0.101	0.357	0.613	0.529
Fraction CO_2 Mobile 50 years	0.639	0.791	0.942	0.828
Fraction CO_2 Mobile 100 years	0.406	0.629	0.851	0.692
Fraction CO_2 Mobile 1000 years	0.065	0.307	0.549	0.198

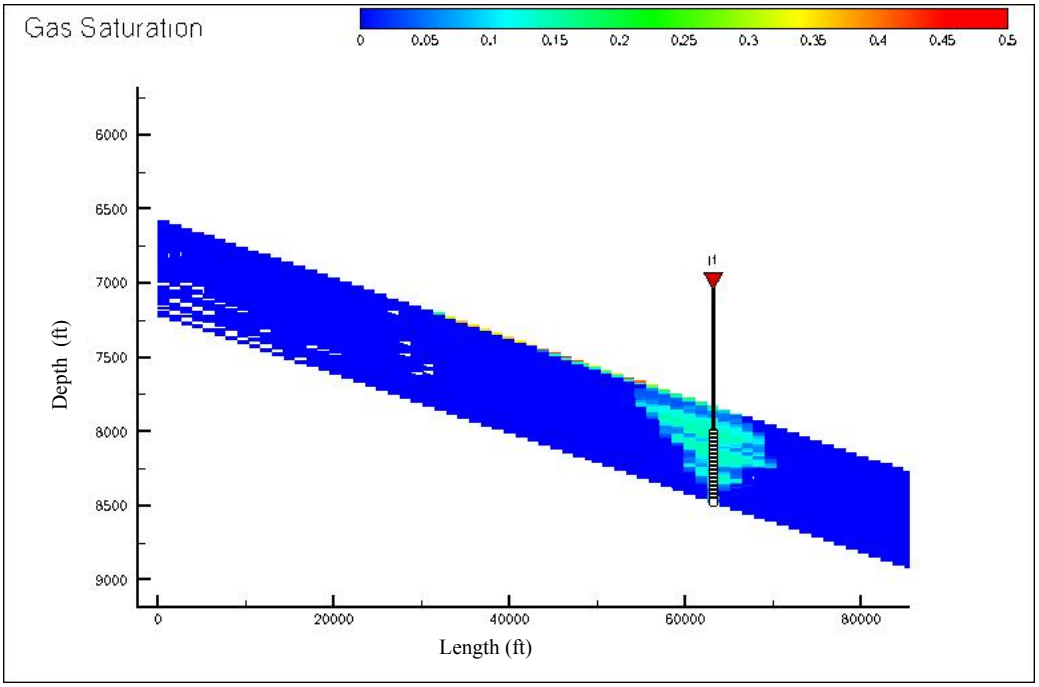

Figure 4-5: Cross section of the mid point simulation model showing gas saturation at 1000 years

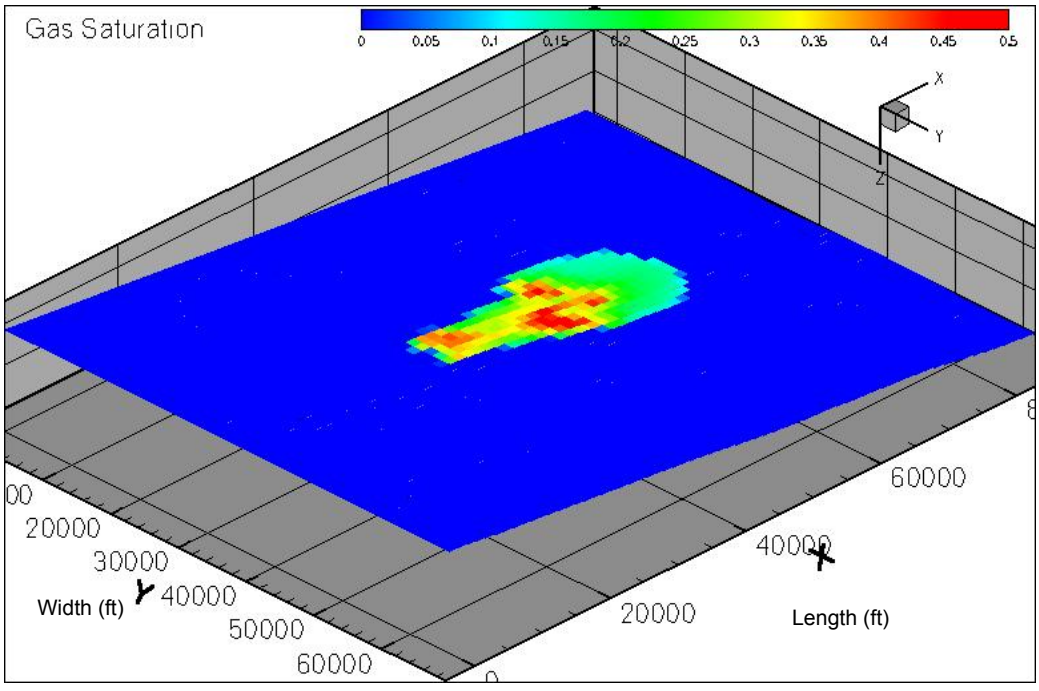

Figure 4-6: Top layer view of the mid point simulation model showing gas saturation at 1000 years

Figures 4-6 and 4-7 are copyright of Society of Petroleum Engineers (2004). Published in SPE Paper 88485, proceedings of 2004 SPE Asia Pacific Oil and Gas

Conference and Exhibition, Perth, Australia. Further figures for Study A are shown in Appendix D – Supplementary Figures.

4.4 Discussion

4.4.1 Migration of CO_2 Plume

The injected CO_2 in the model migrated laterally during injection under influence of the pressure provided by the injection well. Post injection, the lateral expansion of the plume ceased and CO_2 migrated upwards due to the lighter density of the CO_2 compared to the formation water. A significant residual trail of CO_2 remained about the wellbore as water imbibed behind the migrating plume, as shown in Figure 4-5. Thus by visual inspection of these figures, the impact of the mechanism of gas-water relative permeability hysteresis in trapping significant amounts of CO_2 was verified.

4.4.2 Impact of Permeability

As can be expected, the results of this study confirm that permeability has a large impact on the migration of a CO_2 plume and the pressure rise in the formation. High overall permeability increases the overall distance that a plume may migrate. Low permeability impedes CO_2 movement away from the injector post injection. A low permeability reservoir outcome has an effect of increasing the pressure rise in formation, as greater bottom hole pressure is required to inject the target rate of CO_2 through the well into the formation. Large pressure rises in low permeability outcomes can be a concern regarding faults and propagating fractures in the formation. Thus the finding of Law and Bachu (Law and Bachu 1996) is confirmed that a "sweet spot" of high permeability is desirable for injection of CO_2 to lower formation pressure rise with the remainder of the formation of lower permeability to reduce the risk of migrating CO_2 creating a containment breach.

While permeability is important for containment risks during and after injection, it has a diminished role in determining the long term storage fate of CO_2. Permeability, in this study, was not a consistent factor in determining a long term storage status for CO_2 as potentially mobile, dissolved or trapped as a residual phase. This is due to other factors having a more significant effect in the post injection migration stage of simulation, such as the degree of dissolution and residual gas trapping.

Vertical permeability has a significant impact on long term migration and the pressure transmitted to the seal of the model. Generally low vertical permeability reduced the volume of CO_2 reaching the top of the model by impeding vertical flow, allowing more CO_2 to be trapped through greater reservoir contact about the injector.

4.4.3 Impact of Relative Permeability

The range of relative permeability outcomes does have an impact on reservoir performance in terms of pressure rise in the near time after the injection of the CO_2 (less than 100 years post-injection). In the long term timeframe post injection, the differences in relative permeability curve shape has a diminished effect on the movement of the migrating plume. This diminished effect in the post injection phase is due to smaller forces acting on the migration plume (buoyancy forces) compared to the significant viscous forces from the injection well pressure during injection. The shape of the relative permeability curves also has small effect on the long term status of the CO_2 in the formation as the influence of residual gas trapping and dissolution has more significant impact.

4.4.4 Impact of Irreducible Water Saturation, S_{wir}

The irreducible water saturation uncertainty range used in this study had a small effect on the migration of a CO_2 plume and pressure buildup in the formation. S_{wir} has a significant effect during the injection of CO_2 for a low side outcome for S_{wir}. A low side outcome for S_{wir} (although it is a numerically higher value of S_{wir}) enhances reservoir contact for the CO_2, increasing the volume of water available for CO_2 to dissolve in the formation. The long term impact of the S_{wir} is diminished in comparison to the other factors considered in this study.

4.4.5 Impact of Solubility

Uncertainty in solubility has a significant impact on the fraction of mobile or trapped CO_2. Uncertainty in solubility also has an effect on the long term pressure response of the formation. As CO_2 dissolves into the formation the volumetric impact of CO_2 is reduced, hence pressure decreases. It is noted that dissolved CO_2 increases water density by a small fraction as demonstrated by Ennis-King and Paterson (Ennis-King and Paterson 2003). Using a reasonable range of uncertainty in solubility, the p10-

p50-p90 range of CO_2 dissolved into the formation for this study range from 0.094 to 0.330 to 0.566 fraction of CO_2 injected at the 1000 year timeframe. Solubility accounts for the sequestration of a significant fraction of CO_2 injected into a saline formation.

4.4.6 Impact of Trapped Gas Saturation

This study confirmed that trapping through the effects of gas-water relative permeability hysteresis is a post injection process, with most of the significant effects of uncertainty in Land's constant having an effect over the long post injection time frame that was simulated. During injection, uncertainty in Land's constant had a small effect on all metrics. After low values of permeability and vertical permeability effects, high side values of Land's constant limited migration of CO_2, although this measurement did not meet the 95% confidence significance test. From this observation it is worth examining a higher order / non-linear experimental design to resolve Land's constant as a significant factor in terms of migration. The uncertainty in Land's constant has a significant effect on the long term status of CO_2 in the formation. Higher residual phase CO_2 significantly limits the amount of CO_2 potentially mobile in the formation and hence reduces the risk of a containment breach. In this model and study, residual gas trapping was as significant as dissolution in trapping the CO_2. The ranges of CO_2 trapped as a residual phase for this model using a p10-p50-p90 range are 0.101 to 0.357 to 0.617 fraction at the 1000 year time frame. Thus a significant amount of CO_2 can be immobilized by this mechanism.

5. Study B

The objective of the Study B was to investigate the reservoir performance of a heterogeneous saline formation when used for geological storage of CO_2.

5.1 Reservoir Simulation Model

A new model was developed for this study as it was being developed in tandem with the Study A simulation model as it was desirable for the purpose of future publication opportunities to develop two separate models with different static realisations to delineate each study from each other. A conceptual, generic heterogeneous model was populated with siltstone/sand properties consistent with a fine-grained lower shore face shallow-marine sandstone reservoir similar in concept to the Study A model. The summary of generic model properties is shown in Table 5-1. The Study B simulation model does not have the box like structure of the Study A model, instead it has a 4 way enclosure updip in the model with a gentle dip down the lengthways section of the model. Figures 5-1 and 5-2 show the structure of the Study B model.

Table 5-1: Study B model summary

Depositional setting	**Fine-grained lower shoreface shallow marine**
Average horizontal permeability	50 md mean, 20 md median
Average vertical permeability	1.38 md mean , 0.001 md median
Average porosity	0.18
Temperature	212ºF or 100° C
Solubility range	100 scf/bbl varying with uncertainty in formation water properties (Chang et al. 1998)
Average initial formation pressure	3200 psia (22.06 MPa)
Typical grid block size (m)	400 by 400 by 5
Model dimensions	38 by 49 by 28
Model lengths (km)	15.2 by 19.6 by 0.2
Rate of injection	50 MMscf/d or ~0.48 MTPA CO_2
Injection period	60 years

The formation was modelled with a salinity of 30000 ppm, reservoir pressure of 3200 psia and a formation temperature of 212ºF, in keeping with a normally pressured marine sand of some 2 km or 7000 ft in depth. The porosity distribution in the model ranges from 0 to 0.326, with a mean porosity of the formation of 0.180 with a standard deviation of 0.05. The permeability distributed in the model ranges from 0 to 450 md, with a mean permeability of 50 md and a log normally distributed standard deviation of 1.21. Reservoir thickness is 200m. The reservoir model was structured with a shallow dip of 1.5º. As before in Study A, the porosity was distributed geostatistically using the Sequential Gaussian Simulation technique (Olea 1999). Figures 5-1 and 5-2 show the porosity distribution and hence heterogeneity present in the reservoir model. Permeability was distributed using a generic porosity-permeability cloud transform based on lower shore face formation values as in the Study A model.

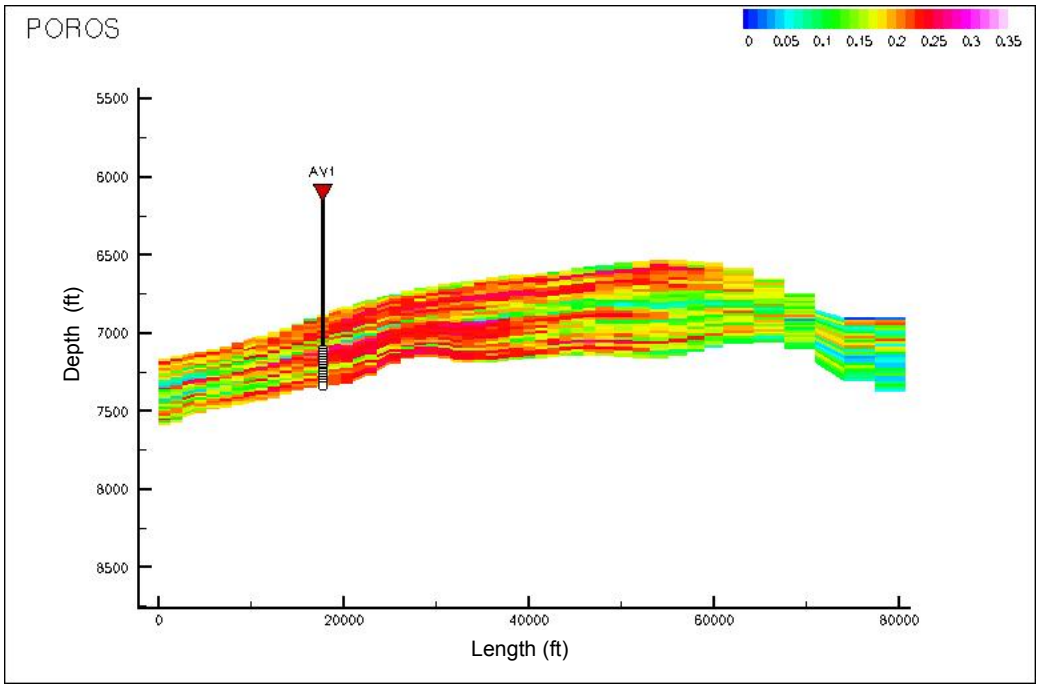

Figure 5-1: Porosity distribution in the Study B model

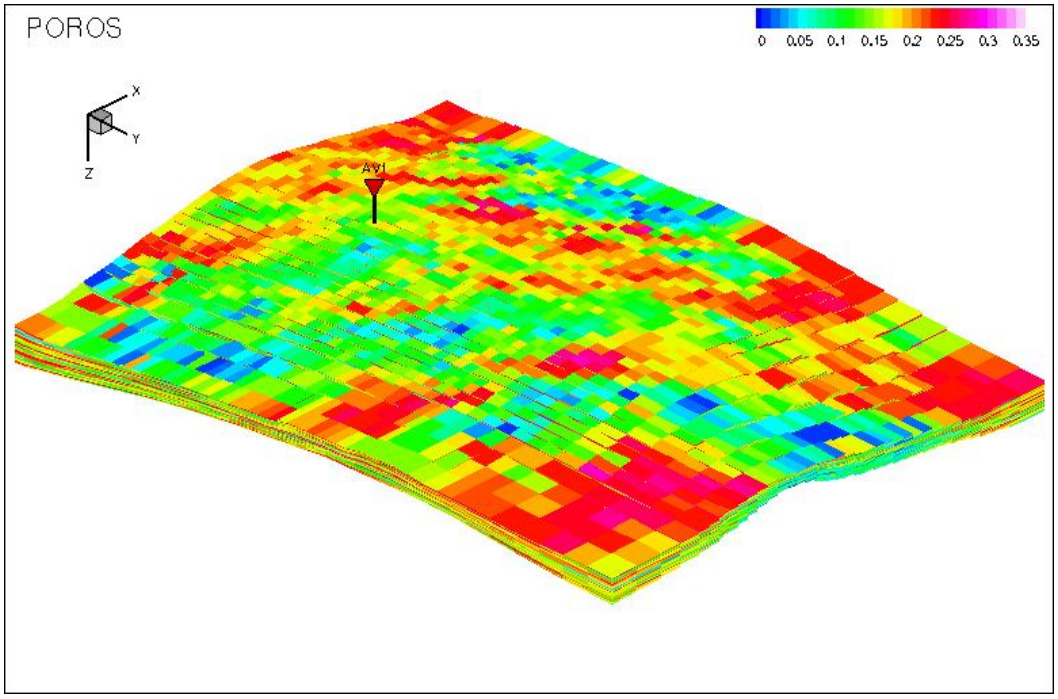

Figure 5-2: **Porosity distribution in the Study B model**

A single vertical well was situated down dip in the reservoir model. The well was completed in the lower half of the model to take advantage of longer reservoir contact between the plume and the formation water. The well placement in the model is shown in Figure 5-2. CO_2 was injected at a rate of 50 MMscf/d for a period of 60 years. Post injection, the simulation was run for 1000 years to monitor long term migration and status of CO_2 in the formation as dissolved, mobile or trapped as a residual phase.

As part of the evaluation of the results of Study A (the responses were in a Plackett Burman design (Plackett and Burman 1946)), some non-linear responses of statistical significance for metrics were observed. To better characterise the non-linear response of the variables examined in this subsequent study, a revised multivariable analysis approach has to be taken. Hence, a second order non-linear Design of Experiments (DOE) (NIST/SEMATECH. 2004) sensitivity study was employed to investigate reservoir performance of this CO_2 storage model.

DOE methodology allows the establishment of statistical significant factors in the results. Second order designs can investigate non-linear responses and interactions

between parameters affecting reservoir performance better than a Plackett Burman design as used in Study A. Plackett Burman designs assume a linear response and as such can be very useful for initial screening studies for multivariable reservoir simulation uncertainty analysis. If non-linear responses are observed with a Plackett Burman design study, a subsequent uncertainty analysis study should take that into account and plan to use a DOE methodology that can examine which interactions between parameters are significant.

The parameters varied were: relative permeability curves, irreducible water saturation (S_{wir}), solubility, maximum trapped gas saturation and permeability. See Table 5-2 for parametric ranges. The ranges reflect a broad range of uncertainty based on petroleum reservoir experience with regards to the range of permeability in the reservoir and irreducible water saturation. A conservative outlook was taken regarding maximum trapped gas saturation, based on literature values (Hamon et al. 2001). The relative permeability curves employed were based on Brook-Corey theory and reflect a wide range of scenarios possible for subsurface CO_2 movement (Brooks and Corey 1966). Solubility uncertainty ranges reflect an appropriate range of uncertainty in formation water properties.

A second order DOE matrix, totalling thirty simulation runs was employed to test reservoir parameter sensitivities. The next step of this second order DOE study was to determine the statistically significant factors at 95% confidence, in the response of these variable changes. Following the significance tests, the reservoir performance response surface or proxy (a polynomial type equation that models the responses of the study) can be developed for each metric. The polynomial for each metric was used in a Monte Carlo simulation to generate a probabilistic range of reservoir responses based on uncertainty in individual parameters used. The range of probabilistic outcomes was ranked to give p10-p50-p90 values for each metric in the simulation study.

Table 5-2: Parametric ranges for Study B

Parameter	Low side	Base Case	High side
Relative permeability	Segregated flow: Corey exponents (ngas 1.5, nwater 1.5)	Rock curves Corey exponents (ngas 2, nwater 4)	Tight rock curves Corey exponents (ngas 2, nwater 6)
Irreducible water saturation	0.6	0.5	0.4
Solubility	- 30% base case	As for Chang, Coats and Nolen (1998)	+ 30 % base case
Land's constant	6	3	1
Permeability multiplier	0.3	1	3

Table 5-3: **Second order design of experiments table used in Study B**

Simulation Run	Relative Permeability	Swir	Solubility	Land trapping	Permeability
1	Low	Low	Low	Low	High
2	Low	Low	Low	High	Low
3	Low	Low	High	Low	Low
4	Low	Low	High	Mid	Mid
5	Low	Low	High	High	High
6	Low	Mid	Low	Mid	Low
7	Low	Mid	Mid	Low	Low
8	Low	High	Low	Low	Low
9	Low	High	Low	High	High
10	Low	High	Mid	High	Mid
11	Low	High	High	Low	High
12	Low	High	High	High	Low
13	Mid	Low	Mid	High	Low
14	Mid	Low	High	Low	High
15	Mid	Mid	Low	High	Mid
16	Mid	Mid	Mid	Mid	High
17	Mid	High	Low	Low	Mid
18	Mid	High	High	Mid	Low
19	High	Low	Low	Low	Low
20	High	Low	Low	High	High
21	High	Low	Mid	Mid	Mid
22	High	Low	High	Mid	High
23	High	Low	High	High	Low
24	High	Mid	Low	Low	High
25	High	Mid	High	High	Mid
26	High	High	Low	Low	High
27	High	High	Low	High	Low
28	High	High	Mid	Low	Low
29	High	High	High	Low	Low
30	High	High	High	High	High

5.2 Study B Metrics

The subsurface metrics for Study B, were carried over from Study A. These selected metrics were used to gauge reservoir performance for the Study B reservoir simulation program:

- Lateral migration of injected carbon dioxide,
- Pressure rise at the seal (i.e top of the formation in reservoir simulation model),
- Fraction of CO_2 injected subsequently dissolved, and
- Fraction of CO_2 injected subsequently trapped as a residual phase.

5.3 Results

Parameters affecting reservoir metrics for Study B are shown in Table 5-4. Examples of Pareto charts diagrammatically showing the significance and ranking of parameters effecting migration of CO_2 at 60 years and the fraction of CO_2 residual trapped at 1000 years are shown in Figures 5-3 and 5-4. The response metrics measured in this study were: migration distance of the CO_2 away from the injector; pressure rise at the seal at the injection well; fraction of CO_2 injected dissolved and fraction of gas trapped as a residual phase. These were evaluated at the end of injection 60 years, and at 1000 years. Visualisations of CO_2 migration for the base case model are shown as cross sections through the injection well in Figures 5-5 to 5-8 and from the top layer in Figures 5-9 to 5-12. Heterogeneities in the formation prevent uniform plume distribution and migration about the well bore. The final step of Design of Experiments methodology is to run Monte Carlo simulations of the response surface. From Monte Carlo simulations expected / probabilistic range of results can be predicted. The results of Monte Carlo simulations are summarised in Table 5-4 for each metric measured in this study.

Table 5-4: **Statistically significant factors and ranking**

Factor	**Migration 60 years**	**Migration 1000 years**	**Pressure rise at seal 60 years**	**Pressure rise at seal 1000 years**
Relative Permeability	**X** (2)	**X** (3)	**X** (3)	**X** (4)
S_{wir}	**X** (4)		**X** (4)	**X** (5)
Solubility	**X** (3)	**X** (4)	**X** (2)	**X** (1)
Land's Constant		**X** (2)		**X** (3)
Permeability	**X** (1)	**X** (1)	**X** (1)	**X** (2)

Factor	**Fraction CO_2 dissolved 60 years**	**Fraction CO_2 dissolved 1000 years**	**Fraction CO_2 trapped 60 years**	**Fraction CO_2 trapped 1000 years**
Relative Permeability	**X** (2)	**X** (3)	**X** (3)	
S_{wir}	**X** (4)	**X** (5)	**X** (1)	**X** (3)
Solubility	**X** (1)	**X** (1)	**X** (4)	**X** (4)
Land's Constant	**X** (5)	**X** (2)	**X** (5)	**X** (1)
Permeability	**X** (3)	**X** (4)	**X** (2)	**X** (2)

X denotes that factor is significant as a first or higher order term at a 95% confidence limit. This Table was created from interpretation of Pareto charts.

In this study, all factors are significant in some manner. The order of significance does change with each metric, e.g. permeability is most significant factor for migration, but less significant for the fraction of CO_2 that is dissolved. The order is of significant factors is in line with expectations from Study B, e.g. permeability most significant for migration, Land's trapping for residual trapping, solubility for dissolution.

Table 5-5: **Monte Carlo ranges of results from Study B**

Parameter	**P10**	**P50**	**P90**
Migration (km) 60 years	2.75	3.82	4.89
Migration (km) 1000 years	3.03	7.52	12.00
Pressure rise at seal 60 years (MPa)	0.90	1.31	1.72
Pressure rise at seal 1000 years (MPa)	0.76	0.88	1.00
Fraction CO_2 dissolved 60 years	0.052	0.123	0.204
Fraction CO_2 dissolved 1000 years	0.083	0.217	0.351
Fraction CO_2 trapped 60 years	0.000	0.031	0.080
Fraction CO_2 trapped 1000 years	0.118	0.461	0.804

Table 5-5 shows the results of Monte Carlo simulations based on the DOE proxy equation. The table shows the expected low to high range of results for each metric measured.

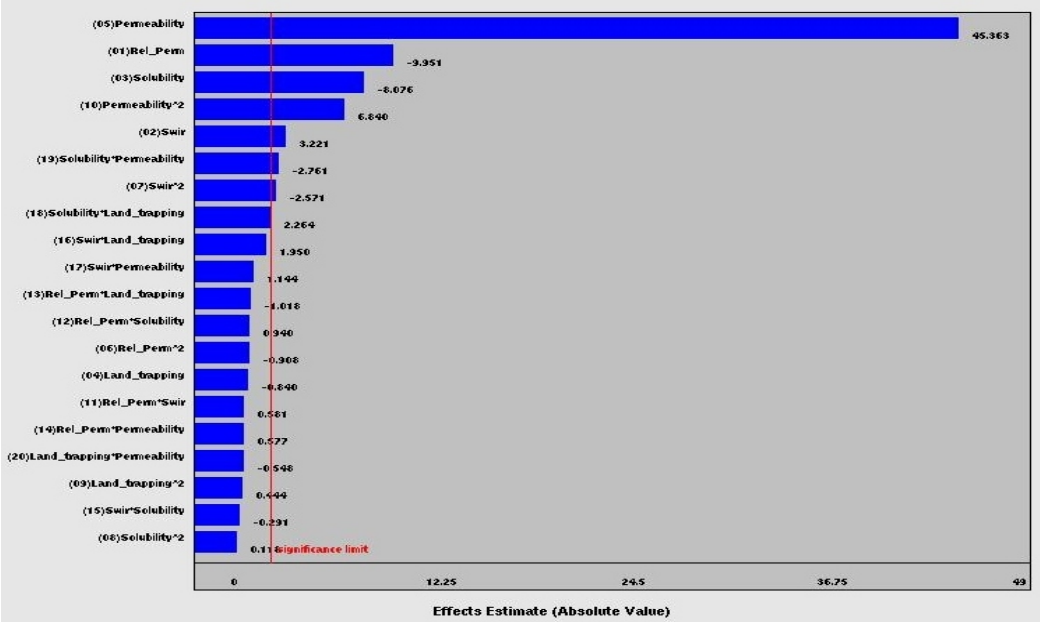

Figure 5-3: Pareto chart for migration of CO_2 at 60 years

In Figure 5-3 the influence of permeability on migration is paramount and is the most significant effect.

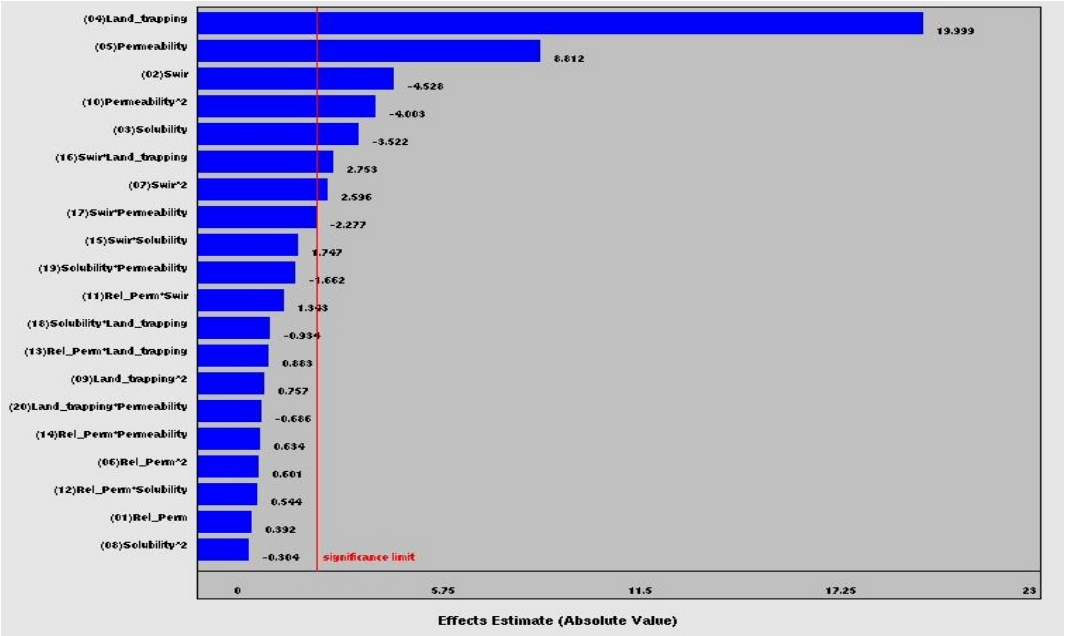

Figure 5-4: **Pareto chart for residual trapping of CO_2 at 1000 years**

In Figure 5-4 the influence of Land's constant in residual trapping is the most significant effect, however permeability (which controls rate of migration) is also quite significant.

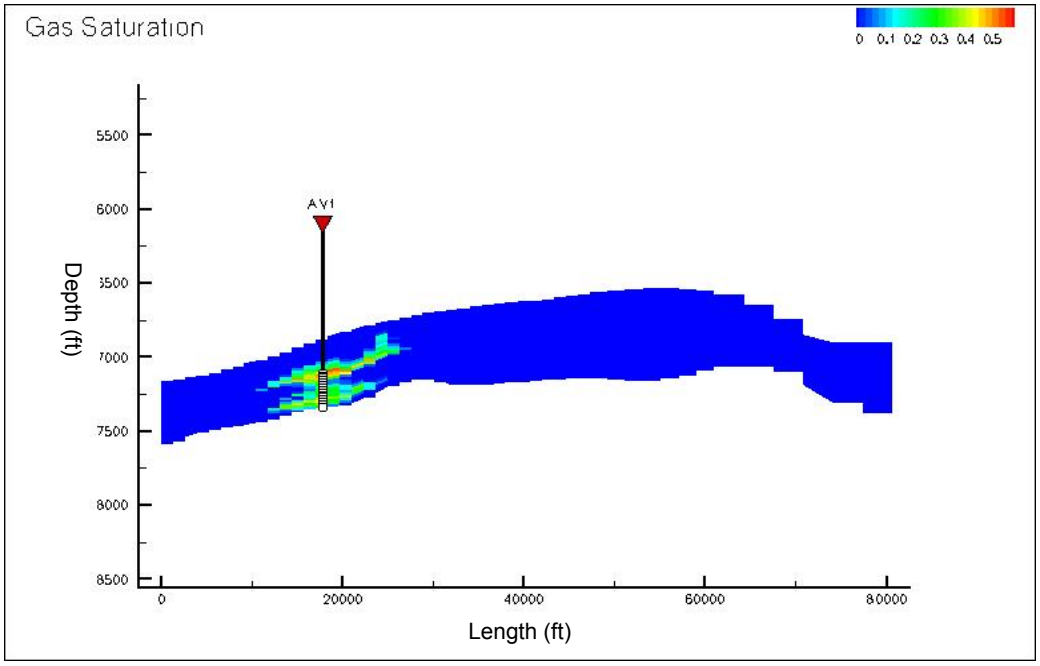

Figure 5-5: Cross section showing CO_2 migration for the reference case model – 30 years.

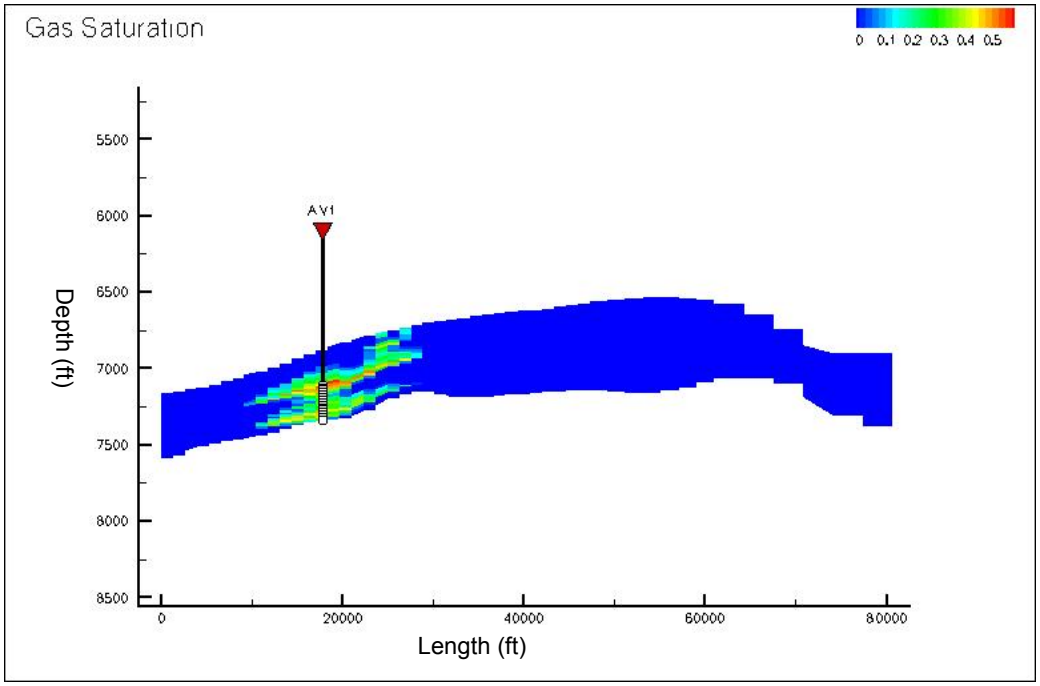

Figure 5-6: Cross section showing CO_2 migration for the reference case model – 60 years

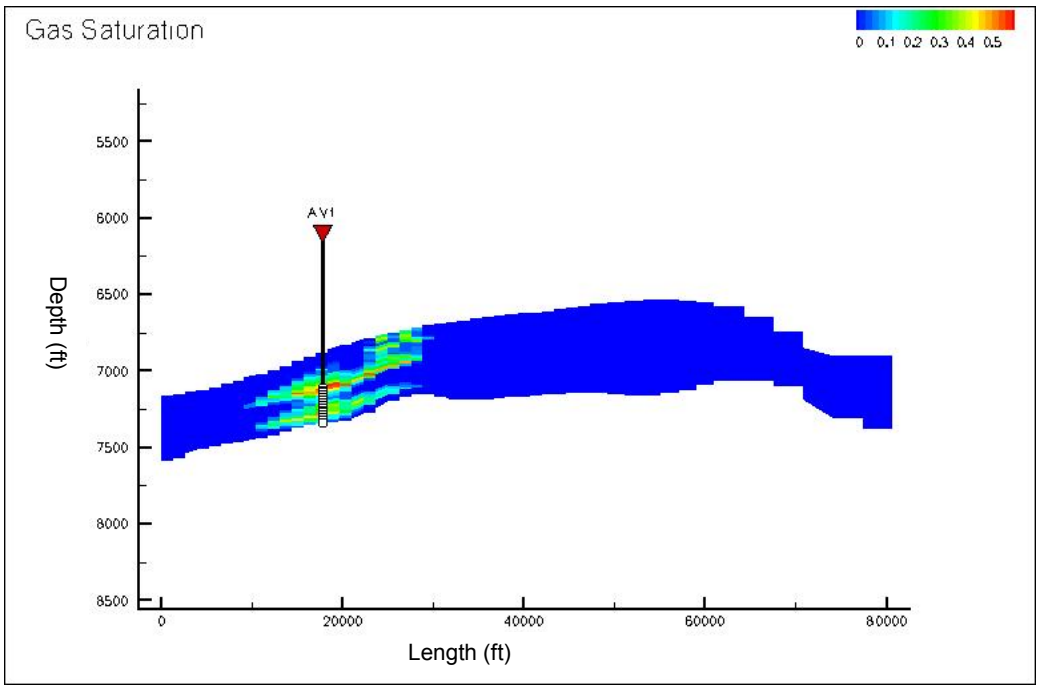

Figure 5-7: Cross section showing CO_2 migration for the reference case model – 100 years

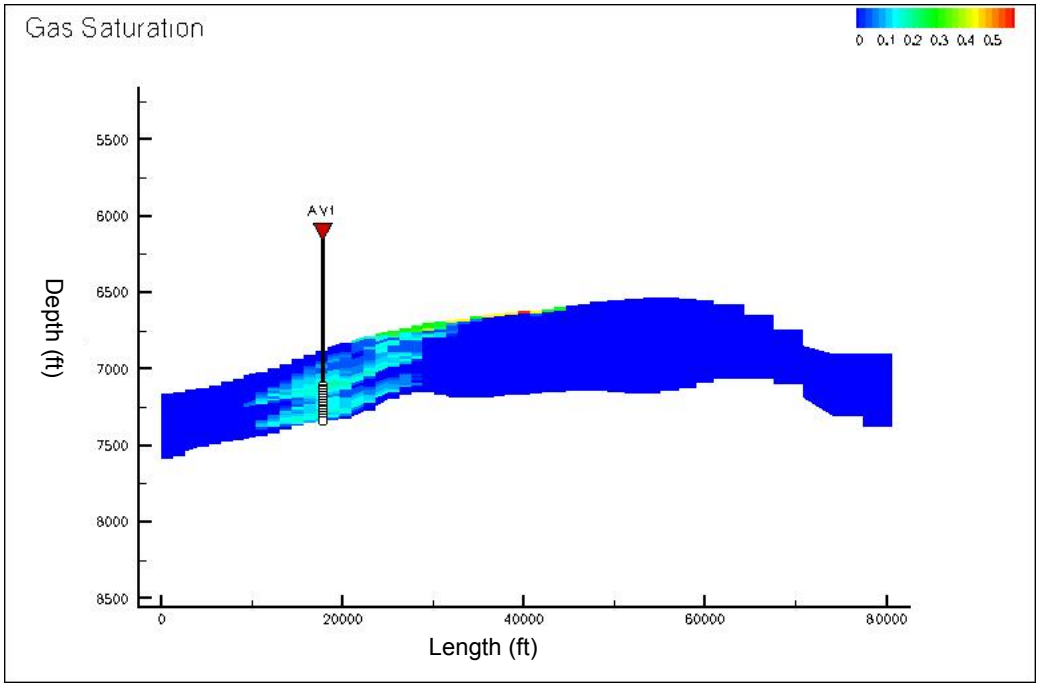

Figure 5-8: Cross section showing CO_2 migration for the reference case model – 1000 years

In Figures 5-5 to 5-8, the movement up dip by the migrating CO_2 plume is shown. At 1000 years, in Figure 5-8, a trail of residual gas can be seen about the injection well bore.

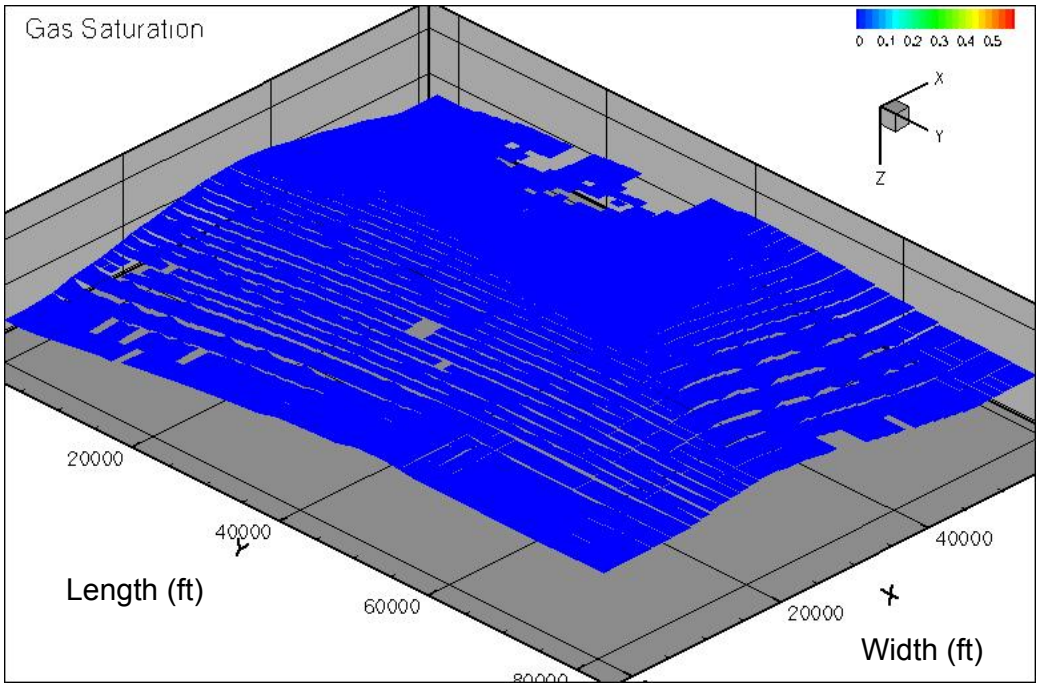

Figure 5-9: **Top layer of the reference model at 30 years**

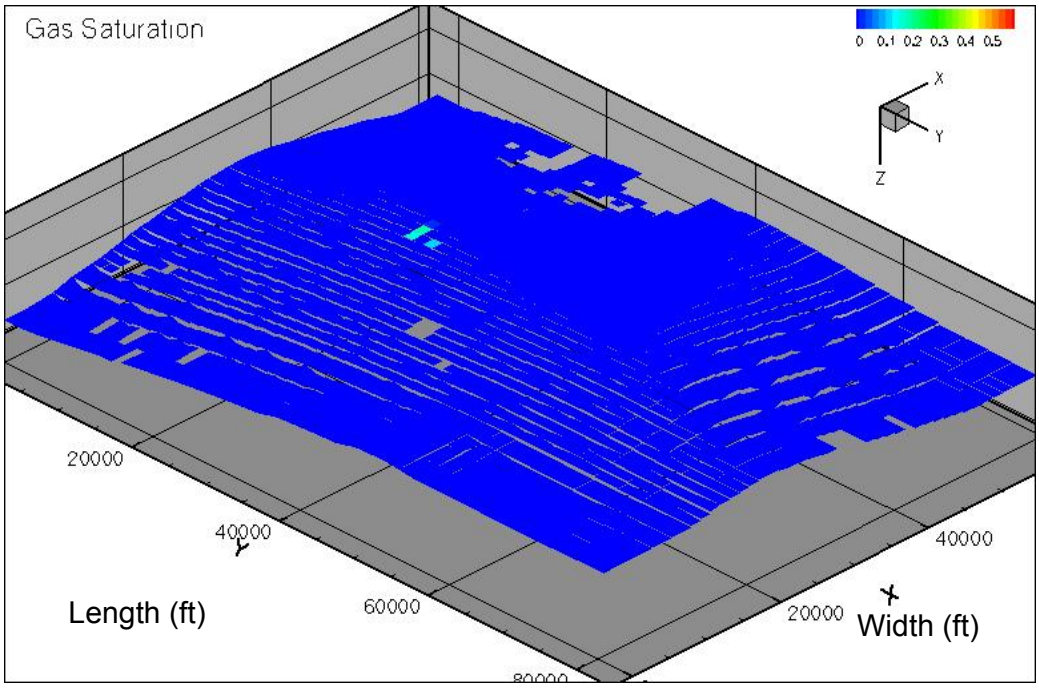

Figure 5-10: Top layer of the reference model at 60 years – end of injection.

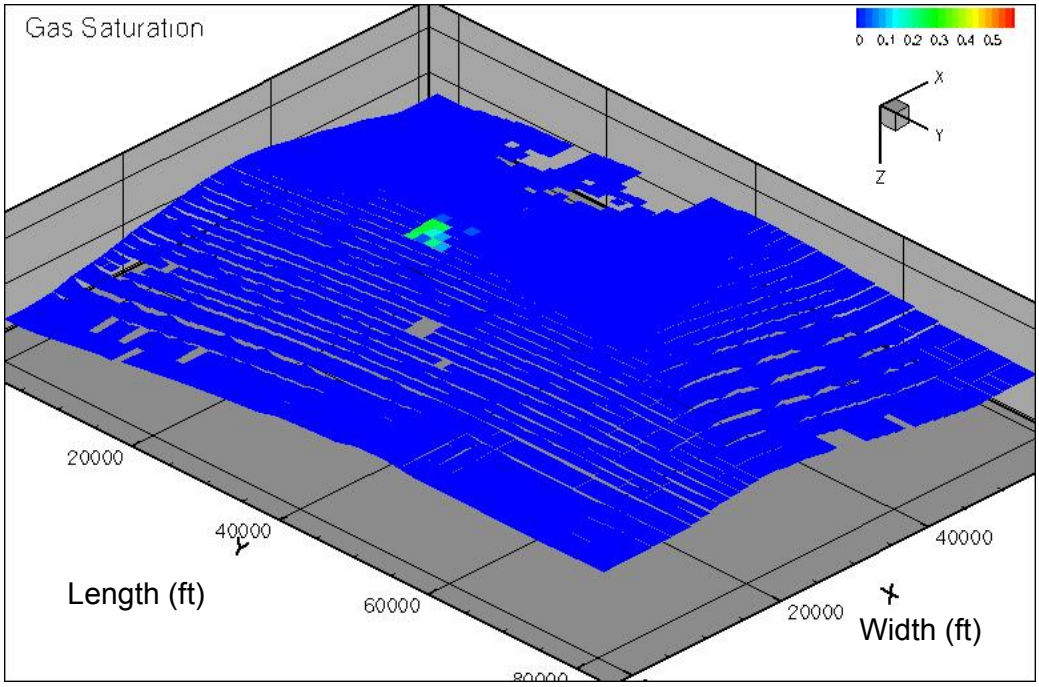

Figure 5-11: Top layer of the reference model at 100 years

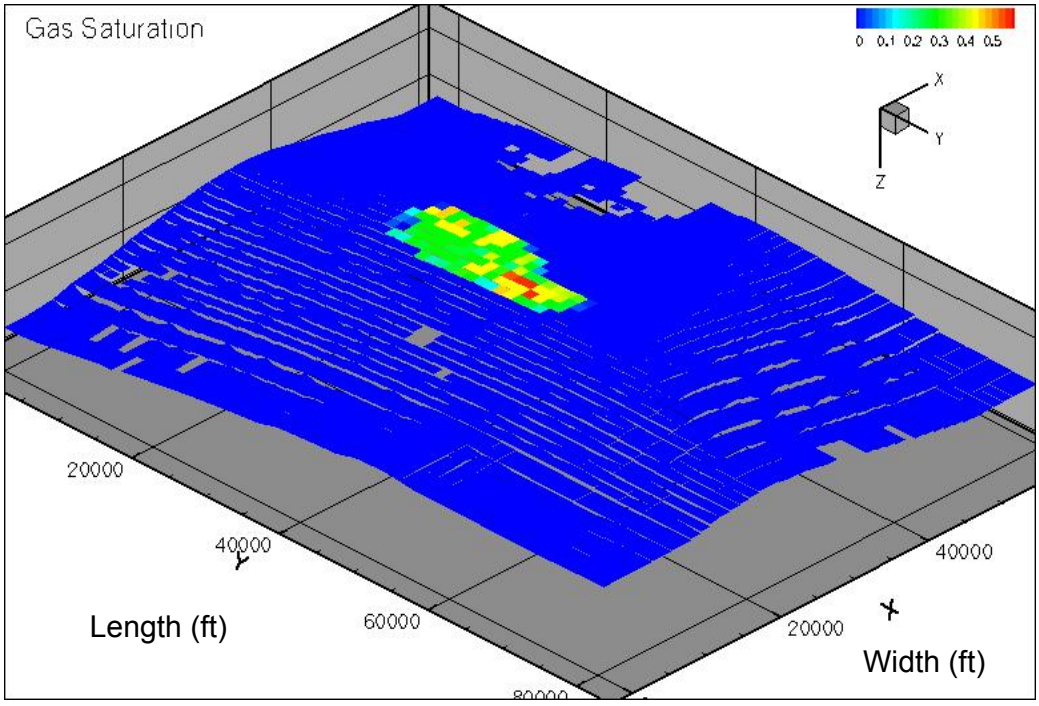

Figure 5-12: Top layer of the reference model at 1000 years

Up dip is towards the right in Figures 5-9 to 5-12.

In Figure 5-9 to 5-12, the migrating CO_2 plume hits the top layer/seal at 60 years and migrates up dip over the next 1000 years.

5.4 Reservoir Performance Metrics Summary

5.4.1 Migration

Over the 60 year injection program, the probabilistic range of migration from the injection well was 2.75 km to 3.82 km to 4.89 km on a p10-p50-p90 basis. Over the 1000 years injection well shut-in period the probabilistic range of migration distances widened from 3.03 km to 7.52 km to 12.00 km on a p10-p50-p90 basis.

5.4.2 Pressure Rise at the Seal

The p10-p50-p90 range of pressure rise at the formation seal at the 60 year mark was 0.90 MPa to 1.31 MPa to 1.72 MPa. Post injection at the 1000 year mark with pressure response equilibrated in the model, the pressure rise at the seal p10-p50-p90 range had decreased to 0.76 MPa to 0.88 MPa to 1.00 MPa as the reservoir pressure equalised.

5.4.3 Fraction of CO_2 Injected Dissolved

The fraction of CO_2 injected that had dissolved into the formation brine at 60 years ranges on a p10-p50-p90 basis from 0.052 to 0.123 to 0.204. The fraction of CO_2 dissolved at 1000 years ranges on a p10-p50-p90 basis from 0.083 to 0.217 to 0.351.

5.4.4 Fraction of CO_2 Injected Residually Trapped

The fraction of CO_2 trapped as a residual phase at the end of injection at 60 years ranges on a p10-p50-p90 basis from 0.000 to 0.031 to 0.080. At the end of simulation period of 1000 years the probabilistic p10-p50-p90 range is from 0.118 to 0.461 to 0.804.

5.5 Discussion

When examining the pareto charts, some of the factors shown to statistically significant for each reservoir performance metric appear simple and straightforward, such as permeability affecting migration distance and solubility effecting fraction of CO_2 dissolved. What is not trivial is the interaction of individual parameters affecting model response; reservoir simulation models are required to predict plume behaviour with heterogeneous rock properties and multiple CO_2 trapping mechanisms. However permeability appears to be a key factor for several reservoir performance

metrics: migration away from the injection well, pressure rise in the formation (this can incur a well injectivity problem in tight formations) and also for the long term fate of CO_2 as trapped residual phase, mobile or dissolved in formation water.

The reservoir performance of injected CO_2 in heterogeneous formations such as this model suite can be summarised as: mobile CO_2 migrates up dip due to buoyancy with a tortuous migration path due to heterogeneity, dissolves into the formation waters and can be trapped as a residual phase. Before possible significant mineralisation occurs over a 1000 year time frame, dissolution and residual gas trapping are effective in sequestering the CO_2 in the subsurface. The quantities of residual and dissolved CO_2, representing effectively sequestered CO_2, can be significant.

The heterogeneous formation used for this study was successful for CO_2 storage due to sufficient injectivity in to the formation and effective trapping over simulated time frame. The next step from a single successful heterogeneous formation simulation was to determine how varying formation heterogeneity impacts CO_2 migration and influences trapping mechanisms through a range of models with varying formation heterogeneity. This next step is evaluated in Chapter 6.

6. Major Study

The two enabling studies investigated aspects of trapping mechanisms for CO_2 injection into saline formations and formation heterogeneity on reservoir performance. The main questions to arise from both sets of studies were: firstly, how does variation in formation heterogeneity impact the success of a geological disposal project? Secondly, how do variations in formation heterogeneity impact the migration of an injected plume and influence the trapping mechanisms that can potentially contain the plume?

Thus the objective of the major study is to evaluate the role of formation heterogeneity in the reservoir performance of carbon dioxide disposal project in a saline formation. In particular the reservoir characterisation of the formation was evaluated though variation of the content of shale in the formation (or net-to-gross), length of shale intervals that can influence injected CO_2 and the formation dip.

6.1 Development of Reservoir Simulation Models

A new suite of simulation models were required to set up this study. To start, a conceptual fine scale model was developed of a notional marine sand system that was 10 km long, 5 km wide and had a total thickness of 120 m. The original cell sizes in the geological model were 50 m by 50 m by 0.4 m thickness, so that the number of grid cells was 200 by 100 by 300 (i.e. 6 million). The model contained a dip of one degree, aligned with the length of the model.

As before in Studies A and B, Sequential Gaussian Simulation (SGS), was used to generate porosity values for sand. A mean sand porosity of 0.22 with a standard deviation of 0.02 were used as inputs and a single distribution was generated, which was used to populate all the models.

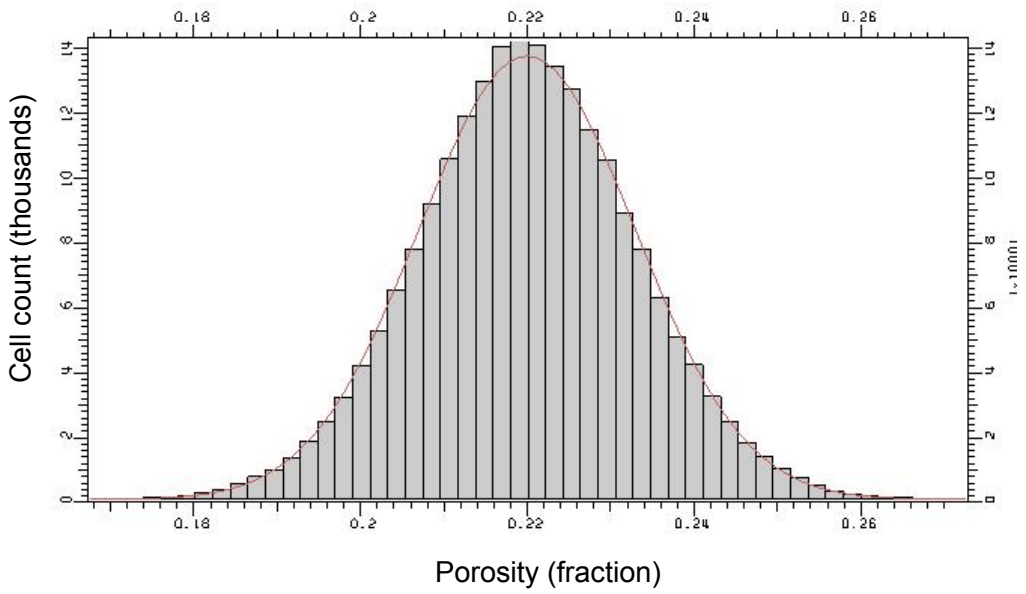

Figure 6-1: Porosity in the sand of the major study model

A logarithmic function was developed to populate the sand in the model with horizontal permeability in what was deemed an appropriate non-linear fashion, based on the assigned porosity values,

$$k = 6e^{70\phi} \times 10^{-6} \qquad (6.1)$$

The resulting mean horizontal permeability for sand was 68 md. A k_v/k_h ratio of 0.1 was used to set the vertical permeability.

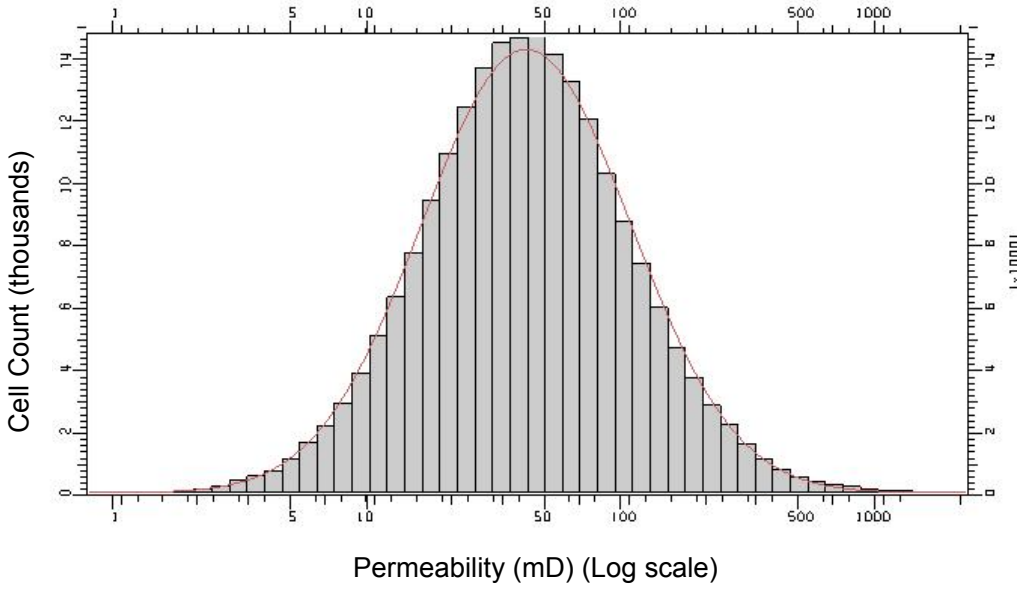

Figure 6-2: Permeability in the sand of the homogeneous model

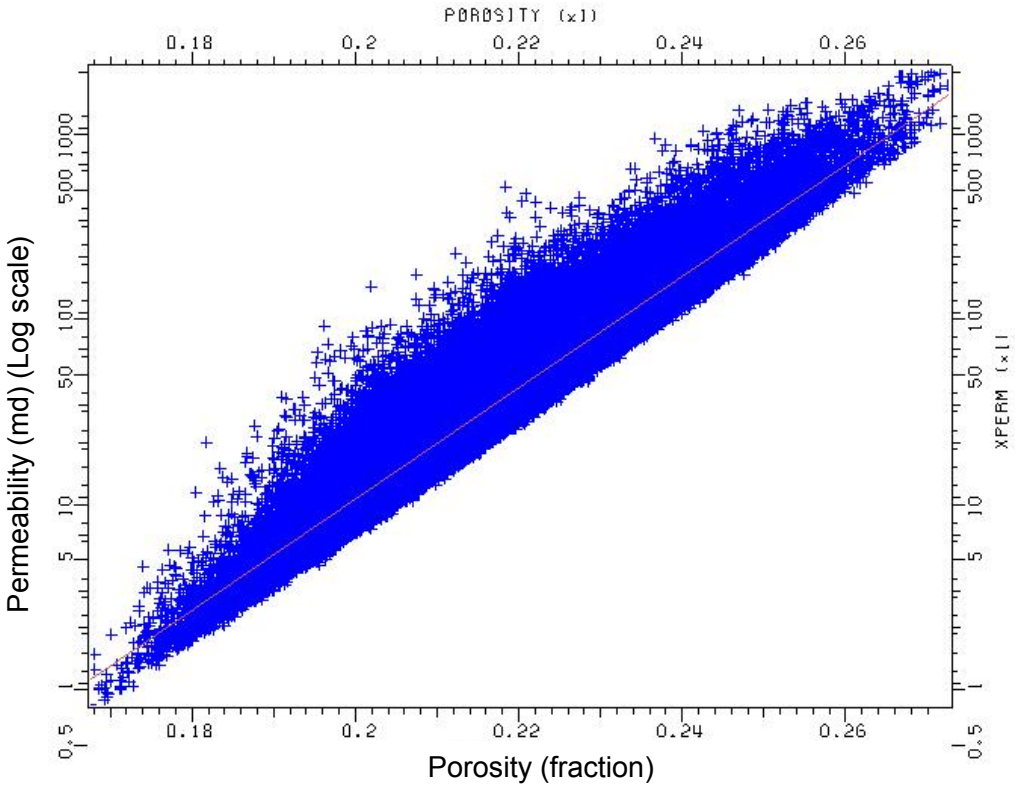

Figure 6-3: Porosity permeability in the sand of upscaled homogeneous model

Different geostatistical realizations of the fine scale model were developed for different net–to-gross ratios and shale lengths. Net to gross ratios were varied from 80:20 to 40:60 ratios of net sand to shale. Rock heterogeneity was further characterized by varying the lengths of shale populated in the models, which was achieved by changing the geostatistical variogram range used in the model for each net-to-gross ratio. The radial shale variogram ranges used in each net to gross realization were 100m, 300m, 1000m and 3000m in length, to simulate the effect of short and longer shale barriers. Thus, for each net to gross ratio four shale length variations were developed. The shale populated in the fine scale model has no porosity or permeability, thus would act as an impermeable barrier to rising injected CO_2. Increased shale lengths should increase the tortuousity in the vertical migration path of the injected CO_2. Note that since the facies were geostatistically populated, the shales were not necessarily continuous, but could contain "holes".

All of the fine scale models were upscaled to a more manageable size for reservoir simulation using the flow based methods of Durlofsky et al. (1996). The upscaling

algorithm developed by Durlofsky et al. (1996) examines the three dimensional flow properties in the fine scale model and seeks to have the same flow behaviour in the upscaled coarse grid model, while maintaining the same pore volume. Hence, the overall fluid movement in the upscaled grid is expected to be similar to fine scale fluid flow.

Each upscaled reservoir model had cell sizes of 100m by 100m by 2.8m, so that the number of cells was (50 x 100 x 43 =) 215,000. Each upscaled model was replicated with geologic dip values of 0, 1, 2, 5, or 10 degrees, so the influence of formation dip on plume migration could be evaluated.

Thus an overall total of one hundred separate coarse simulation models were built, encapsulating five net-to-gross ratios representing low-to-high reservoir quality, four shale length values and five formation dip ranges.

Figures 6-4 to 6-10 show the formation variability or heterogeneity for different amounts of net-to-gross with the same shale length (300m in this case). Figure 6-11 to 6-14 shows the variation in heterogeneity (shown as porosity variation) due to the different shale lengths applied for the same net-to-gross value. Note that for Figures 6-4 to 6-14 that blue represents good reservoir quality / high porosity while red represents poor reservoir quality / low porosity.

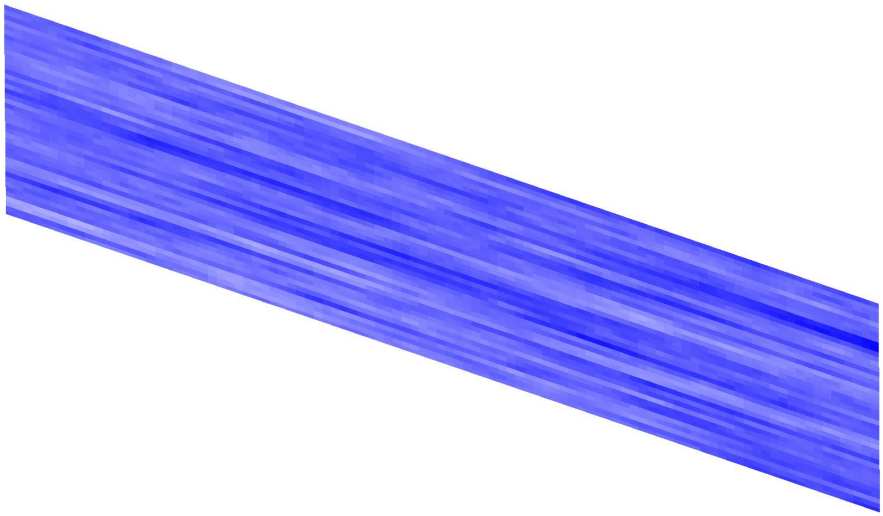

Figure 6-4: Cross section of upscaled reservoir models showing the variation of porosity – homogeneous (sand only)

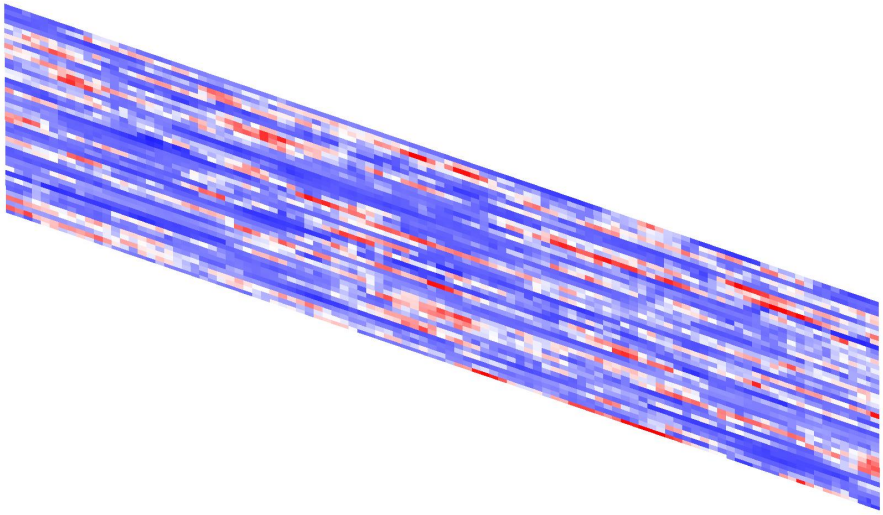

Figure 6-5: Cross section of upscaled reservoir models showing the variation of porosity – 80:20 net sand to shale

Shale length variogram 300m.

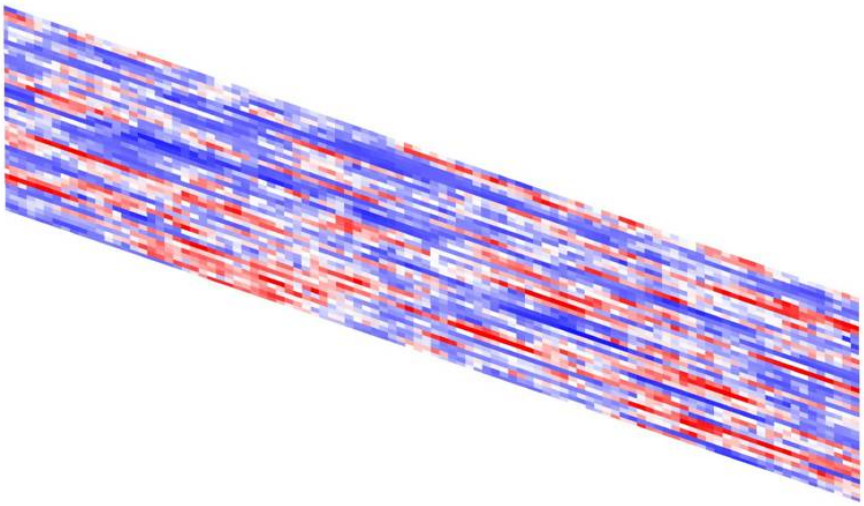

Figure 6-6: Cross section of upscaled reservoir models showing the variation of porosity – 70:30 net sand to shale

Shale length variogram 300m.

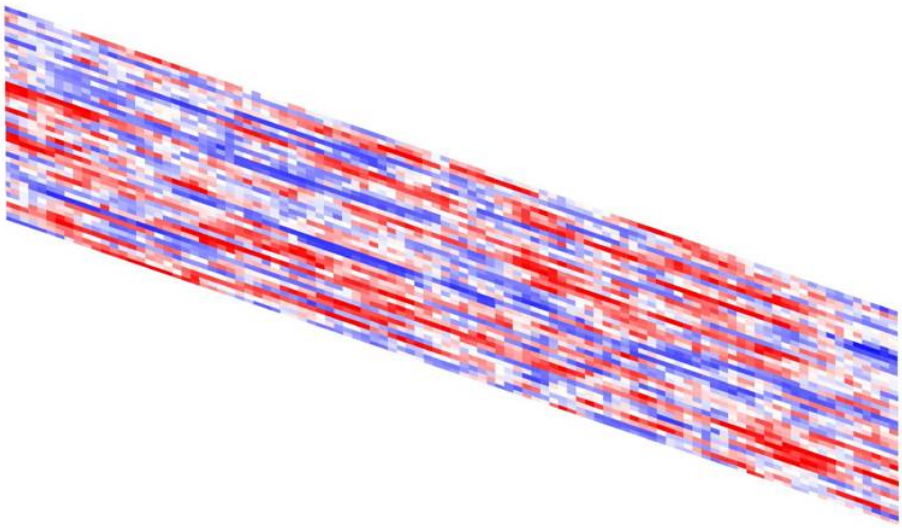

Figure 6-7: Cross section of upscaled reservoir models showing the variation of porosity – 60:40 net sand to shale

Shale length variogram 300m.

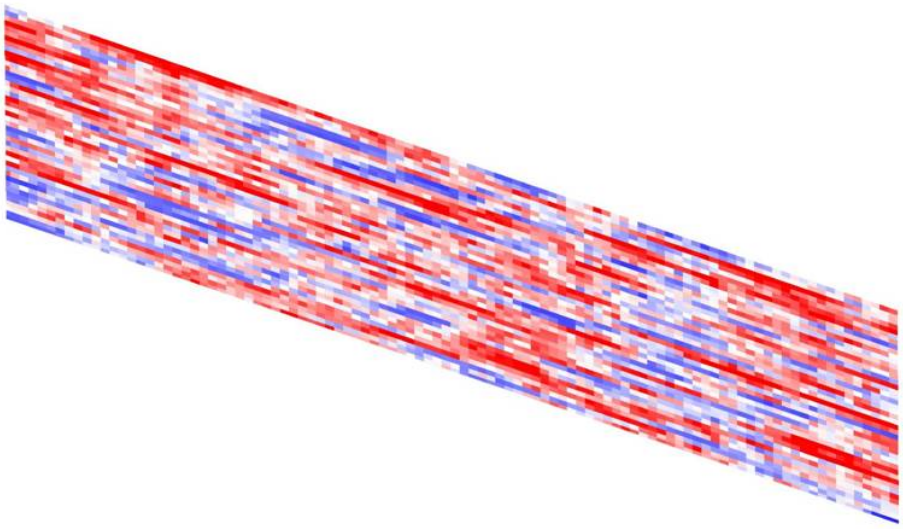

Figure 6-8: Cross section of upscaled reservoir models showing the variation of porosity – 50:50 net sand to shale

Shale length variogram 300m.

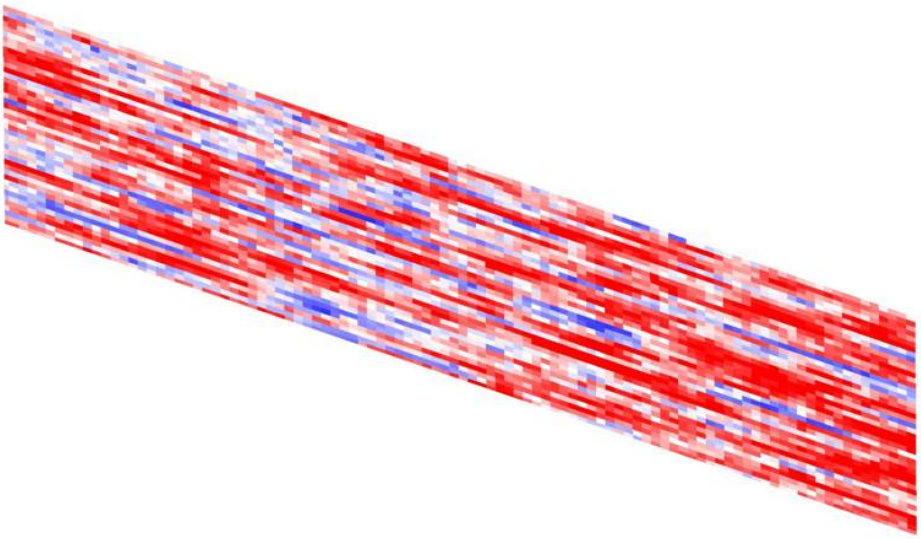

Figure 6-9: Cross section of upscaled reservoir models showing the variation of porosity – 40:60 net sand to shale

Shale length variogram 300m.

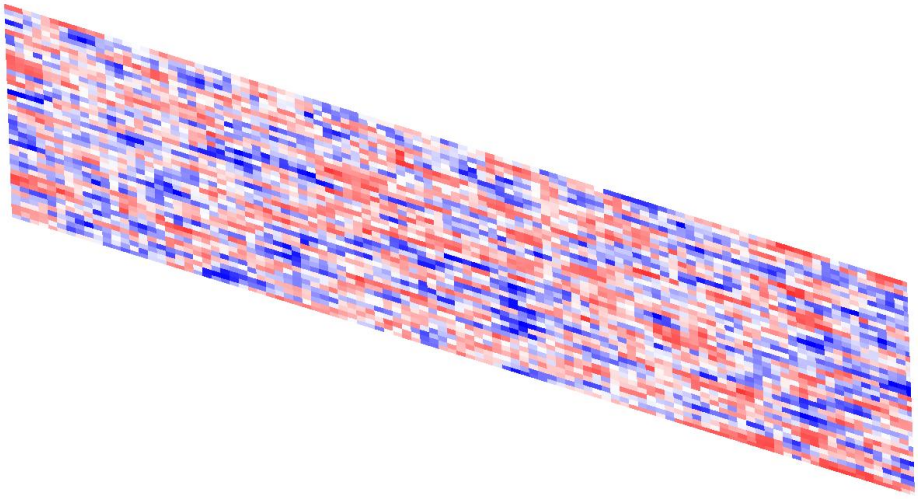

Figure 6-10: Cross section of upscaled reservoir models showing the variation of porosity – 70:30 net sand to shale

Shale length variogram 100m.

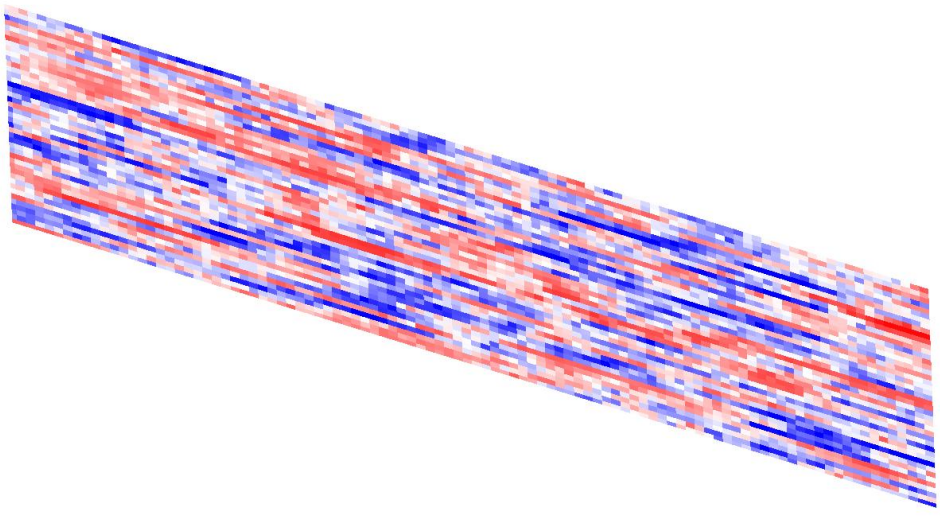

Figure 6-11: Cross section of upscaled reservoir models showing the variation of porosity – 70:30 net sand to shale

Shale length variogram 300m.

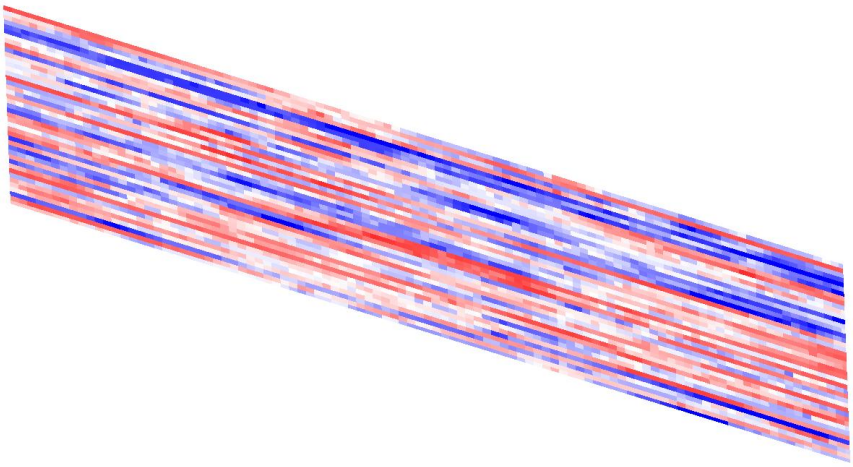

Figure 6-12: Cross section of upscaled reservoir models showing the variation of porosity – 70:30 net sand to shale

Shale length variogram 1000m.

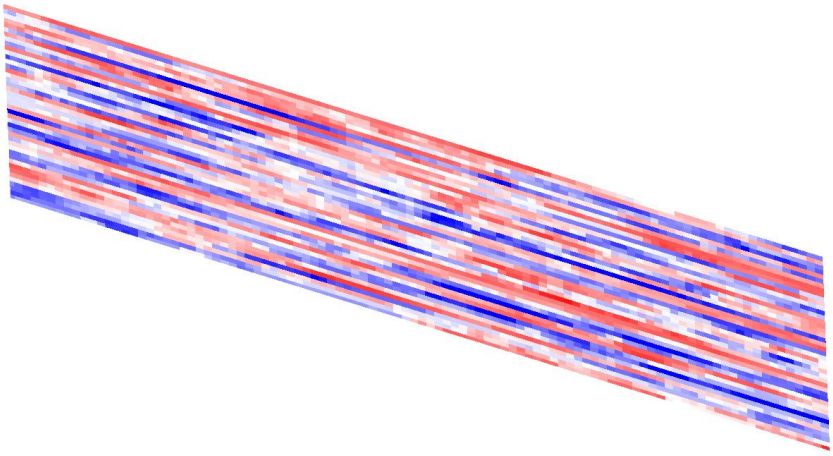

Figure 6-13: Cross section of upscaled reservoir models showing the variation of porosity – 70:30 net sand to shale

Shale length variogram 3000m.

6.2 Reservoir Simulation Formulation

Similar to Study B, a reservoir formation temperature of 212°F (100ºC) and a formation datum pressure of 3200 psia (22.06 MPa) were used for all the models (equivalent to being ~7000ft or 2km in the subsurface under normal hydrostatic conditions). Reservoir simulation was run under isothermal conditions and the models were under normal hydrostatic conditions initially. The lateral edges of the reservoir model used a hundred fold pore volume multipliers to simulate an extensive aquifer extent.

The mid point relative permeability curves used in the preliminary studies A and B of this thesis were used to govern the movement of the CO_2 plume. (See earlier in chapter 2 for derivation of relative permeability curves used in this study.)

The maximum residual CO_2 saturation (S_{grM}) in the study was set at 15%, which is considered a conservative figure when compared with some ranges of residual gas saturation values that have been used previously for heterogeneous formations (Hamon et al. 2001; Hovorka et al. 2004).

6.3 Reservoir Performance Study

In each of the models three CO_2 injection wells were located down dip in the model formation. This is shown in Figure 6-14. The wells injected a total of 50 MMscf of CO_2 per day (~ 1 million tones per annum) over a period of 50 years. The dynamic simulation of each geological scenario was run for 8000 years in order to characterize the very long term migration and trapping mechanism effects. Plume migration and outcomes of various trapping mechanisms, such as effectiveness of dissolution and residual phase gas trapping, were compared between the scenarios. Trends associated with shale length, reservoir quality and formation dip were identified.

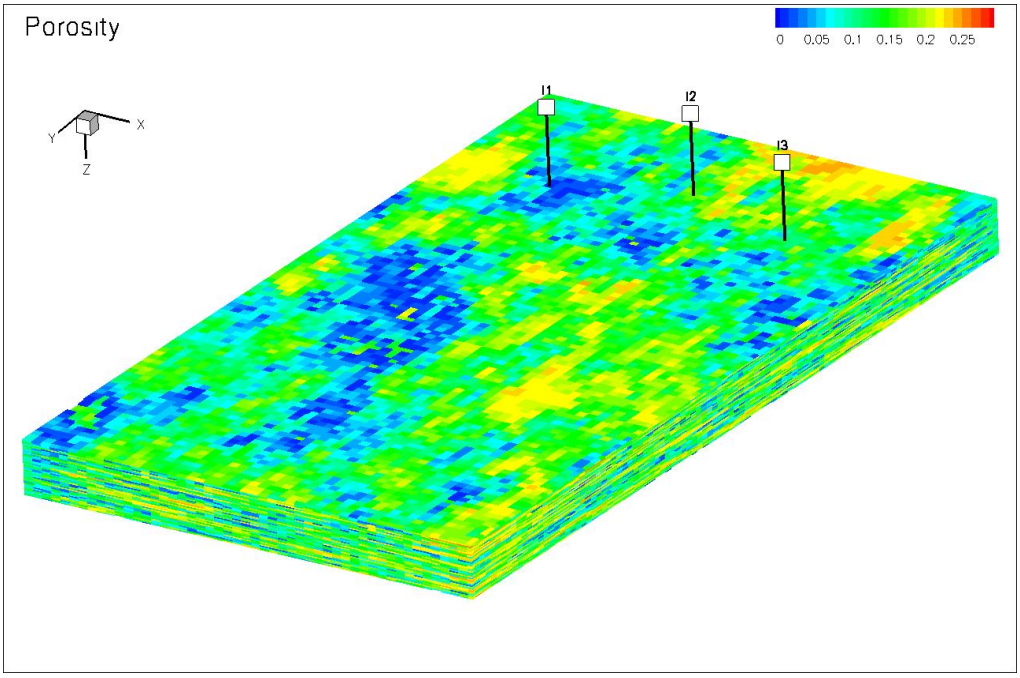

Figure 6-14: Location of wells in the reservoir simulation model

Porosity distribution for 60:40 sand to shale model shown.

6.4 Reservoir Performance Metrics

Technical subsurface metrics focusing on containment were considered for this study. As in Studies A and B possible fiscal incentives, such as the avoidance of a greenhouse gas emission tax, were not considered. Clearly the migration of the CO_2 plume in the formation and the long-term storage of CO_2 are the key outputs that need to be quantified for containment. This involves measuring the vertical/stratigraphic and lateral movement of the plume whilst keeping track of how much gas has dissolved in the water and how much gas has been trapped in a residual gas phase.

6.5 Results

Basic data for the Major Study is in Appendix C, Section C.3 in Table C-7 to C-70. Multiple supplementary figures describing the range of results observed for lateral and vertical migration, fraction of CO_2 injected that is dissolved, residually trapped and remaining mobile are in Appendix D, Figures D-15 to D-237.

6.5.1 Migration

Comparisons can be made into the impact of the range of net-sand-to-gross-shale ratios being considered for the Major Study. Figures 6-15 to 6-20 show the CO_2 plume for each net-to-gross reservoir model with the shale length maintained at 300m, at the end of injection (50 years) and at the end of the simulation (1000 years). The impact of the varying amounts of shale is apparent on the development of the shape of the plume, with vertical movement being restricted and lateral movement encouraged as the amount of shale increases in the model.

Figures 6-21 to 6-24 show how in an environment with the same net-to-gross or sand to shale ratio, in this case 70:30, how plume movement is effect by varying the length of the shale variogram. Generally, it can be noted that the longer the variogram, the less vertical stratigraphic flow in the formation as the longer shale in the formation impedes the direct vertical movement of CO_2. This is despite the ratio of sand to shale in all of the models shown being held constant (70:30 sand to shale for these figures).

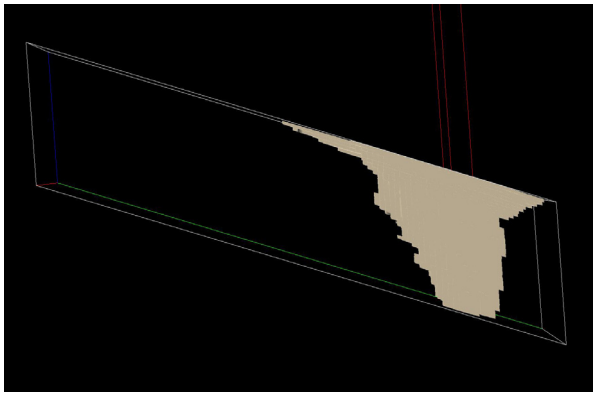

Side on 50 years

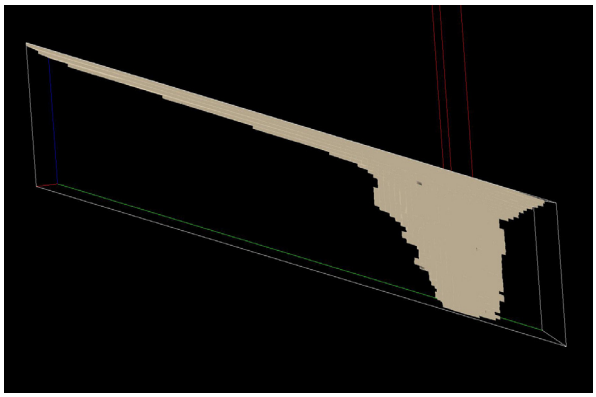

Side on 1000 years

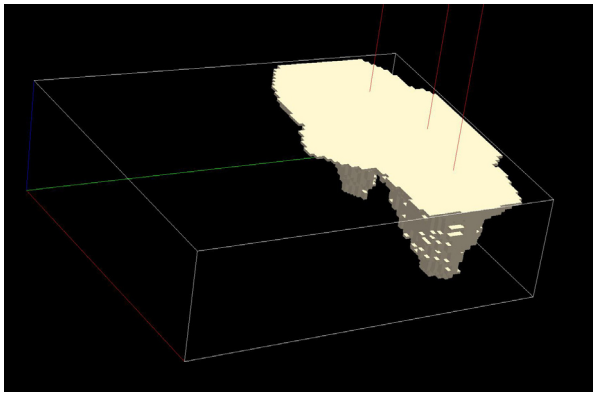

Oblique view 50 years

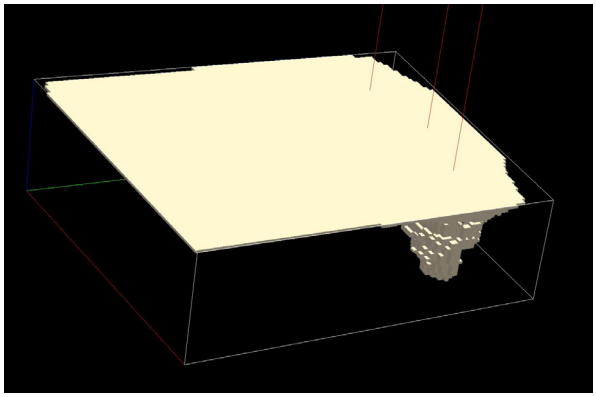

Oblique view 1000 years

Figure 6-15: Development of gaseous phase CO_2 plume in the homogeneous model

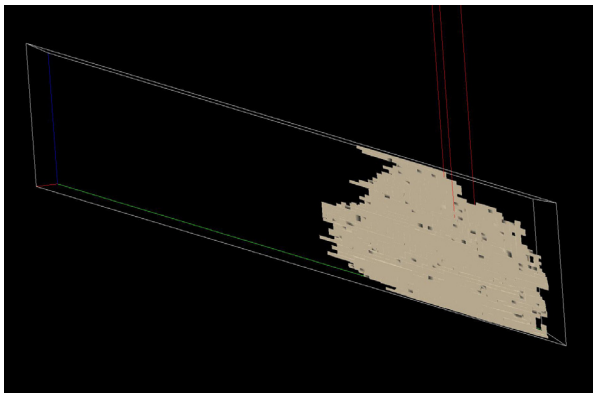

Side on 50 years

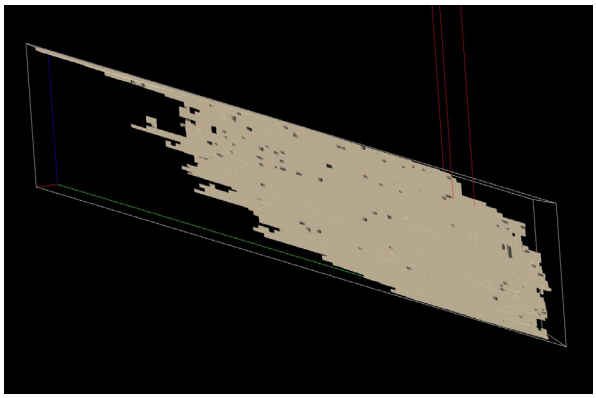

Side on 1000 years

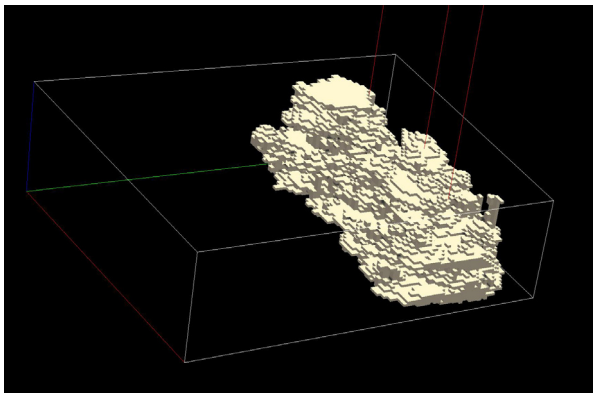

Oblique view 50 years

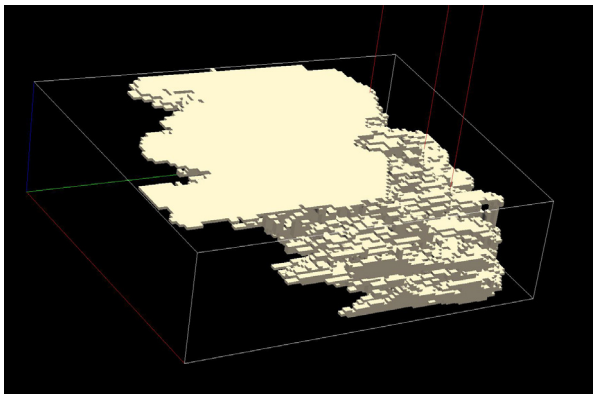

Oblique view 1000 years

Figure 6-16: Development of gaseous phase CO_2 plume in the 80:20 sand to shale model, shale length 300m

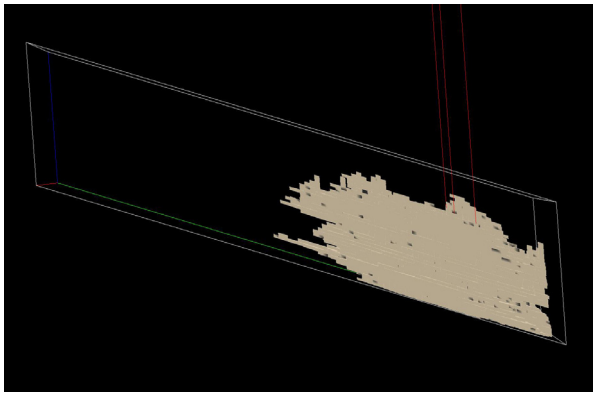

Side on 50 years

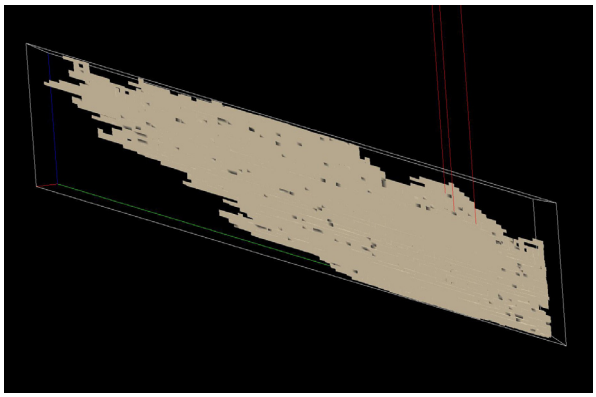

Side on 1000 years

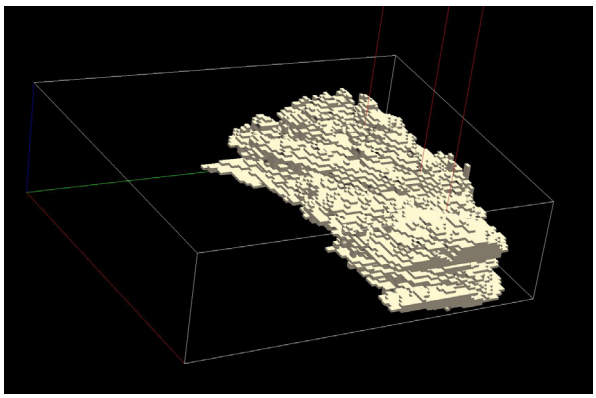

Oblique view 50 years

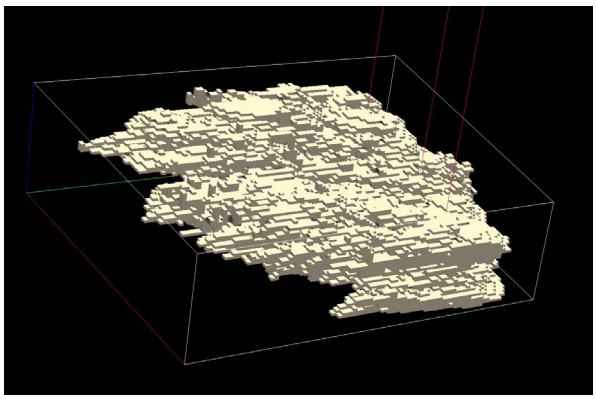

Oblique view 1000 years

Figure 6-17: Development of gaseous phase CO_2 plume in the 70:30 sand to shale model, shale length 300m

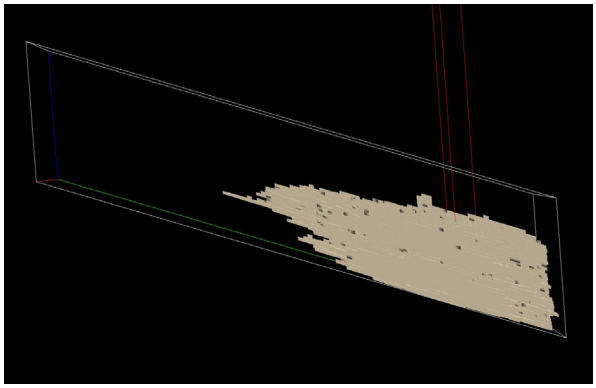

Side on 50 years

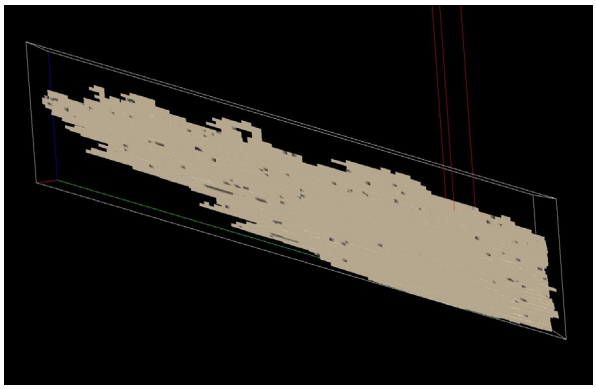

Side on 1000 years

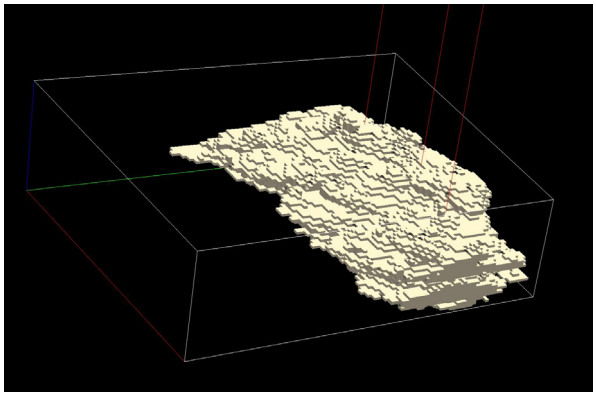

Oblique view 50 years

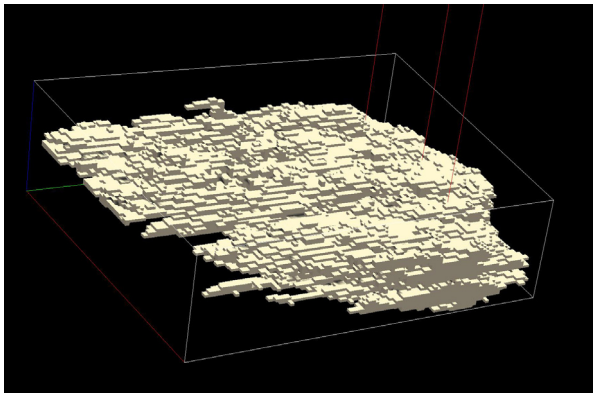

Oblique view 1000 years

Figure 6-18: Development of gaseous phase CO_2 plume in the 60:40 sand to shale model, shale length 300m

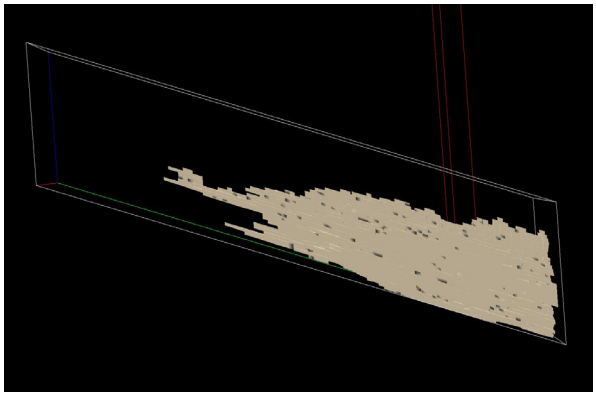

Side on 50 years

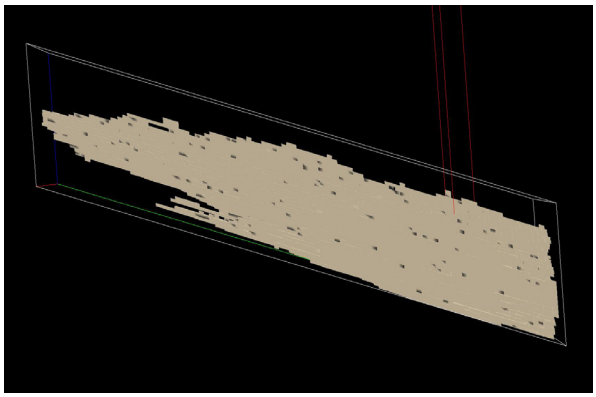

Side on 1000 years

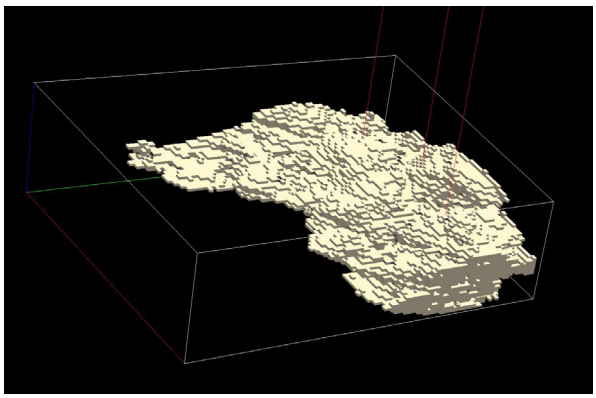

Oblique view 50 years

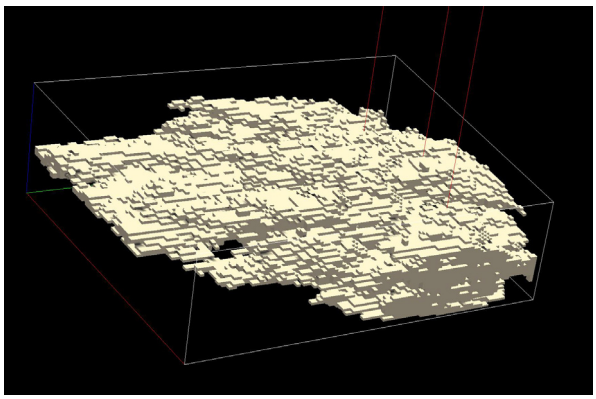

Oblique view 1000 years

Figure 6-19: Development of gaseous phase CO_2 plume in the 50:50 sand to shale model, shale length 300m.

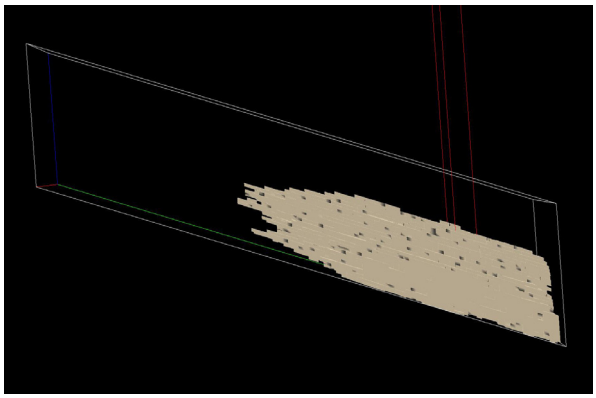

Side on 50 years

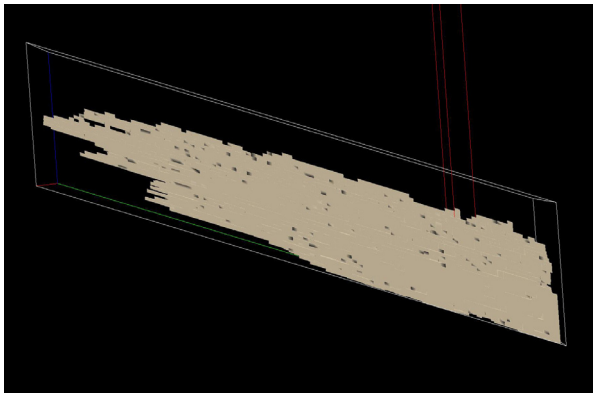

Side on 1000 years

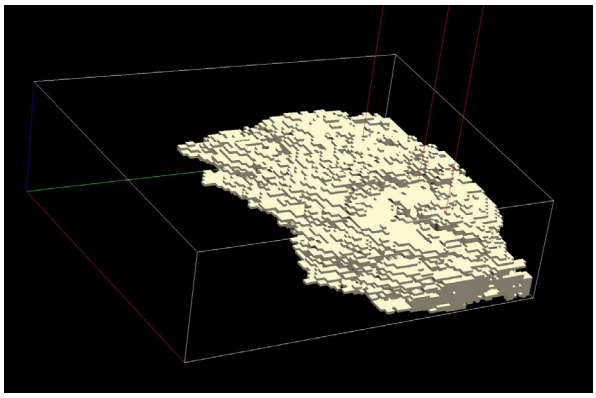

Oblique view 50 years

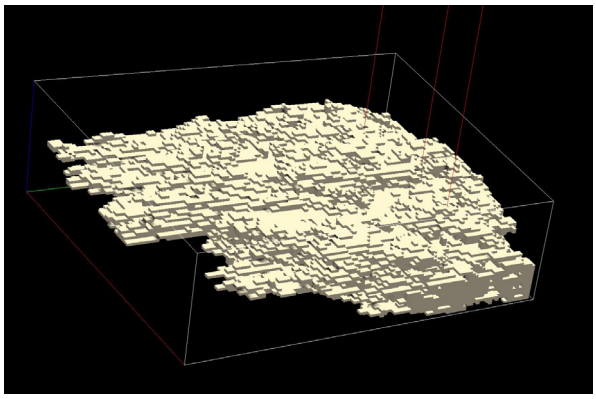

Oblique view 1000 years

Figure 6-20: Development of gaseous phase CO_2 plume in the 40:60 sand to shale model, shale length 300m

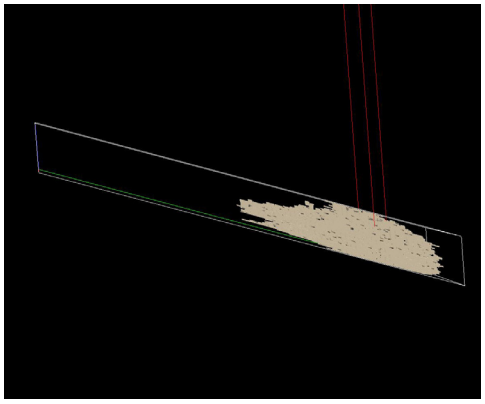

Side on 50 years

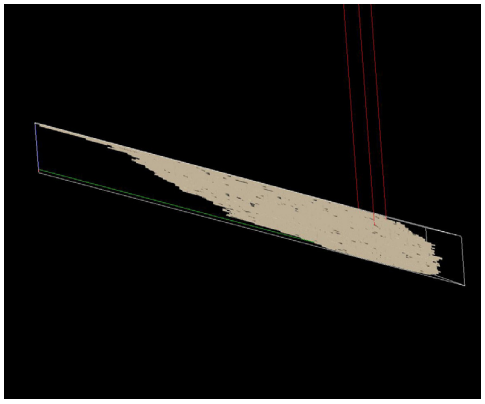

Side on 1000 years

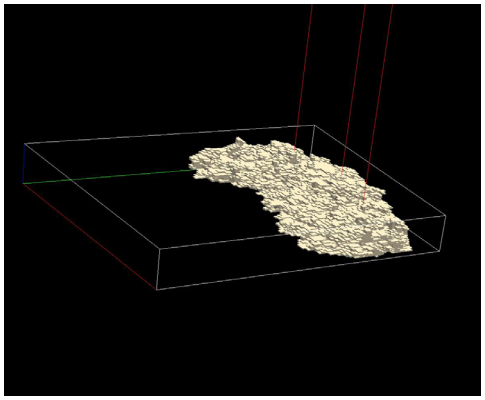

Oblique view 50 years

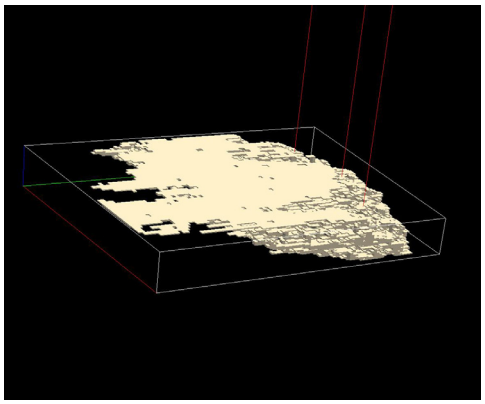

Oblique view 1000 years

Figure 6-21: Development of gaseous phase CO_2 plume in the 70:30 sand to shale model with 100m shale length

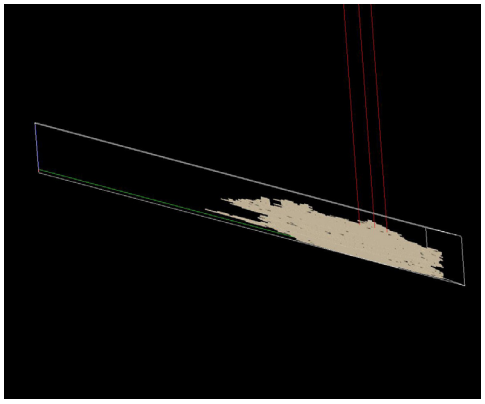

Side on 50 years

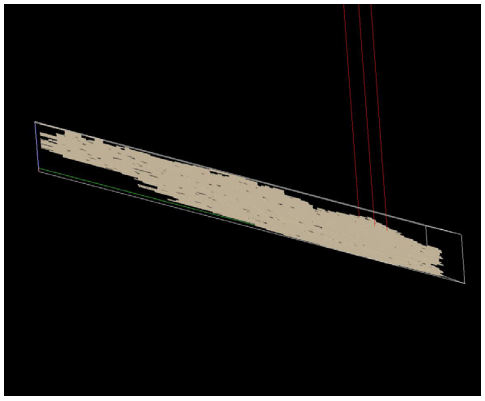

Side on 1000 years

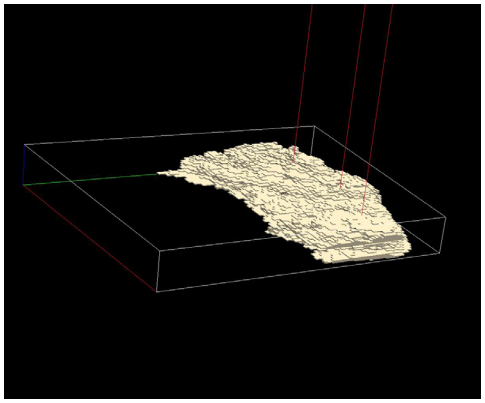

Oblique view 50 years

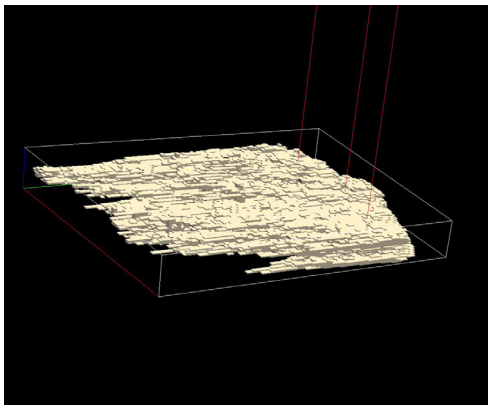

Oblique view 1000 years

Figure 6-22: Development of gaseous phase CO_2 plume in the 70:30 sand to shale model with 300m shale length

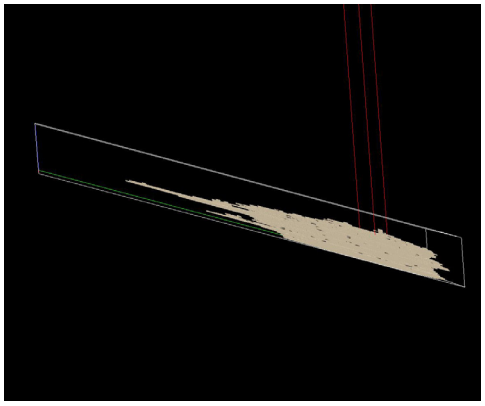

Side on 50 years

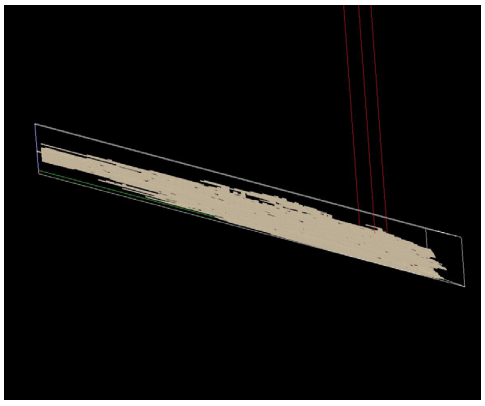

Side on 1000 years

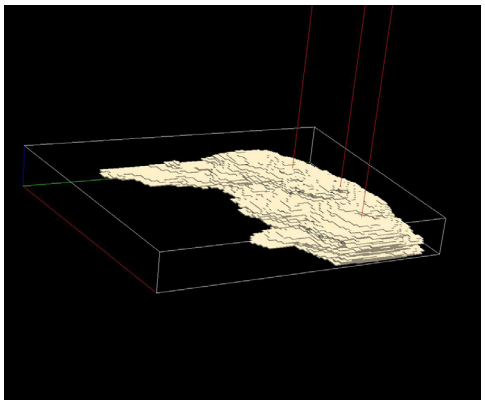

Oblique view 50 years

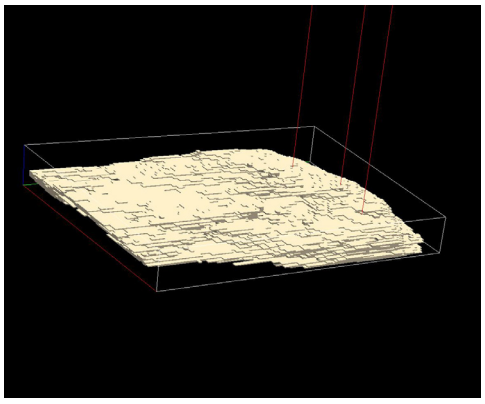

Oblique view 1000 years

Figure 6-23: Development of gaseous phase CO_2 plume in the 70:30 sand to shale model with 1000m shale length

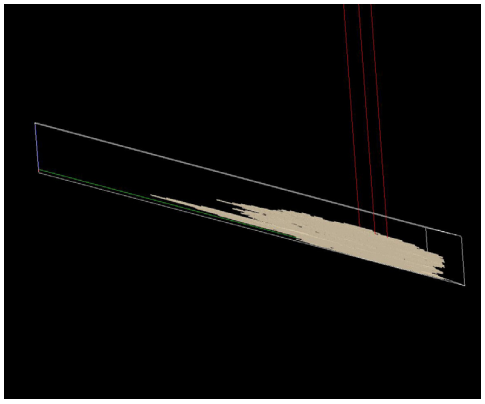

Side on 50 years

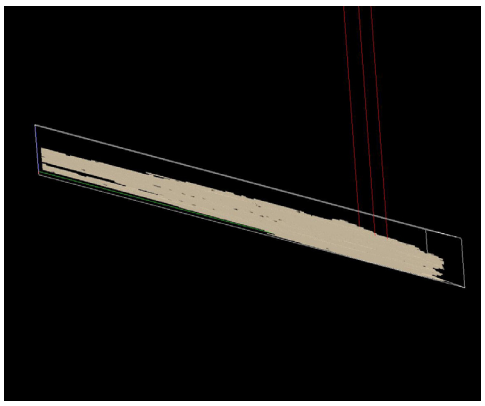

Side on 1000 years

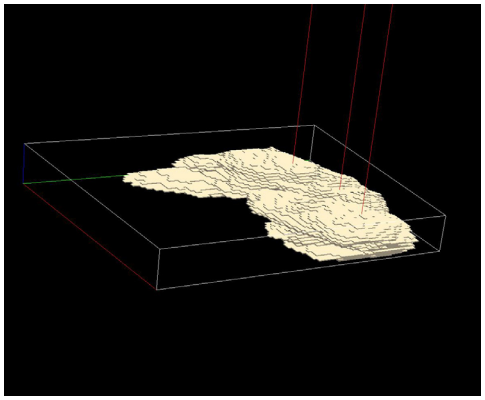

Oblique view 50 years

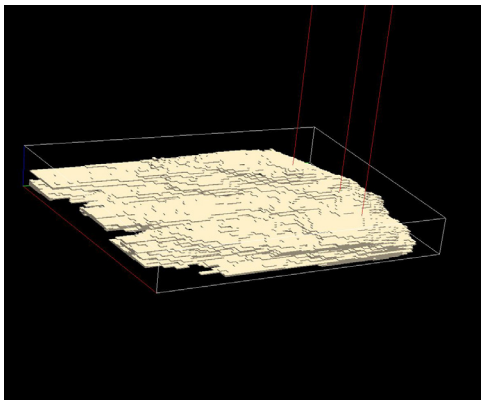

Oblique view 1000 years

Figure 6-24: Development of gaseous phase CO_2 plume in the 70:30 sand to shale model with 3000m shale length

The following Figures 6-25 to 6-32, the lateral distance travelled by the injected plume of CO_2 from the injection well is compared for several models. Figures 6-25 and 6-26 compare models with the same net to gross and dip but different shale variogram lengths (100m, 300m, 1000m and 3000m). During the first 100 years, the models with longer variograms (1000 or 3000m) have faster laterally migration. This is due to the long shale baffles directing migrating CO_2 laterally up dip until it reaches the end of a shale break when the CO_2 moves up stratigraphically. In the shorter variogram models (100m, 300m and the homogeneous model) the pathway to the top of model is less tortuous, the lateral migration is slow until the plume hits the top layer of model. When migrating CO_2 touches the seal, or top layer of the simulation model, the only migration movement physically possible is laterally up dip. This observation is shown diagrammatically for migrating plumes in the homogeneous model in Figure 6-15 and Figure 6-16 for the 80:20 net to gross, 300m shale length model. The legend for Figures 6-15 to 6-44 are similar in scope; the first term refers to the ratio of net sand to shale, the second term the length of shale variogram, the final term the formation dip. For example "8020_1000_1" refers to the model with 80:20 ratio of net sand to shale, 1000m shale variogram and formation dip of 1 degrees.

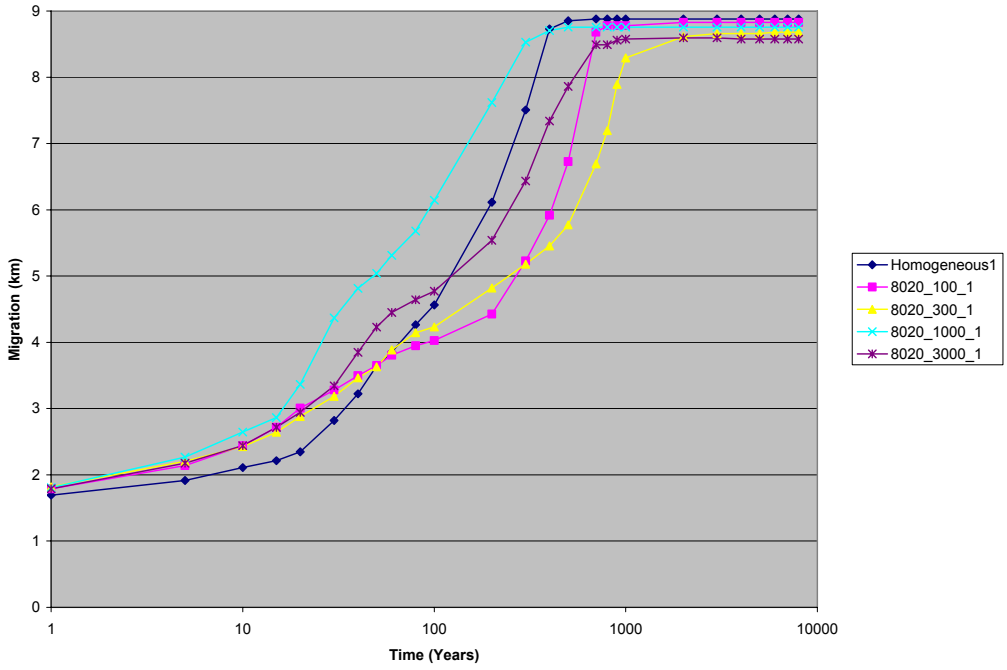

Figure 6-25: Migration comparison of the 80:20 net-to-gross models, 1 degree slope

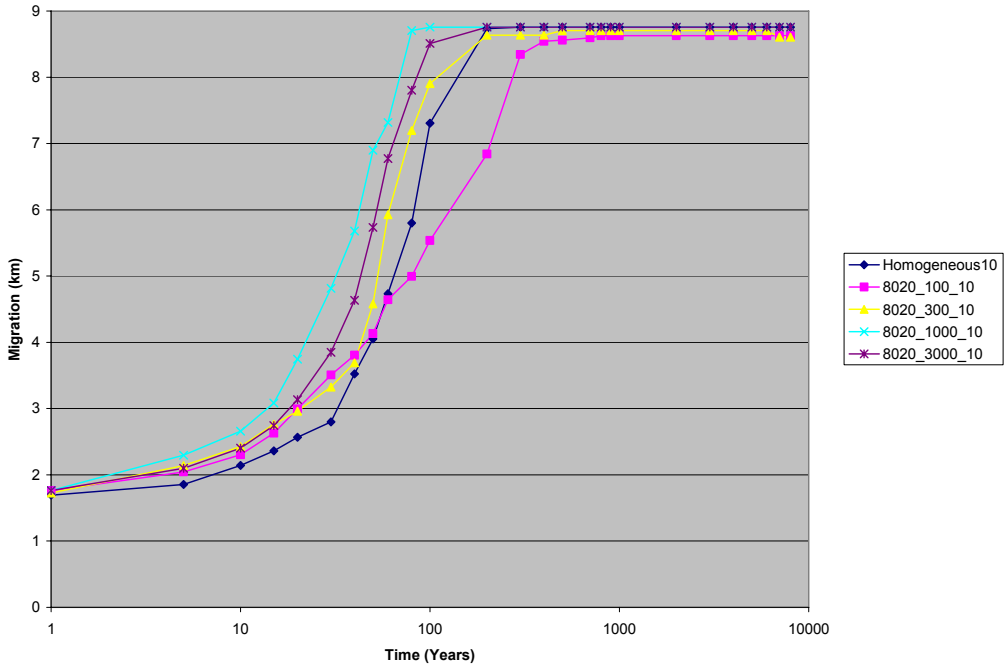

Figure 6-26: Migration comparison of the 80:20 net-to-gross models, 10 degree slope

In comparing Figures 6-25 and 6-26, the influence of increased formation dip from 1 degree in Figure 6-25 to 10 degrees in Figure 6-26 can be seen in accelerating the lateral migration of the plume.

Figures 6-27 and 6-28 are similar to 6-25 and 6-26 except being for a model with poorer reservoir quality, 50:50 net sand to gross. In these figures, the change of the shale variogram length has an impact on lateral migration, due to more shale being in the model (and hence more flow barriers) compared to the 80:20 net to gross models in Figures 6-25 and 6-26. For the 50:50 net sand to shale models, the longer length variograms have faster lateral migration than the homogeneous and the 100 m shale length models. The increase in formation dip from 1 to 10 degrees from Figure 6-27 to 6-28 again shows that increased formation dip accelerates migration of an injected plume.

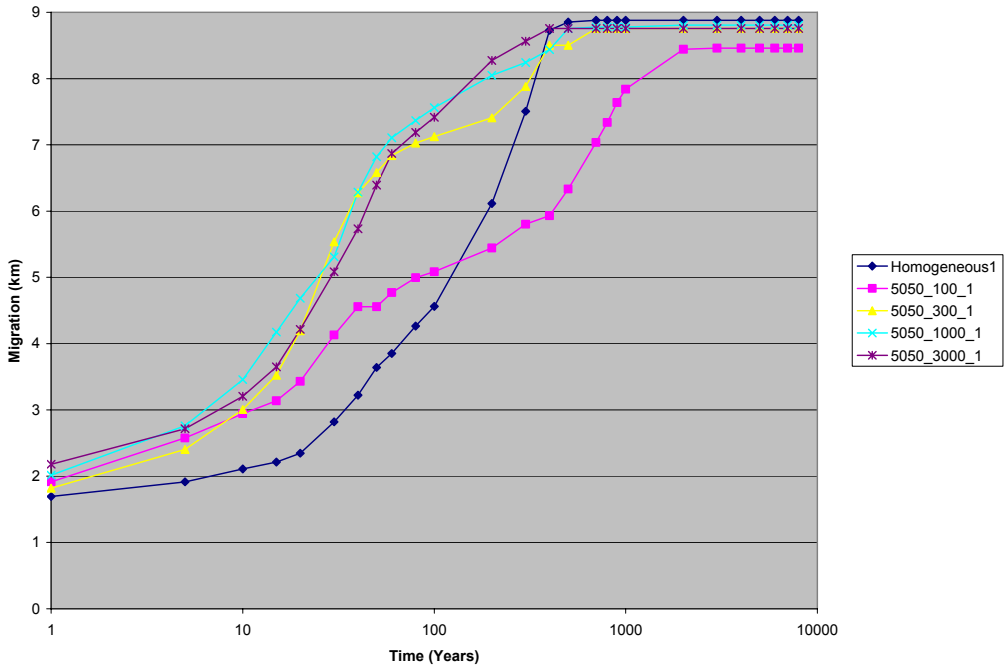

Figure 6-27: Migration comparison of the 50:50 net-to-gross models, 1 degree slope

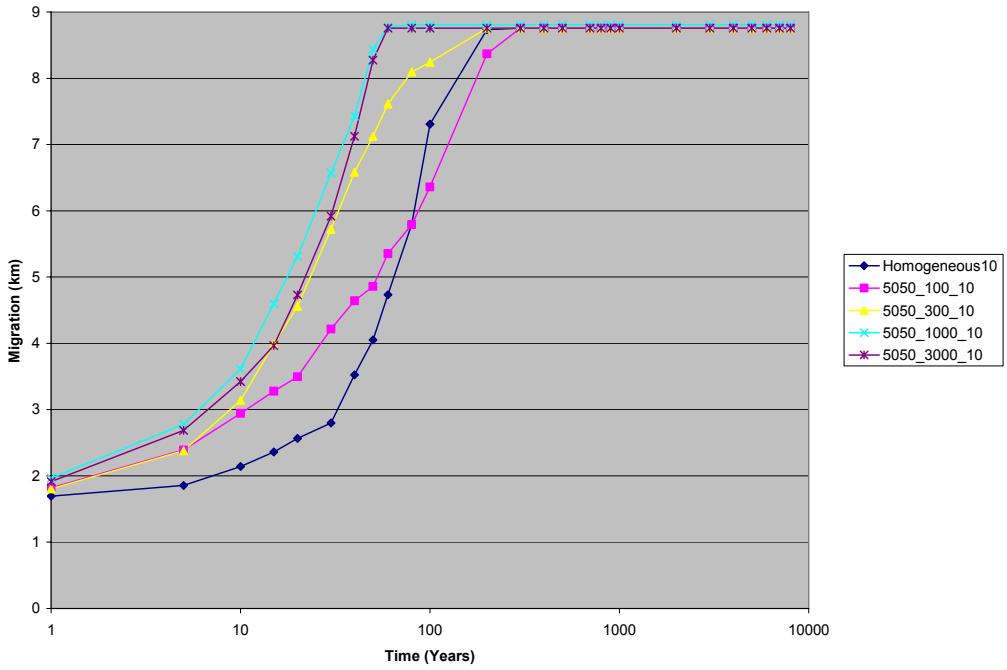

Figure 6-28: Migration comparison of the 50:50 net-to-gross models, 10 degree slope

In Figures 6-29 to 6-32, the rate of lateral migration is compared for differing amounts of net to gross, with the shale variogram length held constant.

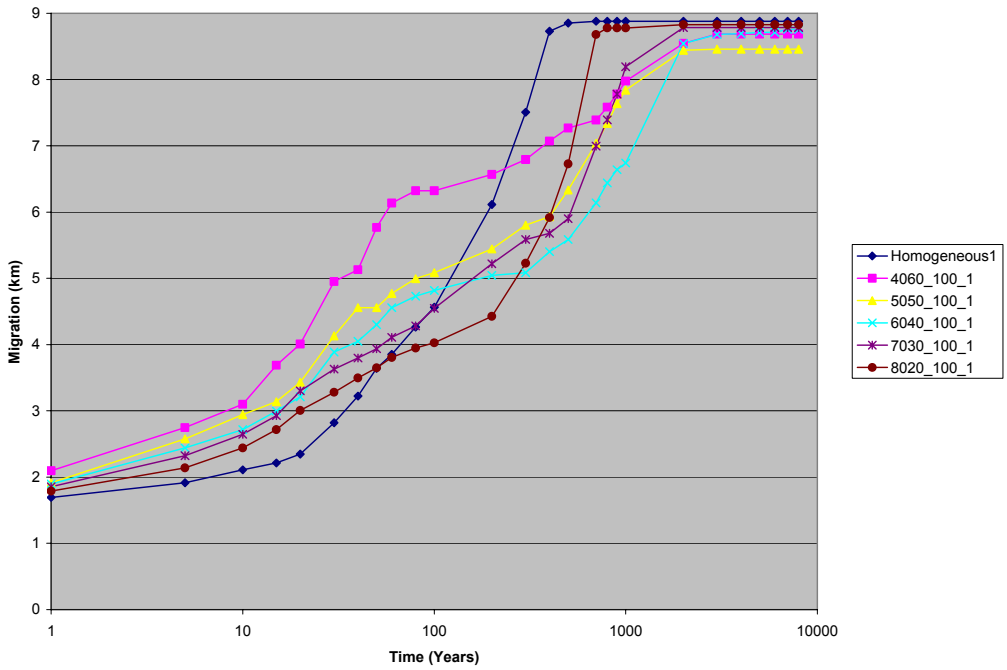

Figure 6-29: Migration comparison of the 100 m facies models, various net-to-gross, 1 degree slope

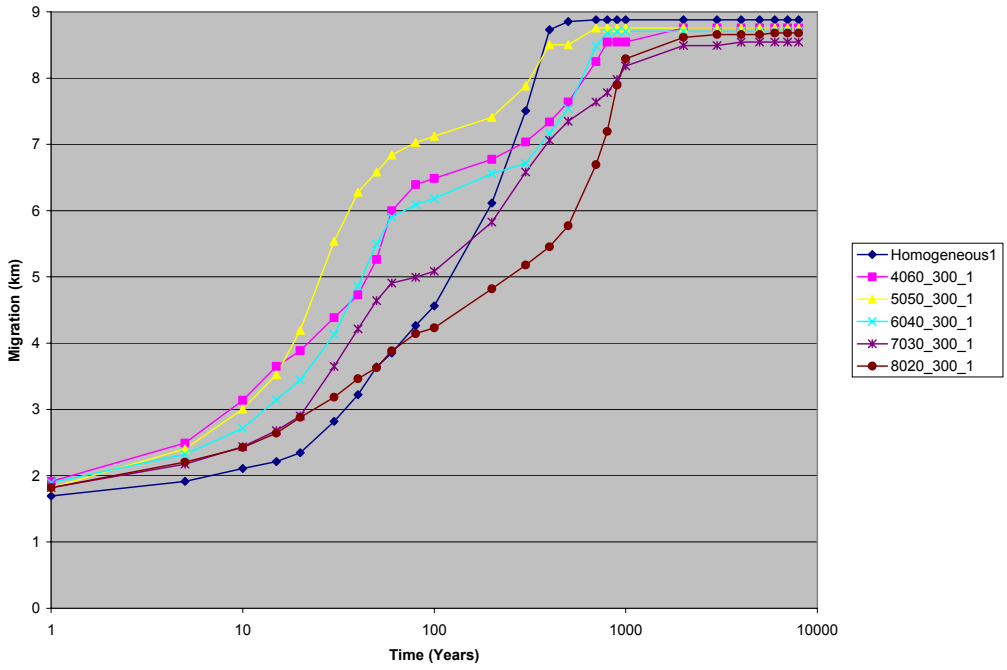

Figure 6-30: Migration comparison of the 300 m facies models, various net-to-gross, 1 degree slope

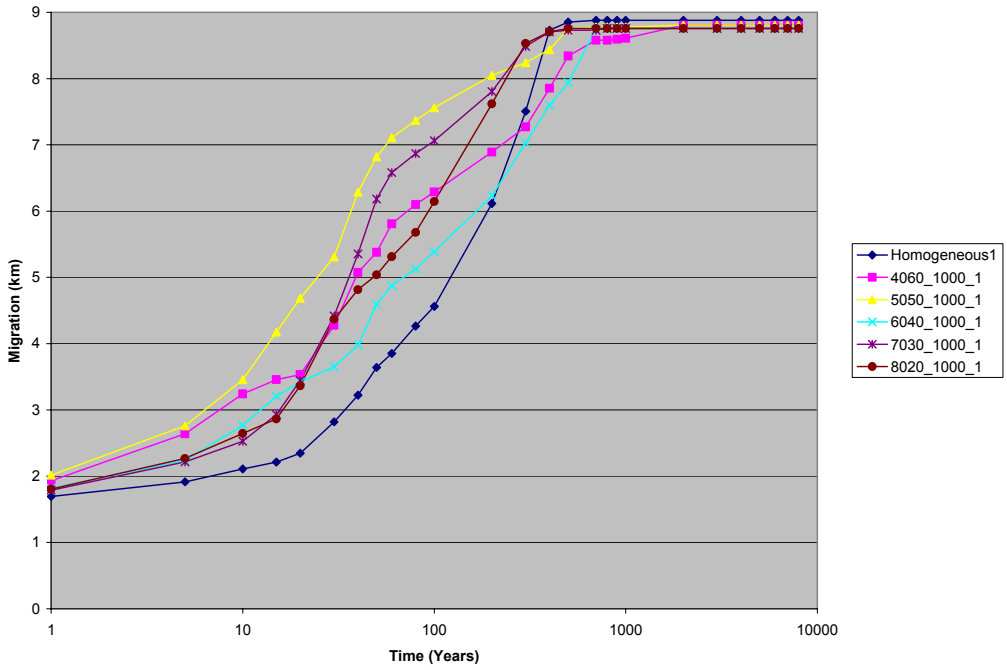

Figure 6-31: Migration comparison of the 1000 m facies models, various net-to-gross, 1 degree slope

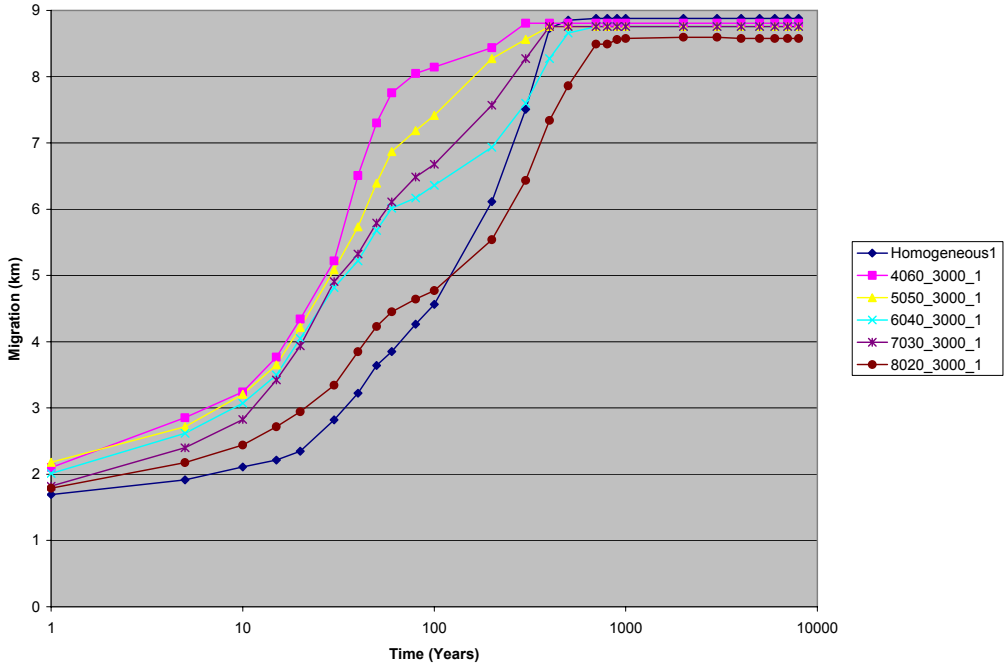

Figure 6-32: Migration comparison of the 3000 m facies models, various net-to-gross, 1 degree slope

In Figures 6-29 to 6-32, the impact of increasing the amount of shale influences the rate of lateral migration by the injected plume. Poorer reservoir quality rock (e.g 40:60 net to gross) is favourable to lateral migration than the higher quality rock.

6.5.2 Vertical Migration

Figures 6-33 to 6-36 show the vertical migration of the CO_2 plume in the models. When the CO_2 plume touches the value of 100% is the point that the CO_2 plume has reached the geological seal in the model. Each model has the same well completions; the differences in the initial vertical position on the plot for different models are due to the initial well performance.

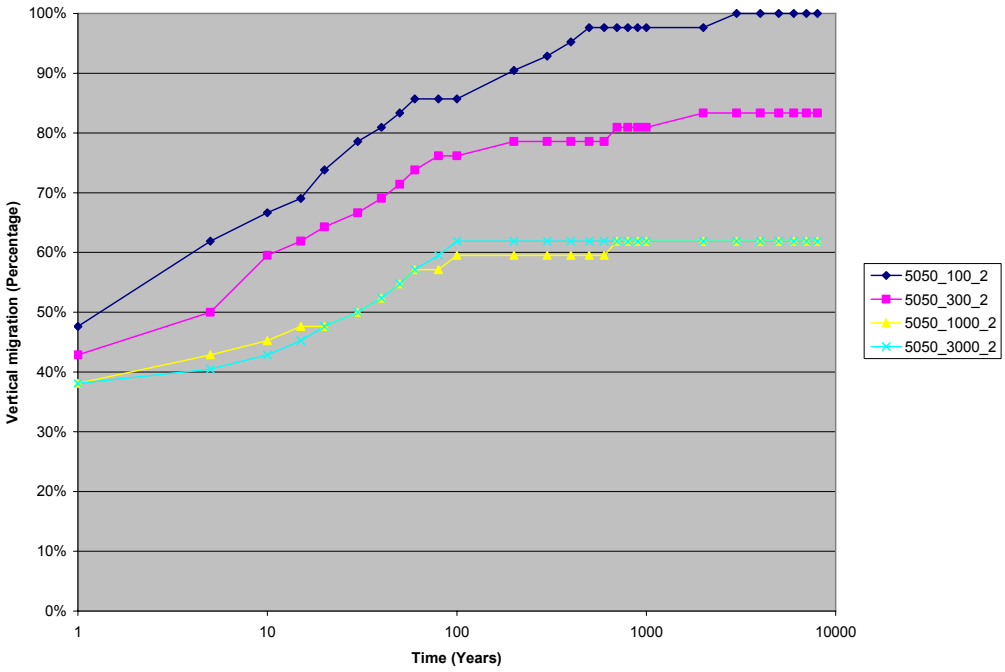

Figure 6-33: Vertical migration comparison of the 50:50 net to gross models, various shale lengths, 2 degree slope

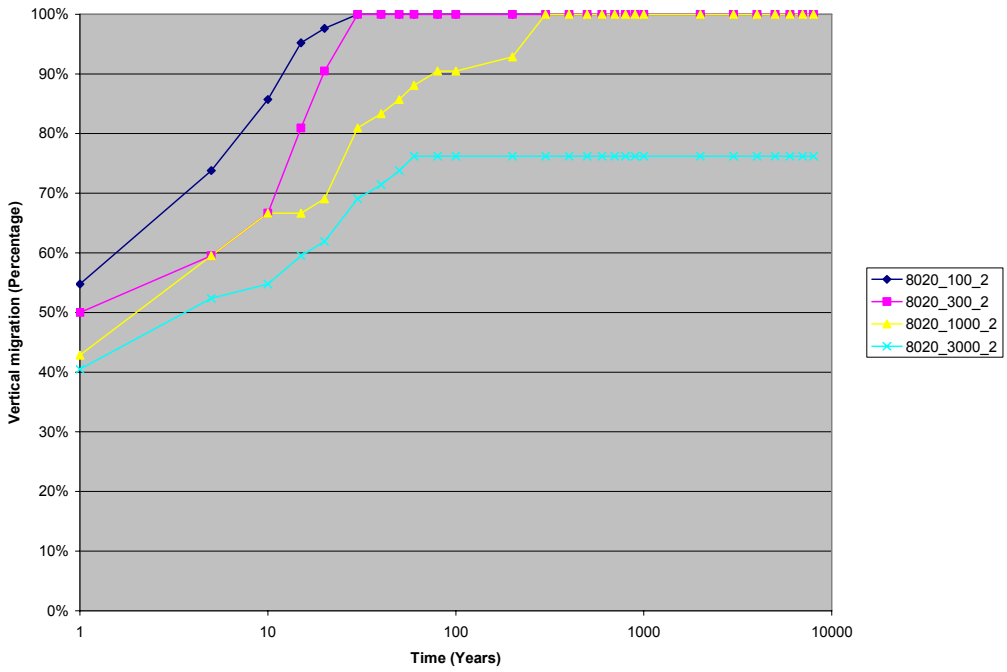

Figure 6-34: Vertical migration comparison of the 80:20 net to gross models, various shale lengths, 2 degree slope

From Figures 6-33 and 6-34, a low and high reservoir quality reservoirs (50:50 and 80:20 net sand to gross respectively), the impact of shale length variograms is apparent. The longer the shale length variogram is in the model the slower vertical stratigraphic migration of the injected CO_2 plume.

In Figure 6-35 and 6-36, the ratio of sand to shale was varied for two variogram lengths, 300m and 3000m. From these figures it shown that with a reduction in reservoir quality, with steadier increases in the amount of non-reservoir shale in the formation, the ability of the migrating plume to stratigraphically move up the formation is diminished.

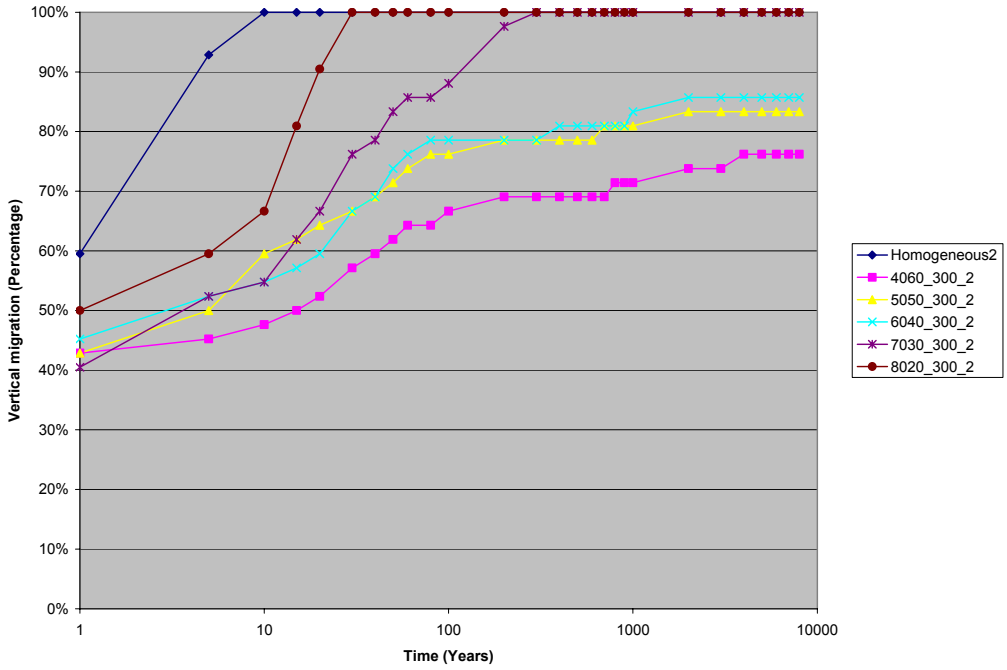

Figure 6-35: Vertical migration comparison of the 300 m shale length models, various sand to shale contents, 2 degree slope

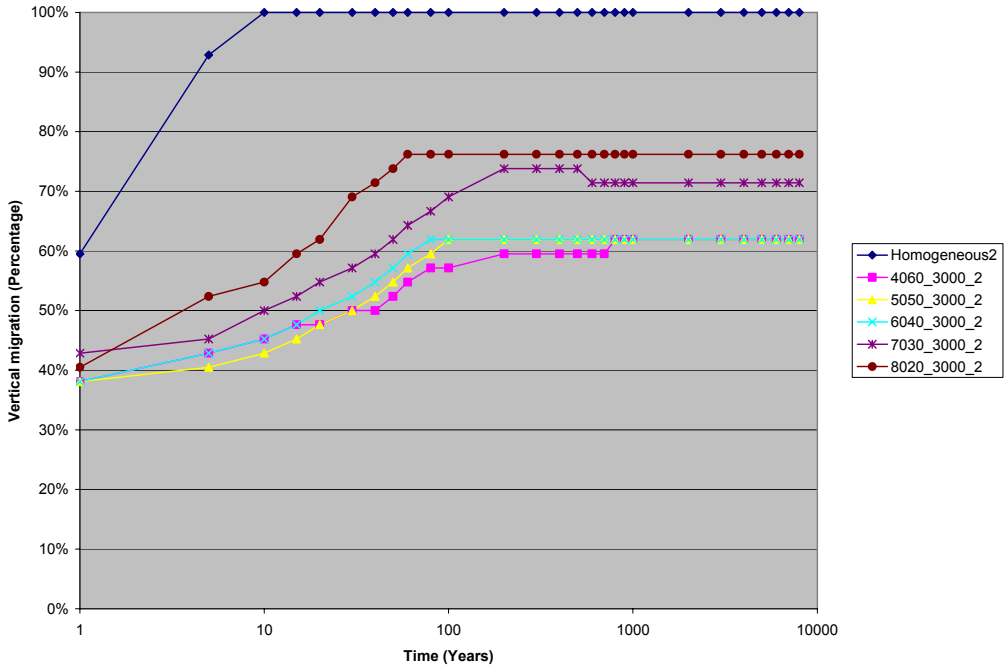

Figure 6-36: Vertical migration comparison of the 3000 m shale length models, various sand to shale contents, 2 degree slope

6.5.3 Trapping Mechanism

Figures 6-37 to 6-40 show the fraction of CO_2 trapped as a residual phase for changes in shale length variogram and changes in the amount of net to gross for a selection of models.

Note that residual phase trapped gas is not based on a direct calculation of trapped gas volumes in cells but instead is defined by a practically immobile gas relative permeability k_{rg} of 0.0001. When CO_2 is present in a model cell, but the k_{rg} of the cell is less than 0.0001, as occurs at the end of the hysteresis cycle, the gaseous volume of CO_2 in that cell is regarded as residually trapped.

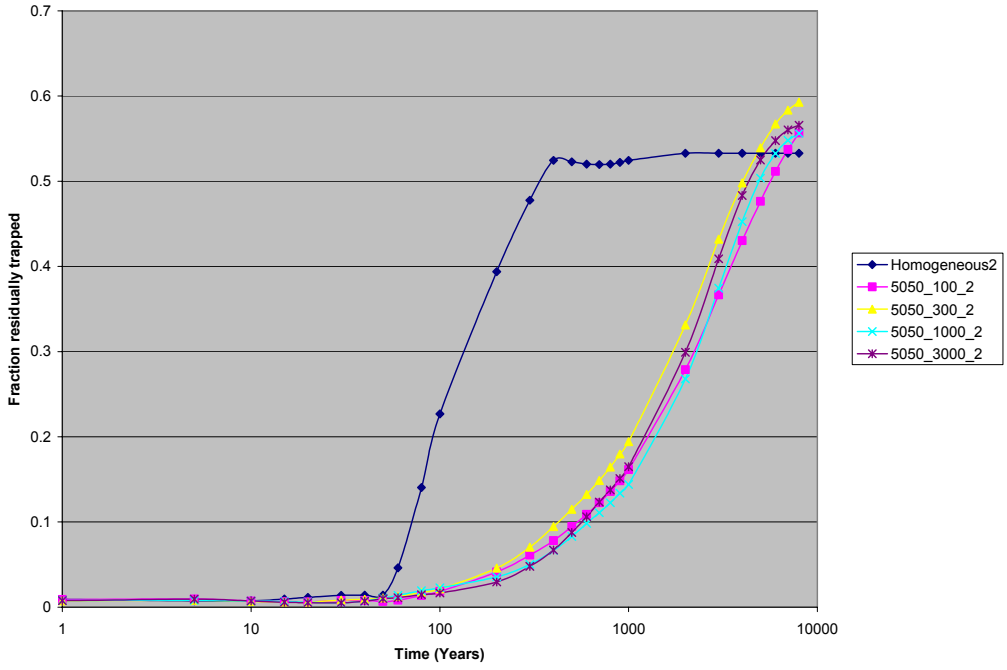

Figure 6-37: Fraction of residually trapped CO_2 for 50:50 ratio of sand to shale, formation dip of 2 degrees

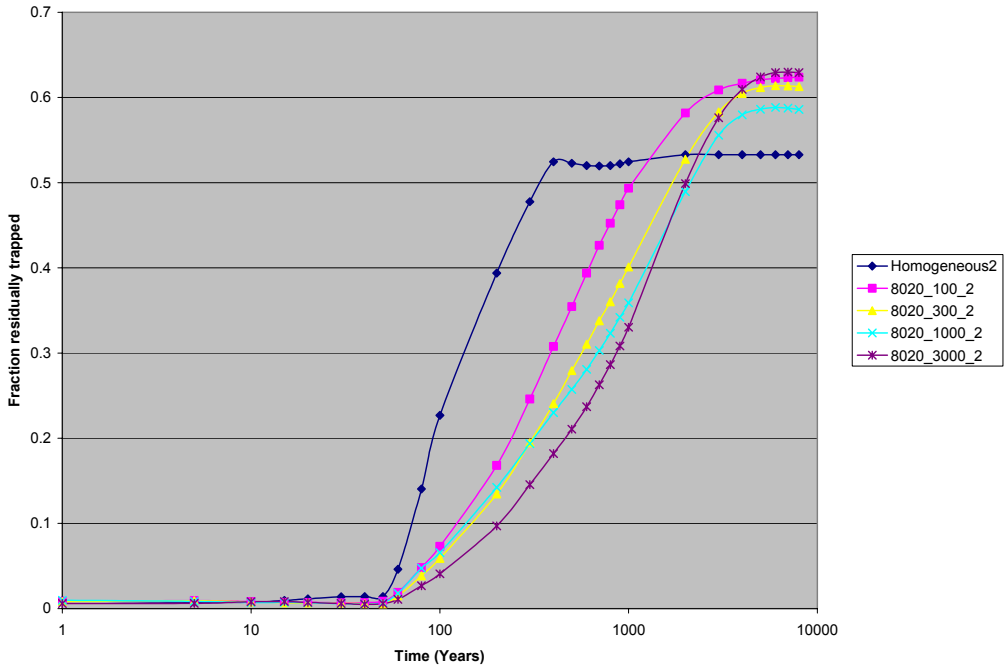

Figure 6-38: Fraction of residually trapped CO_2 for 80:20 ratio of sand to shale, formation dip of 2 degrees

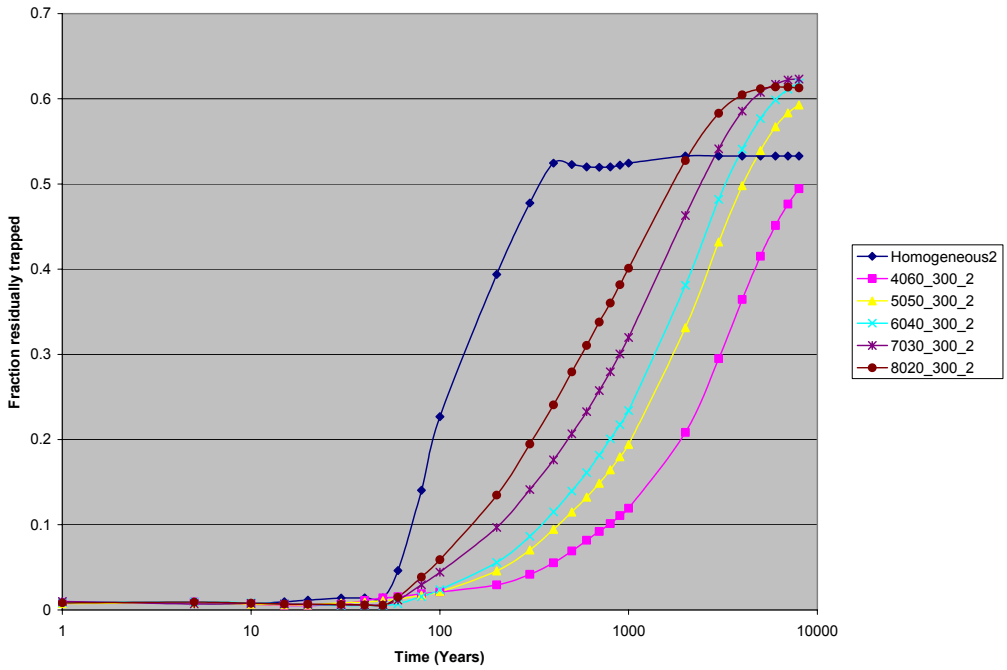

Figure 6-39: Fraction of residually trapped CO_2 for 300m shale length variogram, formation dip of 2 degrees

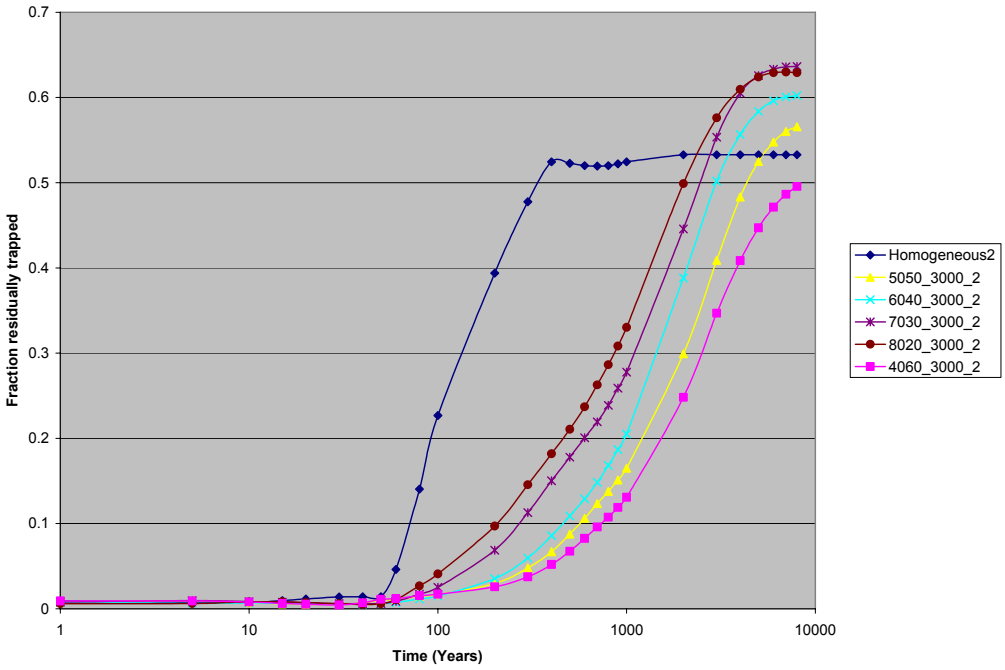

Figure 6-40: Fraction of residually trapped CO_2 for 3000m shale length variogram, formation dip of 2 degrees

From Figures 6-37 and 6-38 it is shown that heterogeneity present in the model significantly delays residual phase gas trapping compared to the homogeneous model. Where differentiation occurs between the heterogeneous models in Figure 6-38, the longer the shale breaks are in the model the slower the residual trapping is occurring. From Figures 6-39 and 6-40 it is apparent that increasing the shale fraction in model appears to delay the process of residual gas trapping.

For a selection of results, Figure 6-41 shows the amount of CO_2 dissolved and Figure 6-42 shows that amount of CO_2 remaining mobile for the 50:50 net sand to shale models (with varying shale length). Figure 6-43 shows the amount of CO_2 dissolved and Figure 6-44 shows that amount of CO_2 remaining mobile for the range of net-gross values with the 300m shale length variogram.

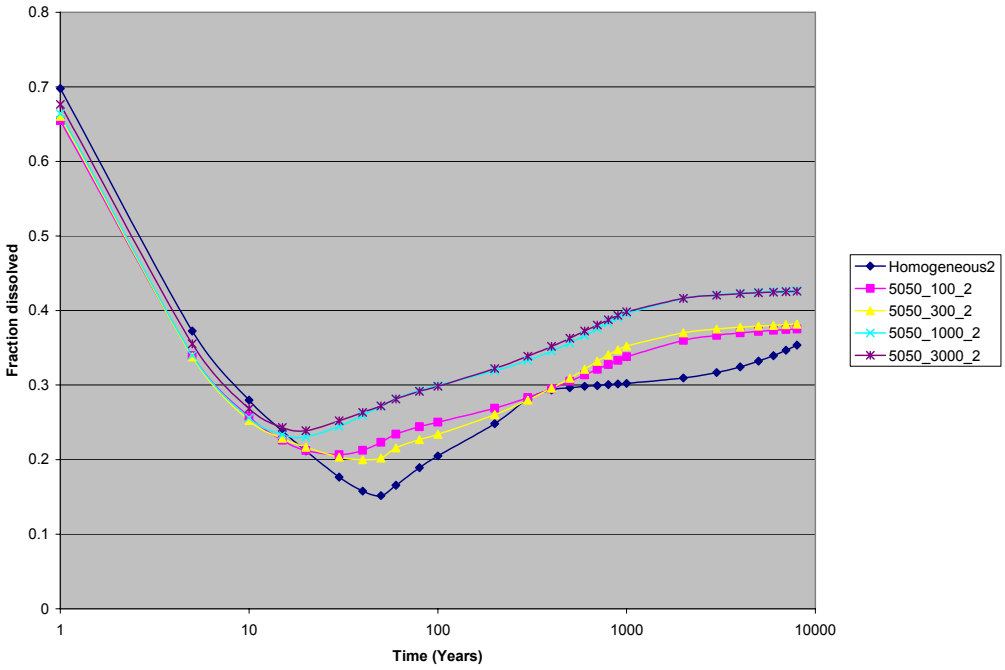

Figure 6-41: Fraction of dissolved CO_2 for 50:50 ratio of sand to shale, formation dip of 2 degrees

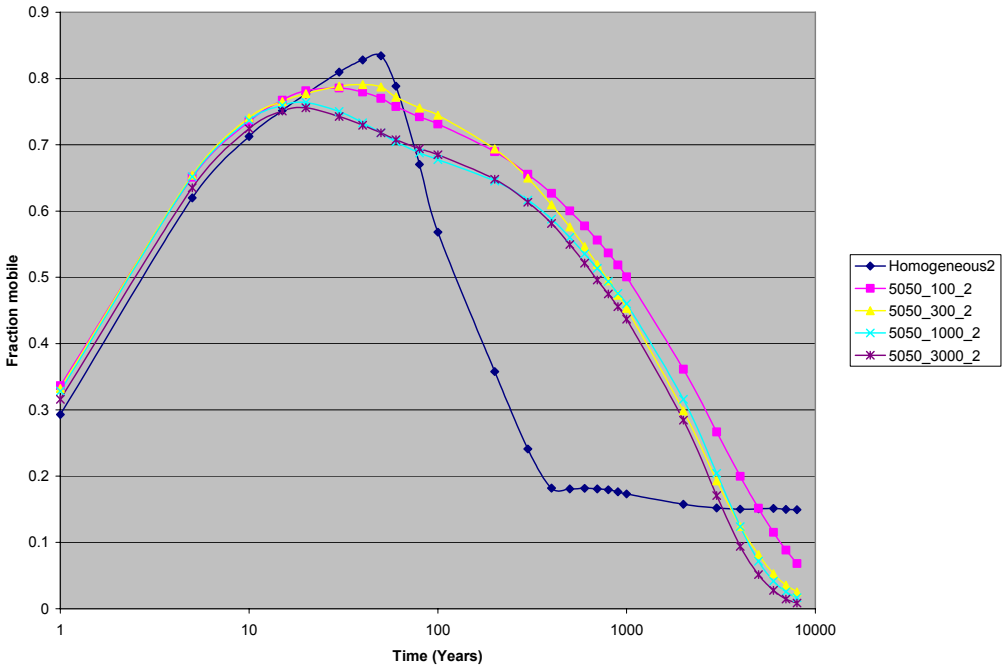

Figure 6-42: Fraction of mobile CO_2 for 50:50 ratio of sand to shale, formation dip of 2 degrees

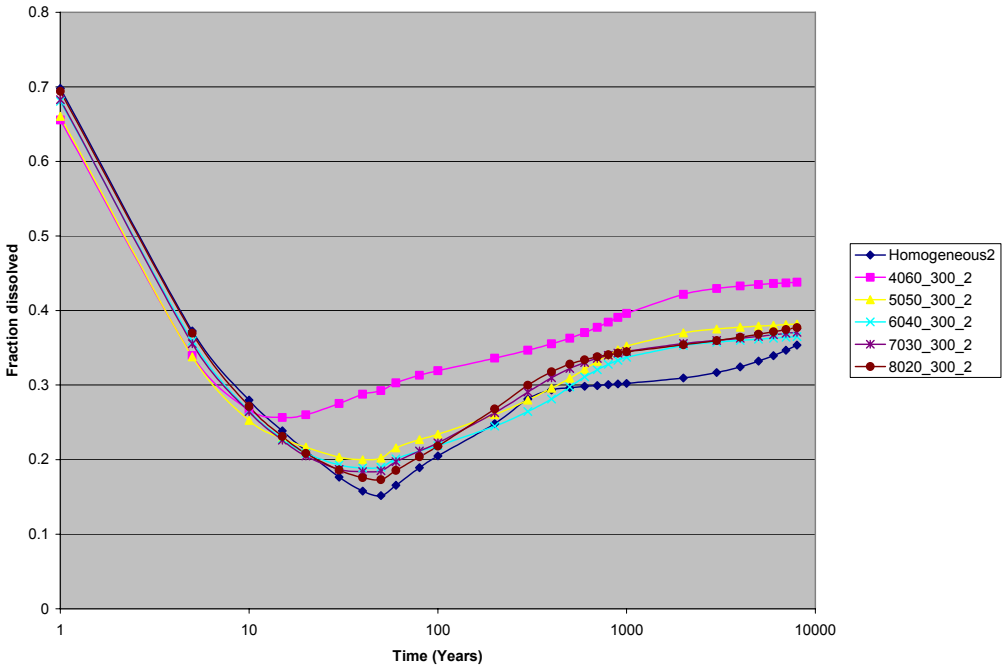

Figure 6-43: Fraction of injection CO_2 dissolved - comparison of the 300 m shale length models, various sand to shale ratios, 2 degree slope

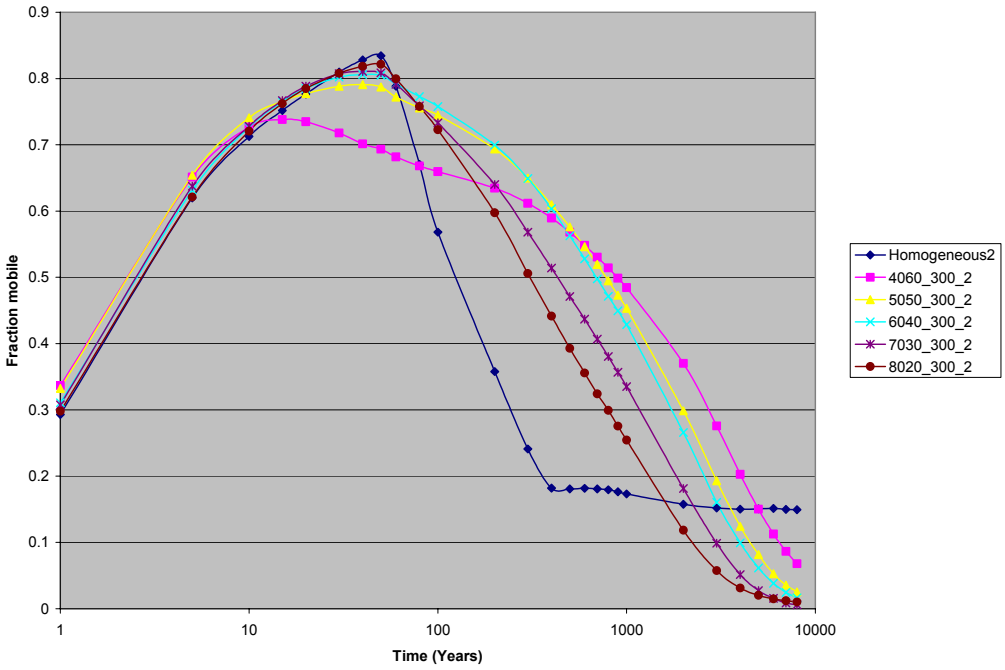

Figure 6-44: Fraction of injection CO_2 remaining mobile - comparison of the 300 m shale length models, various sand to shale lengths, 2 degree slope

6.6 Discussion

The homogeneous reservoir model shows the development of the CO_2 plume as being quite symmetrical, with the plume migrating upwards with no hindrance until the formation seal is reached. The plume then spreads underneath the seal and moves upwards due to the formation dip. With the introduction of a modest amount of shale (such as the 80:20 models in Figure 6-16) the impedance of vertical migration of the plume is noticeable. With increasing amounts of shale as seen in Figure 6-15 to 6-20 the ability of the plume to migrate upwards is progressively limited due to the increasingly tortuous migration path. This effect is amplified with the lengthening of the shale variograms from 100m to lengths of 3000m as seen in Figure 6-21 to 6-24, with lengthening shale length increasing the impedence to vertical migration. In essence the shale serves to guide the plume up dip and thereby enhance overall reservoir contact between the plume and the formation, which, in turn, leads to larger dissolution of the injected gas. Although decreasing reservoir quality diminishes the ability of the plume to migrate vertically upwards, the plume can still move structurally higher through lateral migration up dip. Note that the reduction of reservoir quality with decreasing net-to-gross ratios accelerates lateral migration by reducing the amount of net sand in the model about the well bore, leading to an acceleration of near well bore migration.

Formation dip influences the subsurface migration of injected CO_2 by changing the role of vertical force acting on the plume. Increasing formation dip, increased the ability of the density constract between the plume and water to drive lateral migration of carbon dioxide through the target formation. This contrast is shown in comparing Figure 6-27 and 6-28; a low formation dip (1º) case in Figure 6-27 has lower rates of lateral migration compared to a high formation dip case (10º) in Figure 6-28. Therefore the selection of a candidate low dipping formation for containment for disposed CO_2 would appear to be superior over a formation with a high formation dip.

Figures 6-41 and 6-43 shows that during injection the CO_2 plume dissolves into the formation water. The water surrounding the injection wells becomes saturated with the gas as the CO_2 laterally permeates the reservoir, with reservoir contact of the

plume guided by the formation heterogeneity. This process continues until the injection of CO_2 ceases and the plume migrates upwards, due to gravity, and contacts virgin formation water. It is apparent that the level of dissolution is flattening out in all cases.

Figures 6-37 to 6-40 confirm that residual phase gas trapping as a means of storage is, essentially, a post injection process, since the CO_2 plume is required to be migrating for effective trapping to occur, with water imbibing behind the plume causing the relative permeability of the CO_2 to reduce to zero. The differences in net-to-gross and shale length have an impact on the rate of residual phase trapping, as increasing shale amount or length of shale in the formation limits the ability of the plume to migrate, delaying the gas-water relative permeability hysteresis cycle. It would appear that for the homogeneous case the fraction of trapped CO_2 is reaching a limit of around 55%, while for heterogeneous models the amount trapped can range from 55 to 70% with equilibrium not yet present at late time frame that has been simulated.

The mobile gas in Figure 6-42 is derived from Figures 6-41 and 6-37, as is the mobile gas plot Figure 6-44 derived from Figures 6-43 and 6-39, since the mobile CO_2 accounts for the remaining CO_2 that, by definition, is mobile (by not being residually trapped or dissolved). Given that approximately 30 to 45% of the CO_2 dissolves (as in Figure 6-43), and more than 60% may eventually become trapped in a residual phase (as Figure 6-39), it is reasonable to suppose that the simulation would need to run for longer, even for another order of magnitude, before formal equilibrium is achieved.

The degree of reservoir heterogeneity has a quantifiable effect on the migration and containment of injected CO_2. In terms of site selection for potential geological disposal targets, the impact of heterogeneity in the formation geology should be considered. Provided that a heterogeneous formation has sufficient injectivity and meets other containment criteria, such as a formation seal, heterogeneity in the target formation acts to slow the process of CO_2 migration, and can thus delay the reliance of the formation seal for containment. Compared to heterogeneous formations, a homogeneous formation has faster rates of migration and hence an increased rate of

residual phase gas trapping and earlier reliance on the formation seal. As to an overall comparison of heterogeneous and homogeneous formations for comparisons of containment of CO_2 by dissolution and residual phase gas trapping, long time scale simulations are required for equilibrium to be achieved.

That main finding of this study is that the formation qualities that would be beneficial for long term containment of injected CO_2 would be a heterogeneous formation, with sufficient permeability for injection, low formation dip, with long length intrabed shales to impede movement stratigraphic movement of CO_2 and maximise reservoir contact between the plume and the formation. This formation criteria fulfils the research question for this study and will provide guidance for the future selection of formations to be screened and developed for the geological disposal of CO_2.

7. Conclusions

This study has built on previous research by evaluating the roles of several CO_2 trapping mechanisms and the impact of variations in formation heterogeneity through reservoir simulation of CO_2 injection into several models of saline formations.

In the second chapter, aspects of CO_2 physical behaviour in saline formations were explained. Physical means of containing injected CO_2 in saline formation; such as dissolution, geological trap and seal, mineralization, gas-water relative permeability hysteresis were discussed in detail. Reservoir simulation studies in the literature investigating CO_2 geological disposal into saline formations were discussed and compared. These studies were conducted to understand the fundamental processes during CO_2 disposal including a range of various trapping mechanisms. However, simulation models employed in the literature have been mainly generic or homogeneous models based on sparse input data. Integration of full reservoir characterization in reservoir simulation models, where the interaction of formation heterogeneity on the injected plume movement was lacking.

In the third chapter, the general methodology of this thesis was outlined. The physical description and the appropriate use of the black oil formulation reservoir simulation package was explained for this study.

In the fourth, fifth and sixth chapters, reservoir performance metrics for the evaluation of CO_2 underground storage projects in the absence of economic metrics were presented. Two enabling studies in Chapters 4 and 5 evaluated the role of trapping mechanisms in containing CO_2 and also the impact of formation heterogeneity in plume movement separately. Design of Experiments methods were applied and provided estimates for ranges in reservoir performance such amount of CO_2 dissolved and residually trapped. The major study of this report combined the evaluation of trapping mechanisms and role of variations in formations heterogeneity in containing injected CO_2 in a saline formation in determining the favourable characteristics of a formation for disposal of CO_2.

Dissolution of injected carbon dioxide into formation water and the immobilisation of carbon dioxide by imbibition relative permeability forces are significant in reducing the reliance of an overlying geological seal and trap in providing containment for an injected carbon dioxide plume. Initial reservoir simulation demonstrated that formation permeability has significant effect on reservoir performance with regards to; migration, pressure distribution and long term trapping of the CO_2.

Reservoir characterisation of potential geological disposal target is key exercise in providing confident predictions of long term movement of injected carbon dioxide. The degree and distribution of formation heterogeneity has a significant influence on the migration and trapping of an injected carbon dioxide plume. Reservoir characterisation of formation heterogeneity has several influences on containment of an injected plume than one could expect in a simple homogeneous reservoir; rate of stratigraphic migration is decreased by means of tortuous passages through shales barriers for migrating plumes, reservoir contact by the plume with virgin formation water increasing due to further lateral movement delineated by shale breaks, in turn increasing dissolution and residual trapping of the plume. Increased heterogeneity delays the trapping of CO_2 as a residual phase, since the ability of the plume to migrate through a heterogeneous formation can be severely inhibited. Low formation dip is desirable to reduce the rate of migration of an injected plume.

Thus low dipping heterogeneous saline formations (including low net-to-gross systems) are desirable targets for selection for geological disposal of carbon dioxide, provided that there is sufficient permeability to allow for economical injection of the CO_2, as these formations are effective in containing CO_2.

Formation heterogeneity serves to limit the reliance of the formation seal as the only mechanism for containment. For the particular models considered in these studies it would appear that the simulations would need to be run for several tens of thousands of years for equilibrium to be reached.

7.1 Further Work

This study has demonstrated the impact of varying quantities of sand and shale on the migration of CO_2 and the effectiveness of certain storage mechanisms. Although the models are considered realistic there are clearly many other configurations that could be considered. Further studies should be undertaken with regards to:

1. Long term simulation models, of the order of tens of thousand of years should be considered to drive towards the formation of an effective equilibrium state occurring within simulation models in CO_2 disposal site selection and characterization evaluation.

2. Specific screening studies to evaluate potential geological formations for disposal of carbon dioxide from nearby sources of carbon dioxide. This study requires the involvement of geologists and other earth scientists for reservoir modeling and description, to fully characterize the reservoir sufficiently to give plausible outcomes for dynamic forecasts of CO_2 migration and trapping.

3. Relative permeability measurements, both drainage and imbibition, of CO_2 movement in real core samples. There is a paucity of high quality experiments in this fundamental area of fluid movement for CO_2 disposal. While analogues from petroleum literature are adequate and appropriate for the time being to describe CO_2 relative permeability, high quality experiments are desirable to reduce uncertainty in this area.

4. Comparison of fine and coarse scale models for scaling effects in relative permeability and physical processes such as dissolution.

5. Consider the coupling of reservoir simulation with geo-mechanical and temperature effects included, so that possible fracturing and potential fault activity due to thermal (e.g. injection of 'cool' CO_2 into a warm reservoir) and pressure effects could be evaluated for containment at a particular site.

6. Injectivity studies investigating the near wellbore effects as CO_2 is injected into saline formation, including changing mobility of the CO_2, impact of well skin, formation dry-out and salt precipitation.

7.2 Final Remarks

An underlying driver of this work was to demonstrate the requirement of understanding the geology of a formation selected for disposal of carbon dioxide to a wider subsurface community working on the issue of carbon dioxide disposal. In future industrial scale projects examining the disposal of carbon dioxide, reservoir simulation / development engineers need to work collaboratively with their subsurface peers such as geologists, petrophysicists, geophysicists and well engineering to create an acceptable development plan which takes account of variable subsurface outcomes. Reservoir characterisation of selected formations for CO_2 disposal will be a requirement to ensure the disposal of CO_2 in those formations will be successful in keeping CO_2 contained within those formations.

References

Agarwal, R. G., Al-Hussainy, R. and Ramey Jr., H. J. (1965). "The importance of water influx in gas reservoirs." Journal of Petroleum Technology **11**: 1336-1342.

Altunin, V. V. (1975). Thermophysical properties of carbon dioxide Moscow Publishing House of Standards (in Russian).

Angus, S., Armstrong, B. and de Reuck, K. M. (1976). International Thermodynamics Tables of the Fluid State Carbon Dioxide. Oxford, International Union of Pure and Applied Chemistry, Pergamon Press.

Bachu, S. (2000). "Sequestration of CO_2 in geological media: criteria and approach for site selection in response to climate change." Energy Conversion and Management **41**(9): 953-970.

Bachu, S. (2002). "Sequestration of CO_2 in geological media in response to climate change: road map for site selection using the transform of the geological space into the CO_2 phase space." Energy Conversion and Management **43**(1): 87-102.

Bachu, S., Gunter, W. D. and Perkins, E. H. (1994). "Aquifer disposal of CO2: hydrodynamic and mineral trapping." Energy Conversion and Management **35**(4): 269-279.

Baklid, A., Korbol, R. and Owren, G. (1996). Sleipner Vest CO_2 disposal, CO_2 injection into a shallow underground aquifer. SPE Annual Technical Conference. Denver, Colorado, USA, Society of Petroleum Engineers: SPE 36600.

Battistelli, A., Calore, C. and Preuss, K. (1997). "The simulator TOUGH2/EWASG for modelling geothermal reservoirs with brines and non-condensable gas." Geothermics **26**(4): 437-464.

Bennion, D. B. and Bachu, S. (2006). Supercritical CO_2 and H_2S-Brine Drainage and Imbibition Relative Permeability relationships for Intragranular Sandstone and Carbonate Formations. SPE Europe/EAGE Annual Conference and Exhibition. Vienna, Austria, Society of Petroleum Engineers: SPE Paper 99326.

Bradshaw, J., Bradshaw, B., Allison, G., Rigg, A., Nguyen, V. and Spencer, L. (2002). "The potential for geological sequestration of CO_2 in Australia: preliminary findings and implications for new gas field development." APPEA J. **1**(2002): 25-46.

Brinks, J. and Fanchi, J. (2001). Geologic Sequestration: Modeling and Monitoring Injected CO_2. SPE/EPA/DOE Exploration and Production Environmental Conference. San Antonio, Texas, Society of Petroleum Engineers: SPE Paper 66749.

Brooks, R. H. and Corey, A. T. (1966). "Properties of porous media affecting fluid flow." Journal of Irrigation and Drainage Engineering **6**(61).

Chang, Y.-B., Lim, M. T., Pope, G. A. and Sepehrnoori, K. (1994). "CO_2 Flow Patterns Under Multiphase Flow: Heterogeneous Field-Scale Conditions." SPE Reservoir Eng **9**: 208-216.

Chang, Y., Coats, B. and Nolen, J. (1998). "A compositional model for CO_2 floods including CO_2 solubility in water." SPE Reservoir Evaluation & Engineering **4**: 155-160.

Chevron (2006). Draft Environmental Impact Statement / Environmental Review and Management Programme for the Proposed Gorgon Development: Main Report. Perth, Western Australia, Chevron Australia Pty Ltd.

Cook, A., Rigg, A. and Bradshaw, J. (2000). "Putting it back where it came from: is geological disposal of carbon dioxide an option for Australia?" APPEA Journal **1**: 1-13.

Davis, N., Riddiford, F., Bishop, C., Taylor, B. and Froukhi, R. (2001). The In Salah Gas Project, Central Algeria: Bringing an Eight Field Gas Development to Sanction. SPE Middle East Show. Bahrain, Society of Petroleum Engineers: SPE Paper 68180.

Deo, M. D. and Deans, H. A. (1990). Experimental and Theoretical Determination of Residual Saturation After a Water-Driven Carbon Dioxide flood. SPE/DOE Seventh Symposium on Enhanced Oil Recovery. Tulsa, Oklahoma, Society of Petroleum Engineers: SPE Paper 20266.

Doughty, C. and Preuss, K. (2004). "Modeling supercritical carbon dioxide injection in heterogeneous porous media." Vadose Zone J **3**: 837-847.

Durlofsky, L., Behrens, R., RC, J. and Bernath, A. (1996). "Scale up of heterogeneous three dimensional reservoir descriptions." SPE Journal **3**(September): 313-326.

Engebretsen, H., Fossan, B. and Nesse, S. (2002). EIA for the world's northernmost LNG plant, the Snohvit project in an environmental sensitive area at 71°N. SPE International Conference on Health, Safety and Environment in Oil and gas Exploration and Production. Kuala Lumpur, Malaysia, Society of Petroleum Engineers: SPE paper 74027.

Enick, R. and Klara, S. (1990). "CO_2 solubility in water and brine under reservoir conditions." Chem. Eng. Commun. 90 (1990), pp. 23-33. .

Ennis-King, J. and Paterson, L. (2002). Engineering aspects of geological sequestration of carbon dioxide. SPE Asia Pacific Oil and Gas Conference & Exhibition. Melbourne, Victoria, Australia, Society of Petroleum Engineers: SPE Paper 77809.

Ennis-King, J. and Paterson, L. (2003). "Role of convective mixing in the long-term storage of carbon dioxide in deep saline formations." SPE Journal **10**(3): 349-356.

Fenghour, A., Wakeham, W. A. and Vesovic, V. (1998). "The Viscosity of Carbon Dioxide." J. Phys. Chem. Ref. Data **27**(1): 31-44.

Firoozabadi, A., Olsen, G. and van Golf-Racht, T. (1987). Residual gas saturation in water-drive gas reservoirs. SPE California Regional Meeting. Ventura, CA, USA, Society of Petroleum Engineers: SPE Paper 16355.

Firoozabadi, A. and Thomas, L. K. (1989). Sixth SPE Comparative Solution Project: A Comparison of Dual-Porosity Simulators. Tenth SPE Symposium on Reservoir Simulation. Houston, Texas, Society of Petroleum Engineers, SPE paper 18741.

Flett, M., Gurton, R. and Taggart, I. (2004). The function of gas-water relative permeability hysteresis in the sequestration of carbon dioxide in saline formations. SPE Asia-Pacific Oil and Gas Conference and Exhibition, Perth, Australia.

Flett, M., Gurton, R. and Taggart, I. (2004). Heterogeneous saline formations: long term benefits for geo-sequestration of greenhouse gases. Seventh International Conference on Greenhouse Gas Control Technologies (GHGT-7), Vancouver, Canada., Elsevier.

Flett, M., Gurton, R. and Weir, G. (2006). Reservoir performance of disposed carbon dioxide in saline formations: impact of heterogeneity and dip. 8th International conference on Greenhouse Gas Control Technologies, Trondheim, Norway.

Flett, M., Gurton, R. and Weir, G. (2007). "Heterogeneous saline formations for carbon dioxide disposal: Impact of varying heterogeneity on containment and trapping." Journal of Petroleum Science and Engineering **57**(1-2): 106-118.

Floris, F. J. T., Bush, M. D., Cuypers, M., Roggero, F. and Syversveen, A. R. (2001). "Methods for quantifying the uncertainty of production forecasts: a comparative study." Petroleum Geoscience **7**: S87-S96.

Garcia, J. E. (2003). Fluid Dynamics of Carbon Dioxide Disposal into Saline Aquifers. Civil and Environmental Engineering. Berkeley, University of California, Berkeley.

Gunter, W. D., Perkins, E. H. and McCann, T. J. (1993). "Aquifer disposal of CO_2-rich gases: reaction design for added capacity." Energy Conversion and Management **34**(9-11): 941-948.

Hamon, G., Suzanne, K., Billiotte, J. and Trocme, V. (2001). Field-wide variations of trapped gas saturation in heterogeneous sandstone reservoirs SPE Annual Technical Conference and Exhibition, New Orleans, Louisiana, USA.

Hendriks, C. A. and Blok, K. (1995). "Underground Storage of Carbon Dioxide." Energy Conversion and Management **36**(6-9): 539-542.

Hitchon, B., Ed. (1996). Aquifer Disposal of Carbon Dioxide, Hydrodynamic and Mineral Trapping - Proof of Concept. Sherwood Park, Alberta, Canada Geoscience Publishing Ltd.

Holloway, S. and van der Straaten, R. (1995). "The Joule II Project: The Underground Disposal of Carbon Dioxide " Energy Conversion and Management **36**(6-9): 519-522.

Honarpour, M., Koederitz, L. and Harvey, A. (1986). Relative Permeability of Petroleum Reservoirs. USA CRC Press Inc.

Houghton, J., Ed. (2001). The Scientific Basis. Climate Change 2001. Cambridge, United Kingdom, Cambridge University Press.

Hovorka, S., Doughty, C. and Holtz, M. (2004). Testing efficiency of storage in the subsurface: Frio Brine Pilot experiment. Paper 574, Presented at the Seventh

International Conference on Greenhouse Gas Control Technologies, Vancouver, Canada, September 5-9 (2004).

Hovorka, S. D., Doughty, C., Benson, S. M., Preuss, K. and Knox, P. R. (2004). The impact of geological heterogeneity on CO_2 storage in brine formations: a case study from the Texas Gulf Coast. Geological Storage of Carbon Dioxide. S. J. Baines and R. H. Worden. London, Geological Society. **Special Publications:** 147-163.

Imperial College (2008). PUNQ-S3 Model online data set, Imperial College.

Jacobs, M. A. (2005). Measurement and modeling of thermodynamic properties for the processing of polymers in supercritical fluids. Eindhoven, Eindhoven University of Technology.

Jerauld, G. R. (1997). "General three-phase relative permeability model for Prudhoe Bay." SPE Reservoir Eng **12**(4): 255-263.

Juanes, R., Spiteri, E. J., F.M., O. J. and Blunt, M. J. (2006). "Impact of relative permeability hysteresis on geological CO_2 storage." Water Resource Research **42**.

Keelan, D. K. and Pugh, V. J. (1975). "Trapped gas saturation in carbonate formations." SPE Journal **4**: 149-160.

Killough, J. E. (1976). "Reservoir simulation with history-dependant saturation functions." Petrol. Trans. AIME(261): 37-48.

Koide, H., Takahashi, M. and Tsukamoto, H. (1995). "Self-Trapping Mechanisms of Carbon Dioxide in the Aquifer Disposal." Energy Conversion and Management **36**(6-9): 505-508.

Koide, H., Tazaki, Y., Noguchi, Y., Iijima, M., Ito, K. and Shindo, Y. (1993). "Underground storage of carbon dioxide in depleted natural gas reservoirs and useless aquifers." Engineering Geology **34**: 175-179.

Korbol, R. and Kaddour, A. (1995). "Sleipner Vest CO_2 disposal - injection of removed CO_2 into the Utsira formation." Energy Conversion and Management **36**(6-9): 509-512.

Kralik, J. G., Manak, L. J., Jerauld, G. R. and Spence, A. P. (2000). Effect of trapped gas on relative permeability and residual oil saturation in an oil-wet sandstone. SPE Annual Technical Conference & Exhibition,. Dallas, TX, USA, Society of Petroleum Engineers: SPE Paper 62997.

Kumar, A., Noh, M., Pope, G., Sepehrnoori, K., Bryant, S. and Lake, L. (2004). Reservoir simulation of CO_2 storage in deep saline aquifers. SPE/DOE Fourteenth Symposium on Improved Oil Recovery.. Tulsa, Oklahoma, U.S.A. 17-21 April (2004).

Land, C. S. (1968). "Calculation of imbibition relative permeability for two- and three-phase flow from rock properties." SPE J.: (1968), pp. 149-156 (June, SPE paper 1942).

Law, D. H. S. and Bachu, S. (1996). "Hydrogeological and numerical analysis of CO_2 disposal in deep aquifers in the Alberta sedimentary basin." Energy Conversion and Management **37**(6-8): 1167-1174.

Leonenko, Y., Keith, D. W., Pooladi-Darvish, M. and Hassanzadeh, H. (2006). Accelerating the dissolution of CO_2 in aquifers. 8th International conference of Greenhouse Gas Control Technologies. Trondheim, Norway, IEA

Lindeberg, E. (1997). "Escape of CO_2 from aquifers." Energy Conversion and Management **38**(Supplement 1): S235-S240.

Lindeberg, E. and Wessel-Berg, D. (1997). "Vertical convection in an aquifer column under a gas cap of CO_2." Energy Conversion and Management **38S**: S229-234.

Mansoori, J. (1982). "Compositional Modeling of CO_2 flooding and the Effect of CO_2 Water Solubility." SPE Journal **SPE paper 11438**.

Mo, S., Zweigel, P., Lindeberg, E. and Akervoll, I. (2005). Modeling long-term CO_2 storage in aquifer with a black-oil reservoir simulator. SPE Europe/EAGE Annual Conference. Madrid, Spain, Society of Petroleum Engineers: SPE Paper 93952.

Nghiem, L. (2002). Compositional Simulator for Carbon Dioxide Sequestration. Calgary, Computer Modelling Group Ltd.

Nghiem, L., Sammon, P., Grabenstetter, J. and Ohkuma, H. (2004). Modeling CO_2 storage in Aquifers with a Fully-Coupled Geochemical EOS Compositional Simulator. SPE/DOE Symposium on Improved Oil Recovery. Tulsa, Oklahoma, Society of Petroleum Engineers, SPE Paper 89474.

NIST/SEMATECH. (2004). "e-Handbook of Statistical Methods, http://www.itl.nist.gov/div898/handbook/." Retrieved May 31 2004

Olea, R. A. (1999). Geostatistics for Engineers and Earth Scientists, Springer; 1st edition.

Pasala, S. M., Forster, C. B., Lim, S. J. and Deo, M. D. (2003). Simulating the Impacts of Faults on CO_2 Sequestration and Enhanced Oil Recovery in Sandstone Aquifers. SPE Annual Conference and Exhibition. Denver, Colorado, Society of Petroleum Engineers: SPE Paper 84186.

Perry, R. H. and Green, D. W. (1997). Perry's Chemical Engineers' Handbook, McGraw-Hill.

Plackett, R. L. and Burman, J. P. (1946). "The Design of Optimum Multifactorial Experiments." Biometrika **33**(4): 305-25.

Preuss, K. (2004). "Numerical simulation of CO_2 leakage froma geological disposal reservoir, including transitions from super- to subcritical conditions, and boiling of liquid CO_2." SPE Journal **9**(2): 237-248.

Preuss, K. and Garcia, J. (2002). "Multiphase flow dynamics during CO_2 disposal into saline aquifers." Environmental Geology **42**(2-3): 282-295.

Preuss, K., Garcia, J., Kovscek, T., Oldenburg, C., Rutqvist, J., Steefel, C. and Xu, T. (2002). Intercomparison of Numerical Simulation Codes for Geological Disposal. Berkeley, Lawrence Berkeley National Laboratory.

Preuss, K., Xu, T., Apps, J. and Garcia, J. (2003). "Numerical modeling of aquifer disposal of CO2." SPE Journal **49**(March).

Prieditis, J., Yang, A. P. and Wilkins, M. D. (1996). Simulation of a CO_2 Flood in the Slaughter Field with Geostatisical Reservoir Characterization. SPE Annual Conference and Exhibition. New Orleans, Louisiana, Society of Petroleum Engineers: SPE Paper 49168.

Rigg, A., Allinson, G., Bradshaw, J., Ennis-King, J., Gibson-Poole, C. M. and Hillis, R. R. (2001). "The Search for Sites for Geological Sequestration for CO_2 in Australia: A Progress Report on GEODISC." APPEA Journal: 711-725.

Span, R. and Wagner, W. (1996). " A new equation of state for carbon dioxide covering the fluid region from the triple-point temperature to 1100 K at pressures up to 800 MPa." J. Phys. Chem. Ref. Data **25**(6): 1509-1596.

Spiteri, E. J. (2005). Relative permeability hysteresis: a new model and impact on reservoir simulation. Petroleum Engineering, Stanford University, California.

Spiteri, E. J. and Juanes, R. (2006). "Impact of relative permeability hysteresis on the numerical simulation of WAG injection." Journal of Petroleum Science and Engineering **50**(2): 115-139.

Spiteri, E. J., Juanes, R., Blunt, M. J. and Orr Jr., F. M. (2005). Relative Permeability Hysteresis: Trapping models and application to geological CO_2 sequestration. SPE Annual Technical Conference and Exhibition. Dallas, Texas, USA, Society of Petroleum Engineers :SPE Paper 96448.

Standing, M. B. (1975). Notes on Relative Permeability Relationships. Stanford, California, Stanford University.

Suzanne, K., Hamon, G., Billiotte, J. and V., T. (2003). Experimental relationships between residual gas saturation and initial gas saturation in heterogeneous sandstone reservoirs. SPE Annual Technical Conference & Exhibition. Denver, Colorado, USA, Society of Petroleum Engineers: SPE Paper 84038.

van der Meer, L. G. H. (1995). "The CO_2 storage efficiency of aquifers." Energy Conversion and Management **36**(6-9): 513-518.

van der Meer, L. G. H. (1996). "Computer modelling of underground CO_2 storage." Energy Conversion and Management **37**(6-8): 1155-1160.

Vargaftik, N. B., Vinogradov, Y. K. and Yargin, V. S. (1996). Handbook of Physical Properties of Liquids and Gases. New York, Begell House.

Vesovic, V., Wakeham, W. A., Olchowy, G. A., Sengers, J. V., Watson, J. T. R. and Millol, J. (1990). "The Transport Properties of Carbon Dioxide." J. Phys. Chem. Ref. Data **19**(3): 763-808.

Wegener, D. C. and Harpole, K. J. (1996). Determination of relative permeability and trapped gas saturation for predictions of WAG performance in the South Cowden CO_2 flood. SPE/DOE Tenth Symposium on Improved Oil Recovery. Tulsa, Oklahoma, USA,, Society of Petroleum Engineers: SPE Paper 35429.

Weir, G. J., White, S. P. and Kissling, W. M. (1995). "Reservoir Storage and Containment of Greenhouse gases." Energy Conversion and Management **36**(6-9): 531-534.

Wright, I. W. (2007). The In Salah Gas CO_2 Storage Project. International Petroleum Technology Conference, Dubai, UAE.

Xu, T., Apps, J. A. and Pruess, K. (2004). "Numerical simulation of CO_2 disposal by mineral trapping in deep aquifers." Applied Geochemistry **19**(6): 917-936.

APPENDIX A – PEER REVIEWED PAPERS

1. Flett, M., Gurton, R. and Taggart, I. (2004). Heterogeneous saline formations: long term benefits for geo-sequestration of greenhouse gases. Seventh International Conference on Greenhouse Gas Control Technologies (GHGT-7), Vancouver, Canada., Elsevier.
   ISBN 0-080-44881-X

   Paper not included due to copyright restriction.

2. Flett, M., Gurton, R. and Weir, G. (2007). "Heterogeneous saline formations for carbon dioxide disposal: Impact of varying heterogeneity on containment and trapping." Journal of Petroleum Science and Engineering **57**(1-2): 106-118.
   doi:10.1016/j.petrol.2006.08.016

   Paper not included due to copyright restriction.

APPENDIX B – CONFERENCE PAPERS

1. Flett, M., Gurton, R. and Taggart, I. (2004). The function of gas-water relative permeability hysteresis in the sequestration of carbon dioxide in saline formations. SPE Asia-Pacific Oil and Gas Conference and Exhibition, Perth, Australia.

doi:10.2118/88485-MS

Paper not included due to copyright restriction.

2. Flett, M., Gurton, R. and Weir, G. (2006). Reservoir performance of disposed carbon dioxide in saline formations: impact of heterogeneity and dip. 8th International conference on Greenhouse Gas Control Technologies, Trondheim, Norway.

Paper not included due to copyright restriction.

APPENDIX C – DATA

C.1 Study A.

TABLE C-1: Simulation study results for migration of the CO_2 plume and pressure rise at 50, 100 and 1000 years for Study A

Simulation Run	Migration 50 years (km)	Migration 100 years (km)	Migration 1000 years (km)	Pressure Rise 50 years (MPa)	Pressure Rise 100 years (MPa)	Pressure Rise 1000 years (MPa)
Run 1	4.62	6.84	15.53	1.068	0.888	0.844
Run 2	5.88	9.50	19.47	1.210	0.896	0.927
Run 3	2.65	3.30	8.33	2.728	1.045	0.913
Run 4	3.08	4.34	4.51	0.901	0.742	0.674
Run 5	5.07	7.12	19.17	1.229	0.910	0.945
Run 6	5.47	7.89	17.10	1.107	0.851	0.809
Run 7	2.27	2.91	6.67	2.683	0.868	0.722
Run 8	2.76	2.86	3.84	1.621	0.956	0.821
Run 9	2.37	2.40	3.97	1.328	0.758	0.565
Run 10	3.09	4.90	15.93	0.979	0.784	0.604
Run 11	2.65	3.30	9.93	2.496	0.886	0.699
Run 12	3.40	3.59	7.23	1.715	0.986	0.801
Mid point	2.79	2.79	9.93	1.641	0.886	0.764

TABLE C-2: Simulation study results for fraction of CO_2 dissolved and fraction of gas trapped as a residual phase at 50, 100 and 1000 years for Study A

Simulation Run	Fraction CO_2 dissolved 50 years	Fraction CO_2 dissolved 100 years	Fraction CO_2 dissolved 1000 years	Fraction CO_2 trapped 50 years	Fraction CO_2 trapped 100 years	Fraction CO_2 trapped 1000 years
Run 1	0.1045	0.1380	0.1682	0.0161	0.2941	0.7114
Run 2	0.0770	0.1060	0.1934	0.0160	0.1009	0.2233
Run 3	0.0654	0.0722	0.0887	0.0072	0.1912	0.6123
Run 4	0.3902	0.4664	0.5233	0.0059	0.2261	0.4708
Run 5	0.0603	0.0789	0.1454	0.0127	0.0963	0.2106
Run 6	0.1912	0.2455	0.3351	0.0039	0.2587	0.3968
Run 7	0.3610	0.4027	0.4581	0.0056	0.2149	0.4398
Run 8	0.0948	0.1043	0.1267	0.0139	0.0381	0.6203
Run 9	0.3308	0.3587	0.5058	0.0061	0.0077	0.0879
Run 10	0.2957	0.4025	0.6660	0.0044	0.0407	0.2001
Run 11	0.2988	0.3439	0.5114	0.0028	0.0464	0.1147
Run 12	0.1069	0.1250	0.2127	0.0152	0.0309	0.1970
Mid point	0.1650	0.1986	0.2736	0.0071	0.1092	0.5287

TABLE C-3: Simulation study results for fraction of CO_2 mobile in the formation for Study A

Simulation Run	Fraction CO_2 mobile 50 years	Fraction CO_2 mobile 100 years	Fraction CO_2 mobile 1000 years
Run 1	0.8795	0.5679	0.1204
Run 2	0.9069	0.7932	0.5833
Run 3	0.9274	0.7366	0.2990
Run 4	0.6039	0.3075	0.0059
Run 5	0.9270	0.8248	0.6440
Run 6	0.8049	0.4958	0.2681
Run 7	0.6334	0.3824	0.1021
Run 8	0.8914	0.8576	0.2530
Run 9	0.6631	0.6336	0.4063
Run 10	0.6999	0.5568	0.1338
Run 11	0.6984	0.6097	0.3739
Run 12	0.8778	0.8441	0.5903
Mid point	0.8279	0.6923	0.1977

C.2 Study B

TABLE C-4: Results of statistical ranges of results from the Study B simulation study

Parameter	**P10**	**P50**	**P90**
Migration (km) 60 years	2.75	3.82	4.89
Migration (km) 1000 years	3.03	7.52	12.00
Pressure rise at seal 60 years (MPa)	0.90	1.31	1.72
Pressure rise at seal 1000 years (MPa)	0.76	0.88	1.00
Fraction CO_2 dissolved 60 years	0.052	0.123	0.204
Fraction CO_2 dissolved 1000 years	0.083	0.217	0.351
Fraction CO_2 trapped 60 years	0.000	0.031	0.080
Fraction CO_2 trapped 1000 years	0.118	0.461	0.804

TABLE C-5: Results from the Study B simulation study: migration in kilometres and Pressure above datum in MPa at 60, 100 and 1000 years

RUN	Migration 60 years (km)	Migration 100 years (km)	Migration 1000 years (km)	Pressure at seal 60 years (MPa)	Pressure at seal 100 years (MPa	Pressure at seal 1000 years (MPa)
1	4.86	5.60	12.91	1.107	1.014	1.007
2	3.29	3.41	4.86	1.660	1.017	0.936
3	3.21	3.29	4.86	1.488	0.899	0.738
4	3.41	3.79	8.00	1.123	0.889	0.802
5	4.46	4.86	8.87	1.025	0.900	0.871
6	3.44	3.68	6.00	1.677	1.008	0.926
7	3.29	3.41	6.00	1.575	0.931	0.820
8	3.41	3.68	6.00	1.714	1.022	0.921
9	4.86	6.00	11.10	1.137	1.016	1.008
10	3.79	4.07	6.40	1.197	0.945	0.900
11	4.46	5.60	12.32	1.038	0.910	0.845
12	3.29	3.29	4.07	1.552	0.900	0.781
13	3.04	3.29	4.46	1.490	0.932	0.840
14	4.30	4.86	11.10	0.994	0.875	0.782
15	3.79	4.07	7.60	1.212	0.991	0.952
16	4.67	5.25	11.70	1.022	0.921	0.872
17	3.79	4.07	9.30	1.223	0.988	0.921
18	3.04	3.22	4.46	1.480	0.890	0.740
19	3.04	3.22	4.86	1.530	0.993	0.920
20	4.30	4.86	8.48	1.073	0.992	0.969
21	3.41	3.79	6.80	1.114	0.929	0.847
22	4.17	4.46	9.30	1.000	0.901	0.792
23	2.82	3.04	4.07	1.373	0.875	0.788
24	4.67	5.05	12.35	1.081	0.993	0.941
25	3.41	3.79	4.55	1.125	0.903	0.833
26	4.67	4.86	11.72	1.092	0.998	0.956
27	3.04	3.22	4.07	1.606	1.011	0.938
28	2.91	3.04	4.86	1.525	0.947	0.829
29	2.91	3.04	4.86	1.452	0.898	0.754
30	4.30	4.46	8.00	1.014	0.902	0.861

TABLE C-6: Results from the Study B simulation study: Fraction of CO_2 injected that has dissolved and residually trapped at 60, 100 and 1000 years.

Run	Fraction CO_2 dissolved 60 years	Fraction CO_2 dissolved 100 years	Fraction CO_2 dissolved 1000 years	Fraction CO_2 trapped 60 years	Fraction CO_2 trapped 100 years	Fraction CO_2 trapped 1000 years
1	0.0768	0.0989	0.1363	0.0920	0.1910	0.5430
2	0.0685	0.0740	0.1121	0.0446	0.1089	0.6180
3	0.1718	0.1870	0.3350	0.0336	0.0580	0.2238
4	0.1700	0.2085	0.3189	0.0422	0.1078	0.5362
5	0.1912	0.2477	0.2799	0.0656	0.2751	0.6556
6	0.0769	0.0850	0.1417	0.0007	0.0347	0.2888
7	0.1344	0.1499	0.2749	0.0004	0.0140	0.0974
8	0.0701	0.0776	0.1371	0.0134	0.0386	0.1630
9	0.0796	0.0923	0.1005	0.0274	0.2233	0.6874
10	0.1278	0.1568	0.2002	0.0098	0.1230	0.6944
11	0.1997	0.2574	0.3381	0.0167	0.0624	0.2183
12	0.1711	0.1894	0.2815	0.0077	0.0678	0.5611
13	0.1403	0.1500	0.2112	0.0248	0.1135	0.5437
14	0.1945	0.2659	0.3933	0.0395	0.1017	0.3745
15	0.0736	0.0893	0.1249	0.0052	0.1488	0.7517
16	0.1471	0.1961	0.2547	0.0054	0.1162	0.4974
17	0.0712	0.0894	0.1517	0.0048	0.0301	0.2195
18	0.1798	0.1958	0.3217	0.0025	0.0477	0.3031
19	0.0794	0.0838	0.1294	0.0339	0.0600	0.2319
20	0.0745	0.0937	0.1142	0.0471	0.3232	0.8356
21	0.1371	0.1549	0.2437	0.0324	0.1135	0.5575
22	0.1894	0.2519	0.3944	0.0339	0.1001	0.3906
23	0.1998	0.2113	0.2731	0.0247	0.1137	0.5073
24	0.0743	0.1018	0.1682	0.0155	0.0581	0.2885
25	0.1803	0.2081	0.2905	0.0086	0.1641	0.6694
26	0.0704	0.0946	0.1453	0.0192	0.0723	0.3391
27	0.0709	0.0755	0.1044	0.0151	0.1193	0.5848
28	0.1298	0.1395	0.2319	0.0116	0.0333	0.1509
29	0.1795	0.1931	0.3201	0.0082	0.0311	0.1378
30	0.1781	0.2306	0.2719	0.0124	0.2557	0.6681

Note: Fraction of mobile CO_2 at any point of time is defined as the sum of fraction of dissolved CO_2 and fraction of residually trapped CO_2 subtracted from unity. As the fraction of mobile CO_2 is derived from the fractions of both residual CO_2 and dissolved CO_2 it is not a direct product of reservoir simulation but is inferred from simulation results.

C.3 Major Study

Results from the Major Study reservoir simulation study: Fraction of CO_2 injected that has dissolved, residually trapped and mobile at various years:

Table C-7: Results for CO_2 states for the Homogeneous model with 0, 1, 2, 5 and 10 degree dips. 1-100 years

Fraction	Year	1	5	10	15	20	30	40	50	60	80	100
Dissolved	Homogeneous0	0.9011	0.6494	0.5021	0.4173	0.3605	0.2887	0.2519	0.2297	0.2424	0.2588	0.2680
Trapped	Homogeneous0	0.0028	0.0034	0.0053	0.0076	0.0104	0.0133	0.0133	0.0214	0.0600	0.1461	0.2054
Mobile	Homogeneous0	0.0961	0.3472	0.4926	0.5752	0.6291	0.6980	0.7348	0.7490	0.6976	0.5950	0.5267
Dissolved	Homogeneous1	0.7120	0.3857	0.2896	0.2455	0.2165	0.1787	0.1614	0.1563	0.1695	0.1900	0.2016
Trapped	Homogeneous1	0.0086	0.0066	0.0077	0.0104	0.0122	0.0148	0.0147	0.0155	0.0494	0.1309	0.2011
Mobile	Homogeneous1	0.2794	0.6077	0.7027	0.7442	0.7713	0.8065	0.8239	0.8282	0.7811	0.6791	0.5973
Dissolved	Homogeneous2	0.6979	0.3726	0.2799	0.2385	0.2118	0.1766	0.1577	0.1518	0.1656	0.1892	0.2050
Trapped	Homogeneous2	0.0091	0.0075	0.0075	0.0097	0.0116	0.0138	0.0141	0.0140	0.0461	0.1404	0.2268
Mobile	Homogeneous2	0.2930	0.6199	0.7126	0.7518	0.7766	0.8096	0.8282	0.8343	0.7883	0.6704	0.5682
Dissolved	Homogeneous5	0.6788	0.3518	0.2619	0.2264	0.2048	0.1780	0.1597	0.1483	0.1650	0.1923	0.2126
Trapped	Homogeneous5	0.0096	0.0076	0.0067	0.0077	0.0092	0.0127	0.0147	0.0167	0.0444	0.1399	0.2634
Mobile	Homogeneous5	0.3116	0.6406	0.7313	0.7659	0.7860	0.8093	0.8255	0.8351	0.7906	0.6678	0.5240
Dissolved	Homogeneous10	0.6878	0.3565	0.2631	0.2269	0.2069	0.1850	0.1708	0.1600	0.1788	0.2049	0.2234
Trapped	Homogeneous10	0.0090	0.0054	0.0076	0.0068	0.0078	0.0107	0.0134	0.0142	0.0324	0.1173	0.2345
Mobile	Homogeneous10	0.3033	0.6381	0.7293	0.7663	0.7853	0.8043	0.8158	0.8259	0.7888	0.6778	0.5421

Table C-8: Results for CO_2 states for the Homogeneous model with 0, 1, 2, 5 and 10 degree dips. 200-8000 years

Fraction	Year	200	300	400	500	600	700	800	900	1000	2000	3000	4000	5000	6000	7000	8000
Dissolved	Homogeneous0	0.2838	0.2895	0.2925	0.2943	0.2958	0.2968	0.2979	0.2988	0.2993	0.3041	0.3090	0.3139	0.3186	0.3231	0.3273	0.3313
Trapped	Homogeneous0	0.2755	0.3029	0.3226	0.3295	0.3310	0.3351	0.3403	0.3455	0.3461	0.3415	0.3372	0.3332	0.3296	0.3264	0.3235	0.3208
Mobile	Homogeneous0	0.4407	0.4076	0.3849	0.3761	0.3733	0.3681	0.3618	0.3556	0.3546	0.3545	0.3539	0.3530	0.3518	0.3505	0.3492	0.3479
Dissolved	Homogeneous1	0.2320	0.2521	0.2662	0.2834	0.2944	0.2993	0.3020	0.3038	0.3052	0.3139	0.3205	0.3271	0.3336	0.3398	0.3459	0.3517
Trapped	Homogeneous1	0.3246	0.3753	0.4089	0.4426	0.4720	0.4737	0.4768	0.4757	0.4733	0.4721	0.4671	0.4633	0.4590	0.4548	0.4502	0.4455
Mobile	Homogeneous1	0.4434	0.3725	0.3249	0.2741	0.2337	0.2270	0.2211	0.2206	0.2215	0.2140	0.2124	0.2096	0.2074	0.2054	0.2039	0.2028
Dissolved	Homogeneous2	0.2482	0.2814	0.2935	0.2964	0.2983	0.2994	0.3005	0.3015	0.3024	0.3097	0.3169	0.3245	0.3321	0.3395	0.3466	0.3535
Trapped	Homogeneous2	0.3939	0.4777	0.5245	0.5228	0.5201	0.5197	0.5201	0.5221	0.5245	0.5327	0.5327	0.5327	0.5327	0.5327	0.5327	0.5327
Mobile	Homogeneous2	0.3579	0.2410	0.1820	0.1808	0.1816	0.1809	0.1794	0.1764	0.1732	0.1576	0.1520	0.1502	0.1507	0.1512	0.1499	0.1493
Dissolved	Homogeneous5	0.2849	0.2833	0.2852	0.2864	0.2876	0.2887	0.2897	0.2907	0.2917	0.3010	0.3104	0.3198	0.3291	0.3379	0.3460	0.3534
Trapped	Homogeneous5	0.5506	0.5976	0.5954	0.5993	0.6043	0.6035	0.6060	0.6073	0.6088	0.6180	0.6153	0.6063	0.5949	0.5860	0.5764	0.5678
Mobile	Homogeneous5	0.1644	0.1192	0.1195	0.1143	0.1080	0.1077	0.1042	0.1019	0.0995	0.0810	0.0743	0.0739	0.0760	0.0761	0.0776	0.0787
Dissolved	Homogeneous10	0.2646	0.2685	0.2707	0.2724	0.2740	0.2755	0.2770	0.2785	0.2799	0.2932	0.3058	0.3175	0.3283	0.3380	0.3466	0.3545
Trapped	Homogeneous10	0.6061	0.6206	0.6252	0.6288	0.6320	0.6342	0.6374	0.6392	0.6406	0.6520	0.6426	0.6325	0.6223	0.6132	0.6053	0.5981
Mobile	Homogeneous10	0.1293	0.1109	0.1040	0.0989	0.0940	0.0902	0.0856	0.0824	0.0795	0.0548	0.0517	0.0499	0.0494	0.0488	0.0481	0.0474

Table C-9: Results for CO_2 states for the 40:60 net-to-gross model with 100m shale length. 0, 1, 2, 5 and 10 degree dips. 1-100 years

Fraction	Year	1	5	10	15	20	30	40	50	60	80	100
Dissolved	4060_100_0	0.8806	0.6166	0.4827	0.4220	0.3953	0.3766	0.3693	0.3687	0.3820	0.3908	0.3953
Trapped	4060_100_0	0.0032	0.0054	0.0052	0.0053	0.0056	0.0057	0.0079	0.0115	0.0130	0.0157	0.0178
Mobile	4060_100_0	0.1163	0.3781	0.5121	0.5727	0.5991	0.6177	0.6227	0.6198	0.6050	0.5935	0.5869
Dissolved	4060_100_1	0.6385	0.3378	0.2688	0.2460	0.2413	0.2472	0.2513	0.2526	0.2668	0.2773	0.2831
Trapped	4060_100_1	0.0077	0.0086	0.0067	0.0070	0.0080	0.0086	0.0131	0.0194	0.0213	0.0248	0.0274
Mobile	4060_100_1	0.3538	0.6536	0.7245	0.7470	0.7507	0.7442	0.7357	0.7280	0.7119	0.6979	0.6896
Dissolved	4060_100_2	0.6338	0.3380	0.2685	0.2461	0.2428	0.2474	0.2646	0.2781	0.2890	0.2990	0.3050
Trapped	4060_100_2	0.0094	0.0096	0.0073	0.0070	0.0072	0.0056	0.0071	0.0103	0.0121	0.0155	0.0178
Mobile	4060_100_2	0.3568	0.6523	0.7241	0.7468	0.7500	0.7469	0.7283	0.7117	0.6990	0.6855	0.6772
Dissolved	4060_100_5	0.6656	0.3435	0.2643	0.2380	0.2275	0.2244	0.2280	0.2334	0.2438	0.2546	0.2619
Trapped	4060_100_5	0.0086	0.0073	0.0074	0.0076	0.0072	0.0063	0.0077	0.0089	0.0110	0.0155	0.0197
Mobile	4060_100_5	0.3258	0.6492	0.7283	0.7544	0.7654	0.7693	0.7642	0.7576	0.7453	0.7298	0.7184
Dissolved	4060_100_10	0.6808	0.3453	0.2566	0.2249	0.2095	0.1969	0.1937	0.1944	0.2061	0.2186	0.2275
Trapped	4060_100_10	0.0074	0.0097	0.0082	0.0071	0.0072	0.0076	0.0087	0.0076	0.0093	0.0146	0.0198
Mobile	4060_100_10	0.3118	0.6450	0.7353	0.7680	0.7833	0.7955	0.7976	0.7980	0.7847	0.7669	0.7527

For this section and the following sections, the model description, the first term stand for the ratio of net sand to shale, the second term stands for the shale length variogram and the third term stands for the degree of dip. E.g. “4060_100_5” is the model with 40:60 net sand to shale, with 100m shale variogram and 5 degree dip.

Table C-10: Results for CO_2 states for the 40:60 net-to-gross model with 100m shale length, 0, 1, 2, 5 and 10 degree dips.200-8000 years

Fraction	Year	200	300	400	500	600	700	800	900	1000	2000	3000	4000	5000	6000	7000	8000
Dissolved	4060_100_0	0.4041	0.4075	0.4099	0.4120	0.4141	0.4162	0.4181	0.4200	0.4217	0.4376	0.4494	0.4561	0.4591	0.4607	0.4619	0.4630
Trapped	4060_100_0	0.0237	0.0280	0.0301	0.0314	0.0330	0.0343	0.0358	0.0380	0.0400	0.0650	0.0900	0.1167	0.1445	0.1736	0.2003	0.2251
Mobile	4060_100_0	0.5722	0.5645	0.5600	0.5565	0.5529	0.5495	0.5460	0.5420	0.5383	0.4974	0.4606	0.4273	0.3964	0.3657	0.3378	0.3119
Dissolved	4060_100_1	0.2958	0.3021	0.3072	0.3117	0.3158	0.3198	0.3236	0.3272	0.3307	0.3589	0.3738	0.3799	0.3829	0.3849	0.3862	0.3872
Trapped	4060_100_1	0.0329	0.0412	0.0488	0.0557	0.0622	0.0686	0.0743	0.0800	0.0857	0.1460	0.2087	0.2659	0.3137	0.3543	0.3899	0.4203
Mobile	4060_100_1	0.6712	0.6567	0.6440	0.6326	0.6220	0.6115	0.6021	0.5928	0.5836	0.4951	0.4175	0.3542	0.3034	0.2608	0.2239	0.1925
Dissolved	4060_100_2	0.3196	0.3282	0.3352	0.3413	0.3470	0.3522	0.3570	0.3617	0.3661	0.3946	0.4042	0.4084	0.4108	0.4124	0.4136	0.4145
Trapped	4060_100_2	0.0285	0.0404	0.0527	0.0637	0.0734	0.0823	0.0905	0.0984	0.1058	0.1887	0.2650	0.3248	0.3730	0.4125	0.4417	0.4643
Mobile	4060_100_2	0.6520	0.6315	0.6121	0.5950	0.5796	0.5655	0.5525	0.5399	0.5281	0.4168	0.3308	0.2668	0.2162	0.1751	0.1447	0.1212
Dissolved	4060_100_5	0.2827	0.2964	0.3071	0.3163	0.3244	0.3314	0.3374	0.3425	0.3466	0.3666	0.3740	0.3778	0.3801	0.3818	0.3831	0.3842
Trapped	4060_100_5	0.0446	0.0707	0.0933	0.1113	0.1262	0.1392	0.1509	0.1631	0.1752	0.2874	0.3661	0.4274	0.4688	0.4979	0.5183	0.5332
Mobile	4060_100_5	0.6727	0.6329	0.5996	0.5724	0.5494	0.5294	0.5117	0.4944	0.4782	0.3460	0.2599	0.1949	0.1511	0.1203	0.0986	0.0826
Dissolved	4060_100_10	0.2550	0.2725	0.2853	0.2954	0.3032	0.3090	0.3134	0.3168	0.3197	0.3366	0.3446	0.3493	0.3525	0.3549	0.3569	0.3585
Trapped	4060_100_10	0.0547	0.0956	0.1302	0.1558	0.1727	0.1882	0.2025	0.2169	0.2309	0.3375	0.4099	0.4607	0.4991	0.5265	0.5453	0.5586
Mobile	4060_100_10	0.6903	0.6319	0.5845	0.5488	0.5241	0.5027	0.4841	0.4663	0.4494	0.3258	0.2455	0.1900	0.1484	0.1186	0.0978	0.0829

Table C-11: Results for CO_2 states for the 40:60 net-to-gross model with 300m shale length. 0, 1, 2, 5 and 10 degree dips. 1-100 years

Fraction	Year	1	5	10	15	20	30	40	50	60	80	100
Dissolved	4060_300_0	0.8756	0.5988	0.4667	0.4120	0.3870	0.3689	0.3663	0.3669	0.3793	0.3883	0.3930
Trapped	4060_300_0	0.0026	0.0048	0.0048	0.0045	0.0038	0.0046	0.0072	0.0099	0.0107	0.0138	0.0154
Mobile	4060_300_0	0.1218	0.3964	0.5285	0.5835	0.6092	0.6265	0.6265	0.6231	0.6100	0.5979	0.5916
Dissolved	4060_300_1	0.6657	0.3464	0.2754	0.2649	0.2689	0.2853	0.2978	0.3077	0.3187	0.3285	0.3340
Trapped	4060_300_1	0.0075	0.0070	0.0064	0.0051	0.0047	0.0066	0.0104	0.0142	0.0152	0.0187	0.0205
Mobile	4060_300_1	0.3268	0.6465	0.7182	0.7300	0.7263	0.7081	0.6918	0.6781	0.6661	0.6528	0.6455
Dissolved	4060_300_2	0.6556	0.3395	0.2668	0.2566	0.2601	0.2752	0.2877	0.2925	0.3030	0.3131	0.3194
Trapped	4060_300_2	0.0076	0.0091	0.0065	0.0054	0.0051	0.0069	0.0110	0.0141	0.0153	0.0190	0.0211
Mobile	4060_300_2	0.3368	0.6514	0.7267	0.7380	0.7348	0.7179	0.7013	0.6934	0.6817	0.6679	0.6595
Dissolved	4060_300_5	0.6602	0.3381	0.2555	0.2393	0.2402	0.2454	0.2477	0.2472	0.2577	0.2696	0.2776
Trapped	4060_300_5	0.0086	0.0085	0.0069	0.0056	0.0056	0.0068	0.0094	0.0108	0.0123	0.0163	0.0192
Mobile	4060_300_5	0.3313	0.6534	0.7376	0.7550	0.7542	0.7479	0.7430	0.7420	0.7301	0.7141	0.7032
Dissolved	4060_300_10	0.6804	0.3353	0.2457	0.2196	0.2106	0.2082	0.2086	0.2083	0.2201	0.2353	0.2464
Trapped	4060_300_10	0.0072	0.0088	0.0071	0.0071	0.0059	0.0064	0.0079	0.0078	0.0091	0.0140	0.0186
Mobile	4060_300_10	0.3124	0.6559	0.7472	0.7733	0.7835	0.7853	0.7835	0.7839	0.7708	0.7507	0.7349

Table C-12: Results for CO_2 states for the 40:60 net-to-gross model with 300m shale length, 0, 1, 2, 5 and 10 degree dips.200-8000 years

Fraction	Year	200	300	400	500	600	700	800	900	1000	2000	3000	4000	5000	6000	7000	8000
Dissolved	4060_300_0	0.4012	0.4038	0.4058	0.4075	0.4091	0.4107	0.4123	0.4139	0.4154	0.4299	0.4420	0.4515	0.4581	0.4615	0.4629	0.4638
Trapped	4060_300_0	0.0194	0.0216	0.0225	0.0234	0.0244	0.0254	0.0267	0.0282	0.0300	0.0556	0.0817	0.1073	0.1345	0.1647	0.1956	0.2250
Mobile	4060_300_0	0.5794	0.5746	0.5717	0.5691	0.5665	0.5638	0.5611	0.5580	0.5546	0.5145	0.4763	0.4412	0.4074	0.3738	0.3415	0.3112
Dissolved	4060_300_1	0.3467	0.3542	0.3606	0.3663	0.3711	0.3755	0.3795	0.3833	0.3870	0.4149	0.4269	0.4319	0.4346	0.4361	0.4373	0.4381
Trapped	4060_300_1	0.0264	0.0330	0.0399	0.0469	0.0541	0.0610	0.0679	0.0743	0.0803	0.1381	0.2029	0.2650	0.3196	0.3662	0.4028	0.4312
Mobile	4060_300_1	0.6268	0.6128	0.5995	0.5868	0.5748	0.5635	0.5525	0.5423	0.5326	0.4469	0.3702	0.3031	0.2459	0.1977	0.1599	0.1307
Dissolved	4060_300_2	0.3361	0.3467	0.3552	0.3627	0.3702	0.3775	0.3843	0.3907	0.3962	0.4218	0.4294	0.4328	0.4348	0.4361	0.4371	0.4378
Trapped	4060_300_2	0.0293	0.0416	0.0554	0.0692	0.0817	0.0921	0.1014	0.1107	0.1193	0.2082	0.2949	0.3645	0.4151	0.4512	0.4765	0.4945
Mobile	4060_300_2	0.6345	0.6117	0.5894	0.5681	0.5481	0.5305	0.5143	0.4986	0.4845	0.3700	0.2758	0.2026	0.1501	0.1126	0.0865	0.0677
Dissolved	4060_300_5	0.3026	0.3209	0.3380	0.3520	0.3623	0.3698	0.3751	0.3791	0.3822	0.3970	0.4021	0.4047	0.4064	0.4077	0.4087	0.4096
Trapped	4060_300_5	0.0437	0.0759	0.1070	0.1343	0.1541	0.1699	0.1843	0.1987	0.2146	0.3421	0.4303	0.4877	0.5209	0.5407	0.5520	0.5586
Mobile	4060_300_5	0.6537	0.6032	0.5551	0.5138	0.4835	0.4603	0.4407	0.4222	0.4032	0.2609	0.1676	0.1076	0.0727	0.0516	0.0393	0.0318
Dissolved	4060_300_10	0.2823	0.3100	0.3271	0.3377	0.3442	0.3485	0.3519	0.3547	0.3570	0.3691	0.3743	0.3773	0.3796	0.3813	0.3829	0.3842
Trapped	4060_300_10	0.0617	0.1165	0.1644	0.1966	0.2192	0.2405	0.2595	0.2773	0.2940	0.4250	0.4966	0.5378	0.5630	0.5772	0.5839	0.5876
Mobile	4060_300_10	0.6560	0.5734	0.5085	0.4658	0.4366	0.4110	0.3885	0.3681	0.3490	0.2059	0.1291	0.0849	0.0575	0.0415	0.0333	0.0283

Table C-13: Results for CO_2 states for the 40:60 net-to-gross model with 1000m shale length. 0, 1, 2, 5 and 10 degree dips. 1-100 years

Fraction	Year	1	5	10	15	20	30	40	50	60	80	100
Dissolved	4060_1000_0	0.8696	0.5857	0.4427	0.3797	0.3495	0.3266	0.3251	0.3297	0.3421	0.3523	0.3576
Trapped	4060_1000_0	0.0029	0.0055	0.0053	0.0050	0.0040	0.0035	0.0036	0.0041	0.0050	0.0093	0.0114
Mobile	4060_1000_0	0.1275	0.4088	0.5520	0.6153	0.6465	0.6699	0.6713	0.6662	0.6529	0.6385	0.6310
Dissolved	4060_1000_1	0.6721	0.3525	0.2639	0.2365	0.2311	0.2427	0.2625	0.2812	0.2915	0.3011	0.3067
Trapped	4060_1000_1	0.0057	0.0093	0.0069	0.0057	0.0049	0.0046	0.0055	0.0074	0.0086	0.0128	0.0154
Mobile	4060_1000_1	0.3222	0.6382	0.7292	0.7578	0.7640	0.7528	0.7321	0.7113	0.6999	0.6861	0.6779
Dissolved	4060_1000_2	0.6654	0.3440	0.2554	0.2274	0.2198	0.2275	0.2466	0.2652	0.2750	0.2853	0.2916
Trapped	4060_1000_2	0.0055	0.0097	0.0073	0.0065	0.0052	0.0046	0.0053	0.0074	0.0092	0.0142	0.0167
Mobile	4060_1000_2	0.3291	0.6462	0.7373	0.7661	0.7750	0.7679	0.7481	0.7274	0.7158	0.7005	0.6916
Dissolved	4060_1000_5	0.6646	0.3416	0.2515	0.2206	0.2097	0.2101	0.2205	0.2321	0.2435	0.2563	0.2648
Trapped	4060_1000_5	0.0089	0.0091	0.0078	0.0066	0.0056	0.0046	0.0049	0.0067	0.0093	0.0156	0.0208
Mobile	4060_1000_5	0.3265	0.6493	0.7408	0.7728	0.7847	0.7854	0.7746	0.7613	0.7472	0.7280	0.7144
Dissolved	4060_1000_10	0.6498	0.3279	0.2398	0.2071	0.1937	0.1872	0.1879	0.1930	0.2058	0.2213	0.2329
Trapped	4060_1000_10	0.0084	0.0097	0.0083	0.0070	0.0063	0.0052	0.0046	0.0050	0.0072	0.0151	0.0216
Mobile	4060_1000_10	0.3418	0.6624	0.7519	0.7859	0.8000	0.8077	0.8075	0.8020	0.7871	0.7636	0.7455

Table C-14: Results for CO_2 states for the 40:60 net-to-gross model with 1000m shale length, 0, 1, 2, 5 and 10 degree dips. 200-8000 years

Fraction	Year	200	300	400	500	600	700	800	900	1000	2000	3000	4000	5000	6000	7000	8000
Dissolved	4060_1000_0	0.3679	0.3713	0.3733	0.3751	0.3769	0.3787	0.3804	0.3822	0.3838	0.3990	0.4116	0.4212	0.4275	0.4312	0.4333	0.4345
Trapped	4060_1000_0	0.0161	0.0194	0.0206	0.0215	0.0226	0.0239	0.0255	0.0270	0.0290	0.0550	0.0822	0.1118	0.1402	0.1682	0.1980	0.2272
Mobile	4060_1000_0	0.6160	0.6093	0.6061	0.6034	0.6005	0.5974	0.5941	0.5908	0.5872	0.5460	0.5062	0.4670	0.4323	0.4006	0.3686	0.3384
Dissolved	4060_1000_1	0.3200	0.3278	0.3347	0.3410	0.3470	0.3531	0.3586	0.3641	0.3697	0.4188	0.4292	0.4332	0.4355	0.4369	0.4379	0.4386
Trapped	4060_1000_1	0.0231	0.0318	0.0411	0.0503	0.0590	0.0684	0.0775	0.0869	0.0953	0.1568	0.2362	0.3175	0.3822	0.4290	0.4623	0.4855
Mobile	4060_1000_1	0.6568	0.6404	0.6242	0.6087	0.5940	0.5785	0.5638	0.5490	0.5351	0.4244	0.3346	0.2493	0.1823	0.1341	0.0998	0.0759
Dissolved	4060_1000_2	0.3096	0.3218	0.3338	0.3453	0.3570	0.3687	0.3806	0.3911	0.3993	0.4243	0.4300	0.4326	0.4340	0.4350	0.4358	0.4363
Trapped	4060_1000_2	0.0290	0.0442	0.0604	0.0775	0.0945	0.1094	0.1210	0.1309	0.1421	0.2516	0.3655	0.4394	0.4839	0.5084	0.5233	0.5328
Mobile	4060_1000_2	0.6614	0.6339	0.6058	0.5772	0.5485	0.5219	0.4984	0.4780	0.4586	0.3242	0.2045	0.1281	0.0821	0.0566	0.0410	0.0308
Dissolved	4060_1000_5	0.2949	0.3231	0.3499	0.3699	0.3813	0.3881	0.3928	0.3961	0.3987	0.4096	0.4129	0.4147	0.4159	0.4168	0.4175	0.4182
Trapped	4060_1000_5	0.0499	0.0837	0.1161	0.1427	0.1660	0.1864	0.2066	0.2272	0.2476	0.4179	0.5014	0.5390	0.5556	0.5633	0.5668	0.5688
Mobile	4060_1000_5	0.6552	0.5932	0.5340	0.4874	0.4527	0.4255	0.4006	0.3767	0.3536	0.1725	0.0856	0.0463	0.0285	0.0199	0.0157	0.0130
Dissolved	4060_1000_10	0.2834	0.3273	0.3498	0.3606	0.3669	0.3711	0.3743	0.3767	0.3787	0.3878	0.3911	0.3931	0.3946	0.3958	0.3969	0.3978
Trapped	4060_1000_10	0.0657	0.1177	0.1586	0.1931	0.2235	0.2536	0.2810	0.3061	0.3305	0.4930	0.5503	0.5731	0.5837	0.5881	0.5901	0.5910
Mobile	4060_1000_10	0.6509	0.5551	0.4916	0.4463	0.4096	0.3753	0.3447	0.3172	0.2909	0.1192	0.0586	0.0338	0.0217	0.0161	0.0130	0.0112

Table C-15: Results for CO_2 states for the 40:60 net-to-gross model with 3000m shale length. 0, 1, 2, 5 and 10 degree dips. 1-100 years

Fraction	Year	1	5	10	15	20	30	40	50	60	80	100
Dissolved	4060_3000_0	0.8899	0.6301	0.4941	0.4355	0.4112	0.4008	0.3990	0.3986	0.4078	0.4150	0.4190
Trapped	4060_3000_0	0.0027	0.0036	0.0047	0.0044	0.0039	0.0041	0.0060	0.0089	0.0096	0.0116	0.0129
Mobile	4060_3000_0	0.1074	0.3663	0.5012	0.5601	0.5849	0.5951	0.5950	0.5925	0.5826	0.5734	0.5681
Dissolved	4060_3000_1	0.6396	0.3345	0.2655	0.2548	0.2645	0.2981	0.3162	0.3329	0.3411	0.3489	0.3539
Trapped	4060_3000_1	0.0085	0.0091	0.0062	0.0060	0.0048	0.0052	0.0084	0.0132	0.0140	0.0168	0.0182
Mobile	4060_3000_1	0.3519	0.6564	0.7283	0.7392	0.7308	0.6967	0.6754	0.6539	0.6450	0.6343	0.6279
Dissolved	4060_3000_2	0.6346	0.3269	0.2565	0.2426	0.2487	0.2796	0.2972	0.3133	0.3215	0.3309	0.3375
Trapped	4060_3000_2	0.0091	0.0092	0.0079	0.0063	0.0053	0.0045	0.0070	0.0111	0.0119	0.0152	0.0171
Mobile	4060_3000_2	0.3563	0.6639	0.7356	0.7511	0.7461	0.7158	0.6959	0.6757	0.6666	0.6538	0.6454
Dissolved	4060_3000_5	0.6346	0.3247	0.2493	0.2307	0.2282	0.2427	0.2607	0.2785	0.2894	0.3023	0.3127
Trapped	4060_3000_5	0.0094	0.0100	0.0071	0.0059	0.0058	0.0047	0.0060	0.0090	0.0103	0.0159	0.0202
Mobile	4060_3000_5	0.3559	0.6654	0.7436	0.7633	0.7660	0.7526	0.7332	0.7124	0.7003	0.6818	0.6671
Dissolved	4060_3000_10	0.6185	0.3109	0.2351	0.2114	0.2060	0.2094	0.2193	0.2361	0.2500	0.2697	0.2857
Trapped	4060_3000_10	0.0079	0.0086	0.0088	0.0076	0.0066	0.0049	0.0053	0.0068	0.0087	0.0152	0.0200
Mobile	4060_3000_10	0.3736	0.6804	0.7561	0.7811	0.7874	0.7857	0.7754	0.7572	0.7413	0.7152	0.6943

Table C-16: Results for CO_2 states for the 40:60 net-to-gross model with 3000m shale length, 0, 1, 2, 5 and 10 degree dips. 200-8000 years

Fraction	Year	200	300	400	500	600	700	800	900	1000	2000	3000	4000	5000	6000	7000	8000
Dissolved	4060_3000_0	0.4273	0.4301	0.4317	0.4331	0.4344	0.4358	0.4372	0.4385	0.4399	0.4549	0.4719	0.4860	0.4937	0.4980	0.5003	0.5016
Trapped	4060_3000_0	0.0161	0.0174	0.0177	0.0180	0.0183	0.0187	0.0192	0.0198	0.0204	0.0357	0.0575	0.0778	0.1016	0.1310	0.1659	0.1976
Mobile	4060_3000_0	0.5566	0.5525	0.5506	0.5490	0.5473	0.5454	0.5436	0.5418	0.5397	0.5094	0.4706	0.4362	0.4046	0.3710	0.3338	0.3008
Dissolved	4060_3000_1	0.3686	0.3798	0.3898	0.3984	0.4063	0.4140	0.4209	0.4276	0.4345	0.4738	0.4817	0.4850	0.4869	0.4880	0.4888	0.4894
Trapped	4060_3000_1	0.0239	0.0298	0.0368	0.0446	0.0530	0.0608	0.0684	0.0758	0.0826	0.1536	0.2348	0.3101	0.3653	0.4025	0.4296	0.4498
Mobile	4060_3000_1	0.6074	0.5904	0.5734	0.5570	0.5407	0.5253	0.5107	0.4965	0.4829	0.3726	0.2835	0.2049	0.1479	0.1095	0.0816	0.0608
Dissolved	4060_3000_2	0.3604	0.3776	0.3928	0.4071	0.4208	0.4331	0.4437	0.4512	0.4568	0.4749	0.4796	0.4818	0.4830	0.4839	0.4845	0.4850
Trapped	4060_3000_2	0.0258	0.0374	0.0519	0.0674	0.0825	0.0960	0.1075	0.1190	0.1308	0.2480	0.3468	0.4086	0.4471	0.4714	0.4864	0.4956
Mobile	4060_3000_2	0.6138	0.5850	0.5553	0.5254	0.4967	0.4709	0.4487	0.4298	0.4125	0.2771	0.1736	0.1097	0.0699	0.0448	0.0291	0.0195
Dissolved	4060_3000_5	0.3537	0.3887	0.4141	0.4288	0.4373	0.4428	0.4466	0.4493	0.4514	0.4607	0.4637	0.4652	0.4662	0.4670	0.4676	0.4682
Trapped	4060_3000_5	0.0437	0.0722	0.1045	0.1322	0.1585	0.1822	0.2035	0.2226	0.2407	0.3901	0.4649	0.5000	0.5159	0.5226	0.5254	0.5266
Mobile	4060_3000_5	0.6027	0.5392	0.4814	0.4389	0.4042	0.3750	0.3499	0.3281	0.3079	0.1492	0.0714	0.0348	0.0179	0.0104	0.0070	0.0053
Dissolved	4060_3000_10	0.3546	0.3944	0.4115	0.4199	0.4250	0.4286	0.4313	0.4334	0.4350	0.4428	0.4457	0.4475	0.4488	0.4499	0.4508	0.4516
Trapped	4060_3000_10	0.0542	0.0994	0.1402	0.1792	0.2141	0.2412	0.2649	0.2871	0.3096	0.4563	0.5101	0.5312	0.5401	0.5432	0.5443	0.5445
Mobile	4060_3000_10	0.5912	0.5062	0.4483	0.4008	0.3608	0.3301	0.3038	0.2795	0.2553	0.1009	0.0442	0.0213	0.0111	0.0069	0.0049	0.0038

Table C-17: Results for CO_2 states for the 50:50 net-to-gross model with 100m shale length. 0, 1, 2, 5 and 10 degree dips. 1-100 years

Fraction	Year	1	5	10	15	20	30	40	50	60	80	100
Dissolved	5050_100_0	0.8861	0.6224	0.4787	0.4061	0.3663	0.3287	0.3145	0.3107	0.3221	0.3302	0.3341
Trapped	5050_100_0	0.0024	0.0053	0.0050	0.0053	0.0049	0.0061	0.0064	0.0046	0.0062	0.0107	0.0143
Mobile	5050_100_0	0.1115	0.3723	0.5163	0.5886	0.6288	0.6652	0.6790	0.6847	0.6717	0.6592	0.6516
Dissolved	5050_100_1	0.6627	0.3481	0.2643	0.2331	0.2207	0.2176	0.2251	0.2365	0.2476	0.2567	0.2616
Trapped	5050_100_1	0.0081	0.0098	0.0073	0.0068	0.0063	0.0078	0.0067	0.0069	0.0073	0.0123	0.0166
Mobile	5050_100_1	0.3293	0.6422	0.7284	0.7602	0.7729	0.7747	0.7682	0.7567	0.7451	0.7310	0.7217
Dissolved	5050_100_2	0.6546	0.3395	0.2577	0.2261	0.2123	0.2066	0.2126	0.2232	0.2343	0.2442	0.2501
Trapped	5050_100_2	0.0089	0.0095	0.0073	0.0065	0.0062	0.0079	0.0078	0.0066	0.0081	0.0136	0.0185
Mobile	5050_100_2	0.3366	0.6510	0.7350	0.7674	0.7815	0.7856	0.7796	0.7701	0.7576	0.7423	0.7314
Dissolved	5050_100_5	0.6533	0.3369	0.2522	0.2205	0.2045	0.1921	0.1943	0.2009	0.2121	0.2236	0.2312
Trapped	5050_100_5	0.0029	0.0095	0.0079	0.0066	0.0064	0.0081	0.0057	0.0074	0.0091	0.0167	0.0247
Mobile	5050_100_5	0.3438	0.6536	0.7399	0.7729	0.7892	0.7998	0.8000	0.7917	0.7788	0.7597	0.7441
Dissolved	5050_100_10	0.6434	0.3226	0.2377	0.2061	0.1903	0.1736	0.1717	0.1766	0.1891	0.2026	0.2127
Trapped	5050_100_10	0.0095	0.0091	0.0077	0.0069	0.0060	0.0070	0.0060	0.0052	0.0067	0.0145	0.0222
Mobile	5050_100_10	0.3472	0.6684	0.7545	0.7870	0.8037	0.8193	0.8224	0.8182	0.8042	0.7829	0.7651

Table C-18: Results for CO_2 states for the 50:50 net-to-gross model with 100m shale length, 0, 1, 2, 5 and 10 degree dips. 200-8000 years

Fraction	Year	200	300	400	500	600	700	800	900	1000	2000	3000	4000	5000	6000	7000	8000
Dissolved	5050_100_0	0.3417	0.3465	0.3507	0.3547	0.3584	0.3619	0.3652	0.3683	0.3713	0.3926	0.4038	0.4078	0.4099	0.4112	0.4122	0.4129
Trapped	5050_100_0	0.0270	0.0320	0.0356	0.0392	0.0428	0.0465	0.0503	0.0546	0.0583	0.0965	0.1308	0.1648	0.1970	0.2263	0.2534	0.2782
Mobile	5050_100_0	0.6313	0.6215	0.6137	0.6061	0.5988	0.5916	0.5845	0.5771	0.5704	0.5109	0.4654	0.4274	0.3931	0.3626	0.3344	0.3088
Dissolved	5050_100_1	0.2753	0.2855	0.2943	0.3022	0.3092	0.3155	0.3214	0.3269	0.3319	0.3613	0.3707	0.3749	0.3773	0.3789	0.3801	0.3810
Trapped	5050_100_1	0.0331	0.0469	0.0572	0.0669	0.0761	0.0855	0.0949	0.1041	0.1134	0.2044	0.2829	0.3444	0.3960	0.4368	0.4690	0.4962
Mobile	5050_100_1	0.6917	0.6676	0.6485	0.6308	0.6147	0.5989	0.5837	0.5690	0.5548	0.4343	0.3464	0.2808	0.2267	0.1843	0.1509	0.1228
Dissolved	5050_100_2	0.2689	0.2833	0.2950	0.3051	0.3137	0.3211	0.3276	0.3331	0.3379	0.3599	0.3667	0.3700	0.3720	0.3734	0.3744	0.3753
Trapped	5050_100_2	0.0413	0.0612	0.0782	0.0948	0.1089	0.1227	0.1358	0.1482	0.1614	0.2787	0.3667	0.4302	0.4764	0.5115	0.5372	0.5567
Mobile	5050_100_2	0.6898	0.6556	0.6268	0.6002	0.5774	0.5562	0.5367	0.5187	0.5007	0.3614	0.2667	0.1998	0.1516	0.1151	0.0884	0.0680
Dissolved	5050_100_5	0.2592	0.2790	0.2939	0.3060	0.3158	0.3230	0.3283	0.3323	0.3356	0.3512	0.3568	0.3598	0.3619	0.3636	0.3649	0.3660
Trapped	5050_100_5	0.0649	0.1004	0.1298	0.1544	0.1754	0.1951	0.2137	0.2336	0.2512	0.3851	0.4695	0.5231	0.5562	0.5768	0.5904	0.5987
Mobile	5050_100_5	0.6759	0.6206	0.5763	0.5395	0.5088	0.4820	0.4580	0.4340	0.4132	0.2637	0.1737	0.1170	0.0819	0.0596	0.0448	0.0353
Dissolved	5050_100_10	0.2475	0.2710	0.2889	0.3005	0.3080	0.3134	0.3174	0.3207	0.3235	0.3382	0.3444	0.3481	0.3507	0.3528	0.3546	0.3561
Trapped	5050_100_10	0.0736	0.1262	0.1653	0.1928	0.2176	0.2391	0.2595	0.2786	0.2963	0.4262	0.5001	0.5456	0.5741	0.5910	0.6007	0.6075
Mobile	5050_100_10	0.6789	0.6028	0.5458	0.5067	0.4743	0.4476	0.4231	0.4007	0.3803	0.2356	0.1555	0.1063	0.0752	0.0562	0.0447	0.0363

Table C-19: Results for CO_2 states for the 50:50 net-to-gross model with 300m shale length. 0, 1, 2, 5 and 10 degree dips. 1-100 years

Fraction	Year	1	5	10	15	20	30	40	50	60	80	100
Dissolved	5050_300_0	0.8797	0.6056	0.4601	0.3904	0.3516	0.3147	0.3009	0.2925	0.3065	0.3158	0.3197
Trapped	5050_300_0	0.0026	0.0045	0.0044	0.0047	0.0048	0.0053	0.0062	0.0106	0.0115	0.0162	0.0193
Mobile	5050_300_0	0.1177	0.3899	0.5355	0.6049	0.6435	0.6800	0.6929	0.6970	0.6820	0.6680	0.6610
Dissolved	5050_300_1	0.6684	0.3459	0.2600	0.2349	0.2233	0.2129	0.2158	0.2190	0.2341	0.2446	0.2500
Trapped	5050_300_1	0.0069	0.0081	0.0067	0.0057	0.0060	0.0074	0.0080	0.0112	0.0131	0.0182	0.0218
Mobile	5050_300_1	0.3247	0.6460	0.7333	0.7593	0.7707	0.7797	0.7762	0.7698	0.7529	0.7372	0.7282
Dissolved	5050_300_2	0.6604	0.3380	0.2526	0.2286	0.2168	0.2032	0.2000	0.2020	0.2156	0.2269	0.2340
Trapped	5050_300_2	0.0074	0.0081	0.0067	0.0061	0.0059	0.0084	0.0091	0.0108	0.0125	0.0174	0.0214
Mobile	5050_300_2	0.3322	0.6539	0.7407	0.7654	0.7773	0.7884	0.7909	0.7872	0.7719	0.7557	0.7447
Dissolved	5050_300_5	0.6663	0.3388	0.2515	0.2222	0.2125	0.2093	0.2185	0.2283	0.2407	0.2542	0.2642
Trapped	5050_300_5	0.0068	0.0087	0.0073	0.0058	0.0061	0.0076	0.0077	0.0075	0.0106	0.0165	0.0245
Mobile	5050_300_5	0.3268	0.6525	0.7412	0.7721	0.7814	0.7831	0.7738	0.7642	0.7487	0.7293	0.7113
Dissolved	5050_300_10	0.6506	0.3242	0.2380	0.2084	0.1976	0.1921	0.1976	0.2010	0.2155	0.2328	0.2465
Trapped	5050_300_10	0.0093	0.0070	0.0072	0.0064	0.0058	0.0083	0.0084	0.0060	0.0085	0.0168	0.0271
Mobile	5050_300_10	0.3401	0.6688	0.7547	0.7852	0.7966	0.7997	0.7940	0.7930	0.7760	0.7504	0.7265

Table C-20: Results for CO_2 states for the 50:50 net-to-gross model with 300m shale length, 0, 1, 2, 5 and 10 degree dips. 200-8000 years

Fraction	Year	200	300	400	500	600	700	800	900	1000	2000	3000	4000	5000	6000	7000	8000
Dissolved	5050_300_0	0.3265	0.3316	0.3360	0.3400	0.3441	0.3480	0.3518	0.3557	0.3594	0.3862	0.4015	0.4096	0.4135	0.4154	0.4163	0.4171
Trapped	5050_300_0	0.0289	0.0318	0.0339	0.0365	0.0390	0.0417	0.0443	0.0471	0.0499	0.0821	0.1133	0.1432	0.1747	0.2059	0.2354	0.2622
Mobile	5050_300_0	0.6446	0.6367	0.6301	0.6235	0.6169	0.6103	0.6039	0.5972	0.5907	0.5317	0.4852	0.4472	0.4118	0.3787	0.3482	0.3207
Dissolved	5050_300_1	0.2662	0.2792	0.2897	0.2989	0.3071	0.3151	0.3224	0.3293	0.3357	0.3702	0.3786	0.3822	0.3842	0.3855	0.3865	0.3872
Trapped	5050_300_1	0.0362	0.0493	0.0604	0.0723	0.0839	0.0935	0.1020	0.1114	0.1207	0.2121	0.3021	0.3761	0.4364	0.4802	0.5123	0.5362
Mobile	5050_300_1	0.6976	0.6716	0.6498	0.6287	0.6089	0.5914	0.5755	0.5593	0.5436	0.4177	0.3193	0.2418	0.1794	0.1343	0.1012	0.0766
Dissolved	5050_300_2	0.2605	0.2800	0.2958	0.3091	0.3213	0.3319	0.3407	0.3473	0.3523	0.3701	0.3751	0.3776	0.3791	0.3802	0.3810	0.3817
Trapped	5050_300_2	0.0457	0.0704	0.0947	0.1149	0.1324	0.1487	0.1646	0.1797	0.1943	0.3312	0.4319	0.4982	0.5391	0.5671	0.5833	0.5927
Mobile	5050_300_2	0.6938	0.6496	0.6094	0.5760	0.5463	0.5194	0.4948	0.4730	0.4534	0.2987	0.1930	0.1242	0.0818	0.0527	0.0357	0.0255
Dissolved	5050_300_5	0.3025	0.3300	0.3510	0.3638	0.3715	0.3766	0.3801	0.3828	0.3850	0.3949	0.3984	0.4005	0.4021	0.4033	0.4044	0.4054
Trapped	5050_300_5	0.0745	0.1215	0.1567	0.1860	0.2111	0.2367	0.2595	0.2801	0.3002	0.4456	0.5197	0.5552	0.5713	0.5789	0.5824	0.5842
Mobile	5050_300_5	0.6229	0.5485	0.4923	0.4502	0.4174	0.3867	0.3604	0.3371	0.3148	0.1595	0.0819	0.0443	0.0267	0.0178	0.0132	0.0104
Dissolved	5050_300_10	0.2981	0.3320	0.3480	0.3561	0.3611	0.3647	0.3673	0.3695	0.3712	0.3800	0.3838	0.3864	0.3884	0.3900	0.3914	0.3927
Trapped	5050_300_10	0.0985	0.1600	0.2040	0.2389	0.2713	0.2980	0.3228	0.3446	0.3649	0.4982	0.5539	0.5774	0.5886	0.5937	0.5959	0.5969
Mobile	5050_300_10	0.6034	0.5080	0.4480	0.4050	0.3676	0.3374	0.3099	0.2859	0.2639	0.1218	0.0622	0.0363	0.0230	0.0163	0.0127	0.0104

Table C-21: Results for CO_2 states for the 50:50 net-to-gross model with 1000m shale length. 0, 1, 2, 5 and 10 degree dips. 1-100 years

Fraction	Year	1	5	10	15	20	30	40	50	60	80	100
Dissolved	5050_1000_0	0.8922	0.6297	0.4875	0.4228	0.3900	0.3638	0.3566	0.3523	0.3632	0.3725	0.3771
Trapped	5050_1000_0	0.0025	0.0039	0.0048	0.0047	0.0045	0.0042	0.0061	0.0081	0.0090	0.0142	0.0164
Mobile	5050_1000_0	0.1053	0.3663	0.5077	0.5725	0.6055	0.6321	0.6373	0.6396	0.6278	0.6133	0.6064
Dissolved	5050_1000_1	0.6719	0.3467	0.2650	0.2441	0.2415	0.2564	0.2733	0.2865	0.2969	0.3072	0.3128
Trapped	5050_1000_1	0.0076	0.0070	0.0067	0.0064	0.0052	0.0052	0.0075	0.0108	0.0133	0.0181	0.0209
Mobile	5050_1000_1	0.3204	0.6463	0.7283	0.7495	0.7533	0.7384	0.7192	0.7027	0.6898	0.6748	0.6663
Dissolved	5050_1000_2	0.6640	0.3400	0.2560	0.2337	0.2304	0.2446	0.2595	0.2713	0.2817	0.2928	0.2995
Trapped	5050_1000_2	0.0079	0.0081	0.0070	0.0069	0.0058	0.0050	0.0073	0.0106	0.0137	0.0194	0.0227
Mobile	5050_1000_2	0.3282	0.6519	0.7371	0.7594	0.7637	0.7503	0.7332	0.7181	0.7045	0.6878	0.6777
Dissolved	5050_1000_5	0.6654	0.3377	0.2508	0.2251	0.2177	0.2188	0.2280	0.2371	0.2490	0.2625	0.2715
Trapped	5050_1000_5	0.0066	0.0084	0.0074	0.0072	0.0067	0.0048	0.0052	0.0073	0.0108	0.0181	0.0250
Mobile	5050_1000_5	0.3280	0.6539	0.7418	0.7676	0.7756	0.7764	0.7667	0.7556	0.7403	0.7193	0.7035
Dissolved	5050_1000_10	0.6492	0.3246	0.2365	0.2089	0.1992	0.1937	0.1993	0.1994	0.2128	0.2295	0.2422
Trapped	5050_1000_10	0.0083	0.0093	0.0071	0.0073	0.0070	0.0051	0.0054	0.0064	0.0092	0.0180	0.0265
Mobile	5050_1000_10	0.3425	0.6662	0.7565	0.7838	0.7938	0.8013	0.7953	0.7942	0.7780	0.7524	0.7313

Table C-22: Results for CO_2 states for the 50:50 net-to-gross model with 1000m shale length, 0, 1, 2, 5 and 10 degree dips. 200-8000 years

Fraction	Year	200	300	400	500	600	700	800	900	1000	2000	3000	4000	5000	6000	7000	8000
Dissolved	5050_1000_0	0.3856	0.3885	0.3906	0.3925	0.3943	0.3961	0.3978	0.3995	0.4011	0.4162	0.4286	0.4378	0.4446	0.4493	0.4518	0.4531
Trapped	5050_1000_0	0.0228	0.0251	0.0262	0.0274	0.0291	0.0310	0.0333	0.0356	0.0380	0.0673	0.1002	0.1316	0.1581	0.1840	0.2101	0.2355
Mobile	5050_1000_0	0.5915	0.5864	0.5832	0.5801	0.5766	0.5729	0.5689	0.5649	0.5609	0.5165	0.4712	0.4306	0.3973	0.3668	0.3382	0.3114
Dissolved	5050_1000_1	0.3267	0.3356	0.3434	0.3507	0.3576	0.3639	0.3699	0.3754	0.3806	0.4112	0.4201	0.4238	0.4258	0.4271	0.4280	0.4287
Trapped	5050_1000_1	0.0302	0.0384	0.0476	0.0557	0.0638	0.0722	0.0807	0.0890	0.0969	0.1678	0.2533	0.3287	0.3905	0.4399	0.4766	0.5028
Mobile	5050_1000_1	0.6430	0.6259	0.6090	0.5936	0.5786	0.5639	0.5494	0.5356	0.5225	0.4211	0.3266	0.2475	0.1837	0.1330	0.0954	0.0685
Dissolved	5050_1000_2	0.3191	0.3330	0.3455	0.3566	0.3665	0.3755	0.3836	0.3905	0.3959	0.4161	0.4211	0.4235	0.4248	0.4258	0.4265	0.4271
Trapped	5050_1000_2	0.0355	0.0503	0.0665	0.0831	0.0983	0.1109	0.1226	0.1338	0.1440	0.2679	0.3745	0.4526	0.5036	0.5326	0.5482	0.5561
Mobile	5050_1000_2	0.6454	0.6167	0.5880	0.5604	0.5353	0.5136	0.4937	0.4756	0.4601	0.3160	0.2043	0.1239	0.0715	0.0416	0.0253	0.0168
Dissolved	5050_1000_5	0.3056	0.3318	0.3527	0.3676	0.3774	0.3842	0.3885	0.3916	0.3940	0.4039	0.4070	0.4087	0.4099	0.4109	0.4116	0.4123
Trapped	5050_1000_5	0.0530	0.0871	0.1210	0.1492	0.1736	0.1954	0.2164	0.2377	0.2582	0.4278	0.5200	0.5608	0.5742	0.5795	0.5812	0.5818
Mobile	5050_1000_5	0.6415	0.5810	0.5264	0.4833	0.4490	0.4204	0.3951	0.3707	0.3478	0.1683	0.0729	0.0305	0.0159	0.0096	0.0072	0.0059
Dissolved	5050_1000_10	0.2952	0.3278	0.3466	0.3570	0.3632	0.3673	0.3702	0.3724	0.3741	0.3823	0.3856	0.3878	0.3894	0.3908	0.3921	0.3932
Trapped	5050_1000_10	0.0697	0.1268	0.1742	0.2113	0.2430	0.2700	0.2966	0.3236	0.3486	0.5133	0.5742	0.5927	0.5997	0.6017	0.6022	0.6022
Mobile	5050_1000_10	0.6352	0.5453	0.4792	0.4316	0.3938	0.3628	0.3332	0.3041	0.2773	0.1043	0.0402	0.0196	0.0108	0.0074	0.0057	0.0047

Table C-23: Results for CO_2 states for the 50:50 net-to-gross model with 3000m shale length. 0, 1, 2, 5 and 10 degree dips. 1-100 years

Fraction	Year	1	5	10	15	20	30	40	50	60	80	100
Dissolved	5050_3000_0	0.8794	0.6058	0.4666	0.4051	0.3758	0.3539	0.3444	0.3458	0.3547	0.3621	0.3659
Trapped	5050_3000_0	0.0031	0.0043	0.0053	0.0045	0.0045	0.0042	0.0054	0.0065	0.0068	0.0091	0.0104
Mobile	5050_3000_0	0.1175	0.3900	0.5281	0.5905	0.6197	0.6419	0.6502	0.6478	0.6385	0.6288	0.6237
Dissolved	5050_3000_1	0.6829	0.3636	0.2772	0.2537	0.2548	0.2673	0.2800	0.2904	0.2995	0.3080	0.3132
Trapped	5050_3000_1	0.0065	0.0089	0.0065	0.0055	0.0049	0.0052	0.0075	0.0099	0.0106	0.0136	0.0153
Mobile	5050_3000_1	0.3106	0.6275	0.7163	0.7408	0.7403	0.7275	0.7125	0.6997	0.6899	0.6784	0.6715
Dissolved	5050_3000_2	0.6764	0.3553	0.2684	0.2433	0.2388	0.2522	0.2633	0.2720	0.2813	0.2914	0.2984
Trapped	5050_3000_2	0.0077	0.0094	0.0073	0.0058	0.0053	0.0051	0.0071	0.0099	0.0110	0.0146	0.0166
Mobile	5050_3000_2	0.3159	0.6352	0.7243	0.7509	0.7559	0.7427	0.7296	0.7181	0.7076	0.6939	0.6851
Dissolved	5050_3000_5	0.6761	0.3519	0.2620	0.2324	0.2224	0.2242	0.2346	0.2432	0.2540	0.2681	0.2790
Trapped	5050_3000_5	0.0068	0.0090	0.0070	0.0063	0.0060	0.0055	0.0075	0.0106	0.0128	0.0173	0.0221
Mobile	5050_3000_5	0.3171	0.6391	0.7310	0.7613	0.7716	0.7703	0.7579	0.7462	0.7332	0.7146	0.6989
Dissolved	5050_3000_10	0.6615	0.3369	0.2476	0.2168	0.2045	0.2012	0.2067	0.2119	0.2253	0.2446	0.2602
Trapped	5050_3000_10	0.0066	0.0093	0.0081	0.0071	0.0068	0.0059	0.0067	0.0092	0.0113	0.0170	0.0234
Mobile	5050_3000_10	0.3319	0.6538	0.7443	0.7761	0.7887	0.7929	0.7866	0.7789	0.7635	0.7384	0.7164

Table C-24: Results for CO_2 states for the 50:50 net-to-gross model with 3000m shale length, 0, 1, 2, 5 and 10 degree dips. 200-8000 years

Fraction	Year	200	300	400	500	600	700	800	900	1000	2000	3000	4000	5000	6000	7000	8000
Dissolved	5050_3000_0	0.3725	0.3755	0.3779	0.3802	0.3826	0.3849	0.3870	0.3892	0.3912	0.4082	0.4214	0.4317	0.4393	0.4431	0.4446	0.4454
Trapped	5050_3000_0	0.0133	0.0140	0.0145	0.0151	0.0162	0.0170	0.0185	0.0198	0.0216	0.0466	0.0721	0.0982	0.1304	0.1605	0.1896	0.2162
Mobile	5050_3000_0	0.6142	0.6106	0.6075	0.6047	0.6013	0.5981	0.5945	0.5911	0.5872	0.5452	0.5065	0.4702	0.4303	0.3964	0.3658	0.3384
Dissolved	5050_3000_1	0.3284	0.3402	0.3505	0.3590	0.3664	0.3729	0.3787	0.3840	0.3888	0.4168	0.4238	0.4267	0.4282	0.4292	0.4300	0.4305
Trapped	5050_3000_1	0.0221	0.0318	0.0414	0.0518	0.0620	0.0721	0.0829	0.0934	0.1026	0.1871	0.2833	0.3697	0.4347	0.4794	0.5083	0.5277
Mobile	5050_3000_1	0.6496	0.6280	0.6081	0.5892	0.5716	0.5550	0.5384	0.5227	0.5086	0.3961	0.2928	0.2037	0.1370	0.0914	0.0617	0.0418
Dissolved	5050_3000_2	0.3223	0.3388	0.3517	0.3627	0.3725	0.3806	0.3876	0.3934	0.3983	0.4163	0.4205	0.4225	0.4237	0.4246	0.4253	0.4258
Trapped	5050_3000_2	0.0296	0.0478	0.0671	0.0877	0.1062	0.1233	0.1376	0.1510	0.1649	0.2992	0.4089	0.4833	0.5248	0.5477	0.5602	0.5658
Mobile	5050_3000_2	0.6482	0.6134	0.5812	0.5496	0.5213	0.4960	0.4748	0.4556	0.4368	0.2845	0.1706	0.0942	0.0515	0.0277	0.0145	0.0084
Dissolved	5050_3000_5	0.3168	0.3431	0.3627	0.3757	0.3841	0.3898	0.3935	0.3961	0.3981	0.4065	0.4092	0.4108	0.4119	0.4129	0.4137	0.4144
Trapped	5050_3000_5	0.0538	0.0946	0.1323	0.1663	0.1967	0.2221	0.2458	0.2681	0.2884	0.4529	0.5371	0.5686	0.5790	0.5825	0.5834	0.5834
Mobile	5050_3000_5	0.6295	0.5623	0.5049	0.4580	0.4193	0.3882	0.3606	0.3358	0.3135	0.1406	0.0536	0.0206	0.0091	0.0046	0.0030	0.0022
Dissolved	5050_3000_10	0.3142	0.3489	0.3659	0.3748	0.3800	0.3834	0.3858	0.3876	0.3891	0.3958	0.3987	0.4008	0.4024	0.4038	0.4051	0.4063
Trapped	5050_3000_10	0.0710	0.1315	0.1825	0.2244	0.2581	0.2881	0.3154	0.3418	0.3661	0.5204	0.5714	0.5864	0.5911	0.5924	0.5921	0.5916
Mobile	5050_3000_10	0.6148	0.5196	0.4517	0.4007	0.3619	0.3285	0.2988	0.2705	0.2448	0.0838	0.0299	0.0128	0.0065	0.0038	0.0028	0.0022

Table C-25: Results for CO_2 states for the 60:40 net-to-gross model with 100m shale length. 0, 1, 2, 5 and 10 degree dips. 1-100 years

Fraction	Year	1	5	10	15	20	30	40	50	60	80	100
Dissolved	6040_100_0	0.8932	0.6361	0.4889	0.4131	0.3680	0.3189	0.2955	0.2826	0.2913	0.2982	0.3020
Trapped	6040_100_0	0.0030	0.0057	0.0050	0.0055	0.0053	0.0052	0.0059	0.0061	0.0089	0.0185	0.0260
Mobile	6040_100_0	0.1038	0.3582	0.5061	0.5814	0.6267	0.6759	0.6986	0.7114	0.6999	0.6833	0.6719
Dissolved	6040_100_1	0.7014	0.3780	0.2816	0.2439	0.2255	0.2116	0.2072	0.2076	0.2178	0.2271	0.2332
Trapped	6040_100_1	0.0085	0.0069	0.0077	0.0072	0.0067	0.0059	0.0061	0.0076	0.0105	0.0211	0.0299
Mobile	6040_100_1	0.2901	0.6151	0.7107	0.7489	0.7678	0.7826	0.7867	0.7848	0.7717	0.7517	0.7369
Dissolved	6040_100_2	0.6865	0.3653	0.2716	0.2347	0.2164	0.2023	0.1990	0.1989	0.2100	0.2213	0.2295
Trapped	6040_100_2	0.0086	0.0094	0.0085	0.0074	0.0068	0.0056	0.0059	0.0068	0.0101	0.0211	0.0303
Mobile	6040_100_2	0.3049	0.6253	0.7199	0.7580	0.7767	0.7921	0.7952	0.7943	0.7799	0.7576	0.7402
Dissolved	6040_100_5	0.6805	0.3560	0.2622	0.2242	0.2049	0.1888	0.1849	0.1864	0.1988	0.2142	0.2254
Trapped	6040_100_5	0.0067	0.0096	0.0078	0.0072	0.0070	0.0059	0.0054	0.0055	0.0096	0.0228	0.0365
Mobile	6040_100_5	0.3128	0.6344	0.7299	0.7686	0.7881	0.8053	0.8097	0.8081	0.7916	0.7630	0.7381
Dissolved	6040_100_10	0.6743	0.3477	0.2523	0.2135	0.1925	0.1707	0.1598	0.1538	0.1688	0.1886	0.2033
Trapped	6040_100_10	0.0091	0.0088	0.0081	0.0069	0.0069	0.0062	0.0051	0.0054	0.0090	0.0233	0.0391
Mobile	6040_100_10	0.3166	0.6435	0.7396	0.7795	0.8006	0.8231	0.8351	0.8408	0.8222	0.7880	0.7576

Table C-26: Results for CO_2 states for the 60:40 net-to-gross model with 100m shale length, 0, 1, 2, 5 and 10 degree dips. 200-8000 years

Fraction	Year	200	300	400	500	600	700	800	900	1000	2000	3000	4000	5000	6000	7000	8000
Dissolved	6040_100_0	0.3143	0.3246	0.3336	0.3413	0.3478	0.3535	0.3584	0.3627	0.3663	0.3833	0.3890	0.3920	0.3937	0.3949	0.3958	0.3964
Trapped	6040_100_0	0.0422	0.0527	0.0614	0.0699	0.0777	0.0854	0.0930	0.0993	0.1054	0.1571	0.1971	0.2301	0.2628	0.2886	0.3134	0.3364
Mobile	6040_100_0	0.6435	0.6227	0.6050	0.5888	0.5746	0.5612	0.5486	0.5380	0.5283	0.4596	0.4139	0.3779	0.3434	0.3166	0.2908	0.2672
Dissolved	6040_100_1	0.2544	0.2706	0.2840	0.2950	0.3044	0.3125	0.3197	0.3255	0.3303	0.3492	0.3556	0.3588	0.3608	0.3621	0.3634	0.3644
Trapped	6040_100_1	0.0563	0.0740	0.0886	0.1043	0.1191	0.1332	0.1476	0.1624	0.1766	0.2969	0.3787	0.4398	0.4880	0.5236	0.5490	0.5682
Mobile	6040_100_1	0.6893	0.6554	0.6273	0.6008	0.5765	0.5542	0.5327	0.5121	0.4930	0.3539	0.2657	0.2014	0.1512	0.1143	0.0876	0.0674
Dissolved	6040_100_2	0.2590	0.2800	0.2965	0.3098	0.3202	0.3277	0.3332	0.3372	0.3404	0.3535	0.3581	0.3608	0.3626	0.3640	0.3653	0.3664
Trapped	6040_100_2	0.0671	0.0945	0.1187	0.1422	0.1651	0.1870	0.2079	0.2266	0.2455	0.3841	0.4694	0.5255	0.5621	0.5852	0.5994	0.6082
Mobile	6040_100_2	0.6739	0.6254	0.5848	0.5480	0.5146	0.4853	0.4589	0.4361	0.4141	0.2624	0.1724	0.1137	0.0753	0.0508	0.0353	0.0254
Dissolved	6040_100_5	0.2661	0.2923	0.3077	0.3170	0.3228	0.3270	0.3302	0.3327	0.3347	0.3446	0.3488	0.3517	0.3540	0.3559	0.3576	0.3591
Trapped	6040_100_5	0.0976	0.1443	0.1840	0.2182	0.2509	0.2787	0.3058	0.3297	0.3507	0.4939	0.5661	0.6010	0.6177	0.6254	0.6296	0.6313
Mobile	6040_100_5	0.6363	0.5634	0.5083	0.4648	0.4263	0.3943	0.3640	0.3376	0.3145	0.1615	0.0851	0.0474	0.0283	0.0186	0.0128	0.0096
Dissolved	6040_100_10	0.2521	0.2765	0.2878	0.2945	0.2991	0.3026	0.3052	0.3075	0.3093	0.3196	0.3250	0.3291	0.3324	0.3351	0.3374	0.3395
Trapped	6040_100_10	0.1229	0.1837	0.2303	0.2695	0.3045	0.3363	0.3636	0.3886	0.4116	0.5510	0.6080	0.6319	0.6423	0.6472	0.6493	0.6498
Mobile	6040_100_10	0.6250	0.5399	0.4820	0.4360	0.3964	0.3611	0.3312	0.3039	0.2791	0.1294	0.0670	0.0391	0.0254	0.0177	0.0132	0.0107

Table C-27: Results for CO_2 states for the 60:40 net-to-gross model with 300m shale length. 0, 1, 2, 5 and 10 degree dips. 1-100 years

Fraction	Year	1	5	10	15	20	30	40	50	60	80	100
Dissolved	6040_300_0	0.8924	0.6310	0.4828	0.4057	0.3599	0.3144	0.2936	0.2866	0.2956	0.3019	0.3045
Trapped	6040_300_0	0.0026	0.0041	0.0053	0.0053	0.0050	0.0039	0.0044	0.0045	0.0058	0.0112	0.0163
Mobile	6040_300_0	0.1050	0.3649	0.5119	0.5890	0.6351	0.6817	0.7020	0.7090	0.6986	0.6869	0.6792
Dissolved	6040_300_1	0.6911	0.3672	0.2721	0.2346	0.2154	0.2014	0.1991	0.2029	0.2136	0.2220	0.2269
Trapped	6040_300_1	0.0085	0.0074	0.0077	0.0072	0.0060	0.0049	0.0053	0.0052	0.0066	0.0143	0.0205
Mobile	6040_300_1	0.3005	0.6254	0.7202	0.7582	0.7787	0.7937	0.7955	0.7919	0.7798	0.7637	0.7526
Dissolved	6040_300_2	0.6807	0.3592	0.2654	0.2282	0.2086	0.1927	0.1889	0.1898	0.2011	0.2116	0.2185
Trapped	6040_300_2	0.0087	0.0093	0.0083	0.0070	0.0064	0.0052	0.0052	0.0052	0.0072	0.0156	0.0238
Mobile	6040_300_2	0.3106	0.6314	0.7263	0.7649	0.7850	0.8021	0.8059	0.8049	0.7917	0.7728	0.7577
Dissolved	6040_300_5	0.6807	0.3557	0.2609	0.2224	0.2022	0.1845	0.1805	0.1786	0.1911	0.2056	0.2168
Trapped	6040_300_5	0.0095	0.0103	0.0084	0.0073	0.0069	0.0056	0.0048	0.0053	0.0091	0.0227	0.0361
Mobile	6040_300_5	0.3098	0.6339	0.7308	0.7702	0.7908	0.8099	0.8147	0.8161	0.7998	0.7717	0.7472
Dissolved	6040_300_10	0.6658	0.3409	0.2489	0.2112	0.1914	0.1735	0.1687	0.1658	0.1802	0.1988	0.2136
Trapped	6040_300_10	0.0097	0.0079	0.0080	0.0069	0.0066	0.0054	0.0053	0.0056	0.0092	0.0257	0.0435
Mobile	6040_300_10	0.3245	0.6512	0.7431	0.7818	0.8020	0.8211	0.8260	0.8287	0.8106	0.7755	0.7429

Table C-28: Results for CO_2 states for the 60:40 net-to-gross model with 300m shale length, 0, 1, 2, 5 and 10 degree dips. 200-8000 years

Fraction	Year	200	300	400	500	600	700	800	900	1000	2000	3000	4000	5000	6000	7000	8000
Dissolved	6040_300_0	0.3109	0.3166	0.3218	0.3269	0.3317	0.3365	0.3408	0.3453	0.3497	0.3775	0.3924	0.3997	0.4032	0.4049	0.4062	0.4072
Trapped	6040_300_0	0.0269	0.0317	0.0361	0.0410	0.0463	0.0517	0.0567	0.0613	0.0657	0.1036	0.1413	0.1798	0.2132	0.2446	0.2735	0.3002
Mobile	6040_300_0	0.6622	0.6518	0.6421	0.6320	0.6220	0.6118	0.6024	0.5934	0.5846	0.5189	0.4663	0.4205	0.3836	0.3505	0.3203	0.2926
Dissolved	6040_300_1	0.2443	0.2587	0.2710	0.2817	0.2913	0.3004	0.3089	0.3166	0.3232	0.3513	0.3584	0.3617	0.3638	0.3652	0.3664	0.3673
Trapped	6040_300_1	0.0411	0.0573	0.0734	0.0897	0.1047	0.1175	0.1307	0.1433	0.1544	0.2658	0.3615	0.4355	0.4887	0.5278	0.5569	0.5780
Mobile	6040_300_1	0.7145	0.6840	0.6556	0.6286	0.6041	0.5821	0.5604	0.5401	0.5225	0.3829	0.2801	0.2028	0.1474	0.1070	0.0768	0.0548
Dissolved	6040_300_2	0.2449	0.2646	0.2813	0.2975	0.3109	0.3206	0.3278	0.3332	0.3373	0.3529	0.3575	0.3600	0.3616	0.3629	0.3640	0.3649
Trapped	6040_300_2	0.0557	0.0864	0.1152	0.1397	0.1610	0.1818	0.2009	0.2174	0.2341	0.3811	0.4819	0.5408	0.5768	0.5988	0.6113	0.6186
Mobile	6040_300_2	0.6994	0.6490	0.6035	0.5628	0.5281	0.4976	0.4713	0.4494	0.4286	0.2660	0.1605	0.0992	0.0616	0.0383	0.0247	0.0165
Dissolved	6040_300_5	0.2570	0.2913	0.3119	0.3235	0.3304	0.3348	0.3379	0.3404	0.3423	0.3512	0.3547	0.3571	0.3590	0.3607	0.3621	0.3634
Trapped	6040_300_5	0.1013	0.1579	0.2018	0.2403	0.2723	0.3018	0.3276	0.3513	0.3740	0.5263	0.5910	0.6172	0.6273	0.6310	0.6321	0.6322
Mobile	6040_300_5	0.6417	0.5509	0.4863	0.4362	0.3973	0.3634	0.3345	0.3083	0.2837	0.1225	0.0543	0.0257	0.0136	0.0084	0.0058	0.0044
Dissolved	6040_300_10	0.2727	0.3038	0.3170	0.3239	0.3282	0.3312	0.3335	0.3353	0.3368	0.3451	0.3496	0.3531	0.3559	0.3584	0.3605	0.3625
Trapped	6040_300_10	0.1346	0.2094	0.2640	0.3082	0.3471	0.3785	0.4072	0.4327	0.4556	0.5839	0.6207	0.6315	0.6351	0.6355	0.6348	0.6338
Mobile	6040_300_10	0.5927	0.4868	0.4190	0.3679	0.3247	0.2902	0.2593	0.2320	0.2076	0.0710	0.0297	0.0154	0.0090	0.0061	0.0047	0.0037

Table C-29: Results for CO_2 states for the 60:40 net-to-gross model with 1000m shale length. 0, 1, 2, 5 and 10 degree dips. 1-100 years

Fraction	Year	1	5	10	15	20	30	40	50	60	80	100
Dissolved	6040_1000_0	0.8963	0.6419	0.4939	0.4176	0.3743	0.3307	0.3102	0.2986	0.3069	0.3135	0.3166
Trapped	6040_1000_0	0.0030	0.0050	0.0053	0.0052	0.0048	0.0040	0.0041	0.0047	0.0051	0.0069	0.0092
Mobile	6040_1000_0	0.1007	0.3531	0.5008	0.5772	0.6210	0.6653	0.6856	0.6967	0.6880	0.6796	0.6743
Dissolved	6040_1000_1	0.7045	0.3804	0.2810	0.2429	0.2271	0.2193	0.2185	0.2217	0.2313	0.2403	0.2456
Trapped	6040_1000_1	0.0079	0.0084	0.0078	0.0066	0.0061	0.0049	0.0049	0.0058	0.0066	0.0101	0.0130
Mobile	6040_1000_1	0.2876	0.6112	0.7112	0.7505	0.7668	0.7758	0.7766	0.7726	0.7621	0.7497	0.7414
Dissolved	6040_1000_2	0.6907	0.3671	0.2711	0.2331	0.2163	0.2083	0.2068	0.2090	0.2194	0.2306	0.2381
Trapped	6040_1000_2	0.0086	0.0089	0.0077	0.0064	0.0062	0.0051	0.0047	0.0057	0.0066	0.0103	0.0138
Mobile	6040_1000_2	0.3007	0.6241	0.7212	0.7605	0.7774	0.7866	0.7886	0.7853	0.7739	0.7591	0.7481
Dissolved	6040_1000_5	0.6831	0.3578	0.2627	0.2240	0.2060	0.1948	0.1942	0.1954	0.2075	0.2226	0.2341
Trapped	6040_1000_5	0.0080	0.0092	0.0081	0.0074	0.0065	0.0055	0.0045	0.0058	0.0077	0.0152	0.0245
Mobile	6040_1000_5	0.3089	0.6330	0.7293	0.7686	0.7875	0.7998	0.8013	0.7988	0.7848	0.7622	0.7414
Dissolved	6040_1000_10	0.6813	0.3541	0.2579	0.2173	0.1969	0.1815	0.1785	0.1760	0.1899	0.2092	0.2244
Trapped	6040_1000_10	0.0103	0.0104	0.0089	0.0071	0.0070	0.0057	0.0049	0.0056	0.0082	0.0177	0.0292
Mobile	6040_1000_10	0.3084	0.6355	0.7333	0.7756	0.7960	0.8128	0.8166	0.8183	0.8019	0.7731	0.7464

Table C-30: Results for CO_2 states for the 60:40 net-to-gross model with 1000m shale length, 0, 1, 2, 5 and 10 degree dips. 200-8000 years

Fraction	Year	200	300	400	500	600	700	800	900	1000	2000	3000	4000	5000	6000	7000	8000
Dissolved	6040_1000_0	0.3224	0.3265	0.3305	0.3344	0.3383	0.3421	0.3459	0.3497	0.3535	0.3834	0.4019	0.4123	0.4174	0.4197	0.4209	0.4217
Trapped	6040_1000_0	0.0146	0.0163	0.0178	0.0194	0.0212	0.0235	0.0261	0.0288	0.0317	0.0576	0.0843	0.1139	0.1437	0.1753	0.2096	0.2404
Mobile	6040_1000_0	0.6629	0.6573	0.6517	0.6462	0.6406	0.6344	0.6280	0.6215	0.6148	0.5590	0.5138	0.4739	0.4388	0.4050	0.3695	0.3378
Dissolved	6040_1000_1	0.2625	0.2760	0.2876	0.2981	0.3073	0.3160	0.3248	0.3333	0.3407	0.3675	0.3733	0.3759	0.3773	0.3783	0.3790	0.3795
Trapped	6040_1000_1	0.0255	0.0393	0.0528	0.0671	0.0810	0.0943	0.1065	0.1175	0.1284	0.2514	0.3691	0.4594	0.5176	0.5553	0.5797	0.5960
Mobile	6040_1000_1	0.7120	0.6847	0.6596	0.6348	0.6117	0.5897	0.5688	0.5492	0.5309	0.3811	0.2577	0.1648	0.1051	0.0665	0.0413	0.0245
Dissolved	6040_1000_2	0.2646	0.2844	0.3004	0.3150	0.3279	0.3374	0.3446	0.3499	0.3538	0.3671	0.3706	0.3724	0.3734	0.3742	0.3748	0.3754
Trapped	6040_1000_2	0.0378	0.0648	0.0950	0.1195	0.1413	0.1628	0.1815	0.2002	0.2192	0.3901	0.5091	0.5685	0.5995	0.6144	0.6202	0.6224
Mobile	6040_1000_2	0.6976	0.6508	0.6046	0.5655	0.5308	0.4998	0.4739	0.4499	0.4270	0.2428	0.1202	0.0592	0.0271	0.0114	0.0050	0.0022
Dissolved	6040_1000_5	0.2740	0.3030	0.3221	0.3340	0.3408	0.3450	0.3478	0.3499	0.3515	0.3583	0.3607	0.3623	0.3635	0.3646	0.3656	0.3664
Trapped	6040_1000_5	0.0847	0.1447	0.1877	0.2251	0.2625	0.2943	0.3237	0.3506	0.3779	0.5587	0.6180	0.6309	0.6344	0.6346	0.6340	0.6332
Mobile	6040_1000_5	0.6412	0.5523	0.4901	0.4408	0.3966	0.3608	0.3284	0.2995	0.2706	0.0830	0.0213	0.0068	0.0021	0.0009	0.0004	0.0003
Dissolved	6040_1000_10	0.2768	0.3066	0.3210	0.3281	0.3323	0.3351	0.3371	0.3387	0.3399	0.3459	0.3489	0.3513	0.3533	0.3551	0.3567	0.3582
Trapped	6040_1000_10	0.1214	0.1937	0.2513	0.2996	0.3400	0.3769	0.4118	0.4431	0.4708	0.6183	0.6435	0.6466	0.6460	0.6445	0.6430	0.6415
Mobile	6040_1000_10	0.6018	0.4997	0.4277	0.3723	0.3277	0.2880	0.2510	0.2182	0.1893	0.0359	0.0076	0.0021	0.0007	0.0004	0.0003	0.0002

Table C-31: Results for CO_2 states for the 60:40 net-to-gross model with 3000m shale length. 0, 1, 2, 5 and 10 degree dips. 1-100 years

Fraction	Year	1	5	10	15	20	30	40	50	60	80	100
Dissolved	6040_3000_0	0.8966	0.6416	0.4970	0.4228	0.3805	0.3382	0.3226	0.3151	0.3245	0.3325	0.3361
Trapped	6040_3000_0	0.0023	0.0033	0.0051	0.0053	0.0047	0.0043	0.0044	0.0049	0.0054	0.0078	0.0094
Mobile	6040_3000_0	0.1011	0.3551	0.4979	0.5719	0.6148	0.6575	0.6730	0.6801	0.6701	0.6597	0.6545
Dissolved	6040_3000_1	0.6871	0.3636	0.2738	0.2413	0.2292	0.2297	0.2350	0.2419	0.2522	0.2621	0.2675
Trapped	6040_3000_1	0.0075	0.0057	0.0067	0.0066	0.0060	0.0049	0.0059	0.0072	0.0077	0.0115	0.0141
Mobile	6040_3000_1	0.3054	0.6307	0.7195	0.7522	0.7648	0.7654	0.7591	0.7509	0.7401	0.7264	0.7184
Dissolved	6040_3000_2	0.6796	0.3552	0.2657	0.2323	0.2187	0.2168	0.2208	0.2248	0.2360	0.2478	0.2551
Trapped	6040_3000_2	0.0076	0.0065	0.0069	0.0062	0.0061	0.0053	0.0055	0.0061	0.0073	0.0114	0.0149
Mobile	6040_3000_2	0.3128	0.6384	0.7275	0.7615	0.7752	0.7779	0.7737	0.7692	0.7567	0.7407	0.7299
Dissolved	6040_3000_5	0.6787	0.3518	0.2597	0.2248	0.2094	0.2016	0.2007	0.2054	0.2182	0.2334	0.2442
Trapped	6040_3000_5	0.0083	0.0072	0.0079	0.0069	0.0066	0.0054	0.0057	0.0055	0.0078	0.0146	0.0220
Mobile	6040_3000_5	0.3131	0.6410	0.7324	0.7683	0.7840	0.7930	0.7936	0.7891	0.7740	0.7520	0.7337
Dissolved	6040_3000_10	0.6635	0.3381	0.2474	0.2128	0.1957	0.1836	0.1800	0.1852	0.1999	0.2192	0.2341
Trapped	6040_3000_10	0.0092	0.0087	0.0079	0.0076	0.0068	0.0061	0.0058	0.0053	0.0072	0.0158	0.0262
Mobile	6040_3000_10	0.3273	0.6531	0.7448	0.7796	0.7975	0.8102	0.8142	0.8095	0.7930	0.7651	0.7397

Table C-32: Results for CO_2 states for the 60:40 net-to-gross model with 3000m shale length, 0, 1, 2, 5 and 10 degree dips. 200-8000 years

Fraction	Year	200	300	400	500	600	700	800	900	1000	2000	3000	4000	5000	6000	7000	8000
Dissolved	6040_3000_0	0.3420	0.3451	0.3481	0.3511	0.3541	0.3571	0.3601	0.3631	0.3662	0.3927	0.4099	0.4216	0.4288	0.4321	0.4338	0.4349
Trapped	6040_3000_0	0.0137	0.0160	0.0179	0.0196	0.0218	0.0243	0.0267	0.0290	0.0316	0.0643	0.0950	0.1255	0.1554	0.1869	0.2182	0.2449
Mobile	6040_3000_0	0.6443	0.6388	0.6340	0.6293	0.6242	0.6186	0.6132	0.6079	0.6022	0.5430	0.4951	0.4530	0.4159	0.3811	0.3480	0.3202
Dissolved	6040_3000_1	0.2834	0.2960	0.3076	0.3185	0.3292	0.3397	0.3494	0.3582	0.3656	0.3916	0.3971	0.3996	0.4011	0.4020	0.4027	0.4033
Trapped	6040_3000_1	0.0261	0.0387	0.0510	0.0637	0.0772	0.0892	0.1005	0.1119	0.1228	0.2420	0.3652	0.4523	0.5059	0.5411	0.5654	0.5797
Mobile	6040_3000_1	0.6905	0.6653	0.6414	0.6179	0.5936	0.5711	0.5501	0.5300	0.5116	0.3664	0.2376	0.1481	0.0930	0.0568	0.0318	0.0170
Dissolved	6040_3000_2	0.2804	0.3009	0.3209	0.3378	0.3515	0.3611	0.3676	0.3722	0.3756	0.3880	0.3914	0.3931	0.3942	0.3949	0.3956	0.3961
Trapped	6040_3000_2	0.0352	0.0596	0.0858	0.1090	0.1289	0.1483	0.1684	0.1867	0.2051	0.3882	0.5019	0.5567	0.5837	0.5962	0.6005	0.6021
Mobile	6040_3000_2	0.6844	0.6395	0.5932	0.5532	0.5196	0.4906	0.4640	0.4410	0.4192	0.2238	0.1067	0.0502	0.0222	0.0088	0.0039	0.0018
Dissolved	6040_3000_5	0.2895	0.3242	0.3439	0.3546	0.3608	0.3648	0.3675	0.3696	0.3712	0.3779	0.3802	0.3817	0.3829	0.3840	0.3849	0.3858
Trapped	6040_3000_5	0.0713	0.1208	0.1642	0.2034	0.2383	0.2722	0.3033	0.3349	0.3654	0.5465	0.5966	0.6117	0.6150	0.6151	0.6145	0.6138
Mobile	6040_3000_5	0.6392	0.5550	0.4920	0.4420	0.4009	0.3630	0.3291	0.2955	0.2634	0.0757	0.0232	0.0066	0.0021	0.0010	0.0006	0.0005
Dissolved	6040_3000_10	0.2978	0.3290	0.3421	0.3487	0.3527	0.3554	0.3574	0.3590	0.3601	0.3660	0.3690	0.3713	0.3733	0.3751	0.3767	0.3781
Trapped	6040_3000_10	0.1019	0.1693	0.2262	0.2768	0.3210	0.3615	0.3998	0.4336	0.4640	0.5968	0.6202	0.6247	0.6248	0.6239	0.6228	0.6215
Mobile	6040_3000_10	0.6004	0.5017	0.4317	0.3745	0.3263	0.2830	0.2428	0.2074	0.1759	0.0372	0.0108	0.0039	0.0018	0.0010	0.0006	0.0004

Table C-33: Results for CO_2 states for the 70:30 net-to-gross model with 100m shale length. 0, 1, 2, 5 and 10 degree dips. 1-100 years

Fraction	Year	1	5	10	15	20	30	40	50	60	80	100
Dissolved	7030_100_0	0.8969	0.6417	0.4947	0.4153	0.3673	0.3141	0.2873	0.2710	0.2799	0.2890	0.2952
Trapped	7030_100_0	0.0030	0.0056	0.0056	0.0056	0.0057	0.0056	0.0058	0.0072	0.0144	0.0314	0.0419
Mobile	7030_100_0	0.1001	0.3527	0.4997	0.5791	0.6271	0.6804	0.7069	0.7218	0.7057	0.6797	0.6630
Dissolved	7030_100_1	0.6922	0.3702	0.2761	0.2377	0.2173	0.2012	0.1949	0.1918	0.2028	0.2153	0.2247
Trapped	7030_100_1	0.0082	0.0098	0.0083	0.0075	0.0070	0.0067	0.0073	0.0080	0.0149	0.0333	0.0451
Mobile	7030_100_1	0.2997	0.6199	0.7157	0.7548	0.7756	0.7921	0.7978	0.8001	0.7823	0.7514	0.7302
Dissolved	7030_100_2	0.6848	0.3619	0.2694	0.2316	0.2112	0.1939	0.1874	0.1842	0.1965	0.2112	0.2231
Trapped	7030_100_2	0.0101	0.0078	0.0076	0.0076	0.0068	0.0064	0.0068	0.0071	0.0136	0.0317	0.0453
Mobile	7030_100_2	0.3051	0.6303	0.7229	0.7608	0.7821	0.7997	0.8058	0.8087	0.7900	0.7570	0.7316
Dissolved	7030_100_5	0.6845	0.3570	0.2631	0.2243	0.2033	0.1830	0.1760	0.1733	0.1875	0.2080	0.2244
Trapped	7030_100_5	0.0095	0.0082	0.0077	0.0075	0.0069	0.0063	0.0060	0.0068	0.0136	0.0351	0.0559
Mobile	7030_100_5	0.3060	0.6348	0.7292	0.7682	0.7898	0.8107	0.8179	0.8200	0.7990	0.7569	0.7197
Dissolved	7030_100_10	0.6688	0.3429	0.2510	0.2134	0.1937	0.1726	0.1634	0.1599	0.1765	0.2010	0.2201
Trapped	7030_100_10	0.0111	0.0101	0.0080	0.0075	0.0066	0.0066	0.0059	0.0054	0.0107	0.0337	0.0595
Mobile	7030_100_10	0.3201	0.6470	0.7410	0.7790	0.7997	0.8208	0.8307	0.8347	0.8128	0.7653	0.7204

Table C-34: Results for CO_2 states for the 70:30 net-to-gross model with 100m shale length, 0, 1, 2, 5 and 10 degree dips. 200-8000 years

Fraction	Year	200	300	400	500	600	700	800	900	1000	2000	3000	4000	5000	6000	7000	8000
Dissolved	7030_100_0	0.3166	0.3295	0.3384	0.3441	0.3489	0.3527	0.3556	0.3580	0.3600	0.3677	0.3712	0.3730	0.3742	0.3752	0.3761	0.3769
Trapped	7030_100_0	0.0724	0.0945	0.1125	0.1310	0.1463	0.1592	0.1700	0.1786	0.1878	0.2531	0.2927	0.3249	0.3515	0.3754	0.3967	0.4160
Mobile	7030_100_0	0.6110	0.5761	0.5491	0.5249	0.5048	0.4882	0.4744	0.4634	0.4523	0.3792	0.3360	0.3021	0.2743	0.2494	0.2272	0.2072
Dissolved	7030_100_1	0.2557	0.2763	0.2908	0.3010	0.3082	0.3138	0.3178	0.3208	0.3232	0.3384	0.3436	0.3459	0.3479	0.3497	0.3512	0.3525
Trapped	7030_100_1	0.0854	0.1185	0.1503	0.1812	0.2081	0.2324	0.2549	0.2752	0.2943	0.4217	0.4938	0.5398	0.5685	0.5865	0.5984	0.6053
Mobile	7030_100_1	0.6588	0.6052	0.5588	0.5178	0.4837	0.4538	0.4273	0.4040	0.3826	0.2399	0.1627	0.1142	0.0836	0.0638	0.0505	0.0422
Dissolved	7030_100_2	0.2641	0.2902	0.3064	0.3160	0.3219	0.3258	0.3287	0.3314	0.3336	0.3436	0.3471	0.3500	0.3523	0.3541	0.3557	0.3572
Trapped	7030_100_2	0.1030	0.1531	0.1970	0.2368	0.2709	0.3017	0.3270	0.3496	0.3702	0.4949	0.5565	0.5902	0.6067	0.6153	0.6194	0.6220
Mobile	7030_100_2	0.6328	0.5567	0.4966	0.4472	0.4073	0.3725	0.3443	0.3190	0.2961	0.1615	0.0964	0.0598	0.0411	0.0306	0.0249	0.0208
Dissolved	7030_100_5	0.2782	0.3035	0.3144	0.3203	0.3240	0.3266	0.3286	0.3302	0.3315	0.3389	0.3434	0.3470	0.3501	0.3528	0.3552	0.3573
Trapped	7030_100_5	0.1515	0.2250	0.2831	0.3301	0.3699	0.4015	0.4295	0.4541	0.4745	0.5889	0.6270	0.6400	0.6429	0.6425	0.6414	0.6398
Mobile	7030_100_5	0.5704	0.4715	0.4026	0.3497	0.3061	0.2718	0.2419	0.2157	0.1939	0.0722	0.0296	0.0130	0.0070	0.0047	0.0035	0.0029
Dissolved	7030_100_10	0.2768	0.2957	0.3039	0.3088	0.3121	0.3147	0.3167	0.3184	0.3198	0.3294	0.3360	0.3413	0.3457	0.3494	0.3526	0.3553
Trapped	7030_100_10	0.1761	0.2605	0.3265	0.3766	0.4190	0.4553	0.4846	0.5090	0.5296	0.6260	0.6475	0.6498	0.6487	0.6466	0.6443	0.6420
Mobile	7030_100_10	0.5471	0.4438	0.3696	0.3146	0.2688	0.2300	0.1988	0.1726	0.1506	0.0445	0.0165	0.0089	0.0056	0.0040	0.0031	0.0026

Table C-35: Results for CO_2 states for the 70:30 net-to-gross model with 300m shale length. 0, 1, 2, 5 and 10 degree dips. 1-100 years

Fraction	Year	1	5	10	15	20	30	40	50	60	80	100
Dissolved	7030_300_0	0.8941	0.6332	0.4853	0.4058	0.3570	0.3052	0.2812	0.2694	0.2789	0.2866	0.2922
Trapped	7030_300_0	0.0032	0.0051	0.0049	0.0058	0.0051	0.0048	0.0050	0.0053	0.0087	0.0222	0.0309
Mobile	7030_300_0	0.1027	0.3617	0.5098	0.5884	0.6378	0.6900	0.7138	0.7253	0.7124	0.6912	0.6769
Dissolved	7030_300_1	0.6908	0.3640	0.2707	0.2318	0.2104	0.1930	0.1898	0.1931	0.2039	0.2156	0.2237
Trapped	7030_300_1	0.0105	0.0083	0.0077	0.0071	0.0065	0.0061	0.0057	0.0064	0.0112	0.0264	0.0382
Mobile	7030_300_1	0.2986	0.6276	0.7216	0.7611	0.7831	0.8010	0.8045	0.8005	0.7849	0.7581	0.7381
Dissolved	7030_300_2	0.6827	0.3556	0.2644	0.2261	0.2048	0.1869	0.1838	0.1851	0.1972	0.2115	0.2225
Trapped	7030_300_2	0.0100	0.0070	0.0077	0.0071	0.0067	0.0059	0.0058	0.0063	0.0114	0.0296	0.0443
Mobile	7030_300_2	0.3073	0.6375	0.7278	0.7668	0.7885	0.8072	0.8104	0.8087	0.7913	0.7589	0.7331
Dissolved	7030_300_5	0.6826	0.3525	0.2591	0.2211	0.1996	0.1804	0.1770	0.1791	0.1940	0.2149	0.2318
Trapped	7030_300_5	0.0087	0.0092	0.0079	0.0074	0.0073	0.0063	0.0058	0.0053	0.0124	0.0374	0.0600
Mobile	7030_300_5	0.3087	0.6383	0.7330	0.7715	0.7931	0.8134	0.8172	0.8156	0.7936	0.7477	0.7083
Dissolved	7030_300_10	0.6672	0.3393	0.2473	0.2119	0.1917	0.1707	0.1656	0.1650	0.1828	0.2089	0.2292
Trapped	7030_300_10	0.0084	0.0099	0.0071	0.0078	0.0071	0.0061	0.0059	0.0056	0.0117	0.0389	0.0698
Mobile	7030_300_10	0.3244	0.6508	0.7456	0.7803	0.8012	0.8231	0.8285	0.8294	0.8055	0.7521	0.7010

Table C-36: Results for CO_2 states for the 70:30 net-to-gross model with 300m shale length, 0, 1, 2, 5 and 10 degree dips. 200-8000 years

Fraction	Year	200	300	400	500	600	700	800	900	1000	2000	3000	4000	5000	6000	7000	8000
Dissolved	7030_300_0	0.3120	0.3255	0.3355	0.3437	0.3503	0.3560	0.3609	0.3653	0.3691	0.3924	0.4031	0.4074	0.4098	0.4114	0.4126	0.4137
Trapped	7030_300_0	0.0507	0.0635	0.0737	0.0824	0.0905	0.0973	0.1022	0.1079	0.1135	0.1654	0.2099	0.2471	0.2782	0.3078	0.3348	0.3588
Mobile	7030_300_0	0.6373	0.6111	0.5908	0.5740	0.5592	0.5466	0.5368	0.5267	0.5174	0.4421	0.3870	0.3454	0.3119	0.2808	0.2526	0.2275
Dissolved	7030_300_1	0.2536	0.2748	0.2915	0.3054	0.3164	0.3252	0.3321	0.3375	0.3419	0.3595	0.3651	0.3684	0.3708	0.3728	0.3745	0.3760
Trapped	7030_300_1	0.0729	0.1000	0.1231	0.1450	0.1641	0.1821	0.1992	0.2147	0.2292	0.3539	0.4412	0.5033	0.5466	0.5742	0.5903	0.6001
Mobile	7030_300_1	0.6735	0.6252	0.5853	0.5496	0.5195	0.4927	0.4687	0.4478	0.4289	0.2866	0.1937	0.1284	0.0826	0.0530	0.0352	0.0239
Dissolved	7030_300_2	0.2629	0.2906	0.3098	0.3222	0.3302	0.3358	0.3399	0.3428	0.3452	0.3557	0.3600	0.3629	0.3653	0.3674	0.3693	0.3709
Trapped	7030_300_2	0.0969	0.1412	0.1762	0.2068	0.2328	0.2574	0.2796	0.3004	0.3197	0.4629	0.5414	0.5856	0.6075	0.6171	0.6222	0.6231
Mobile	7030_300_2	0.6403	0.5682	0.5141	0.4710	0.4369	0.4068	0.3806	0.3568	0.3351	0.1815	0.0987	0.0515	0.0272	0.0155	0.0086	0.0059
Dissolved	7030_300_5	0.2879	0.3147	0.3261	0.3329	0.3373	0.3404	0.3428	0.3446	0.3460	0.3540	0.3586	0.3624	0.3656	0.3685	0.3710	0.3733
Trapped	7030_300_5	0.1539	0.2196	0.2672	0.3074	0.3436	0.3770	0.4066	0.4314	0.4534	0.5793	0.6196	0.6300	0.6307	0.6293	0.6274	0.6255
Mobile	7030_300_5	0.5582	0.4658	0.4067	0.3597	0.3191	0.2825	0.2506	0.2241	0.2006	0.0667	0.0217	0.0076	0.0037	0.0022	0.0016	0.0012
Dissolved	7030_300_10	0.2906	0.3103	0.3194	0.3248	0.3283	0.3310	0.3331	0.3349	0.3364	0.3463	0.3531	0.3588	0.3635	0.3676	0.3712	0.3744
Trapped	7030_300_10	0.1896	0.2656	0.3240	0.3698	0.4116	0.4472	0.4761	0.5006	0.5210	0.6191	0.6374	0.6370	0.6339	0.6306	0.6273	0.6244
Mobile	7030_300_10	0.5198	0.4241	0.3566	0.3054	0.2600	0.2218	0.1908	0.1645	0.1426	0.0346	0.0095	0.0043	0.0026	0.0018	0.0014	0.0012

Table C-37: Results for CO_2 states for the 70:30 net-to-gross model with 1000m shale length. 0, 1, 2, 5 and 10 degree dips. 1-100 years

Fraction	Year	1	5	10	15	20	30	40	50	60	80	100
Dissolved	7030_1000_0	0.8899	0.6224	0.4725	0.3925	0.3450	0.2957	0.2723	0.2574	0.2672	0.2740	0.2772
Trapped	7030_1000_0	0.0030	0.0051	0.0052	0.0054	0.0047	0.0043	0.0050	0.0071	0.0102	0.0205	0.0277
Mobile	7030_1000_0	0.1071	0.3725	0.5223	0.6021	0.6503	0.7000	0.7227	0.7355	0.7226	0.7054	0.6951
Dissolved	7030_1000_1	0.6588	0.3397	0.2501	0.2136	0.1955	0.1812	0.1816	0.1816	0.1930	0.2033	0.2104
Trapped	7030_1000_1	0.0092	0.0086	0.0073	0.0063	0.0060	0.0049	0.0047	0.0067	0.0110	0.0221	0.0324
Mobile	7030_1000_1	0.3320	0.6517	0.7426	0.7801	0.7986	0.8139	0.8137	0.8117	0.7960	0.7746	0.7572
Dissolved	7030_1000_2	0.6452	0.3282	0.2421	0.2067	0.1884	0.1730	0.1717	0.1741	0.1867	0.2010	0.2124
Trapped	7030_1000_2	0.0093	0.0071	0.0072	0.0065	0.0061	0.0057	0.0046	0.0052	0.0097	0.0232	0.0361
Mobile	7030_1000_2	0.3455	0.6647	0.7507	0.7867	0.8055	0.8212	0.8237	0.8207	0.8036	0.7758	0.7515
Dissolved	7030_1000_5	0.6257	0.3130	0.2305	0.1976	0.1792	0.1630	0.1590	0.1631	0.1795	0.2021	0.2195
Trapped	7030_1000_5	0.0081	0.0104	0.0084	0.0072	0.0064	0.0055	0.0048	0.0046	0.0111	0.0339	0.0542
Mobile	7030_1000_5	0.3662	0.6765	0.7611	0.7951	0.8144	0.8315	0.8362	0.8323	0.8094	0.7641	0.7262
Dissolved	7030_1000_10	0.6352	0.3168	0.2312	0.1972	0.1788	0.1596	0.1531	0.1548	0.1743	0.2029	0.2258
Trapped	7030_1000_10	0.0099	0.0085	0.0077	0.0074	0.0071	0.0062	0.0055	0.0053	0.0111	0.0389	0.0678
Mobile	7030_1000_10	0.3549	0.6747	0.7610	0.7954	0.8142	0.8342	0.8414	0.8398	0.8146	0.7582	0.7064

Table C-38: Results for CO_2 states for the 70:30 net-to-gross model with 1000m shale length, 0, 1, 2, 5 and 10 degree dips. 200-8000 years

Fraction	Year	200	300	400	500	600	700	800	900	1000	2000	3000	4000	5000	6000	7000	8000
Dissolved	7030_1000_0	0.2875	0.2963	0.3041	0.3113	0.3185	0.3250	0.3310	0.3366	0.3416	0.3786	0.3956	0.4024	0.4055	0.4074	0.4088	0.4100
Trapped	7030_1000_0	0.0413	0.0466	0.0517	0.0573	0.0632	0.0691	0.0758	0.0791	0.0857	0.1329	0.1743	0.2106	0.2479	0.2795	0.3096	0.3352
Mobile	7030_1000_0	0.6712	0.6571	0.6441	0.6315	0.6182	0.6059	0.5933	0.5843	0.5727	0.4885	0.4301	0.3869	0.3467	0.3130	0.2815	0.2549
Dissolved	7030_1000_1	0.2386	0.2592	0.2779	0.2961	0.3116	0.3240	0.3339	0.3412	0.3468	0.3653	0.3702	0.3728	0.3744	0.3757	0.3768	0.3777
Trapped	7030_1000_1	0.0608	0.0823	0.1021	0.1201	0.1366	0.1486	0.1613	0.1732	0.1853	0.3030	0.4145	0.4979	0.5528	0.5813	0.5973	0.6064
Mobile	7030_1000_1	0.7006	0.6586	0.6201	0.5837	0.5518	0.5274	0.5048	0.4856	0.4679	0.3317	0.2152	0.1293	0.0728	0.0430	0.0259	0.0160
Dissolved	7030_1000_2	0.2542	0.2882	0.3160	0.3344	0.3458	0.3526	0.3573	0.3606	0.3630	0.3729	0.3763	0.3782	0.3796	0.3808	0.3819	0.3828
Trapped	7030_1000_2	0.0829	0.1197	0.1476	0.1709	0.1907	0.2091	0.2292	0.2486	0.2665	0.4321	0.5405	0.5848	0.6016	0.6084	0.6114	0.6121
Mobile	7030_1000_2	0.6629	0.5921	0.5364	0.4948	0.4635	0.4383	0.4136	0.3908	0.3705	0.1950	0.0832	0.0370	0.0187	0.0107	0.0067	0.0050
Dissolved	7030_1000_5	0.2906	0.3299	0.3445	0.3521	0.3566	0.3595	0.3616	0.3632	0.3645	0.3706	0.3735	0.3758	0.3777	0.3795	0.3810	0.3825
Trapped	7030_1000_5	0.1372	0.1869	0.2291	0.2640	0.2960	0.3291	0.3603	0.3888	0.4180	0.5745	0.6103	0.6182	0.6187	0.6176	0.6163	0.6150
Mobile	7030_1000_5	0.5722	0.4832	0.4265	0.3839	0.3474	0.3114	0.2781	0.2480	0.2176	0.0550	0.0162	0.0060	0.0036	0.0029	0.0027	0.0025
Dissolved	7030_1000_10	0.3116	0.3337	0.3427	0.3477	0.3508	0.3530	0.3547	0.3561	0.3572	0.3639	0.3682	0.3717	0.3746	0.3772	0.3794	0.3814
Trapped	7030_1000_10	0.1739	0.2381	0.2880	0.3368	0.3792	0.4143	0.4490	0.4782	0.5037	0.6096	0.6238	0.6242	0.6225	0.6202	0.6182	0.6162
Mobile	7030_1000_10	0.5144	0.4281	0.3693	0.3155	0.2701	0.2326	0.1963	0.1657	0.1391	0.0265	0.0080	0.0041	0.0029	0.0026	0.0024	0.0024

Table C-39: Results for CO_2 states for the 70:30 net-to-gross model with 3000m shale length. 0, 1, 2, 5 and 10 degree dips. 1-100 years

Fraction	Year	1	5	10	15	20	30	40	50	60	80	100
Dissolved	7030_3000_0	0.8938	0.6319	0.4846	0.4079	0.3624	0.3113	0.2819	0.2636	0.2728	0.2796	0.2824
Trapped	7030_3000_0	0.0027	0.0041	0.0060	0.0059	0.0055	0.0051	0.0047	0.0051	0.0069	0.0117	0.0164
Mobile	7030_3000_0	0.1035	0.3640	0.5094	0.5862	0.6321	0.6836	0.7134	0.7313	0.7204	0.7087	0.7012
Dissolved	7030_3000_1	0.6835	0.3591	0.2683	0.2343	0.2176	0.2030	0.1956	0.1912	0.2013	0.2108	0.2171
Trapped	7030_3000_1	0.0079	0.0090	0.0077	0.0077	0.0067	0.0057	0.0062	0.0065	0.0089	0.0157	0.0217
Mobile	7030_3000_1	0.3086	0.6319	0.7239	0.7580	0.7756	0.7913	0.7982	0.8023	0.7898	0.7735	0.7612
Dissolved	7030_3000_2	0.6760	0.3522	0.2619	0.2283	0.2112	0.1961	0.1893	0.1851	0.1965	0.2094	0.2188
Trapped	7030_3000_2	0.0079	0.0096	0.0082	0.0076	0.0070	0.0059	0.0062	0.0061	0.0088	0.0169	0.0251
Mobile	7030_3000_2	0.3161	0.6382	0.7299	0.7641	0.7818	0.7980	0.8045	0.8088	0.7947	0.7737	0.7561
Dissolved	7030_3000_5	0.6758	0.3481	0.2565	0.2226	0.2050	0.1905	0.1849	0.1803	0.1940	0.2119	0.2267
Trapped	7030_3000_5	0.0113	0.0098	0.0080	0.0072	0.0069	0.0062	0.0060	0.0058	0.0103	0.0253	0.0424
Mobile	7030_3000_5	0.3129	0.6421	0.7355	0.7702	0.7881	0.8034	0.8091	0.8139	0.7957	0.7627	0.7309
Dissolved	7030_3000_10	0.6600	0.3343	0.2456	0.2114	0.1943	0.1793	0.1730	0.1695	0.1859	0.2098	0.2296
Trapped	7030_3000_10	0.0101	0.0070	0.0093	0.0082	0.0077	0.0065	0.0061	0.0063	0.0103	0.0306	0.0568
Mobile	7030_3000_10	0.3300	0.6587	0.7451	0.7804	0.7980	0.8142	0.8208	0.8242	0.8038	0.7596	0.7136

Table C-40: Results for CO_2 states for the 70:30 net-to-gross model with 3000m shale length, 0, 1, 2, 5 and 10 degree dips. 200-8000 years

Fraction	Year	200	300	400	500	600	700	800	900	1000	2000	3000	4000	5000	6000	7000	8000
Dissolved	7030_3000_0	0.2888	0.2942	0.2993	0.3043	0.3088	0.3134	0.3175	0.3214	0.3257	0.3634	0.3824	0.3925	0.3972	0.3998	0.4015	0.4027
Trapped	7030_3000_0	0.0276	0.0322	0.0359	0.0399	0.0437	0.0476	0.0519	0.0563	0.0606	0.1016	0.1373	0.1740	0.2094	0.2400	0.2759	0.3091
Mobile	7030_3000_0	0.6836	0.6736	0.6648	0.6558	0.6475	0.6389	0.6306	0.6223	0.6137	0.5350	0.4803	0.4335	0.3934	0.3601	0.3226	0.2882
Dissolved	7030_3000_1	0.2415	0.2606	0.2762	0.2890	0.3001	0.3097	0.3176	0.3241	0.3293	0.3502	0.3555	0.3579	0.3595	0.3606	0.3615	0.3622
Trapped	7030_3000_1	0.0452	0.0674	0.0901	0.1109	0.1294	0.1462	0.1611	0.1738	0.1866	0.3121	0.4201	0.5011	0.5544	0.5878	0.6070	0.6176
Mobile	7030_3000_1	0.7133	0.6720	0.6337	0.6001	0.5705	0.5441	0.5212	0.5021	0.4840	0.3378	0.2244	0.1410	0.0861	0.0516	0.0315	0.0202
Dissolved	7030_3000_2	0.2543	0.2798	0.2999	0.3151	0.3252	0.3323	0.3374	0.3409	0.3435	0.3536	0.3566	0.3583	0.3595	0.3605	0.3614	0.3622
Trapped	7030_3000_2	0.0688	0.1128	0.1503	0.1778	0.2007	0.2193	0.2388	0.2589	0.2776	0.4457	0.5534	0.6051	0.6257	0.6333	0.6360	0.6364
Mobile	7030_3000_2	0.6769	0.6075	0.5499	0.5070	0.4741	0.4483	0.4238	0.4002	0.3789	0.2008	0.0899	0.0366	0.0147	0.0062	0.0026	0.0014
Dissolved	7030_3000_5	0.2787	0.3095	0.3250	0.3325	0.3370	0.3400	0.3422	0.3438	0.3451	0.3510	0.3537	0.3557	0.3574	0.3590	0.3603	0.3616
Trapped	7030_3000_5	0.1362	0.1997	0.2440	0.2838	0.3168	0.3475	0.3774	0.4063	0.4343	0.5975	0.6369	0.6424	0.6420	0.6407	0.6394	0.6382
Mobile	7030_3000_5	0.5851	0.4908	0.4310	0.3837	0.3463	0.3125	0.2805	0.2499	0.2206	0.0515	0.0093	0.0019	0.0006	0.0004	0.0002	0.0002
Dissolved	7030_3000_10	0.2911	0.3147	0.3240	0.3292	0.3325	0.3348	0.3365	0.3378	0.3389	0.3453	0.3493	0.3526	0.3554	0.3580	0.3602	0.3623
Trapped	7030_3000_10	0.1801	0.2506	0.3071	0.3525	0.3916	0.4296	0.4642	0.4931	0.5188	0.6349	0.6474	0.6464	0.6440	0.6417	0.6395	0.6376
Mobile	7030_3000_10	0.5287	0.4347	0.3689	0.3183	0.2759	0.2356	0.1993	0.1691	0.1422	0.0198	0.0033	0.0010	0.0005	0.0003	0.0002	0.0001

Table C-41: Results for CO_2 states for the 80:20 net-to-gross model with 100m shale length. 0, 1, 2, 5 and 10 degree dips. 1-100 years

Fraction	Year	1	5	10	15	20	30	40	50	60	80	100
Dissolved	8020_100_0	0.8988	0.6453	0.4991	0.4195	0.3716	0.3163	0.2842	0.2625	0.2725	0.2850	0.2947
Trapped	8020_100_0	0.0028	0.0045	0.0057	0.0054	0.0059	0.0059	0.0068	0.0081	0.0183	0.0455	0.0650
Mobile	8020_100_0	0.0984	0.3502	0.4952	0.5751	0.6225	0.6777	0.7090	0.7294	0.7093	0.6696	0.6404
Dissolved	8020_100_1	0.7099	0.3841	0.2872	0.2458	0.2247	0.2062	0.1959	0.1878	0.1999	0.2153	0.2273
Trapped	8020_100_1	0.0090	0.0092	0.0086	0.0071	0.0071	0.0068	0.0075	0.0091	0.0190	0.0482	0.0704
Mobile	8020_100_1	0.2812	0.6067	0.7042	0.7471	0.7682	0.7871	0.7966	0.8032	0.7810	0.7365	0.7023
Dissolved	8020_100_2	0.6960	0.3711	0.2771	0.2375	0.2169	0.1987	0.1896	0.1817	0.1955	0.2141	0.2288
Trapped	8020_100_2	0.0085	0.0093	0.0084	0.0072	0.0072	0.0068	0.0069	0.0088	0.0189	0.0480	0.0729
Mobile	8020_100_2	0.2955	0.6196	0.7146	0.7553	0.7760	0.7945	0.8035	0.8095	0.7856	0.7379	0.6982
Dissolved	8020_100_5	0.6770	0.3514	0.2602	0.2226	0.2027	0.1856	0.1787	0.1734	0.1913	0.2174	0.2383
Trapped	8020_100_5	0.0083	0.0095	0.0076	0.0071	0.0073	0.0066	0.0061	0.0074	0.0174	0.0496	0.0825
Mobile	8020_100_5	0.3147	0.6390	0.7322	0.7703	0.7900	0.8078	0.8152	0.8192	0.7914	0.7330	0.6792
Dissolved	8020_100_10	0.6861	0.3566	0.2605	0.2217	0.2005	0.1798	0.1711	0.1667	0.1876	0.2193	0.2429
Trapped	8020_100_10	0.0111	0.0096	0.0078	0.0072	0.0072	0.0064	0.0060	0.0063	0.0131	0.0445	0.0809
Mobile	8020_100_10	0.3028	0.6338	0.7316	0.7711	0.7923	0.8138	0.8229	0.8270	0.7993	0.7362	0.6761

Table C-42: Results for CO_2 states for the 80:20 net-to-gross model with 100m shale length, 0, 1, 2, 5 and 10 degree dips. 200-8000 years

Fraction	Year	200	300	400	500	600	700	800	900	1000	2000	3000	4000	5000	6000	7000	8000
Dissolved	8020_100_0	0.3195	0.3280	0.3331	0.3364	0.3387	0.3407	0.3423	0.3437	0.3449	0.3513	0.3534	0.3551	0.3567	0.3577	0.3589	0.3601
Trapped	8020_100_0	0.1369	0.1710	0.1952	0.2188	0.2369	0.2515	0.2674	0.2764	0.2821	0.3326	0.3641	0.3881	0.4073	0.4236	0.4372	0.4466
Mobile	8020_100_0	0.5435	0.5010	0.4717	0.4448	0.4244	0.4077	0.3903	0.3799	0.3730	0.3161	0.2825	0.2568	0.2360	0.2187	0.2038	0.1933
Dissolved	8020_100_1	0.2630	0.2808	0.2921	0.2996	0.3049	0.3089	0.3130	0.3169	0.3200	0.3332	0.3386	0.3418	0.3445	0.3469	0.3490	0.3509
Trapped	8020_100_1	0.1448	0.2028	0.2523	0.2944	0.3288	0.3569	0.3814	0.4031	0.4235	0.5238	0.5625	0.5814	0.5887	0.5934	0.5957	0.5967
Mobile	8020_100_1	0.5922	0.5164	0.4557	0.4060	0.3663	0.3341	0.3056	0.2800	0.2565	0.1431	0.0989	0.0768	0.0668	0.0597	0.0553	0.0524
Dissolved	8020_100_2	0.2737	0.2926	0.3017	0.3075	0.3134	0.3167	0.3192	0.3205	0.3212	0.3280	0.3318	0.3350	0.3378	0.3402	0.3424	0.3443
Trapped	8020_100_2	0.1682	0.2461	0.3076	0.3546	0.3939	0.4263	0.4524	0.4741	0.4933	0.5817	0.6087	0.6166	0.6207	0.6224	0.6232	0.6238
Mobile	8020_100_2	0.5582	0.4613	0.3907	0.3379	0.2927	0.2570	0.2284	0.2054	0.1855	0.0903	0.0595	0.0484	0.0415	0.0374	0.0344	0.0318
Dissolved	8020_100_5	0.2901	0.3032	0.3097	0.3144	0.3172	0.3194	0.3209	0.3222	0.3231	0.3301	0.3354	0.3400	0.3440	0.3475	0.3506	0.3534
Trapped	8020_100_5	0.2207	0.3166	0.3856	0.4350	0.4747	0.5040	0.5266	0.5451	0.5601	0.6236	0.6381	0.6430	0.6444	0.6441	0.6426	0.6410
Mobile	8020_100_5	0.4892	0.3801	0.3047	0.2506	0.2081	0.1767	0.1525	0.1327	0.1168	0.0464	0.0265	0.0170	0.0117	0.0084	0.0067	0.0056
Dissolved	8020_100_10	0.2931	0.3047	0.3106	0.3142	0.3169	0.3187	0.3204	0.3219	0.3233	0.3338	0.3417	0.3483	0.3538	0.3586	0.3627	0.3663
Trapped	8020_100_10	0.2349	0.3419	0.4155	0.4690	0.5094	0.5420	0.5646	0.5824	0.5960	0.6441	0.6510	0.6487	0.6443	0.6400	0.6362	0.6328
Mobile	8020_100_10	0.4720	0.3534	0.2740	0.2168	0.1737	0.1394	0.1150	0.0957	0.0807	0.0221	0.0073	0.0030	0.0019	0.0014	0.0011	0.0009

Table C-43: Results for CO_2 states for the 80:20 net-to-gross model with 300m shale length. 0, 1, 2, 5 and 10 degree dips. 1-100 years

Fraction	Year	1	5	10	15	20	30	40	50	60	80	100
Dissolved	8020_300_0	0.8972	0.6415	0.4931	0.4134	0.3641	0.3077	0.2791	0.2652	0.2737	0.2838	0.2915
Trapped	8020_300_0	0.0026	0.0049	0.0054	0.0053	0.0054	0.0057	0.0054	0.0057	0.0147	0.0334	0.0445
Mobile	8020_300_0	0.1002	0.3537	0.5014	0.5813	0.6305	0.6866	0.7154	0.7291	0.7117	0.6829	0.6639
Dissolved	8020_300_1	0.7075	0.3821	0.2810	0.2394	0.2167	0.1943	0.1849	0.1823	0.1928	0.2070	0.2183
Trapped	8020_300_1	0.0079	0.0090	0.0079	0.0077	0.0068	0.0064	0.0060	0.0057	0.0148	0.0360	0.0508
Mobile	8020_300_1	0.2846	0.6089	0.7111	0.7530	0.7764	0.7993	0.8091	0.8120	0.7923	0.7570	0.7309
Dissolved	8020_300_2	0.6939	0.3696	0.2715	0.2309	0.2085	0.1859	0.1758	0.1730	0.1855	0.2037	0.2182
Trapped	8020_300_2	0.0083	0.0092	0.0079	0.0069	0.0066	0.0063	0.0058	0.0056	0.0148	0.0384	0.0590
Mobile	8020_300_2	0.2978	0.6212	0.7206	0.7622	0.7849	0.8077	0.8183	0.8214	0.7997	0.7579	0.7228
Dissolved	8020_300_5	0.6760	0.3511	0.2570	0.2184	0.1975	0.1763	0.1672	0.1632	0.1791	0.2041	0.2242
Trapped	8020_300_5	0.0078	0.0102	0.0085	0.0068	0.0067	0.0064	0.0057	0.0056	0.0161	0.0523	0.0868
Mobile	8020_300_5	0.3162	0.6387	0.7346	0.7748	0.7958	0.8173	0.8271	0.8312	0.8048	0.7436	0.6889
Dissolved	8020_300_10	0.6864	0.3577	0.2594	0.2191	0.1975	0.1755	0.1653	0.1598	0.1782	0.2074	0.2313
Trapped	8020_300_10	0.0089	0.0098	0.0079	0.0068	0.0066	0.0069	0.0063	0.0058	0.0140	0.0549	0.0962
Mobile	8020_300_10	0.3046	0.6325	0.7327	0.7741	0.7959	0.8176	0.8284	0.8344	0.8078	0.7377	0.6725

Table C-44: Results for CO_2 states for the 80:20 net-to-gross model with 300m shale length, 0, 1, 2, 5 and 10 degree dips. 200-8000 years

Fraction	Year	200	300	400	500	600	700	800	900	1000	2000	3000	4000	5000	6000	7000	8000
Dissolved	8020_300_0	0.3174	0.3327	0.3427	0.3497	0.3554	0.3597	0.3632	0.3661	0.3685	0.3832	0.3872	0.3898	0.3918	0.3933	0.3947	0.3960
Trapped	8020_300_0	0.0742	0.0903	0.1035	0.1176	0.1315	0.1445	0.1568	0.1679	0.1785	0.2424	0.2811	0.3157	0.3422	0.3661	0.3876	0.4042
Mobile	8020_300_0	0.6084	0.5771	0.5538	0.5327	0.5130	0.4958	0.4800	0.4660	0.4531	0.3744	0.3316	0.2945	0.2660	0.2406	0.2176	0.1997
Dissolved	8020_300_1	0.2570	0.2829	0.3025	0.3173	0.3274	0.3341	0.3388	0.3423	0.3450	0.3588	0.3645	0.3689	0.3723	0.3751	0.3775	0.3798
Trapped	8020_300_1	0.0982	0.1335	0.1712	0.2048	0.2335	0.2588	0.2801	0.3002	0.3172	0.4359	0.5081	0.5464	0.5691	0.5810	0.5872	0.5903
Mobile	8020_300_1	0.6449	0.5836	0.5262	0.4778	0.4391	0.4071	0.3810	0.3575	0.3378	0.2053	0.1274	0.0846	0.0586	0.0439	0.0353	0.0299
Dissolved	8020_300_2	0.2680	0.2997	0.3178	0.3279	0.3340	0.3380	0.3407	0.3429	0.3446	0.3540	0.3597	0.3642	0.3680	0.3714	0.3744	0.3771
Trapped	8020_300_2	0.1347	0.1946	0.2407	0.2794	0.3105	0.3378	0.3602	0.3818	0.4011	0.5275	0.5829	0.6046	0.6117	0.6138	0.6136	0.6127
Mobile	8020_300_2	0.5974	0.5057	0.4414	0.3927	0.3556	0.3242	0.2991	0.2754	0.2543	0.1185	0.0574	0.0312	0.0203	0.0148	0.0120	0.0102
Dissolved	8020_300_5	0.2872	0.3103	0.3197	0.3247	0.3280	0.3304	0.3323	0.3339	0.3352	0.3446	0.3517	0.3577	0.3630	0.3677	0.3717	0.3754
Trapped	8020_300_5	0.2122	0.2890	0.3470	0.3925	0.4288	0.4588	0.4851	0.5085	0.5293	0.6246	0.6409	0.6392	0.6349	0.6307	0.6268	0.6234
Mobile	8020_300_5	0.5005	0.4007	0.3333	0.2828	0.2432	0.2107	0.1826	0.1577	0.1354	0.0307	0.0074	0.0031	0.0021	0.0016	0.0014	0.0012
Dissolved	8020_300_10	0.2918	0.3077	0.3148	0.3190	0.3221	0.3245	0.3266	0.3284	0.3300	0.3428	0.3526	0.3607	0.3674	0.3731	0.3781	0.3825
Trapped	8020_300_10	0.2469	0.3378	0.4005	0.4496	0.4887	0.5204	0.5479	0.5707	0.5871	0.6445	0.6439	0.6375	0.6314	0.6259	0.6211	0.6168
Mobile	8020_300_10	0.4613	0.3545	0.2847	0.2314	0.1892	0.1551	0.1256	0.1009	0.0829	0.0127	0.0035	0.0018	0.0012	0.0009	0.0008	0.0006

Table C-45: Results for CO_2 states for the 80:20 net-to-gross model with 1000m shale length. 0, 1, 2, 5 and 10 degree dips. 1-100 years

Fraction	Year	1	5	10	15	20	30	40	50	60	80	100
Dissolved	8020_1000_0	0.8931	0.6275	0.4788	0.3993	0.3492	0.2955	0.2710	0.2564	0.2657	0.2725	0.2772
Trapped	8020_1000_0	0.0028	0.0046	0.0052	0.0056	0.0054	0.0048	0.0049	0.0061	0.0151	0.0364	0.0460
Mobile	8020_1000_0	0.1041	0.3679	0.5160	0.5951	0.6453	0.6996	0.7241	0.7376	0.7192	0.6911	0.6768
Dissolved	8020_1000_1	0.6928	0.3613	0.2670	0.2280	0.2052	0.1859	0.1833	0.1842	0.1955	0.2050	0.2123
Trapped	8020_1000_1	0.0072	0.0074	0.0075	0.0072	0.0067	0.0053	0.0057	0.0073	0.0179	0.0433	0.0579
Mobile	8020_1000_1	0.3000	0.6313	0.7255	0.7647	0.7880	0.8088	0.8110	0.8085	0.7866	0.7517	0.7298
Dissolved	8020_1000_2	0.6844	0.3533	0.2611	0.2226	0.2008	0.1791	0.1769	0.1789	0.1915	0.2057	0.2184
Trapped	8020_1000_2	0.0098	0.0086	0.0071	0.0073	0.0069	0.0056	0.0053	0.0067	0.0180	0.0475	0.0657
Mobile	8020_1000_2	0.3058	0.6381	0.7318	0.7701	0.7923	0.8153	0.8178	0.8144	0.7905	0.7468	0.7159
Dissolved	8020_1000_5	0.6857	0.3511	0.2572	0.2184	0.1967	0.1727	0.1666	0.1677	0.1853	0.2103	0.2322
Trapped	8020_1000_5	0.0079	0.0087	0.0095	0.0072	0.0068	0.0057	0.0056	0.0053	0.0188	0.0614	0.0974
Mobile	8020_1000_5	0.3064	0.6403	0.7333	0.7745	0.7965	0.8216	0.8278	0.8270	0.7959	0.7284	0.6704
Dissolved	8020_1000_10	0.6688	0.3385	0.2479	0.2116	0.1907	0.1688	0.1592	0.1559	0.1775	0.2129	0.2496
Trapped	8020_1000_10	0.0092	0.0094	0.0086	0.0086	0.0075	0.0060	0.0059	0.0056	0.0176	0.0665	0.1098
Mobile	8020_1000_10	0.3220	0.6520	0.7435	0.7798	0.8018	0.8253	0.8348	0.8385	0.8048	0.7206	0.6406

Table C-46: Results for CO_2 states for the 80:20 net-to-gross model with 1000m shale length, 0, 1, 2, 5 and 10 degree dips. 200-8000 years

Fraction	Year	200	300	400	500	600	700	800	900	1000	2000	3000	4000	5000	6000	7000	8000
Dissolved	8020_1000_0	0.2922	0.3021	0.3101	0.3170	0.3233	0.3289	0.3341	0.3387	0.3430	0.3659	0.3737	0.3787	0.3817	0.3838	0.3856	0.3871
Trapped	8020_1000_0	0.0656	0.0792	0.0908	0.1003	0.1078	0.1155	0.1219	0.1294	0.1368	0.2052	0.2449	0.2818	0.3166	0.3451	0.3689	0.3873
Mobile	8020_1000_0	0.6422	0.6187	0.5990	0.5827	0.5689	0.5556	0.5441	0.5318	0.5202	0.4288	0.3814	0.3395	0.3018	0.2711	0.2455	0.2256
Dissolved	8020_1000_1	0.2452	0.2713	0.2953	0.3154	0.3309	0.3420	0.3492	0.3540	0.3574	0.3706	0.3757	0.3793	0.3823	0.3848	0.3871	0.3892
Trapped	8020_1000_1	0.1042	0.1423	0.1699	0.1937	0.2131	0.2292	0.2433	0.2581	0.2722	0.3925	0.4806	0.5358	0.5652	0.5785	0.5845	0.5871
Mobile	8020_1000_1	0.6506	0.5863	0.5349	0.4908	0.4560	0.4288	0.4075	0.3879	0.3705	0.2369	0.1436	0.0848	0.0525	0.0366	0.0284	0.0237
Dissolved	8020_1000_2	0.2715	0.3164	0.3425	0.3571	0.3650	0.3697	0.3728	0.3751	0.3769	0.3854	0.3898	0.3934	0.3966	0.3995	0.4021	0.4045
Trapped	8020_1000_2	0.1423	0.1936	0.2300	0.2572	0.2808	0.3030	0.3233	0.3419	0.3589	0.4894	0.5557	0.5795	0.5862	0.5883	0.5874	0.5860
Mobile	8020_1000_2	0.5862	0.4900	0.4275	0.3858	0.3542	0.3273	0.3039	0.2829	0.2642	0.1251	0.0545	0.0271	0.0172	0.0122	0.0105	0.0096
Dissolved	8020_1000_5	0.3227	0.3551	0.3667	0.3723	0.3757	0.3780	0.3798	0.3812	0.3824	0.3898	0.3951	0.3998	0.4039	0.4076	0.4110	0.4141
Trapped	8020_1000_5	0.2147	0.2792	0.3274	0.3638	0.3934	0.4178	0.4395	0.4599	0.4770	0.5809	0.5973	0.5969	0.5935	0.5901	0.5868	0.5838
Mobile	8020_1000_5	0.4626	0.3657	0.3059	0.2639	0.2309	0.2042	0.1807	0.1589	0.1406	0.0293	0.0076	0.0033	0.0025	0.0023	0.0022	0.0022
Dissolved	8020_1000_10	0.3430	0.3624	0.3693	0.3732	0.3759	0.3779	0.3795	0.3810	0.3822	0.3916	0.3991	0.4054	0.4110	0.4157	0.4198	0.4235
Trapped	8020_1000_10	0.2527	0.3277	0.3794	0.4186	0.4491	0.4745	0.4960	0.5165	0.5346	0.5945	0.5970	0.5921	0.5869	0.5822	0.5782	0.5746
Mobile	8020_1000_10	0.4042	0.3099	0.2514	0.2082	0.1751	0.1476	0.1244	0.1025	0.0832	0.0139	0.0039	0.0024	0.0021	0.0021	0.0020	0.0019

Table C-47: Results for CO_2 states for the 80:20 net-to-gross model with 3000m shale length. 0, 1, 2, 5 and 10 degree dips. 1-100 years

Fraction	Year	1	5	10	15	20	30	40	50	60	80	100
Dissolved	8020_3000_0	0.8983	0.6430	0.4944	0.4126	0.3621	0.3085	0.2803	0.2635	0.2720	0.2788	0.2835
Trapped	8020_3000_0	0.0026	0.0055	0.0051	0.0054	0.0054	0.0050	0.0051	0.0060	0.0097	0.0204	0.0269
Mobile	8020_3000_0	0.0991	0.3515	0.5004	0.5820	0.6325	0.6864	0.7146	0.7305	0.7183	0.7008	0.6895
Dissolved	8020_3000_1	0.7062	0.3777	0.2789	0.2362	0.2128	0.1945	0.1904	0.1895	0.1997	0.2104	0.2187
Trapped	8020_3000_1	0.0063	0.0071	0.0077	0.0071	0.0066	0.0055	0.0057	0.0065	0.0112	0.0252	0.0351
Mobile	8020_3000_1	0.2876	0.6152	0.7134	0.7567	0.7806	0.8000	0.8039	0.8041	0.7891	0.7644	0.7462
Dissolved	8020_3000_2	0.6930	0.3656	0.2699	0.2290	0.2063	0.1860	0.1812	0.1809	0.1929	0.2073	0.2185
Trapped	8020_3000_2	0.0060	0.0062	0.0080	0.0083	0.0071	0.0060	0.0052	0.0059	0.0109	0.0267	0.0409
Mobile	8020_3000_2	0.3010	0.6282	0.7221	0.7627	0.7866	0.8080	0.8136	0.8132	0.7963	0.7660	0.7407
Dissolved	8020_3000_5	0.6725	0.3469	0.2554	0.2179	0.1967	0.1764	0.1690	0.1680	0.1835	0.2050	0.2222
Trapped	8020_3000_5	0.0094	0.0084	0.0080	0.0078	0.0071	0.0062	0.0055	0.0050	0.0112	0.0365	0.0619
Mobile	8020_3000_5	0.3181	0.6448	0.7366	0.7744	0.7962	0.8174	0.8255	0.8270	0.8053	0.7585	0.7160
Dissolved	8020_3000_10	0.6844	0.3534	0.2579	0.2188	0.1970	0.1747	0.1643	0.1602	0.1783	0.2043	0.2248
Trapped	8020_3000_10	0.0096	0.0089	0.0083	0.0081	0.0076	0.0067	0.0058	0.0054	0.0117	0.0444	0.0814
Mobile	8020_3000_10	0.3060	0.6377	0.7337	0.7731	0.7953	0.8186	0.8299	0.8344	0.8100	0.7513	0.6938

Table C-48: Results for CO_2 states for the 80:20 net-to-gross model with 3000m shale length, 0, 1, 2, 5 and 10 degree dips. 200-8000 years

Fraction	Year	200	300	400	500	600	700	800	900	1000	2000	3000	4000	5000	6000	7000	8000
Dissolved	8020_3000_0	0.2995	0.3112	0.3210	0.3298	0.3374	0.3442	0.3503	0.3562	0.3617	0.3915	0.3989	0.4021	0.4041	0.4055	0.4066	0.4076
Trapped	8020_3000_0	0.0455	0.0557	0.0619	0.0677	0.0744	0.0806	0.0876	0.0940	0.0998	0.1514	0.1937	0.2331	0.2691	0.3039	0.3353	0.3615
Mobile	8020_3000_0	0.6549	0.6331	0.6171	0.6024	0.5883	0.5752	0.5620	0.5498	0.5385	0.4571	0.4074	0.3649	0.3268	0.2906	0.2581	0.2310
Dissolved	8020_3000_1	0.2487	0.2733	0.2933	0.3092	0.3218	0.3317	0.3387	0.3438	0.3475	0.3612	0.3655	0.3680	0.3698	0.3712	0.3724	0.3735
Trapped	8020_3000_1	0.0708	0.0979	0.1220	0.1451	0.1656	0.1834	0.1996	0.2148	0.2313	0.3779	0.4836	0.5470	0.5850	0.6058	0.6159	0.6202
Mobile	8020_3000_1	0.6805	0.6289	0.5848	0.5457	0.5126	0.4849	0.4617	0.4414	0.4212	0.2610	0.1509	0.0851	0.0452	0.0231	0.0118	0.0063
Dissolved	8020_3000_2	0.2616	0.2916	0.3127	0.3258	0.3340	0.3395	0.3434	0.3463	0.3484	0.3575	0.3609	0.3633	0.3652	0.3669	0.3684	0.3697
Trapped	8020_3000_2	0.0970	0.1456	0.1820	0.2107	0.2370	0.2627	0.2864	0.3084	0.3302	0.4990	0.5762	0.6097	0.6241	0.6292	0.6297	0.6292
Mobile	8020_3000_2	0.6414	0.5629	0.5053	0.4635	0.4290	0.3978	0.3702	0.3453	0.3214	0.1435	0.0628	0.0270	0.0107	0.0039	0.0019	0.0010
Dissolved	8020_3000_5	0.2807	0.3098	0.3237	0.3316	0.3363	0.3395	0.3418	0.3436	0.3449	0.3520	0.3560	0.3591	0.3618	0.3642	0.3664	0.3683
Trapped	8020_3000_5	0.1697	0.2323	0.2815	0.3227	0.3618	0.3958	0.4271	0.4543	0.4789	0.6009	0.6313	0.6385	0.6377	0.6356	0.6335	0.6316
Mobile	8020_3000_5	0.5497	0.4578	0.3948	0.3457	0.3019	0.2648	0.2311	0.2022	0.1762	0.0471	0.0127	0.0024	0.0005	0.0002	0.0002	0.0001
Dissolved	8020_3000_10	0.2906	0.3130	0.3230	0.3286	0.3322	0.3347	0.3367	0.3382	0.3395	0.3476	0.3530	0.3575	0.3614	0.3647	0.3677	0.3703
Trapped	8020_3000_10	0.2099	0.2841	0.3429	0.3925	0.4332	0.4697	0.4997	0.5248	0.5470	0.6297	0.6435	0.6420	0.6384	0.6352	0.6323	0.6297
Mobile	8020_3000_10	0.4995	0.4030	0.3341	0.2789	0.2346	0.1956	0.1636	0.1370	0.1135	0.0227	0.0035	0.0005	0.0002	0.0001	0.0001	0.0000

Table C-49: Migration results for CO_2 states for the homogeneous models, 0, 1, 2, 5 and 10 degree dips. 1-8000 years (in kilometres)

Year	1	5	10	15	20	30	40	50	60	80	100	200	300	400	500	700	800	900	1000
Homogeneous 0	1.692	1.916	2.108	2.205	2.363	2.716	2.987	3.222	3.350	3.521	3.631	4.066	4.364	4.495	4.594	4.792	4.862	4.891	4.891
Homogeneous 1	1.692	1.916	2.108	2.213	2.347	2.821	3.222	3.641	3.852	4.264	4.563	6.114	7.505	8.730	8.853	8.880	8.880	8.880	8.880
Homogeneous 2	1.692	1.916	2.122	2.239	2.347	2.848	3.423	3.852	4.165	4.762	5.189	7.619	8.802	8.827	8.827	8.827	8.827	8.827	8.827
Homogeneous 5	1.692	1.916	2.158	2.362	2.495	2.780	3.631	4.066	4.563	5.487	6.312	8.705	8.783	8.783	8.783	8.783	8.783	8.783	8.783
Homogeneous 10	1.692	1.856	2.143	2.362	2.565	2.800	3.523	4.052	4.733	5.800	7.306	8.734	8.756	8.756	8.756	8.756	8.756	8.756	8.756

Year	2000	3000	4000	5000	6000	7000	8000
Homogeneous 0	4.891	4.891	4.891	4.891	4.891	4.891	4.891
Homogeneous 1	8.880	8.880	8.880	8.880	8.880	8.880	8.880
Homogeneous 2	8.827	8.827	8.827	8.827	8.827	8.827	8.827
Homogeneous 5	8.783	8.783	8.756	8.756	8.756	8.756	8.756
Homogeneous 10	8.756	8.756	8.756	8.756	8.756	8.756	8.756

Table C-50: Migration results for CO_2 states for all the 40:60 net to gross models. 1-1000 years (in kilometres)

Year	1	5	10	15	20	30	40	50	60	80	100	200	300	400	500	700	800	900	1000
4060_100_0	2.094	2.746	3.170	3.611	3.846	4.600	5.040	5.400	5.687	5.744	5.857	5.857	5.857	5.857	5.857	5.857	5.857	5.818	5.818
4060_100_1	2.094	2.746	3.100	3.688	4.008	4.951	5.129	5.765	6.135	6.322	6.322	6.568	6.792	7.072	7.267	7.388	7.584	7.780	7.976
4060_100_2	2.094	2.679	3.100	3.534	3.846	4.862	5.129	5.129	5.673	5.857	6.042	6.474	6.951	7.365	7.682	8.312	8.609	8.609	8.609
4060_100_5	1.997	2.603	3.032	3.392	3.767	4.427	5.040	5.219	5.673	6.228	6.322	6.853	7.522	7.976	8.611	8.805	8.805	8.805	8.805
4060_100_10	1.900	2.531	2.902	3.175	3.469	4.174	4.951	5.219	5.857	6.322	6.474	7.426	7.810	8.778	8.805	8.805	8.805	8.805	8.805
4060_300_0	1.932	2.604	3.173	3.767	3.951	4.513	4.862	5.491	6.042	6.250	6.345	6.345	6.345	6.345	6.345	6.250	6.250	6.250	6.250
4060_300_1	1.916	2.491	3.139	3.649	3.886	4.385	4.730	5.264	5.996	6.392	6.487	6.773	7.035	7.337	7.638	8.247	8.544	8.544	8.544
4060_300_2	1.932	2.518	3.105	3.688	3.927	4.427	4.862	5.582	6.322	6.725	6.821	7.368	7.996	8.593	8.593	8.805	8.805	8.805	8.805
4060_300_5	1.932	2.416	2.976	3.688	3.927	4.427	4.951	5.491	6.440	6.916	7.271	8.502	8.685	8.805	8.805	8.805	8.805	8.805	8.805
4060_300_10	1.837	2.287	2.753	3.243	3.767	4.203	4.774	5.309	6.042	6.853	7.465	8.685	8.805	8.805	8.805	8.805	8.805	8.805	8.805
4060_1000_0	1.932	2.641	3.173	3.459	3.534	4.276	5.129	5.818	5.911	6.003	6.102	6.122	6.122	6.122	6.122	6.122	6.122	6.122	6.122
4060_1000_1	1.932	2.641	3.242	3.459	3.534	4.276	5.075	5.377	5.806	6.102	6.289	6.891	7.271	7.854	8.341	8.579	8.579	8.593	8.609
4060_1000_2	1.932	2.641	3.242	3.459	3.534	4.377	5.176	5.477	5.905	6.389	6.690	7.783	8.609	8.609	8.708	8.805	8.805	8.805	8.805
4060_1000_5	1.932	2.595	3.313	3.534	3.611	4.477	5.276	5.765	6.382	6.910	7.599	8.805	8.805	8.805	8.805	8.805	8.805	8.805	8.805
4060_1000_10	1.900	2.595	3.313	3.534	3.833	4.804	5.377	6.062	6.690	7.705	8.531	8.805	8.805	8.805	8.805	8.805	8.805	8.805	8.805
4060_3000_0	2.144	2.797	3.173	3.688	4.289	5.219	6.440	7.139	7.561	7.755	7.852	7.852	7.852	7.852	7.852	7.852	7.852	7.852	7.852
4060_3000_1	2.102	2.854	3.242	3.767	4.342	5.219	6.509	7.300	7.755	8.047	8.144	8.436	8.805	8.805	8.805	8.805	8.805	8.805	8.805
4060_3000_2	2.102	2.854	3.242	3.927	4.427	5.400	6.916	7.658	8.047	8.611	8.708	8.805	8.805	8.805	8.805	8.805	8.805	8.805	8.805
4060_3000_5	2.062	2.854	3.313	4.091	4.904	6.509	7.589	8.321	8.805	8.805	8.805	8.805	8.805	8.805	8.805	8.805	8.805	8.805	8.805
4060_3000_10	2.054	2.797	3.317	4.342	5.129	6.792	8.047	8.805	8.805	8.805	8.805	8.805	8.805	8.805	8.805	8.805	8.805	8.805	8.805

Table C-51: Migration results for CO_2 states for all the 40:60 net to gross models. 2000-8000 years (in kilometres)

Year	2000	3000	4000	5000	6000	7000	8000
4060_100_0	5.818	5.818	5.818	5.818	5.818	5.818	5.818
4060_100_1	8.546	8.685	8.685	8.685	8.685	8.685	8.685
4060_100_2	8.778	8.778	8.778	8.778	8.753	8.753	8.753
4060_100_5	8.805	8.805	8.805	8.805	8.805	8.805	8.778
4060_100_10	8.805	8.805	8.805	8.778	8.778	8.778	8.778
4060_300_0	6.250	6.250	6.250	6.250	6.250	6.250	6.250
4060_300_1	8.756	8.756	8.756	8.756	8.756	8.756	8.756
4060_300_2	8.805	8.805	8.805	8.805	8.805	8.805	8.805
4060_300_5	8.805	8.805	8.805	8.805	8.805	8.805	8.805
4060_300_10	8.805	8.805	8.805	8.778	8.778	8.778	8.778
4060_1000_0	6.102	6.102	6.102	6.047	6.047	6.047	6.047
4060_1000_1	8.805	8.805	8.805	8.805	8.805	8.805	8.805
4060_1000_2	8.805	8.805	8.805	8.805	8.805	8.805	8.805
4060_1000_5	8.805	8.805	8.805	8.805	8.805	8.805	8.805
4060_1000_10	8.805	8.805	8.805	8.805	8.805	8.805	8.805
4060_3000_0	7.755	7.755	7.755	7.755	7.755	7.755	7.755
4060_3000_1	8.805	8.805	8.805	8.805	8.805	8.805	8.805
4060_3000_2	8.805	8.805	8.805	8.805	8.805	8.805	8.805
4060_3000_5	8.805	8.805	8.805	8.805	8.805	8.805	8.805
4060_3000_10	8.805	8.805	8.805	8.805	8.805	8.805	8.805

Table C-52: Migration results for CO_2 states for all the 50:50 net to gross models. 1-1000 years (in kilometres)

Year	1	5	10	15	20	30	40	50	60	80	100	200	300	400	500	700	800	900	1000
5050_100_0	1.916	2.618	2.944	3.072	3.430	4.132	4.556	4.643	4.859	4.995	4.995	4.995	4.995	4.995	4.995	4.995	4.995	4.995	4.995
5050_100_1	1.916	2.578	2.944	3.139	3.430	4.132	4.556	4.556	4.770	4.995	5.087	5.445	5.803	5.930	6.332	7.035	7.337	7.638	7.839
5050_100_2	1.916	2.528	2.944	3.139	3.430	4.216	4.556	4.643	4.859	5.174	5.445	5.975	6.556	7.218	7.739	8.466	8.659	8.659	8.756
5050_100_5	1.820	2.528	3.007	3.277	3.430	4.385	4.643	4.859	5.174	5.536	5.885	7.218	8.369	8.756	8.756	8.756	8.756	8.756	8.756
5050_100_10	1.820	2.392	2.944	3.277	3.497	4.216	4.643	4.859	5.354	5.791	6.360	8.369	8.756	8.756	8.756	8.756	8.756	8.756	8.756
5050_300_0	1.820	2.406	3.007	3.497	4.194	5.264	6.182	6.462	6.650	6.650	6.650	6.650	6.650	6.650	6.650	6.650	6.650	6.650	6.650
5050_300_1	1.820	2.406	3.007	3.524	4.194	5.536	6.275	6.582	6.839	7.028	7.123	7.409	7.881	8.502	8.502	8.756	8.756	8.756	8.756
5050_300_2	1.805	2.406	3.007	3.605	4.332	5.354	6.145	6.487	6.678	6.868	7.060	7.871	8.502	8.756	8.756	8.756	8.756	8.756	8.756
5050_300_5	1.805	2.440	3.139	3.909	4.556	5.536	6.298	6.773	7.060	7.513	7.901	8.681	8.756	8.756	8.756	8.756	8.756	8.756	8.756
5050_300_10	1.805	2.380	3.139	3.992	4.556	5.719	6.582	7.123	7.610	8.095	8.243	8.756	8.756	8.756	8.756	8.756	8.756	8.756	8.756
5050_1000_0	2.062	2.797	3.385	4.091	4.600	5.309	6.250	6.725	6.916	7.012	7.012	7.012	7.012	7.012	7.012	7.012	7.012	7.012	7.012
5050_1000_1	2.016	2.760	3.459	4.174	4.687	5.309	6.285	6.821	7.108	7.368	7.561	8.047	8.241	8.436	8.753	8.778	8.778	8.778	8.778
5050_1000_2	2.016	2.797	3.459	4.258	4.862	5.582	6.474	7.012	7.465	8.047	8.241	8.632	8.753	8.778	8.778	8.805	8.805	8.805	8.805
5050_1000_5	2.009	2.839	3.611	4.513	5.129	6.098	7.108	7.949	8.534	8.753	8.778	8.805	8.805	8.805	8.805	8.805	8.805	8.805	8.805
5050_1000_10	1.968	2.779	3.611	4.600	5.309	6.568	7.426	8.436	8.778	8.805	8.805	8.805	8.805	8.805	8.805	8.805	8.805	8.805	8.805
5050_3000_0	2.180	2.665	3.139	3.572	4.216	4.995	5.733	6.298	6.678	6.773	6.773	6.773	6.773	6.773	6.773	6.773	6.773	6.773	6.773
5050_3000_1	2.180	2.716	3.207	3.649	4.216	5.084	5.733	6.392	6.868	7.186	7.416	8.273	8.562	8.756	8.756	8.756	8.756	8.756	8.756
5050_3000_2	2.108	2.716	3.349	3.727	4.385	5.174	5.958	6.744	7.313	8.080	8.273	8.756	8.756	8.756	8.756	8.756	8.756	8.756	8.756
5050_3000_5	2.082	2.743	3.422	3.886	4.556	5.587	6.650	7.504	8.273	8.659	8.756	8.756	8.756	8.756	8.756	8.756	8.756	8.756	8.756
5050_3000_10	1.916	2.685	3.422	3.967	4.730	5.921	7.123	8.273	8.756	8.756	8.756	8.756	8.756	8.756	8.756	8.756	8.756	8.756	8.756

Table C-53: Migration results for CO_2 states for all the 50:50 net to gross models. 2000-8000 years (in kilometres)

Year	2000	3000	4000	5000	6000	7000	8000
5050_100_0	4.995	4.995	4.995	4.995	4.995	4.995	4.995
5050_100_1	8.443	8.457	8.457	8.457	8.457	8.457	8.457
5050_100_2	8.756	8.756	8.756	8.756	8.756	8.756	8.756
5050_100_5	8.756	8.756	8.756	8.756	8.756	8.756	8.756
5050_100_10	8.756	8.756	8.756	8.756	8.756	8.756	8.756
5050_300_0	6.582	6.556	6.556	6.556	6.556	6.556	6.556
5050_300_1	8.756	8.756	8.756	8.756	8.756	8.756	8.756
5050_300_2	8.756	8.756	8.756	8.756	8.756	8.756	8.756
5050_300_5	8.756	8.756	8.756	8.756	8.756	8.756	8.756
5050_300_10	8.756	8.756	8.756	8.756	8.756	8.756	8.756
5050_1000_0	7.012	6.982	6.916	6.916	6.916	6.916	6.916
5050_1000_1	8.805	8.805	8.805	8.805	8.805	8.805	8.805
5050_1000_2	8.805	8.805	8.805	8.805	8.805	8.805	8.805
5050_1000_5	8.805	8.805	8.805	8.805	8.805	8.805	8.805
5050_1000_10	8.805	8.805	8.805	8.805	8.805	8.805	8.805
5050_3000_0	6.678	6.678	6.678	6.678	6.678	6.678	6.678
5050_3000_1	8.756	8.756	8.756	8.756	8.756	8.756	8.756
5050_3000_2	8.756	8.756	8.756	8.756	8.756	8.756	8.756
5050_3000_5	8.756	8.756	8.756	8.756	8.756	8.756	8.756
5050_3000_10	8.756	8.756	8.756	8.756	8.756	8.756	8.756

Table C-54: Migration results for CO_2 states for all the 60:40 net to gross models. 1-1000 years (in kilometres)

Year	1	5	10	15	20	30	40	50	60	80	100	200	300	400	500	700	800	900	1000
6040_100_0	1.896	2.439	2.716	2.944	3.212	3.806	3.967	4.300	4.385	4.506	4.506	4.506	4.506	4.506	4.506	4.419	4.419	4.419	4.419
6040_100_1	1.896	2.439	2.716	2.996	3.212	3.886	4.049	4.300	4.556	4.730	4.818	5.045	5.084	5.403	5.587	6.138	6.439	6.640	6.740
6040_100_2	1.896	2.439	2.743	3.007	3.280	3.886	4.049	4.385	4.730	5.084	5.264	5.996	6.369	6.488	6.841	7.373	7.649	7.749	7.966
6040_100_5	1.886	2.399	2.743	3.065	3.288	3.967	4.216	4.643	5.084	5.628	6.089	6.773	8.004	8.615	8.615	8.615	8.615	8.615	8.615
6040_100_10	1.820	2.347	2.743	3.072	3.444	4.049	4.504	5.155	5.819	6.395	6.588	8.615	8.681	8.681	8.681	8.681	8.681	8.681	8.681
6040_300_0	1.896	2.331	2.665	3.082	3.430	4.132	4.770	5.220	5.403	5.495	5.495	5.495	5.495	5.495	5.495	5.445	5.445	5.445	5.403
6040_300_1	1.896	2.322	2.716	3.146	3.444	4.132	4.859	5.495	5.903	6.089	6.182	6.556	6.712	7.169	7.538	8.481	8.681	8.705	8.705
6040_300_2	1.896	2.380	2.716	3.146	3.497	4.161	5.039	5.811	6.182	6.369	6.556	7.195	8.216	8.538	8.705	8.756	8.756	8.756	8.756
6040_300_5	1.886	2.362	2.769	3.277	3.572	4.320	5.311	6.182	6.462	6.905	7.292	8.658	8.730	8.730	8.730	8.756	8.756	8.756	8.756
6040_300_10	1.856	2.322	2.743	3.280	3.607	4.499	5.416	6.275	6.905	7.513	8.017	8.730	8.756	8.756	8.756	8.756	8.756	8.756	8.756
6040_1000_0	1.856	2.267	2.769	3.139	3.349	3.572	3.849	4.419	4.635	4.732	4.732	4.732	4.709	4.724	4.728	4.824	4.828	4.841	4.841
6040_1000_1	1.820	2.239	2.769	3.207	3.422	3.649	3.978	4.593	4.877	5.126	5.389	6.231	7.028	7.600	7.940	8.756	8.756	8.756	8.756
6040_1000_2	1.820	2.239	2.769	3.277	3.497	3.727	4.134	4.779	5.097	5.584	5.877	7.409	7.950	8.756	8.756	8.756	8.756	8.756	8.756
6040_1000_5	1.789	2.182	2.665	3.349	3.649	3.886	4.421	5.097	5.681	6.521	7.038	8.756	8.756	8.756	8.756	8.756	8.756	8.756	8.756
6040_1000_10	1.789	2.182	2.578	3.277	3.649	3.967	4.585	5.389	6.073	6.861	7.641	8.756	8.756	8.756	8.756	8.756	8.756	8.756	8.756
6040_3000_0	2.082	2.618	3.072	3.430	3.967	4.770	5.174	5.495	5.827	5.921	5.921	5.921	5.921	5.921	5.921	5.921	5.921	5.921	5.921
6040_3000_1	2.012	2.618	3.072	3.497	4.049	4.818	5.220	5.679	6.015	6.169	6.360	6.933	7.600	8.273	8.659	8.756	8.756	8.756	8.756
6040_3000_2	2.012	2.618	3.139	3.572	4.132	4.949	5.403	6.015	6.521	6.710	6.839	8.369	8.756	8.756	8.756	8.756	8.756	8.756	8.756
6040_3000_5	1.984	2.578	3.212	3.649	4.300	5.270	6.051	6.900	7.600	8.080	8.466	8.756	8.756	8.756	8.756	8.756	8.756	8.756	8.756
6040_3000_10	1.950	2.578	3.146	3.686	4.470	5.547	6.805	7.792	8.369	8.756	8.756	8.756	8.756	8.756	8.756	8.756	8.756	8.756	8.756

Table C-55: Migration results for CO_2 states for all the 60:40 net to gross models. 2000-8000 years (in kilometres)

Year	2000	3000	4000	5000	6000	7000	8000
6040_100_0	4.419	4.419	4.419	4.419	4.419	4.419	4.419
6040_100_1	8.544	8.681	8.694	8.714	8.714	8.756	8.756
6040_100_2	8.560	8.544	8.544	8.544	8.544	8.544	8.544
6040_100_5	8.596	8.596	8.596	8.596	8.596	8.596	8.596
6040_100_10	8.681	8.681	8.681	8.681	8.681	8.681	8.596
6040_300_0	5.403	5.403	5.445	5.445	5.445	5.445	5.445
6040_300_1	8.705	8.705	8.705	8.705	8.705	8.705	8.705
6040_300_2	8.756	8.756	8.730	8.730	8.730	8.730	8.730
6040_300_5	8.756	8.756	8.756	8.756	8.730	8.730	8.730
6040_300_10	8.756	8.756	8.756	8.730	8.730	8.730	8.730
6040_1000_0	4.741	4.741	4.741	4.741	4.741	4.741	4.741
6040_1000_1	8.756	8.756	8.756	8.756	8.756	8.756	8.756
6040_1000_2	8.756	8.756	8.756	8.756	8.756	8.730	8.730
6040_1000_5	8.756	8.756	8.730	8.730	8.730	8.730	8.730
6040_1000_10	8.730	8.730	8.730	8.730	8.730	8.730	8.730
6040_3000_0	5.827	5.827	5.827	5.827	5.827	5.827	5.827
6040_3000_1	8.756	8.756	8.756	8.756	8.756	8.756	8.756
6040_3000_2	8.783	8.783	8.783	8.783	8.756	8.756	8.756
6040_3000_5	8.756	8.756	8.756	8.756	8.756	8.756	8.756
6040_3000_10	8.756	8.756	8.756	8.756	8.756	8.756	8.756

Table C-56: Migration results for CO_2 states for all the 70:30 net to gross models. 1-1000 years (in kilometres)

Year	1	5	10	15	20	30	40	50	60	80	100	200	300	400	500	700	800	900	1000
7030_100_0	1.896	2.322	2.646	2.928	3.146	3.546	3.713	3.883	3.937	4.022	4.022	4.056	4.108	4.108	4.022	4.022	4.022	4.022	4.082
7030_100_1	1.856	2.322	2.646	2.928	3.303	3.629	3.798	3.937	4.108	4.281	4.545	5.220	5.587	5.679	5.900	6.994	7.393	7.781	8.193
7030_100_2	1.856	2.322	2.646	3.004	3.383	3.713	3.883	4.056	4.281	4.545	4.814	5.827	6.109	6.455	7.094	8.381	8.529	8.577	8.596
7030_100_5	1.856	2.299	2.707	3.082	3.464	3.883	4.108	4.320	4.770	5.538	6.120	6.804	7.513	7.901	7.901	7.901	8.047	8.145	8.243
7030_100_10	1.856	2.299	2.710	3.146	3.546	4.022	4.410	4.862	5.345	6.608	7.000	7.876	8.636	8.658	8.658	8.658	8.658	8.658	8.658
7030_300_0	1.820	2.205	2.427	2.665	2.884	3.497	3.886	4.470	4.556	4.556	4.556	4.556	4.556	4.556	4.556	4.470	4.470	4.470	4.470
7030_300_1	1.820	2.174	2.438	2.680	2.903	3.649	4.216	4.643	4.906	4.995	5.084	5.827	6.582	7.060	7.348	7.637	7.781	7.981	8.181
7030_300_2	1.820	2.139	2.438	2.680	3.021	3.649	4.385	4.818	5.084	5.354	5.628	7.444	8.705	8.730	8.730	8.730	8.730	8.730	8.730
7030_300_5	1.789	2.139	2.438	2.796	3.285	3.806	4.643	5.174	5.354	6.074	6.868	8.756	8.756	8.756	8.756	8.756	8.756	8.756	8.756
7030_300_10	1.789	2.081	2.517	2.934	3.374	3.944	4.906	5.445	5.996	6.934	8.168	8.756	8.756	8.756	8.756	8.756	8.756	8.756	8.756
7030_1000_0	1.805	2.267	2.531	2.884	3.224	4.076	4.906	5.628	5.864	5.958	5.958	5.958	5.958	5.958	5.958	5.864	5.864	5.864	5.864
7030_1000_1	1.789	2.215	2.528	2.930	3.444	4.419	5.354	6.182	6.582	6.868	7.060	7.804	8.485	8.705	8.730	8.730	8.756	8.756	8.756
7030_1000_2	1.789	2.215	2.528	2.930	3.524	4.818	5.864	6.710	7.156	7.541	7.901	8.705	8.756	8.756	8.756	8.756	8.756	8.756	8.756
7030_1000_5	1.763	2.182	2.541	3.064	3.798	5.311	6.868	7.541	8.193	8.705	8.756	8.756	8.756	8.756	8.756	8.756	8.756	8.756	8.756
7030_1000_10	1.763	2.128	2.458	3.004	3.937	5.719	7.186	7.998	8.705	8.756	8.756	8.756	8.756	8.756	8.756	8.756	8.756	8.756	8.756
7030_3000_0	1.886	2.399	2.884	3.349	3.853	4.859	5.264	5.697	5.885	5.980	5.980	5.958	5.958	5.921	5.921	5.885	5.885	5.885	5.885
7030_3000_1	1.820	2.399	2.825	3.422	3.937	4.906	5.323	5.791	6.109	6.487	6.678	7.570	8.273	8.756	8.756	8.756	8.756	8.756	8.756
7030_3000_2	1.820	2.399	2.944	3.572	4.108	5.084	5.533	6.074	6.582	6.996	7.378	8.730	8.756	8.756	8.756	8.756	8.756	8.756	8.756
7030_3000_5	1.820	2.347	2.944	3.727	4.419	5.285	6.010	6.805	7.474	8.273	8.756	8.756	8.756	8.756	8.756	8.756	8.756	8.756	8.756
7030_3000_10	1.820	2.267	2.930	3.853	4.724	5.628	6.616	7.570	8.342	8.756	8.756	8.756	8.756	8.756	8.756	8.756	8.756	8.756	8.756

Table C-57: Migration results for CO_2 states for all the 70:30 net to gross models. 2000-8000 years (in kilometres)

Year	2000	3000	4000	5000	6000	7000	8000
7030_100_0	4.594	4.891	4.990	4.990	4.990	4.990	4.990
7030_100_1	8.783	8.783	8.783	8.783	8.783	8.783	8.783
7030_100_2	8.681	8.681	8.681	8.681	8.681	8.681	8.658
7030_100_5	8.636	8.636	8.636	8.636	8.636	8.636	8.636
7030_100_10	8.658	8.658	8.658	8.658	8.658	8.560	8.560
7030_300_0	4.470	4.470	4.470	4.470	4.470	4.470	4.470
7030_300_1	8.491	8.491	8.544	8.544	8.544	8.544	8.544
7030_300_2	8.756	8.756	8.756	8.756	8.756	8.756	8.756
7030_300_5	8.756	8.756	8.756	8.756	8.756	8.756	8.756
7030_300_10	8.756	8.756	8.756	8.756	8.756	8.756	8.756
7030_1000_0	5.864	5.864	5.772	5.772	5.772	5.772	5.772
7030_1000_1	8.756	8.756	8.756	8.756	8.756	8.756	8.756
7030_1000_2	8.756	8.756	8.756	8.756	8.756	8.756	8.756
7030_1000_5	8.756	8.756	8.756	8.756	8.756	8.756	8.756
7030_1000_10	8.756	8.756	8.756	8.756	8.756	8.756	8.756
7030_3000_0	5.885	5.885	5.864	5.864	5.864	5.864	5.864
7030_3000_1	8.756	8.756	8.756	8.756	8.756	8.756	8.756
7030_3000_2	8.756	8.756	8.756	8.756	8.756	8.756	8.756
7030_3000_5	8.756	8.756	8.756	8.756	8.756	8.756	8.756
7030_3000_10	8.756	8.756	8.756	8.756	8.756	8.756	8.756

Table C-58: Migration results for CO_2 states for all the 80:20 net to gross models. 1-1000 years (in kilometres)

Year	1	5	10	15	20	30	40	50	60	80	100	200	300	400	500	700	800	900	1000
8020_100_0	1.789	2.139	2.482	2.716	2.884	3.207	3.422	3.572	3.714	3.727	3.791	3.714	3.714	3.824	3.931	4.126	4.226	4.226	4.326
8020_100_1	1.789	2.139	2.440	2.716	3.007	3.280	3.497	3.649	3.806	3.948	4.027	4.427	5.227	5.916	6.726	8.681	8.778	8.778	8.778
8020_100_2	1.789	2.139	2.440	2.743	3.007	3.354	3.586	3.727	3.886	4.049	4.132	5.127	6.367	8.168	8.756	8.778	8.778	8.778	8.778
8020_100_5	1.725	2.082	2.353	2.743	3.072	3.507	3.727	3.909	4.132	4.643	4.730	6.144	8.243	8.658	8.658	8.658	8.658	8.658	8.694
8020_100_10	1.763	2.044	2.303	2.630	2.996	3.507	3.806	4.132	4.643	4.995	5.536	6.841	8.344	8.544	8.560	8.596	8.628	8.628	8.628
8020_300_0	1.886	2.205	2.476	2.644	2.880	3.146	3.383	3.564	3.629	3.665	3.665	3.665	3.649	3.798	3.937	4.161	4.246	4.281	4.332
8020_300_1	1.820	2.205	2.426	2.644	2.880	3.183	3.464	3.629	3.883	4.144	4.232	4.821	5.178	5.454	5.772	6.695	7.193	7.892	8.291
8020_300_2	1.820	2.180	2.426	2.658	2.961	3.224	3.524	3.798	4.144	4.455	4.729	6.218	6.861	7.562	7.762	7.963	8.063	8.081	8.291
8020_300_5	1.789	2.180	2.426	2.721	2.961	3.303	3.605	4.056	4.580	6.315	7.000	8.379	8.577	8.636	8.636	8.705	8.705	8.705	8.705
8020_300_10	1.725	2.139	2.426	2.764	2.961	3.324	3.689	4.580	5.926	7.196	7.906	8.636	8.636	8.636	8.705	8.705	8.705	8.705	8.705
8020_1000_0	1.820	2.267	2.602	2.803	3.137	3.937	4.545	4.814	4.859	4.859	4.859	4.859	4.859	4.859	4.859	4.859	4.859	4.859	4.859
8020_1000_1	1.805	2.267	2.646	2.865	3.366	4.369	4.814	5.039	5.311	5.679	6.145	7.619	8.529	8.705	8.756	8.756	8.756	8.756	8.756
8020_1000_2	1.805	2.299	2.646	2.928	3.546	4.635	4.949	5.403	6.145	6.710	6.996	8.681	8.756	8.756	8.756	8.756	8.756	8.756	8.756
8020_1000_5	1.789	2.299	2.646	3.082	3.659	4.814	5.495	6.521	6.996	7.762	8.658	8.756	8.756	8.756	8.756	8.756	8.756	8.756	8.756
8020_1000_10	1.763	2.296	2.658	3.082	3.745	4.814	5.679	6.900	7.316	8.705	8.756	8.756	8.756	8.756	8.756	8.756	8.756	8.756	8.756
8020_3000_0	1.789	2.213	2.440	2.716	2.884	3.250	3.661	3.978	4.134	4.167	4.167	4.167	4.134	4.134	4.134	4.134	4.134	4.134	4.134
8020_3000_1	1.789	2.174	2.440	2.716	2.944	3.343	3.849	4.229	4.452	4.643	4.770	5.540	6.435	7.339	7.863	8.491	8.491	8.560	8.577
8020_3000_2	1.789	2.174	2.440	2.769	3.007	3.531	4.039	4.470	4.995	5.719	6.182	7.313	8.164	8.659	8.756	8.756	8.756	8.756	8.756
8020_3000_5	1.789	2.128	2.440	2.825	3.135	3.746	4.357	5.264	5.996	6.839	7.313	8.756	8.756	8.756	8.756	8.756	8.756	8.756	8.756
8020_3000_10	1.763	2.098	2.401	2.743	3.135	3.849	4.634	5.733	6.773	7.804	8.510	8.756	8.756	8.756	8.756	8.756	8.756	8.756	8.756

Table C-59: Migration results for CO_2 states for all the 80:20 net to gross models. 2000-8000 years (in kilometres)

Year	2000	3000	4000	5000	6000	7000	8000
8020_100_0	4.563	4.563	4.563	4.563	4.563	4.563	4.563
8020_100_1	8.827	8.827	8.827	8.827	8.827	8.827	8.827
8020_100_2	8.783	8.783	8.783	8.783	8.783	8.783	8.783
8020_100_5	8.734	8.734	8.734	8.734	8.734	8.734	8.734
8020_100_10	8.628	8.628	8.628	8.628	8.628	8.628	8.628
8020_300_0	4.975	4.990	4.990	4.990	4.990	4.990	4.990
8020_300_1	8.615	8.659	8.659	8.659	8.681	8.681	8.681
8020_300_2	8.491	8.491	8.681	8.681	8.681	8.681	8.681
8020_300_5	8.705	8.705	8.705	8.705	8.705	8.636	8.636
8020_300_10	8.705	8.705	8.705	8.705	8.705	8.607	8.607
8020_1000_0	4.859	4.859	4.859	4.876	4.876	4.876	4.876
8020_1000_1	8.756	8.756	8.756	8.756	8.756	8.756	8.756
8020_1000_2	8.756	8.756	8.756	8.756	8.756	8.756	8.756
8020_1000_5	8.756	8.756	8.756	8.756	8.756	8.756	8.756
8020_1000_10	8.756	8.756	8.756	8.756	8.756	8.756	8.756
8020_3000_0	4.073	4.039	4.039	4.039	4.039	4.039	4.039
8020_3000_1	8.596	8.596	8.577	8.577	8.577	8.577	8.577
8020_3000_2	8.756	8.756	8.756	8.756	8.756	8.756	8.756
8020_3000_5	8.756	8.756	8.756	8.756	8.756	8.756	8.756
8020_3000_10	8.756	8.756	8.756	8.756	8.756	8.756	8.756

Table C-60: Vertical migration results for CO_2 states for the homogeneous models, 0, 1, 2, 5 and 10 degree dips. 1-8000 years (in fractional movement through model stratigraphy)

Year	1	5	10	15	20	30	40	50	60	80	100	200	300	400	500	700	800	900	1000
Homogeneous 0	0.595	1.000	1.000	1.000	1.000	1.000	1.000	1.000	1.000	1.000	1.000	1.000	1.000	1.000	1.000	1.000	1.000	1.000	1.000
Homogeneous 1	0.595	0.952	1.000	1.000	1.000	1.000	1.000	1.000	1.000	1.000	1.000	1.000	1.000	1.000	1.000	1.000	1.000	1.000	1.000
Homogeneous 2	0.595	0.929	1.000	1.000	1.000	1.000	1.000	1.000	1.000	1.000	1.000	1.000	1.000	1.000	1.000	1.000	1.000	1.000	1.000
Homogeneous 5	0.571	0.833	1.000	1.000	1.000	1.000	1.000	1.000	1.000	1.000	1.000	1.000	1.000	1.000	1.000	1.000	1.000	1.000	1.000
Homogeneous 10	0.548	0.738	0.929	1.000	1.000	1.000	1.000	1.000	1.000	1.000	1.000	1.000	1.000	1.000	1.000	1.000	1.000	1.000	1.000

Year	2000	3000	4000	5000	6000	7000	8000
Homogeneous0	1.000	1.000	1.000	1.000	1.000	1.000	1.000
Homogeneous1	1.000	1.000	1.000	1.000	1.000	1.000	1.000
Homogeneous2	1.000	1.000	1.000	1.000	1.000	1.000	1.000
Homogeneous5	1.000	1.000	1.000	1.000	1.000	1.000	1.000
Homogeneous10	1.000	1.000	1.000	1.000	1.000	1.000	1.000

Table C-61: Vertical migration results for CO_2 states for all the 40:60 net to gross models. 1-1000 years (in fractional movement through model stratigraphy)

Year	1	5	10	15	20	30	40	50	60	80	100	200	300	400	500	700	800	900	1000
4060_100_0	0.429	0.476	0.548	0.571	0.619	0.667	0.738	0.762	0.762	0.786	0.810	0.833	0.857	0.881	0.881	0.905	0.929	0.929	0.952
4060_100_1	0.405	0.476	0.524	0.571	0.619	0.667	0.714	0.762	0.762	0.762	0.786	0.810	0.833	0.857	0.857	0.881	0.881	0.905	0.905
4060_100_2	0.405	0.476	0.524	0.548	0.619	0.643	0.690	0.738	0.738	0.762	0.762	0.786	0.810	0.810	0.833	0.833	0.833	0.833	0.857
4060_100_5	0.405	0.476	0.500	0.548	0.571	0.643	0.667	0.690	0.714	0.714	0.738	0.738	0.738	0.738	0.738	0.762	0.762	0.762	0.786
4060_100_10	0.405	0.452	0.500	0.524	0.548	0.595	0.643	0.667	0.667	0.667	0.690	0.690	0.690	0.690	0.690	0.690	0.690	0.714	0.714
4060_300_0	0.429	0.452	0.476	0.500	0.524	0.571	0.595	0.619	0.643	0.690	0.714	0.762	0.762	0.786	0.786	0.810	0.810	0.810	0.833
4060_300_1	0.429	0.452	0.476	0.500	0.524	0.571	0.595	0.619	0.643	0.667	0.667	0.714	0.714	0.714	0.714	0.714	0.738	0.738	0.738
4060_300_2	0.429	0.452	0.476	0.500	0.524	0.571	0.595	0.619	0.643	0.643	0.667	0.690	0.690	0.690	0.690	0.690	0.690	0.714	0.714
4060_300_5	0.429	0.452	0.476	0.500	0.524	0.548	0.571	0.595	0.619	0.619	0.643	0.667	0.667	0.667	0.667	0.667	0.667	0.667	0.690
4060_300_10	0.405	0.452	0.476	0.476	0.500	0.524	0.548	0.571	0.595	0.595	0.619	0.619	0.619	0.619	0.619	0.619	0.619	0.643	0.643
4060_1000_0	0.381	0.429	0.452	0.452	0.476	0.524	0.571	0.595	0.619	0.690	0.714	0.762	0.762	0.762	0.786	0.786	0.786	0.786	0.786
4060_1000_1	0.381	0.405	0.452	0.452	0.476	0.524	0.548	0.571	0.595	0.619	0.619	0.667	0.667	0.667	0.667	0.667	0.667	0.667	0.667
4060_1000_2	0.381	0.405	0.429	0.452	0.476	0.500	0.548	0.571	0.595	0.595	0.619	0.643	0.643	0.643	0.643	0.643	0.643	0.643	0.643
4060_1000_5	0.381	0.405	0.429	0.452	0.452	0.500	0.524	0.548	0.571	0.595	0.595	0.619	0.619	0.619	0.619	0.619	0.619	0.619	0.619
4060_1000_10	0.381	0.405	0.429	0.452	0.452	0.476	0.524	0.548	0.548	0.571	0.571	0.595	0.619	0.619	0.619	0.619	0.619	0.619	0.619
4060_3000_0	0.381	0.429	0.452	0.476	0.476	0.500	0.524	0.548	0.548	0.571	0.595	0.619	0.643	0.667	0.667	0.667	0.690	0.690	0.690
4060_3000_1	0.381	0.429	0.452	0.476	0.476	0.500	0.524	0.524	0.548	0.571	0.571	0.595	0.619	0.619	0.619	0.619	0.619	0.619	0.619
4060_3000_2	0.381	0.429	0.452	0.476	0.476	0.500	0.500	0.524	0.548	0.571	0.571	0.595	0.595	0.595	0.595	0.595	0.595	0.619	0.619
4060_3000_5	0.381	0.405	0.452	0.452	0.476	0.476	0.500	0.524	0.548	0.571	0.571	0.571	0.595	0.595	0.595	0.595	0.595	0.595	0.595
4060_3000_10	0.381	0.405	0.429	0.452	0.452	0.476	0.500	0.524	0.548	0.548	0.548	0.571	0.571	0.571	0.571	0.571	0.571	0.595	0.595

Table C-51: Vertical migration results for CO_2 states for all the 40:60 net to gross models. 2000-8000 years (in fractional movement through model stratigraphy)

Year	2000	3000	4000	5000	6000	7000	8000
4060_100_0	1.000	1.000	1.000	1.000	1.000	1.000	1.000
4060_100_1	0.976	1.000	1.000	1.000	1.000	1.000	1.000
4060_100_2	0.905	0.929	0.976	1.000	1.000	1.000	1.000
4060_100_5	0.810	0.810	0.810	0.833	0.833	0.833	0.833
4060_100_10	0.738	0.762	0.762	0.762	0.786	0.786	0.786
4060_300_0	0.905	0.976	1.000	1.000	1.000	1.000	1.000
4060_300_1	0.810	0.810	0.833	0.833	0.857	0.857	0.857
4060_300_2	0.738	0.738	0.762	0.762	0.762	0.762	0.762
4060_300_5	0.690	0.690	0.690	0.690	0.690	0.690	0.690
4060_300_10	0.643	0.643	0.643	0.643	0.643	0.643	0.643
4060_1000_0	0.857	0.952	1.000	1.000	1.000	1.000	1.000
4060_1000_1	0.714	0.714	0.714	0.714	0.714	0.714	0.714
4060_1000_2	0.643	0.643	0.643	0.643	0.643	0.643	0.643
4060_1000_5	0.619	0.619	0.619	0.619	0.619	0.619	0.619
4060_1000_10	0.619	0.619	0.619	0.595	0.595	0.595	0.595
4060_3000_0	0.762	0.833	0.929	1.000	1.000	1.000	1.000
4060_3000_1	0.667	0.667	0.667	0.667	0.667	0.667	0.667
4060_3000_2	0.619	0.619	0.619	0.619	0.619	0.619	0.619
4060_3000_5	0.595	0.595	0.595	0.595	0.595	0.595	0.595
4060_3000_10	0.595	0.595	0.595	0.595	0.595	0.595	0.595

Table C-63: Vertical migration results for CO_2 states for all the 50:50 net to gross models. 1-1000 years (in fractional movement through model stratigraphy)

Year	1	5	10	15	20	30	40	50	60	80	100	200	300	400	500	700	800	900	1000
5050_100_0	0.476	0.643	0.667	0.738	0.762	0.810	0.833	0.881	0.929	0.929	0.952	0.976	1.000	1.000	1.000	1.000	1.000	1.000	1.000
5050_100_1	0.476	0.619	0.667	0.714	0.762	0.810	0.810	0.857	0.881	0.905	0.905	0.929	0.952	0.976	1.000	1.000	1.000	1.000	1.000
5050_100_2	0.476	0.619	0.667	0.690	0.738	0.786	0.810	0.833	0.857	0.857	0.857	0.905	0.929	0.952	0.976	0.976	0.976	0.976	0.976
5050_100_5	0.476	0.571	0.667	0.690	0.738	0.786	0.810	0.810	0.833	0.833	0.833	0.857	0.857	0.857	0.857	0.857	0.857	0.857	0.857
5050_100_10	0.452	0.571	0.619	0.667	0.690	0.762	0.786	0.810	0.810	0.810	0.810	0.810	0.810	0.810	0.810	0.810	0.810	0.810	0.810
5050_300_0	0.429	0.524	0.595	0.643	0.667	0.690	0.738	0.762	0.786	0.810	0.810	0.833	0.857	0.857	0.881	0.905	0.905	0.929	0.929
5050_300_1	0.429	0.524	0.595	0.619	0.643	0.690	0.714	0.762	0.762	0.786	0.786	0.810	0.810	0.810	0.810	0.810	0.833	0.833	0.833
5050_300_2	0.429	0.500	0.595	0.619	0.643	0.667	0.690	0.714	0.738	0.762	0.762	0.786	0.786	0.786	0.786	0.786	0.810	0.810	0.810
5050_300_5	0.405	0.500	0.571	0.619	0.619	0.667	0.667	0.690	0.714	0.738	0.738	0.738	0.762	0.762	0.762	0.762	0.762	0.762	0.762
5050_300_10	0.405	0.476	0.524	0.595	0.619	0.643	0.667	0.667	0.690	0.690	0.714	0.690	0.690	0.690	0.690	0.690	0.690	0.690	0.690
5050_1000_0	0.381	0.429	0.452	0.476	0.500	0.524	0.524	0.548	0.571	0.595	0.619	0.643	0.643	0.667	0.667	0.690	0.690	0.690	0.714
5050_1000_1	0.381	0.429	0.452	0.476	0.476	0.500	0.524	0.548	0.571	0.595	0.595	0.619	0.619	0.619	0.619	0.619	0.643	0.643	0.643
5050_1000_2	0.381	0.429	0.452	0.476	0.476	0.500	0.524	0.548	0.571	0.571	0.595	0.595	0.595	0.595	0.595	0.595	0.619	0.619	0.619
5050_1000_5	0.381	0.405	0.429	0.452	0.476	0.500	0.524	0.548	0.548	0.571	0.571	0.571	0.571	0.571	0.571	0.571	0.571	0.571	0.571
5050_1000_10	0.381	0.405	0.429	0.452	0.476	0.476	0.500	0.524	0.548	0.548	0.548	0.548	0.548	0.548	0.548	0.548	0.548	0.548	0.548
5050_3000_0	0.381	0.429	0.452	0.452	0.476	0.500	0.548	0.595	0.619	0.619	0.643	0.667	0.667	0.690	0.714	0.714	0.714	0.738	0.738
5050_3000_1	0.381	0.429	0.452	0.452	0.476	0.500	0.524	0.548	0.595	0.595	0.619	0.643	0.643	0.667	0.667	0.667	0.667	0.667	0.667
5050_3000_2	0.381	0.405	0.429	0.452	0.476	0.500	0.524	0.548	0.571	0.595	0.619	0.619	0.619	0.619	0.619	0.619	0.619	0.619	0.619
5050_3000_5	0.381	0.405	0.429	0.452	0.476	0.476	0.500	0.524	0.548	0.548	0.548	0.548	0.571	0.571	0.571	0.571	0.571	0.571	0.571
5050_3000_10	0.381	0.405	0.429	0.452	0.452	0.476	0.500	0.500	0.524	0.524	0.524	0.548	0.548	0.571	0.571	0.571	0.571	0.571	0.571

Table C-64: Vertical migration results for CO_2 states for all the 50:50 net to gross models. 2000-8000 years (in fractional movement through model stratigraphy)

Year	2000	3000	4000	5000	6000	7000	8000
5050_100_0	1.000	1.000	1.000	1.000	1.000	1.000	1.000
5050_100_1	1.000	1.000	1.000	1.000	1.000	1.000	1.000
5050_100_2	0.976	1.000	1.000	1.000	1.000	1.000	1.000
5050_100_5	0.881	0.929	0.929	0.929	0.929	0.929	0.929
5050_100_10	0.833	0.833	0.833	0.833	0.857	0.857	0.857
5050_300_0	1.000	1.000	1.000	1.000	1.000	1.000	1.000
5050_300_1	0.881	0.881	0.881	0.881	0.881	0.881	0.881
5050_300_2	0.833	0.833	0.833	0.833	0.833	0.833	0.833
5050_300_5	0.762	0.762	0.762	0.762	0.762	0.762	0.762
5050_300_10	0.714	0.714	0.714	0.714	0.714	0.690	0.690
5050_1000_0	0.810	0.905	1.000	1.000	1.000	1.000	1.000
5050_1000_1	0.643	0.643	0.643	0.643	0.643	0.643	0.643
5050_1000_2	0.619	0.619	0.619	0.619	0.619	0.619	0.619
5050_1000_5	0.571	0.571	0.571	0.571	0.571	0.571	0.571
5050_1000_10	0.548	0.548	0.548	0.548	0.548	0.548	0.548
5050_3000_0	0.833	0.929	0.976	1.000	1.000	1.000	1.000
5050_3000_1	0.667	0.667	0.667	0.667	0.667	0.667	0.667
5050_3000_2	0.619	0.619	0.619	0.619	0.619	0.619	0.619
5050_3000_5	0.571	0.571	0.571	0.571	0.571	0.548	0.548
5050_3000_10	0.571	0.571	0.548	0.548	0.524	0.524	0.524

Table C-65: Vertical migration results for CO_2 states for all the 60:40 net to gross models. 1-1000 years (Fraction)

Year	1	5	10	15	20	30	40	50	60	80	100	200	300	400	500	700	800	900	1000
6040_100_0	0.452	0.571	0.643	0.738	0.762	0.833	0.881	0.905	0.976	1.000	1.000	1.000	1.000	1.000	1.000	1.000	1.000	1.000	1.000
6040_100_1	0.429	0.571	0.643	0.738	0.762	0.833	0.881	0.881	0.929	0.929	0.976	1.000	1.000	1.000	1.000	1.000	1.000	1.000	1.000
6040_100_2	0.429	0.548	0.643	0.690	0.762	0.833	0.857	0.881	0.905	0.952	0.976	1.000	1.000	1.000	1.000	1.000	1.000	1.000	1.000
6040_100_5	0.429	0.548	0.595	0.667	0.738	0.810	0.857	0.857	0.881	0.929	0.976	1.000	1.000	1.000	1.000	1.000	1.000	1.000	1.000
6040_100_10	0.429	0.524	0.571	0.643	0.667	0.762	0.833	0.833	0.857	0.881	0.929	1.000	1.000	1.000	1.000	1.000	1.000	1.000	1.000
6040_300_0	0.452	0.524	0.571	0.595	0.619	0.667	0.690	0.738	0.762	0.762	0.786	0.810	0.833	0.881	0.905	0.929	0.929	0.952	0.952
6040_300_1	0.452	0.524	0.548	0.595	0.595	0.667	0.690	0.738	0.762	0.786	0.786	0.810	0.810	0.833	0.833	0.833	0.833	0.857	0.881
6040_300_2	0.452	0.524	0.548	0.571	0.595	0.667	0.690	0.738	0.762	0.786	0.786	0.786	0.786	0.810	0.810	0.810	0.810	0.810	0.810
6040_300_5	0.452	0.524	0.548	0.571	0.595	0.619	0.667	0.714	0.738	0.762	0.762	0.762	0.762	0.762	0.762	0.762	0.762	0.762	0.762
6040_300_10	0.429	0.524	0.524	0.548	0.571	0.595	0.619	0.667	0.667	0.690	0.690	0.690	0.690	0.690	0.690	0.690	0.690	0.690	0.690
6040_1000_0	0.381	0.429	0.429	0.452	0.476	0.571	0.619	0.619	0.643	0.667	0.667	0.690	0.714	0.714	0.714	0.738	0.738	0.762	0.762
6040_1000_1	0.381	0.429	0.429	0.452	0.476	0.571	0.595	0.619	0.619	0.643	0.667	0.667	0.667	0.667	0.667	0.667	0.667	0.667	0.667
6040_1000_2	0.381	0.405	0.429	0.452	0.476	0.548	0.595	0.619	0.619	0.643	0.643	0.643	0.643	0.643	0.643	0.643	0.643	0.643	0.643
6040_1000_5	0.381	0.405	0.429	0.452	0.452	0.500	0.548	0.571	0.595	0.619	0.619	0.619	0.619	0.619	0.619	0.619	0.619	0.619	0.619
6040_1000_10	0.381	0.405	0.429	0.429	0.452	0.476	0.500	0.524	0.548	0.571	0.571	0.595	0.595	0.595	0.595	0.595	0.595	0.595	0.595
6040_3000_0	0.405	0.429	0.452	0.476	0.500	0.524	0.548	0.595	0.619	0.643	0.667	0.690	0.690	0.714	0.714	0.714	0.738	0.738	0.738
6040_3000_1	0.381	0.429	0.452	0.476	0.500	0.524	0.548	0.571	0.595	0.619	0.643	0.643	0.643	0.643	0.643	0.643	0.643	0.643	0.643
6040_3000_2	0.381	0.429	0.452	0.476	0.500	0.524	0.548	0.571	0.595	0.619	0.619	0.619	0.619	0.619	0.619	0.619	0.619	0.619	0.619
6040_3000_5	0.381	0.429	0.429	0.452	0.476	0.500	0.524	0.548	0.571	0.571	0.571	0.571	0.571	0.571	0.571	0.571	0.571	0.571	0.571
6040_3000_10	0.381	0.405	0.429	0.452	0.476	0.500	0.524	0.524	0.548	0.548	0.548	0.548	0.548	0.548	0.548	0.548	0.548	0.548	0.548

Table C-66: Vertical migration results for CO_2 states for all the 60:40 net to gross models. 2000-8000 years (Fraction)

Year	2000	3000	4000	5000	6000	7000	8000
6040_100_0	1.000	1.000	1.000	1.000	1.000	1.000	1.000
6040_100_1	1.000	1.000	1.000	1.000	1.000	1.000	1.000
6040_100_2	1.000	1.000	1.000	1.000	1.000	1.000	1.000
6040_100_5	1.000	1.000	1.000	1.000	1.000	1.000	1.000
6040_100_10	1.000	1.000	1.000	1.000	1.000	1.000	1.000
6040_300_0	1.000	1.000	1.000	1.000	1.000	1.000	1.000
6040_300_1	0.952	0.976	0.976	0.976	1.000	1.000	1.000
6040_300_2	0.857	0.857	0.857	0.857	0.857	0.857	0.857
6040_300_5	0.762	0.762	0.762	0.762	0.762	0.762	0.762
6040_300_10	0.690	0.667	0.667	0.667	0.667	0.667	0.667
6040_1000_0	0.833	0.929	1.000	1.000	1.000	1.000	1.000
6040_1000_1	0.690	0.690	0.690	0.690	0.690	0.690	0.690
6040_1000_2	0.643	0.643	0.667	0.667	0.667	0.667	0.667
6040_1000_5	0.619	0.619	0.619	0.619	0.619	0.619	0.619
6040_1000_10	0.571	0.571	0.571	0.571	0.571	0.571	0.571
6040_3000_0	0.833	0.905	0.976	1.000	1.000	1.000	1.000
6040_3000_1	0.643	0.643	0.643	0.643	0.643	0.643	0.643
6040_3000_2	0.619	0.619	0.619	0.619	0.619	0.619	0.619
6040_3000_5	0.571	0.571	0.571	0.571	0.571	0.571	0.571
6040_3000_10	0.548	0.548	0.548	0.548	0.548	0.548	0.548

Table C-67: Vertical migration results for CO_2 states for all the 70:30 net to gross models. 1-1000 years (Fraction)

Year	1	5	10	15	20	30	40	50	60	80	100	200	300	400	500	700	800	900	1000
7030_100_0	0.500	0.690	0.810	0.881	0.905	1.000	1.000	1.000	1.000	1.000	1.000	1.000	1.000	1.000	1.000	1.000	1.000	1.000	1.000
7030_100_1	0.500	0.667	0.810	0.881	0.905	1.000	1.000	1.000	1.000	1.000	1.000	1.000	1.000	1.000	1.000	1.000	1.000	1.000	1.000
7030_100_2	0.500	0.667	0.786	0.881	0.905	1.000	1.000	1.000	1.000	1.000	1.000	1.000	1.000	1.000	1.000	1.000	1.000	1.000	1.000
7030_100_5	0.476	0.643	0.762	0.833	0.881	0.929	1.000	1.000	1.000	1.000	1.000	1.000	1.000	1.000	1.000	1.000	1.000	1.000	1.000
7030_100_10	0.476	0.619	0.714	0.786	0.833	0.881	0.929	1.000	1.000	1.000	1.000	1.000	1.000	1.000	1.000	1.000	1.000	1.000	1.000
7030_300_0	0.405	0.524	0.571	0.667	0.690	0.786	0.833	0.857	0.857	0.881	0.881	0.929	1.000	1.000	1.000	1.000	1.000	1.000	1.000
7030_300_1	0.405	0.524	0.548	0.643	0.690	0.762	0.786	0.833	0.857	0.857	0.881	0.929	0.976	1.000	1.000	1.000	1.000	1.000	1.000
7030_300_2	0.405	0.524	0.548	0.619	0.667	0.762	0.786	0.833	0.857	0.857	0.881	0.976	1.000	1.000	1.000	1.000	1.000	1.000	1.000
7030_300_5	0.405	0.500	0.548	0.571	0.619	0.690	0.762	0.786	0.810	0.857	0.881	0.905	0.929	0.952	0.976	1.000	1.000	1.000	1.000
7030_300_10	0.405	0.500	0.524	0.548	0.595	0.643	0.714	0.786	0.786	0.833	0.857	0.881	0.881	0.905	0.905	0.905	0.905	0.905	0.905
7030_1000_0	0.452	0.500	0.524	0.548	0.571	0.595	0.667	0.738	0.786	0.833	0.857	0.881	0.881	0.905	0.905	0.929	0.929	0.929	0.952
7030_1000_1	0.452	0.500	0.500	0.548	0.571	0.595	0.643	0.738	0.762	0.786	0.786	0.786	0.810	0.833	0.833	0.857	0.857	0.881	0.905
7030_1000_2	0.452	0.476	0.500	0.524	0.571	0.595	0.643	0.714	0.738	0.738	0.762	0.762	0.786	0.786	0.810	0.810	0.833	0.833	0.833
7030_1000_5	0.452	0.476	0.500	0.524	0.548	0.571	0.619	0.643	0.667	0.738	0.738	0.738	0.738	0.738	0.738	0.738	0.738	0.738	0.738
7030_1000_10	0.452	0.476	0.500	0.500	0.524	0.571	0.595	0.643	0.643	0.667	0.714	0.738	0.738	0.738	0.738	0.738	0.738	0.738	0.738
7030_3000_0	0.429	0.452	0.500	0.524	0.548	0.595	0.619	0.643	0.690	0.738	0.762	0.786	0.786	0.810	0.810	0.833	0.833	0.857	0.857
7030_3000_1	0.429	0.452	0.500	0.524	0.548	0.571	0.619	0.619	0.667	0.714	0.738	0.762	0.762	0.762	0.762	0.762	0.762	0.762	0.762
7030_3000_2	0.429	0.452	0.500	0.524	0.548	0.571	0.595	0.619	0.643	0.667	0.690	0.738	0.738	0.738	0.738	0.714	0.714	0.714	0.714
7030_3000_5	0.405	0.452	0.476	0.500	0.524	0.571	0.571	0.595	0.619	0.619	0.619	0.643	0.643	0.643	0.643	0.643	0.643	0.643	0.643
7030_3000_10	0.405	0.452	0.476	0.500	0.500	0.548	0.571	0.571	0.595	0.595	0.619	0.619	0.619	0.619	0.619	0.619	0.619	0.619	0.619

Table C-68: Vertical migration results for CO_2 states for all the 70:30 net to gross models. 2000-8000 years (Fraction)

Year	2000	3000	4000	5000	6000	7000	8000
7030_100_0	1.000	1.000	1.000	1.000	1.000	1.000	1.000
7030_100_1	1.000	1.000	1.000	1.000	1.000	1.000	1.000
7030_100_2	1.000	1.000	1.000	1.000	1.000	1.000	1.000
7030_100_5	1.000	1.000	1.000	1.000	1.000	1.000	1.000
7030_100_10	1.000	1.000	1.000	1.000	1.000	1.000	1.000
7030_300_0	1.000	1.000	1.000	1.000	1.000	1.000	1.000
7030_300_1	1.000	1.000	1.000	1.000	1.000	1.000	1.000
7030_300_2	1.000	1.000	1.000	1.000	1.000	1.000	1.000
7030_300_5	1.000	1.000	1.000	1.000	0.952	0.952	0.952
7030_300_10	0.905	0.905	0.881	0.881	0.881	0.881	0.881
7030_1000_0	1.000	1.000	1.000	1.000	1.000	1.000	1.000
7030_1000_1	1.000	1.000	1.000	1.000	1.000	1.000	1.000
7030_1000_2	0.833	0.833	0.833	0.833	0.833	0.833	0.833
7030_1000_5	0.738	0.738	0.738	0.738	0.738	0.738	0.738
7030_1000_10	0.714	0.714	0.714	0.714	0.714	0.714	0.714
7030_3000_0	1.000	1.000	1.000	1.000	1.000	1.000	1.000
7030_3000_1	0.762	0.762	0.762	0.762	0.762	0.762	0.762
7030_3000_2	0.714	0.714	0.714	0.714	0.714	0.714	0.714
7030_3000_5	0.643	0.643	0.643	0.643	0.643	0.643	0.643
7030_3000_10	0.619	0.619	0.619	0.619	0.619	0.619	0.619

Table C-69: Vertical migration results for CO_2 states for all the 80:20 net to gross models. 1-1000 years (Fraction)

Year	1	5	10	15	20	30	40	50	60	80	100	200	300	400	500	700	800	900	1000
8020_100_0	0.548	0.738	0.952	0.976	1.000	1.000	1.000	1.000	1.000	1.000	1.000	1.000	1.000	1.000	1.000	1.000	1.000	1.000	1.000
8020_100_1	0.548	0.738	0.905	0.976	0.976	1.000	1.000	1.000	1.000	1.000	1.000	1.000	1.000	1.000	1.000	1.000	1.000	1.000	1.000
8020_100_2	0.548	0.738	0.857	0.952	0.976	1.000	1.000	1.000	1.000	1.000	1.000	1.000	1.000	1.000	1.000	1.000	1.000	1.000	1.000
8020_100_5	0.548	0.714	0.762	0.833	0.952	1.000	1.000	1.000	1.000	1.000	1.000	1.000	1.000	1.000	1.000	1.000	1.000	1.000	1.000
8020_100_10	0.524	0.667	0.762	0.786	0.833	0.976	1.000	1.000	1.000	1.000	1.000	1.000	1.000	1.000	1.000	1.000	1.000	1.000	1.000
8020_300_0	0.524	0.619	0.738	0.833	0.976	1.000	1.000	1.000	1.000	1.000	1.000	1.000	1.000	1.000	1.000	1.000	1.000	1.000	1.000
8020_300_1	0.500	0.595	0.690	0.833	0.952	1.000	1.000	1.000	1.000	1.000	1.000	1.000	1.000	1.000	1.000	1.000	1.000	1.000	1.000
8020_300_2	0.500	0.595	0.667	0.810	0.905	1.000	1.000	1.000	1.000	1.000	1.000	1.000	1.000	1.000	1.000	1.000	1.000	1.000	1.000
8020_300_5	0.476	0.595	0.643	0.810	0.857	1.000	1.000	1.000	1.000	1.000	1.000	1.000	1.000	1.000	1.000	1.000	1.000	1.000	1.000
8020_300_10	0.476	0.595	0.595	0.714	0.810	0.905	1.000	1.000	1.000	1.000	1.000	1.000	1.000	1.000	1.000	1.000	1.000	1.000	1.000
8020_1000_0	0.429	0.619	0.667	0.690	0.714	0.810	0.857	0.881	0.905	0.929	0.952	1.000	1.000	1.000	1.000	1.000	1.000	1.000	1.000
8020_1000_1	0.429	0.619	0.667	0.690	0.690	0.810	0.857	0.881	0.905	0.929	0.929	1.000	1.000	1.000	1.000	1.000	1.000	1.000	1.000
8020_1000_2	0.429	0.595	0.667	0.667	0.690	0.810	0.833	0.857	0.881	0.905	0.905	0.929	1.000	1.000	1.000	1.000	1.000	1.000	1.000
8020_1000_5	0.429	0.548	0.643	0.667	0.690	0.810	0.833	0.857	0.857	0.857	0.857	1.000	1.000	1.000	1.000	1.000	1.000	1.000	1.000
8020_1000_10	0.429	0.500	0.619	0.643	0.667	0.690	0.810	0.833	0.833	0.833	0.833	1.000	1.000	1.000	1.000	1.000	1.000	1.000	1.000
8020_3000_0	0.405	0.524	0.548	0.619	0.667	0.714	0.738	0.762	0.786	0.810	0.810	0.810	0.833	0.857	0.881	0.929	0.952	0.976	1.000
8020_3000_1	0.405	0.524	0.548	0.619	0.643	0.690	0.738	0.762	0.786	0.786	0.786	0.786	0.786	0.786	0.786	0.786	0.810	0.810	0.810
8020_3000_2	0.405	0.524	0.548	0.595	0.619	0.690	0.714	0.738	0.762	0.762	0.762	0.762	0.762	0.762	0.762	0.762	0.762	0.762	0.762
8020_3000_5	0.405	0.500	0.548	0.571	0.619	0.667	0.690	0.714	0.714	0.714	0.714	0.714	0.714	0.714	0.714	0.714	0.714	0.714	0.714
8020_3000_10	0.405	0.476	0.524	0.548	0.595	0.619	0.667	0.690	0.690	0.690	0.690	0.690	0.690	0.690	0.690	0.690	0.690	0.690	0.690

Table C-70: Vertical migration results for CO_2 states for all the 80:20 net to gross models. 2000-8000 years (Fraction)

Year	2000	3000	4000	5000	6000	7000	8000
8020_100_0	1.000	1.000	1.000	1.000	1.000	1.000	1.000
8020_100_1	1.000	1.000	1.000	1.000	1.000	1.000	1.000
8020_100_2	1.000	1.000	1.000	1.000	1.000	1.000	1.000
8020_100_5	1.000	1.000	1.000	1.000	1.000	1.000	1.000
8020_100_10	1.000	1.000	1.000	1.000	1.000	1.000	1.000
8020_300_0	1.000	1.000	1.000	1.000	1.000	1.000	1.000
8020_300_1	1.000	1.000	1.000	1.000	1.000	1.000	1.000
8020_300_2	1.000	1.000	1.000	1.000	1.000	1.000	1.000
8020_300_5	1.000	1.000	1.000	1.000	1.000	1.000	1.000
8020_300_10	1.000	1.000	1.000	1.000	1.000	1.000	1.000
8020_1000_0	1.000	1.000	1.000	1.000	1.000	1.000	1.000
8020_1000_1	1.000	1.000	1.000	1.000	1.000	1.000	1.000
8020_1000_2	1.000	1.000	1.000	1.000	1.000	1.000	1.000
8020_1000_5	1.000	1.000	1.000	1.000	1.000	1.000	1.000
8020_1000_10	1.000	1.000	0.976	0.976	0.976	0.976	0.976
8020_3000_0	1.000	1.000	1.000	1.000	1.000	1.000	1.000
8020_3000_1	0.833	0.833	0.833	0.833	0.833	0.833	0.833
8020_3000_2	0.762	0.762	0.762	0.762	0.762	0.762	0.762
8020_3000_5	0.714	0.714	0.714	0.714	0.714	0.714	0.714
8020_3000_10	0.690	0.667	0.667	0.667	0.667	0.667	0.667

APPENDIX D – SUPPLEMENTARY IMAGES

D.1 Study A

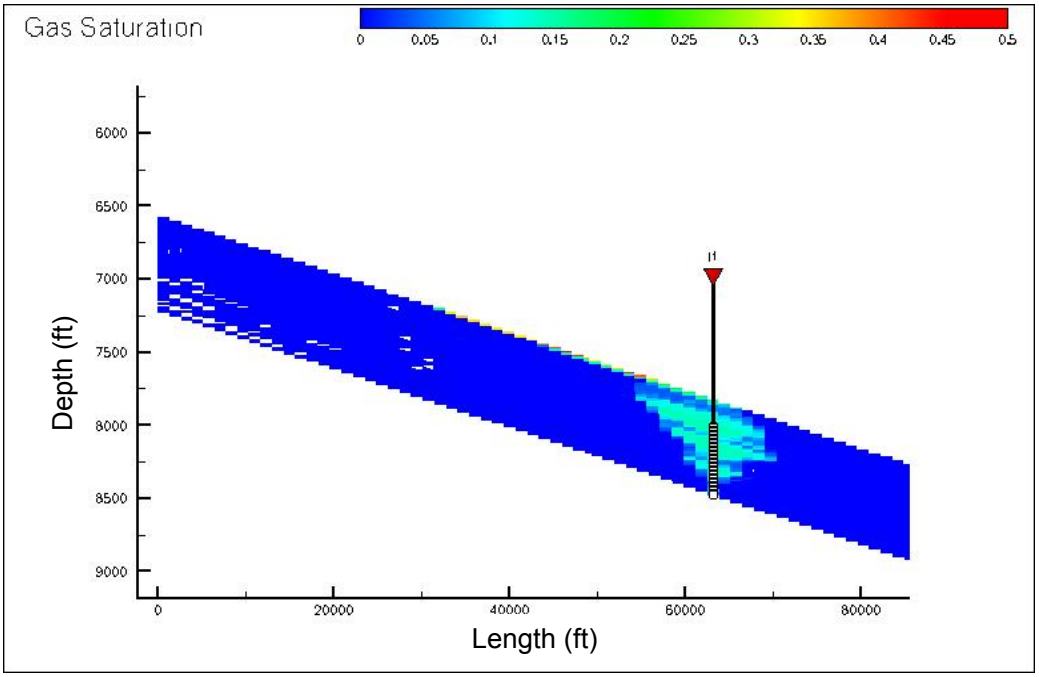

Figure D-1: Cross section of the Study A model, mid point simulation run, showing the gas saturation at 1000 years. (Mid permeability, mid vertical permeability, mid Land's constant, mid relative permeability curves, mid S_{wir}, mid solubility).

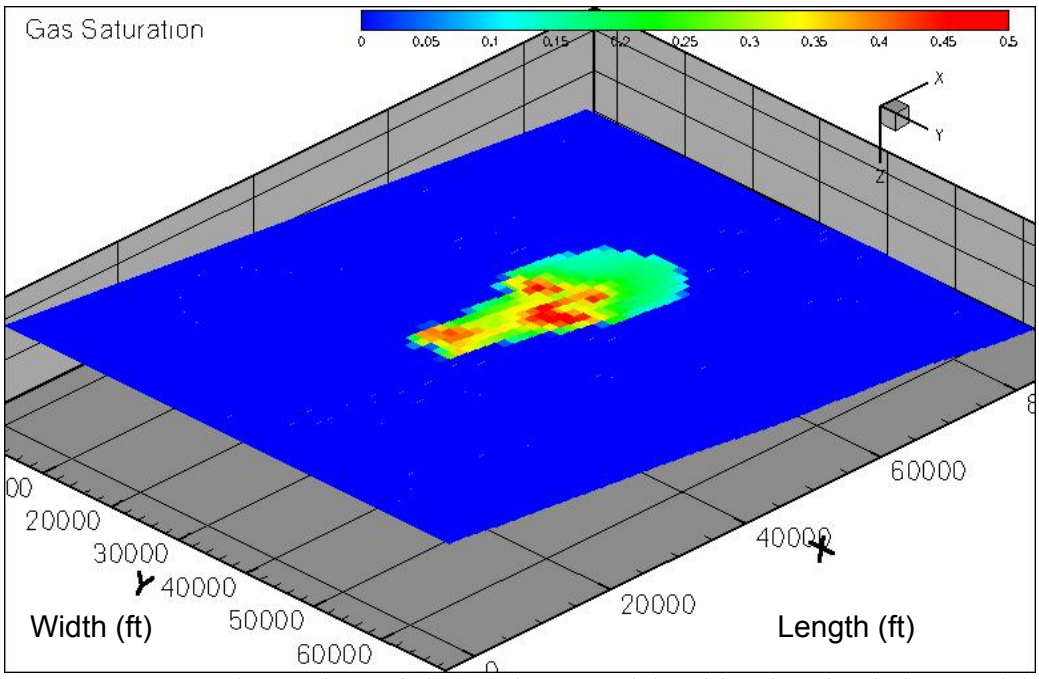

Figure D-2: Top layer view of the Study A model, mid point simulation model, showing the gas saturation at 1000 years. (Mid permeability, mid vertical permeability, mid Land's constant, mid relative permeability curves, mid S_{wir}, mid solubility).

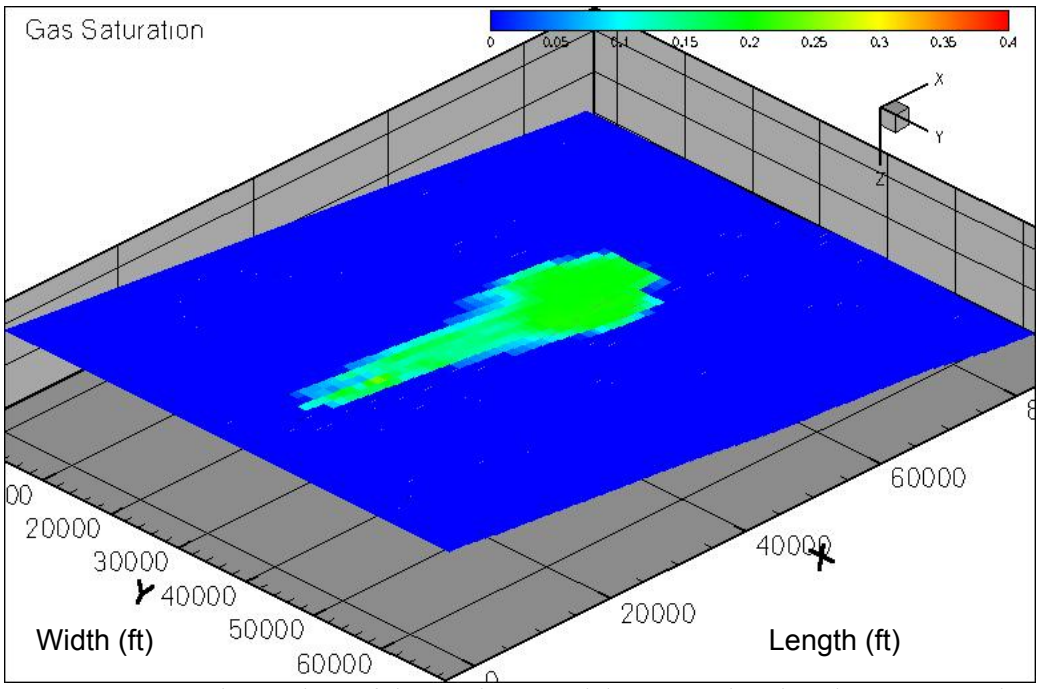

Figure D-3: Top layer view of the Study A model, Run 1, showing the gas saturation at 1000 years. (High permeability, low vertical permeability, high Land's constant, low relative permeability curves, low S_{wir}, low solubility).

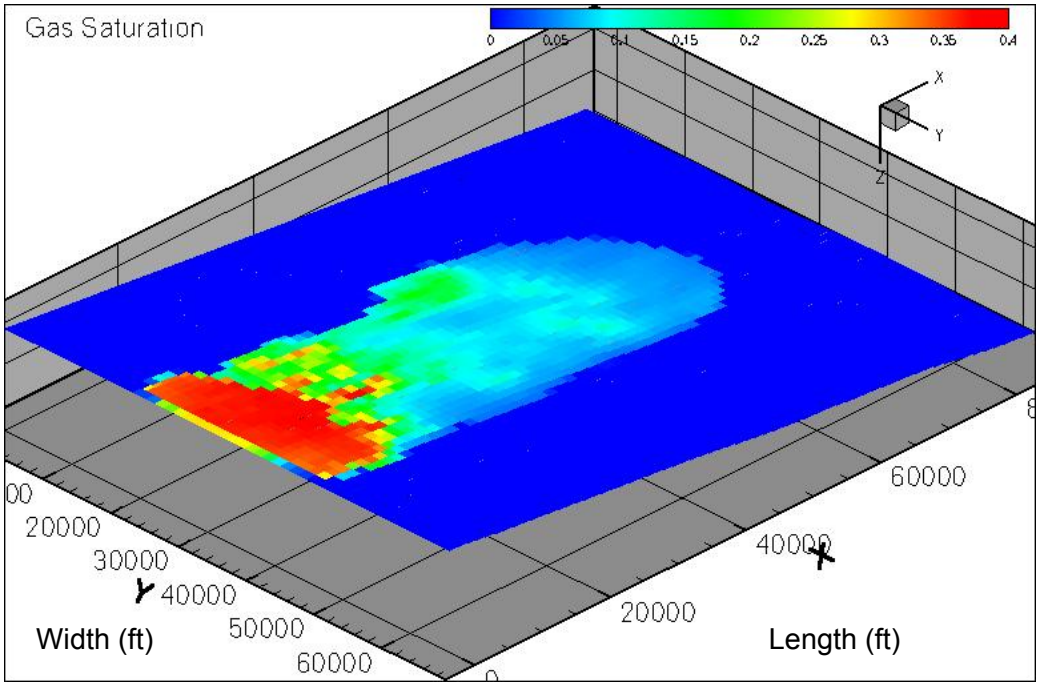

Figure D-4: Top layer view of the Study A model, Run 2, showing the gas saturation at 1000 years. (High permeability, high vertical permeability, low Land's constant, high relative permeability curves, low S_{wir}, low solubility).

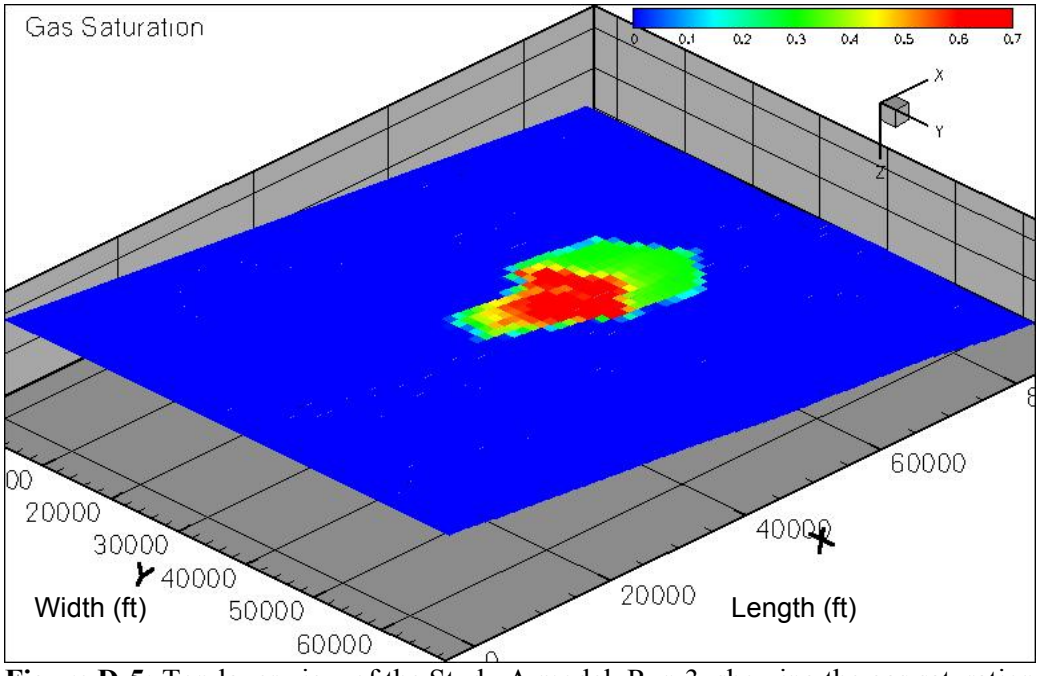

Figure D-5: Top layer view of the Study A model, Run 3, showing the gas saturation at 1000 years. (Low permeability, high vertical permeability, high Land's constant, low relative permeability curves, high S_{wir}, low solubility).

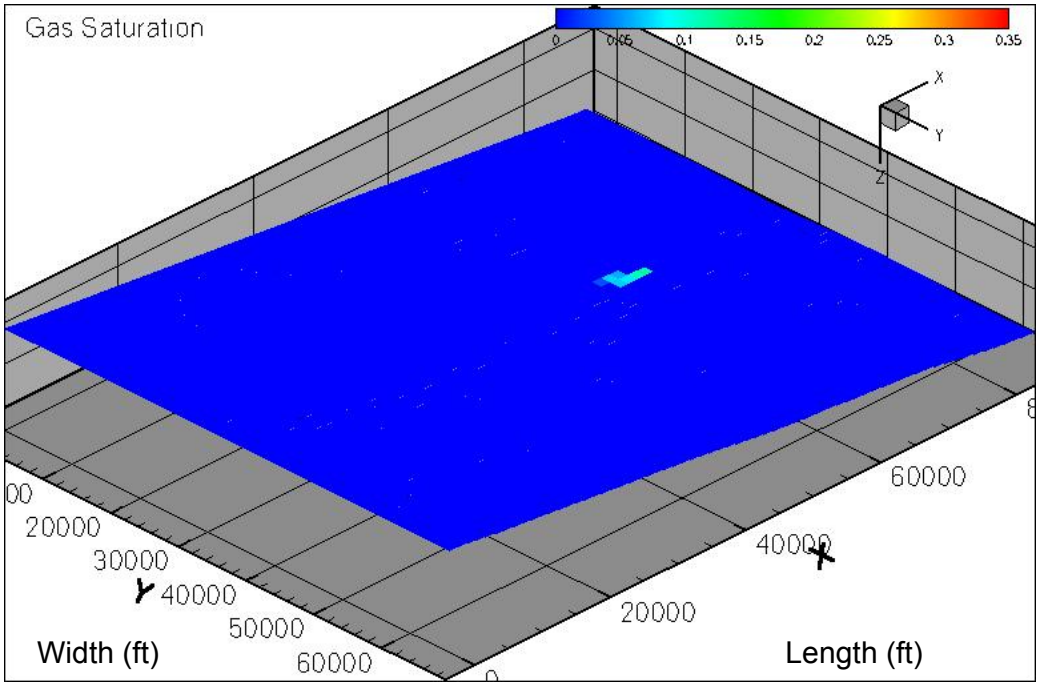

Figure D-6: Top layer view of the Study A model, Run 4, showing the gas saturation at 1000 years. (High permeability, low vertical permeability, high Land's constant, high relative permeability curves, low S_{wir}, high solubility).

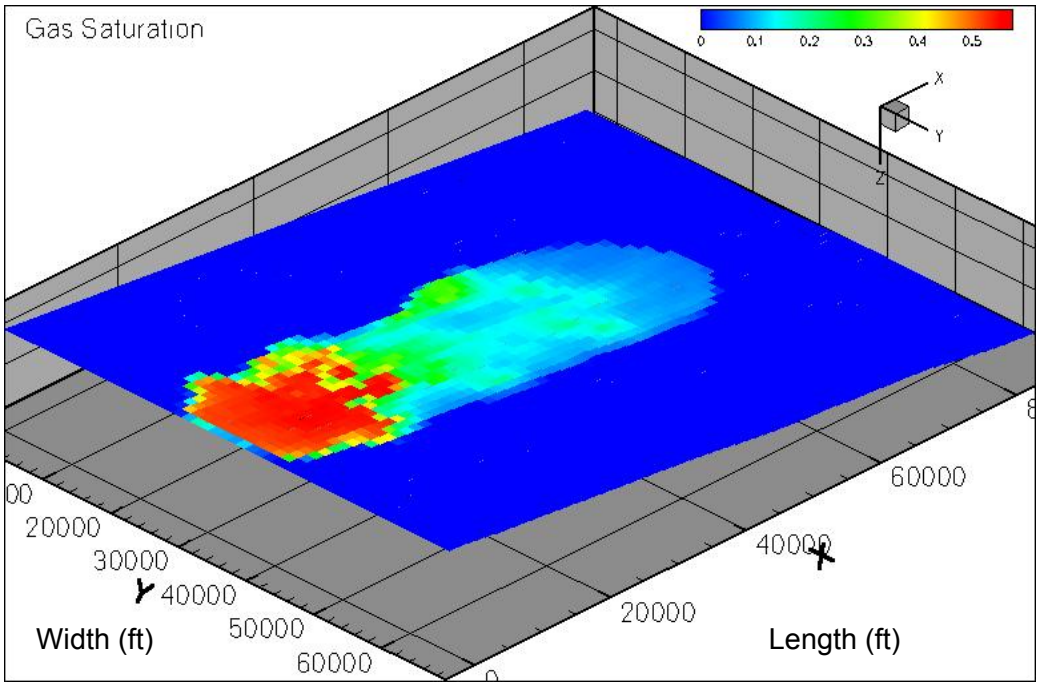

Figure D-7: Top layer view of the Study A model, Run 5, showing the gas saturation at 1000 years. (High permeability, high vertical permeability, low Land's constant, high relative permeability curves, high S_{wir}, low solubility).

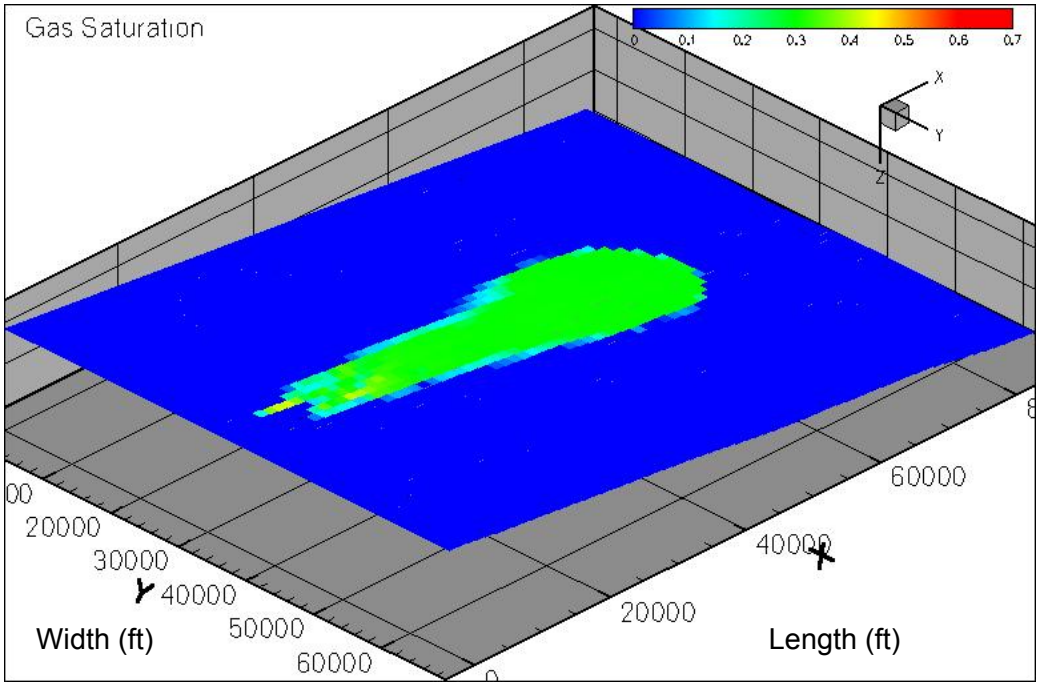

Figure D-8: Top layer view of the Study A model, Run 6, showing the gas saturation at 1000 years. (High permeability, high vertical permeability, high Land's constant, low relative permeability curves, high S_{wir}, high solubility).

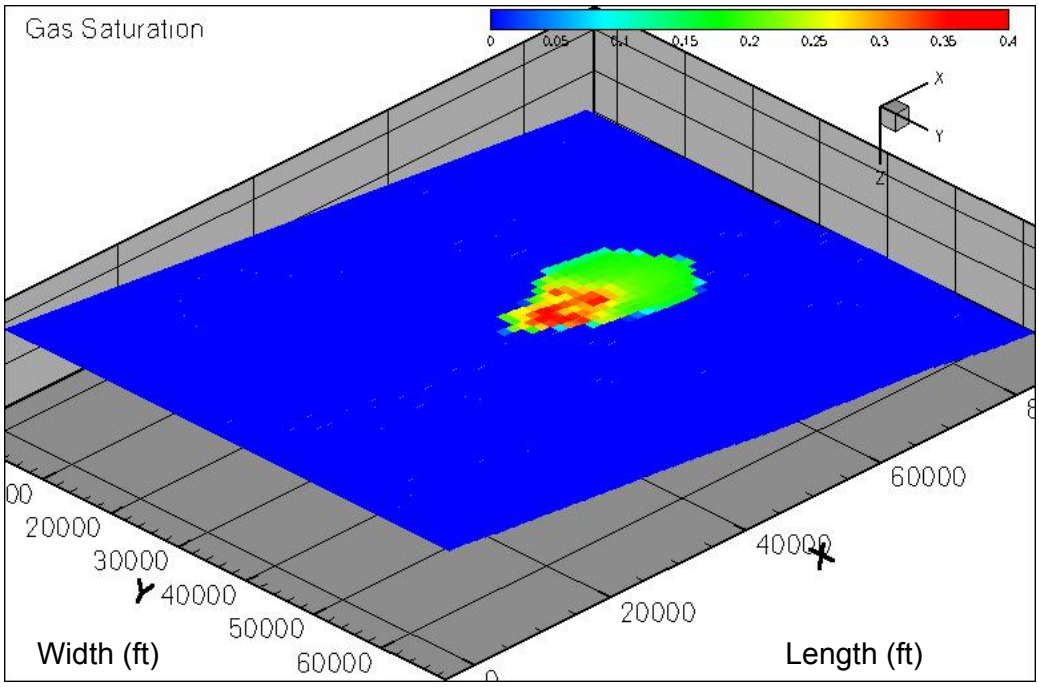

Figure D-9: Top layer view of the Study A model, Run 7, showing the gas saturation at 1000 years. (Low permeability, high vertical permeability, high Land's constant, high relative permeability curves, low S_{wir}, high solubility).

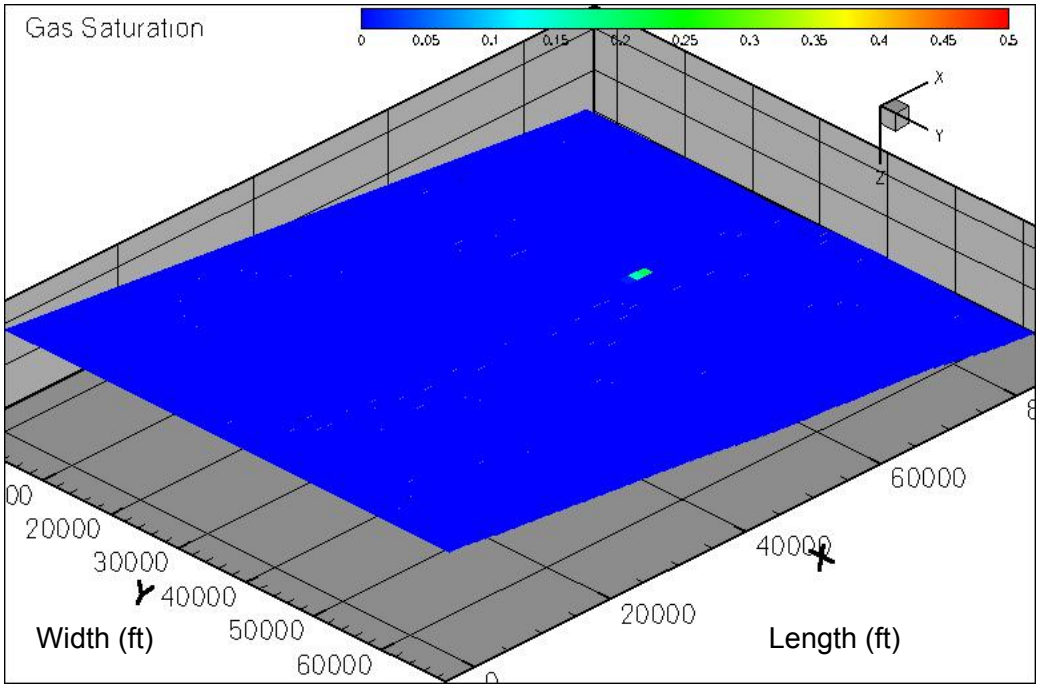

Figure D-10: Top layer view of the Study A model, Run 8, showing the gas saturation at 1000 years. (Low permeability, low vertical permeability, high Land's constant, high relative permeability curves, high S_{wir}, low solubility).

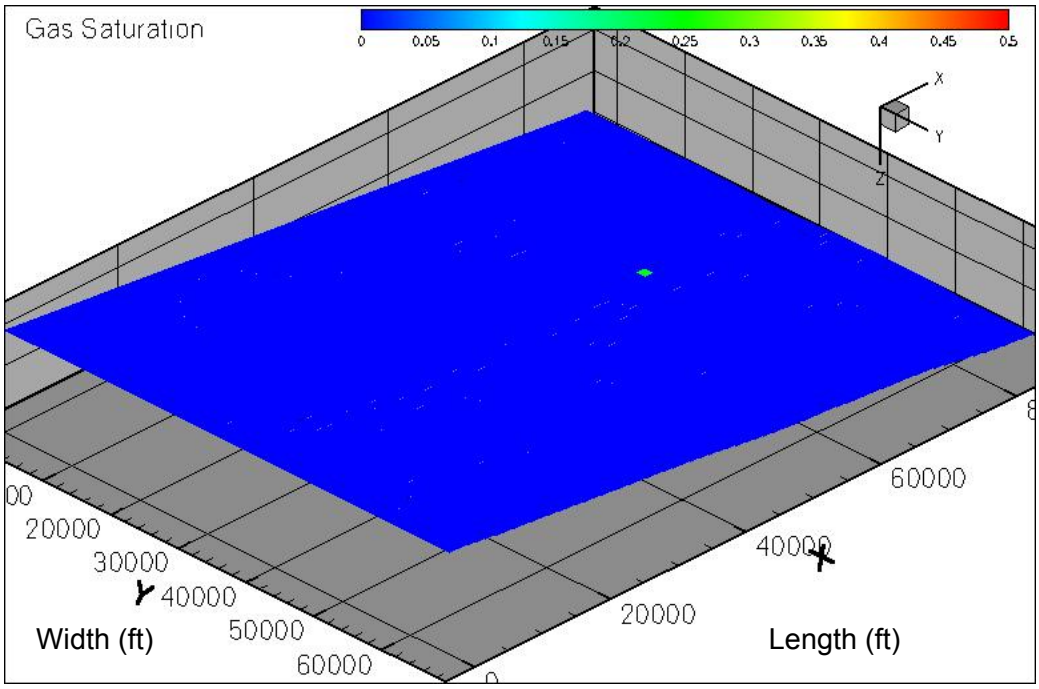

Figure D-11: Top layer view of the Study A model, Run 9, showing the gas saturation at 1000 years. (Low permeability, low vertical permeability, low Land's constant, low relative permeability curves, high S_{wir}, high solubility).

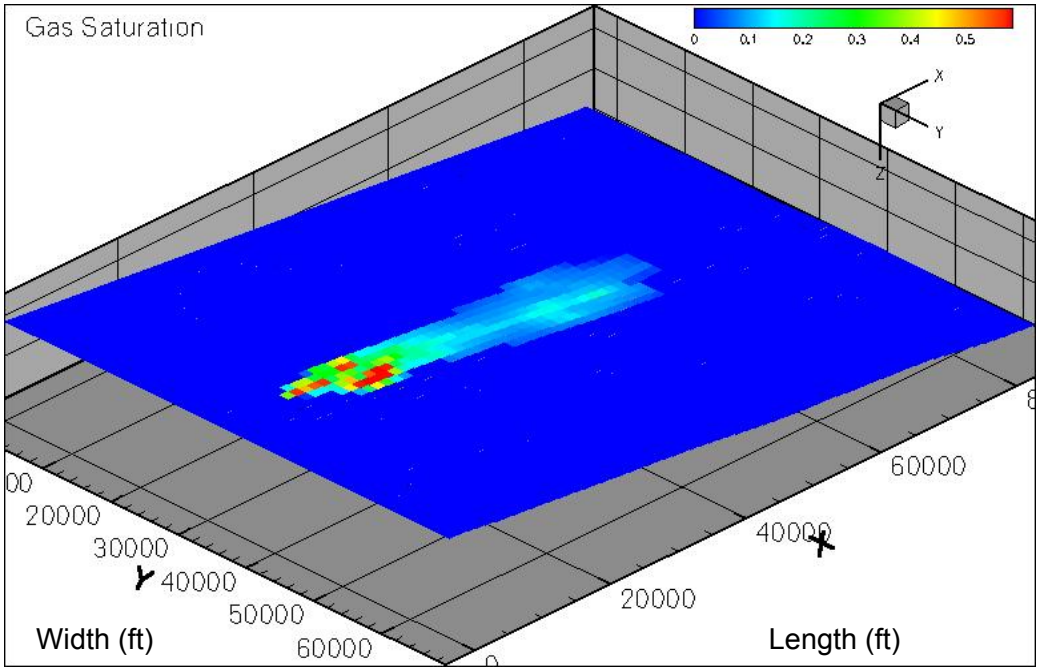

Figure D-12: Top layer view of the Study A model, Run 10, showing the gas saturation at 1000 years. (High permeability, low vertical permeability, low Land's constant, low relative permeability curves, high S_{wir}, high solubility).

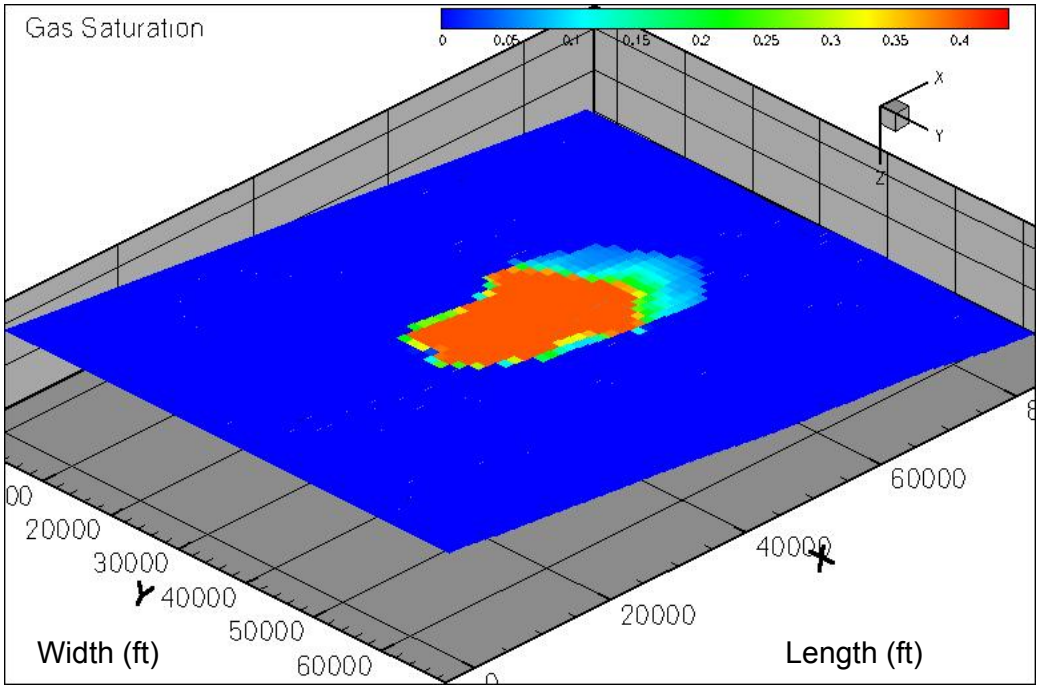

Figure D-13: Top layer view of the Study A model, Run 11, showing the gas saturation at 1000 years. (Low permeability, high vertical permeability, low Land's constant, low relative permeability curves, low S_{wir}, high solubility).

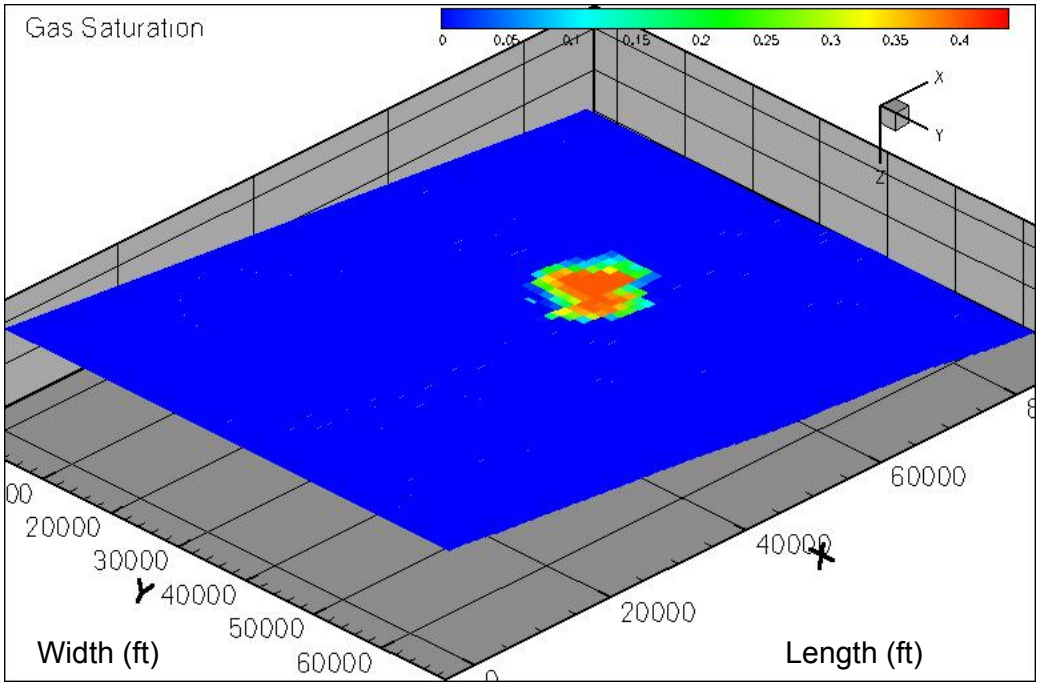

Figure D-14: Top layer view of the Study A model, Run 12, showing the gas saturation at 1000 years. (Low permeability, low vertical permeability, low Land's constant, low relative permeability curves, low S_{wir}, low solubility).

D.2 Major Study

Comparison of migration for various shale lengths:

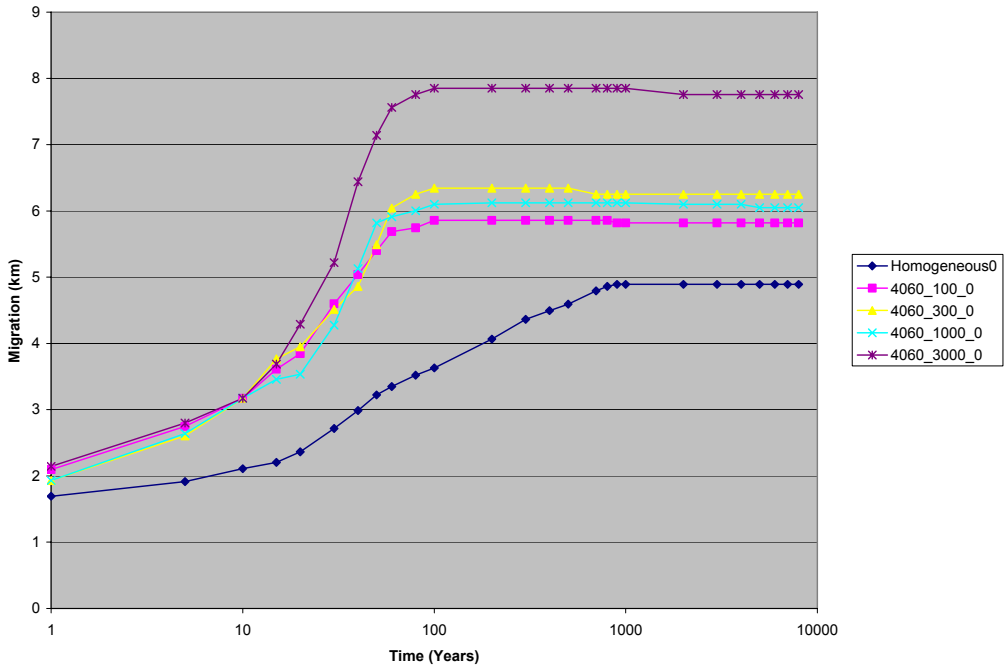

Figure D-15: Migration comparison of the 40:60 net-to-gross models, 0 degree slope

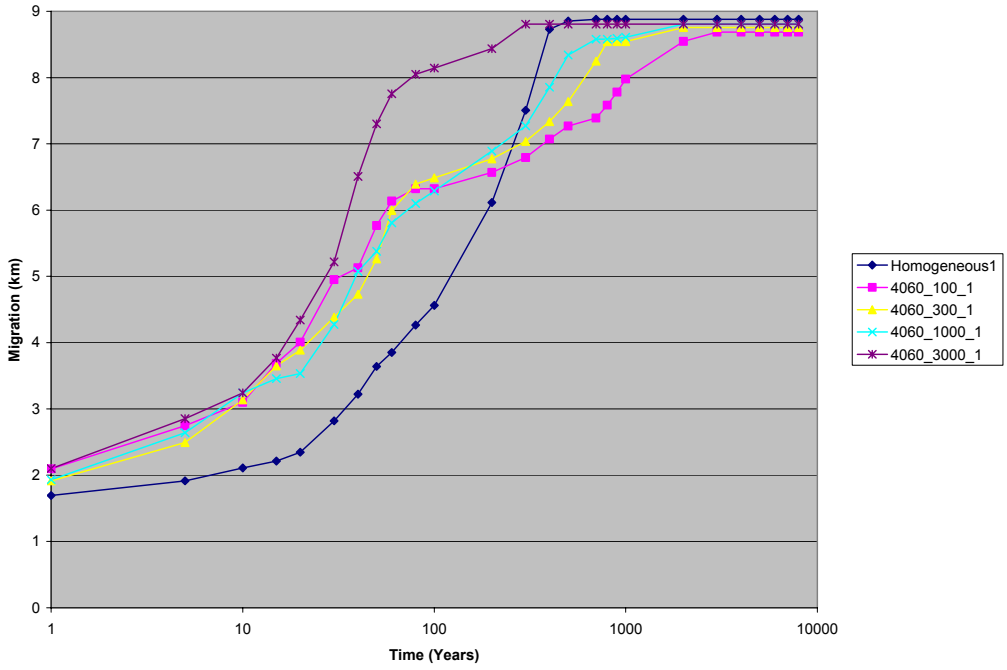

Figure D-16: Migration comparison of the 40:60 net-to-gross models, 1 degree slope

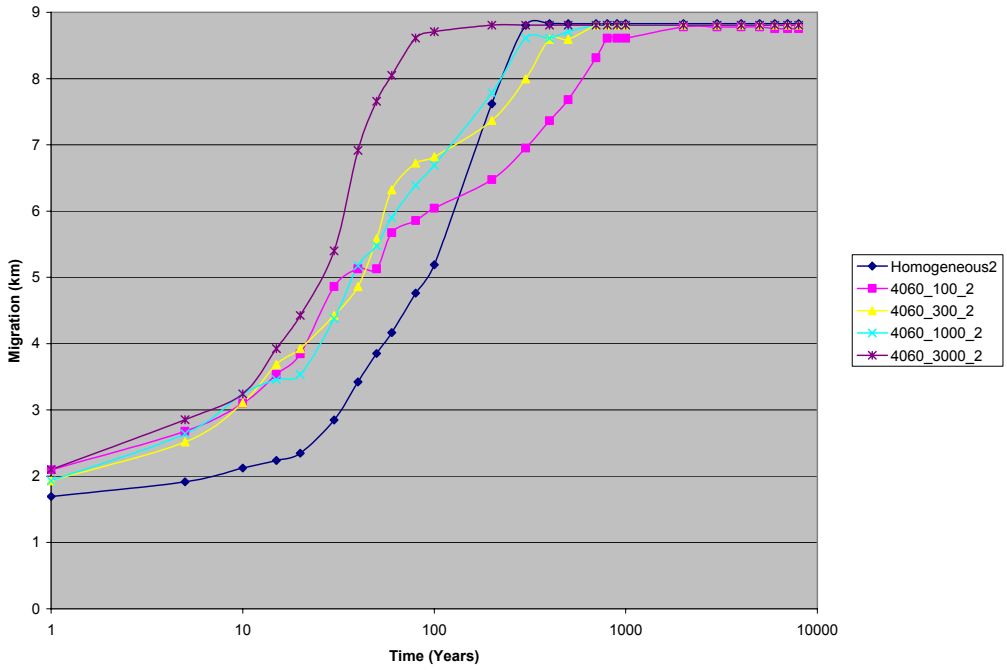

Figure D-17: Migration comparison of the 40:60 net-to-gross models, 2 degree slope

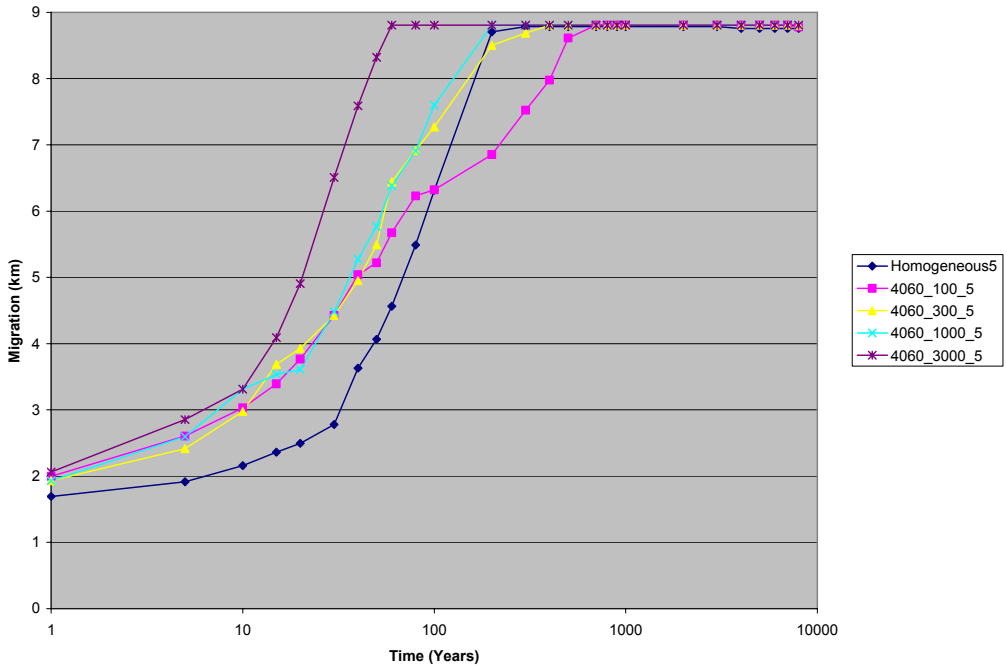

Figure D-18: Migration comparison of the 40:60 net-to-gross models, 5 degree slope

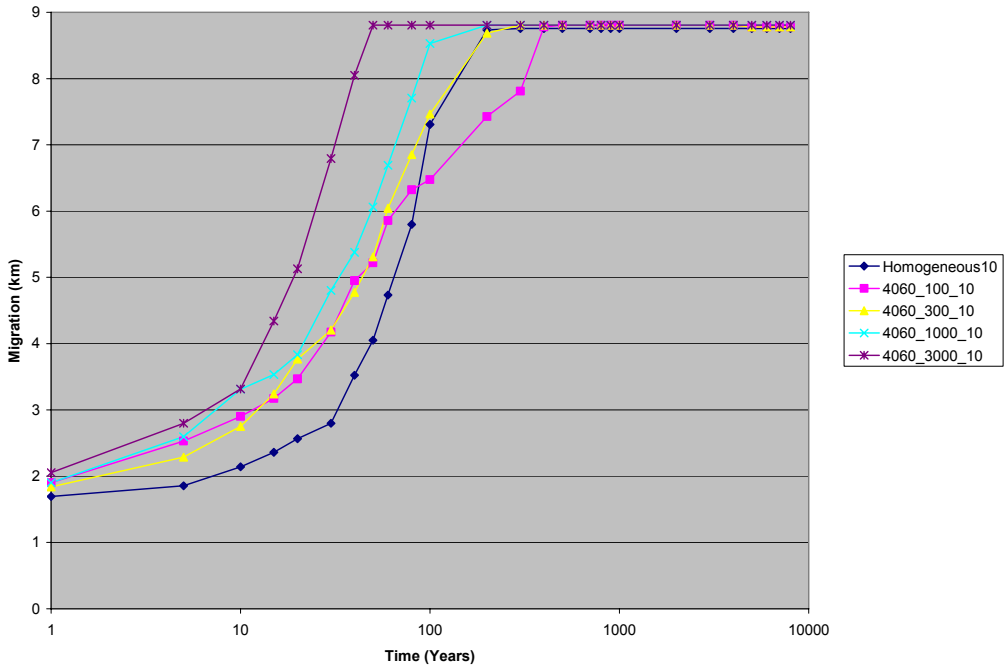

Figure D-19: Migration comparison of the 40:60 net-to-gross models, 10 degree slope

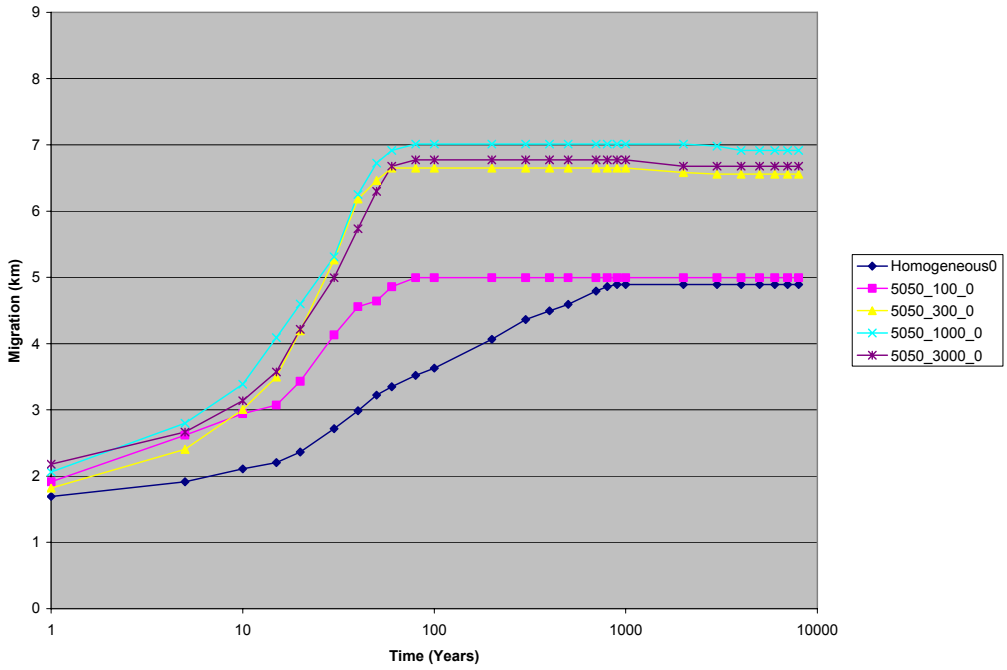

Figure D-20: Migration comparison of the 50:50 net-to-gross models, 0 degree slope

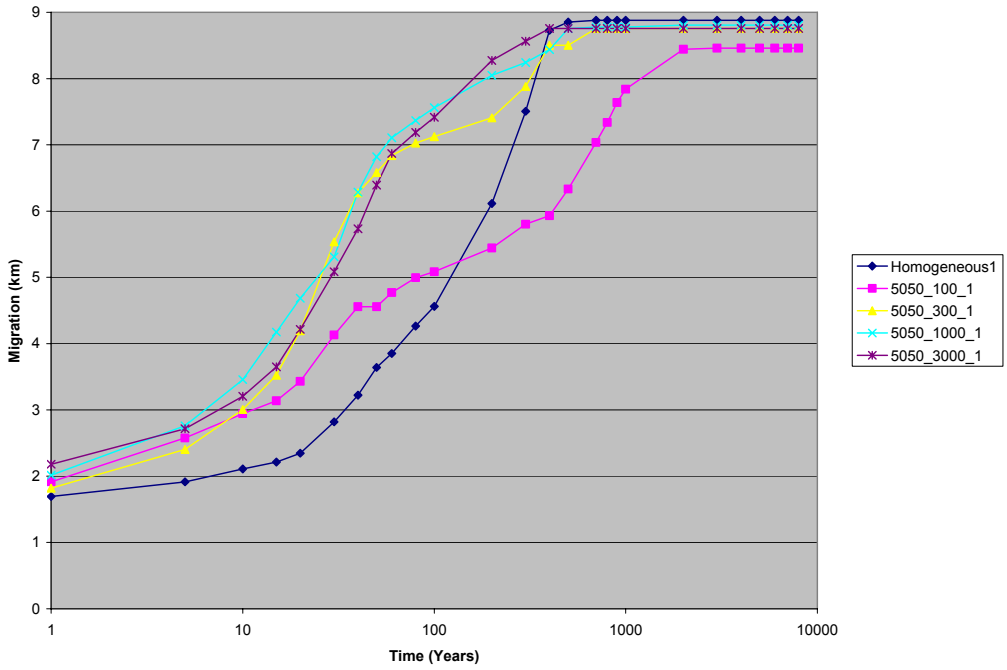

Figure D-21: Migration comparison of the 50:50 net-to-gross models, 1 degree slope

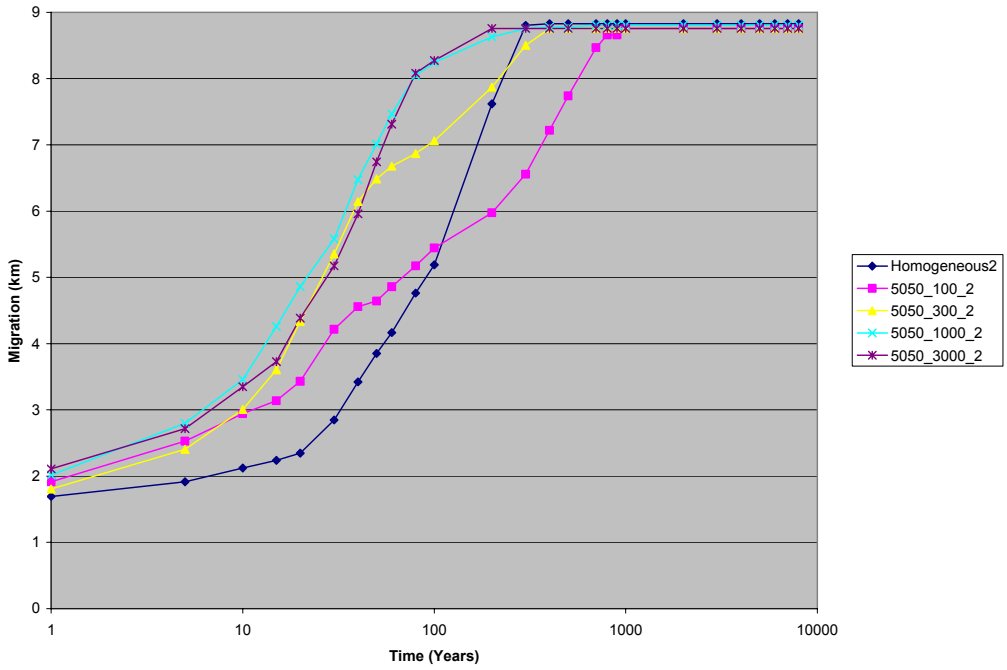

Figure D-22: Migration comparison of the 50:50 net-to-gross models, 2 degree slope

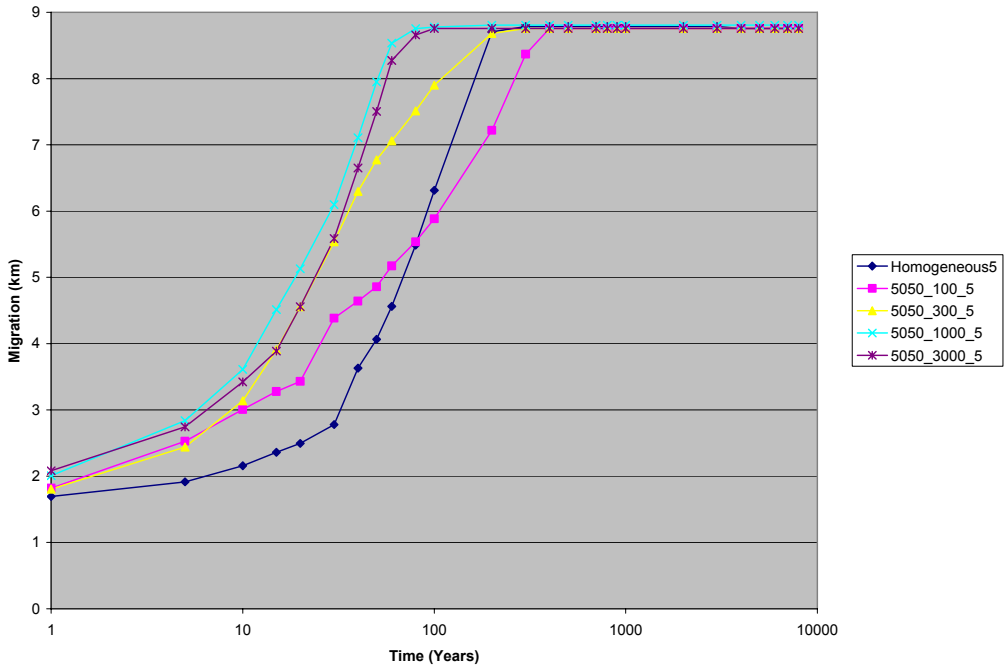

Figure D-23: Migration comparison of the 50:50 net-to-gross models, 5 degree slope

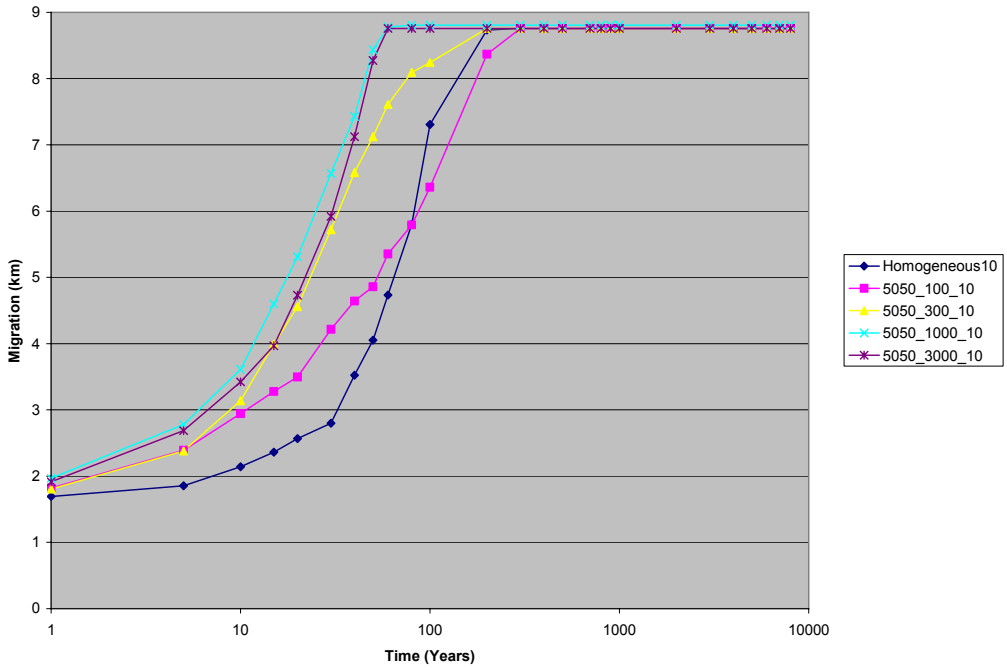

Figure D-24: Migration comparison of the 50:50 net-to-gross models, 10 degree slope

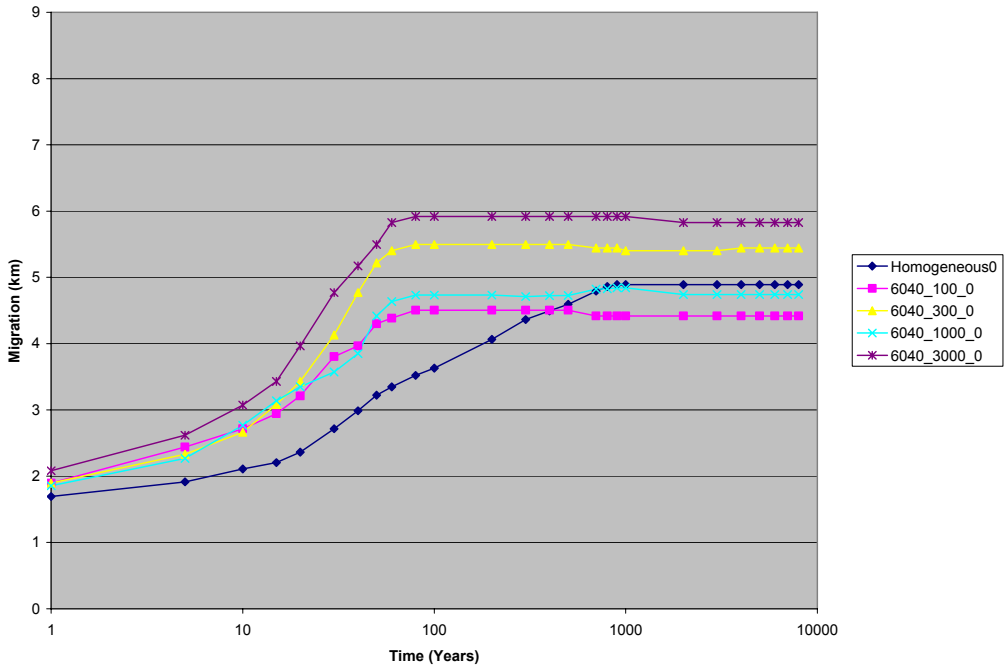

Figure D-25: Migration comparison of the 60:40 net-to-gross models, 0 degree slope

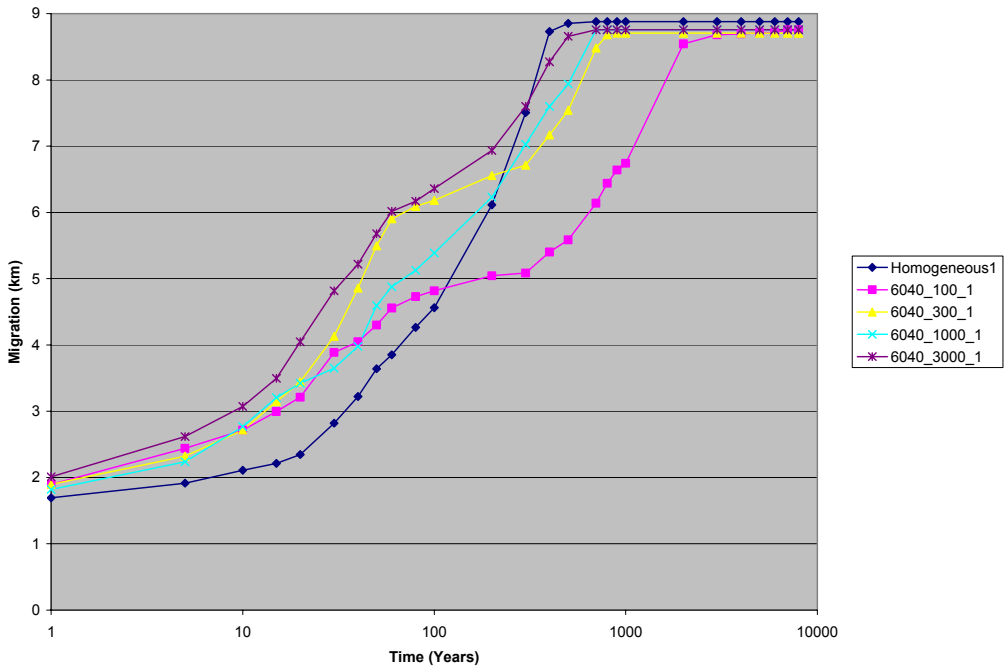

Figure D-26: Migration comparison of the 60:40 net-to-gross models, 1 degree slope

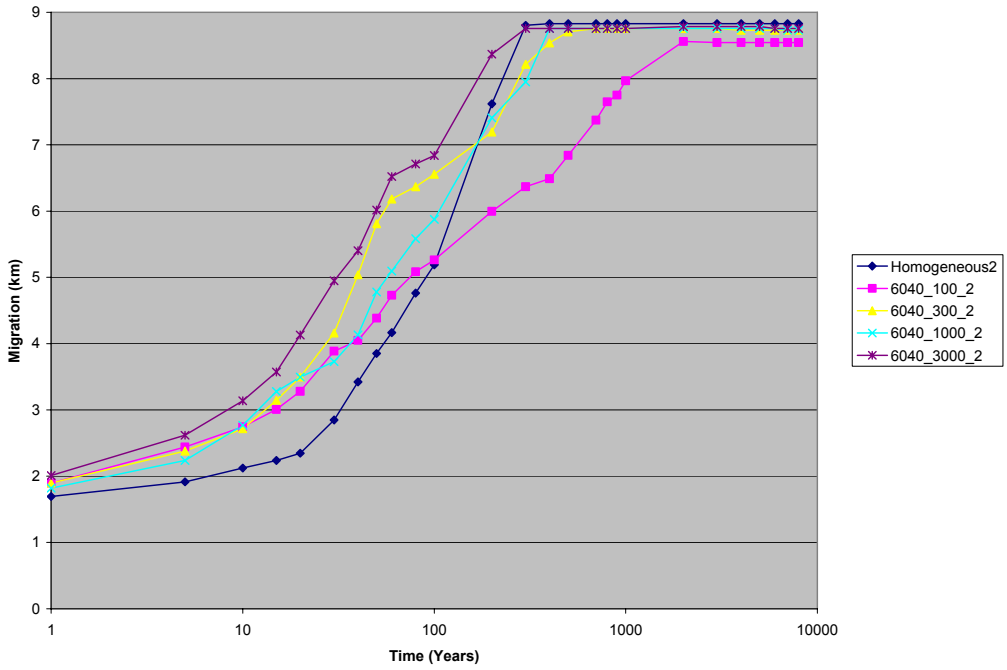

Figure D-27: Migration comparison of the 60:40 net-to-gross models, 2 degree slope

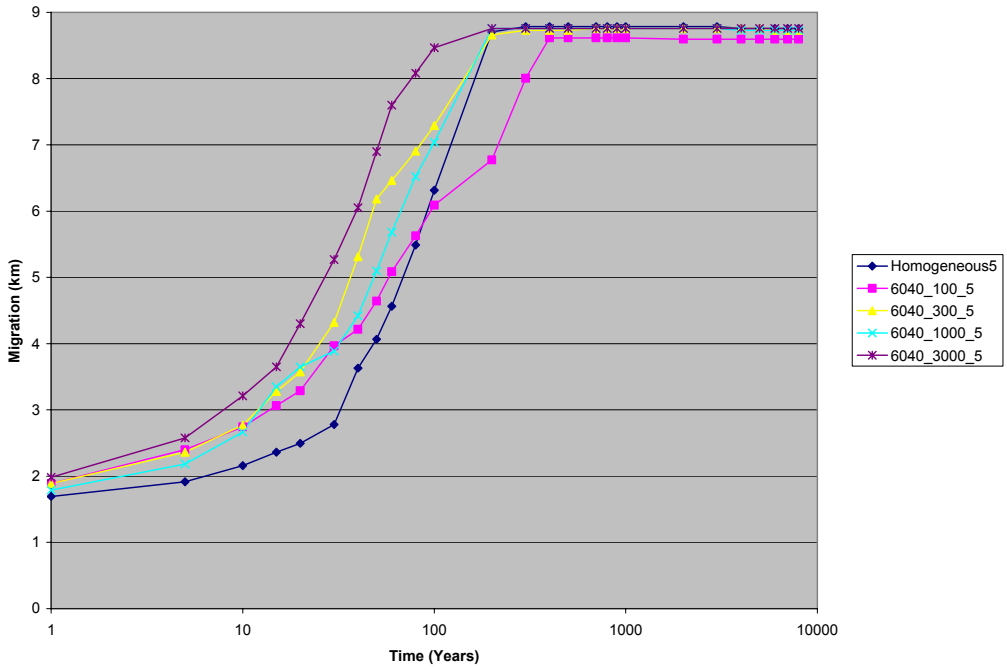

Figure D-28: Migration comparison of the 60:40 net-to-gross models, 5 degree slope

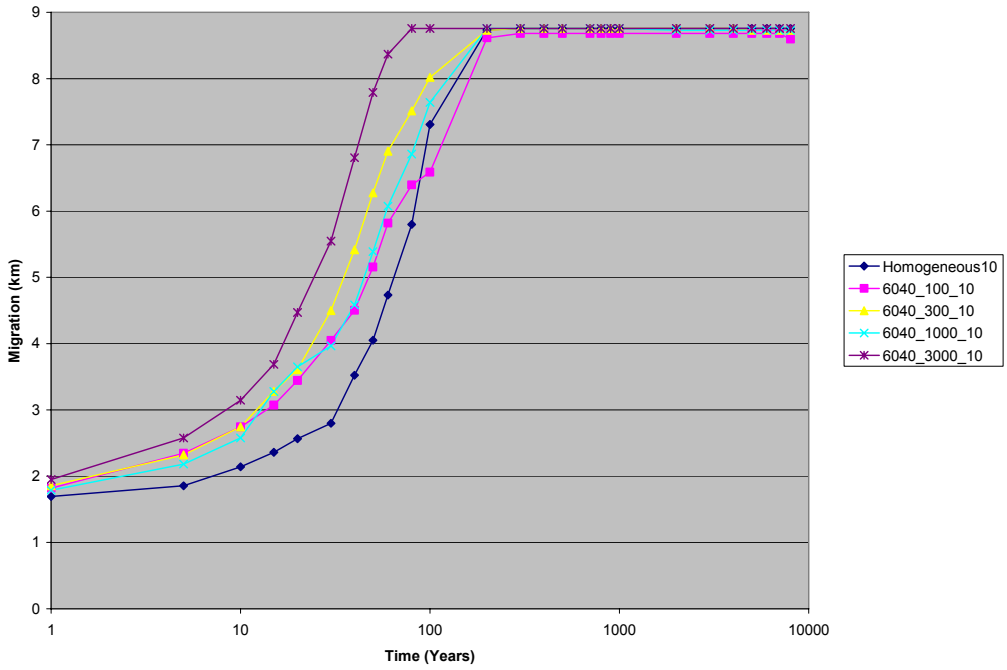

Figure D-29: Migration comparison of the 60:40 net-to-gross models, 10 degree slope

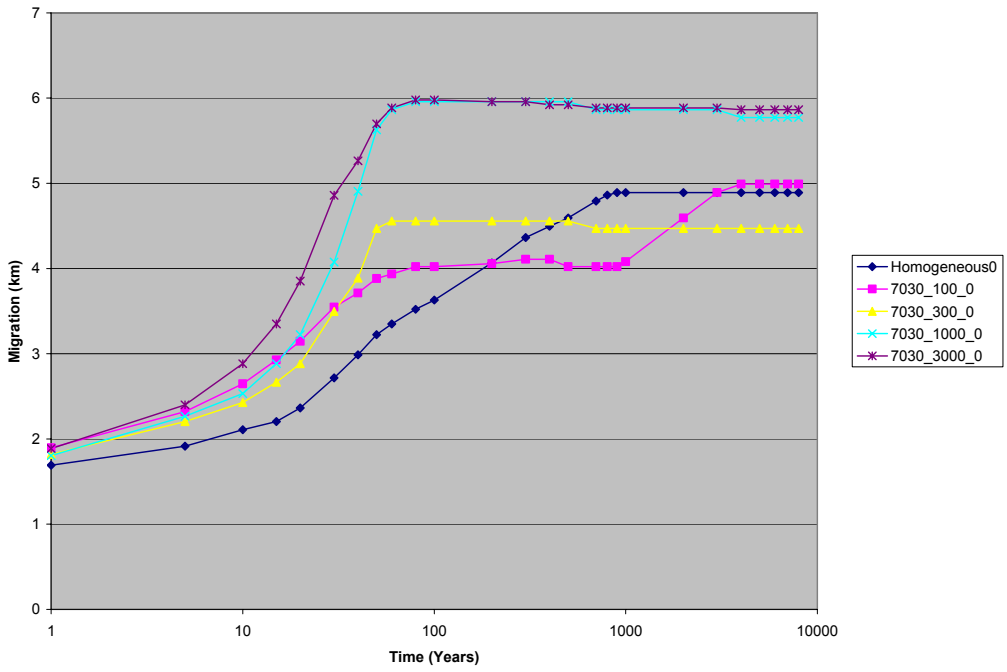

Figure D-30: Migration comparison of the 70:30 net-to-gross models, 0 degree slope

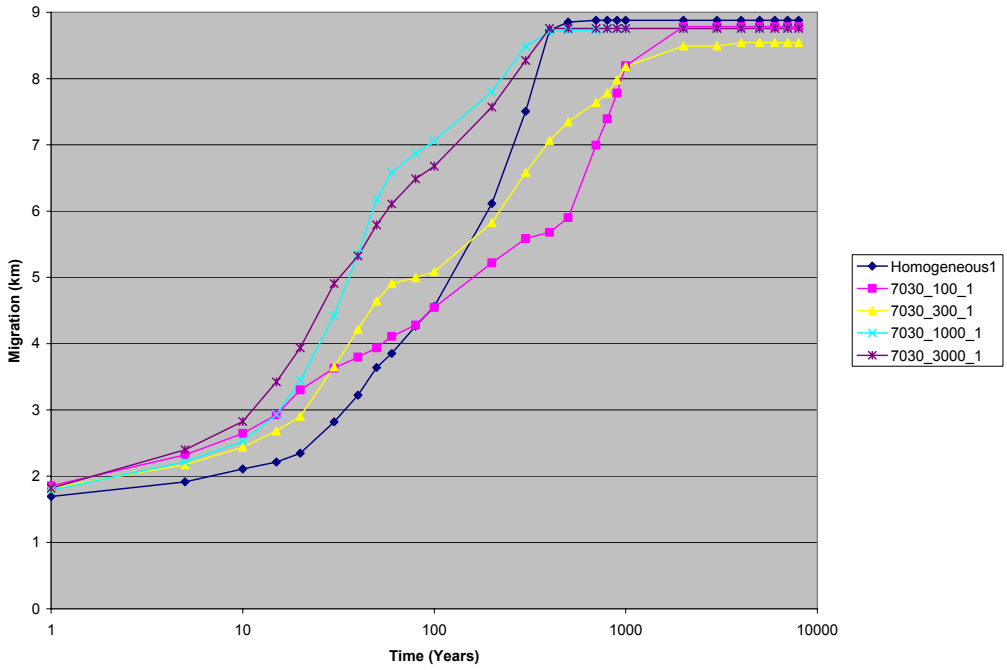

Figure D-31: Migration comparison of the 70:30 net-to-gross models, 1 degree slope

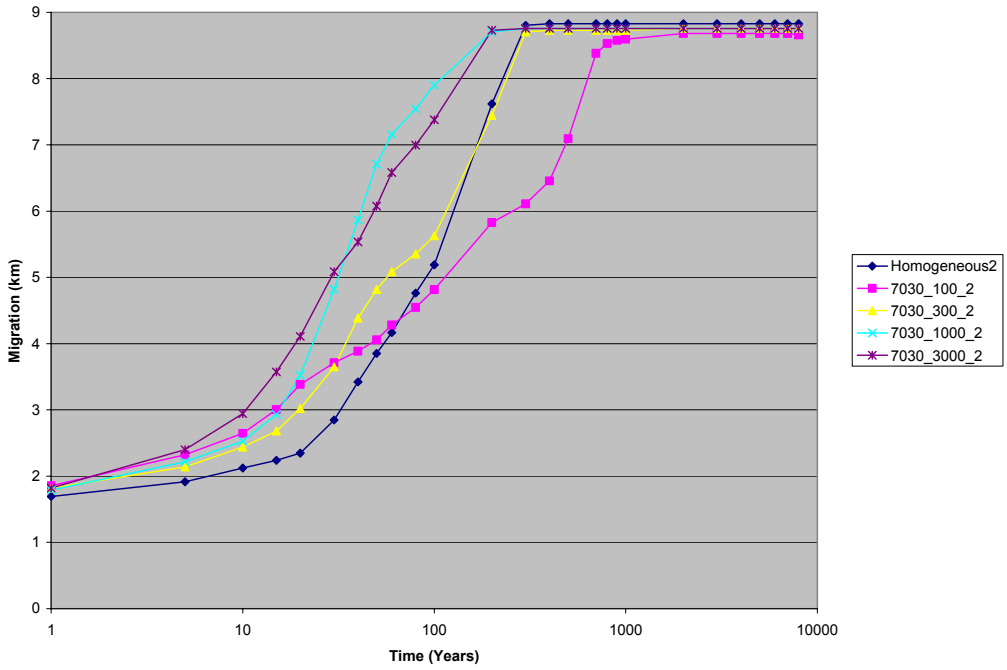

Figure D-32: Migration comparison of the 70:30 net-to-gross models, 2 degree slope

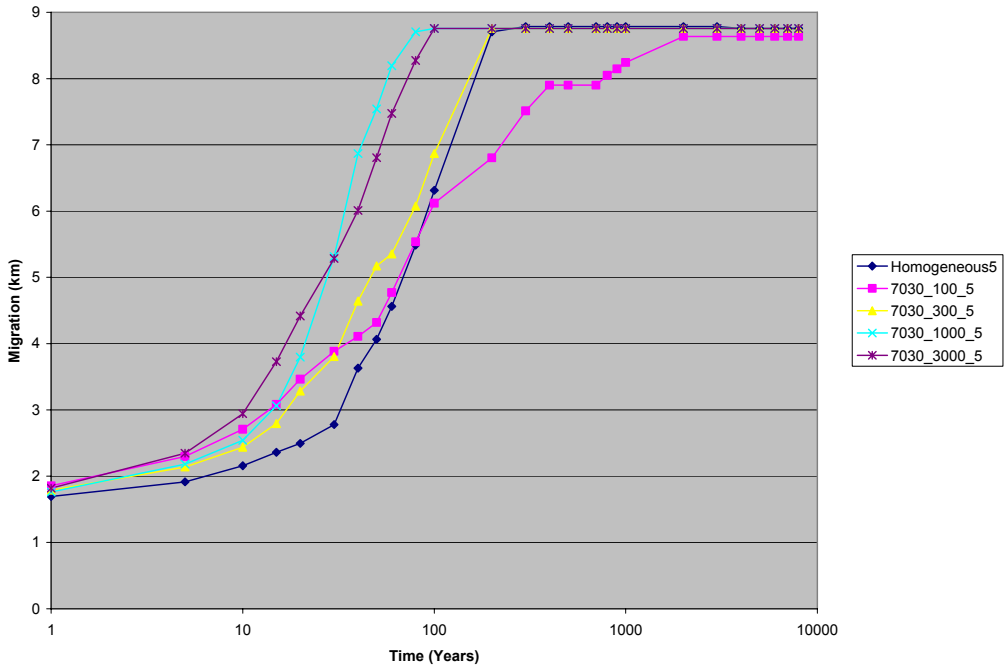

Figure D-33: Migration comparison of the 70:30 net-to-gross models, 5 degree slope

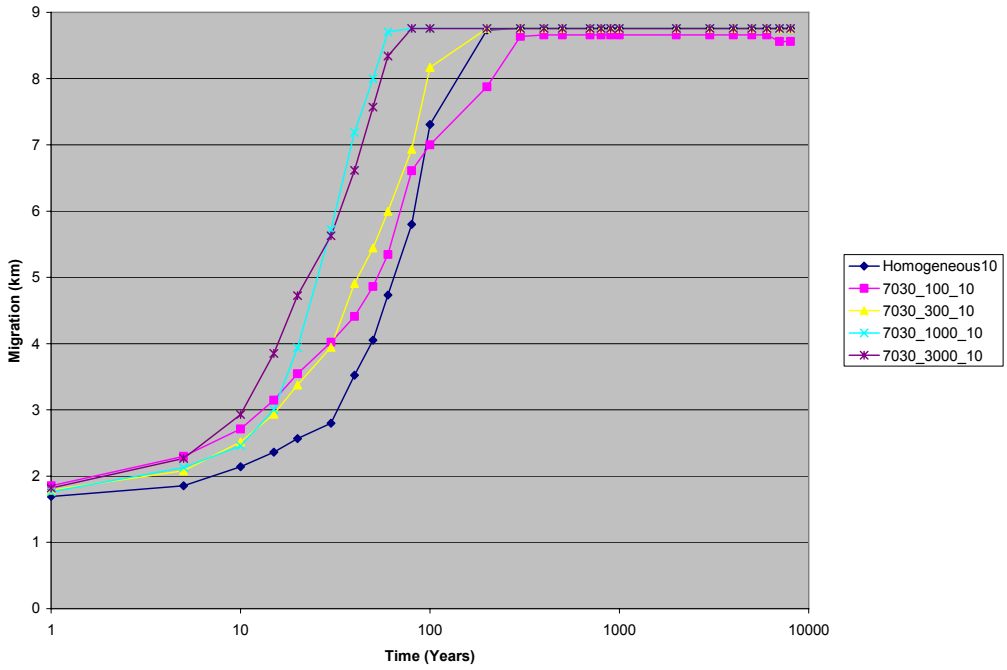

Figure D-34: Migration comparison of the 70:30 net-to-gross models, 10 degree slope

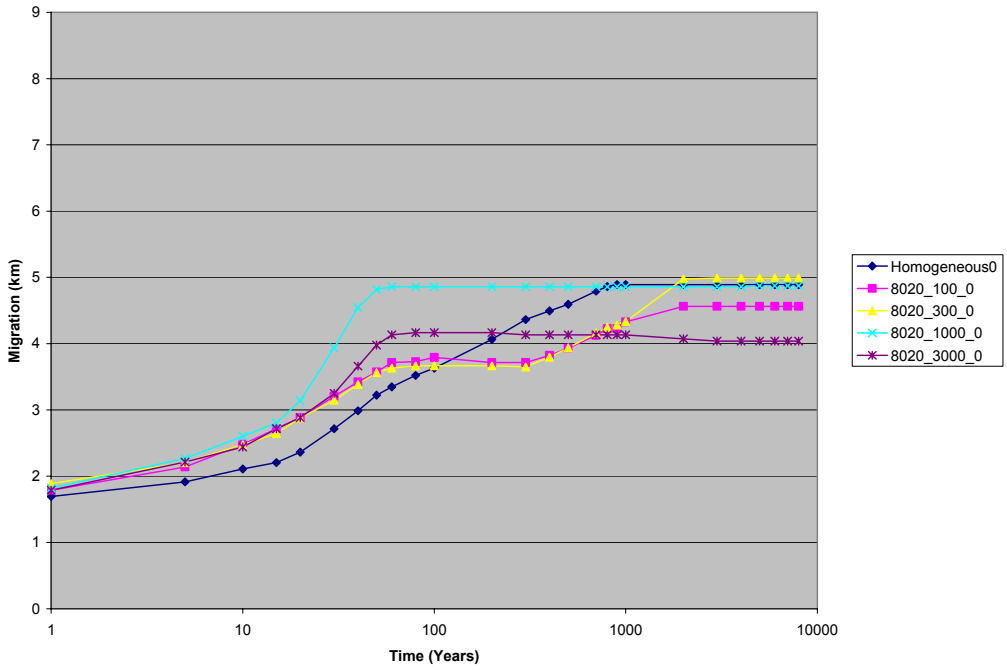

Figure D-35: Migration comparison of the 80:20 net-to-gross models, 0 degree slope

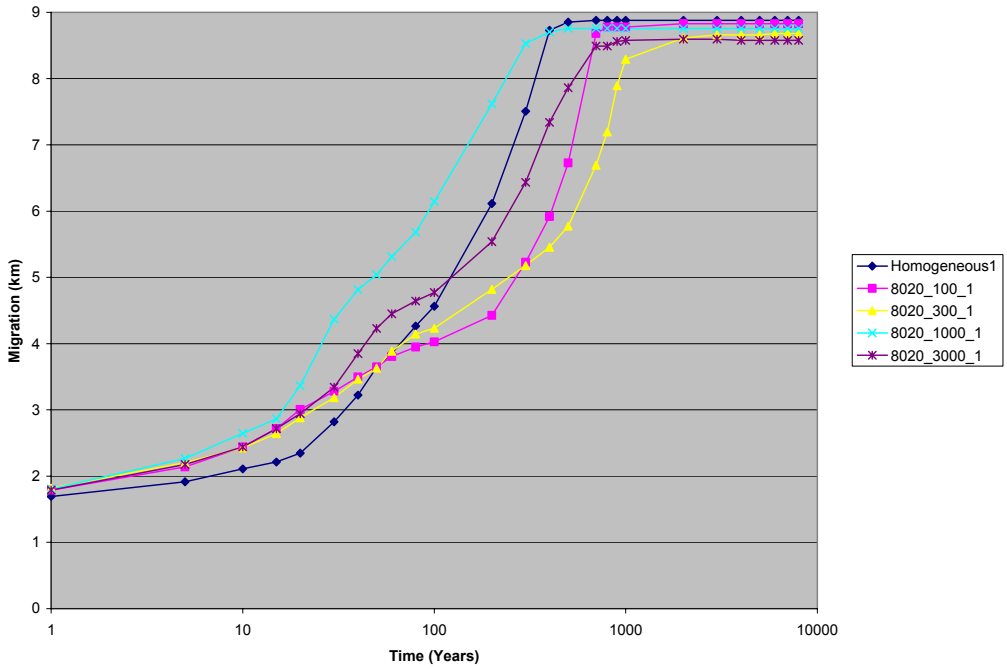

Figure D-36: Migration comparison of the 80:20 net-to-gross models, 1 degree slope

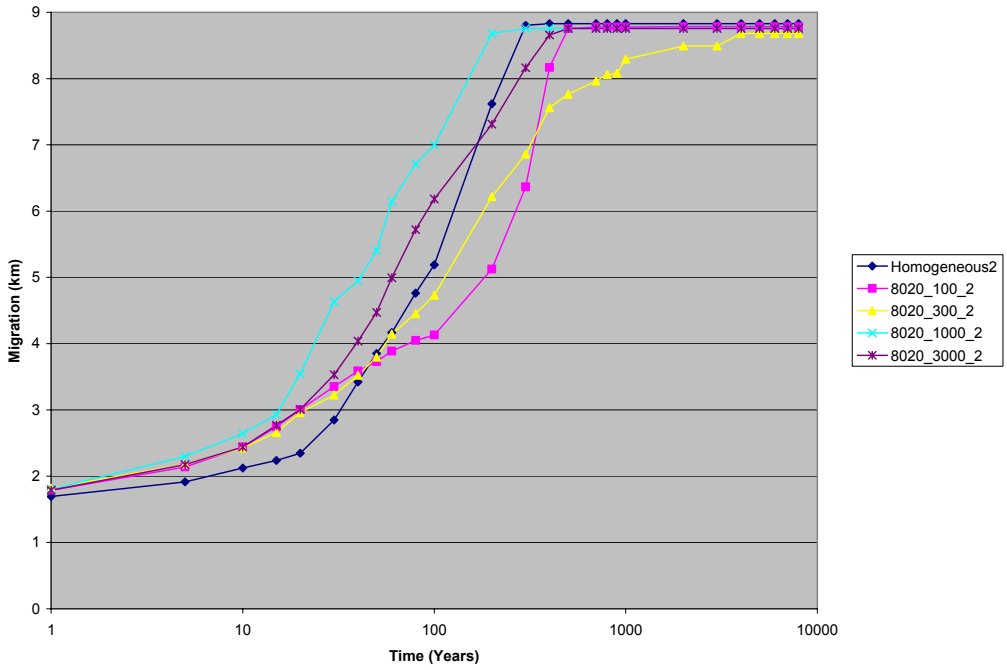

Figure D-37: Migration comparison of the 80:20 net-to-gross models, 2 degree slope

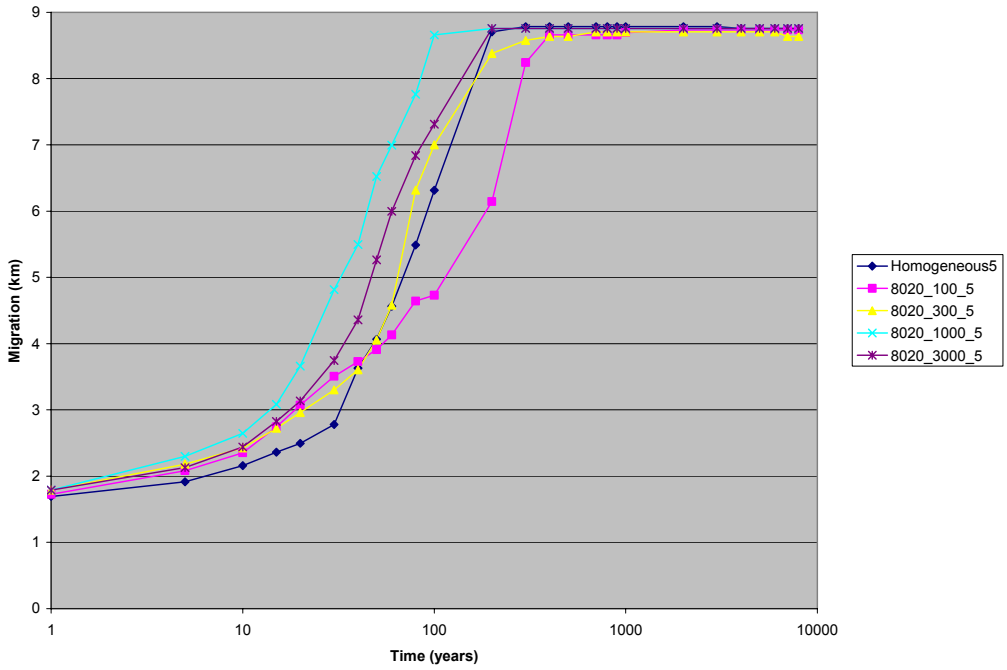

Figure D-38: Migration comparison of the 80:20 net-to-gross models, 5 degree slope

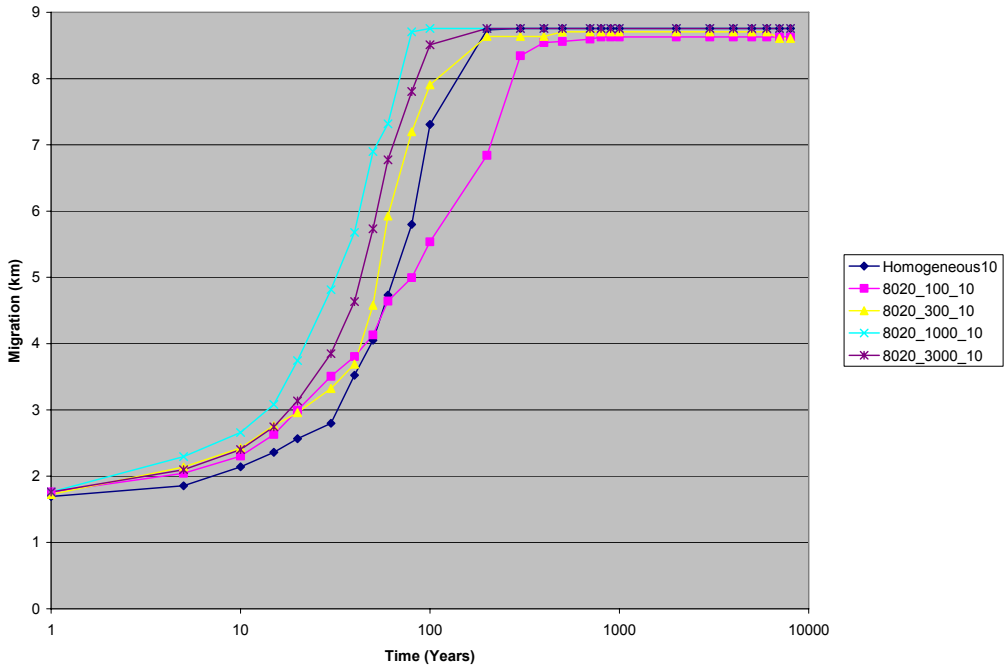

Figure D-39: Migration comparison of the 80:20 net-to-gross models, 10 degree slope

Net to gross comparison on migration

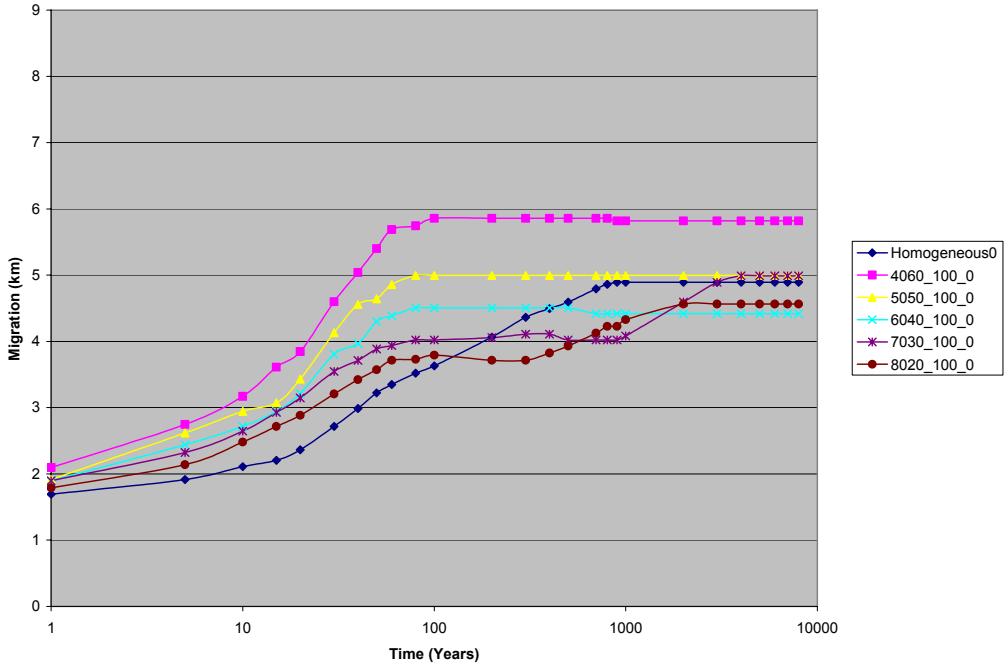

Figure D-40: Migration comparison of the 100 m facies models, various net-to-gross, 0 degree slope

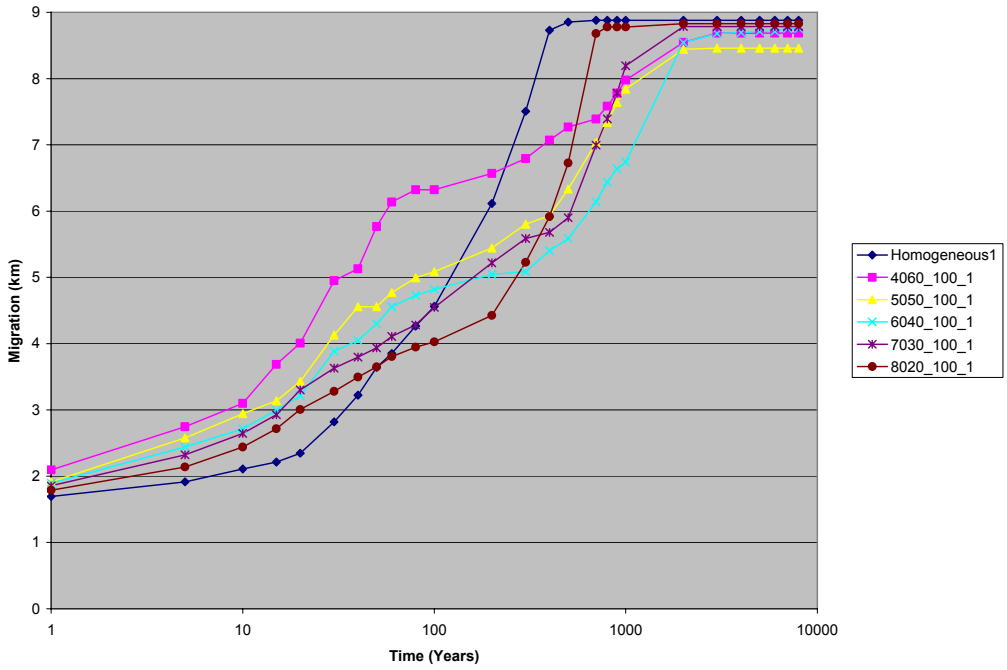

Figure D-41: Migration comparison of the 100 m facies models, various net-to-gross, 1 degree slope

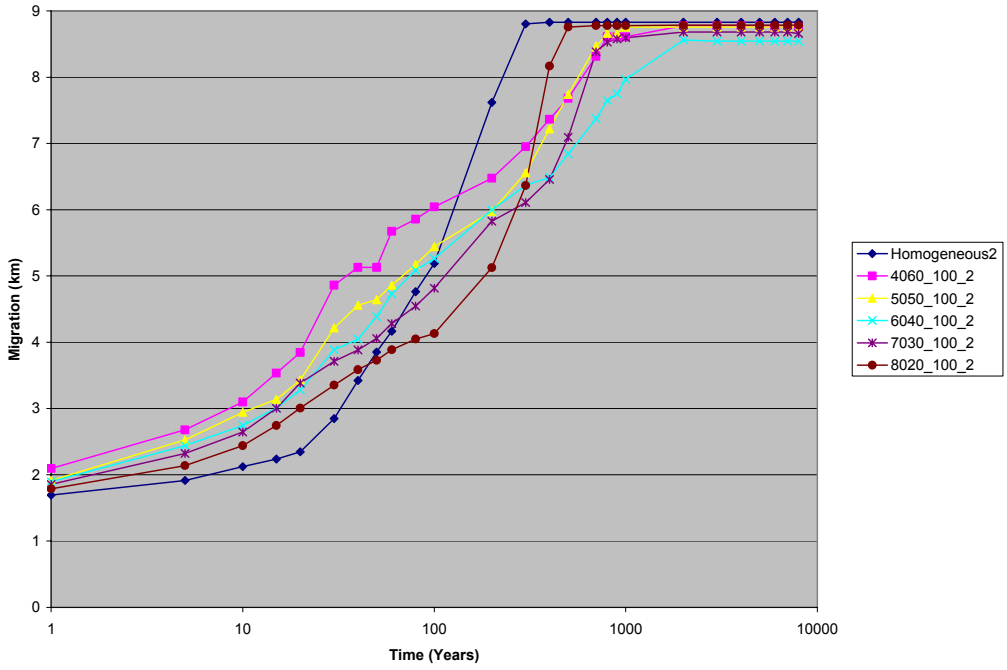

Figure D-42: Migration comparison of the 100 m facies models, various net-to-gross, 2 degree slope

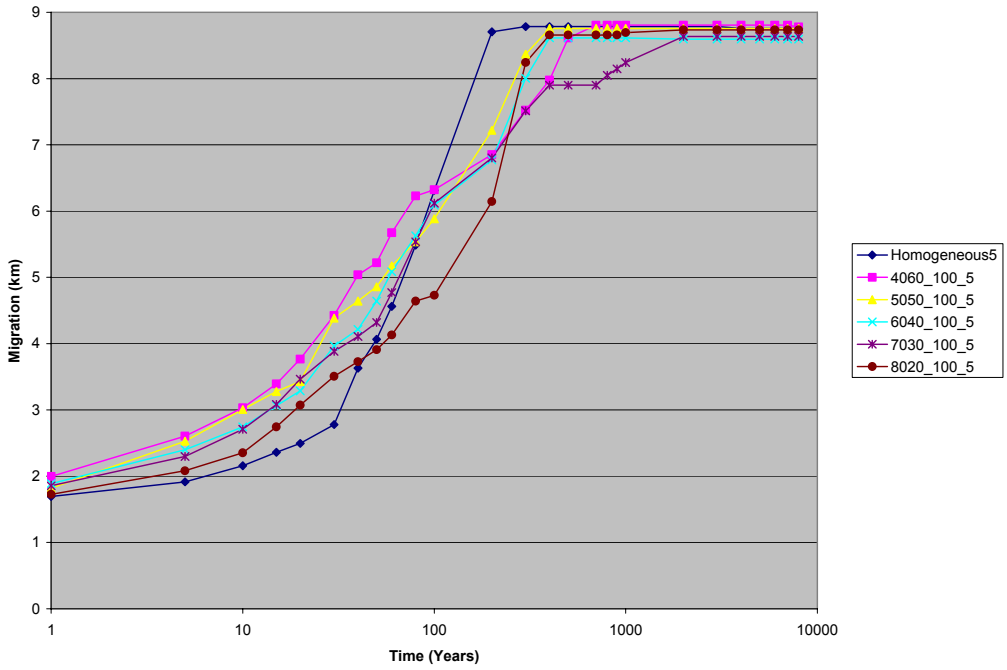

Figure D-43: Migration comparison of the 100 m facies models, various net-to-gross, 5 degree slope

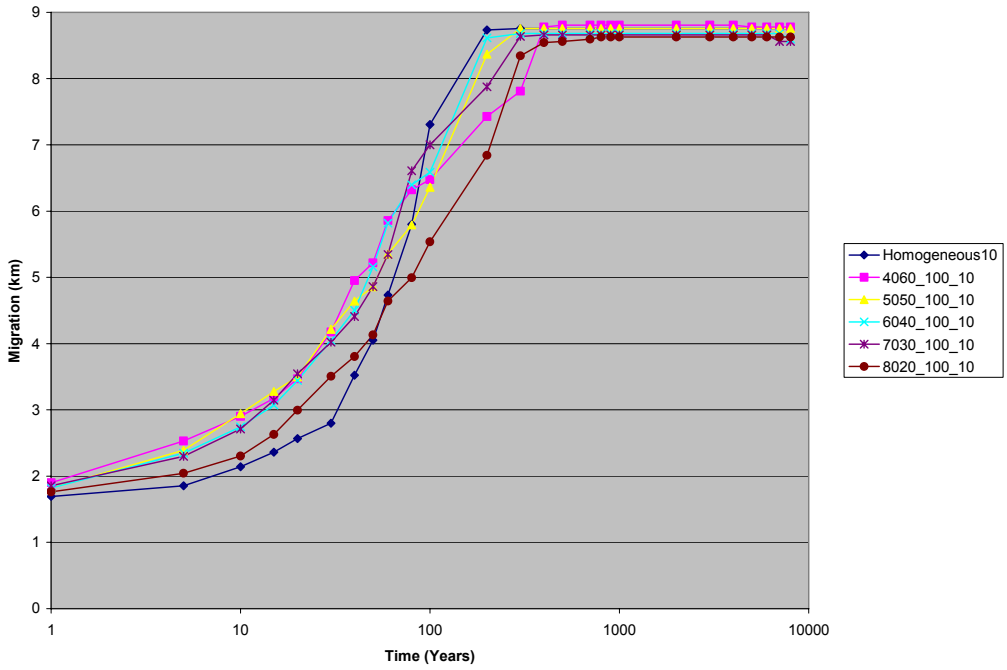

Figure D-44: Migration comparison of the 100 m facies models, various net-to-gross, 10 degree slope

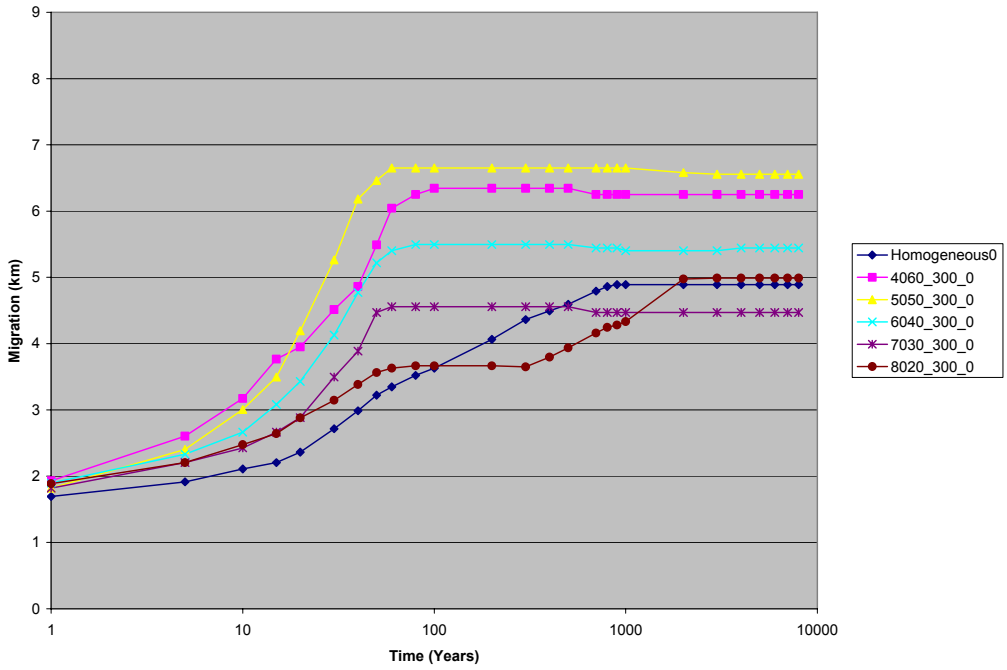

Figure D-45: Migration comparison of the 300 m facies models, various net-to-gross, 0 degree slope

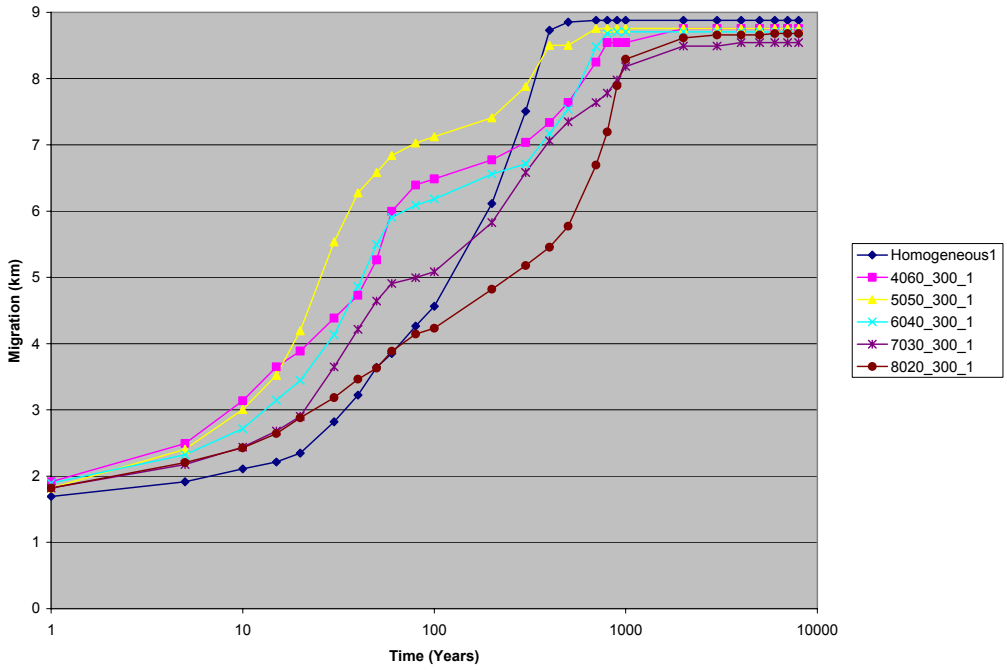

Figure D-46: Migration comparison of the 300 m facies models, various net-to-gross, 1 degree slope

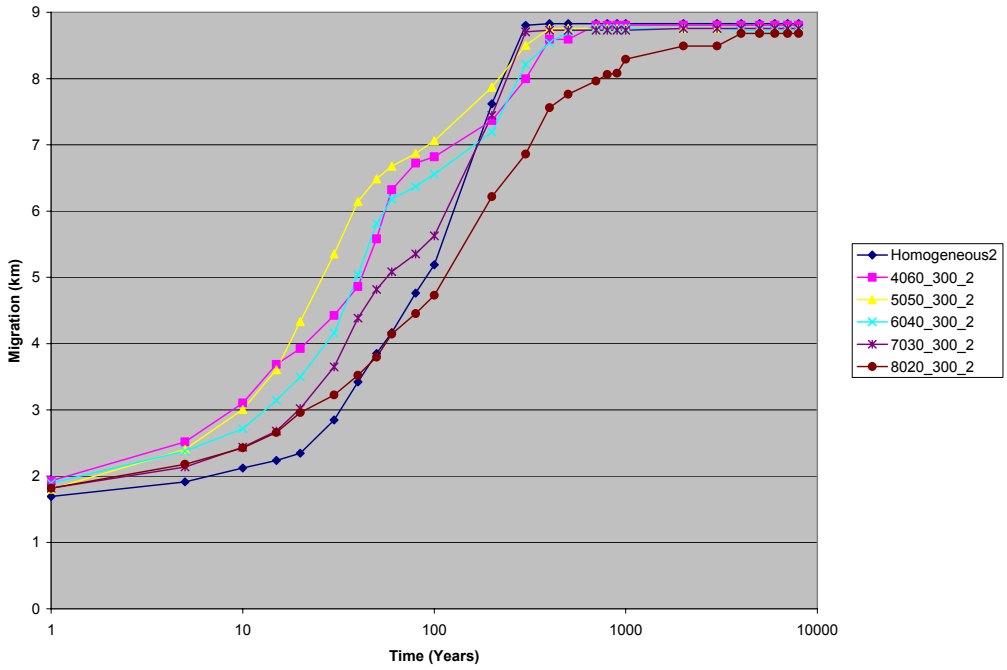

Figure D-47: Migration comparison of the 300 m facies models, various net-to-gross, 2 degree slope

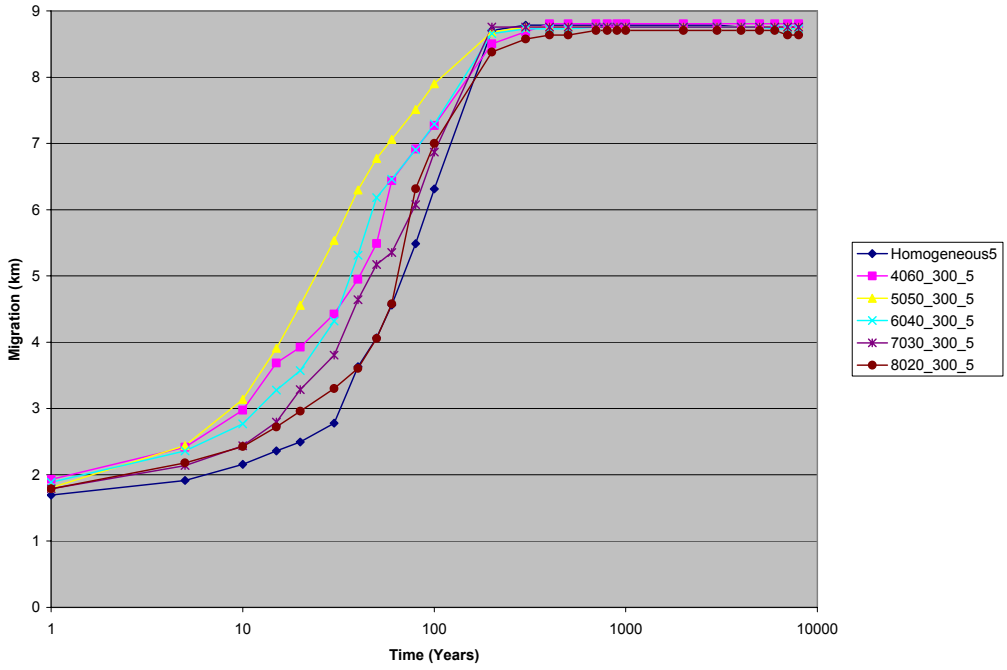

Figure D-48: Migration comparison of the 300 m facies models, various net-to-gross, 5 degree slope

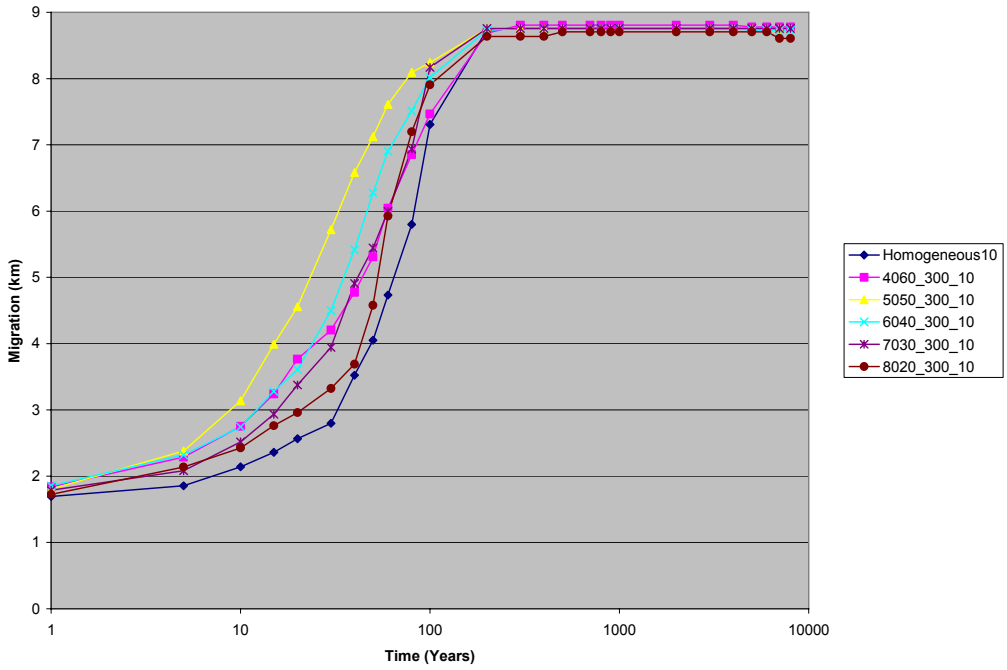

Figure D-49: Migration comparison of the 300 m facies models, various net-to-gross, 10 degree slope

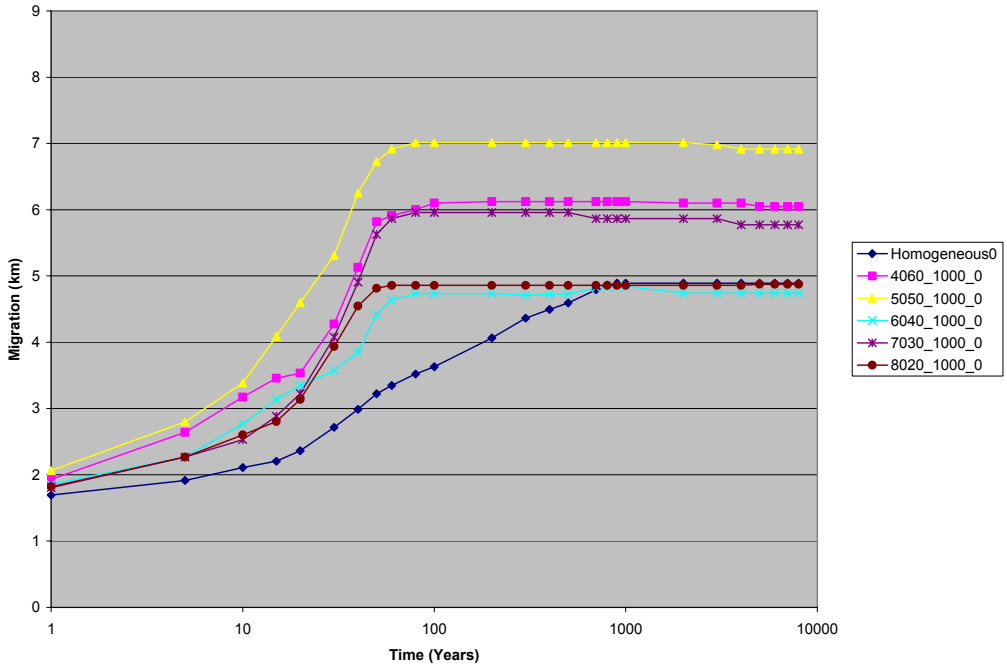

Figure D-50: Migration comparison of the 1000 m facies models, various net-to-gross, 0 degree slope

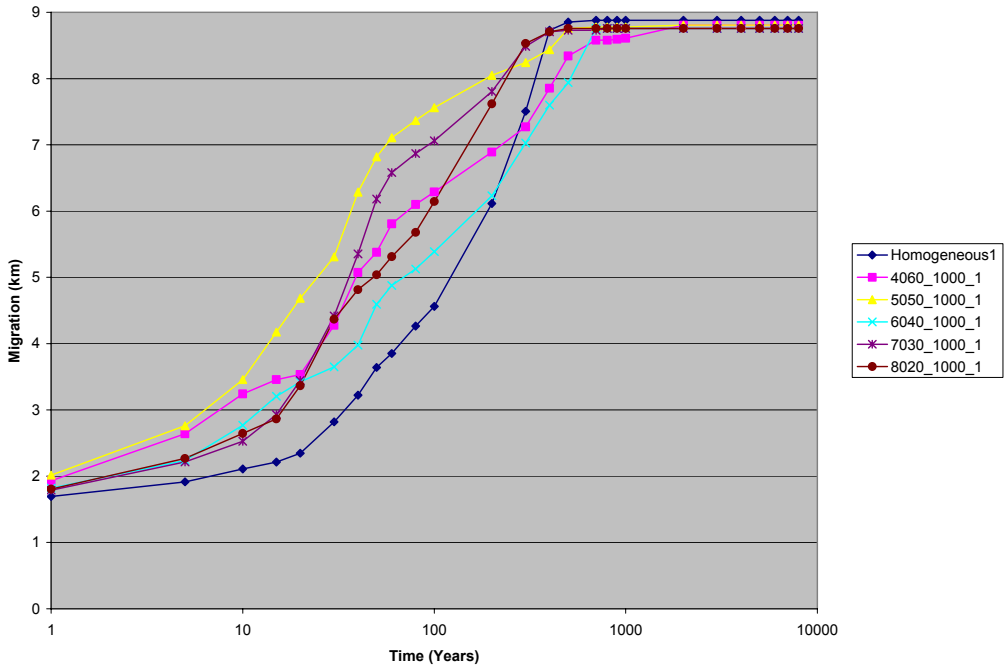

Figure D-51: Migration comparison of the 1000 m facies models, various net-to-gross, 1 degree slope

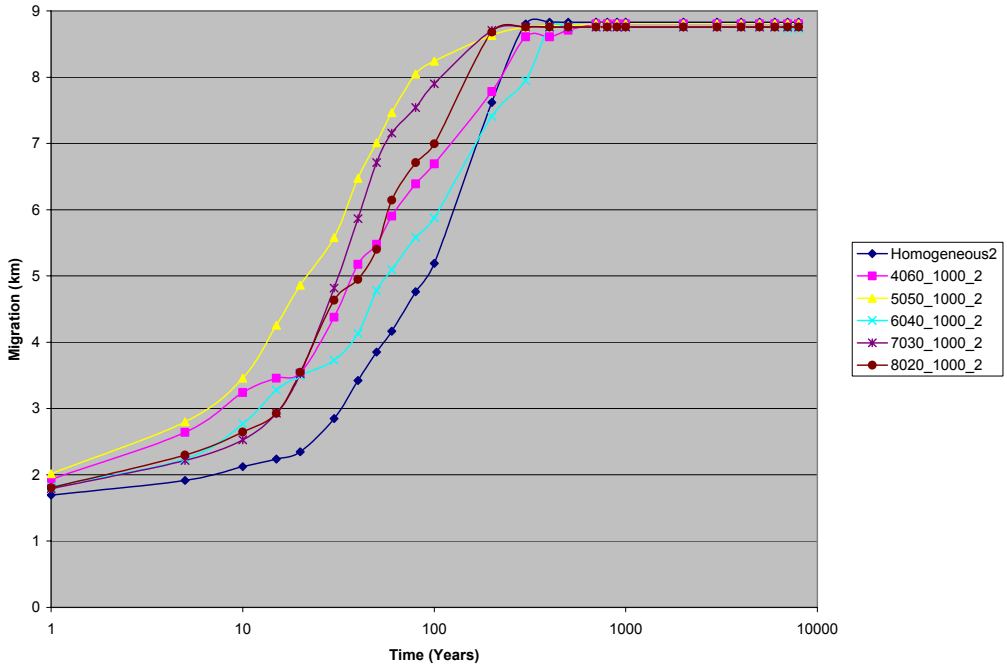

Figure D-52: Migration comparison of the 1000 m facies models, various net-to-gross, 2 degree slope

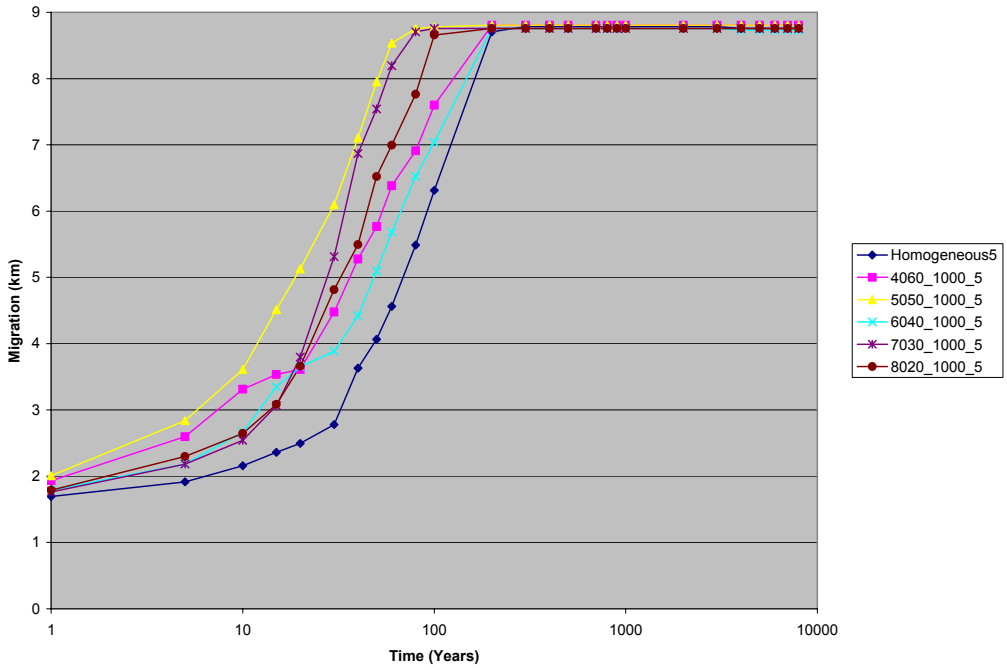

Figure D-53: Migration comparison of the 1000 m facies models, various net-to-gross, 5 degree slope

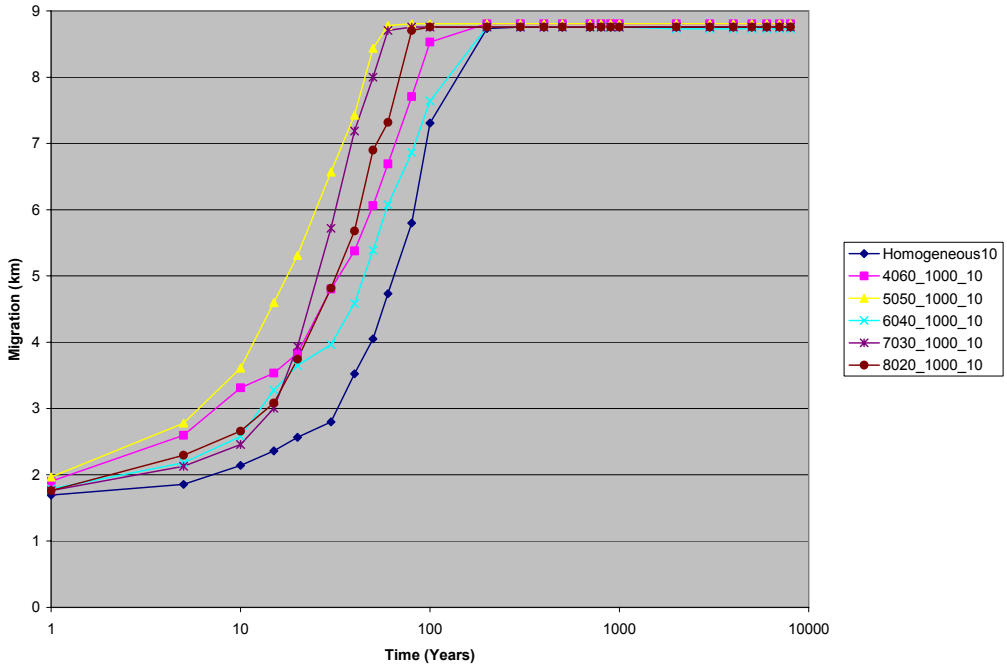

Figure D-54: Migration comparison of the 1000 m facies models, various net-to-gross, 10 degree slope

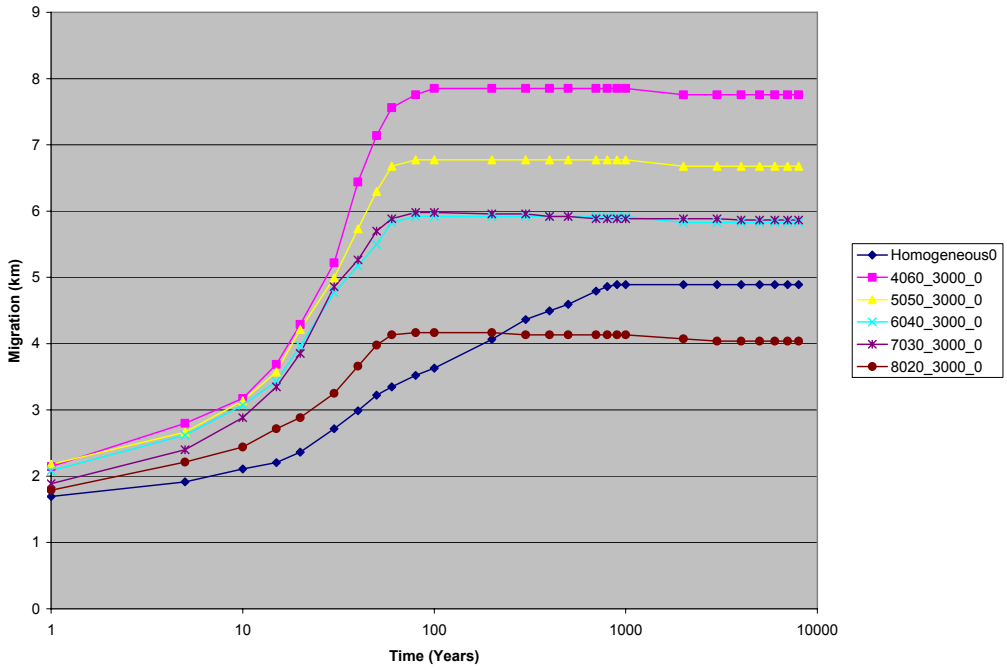

Figure D-55: Migration comparison of the 3000 m facies models, various net-to-gross, 0 degree slope

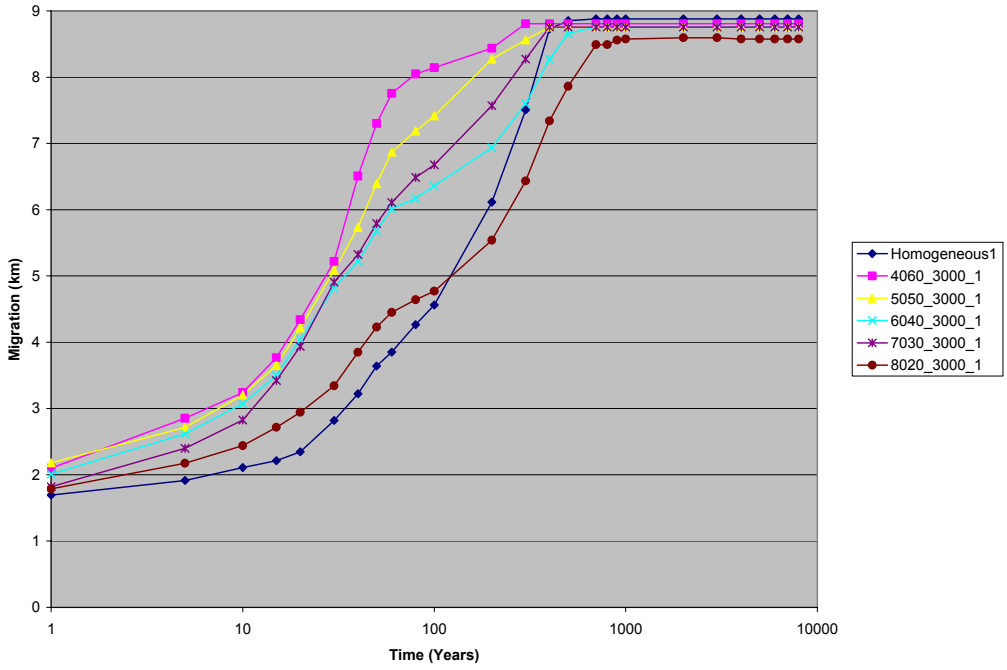

Figure D-56: Migration comparison of the 3000 m facies models, various net-to-gross, 1 degree slope

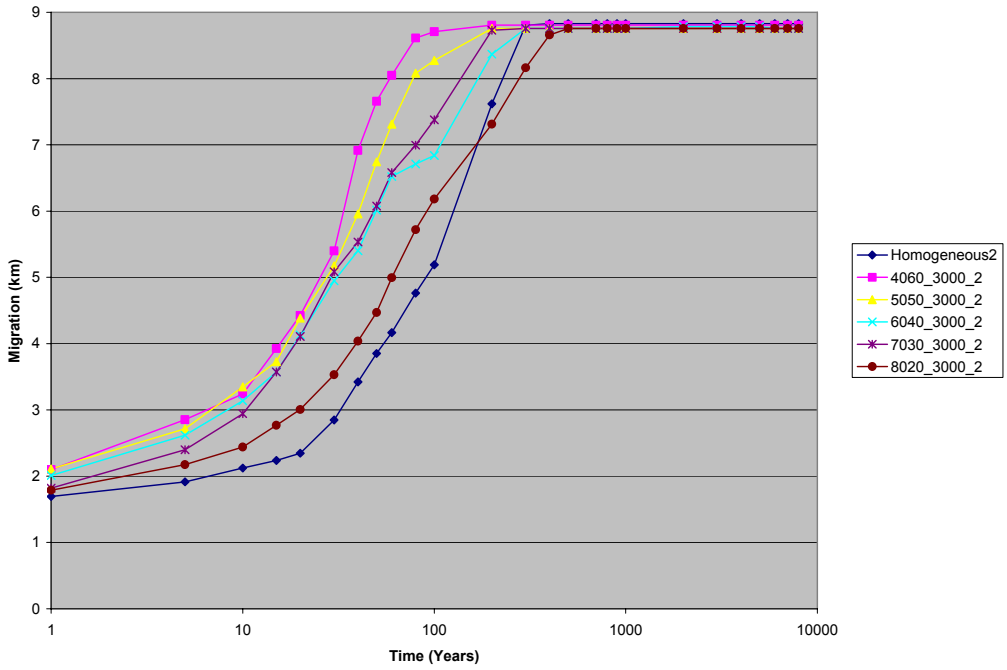

Figure D-57: Migration comparison of the 3000 m facies models, various net-to-gross, 2 degree slope

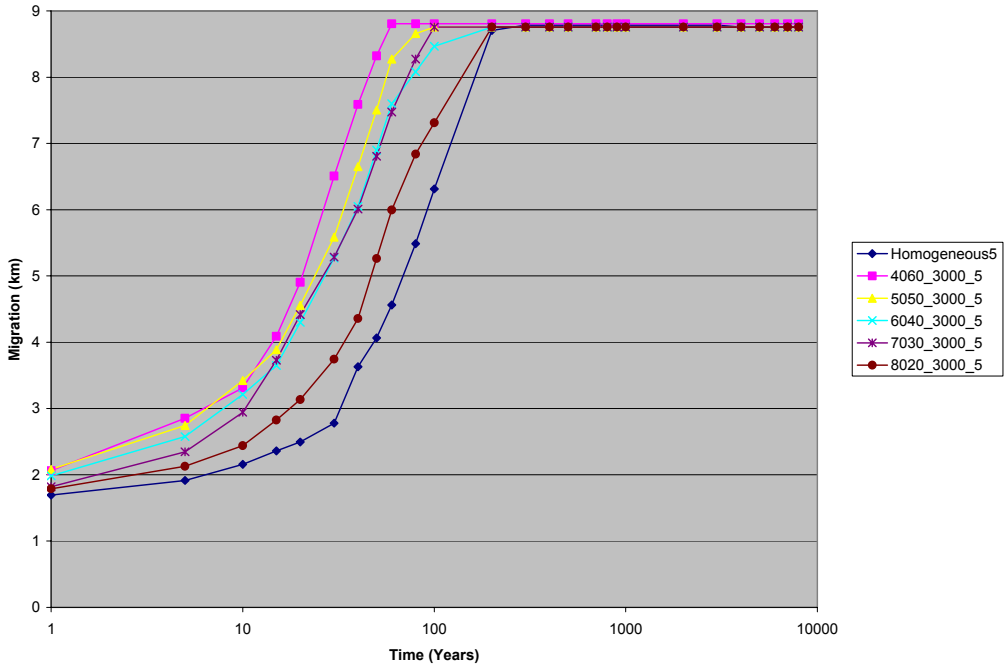

Figure D-58: Migration comparison of the 3000 m facies models, various net-to-gross, 5 degree slope

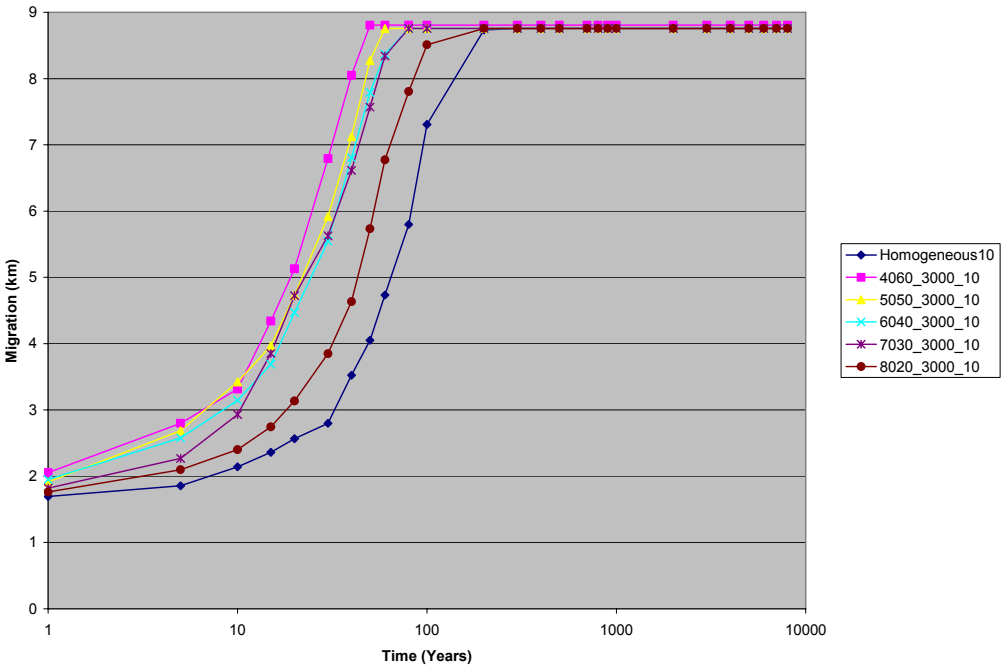

Figure D-59: Migration comparison of the 3000 m facies models, various net-to-gross, 10 degree slope

Vertical Migration

The following figures show the progress of the injected CO_2 plume moving stratigraphically up the model through the layers of the model.
The following figures show the impact of varying shale length for the same net to gross content and formation slope in the model.

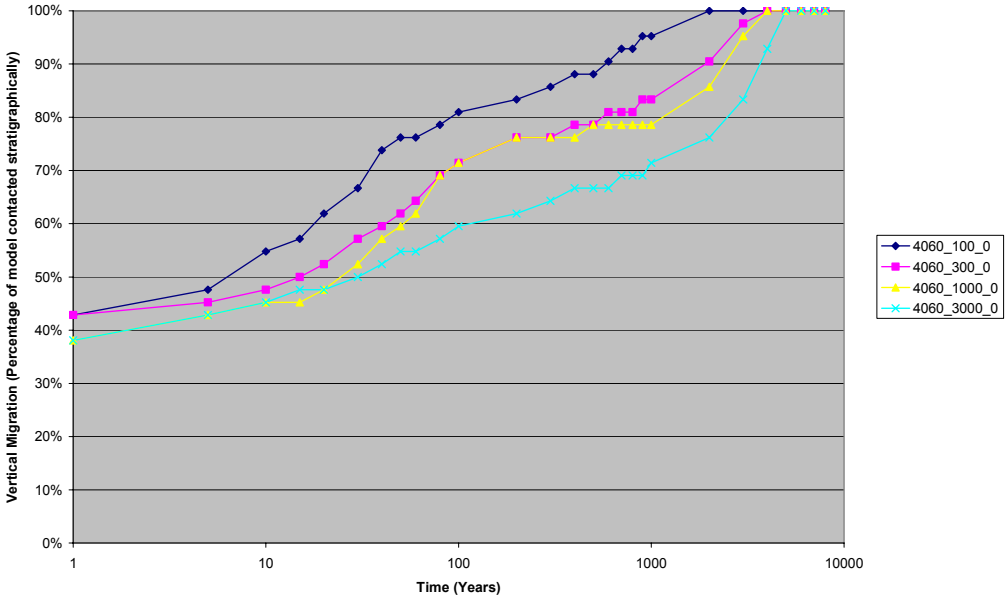

Figure D-60: Vertical migration comparison of the 40:60 net to gross models, various shale lengths, 0 degree slope

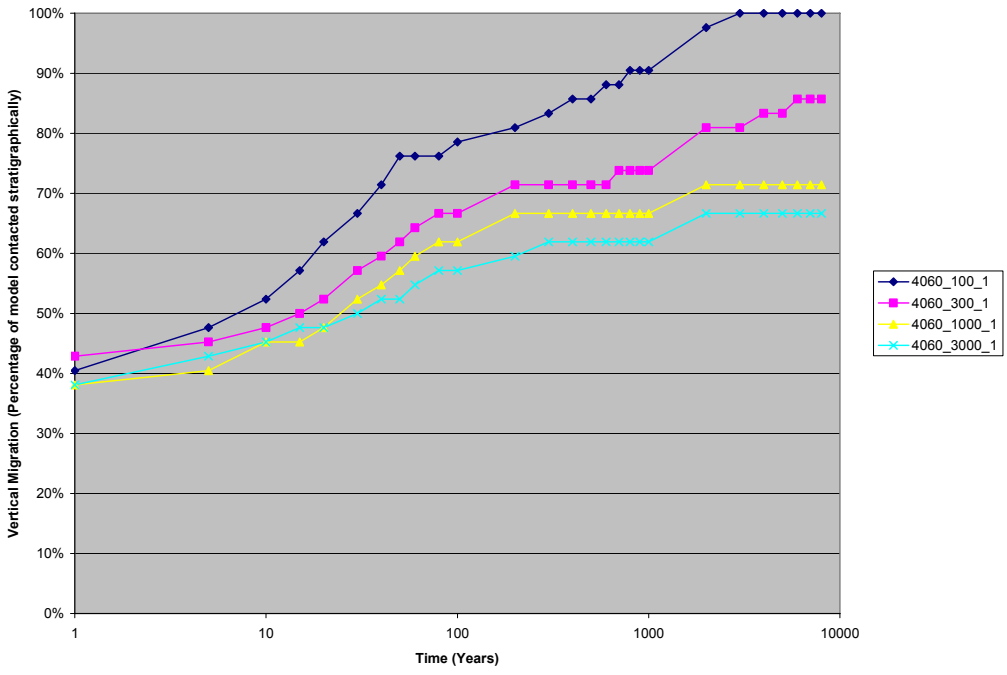

Figure D-61: Vertical migration comparison of the 40:60 net to gross models, various shale lengths, 1 degree slope

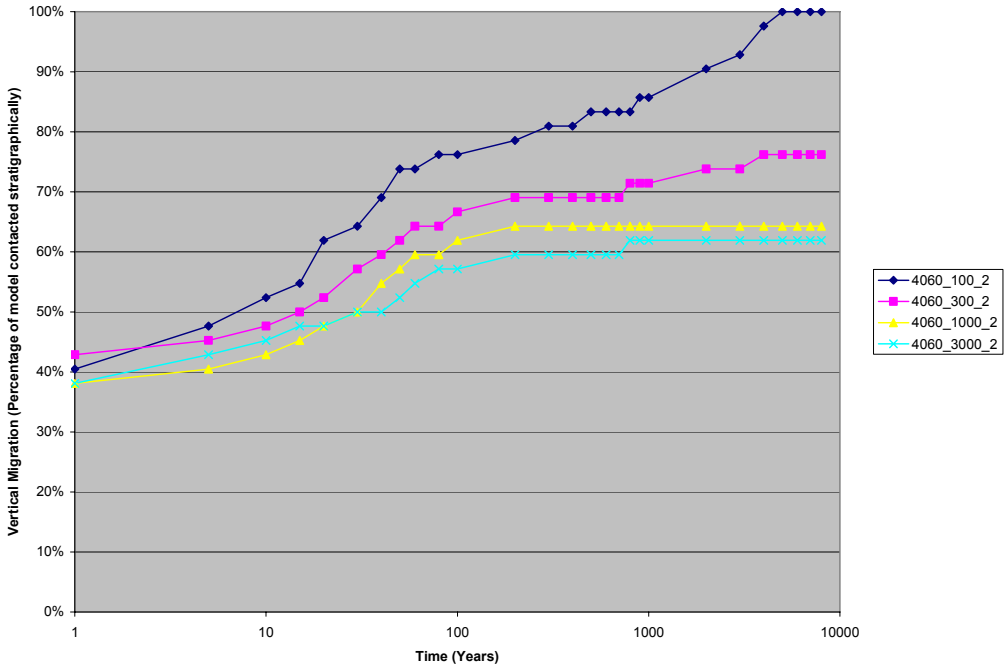

Figure D-62: Vertical migration comparison of the 40:60 net to gross models, various shale lengths, 2 degree slope

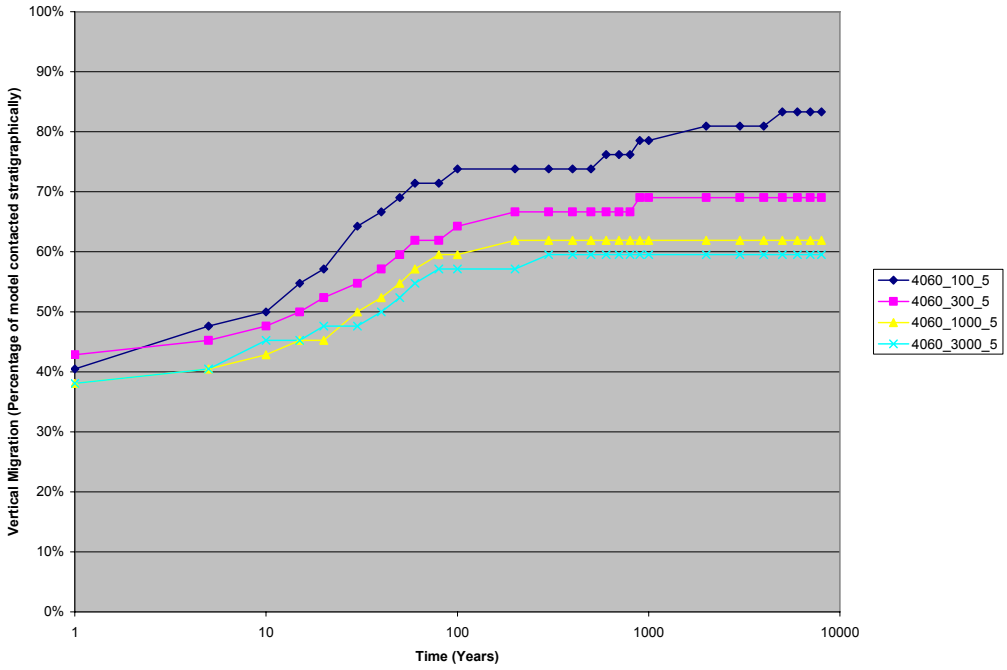

Figure D-63: Vertical migration comparison of the 40:60 net to gross models, various shale lengths, 5 degree slope

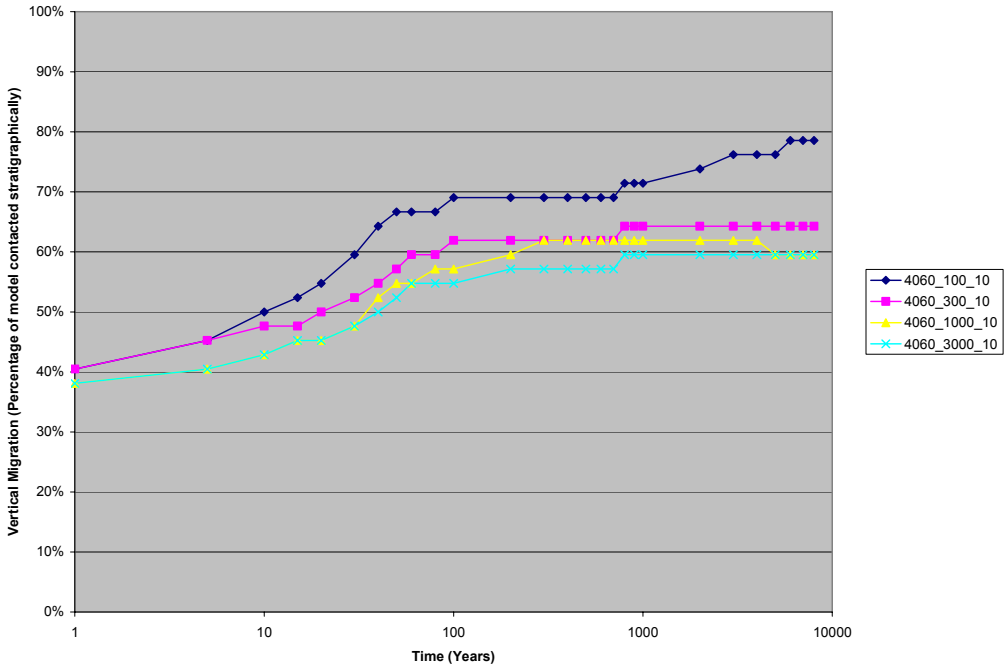

Figure D-64: Vertical migration comparison of the 40:60 net to gross models, various shale lengths, 10 degree slope

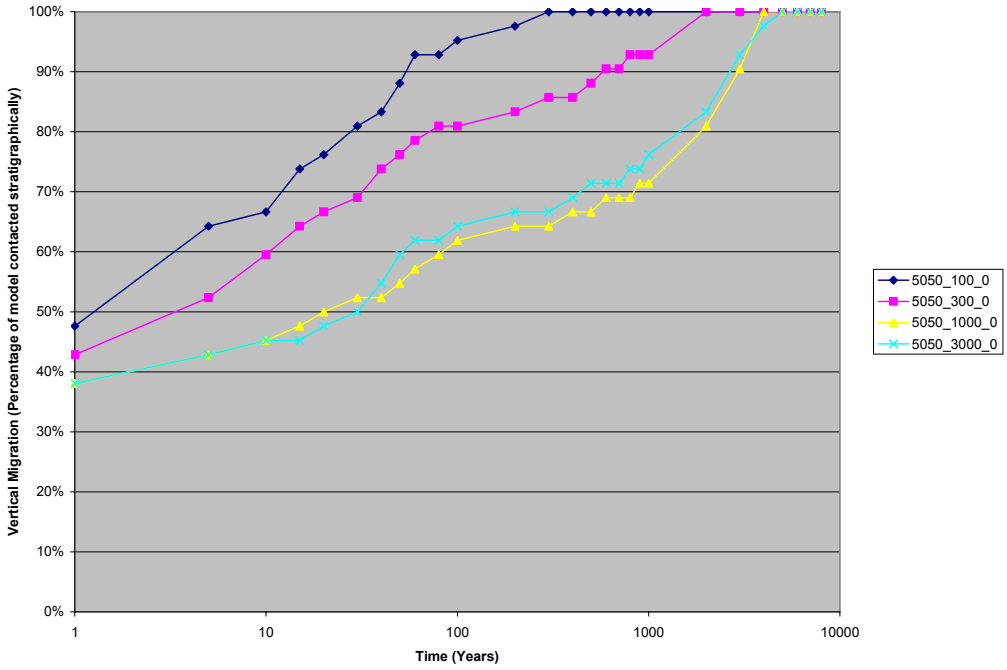

Figure D-65: Vertical migration comparison of the 50:50 net to gross models, various shale lengths, 0 degree slope

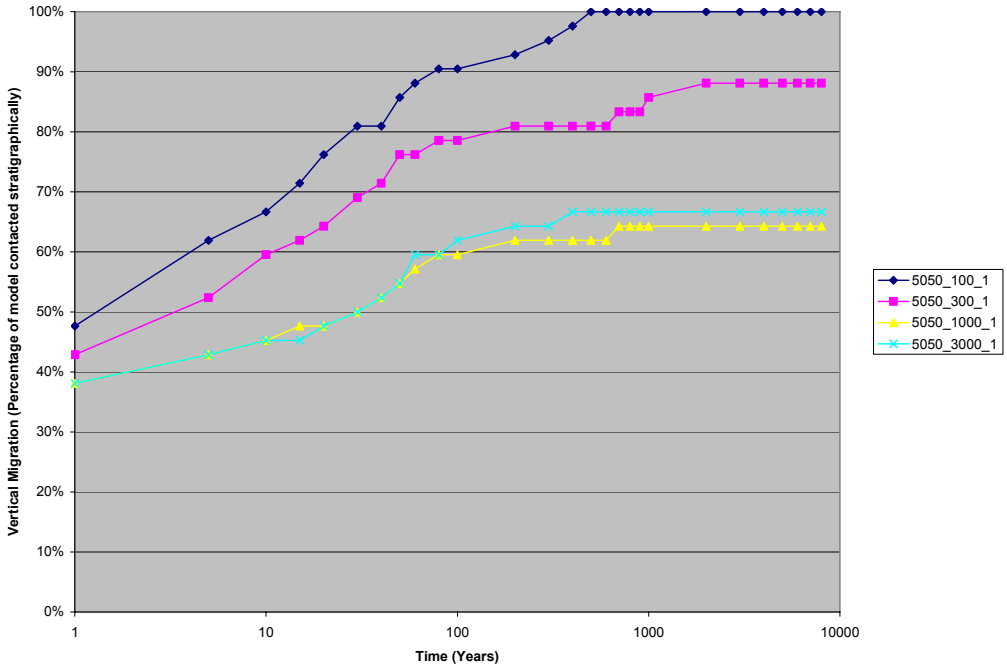

Figure D-66: Vertical migration comparison of the 50:50 net to gross models, various shale lengths, 1 degree slope

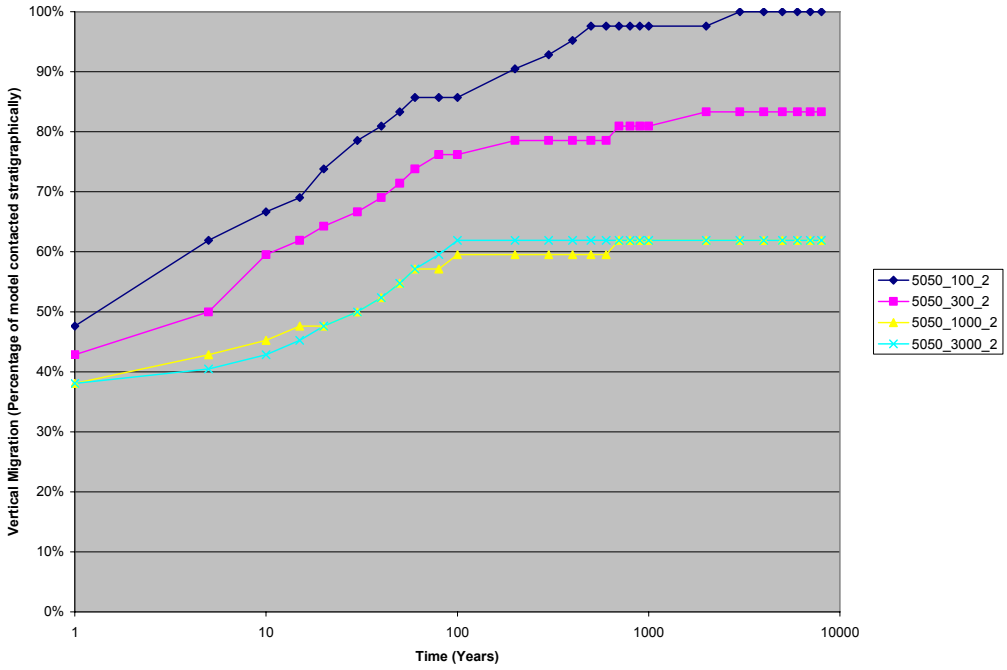

Figure D-67: Vertical migration comparison of the 50:50 net to gross models, various shale lengths, 2 degree slope

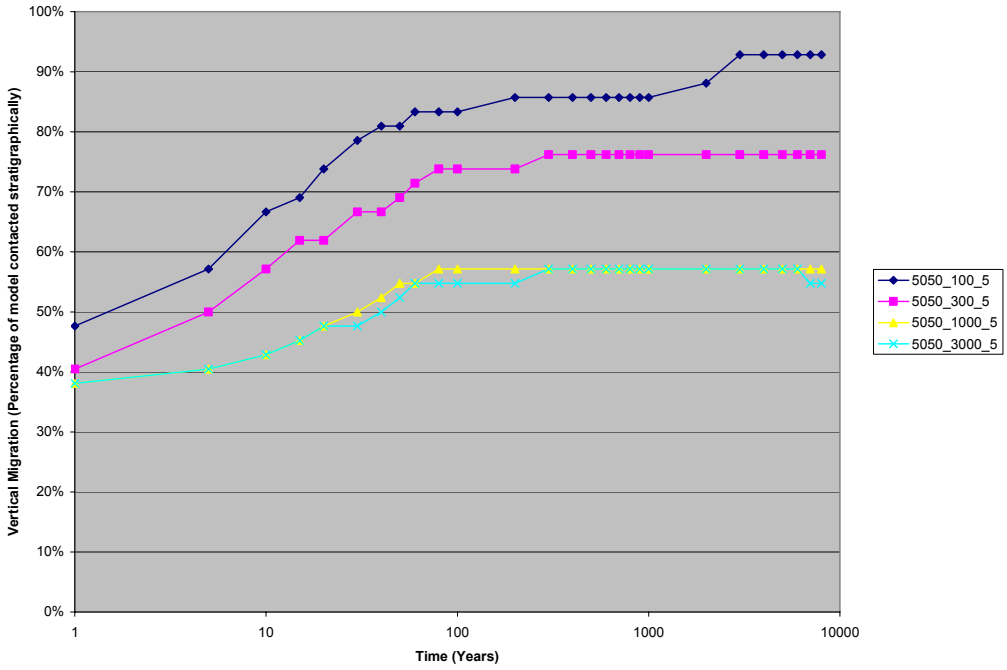

Figure D-68: Vertical migration comparison of the 50:50 net to gross models, various shale lengths, 5 degree slope

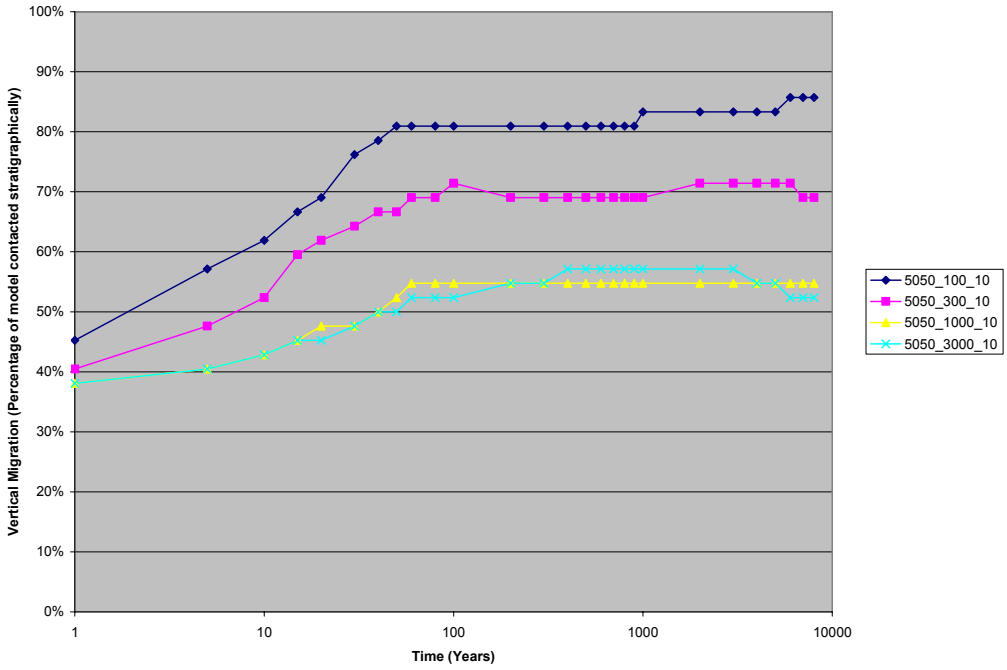

Figure D-69: Vertical migration comparison of the 50:50 net to gross models, various shale lengths, 10 degree slope

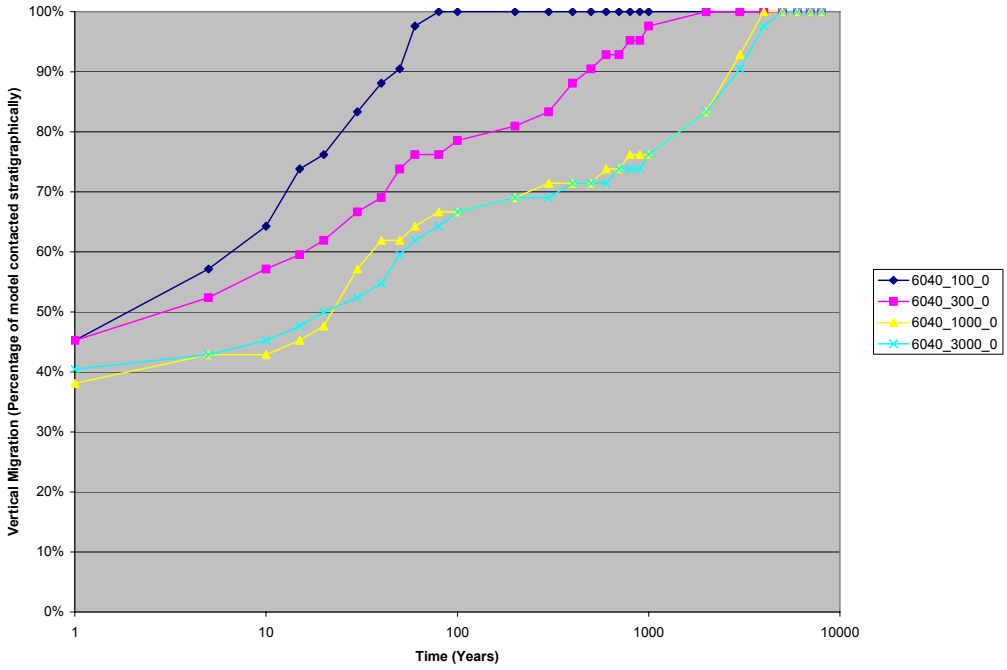

Figure D-70: Vertical migration comparison of the 60:40 net to gross models, various shale lengths, 0 degree slope

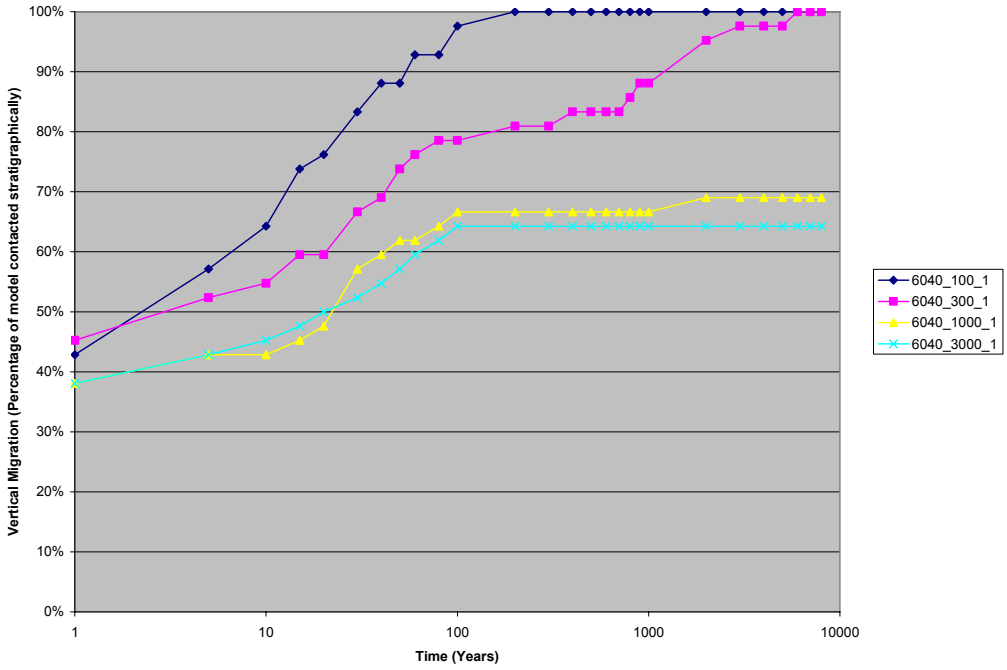

Figure D-71: Vertical migration comparison of the 60:40 net to gross models, various shale lengths, 1 degree slope

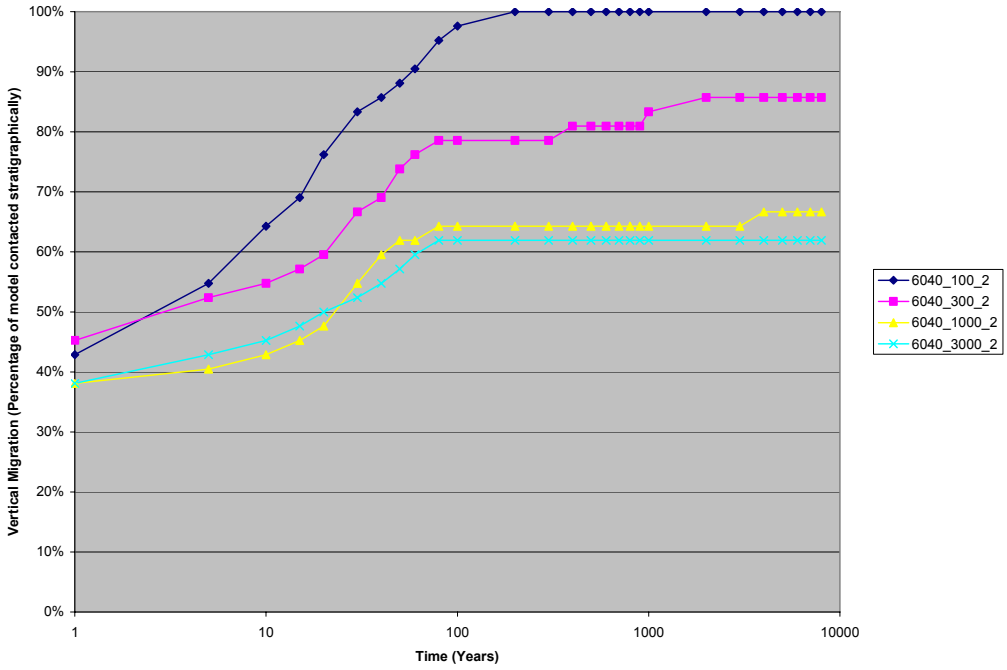

Figure D-72: Vertical migration comparison of the 60:40 net to gross models, various shale lengths, 2 degree slope

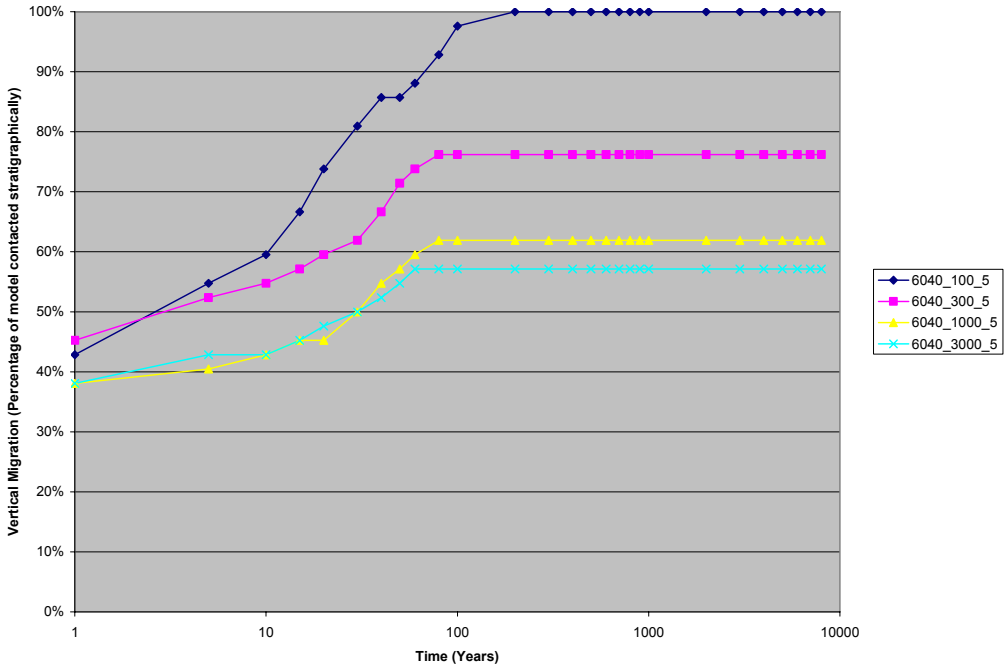

Figure D-73: Vertical migration comparison of the 60:40 net to gross models, various shale lengths, 5 degree slope

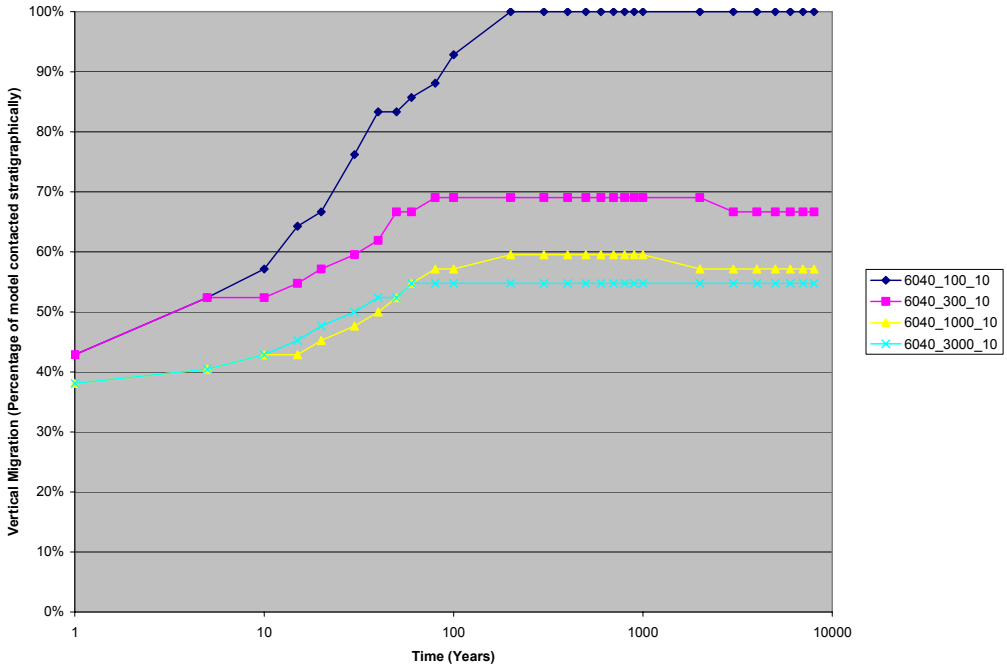

Figure D-74: Vertical migration comparison of the 60:40 net to gross models, various shale lengths, 10 degree slope

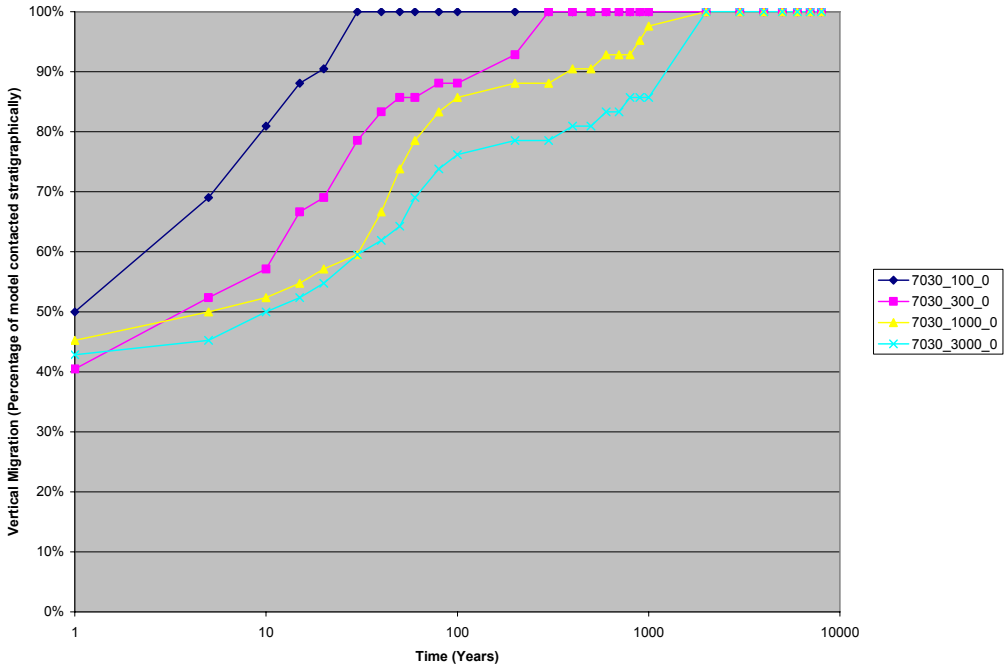

Figure D-75: Vertical migration comparison of the 70:30 net to gross models, various shale lengths, 0 degree slope

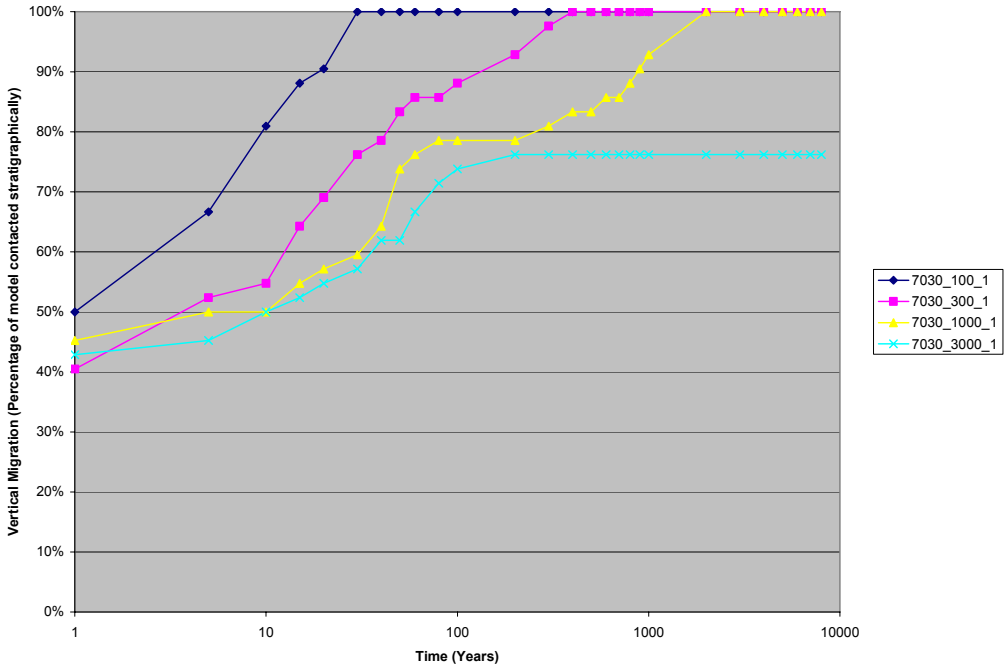

Figure D-76: Vertical migration comparison of the 70:30 net to gross models, various shale lengths, 1 degree slope

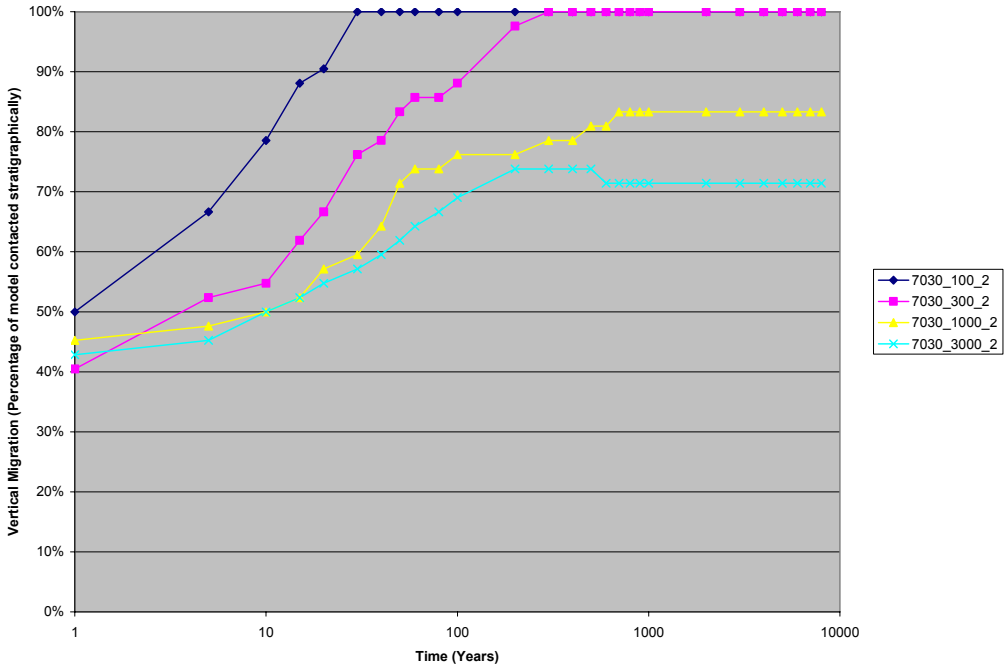

Figure D-77: Vertical migration comparison of the 70:30 net to gross models, various shale lengths, 2 degree slope

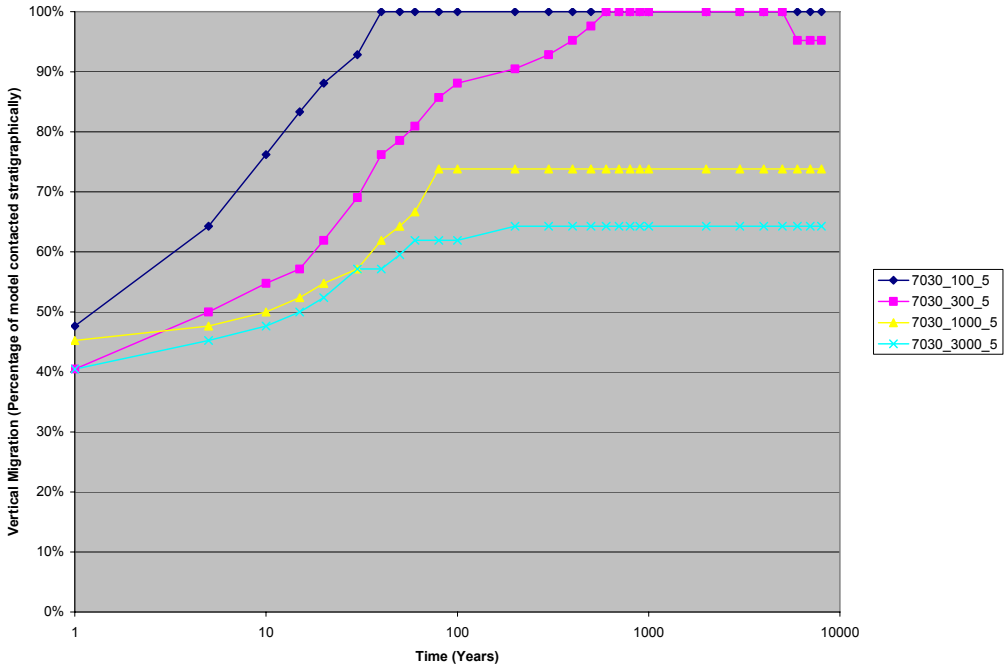

Figure D-78: Vertical migration comparison of the 70:30 net to gross models, various shale lengths, 5 degree slope

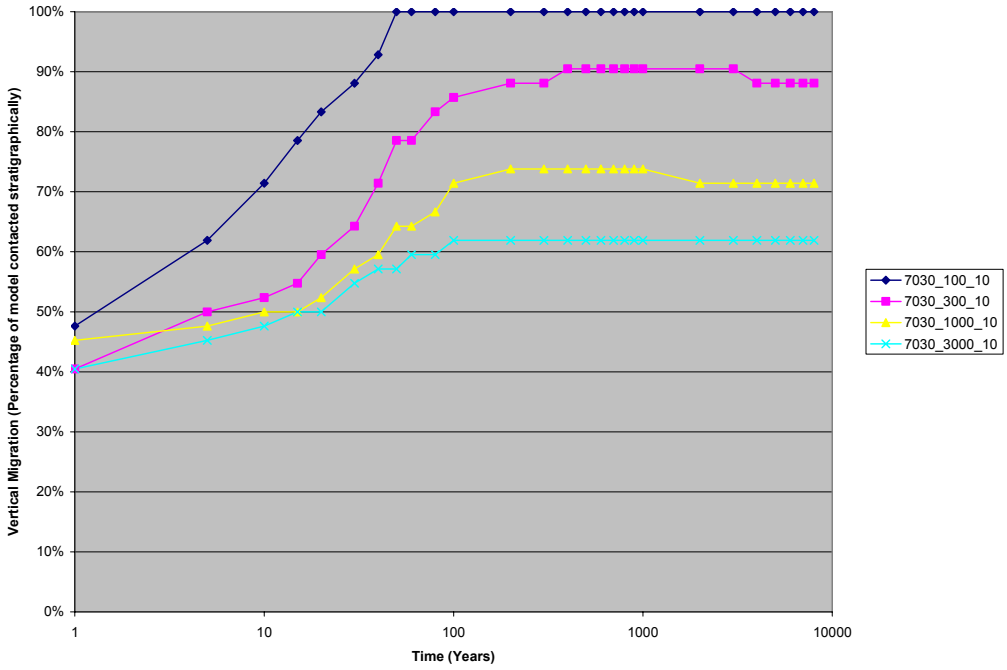

Figure D-79: Vertical migration comparison of the 70:30 net to gross models, various shale lengths, 10 degree slope

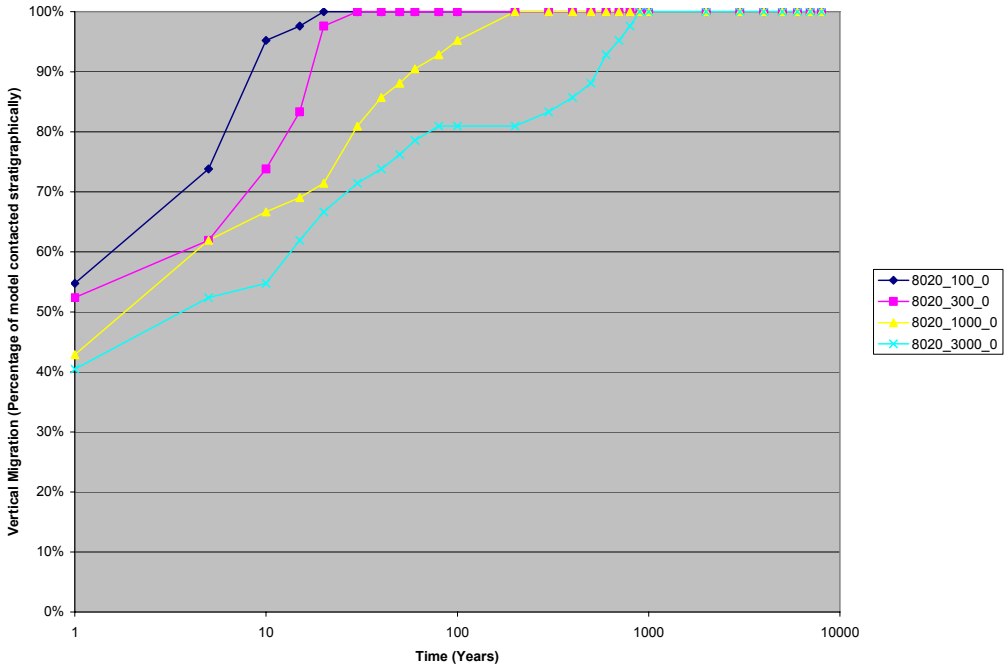

Figure D-80: Vertical migration comparison of the 80:20 net to gross models, various shale lengths, 0 degree slope

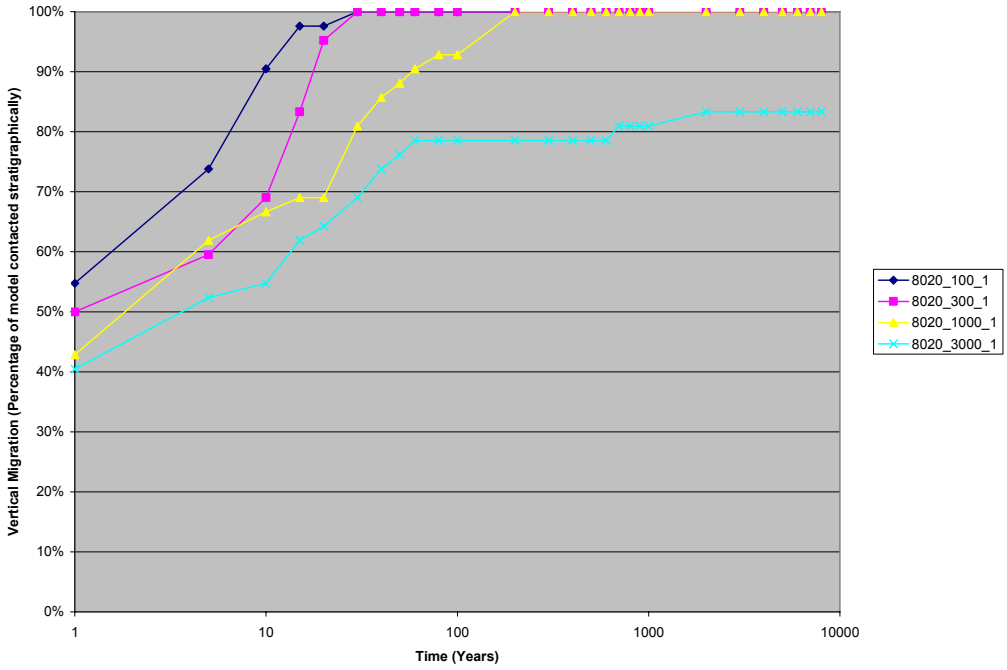

Figure D-81: Vertical migration comparison of the 80:20 net to gross models, various shale lengths, 1 degree slope

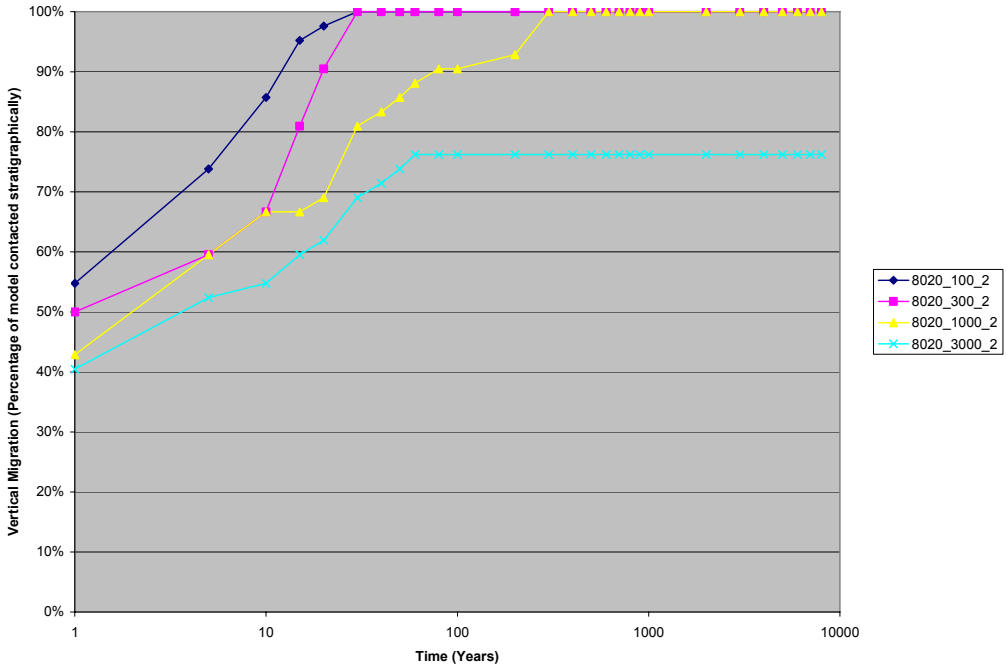

Figure D-82: Vertical migration comparison of the 80:20 net to gross models, various shale lengths, 2 degree slope

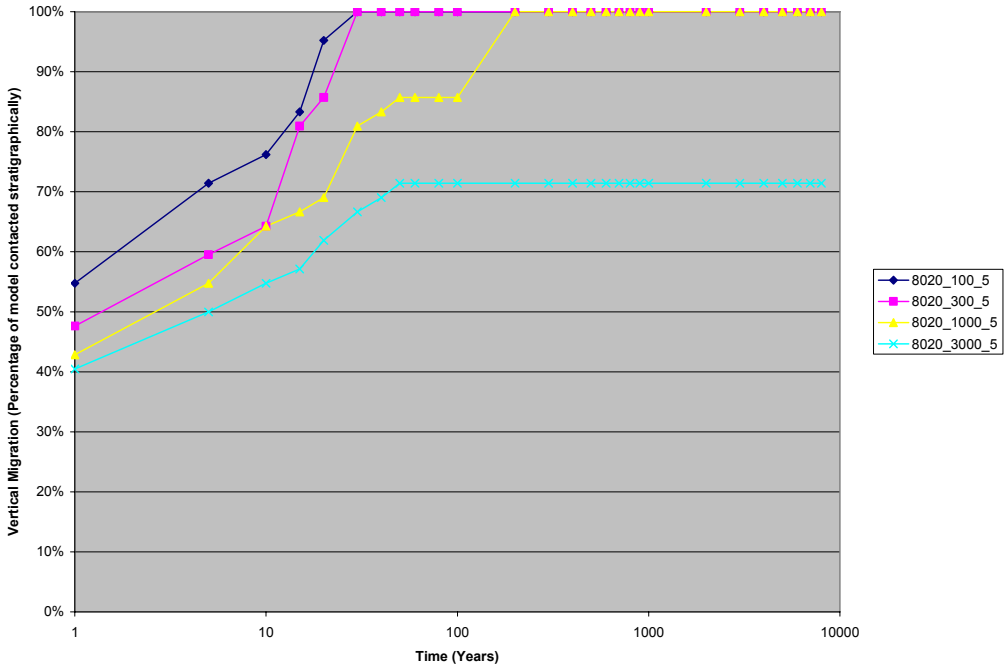

Figure D-83: Vertical migration comparison of the 80:20 net to gross models, various shale lengths, 5 degree slope

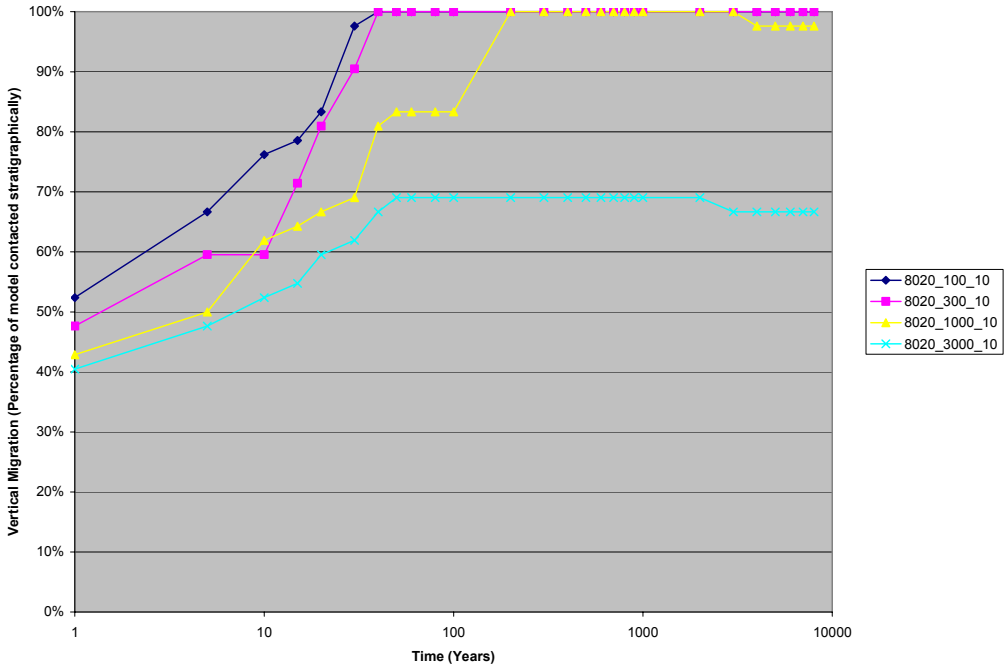

Figure D-84: Vertical migration comparison of the 80:20 net to gross models, various shale lengths, 10 degree slope

The following figures show the impact of changing the sand the shale content in the formation models has for the same shale length variagram used.

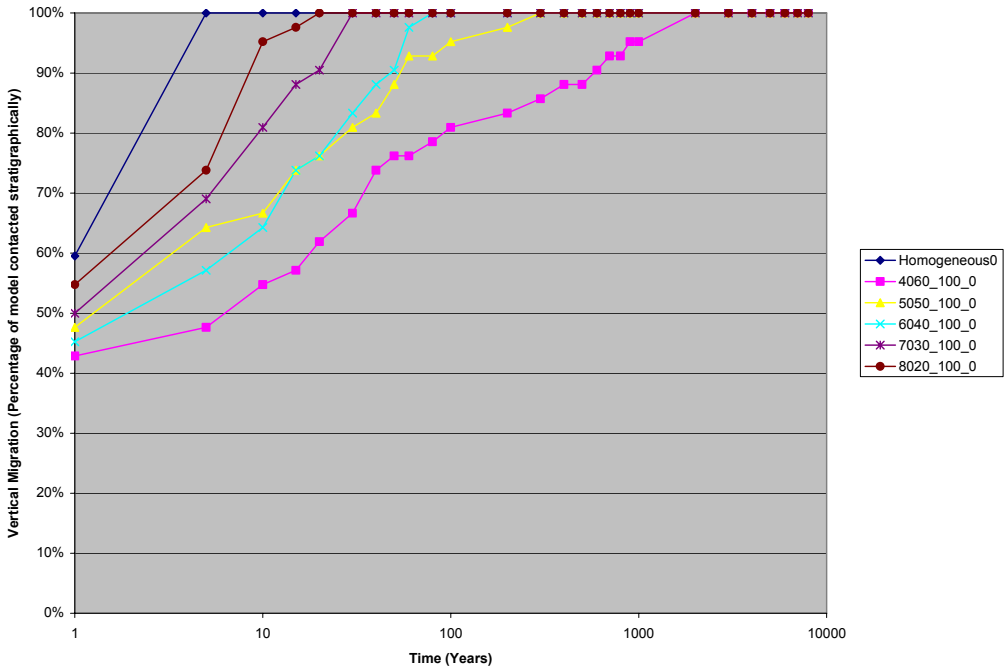

Figure D-85: Vertical migration comparison of the 100 m shale length models, various sand to shale contents, 0 degree slope

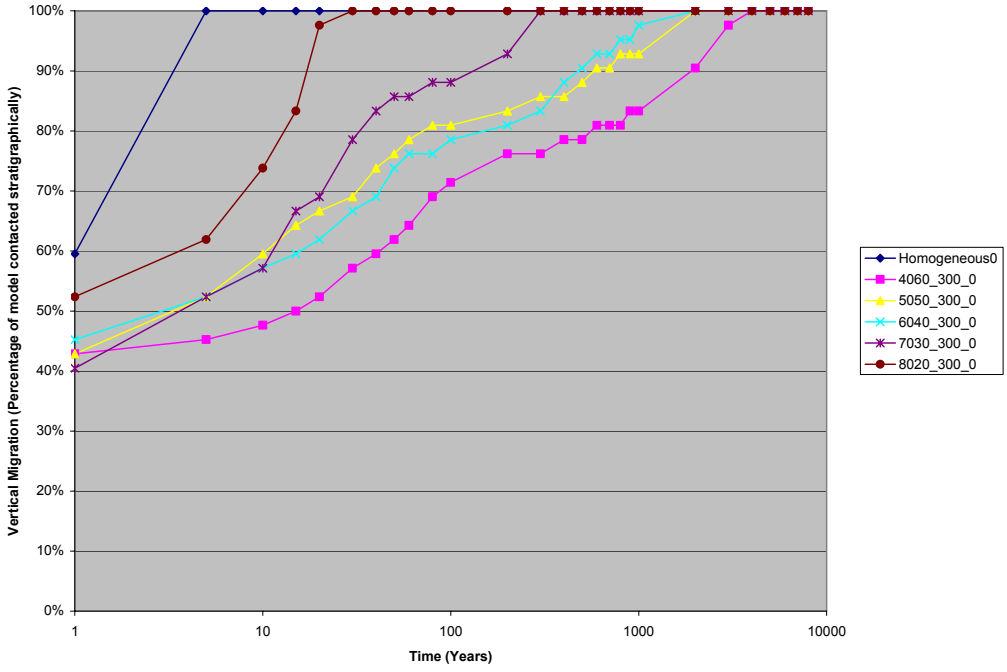

Figure D-86: Vertical migration comparison of the 300 m shale length models, various sand to shale contents, 0 degree slope

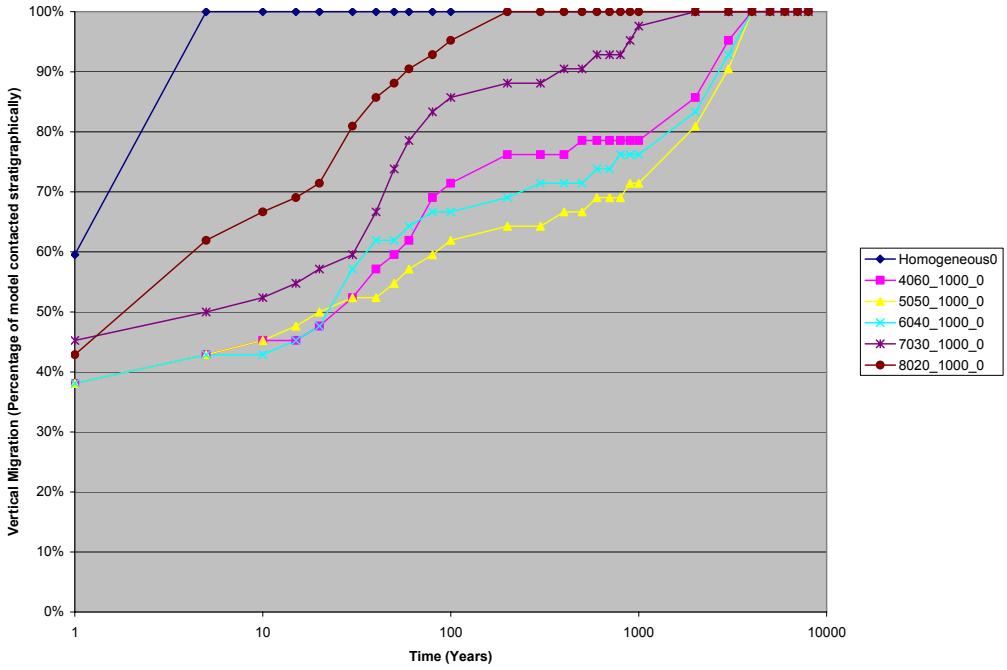

Figure D-87: Vertical migration comparison of the 1000 m shale length models, various sand to shale contents, 0 degree slope

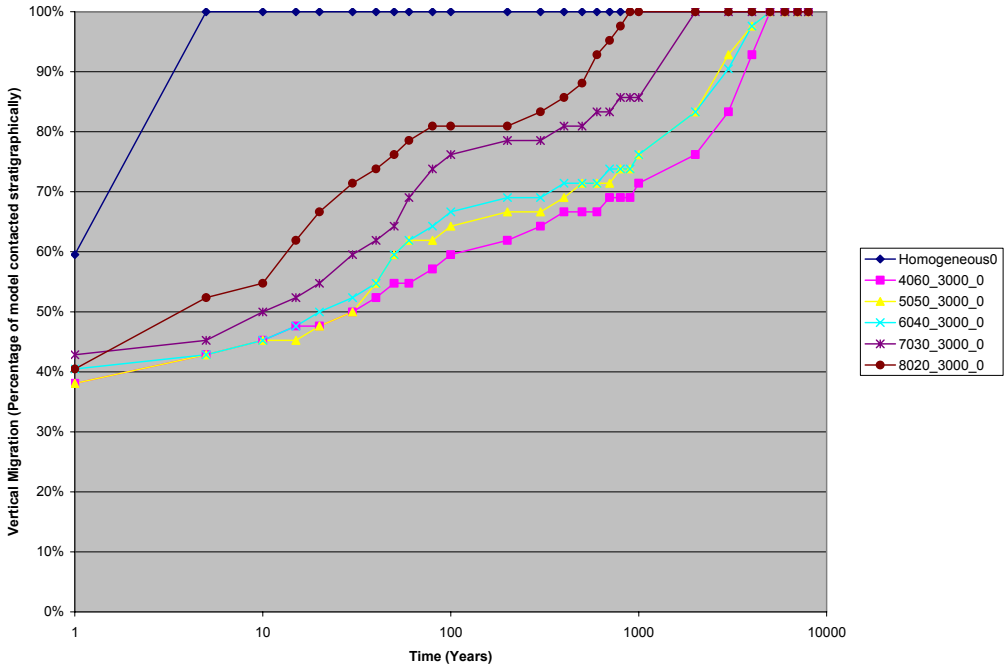

Figure D-88: Vertical migration comparison of the 3000 m shale length models, various sand to shale contents, 0 degree slope

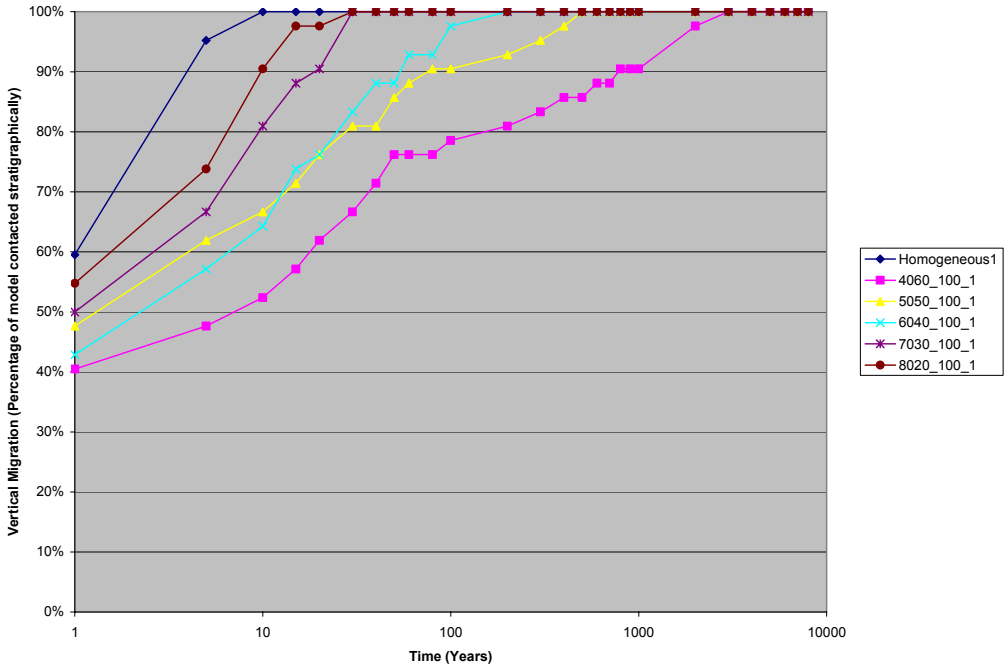

Figure D-89: Vertical migration comparison of the 100 m shale length models, various sand to shale contents, 1 degree slope

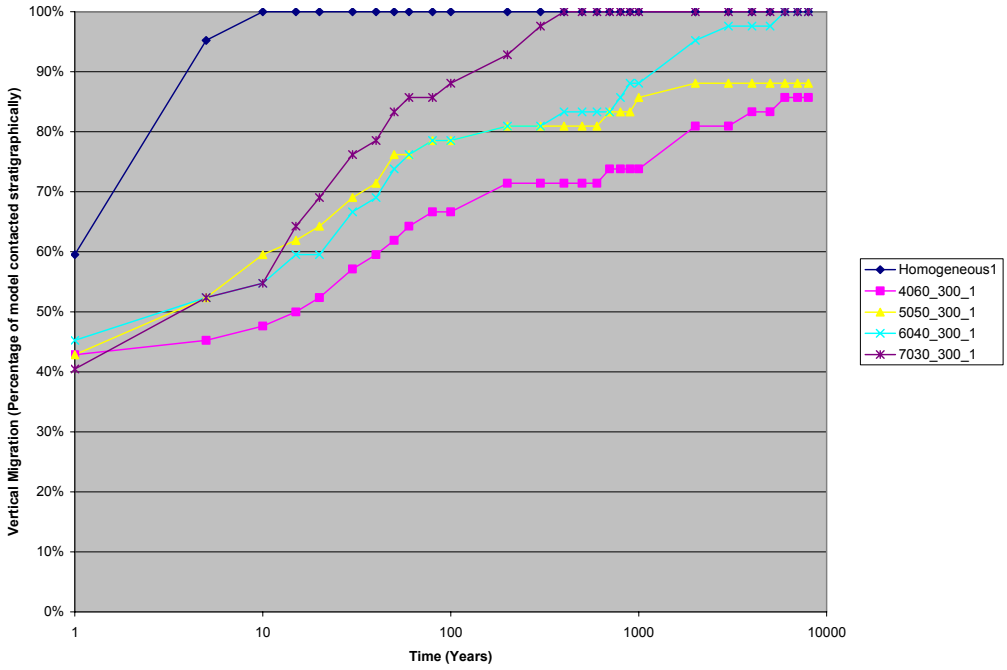

Figure D-90: Vertical migration comparison of the 300 m shale length models, various sand to shale contents, 1 degree slope

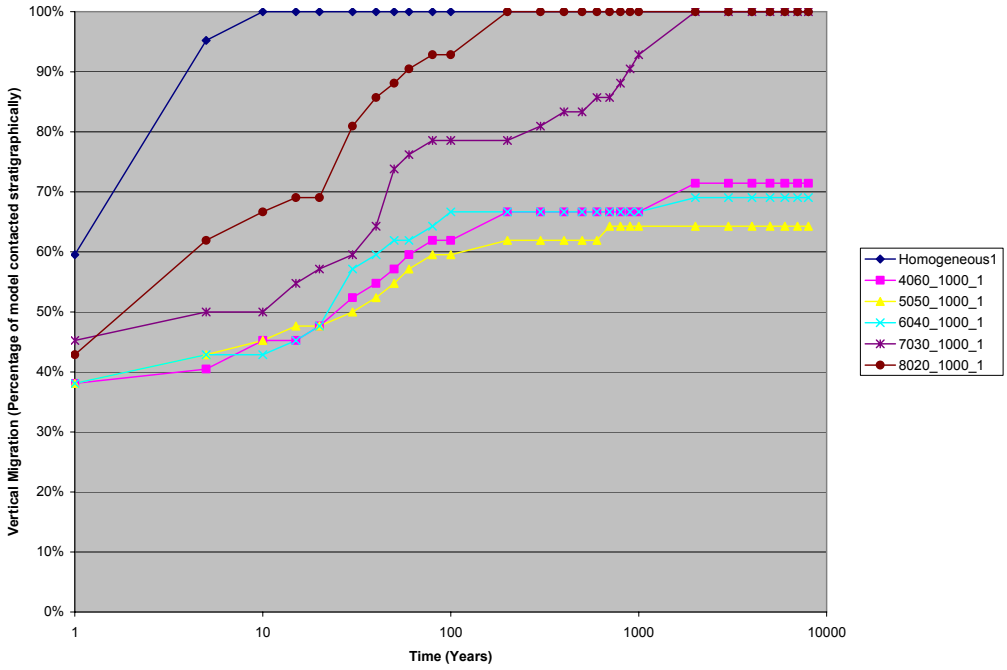

Figure D-91: Vertical migration comparison of the 1000 m shale length models, various sand to shale contents, 1 degree slope

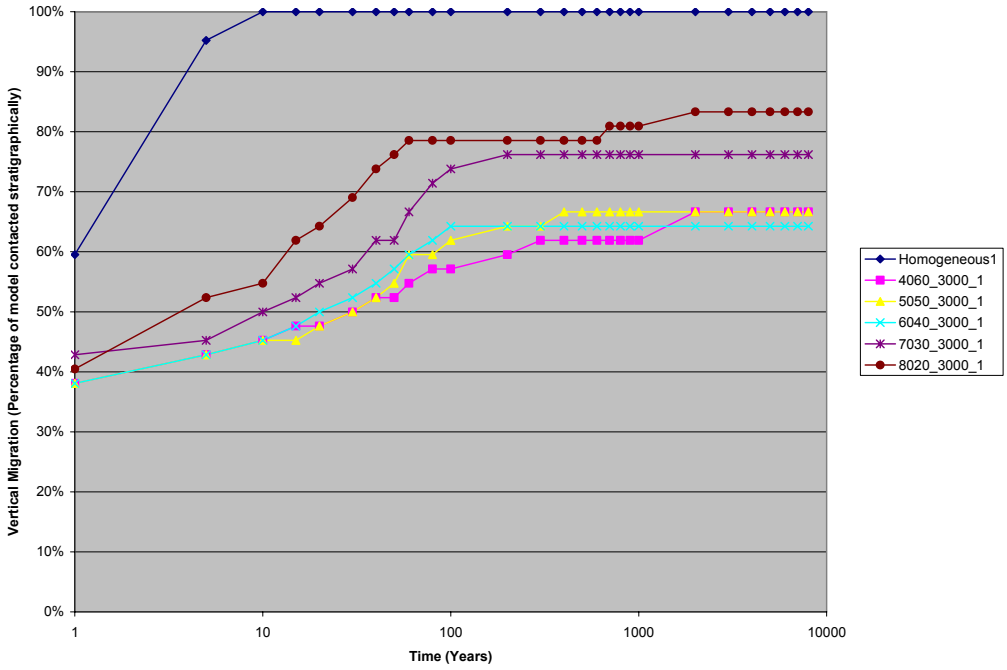

Figure D-92: Vertical migration comparison of the 3000 m shale length models, various sand to shale contents, 1 degree slope

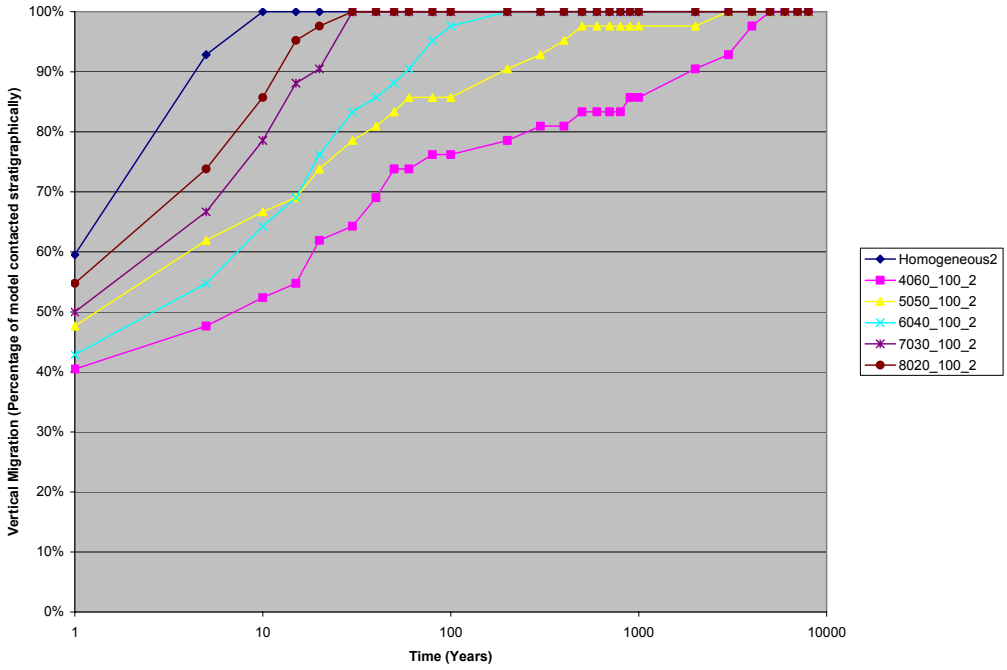

Figure D-93: Vertical migration comparison of the 100 m shale length models, various sand to shale contents, 2 degree slope

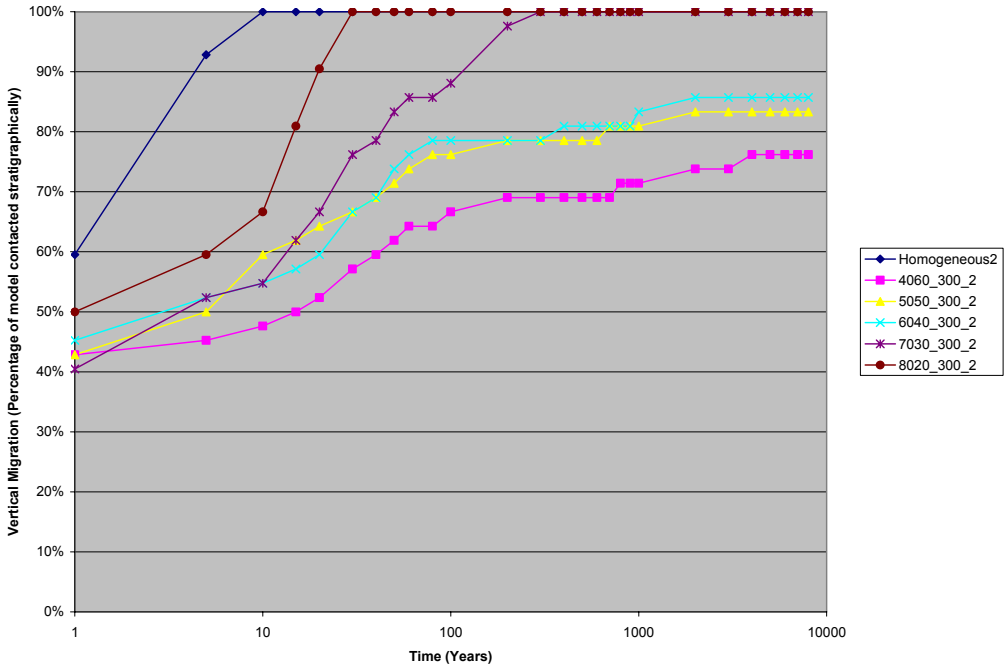

Figure D-94: Vertical migration comparison of the 300 m shale length models, various sand to shale contents, 2 degree slope

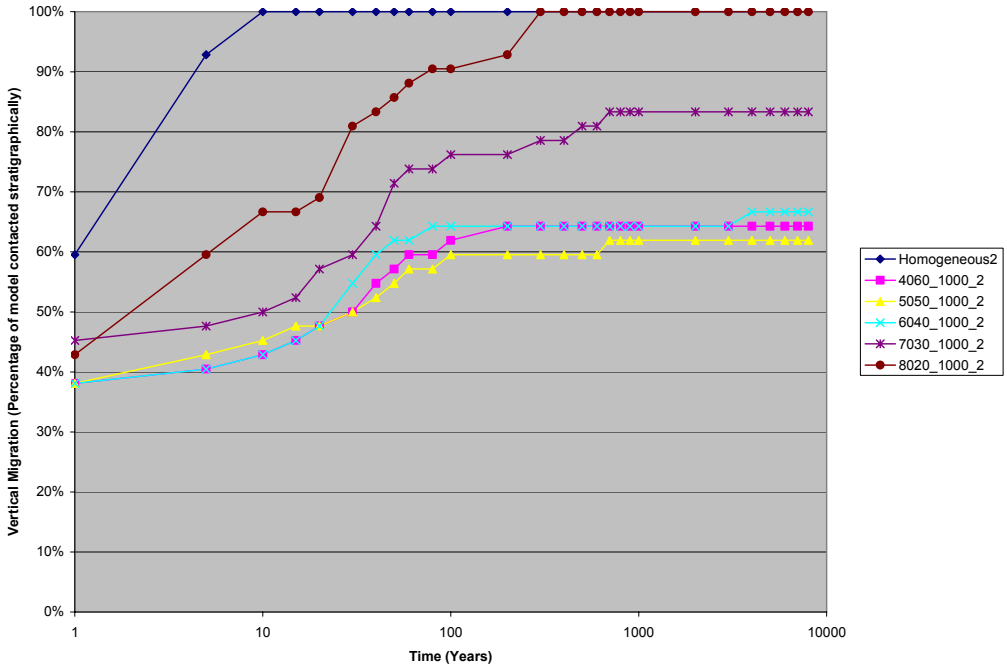

Figure D-95: Vertical migration comparison of the 1000 m shale length models, various sand to shale contents, 2 degree slope

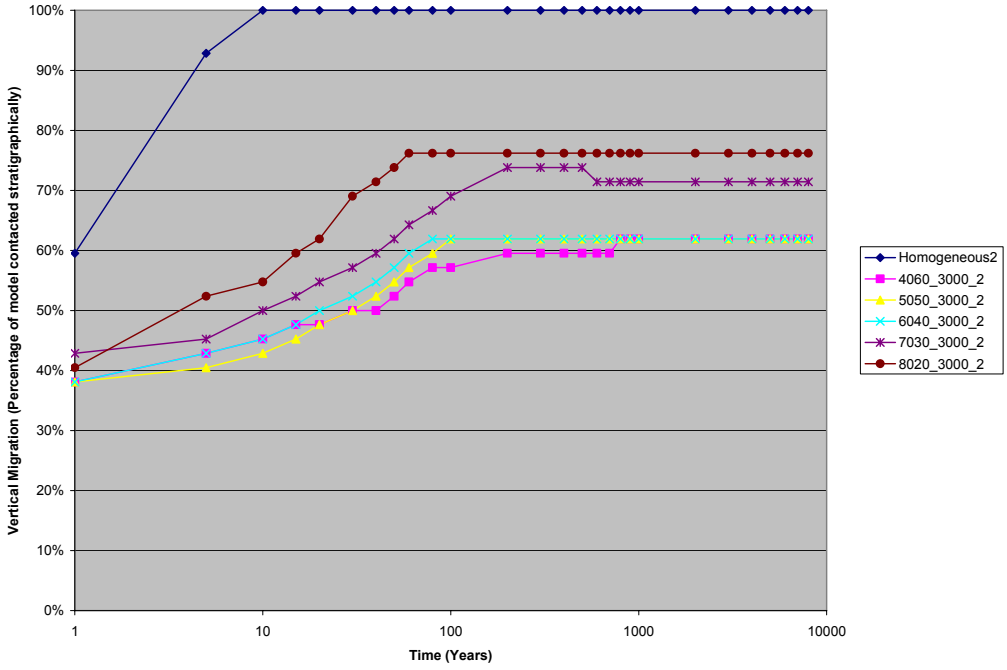

Figure D-96: Vertical migration comparison of the 3000 m shale length models, various sand to shale contents, 2 degree slope

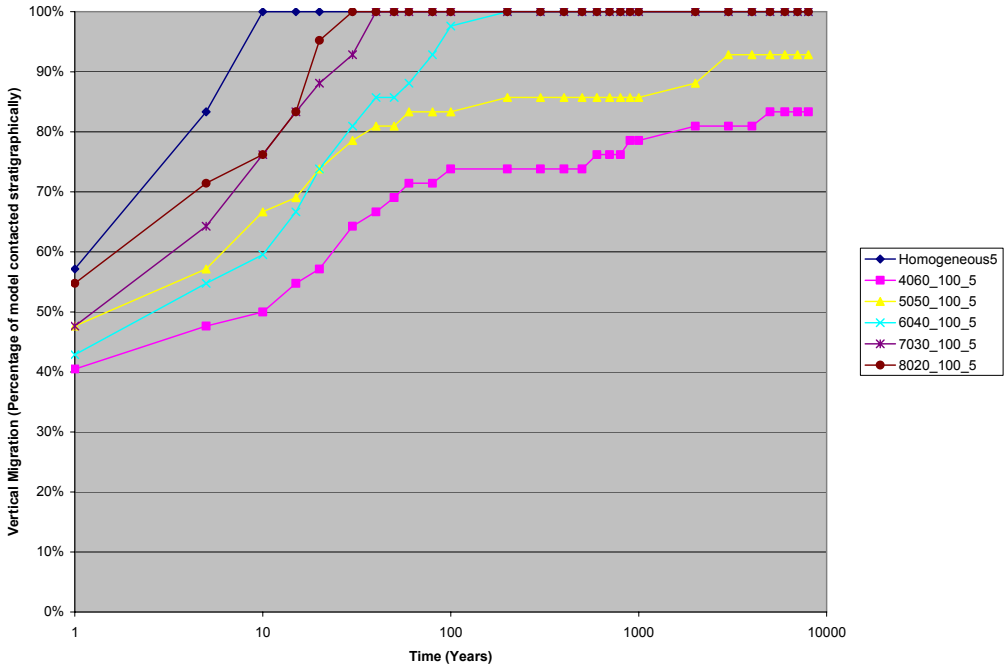

Figure D-97: Vertical migration comparison of the 100 m shale length models, various sand to shale contents, 5 degree slope

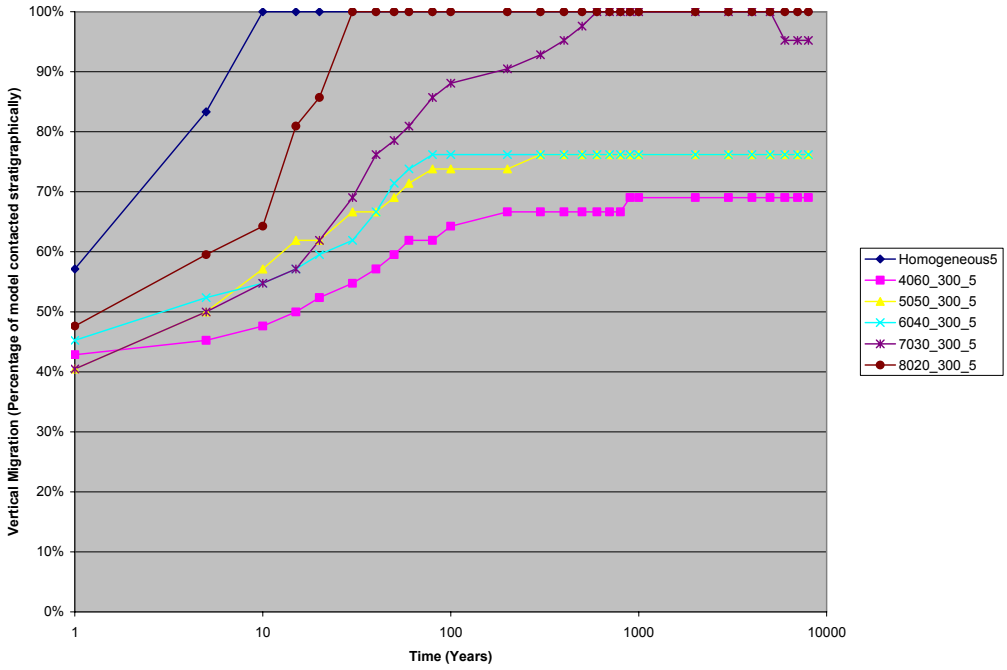

Figure D-98: Vertical migration comparison of the 300 m shale length models, various sand to shale contents, 5 degree slope

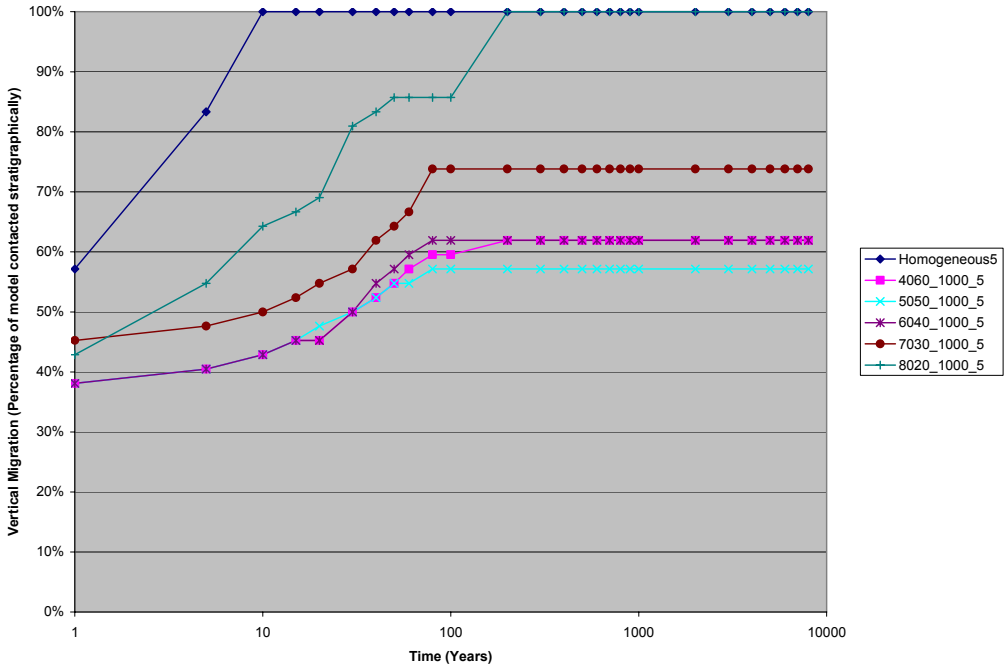

Figure D-99: Vertical migration comparison of the 1000 m shale length models, various sand to shale contents, 5 degree slope

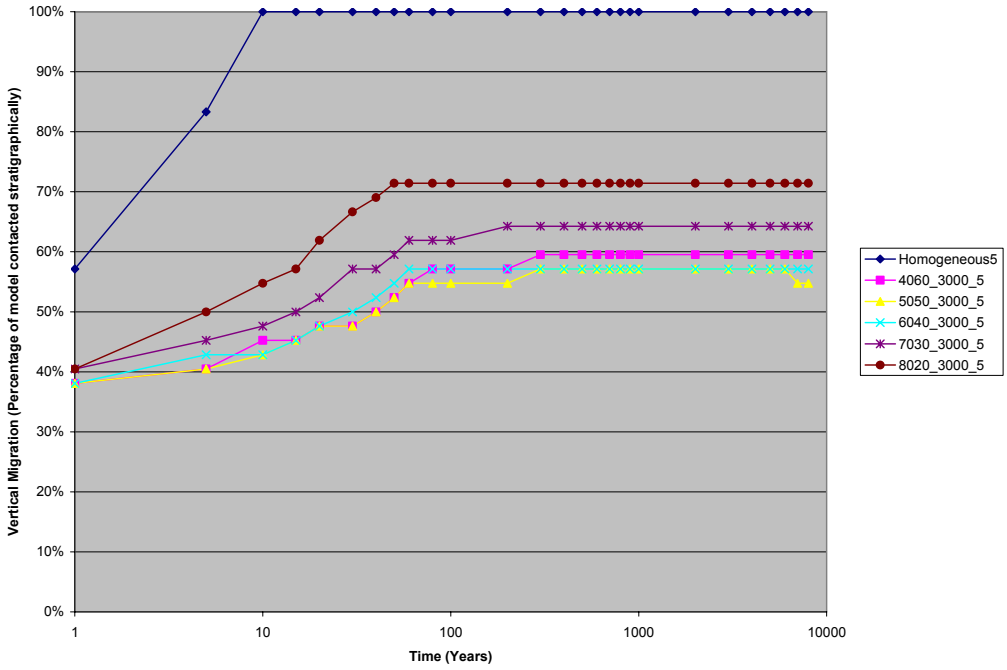

Figure D-100: Vertical migration comparison of the 3000 m shale length models, various sand to shale contents, 5 degree slope

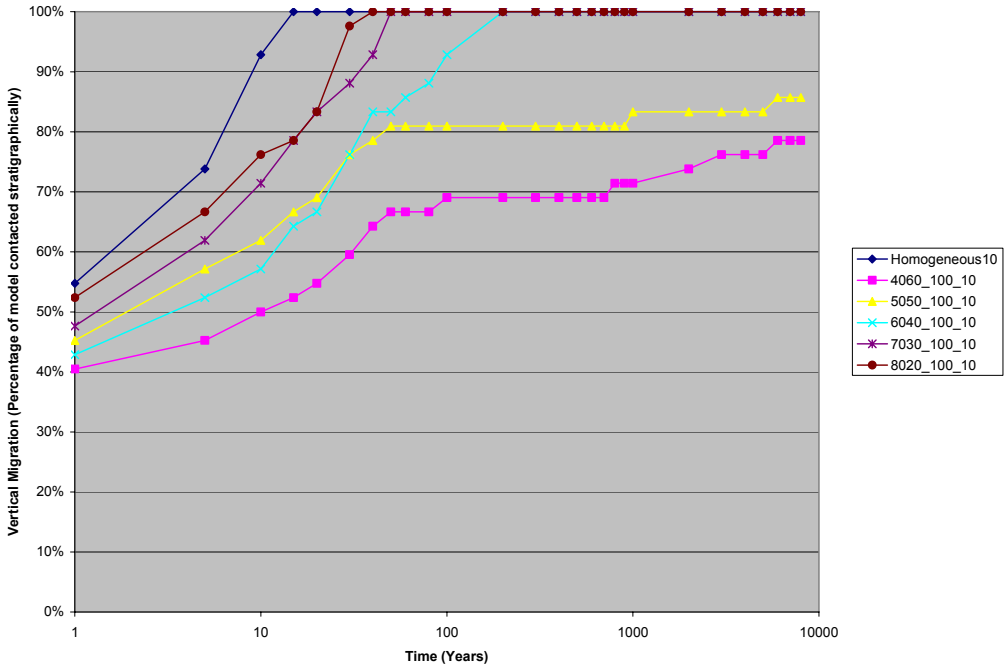

Figure D-101: Vertical migration comparison of the 100 m shale length models, various sand to shale contents, 10 degree slope

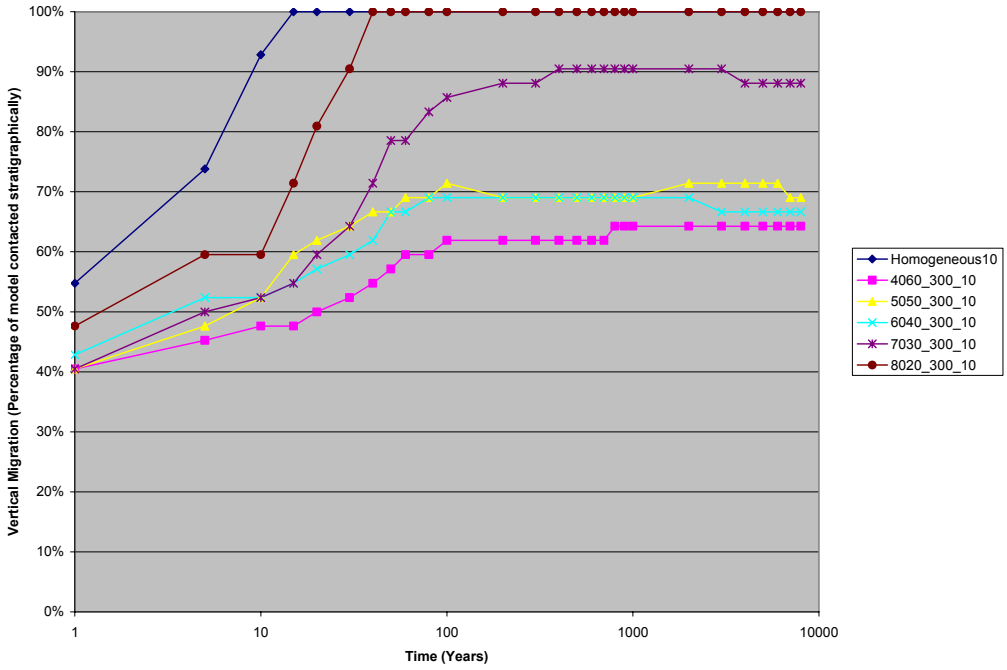

Figure D-102: Vertical migration comparison of the 300 m shale length models, various sand to shale contents, 10 degree slope

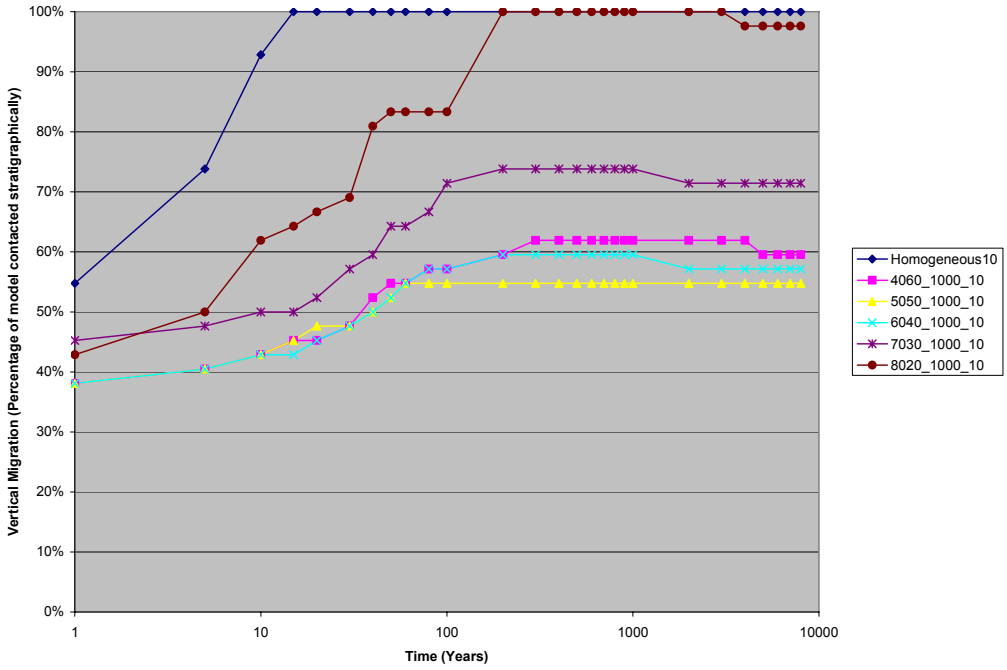

Figure D-103: Vertical migration comparison of the 1000 m shale length models, various sand to shale contents, 10 degree slope

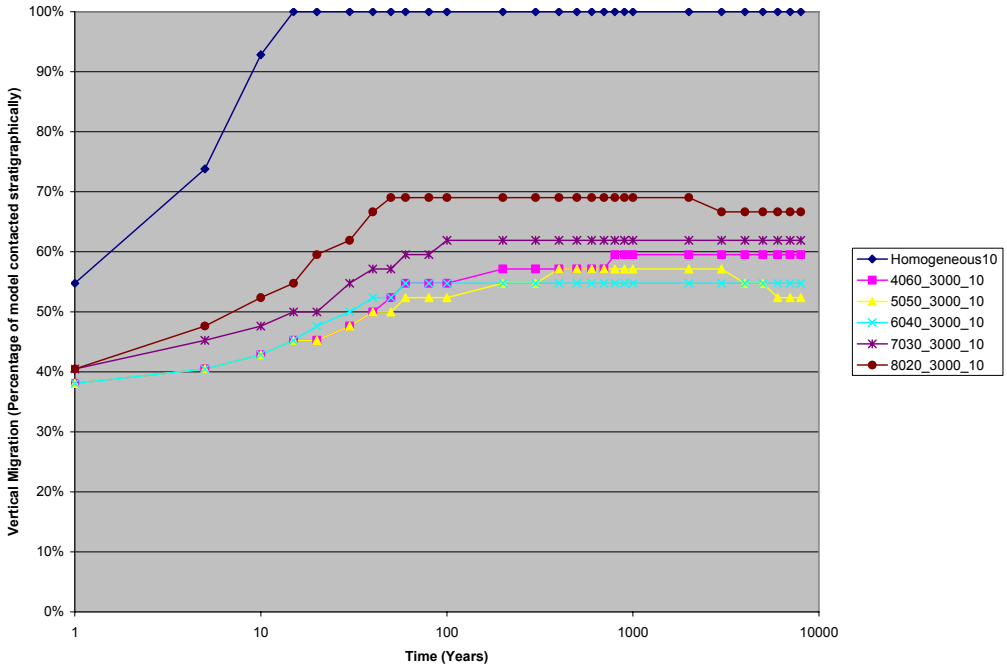

Figure D-104: Vertical migration comparison of the 3000 m shale length models, various sand to shale contents, 10 degree slope

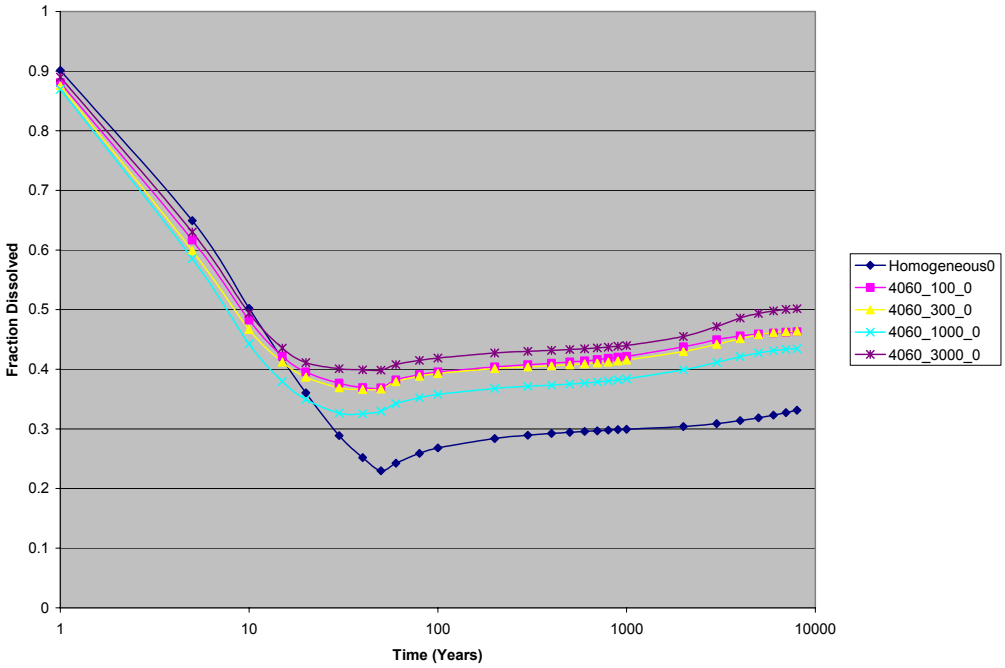

Figure D-104: Fraction of injection CO_2 dissolved - comparison of the 40:60 models, various shale lengths, 0 degree slope

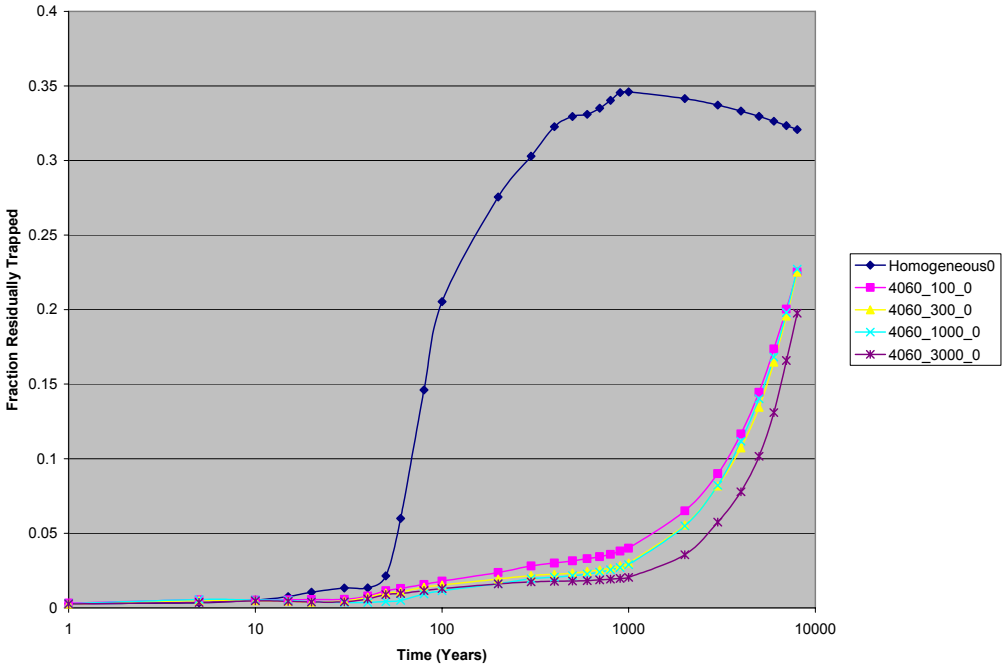

Figure D-105: Fraction of injection CO_2 residually trapped - comparison of the 40:60 models, various shale lengths, 0 degree slope

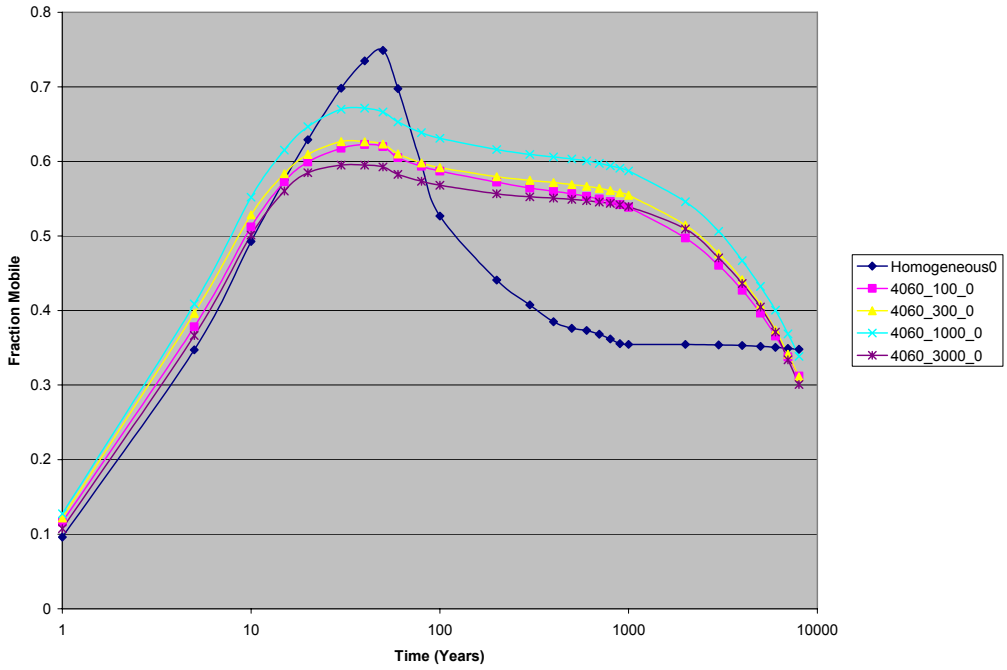

Figure D-105: Fraction of injection CO_2 remaining mobile - comparison of the 40:60 models, various shale lengths, 0 degree slope

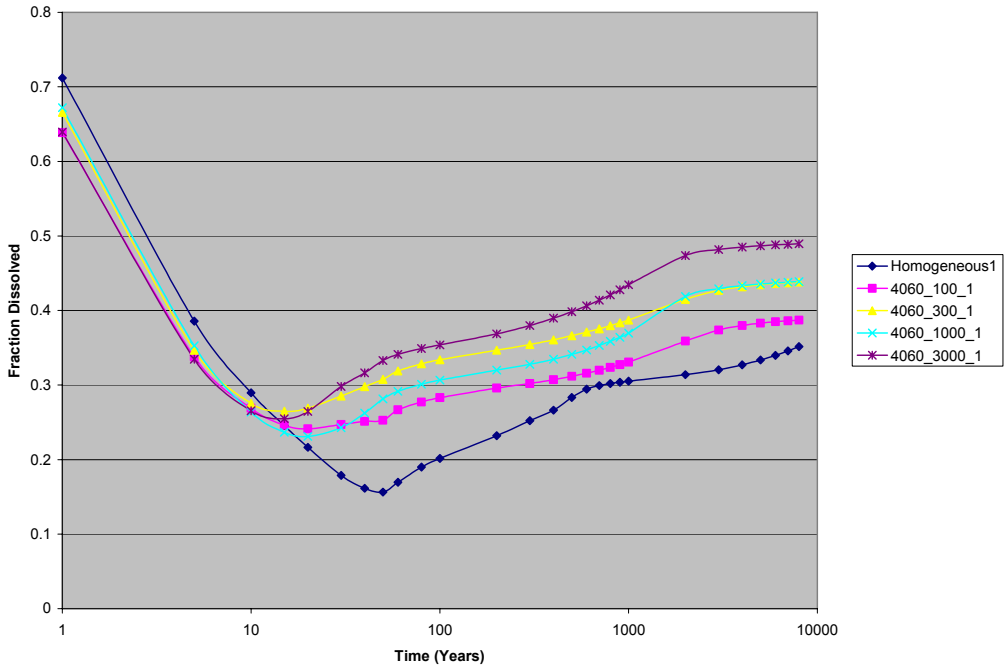

Figure D-106: Fraction of injection CO_2 dissolved - comparison of the 40:60 sand to shale models, various shale lengths, 1 degree slope

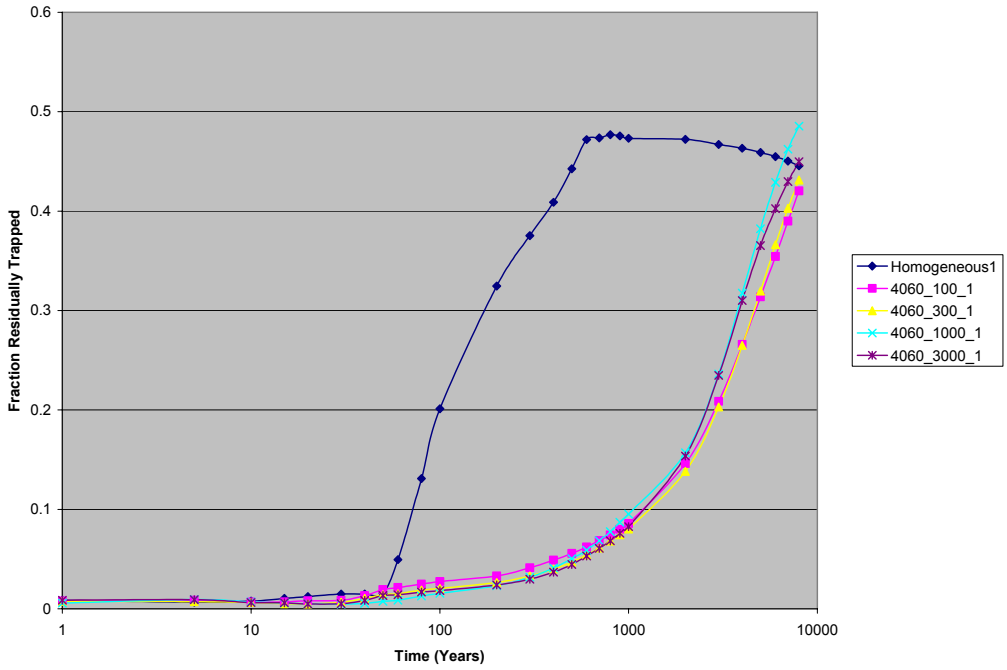

Figure D-107: Fraction of injection CO_2 residually trapped - comparison of the 40:60 sand to shale models, various shale lengths, 1 degree slope

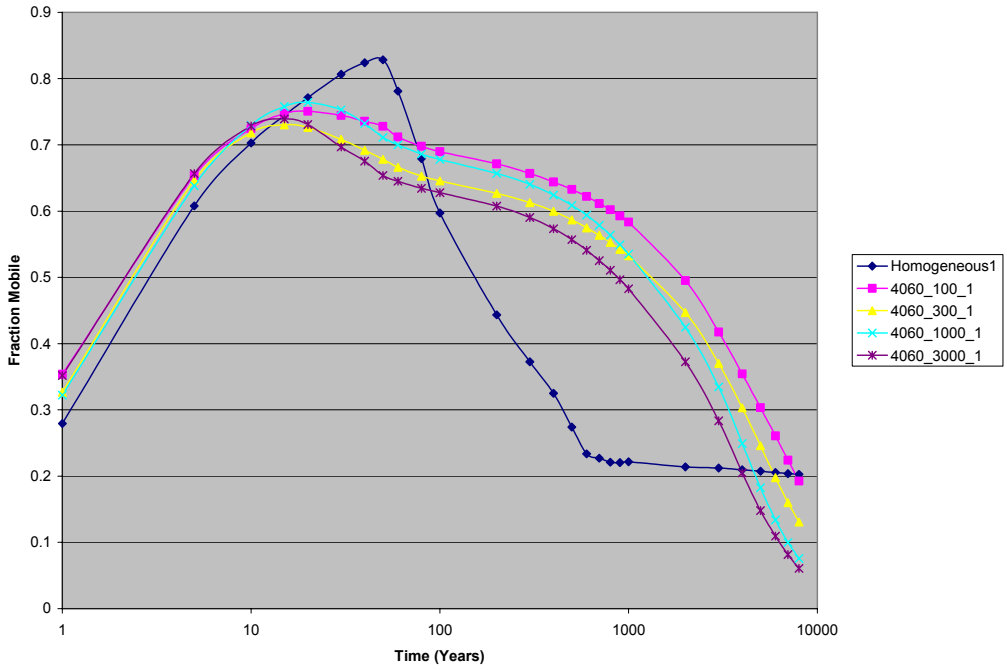

Figure D-108: Fraction of injection CO_2 remaining mobile - comparison of the 40:60 sand to shale models, various shale lengths, 1 degree slope

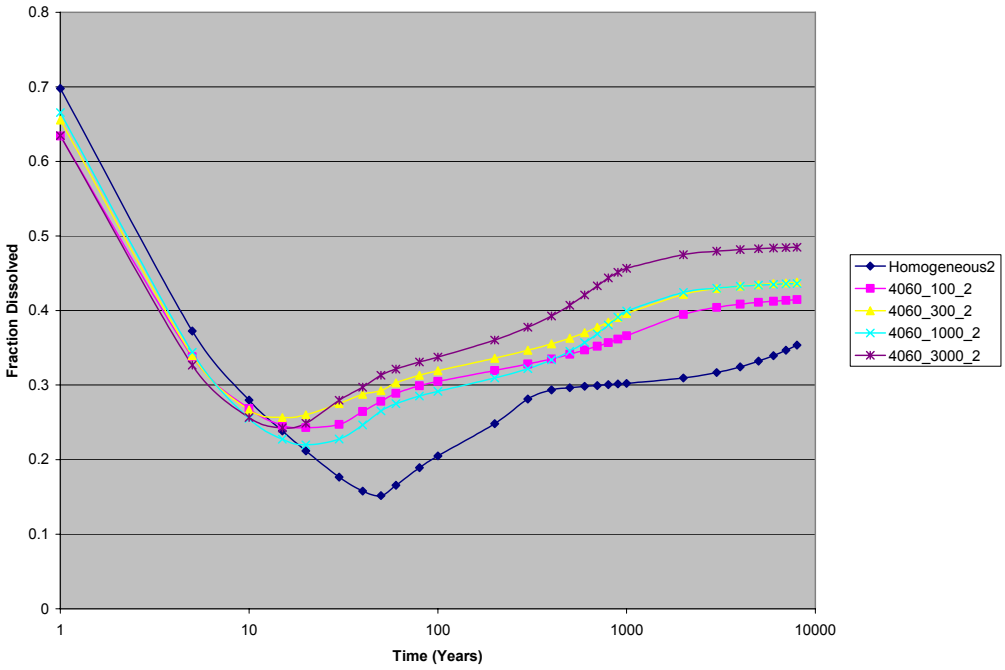

Figure D-109: Fraction of injection CO_2 dissolved - comparison of the 40:60 sand to shale models, various shale lengths, 2 degree slope

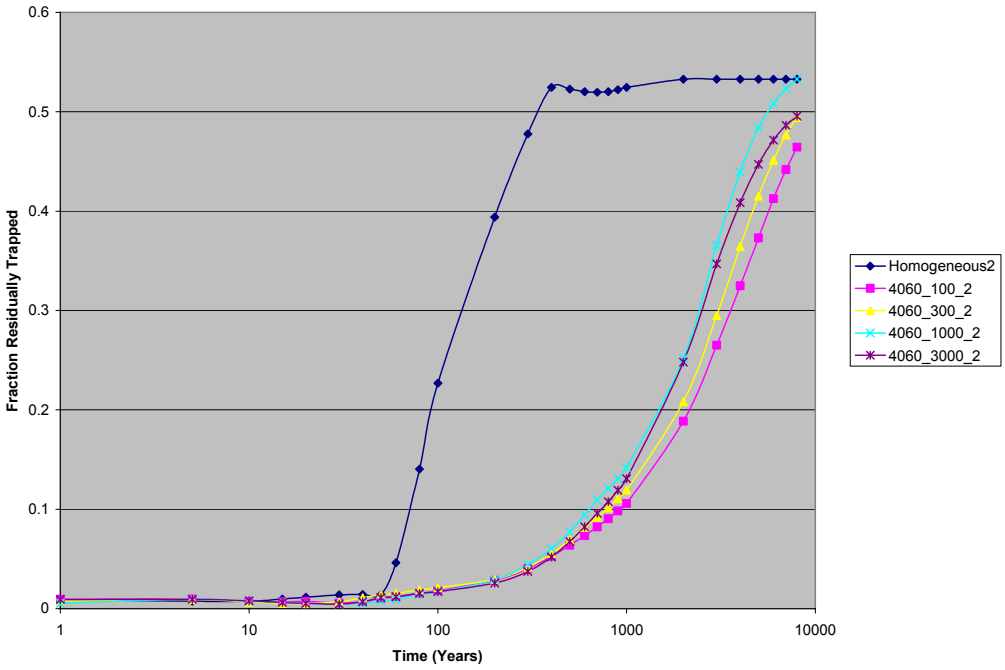

Figure D-110: Fraction of injection CO_2 residually trapped - comparison of the 40:60 sand to shale models, various shale lengths, 2 degree slope

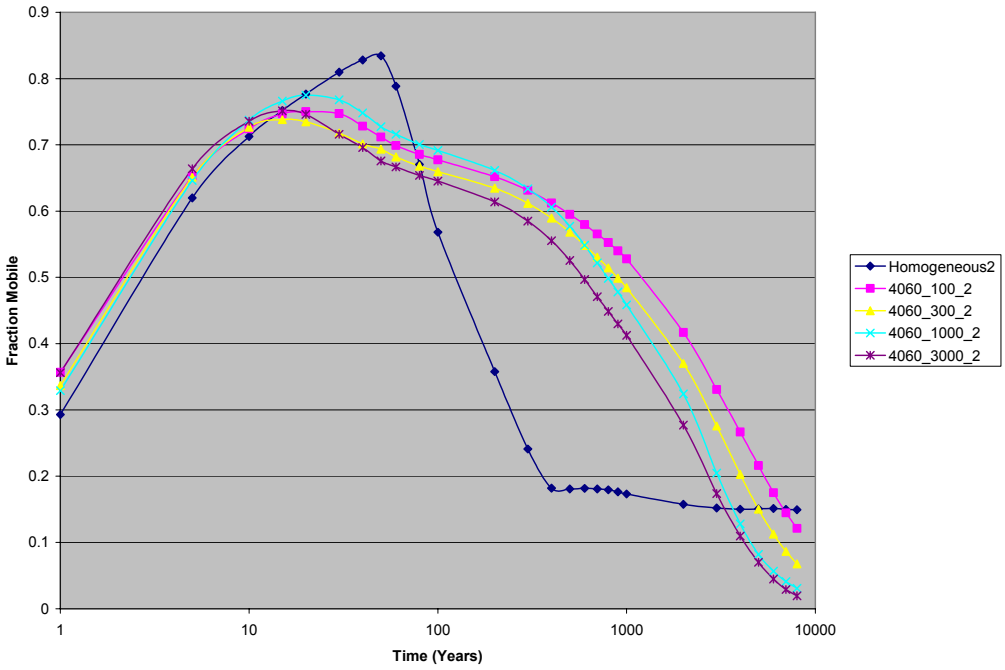

Figure D-111: Fraction of injection CO_2 remaining mobile - comparison of the 40:60 sand to shale models, various shale lengths, 2 degree slope

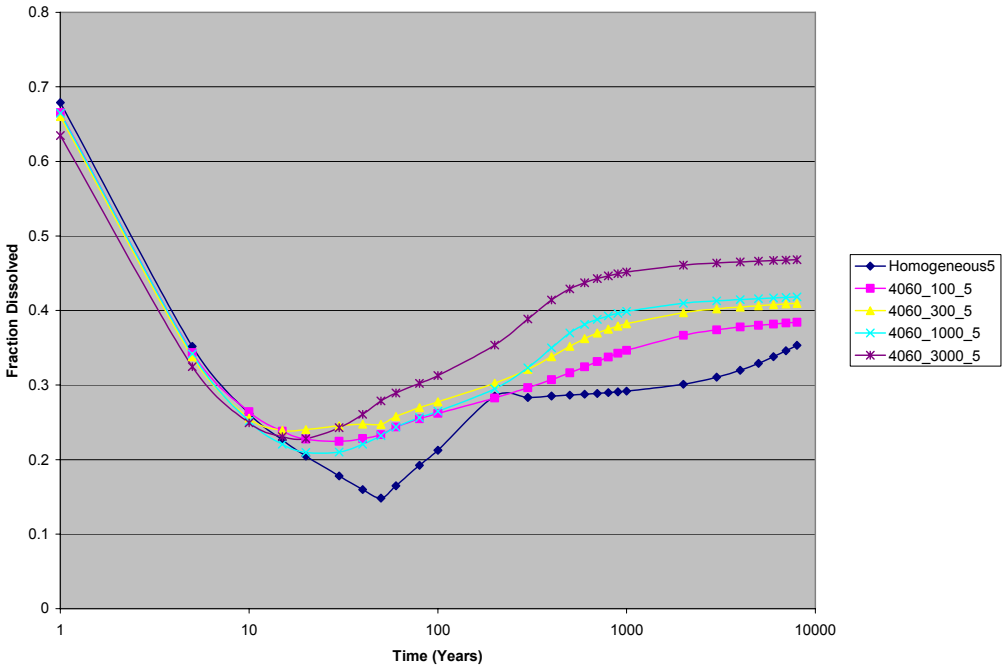

Figure D-112: Fraction of injection CO_2 dissolved - comparison of the 40:60 sand to shale models, various shale lengths, 5 degree slope

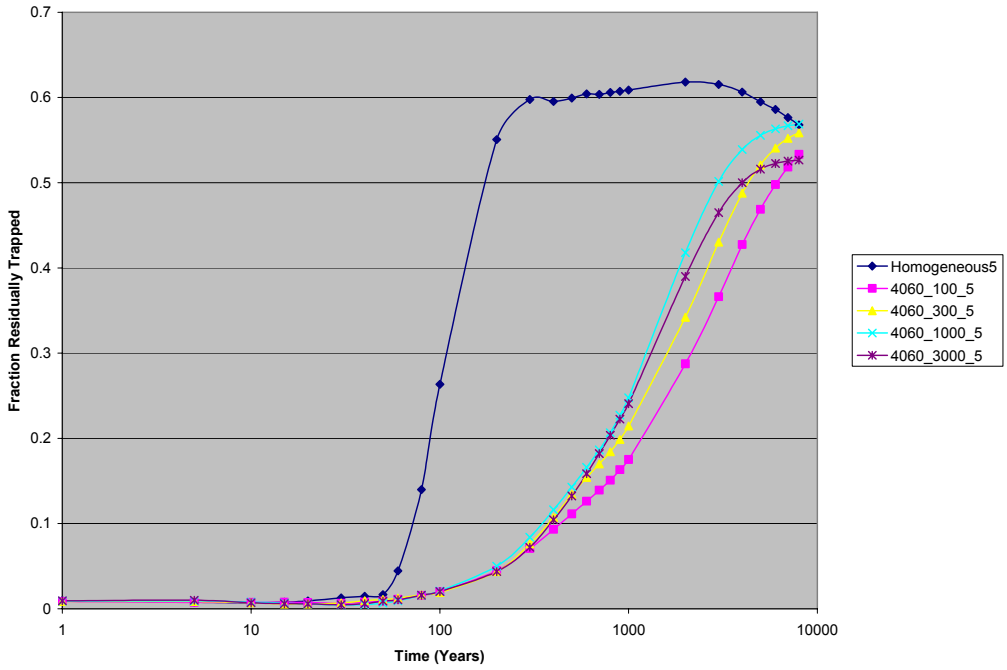

Figure D-113: Fraction of injection CO_2 residually trapped - comparison of the 40:60 sand to shale models, various shale lengths, 5 degree slope

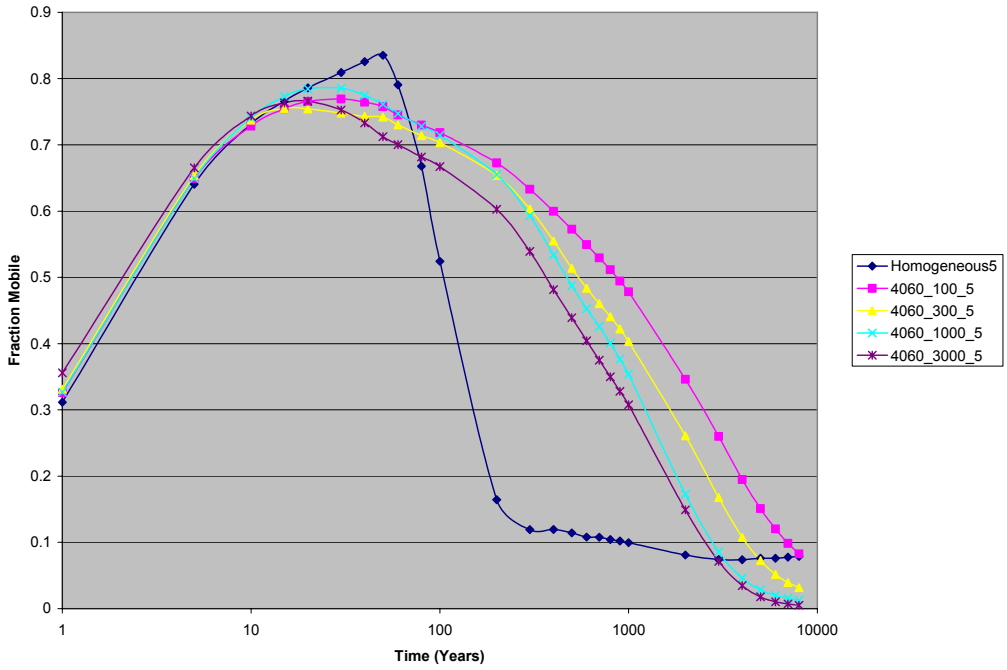

Figure D-114: Fraction of injection CO_2 remaining mobile - comparison of the 40:60 sand to shale models, various shale lengths, 5 degree slope

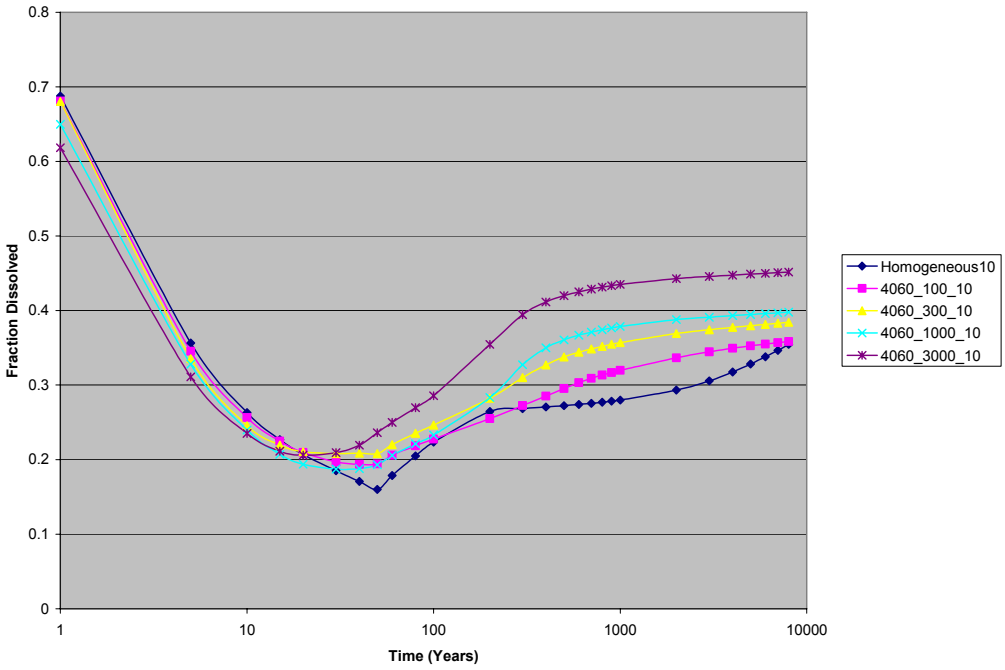

Figure D-115: Fraction of injection CO_2 dissolved - comparison of the 40:60 sand to shale models, various shale lengths, 10 degree slope

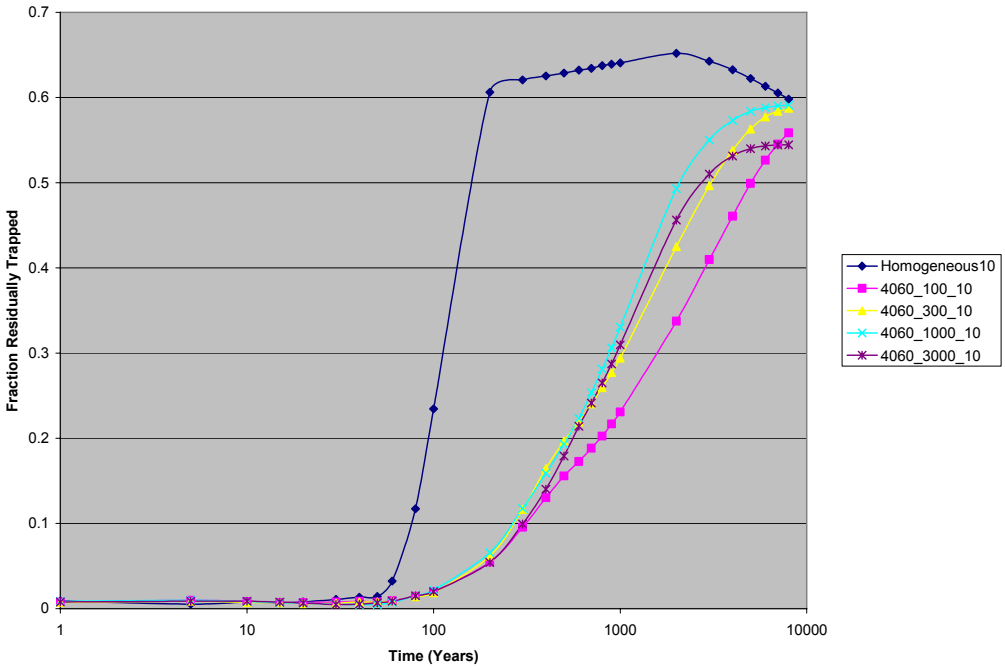

Figure D-116: Fraction of injection CO_2 residually trapped - comparison of the 40:60 sand to shale models, various shale lengths, 10 degree slope

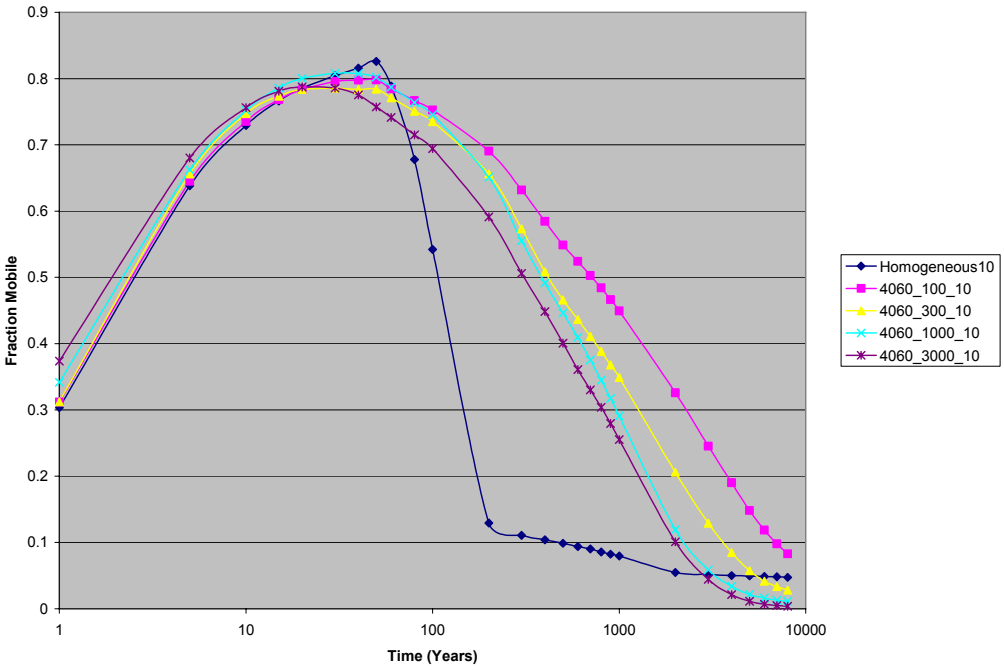

Figure D-117: Fraction of injection CO_2 remaining mobile - comparison of the 40:60 sand to shale models, various shale lengths, 10 degree slope

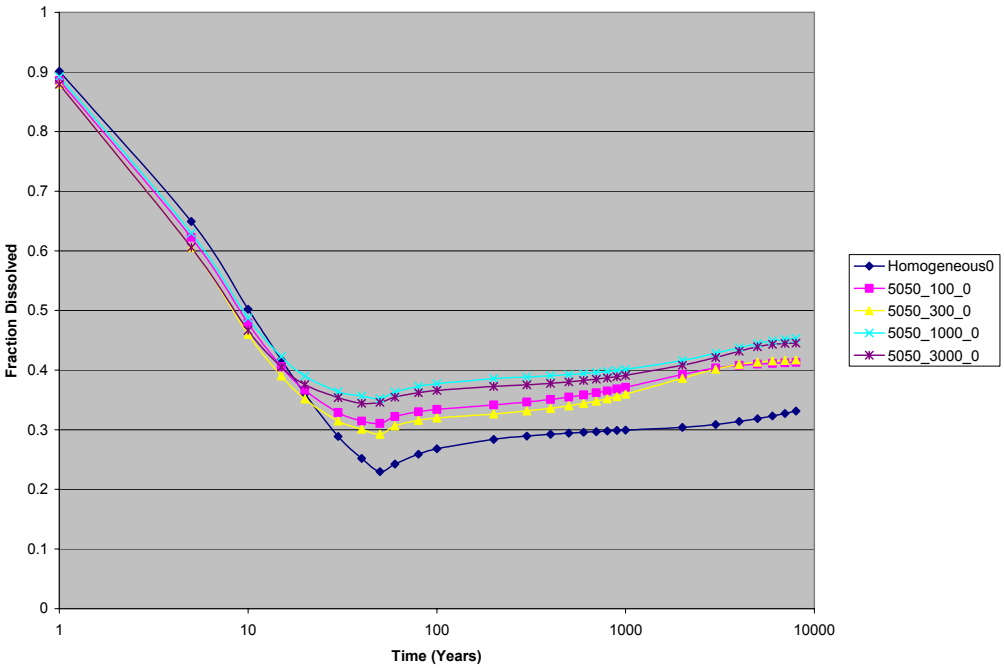

Figure D-118: Fraction of injection CO_2 dissolved - comparison of the 50:50 sand to shale models, various shale lengths, 0 degree slope

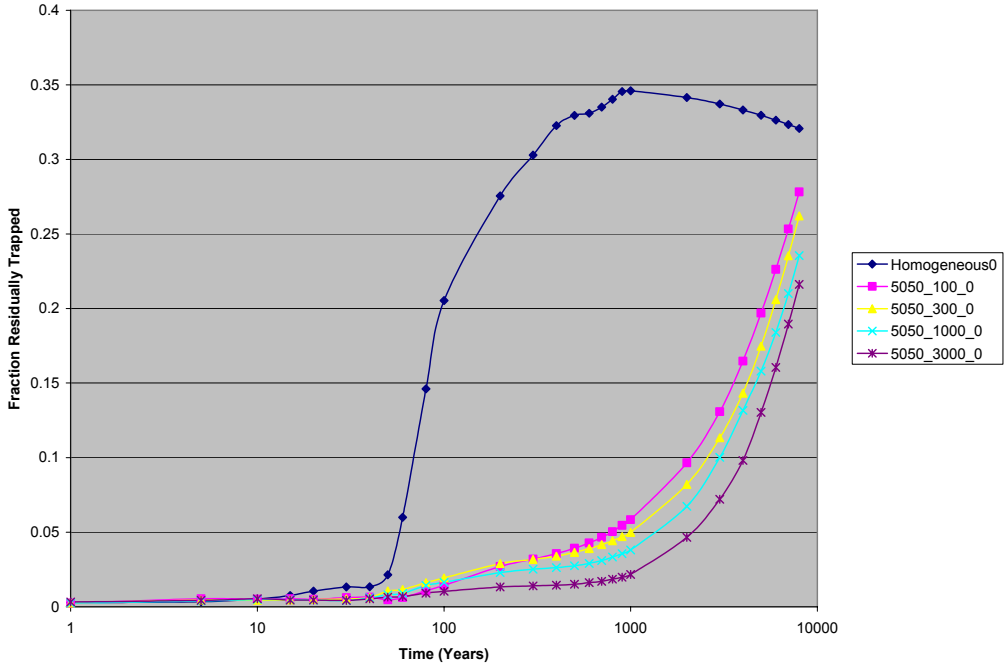

Figure D-119: Fraction of injection CO_2 residually trapped - comparison of the 50:50 sand to shale models, various shale lengths, 0 degree slope

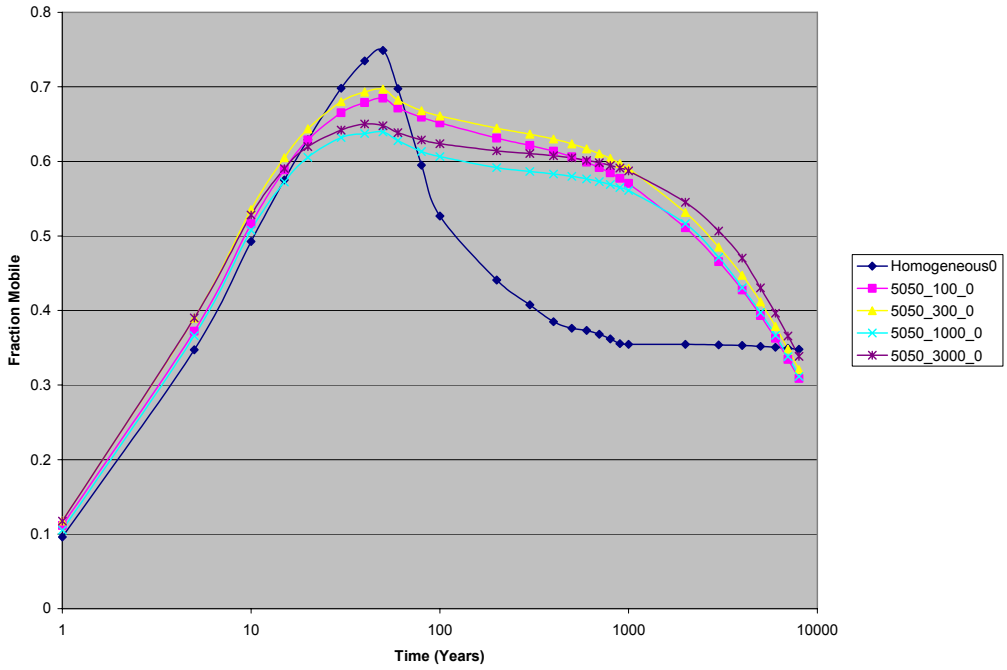

Figure D-120: Fraction of injection CO_2 remaining mobile - comparison of the 50:50 sand to shale models, various shale lengths, 0 degree slope

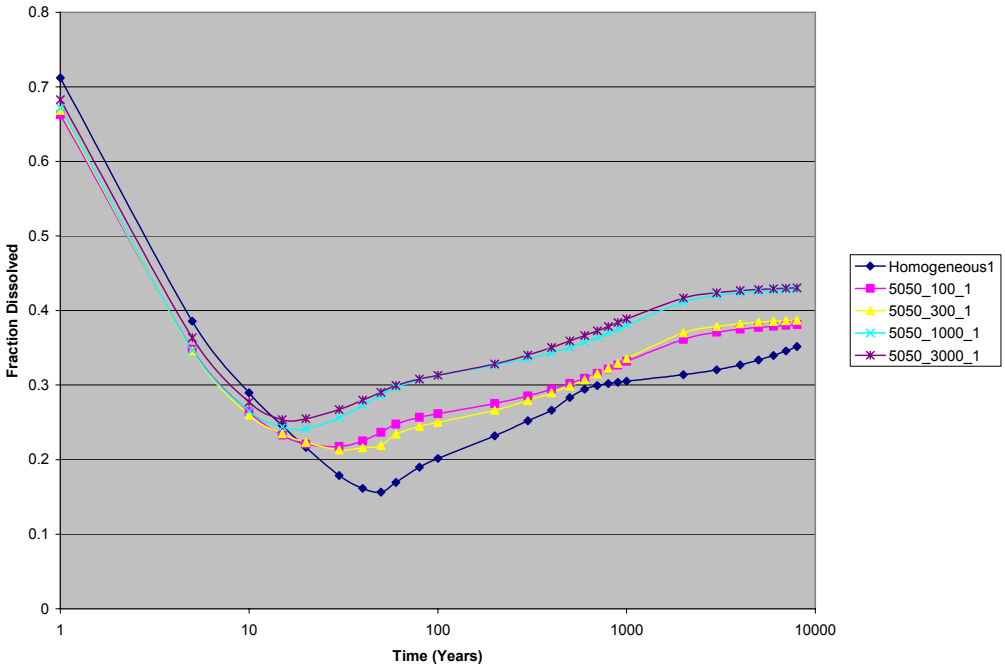

Figure D-121: Fraction of injection CO_2 dissolved - comparison of the 50:50 sand to shale models, various shale lengths, 1 degree slope

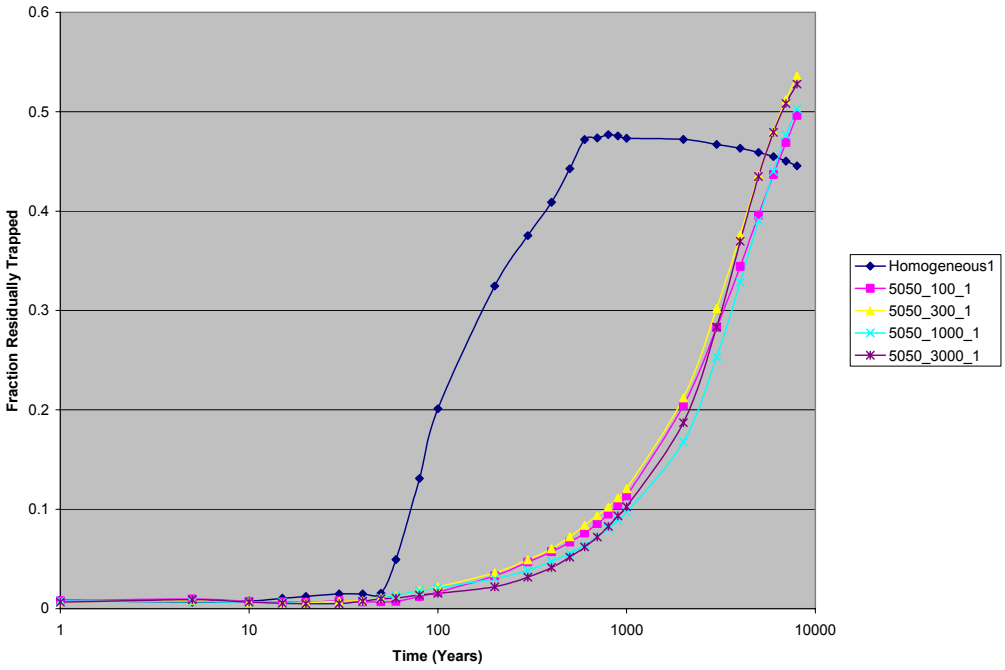

Figure D-122: Fraction of injection CO_2 residually trapped - comparison of the 50:50 sand to shale models, various shale lengths, 1 degree slope

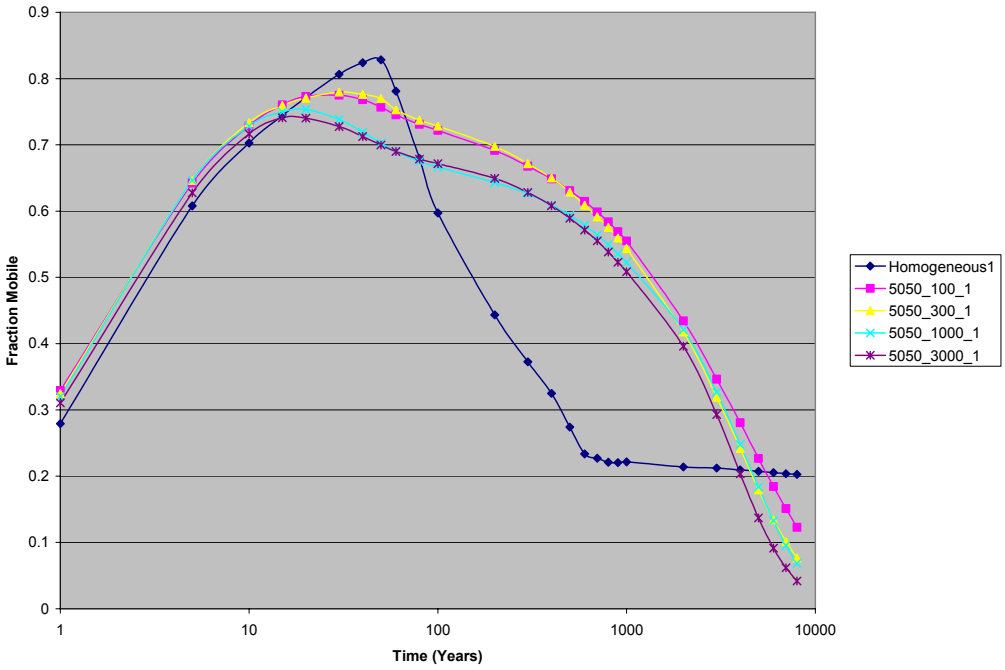

Figure D-123: Fraction of injection CO_2 remaining mobile - comparison of the 50:50 sand to shale models, various shale lengths, 1 degree slope

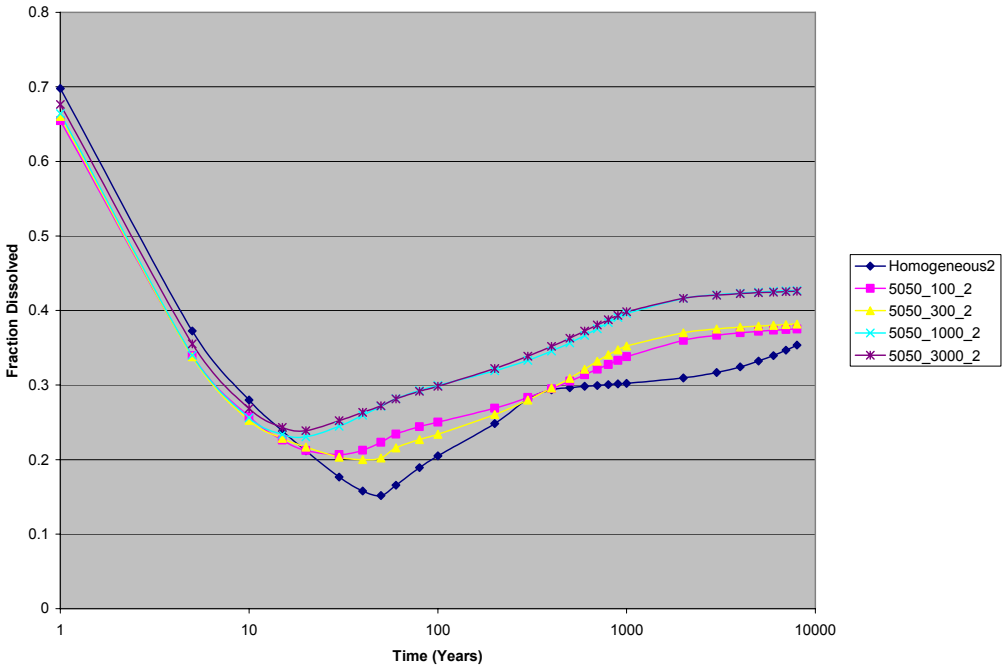

Figure D-124: Fraction of injection CO_2 dissolved - comparison of the 50:50 sand to shale models, various shale lengths, 2 degree slope

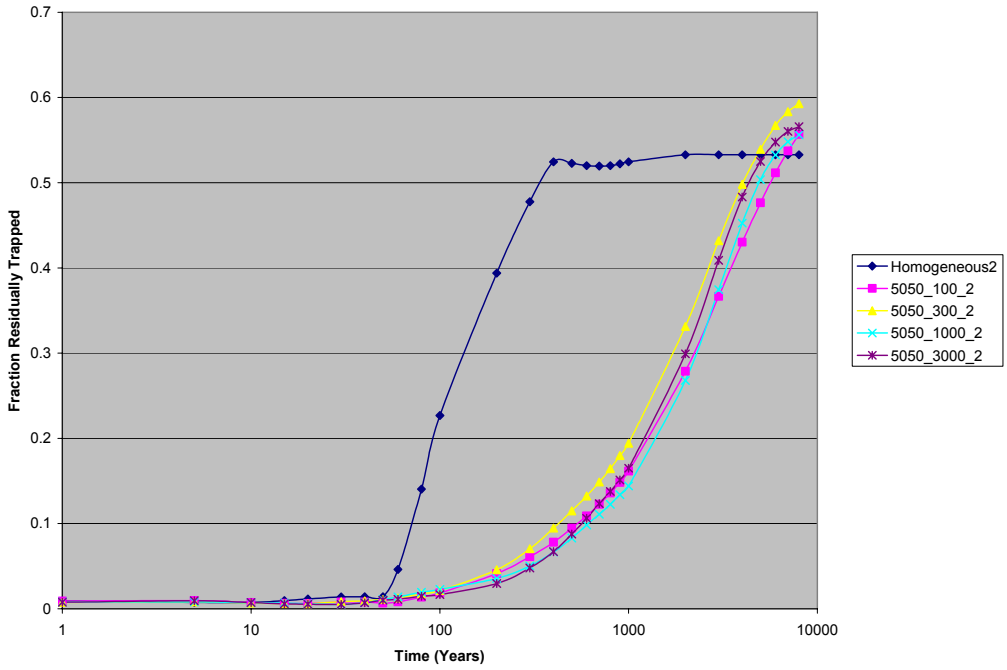

Figure D-125: Fraction of injection CO_2 residually trapped - comparison of the 50:50 sand to shale models, various shale lengths, 2 degree slope

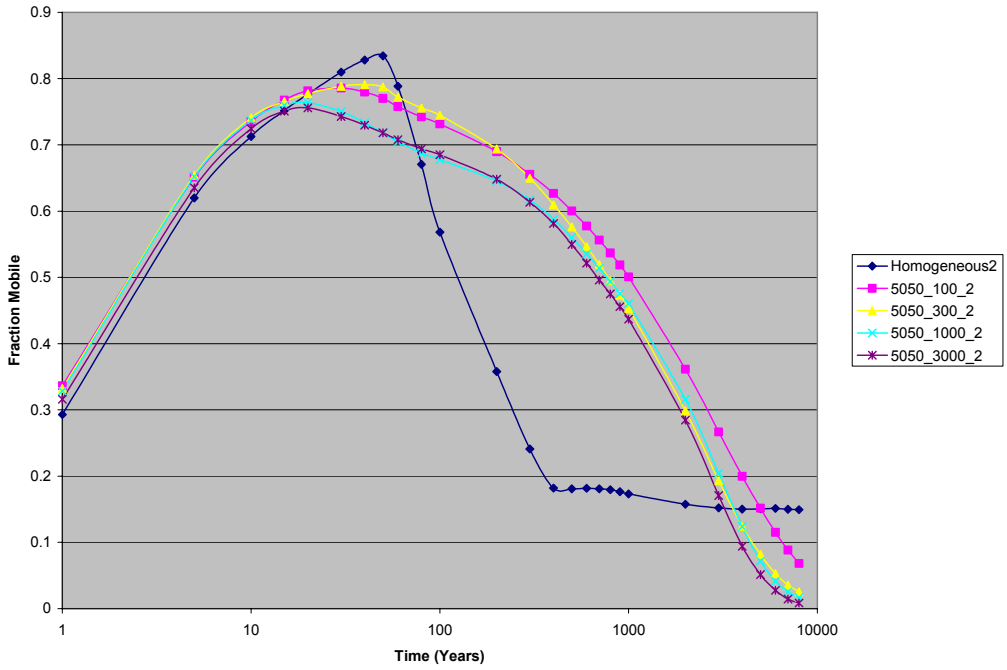

Figure D-126: Fraction of injection CO_2 remaining mobile - comparison of the 50:50 sand to shale models, various shale lengths, 2 degree slope

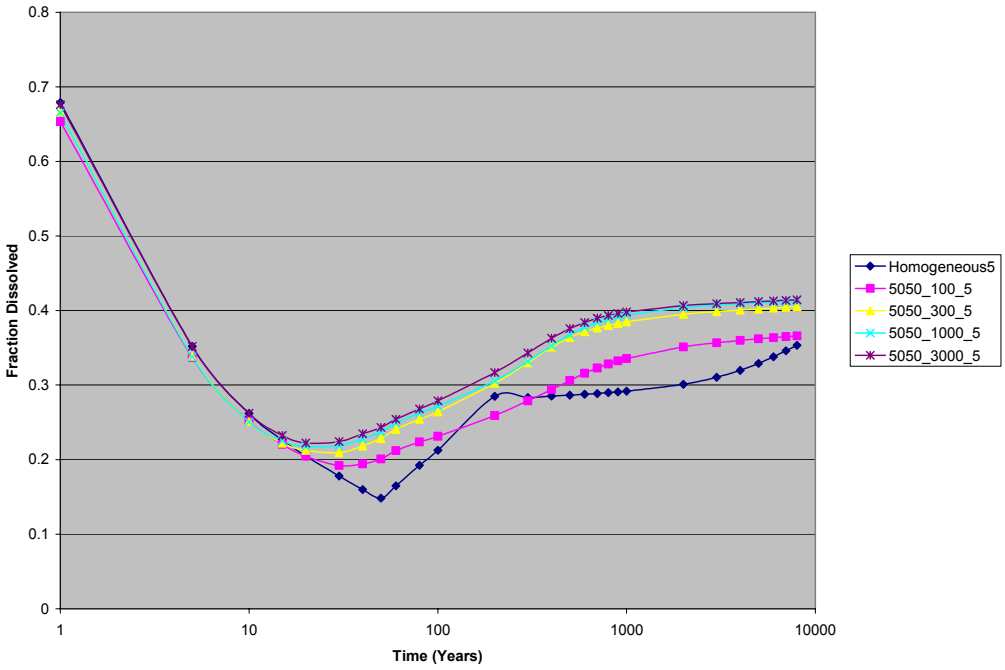

Figure D-127: Fraction of injection CO_2 dissolved - comparison of the 50:50 sand to shale models, various shale lengths, 5 degree slope

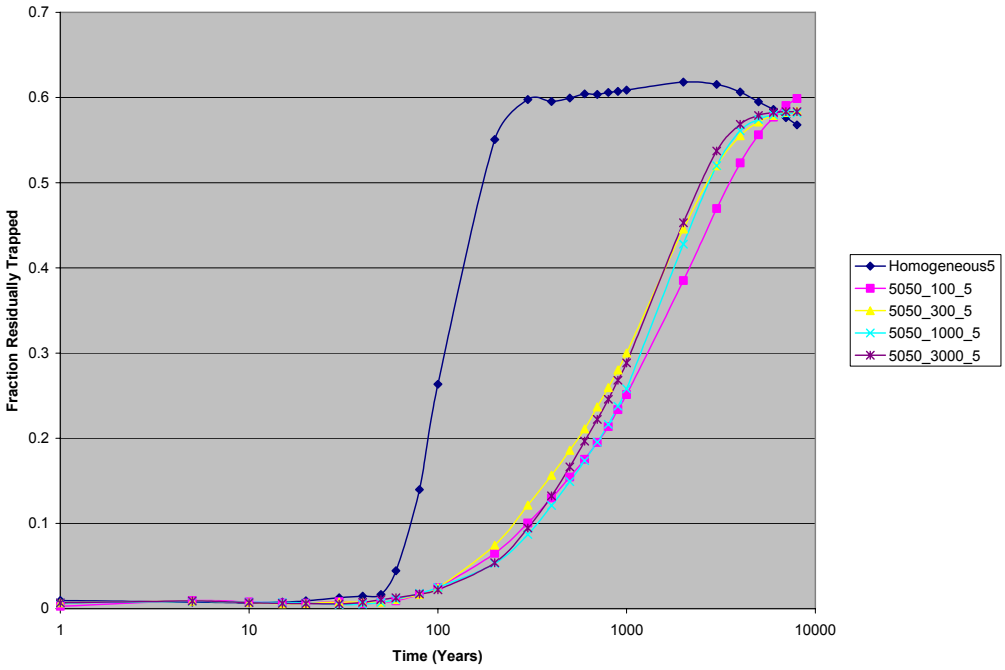

Figure D-128: Fraction of injection CO_2 residually trapped - comparison of the 50:50 sand to shale models, various shale lengths, 5 degree slope

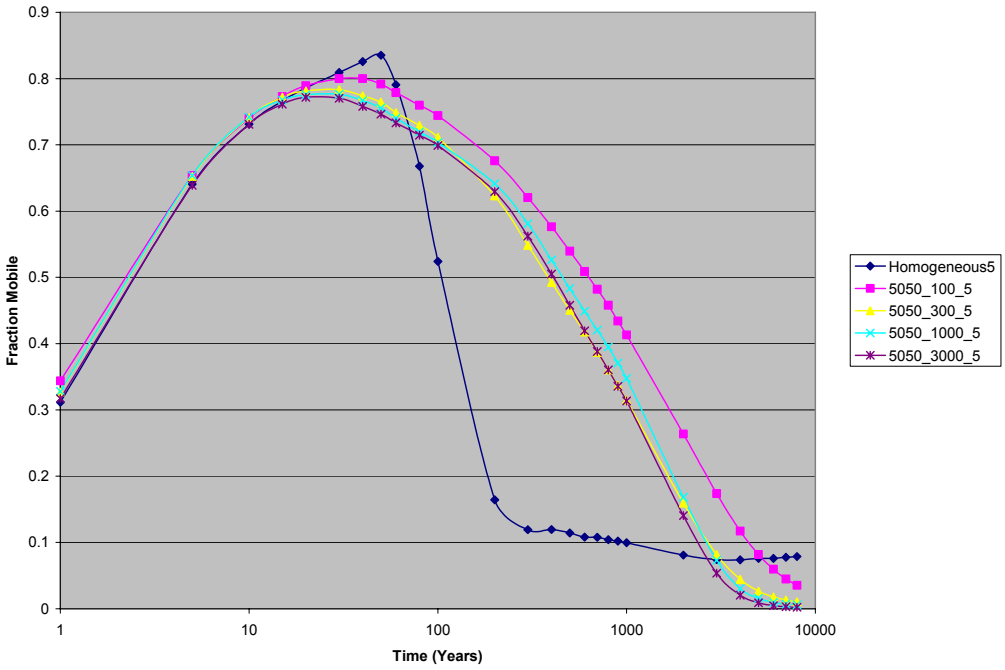

Figure D-129: Fraction of injection CO_2 remaining mobile - comparison of the 50:50 sand to shale models, various shale lengths, 5 degree slope

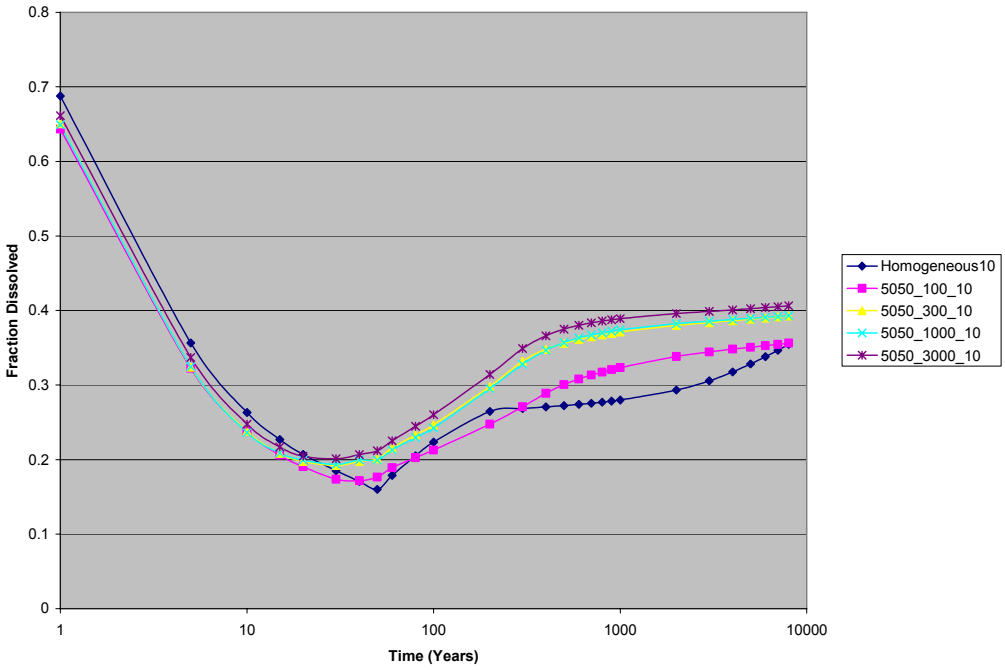

Figure D-130: Fraction of injection CO_2 dissolved - comparison of the 50:50 sand to shale models, various shale lengths, 10 degree slope

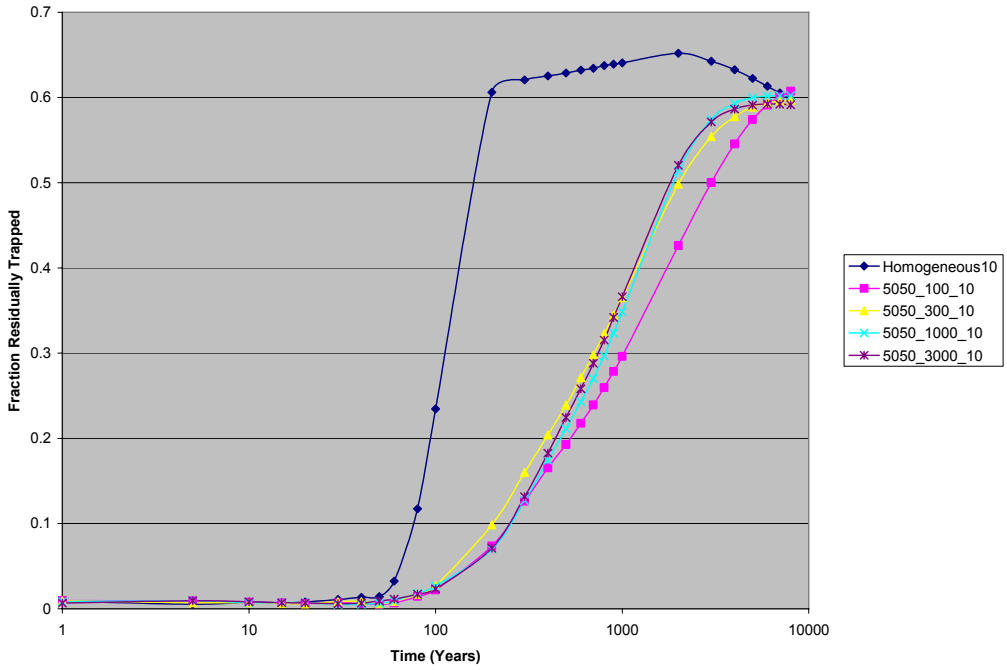

Figure D-131: Fraction of injection CO_2 residually trapped - comparison of the 50:50 sand to shale models, various shale lengths, 10 degree slope

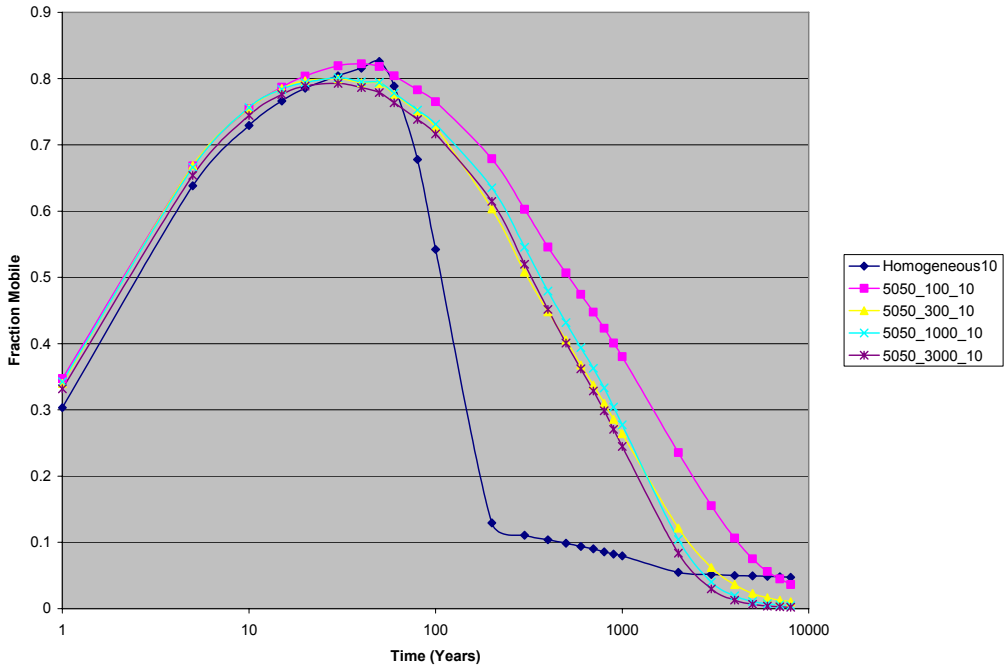

Figure D-132: Fraction of injection CO_2 remaining mobile - comparison of the 50:50 sand to shale models, various shale lengths, 10 degree slope

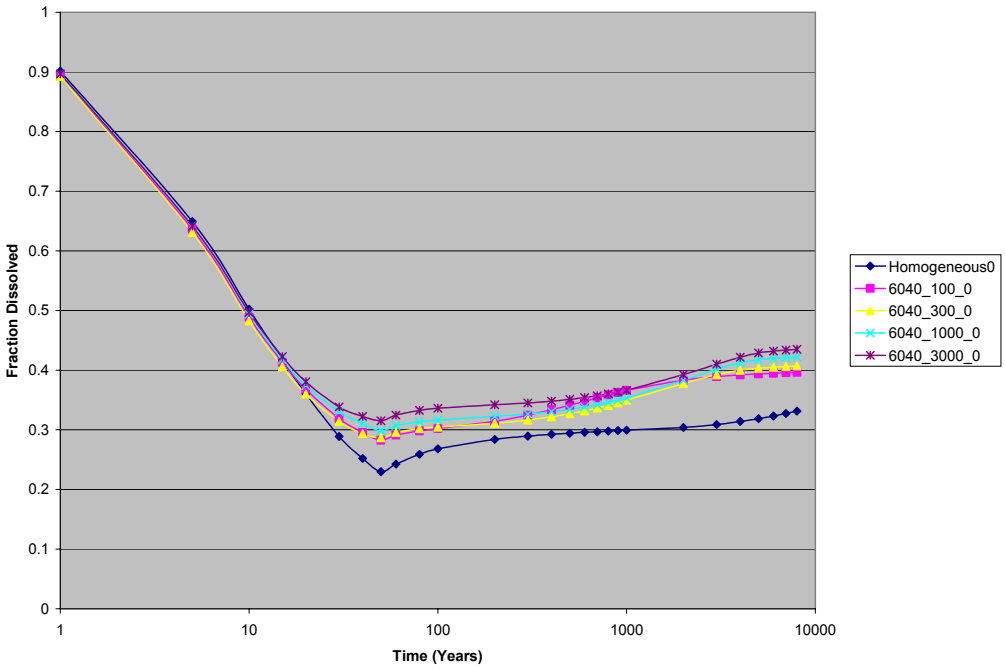

Figure D-133: Fraction of injection CO_2 dissolved - comparison of the 60:40 sand to shale models, various shale lengths, 0 degree slope

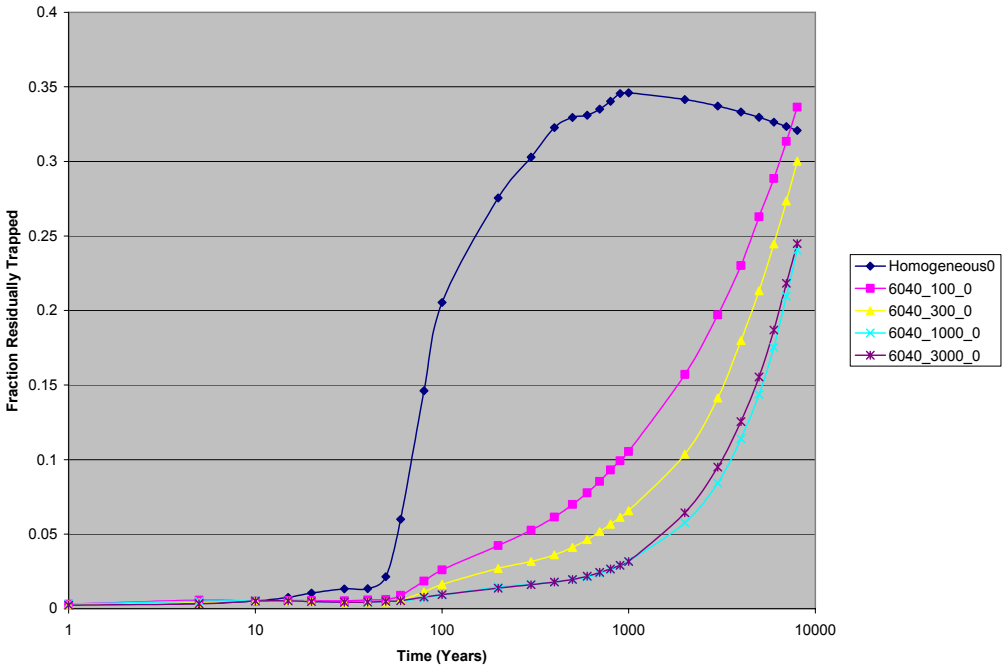

Figure D-134: Fraction of injection CO_2 residually trapped - comparison of the 60:40 sand to shale models, various shale lengths, 0 degree slope

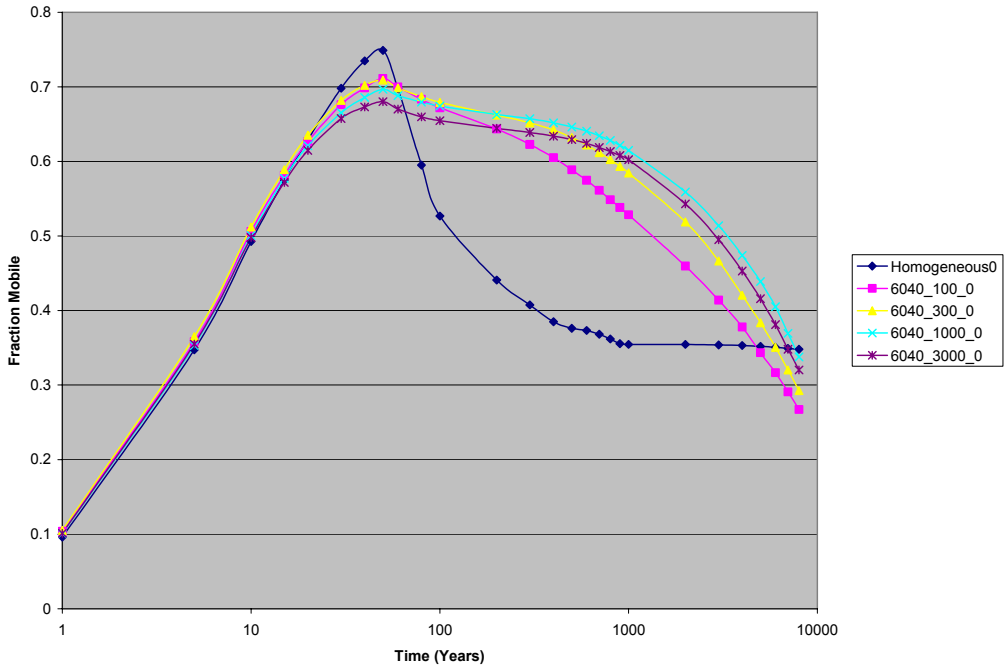

Figure D-135: Fraction of injection CO_2 remaining mobile - comparison of the 60:40 sand to shale models, various shale lengths, 0 degree slope

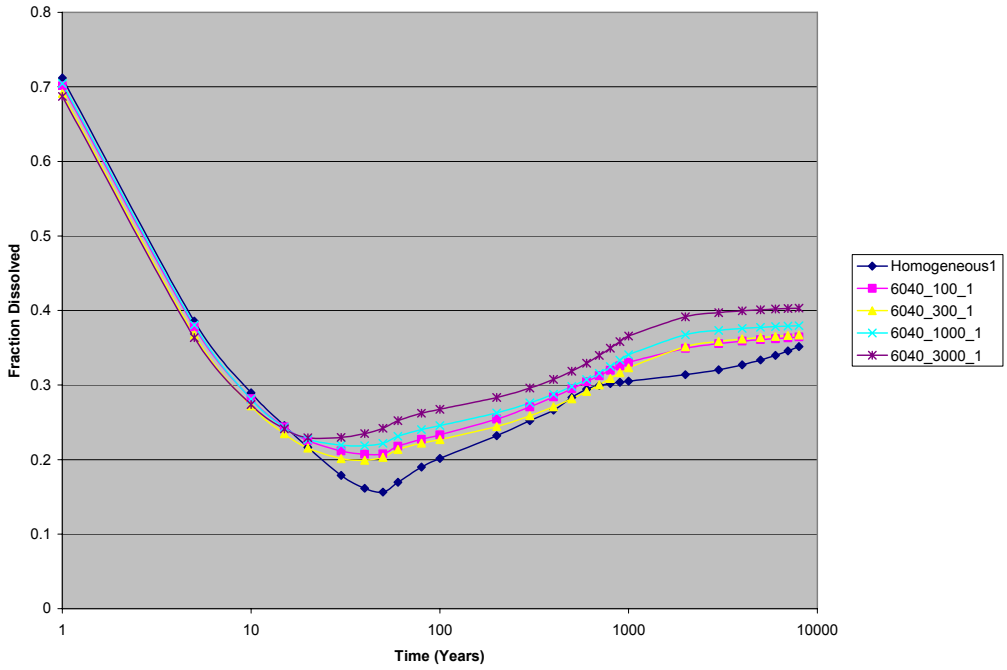

Figure D-136: Fraction of injection CO_2 dissolved - comparison of the 60:40 sand to shale models, various shale lengths, 1 degree slope

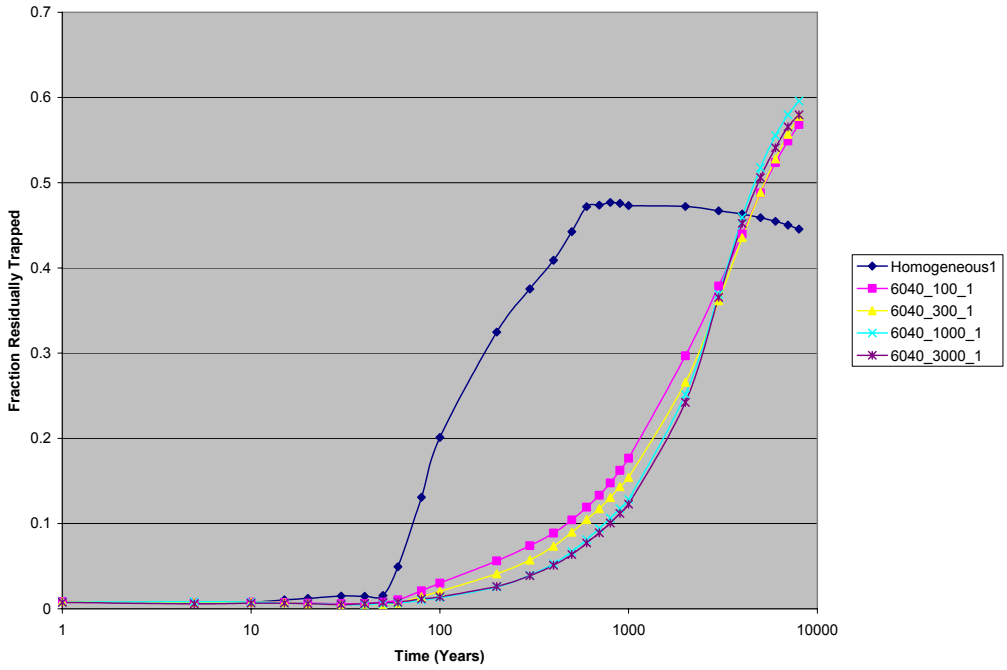

Figure D-137: Fraction of injection CO_2 residually trapped - comparison of the 60:40 sand to shale models, various shale lengths, 1 degree slope

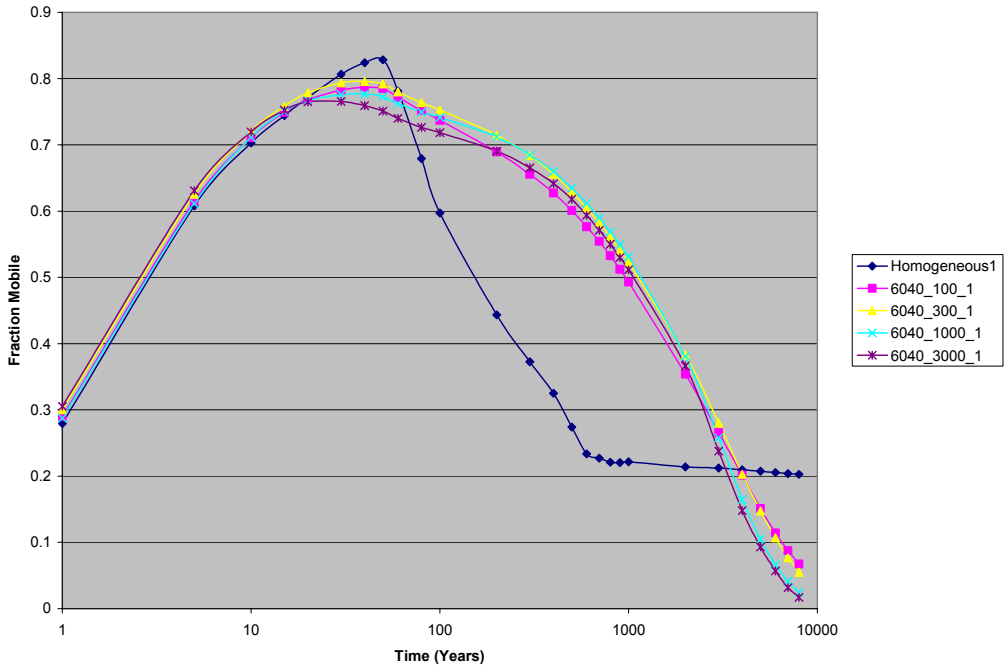

Figure D-138: Fraction of injection CO_2 remaining mobile - comparison of the 60:40 sand to shale models, various shale lengths, 1 degree slope

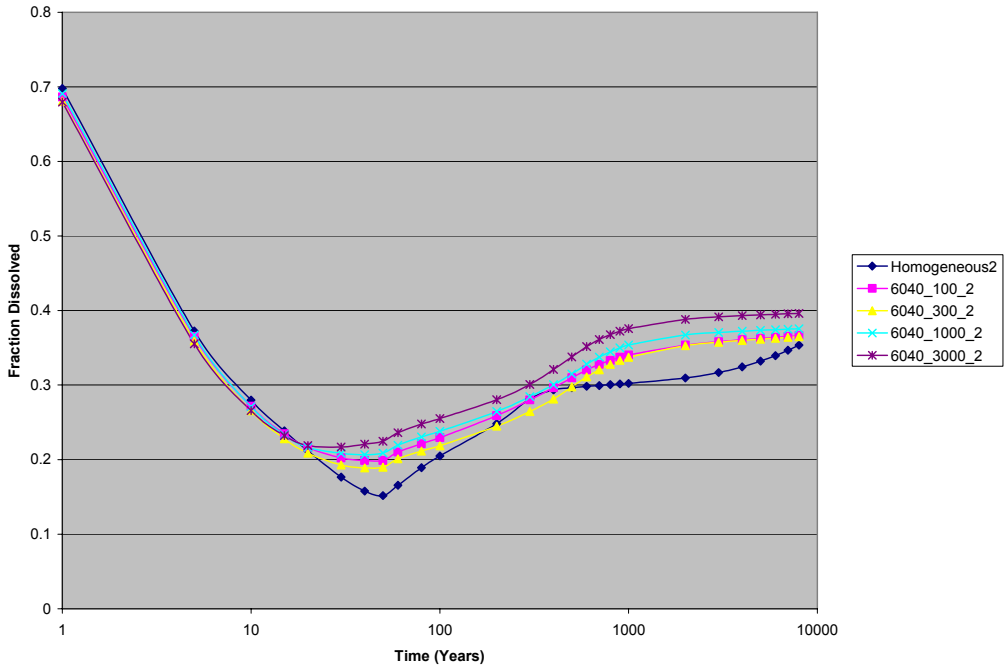

Figure D-139: Fraction of injection CO_2 dissolved - comparison of the 60:40 sand to shale models, various shale lengths, 2 degree slope

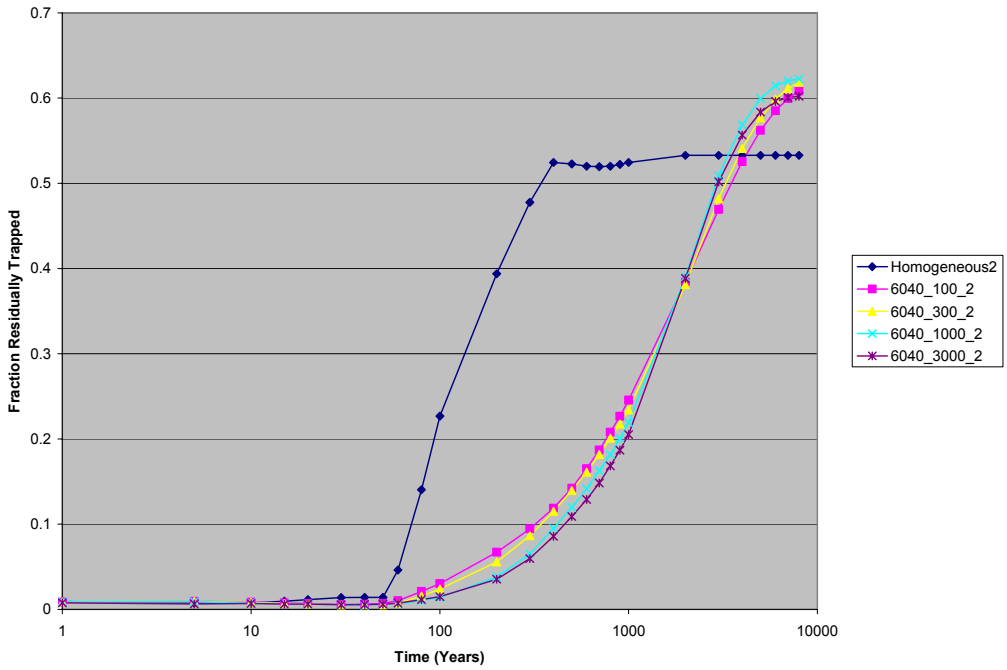

Figure D-140: Fraction of injection CO_2 residually trapped - comparison of the 60:40 sand to shale models, various shale lengths, 2 degree slope

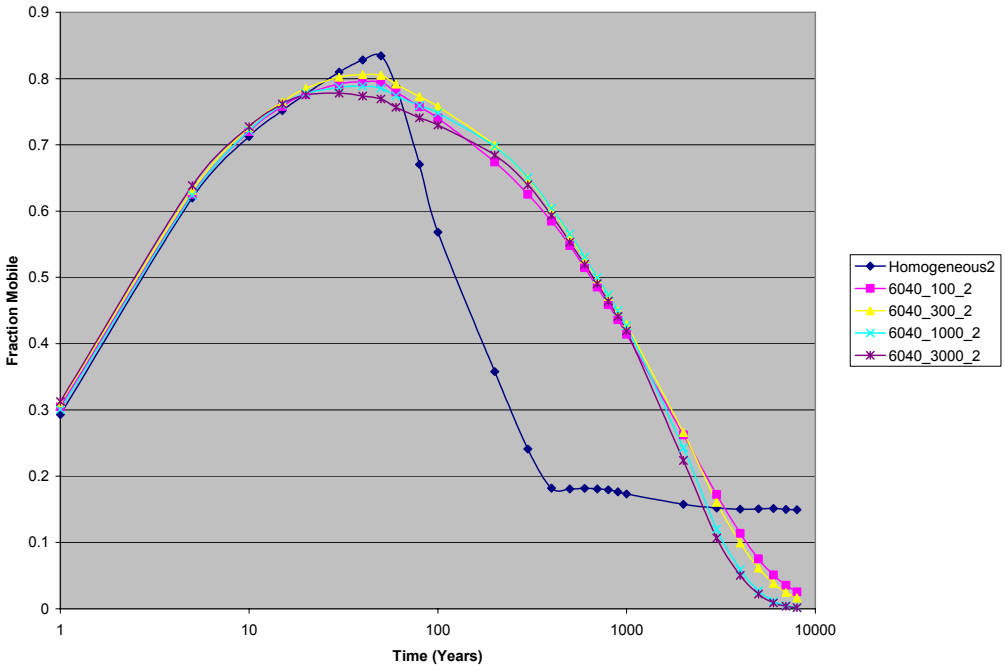

Figure D-141: Fraction of injection CO_2 remaining mobile - comparison of the 60:40 sand to shale models, various shale lengths, 2 degree slope

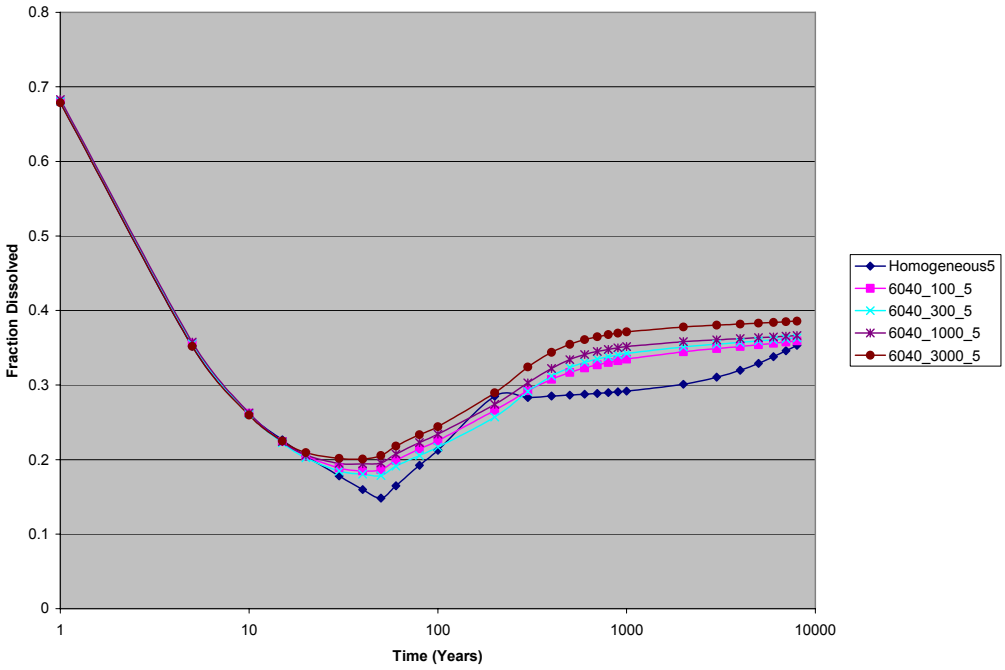

Figure D-142: Fraction of injection CO_2 dissolved - comparison of the 60:40 sand to shale models, various shale lengths, 5 degree slope

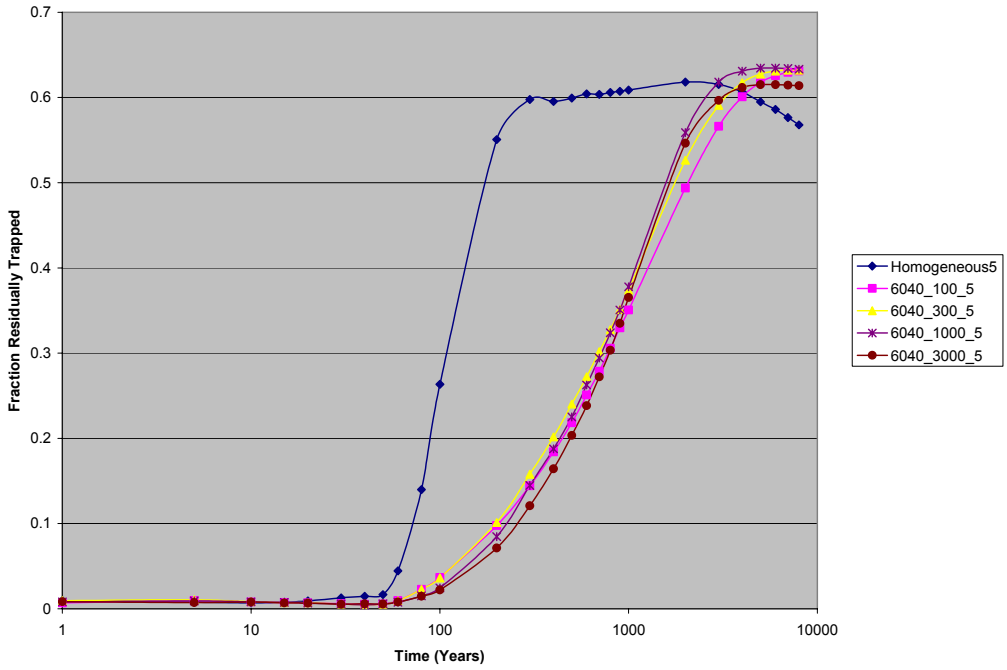

Figure D-143: Fraction of injection CO_2 residually trapped - comparison of the 60:40 sand to shale models, various shale lengths, 5 degree slope

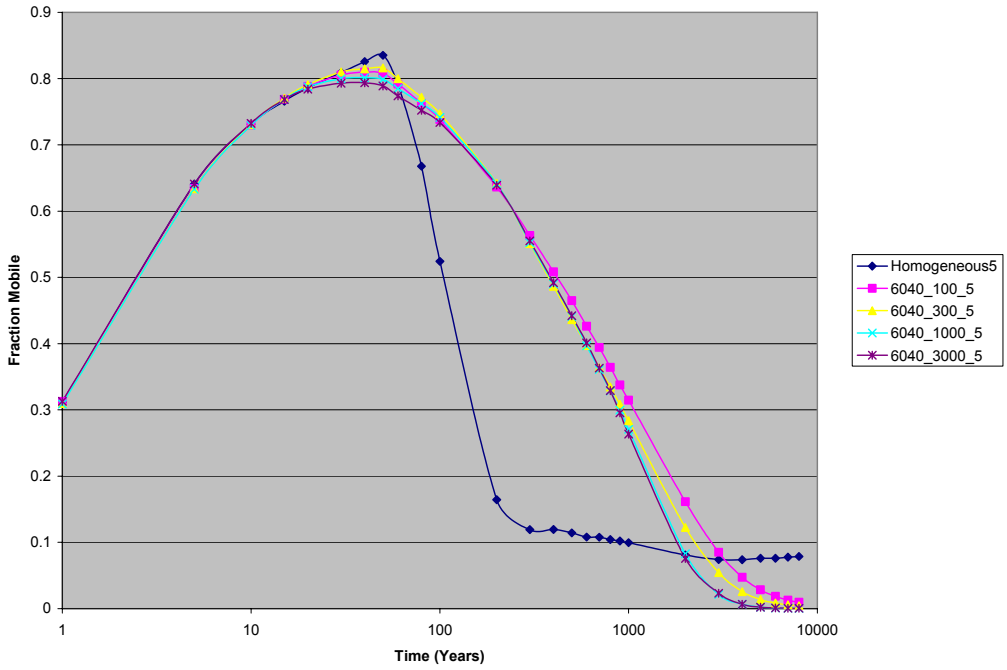

Figure D-144: Fraction of injection CO_2 remaining mobile - comparison of the 60:40 sand to shale models, various shale lengths, 5 degree slope

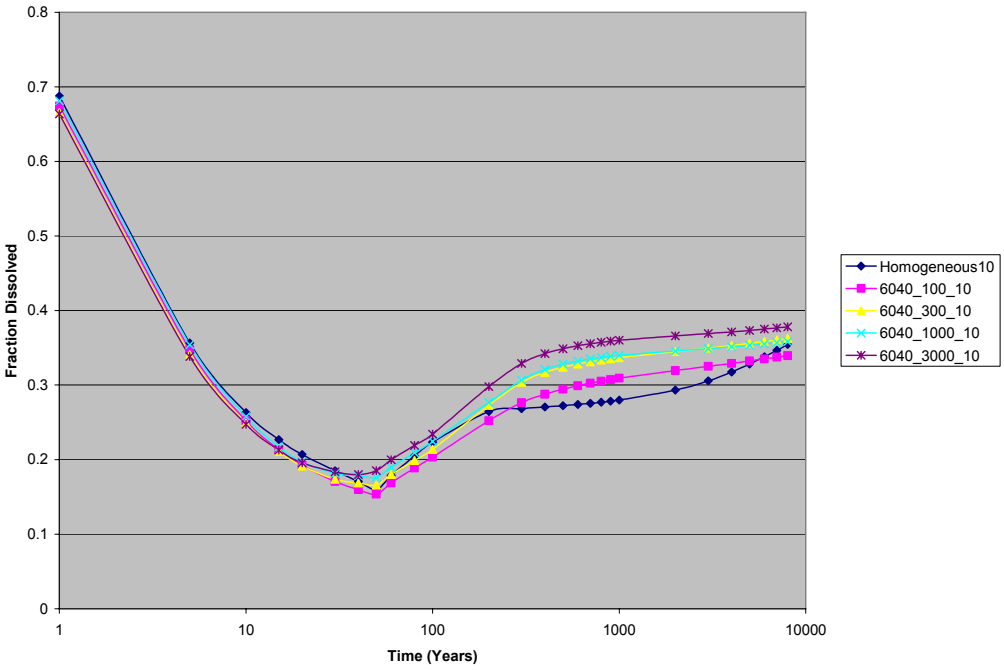

Figure D-145: Fraction of injection CO_2 dissolved - comparison of the 60:40 sand to shale models, various shale lengths, 10 degree slope

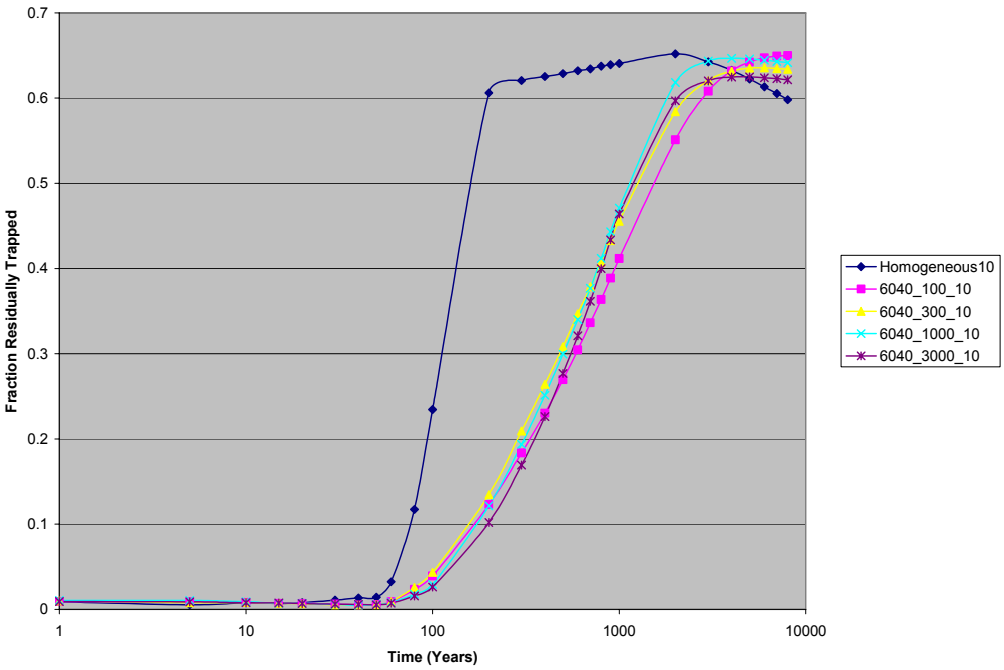

Figure D-146: Fraction of injection CO_2 residually trapped - comparison of the 60:40 sand to shale models, various shale lengths, 10 degree slope

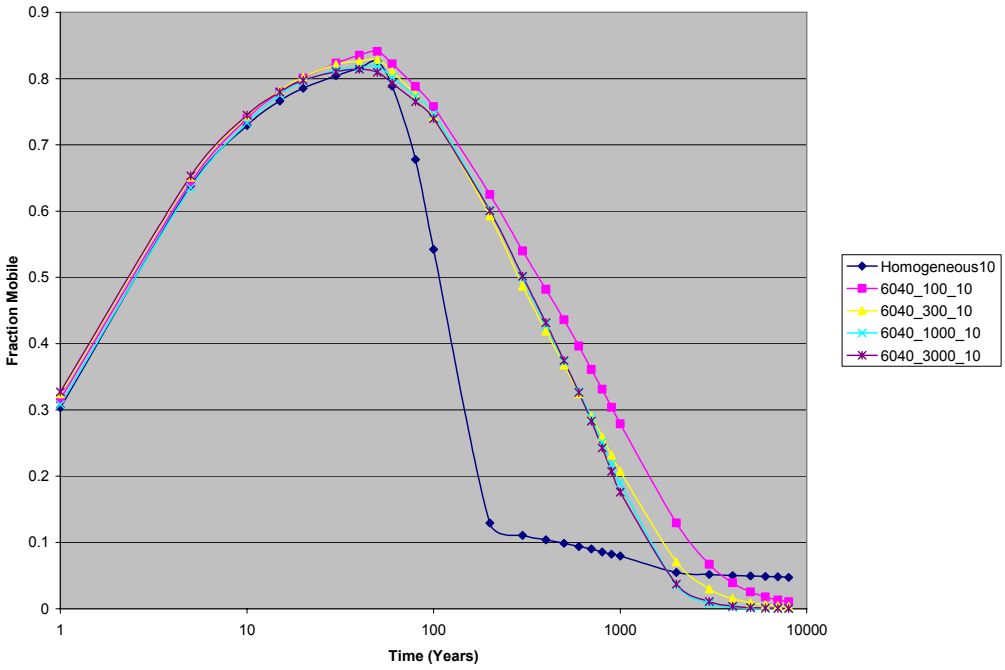

Figure D-147: Fraction of injection CO_2 remaining mobile - comparison of the 60:40 sand to shale models, various shale lengths, 10 degree slope

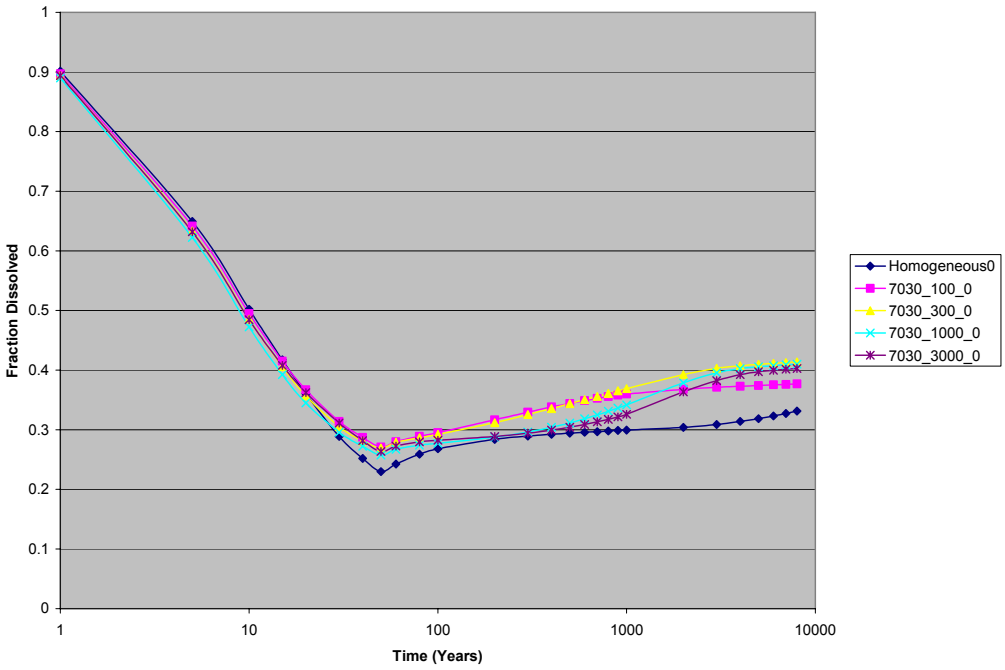

Figure D-148: Fraction of injection CO_2 dissolved - comparison of the 70:30 sand to shale models, various shale lengths, 0 degree slope

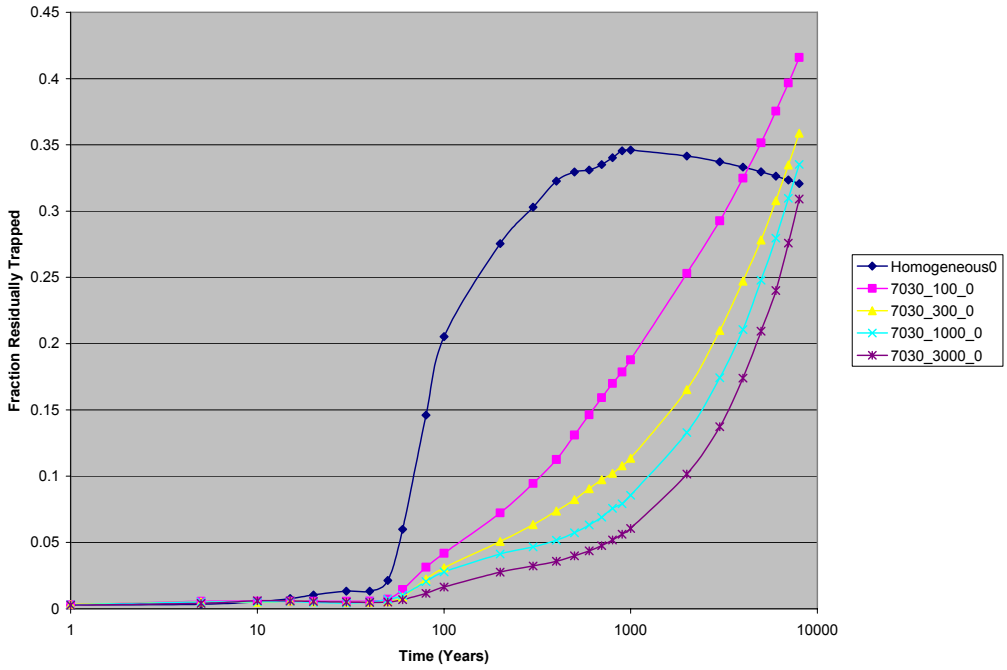

Figure D-149: Fraction of injection CO_2 residually trapped - comparison of the 70:30 sand to shale models, various shale lengths, 0 degree slope

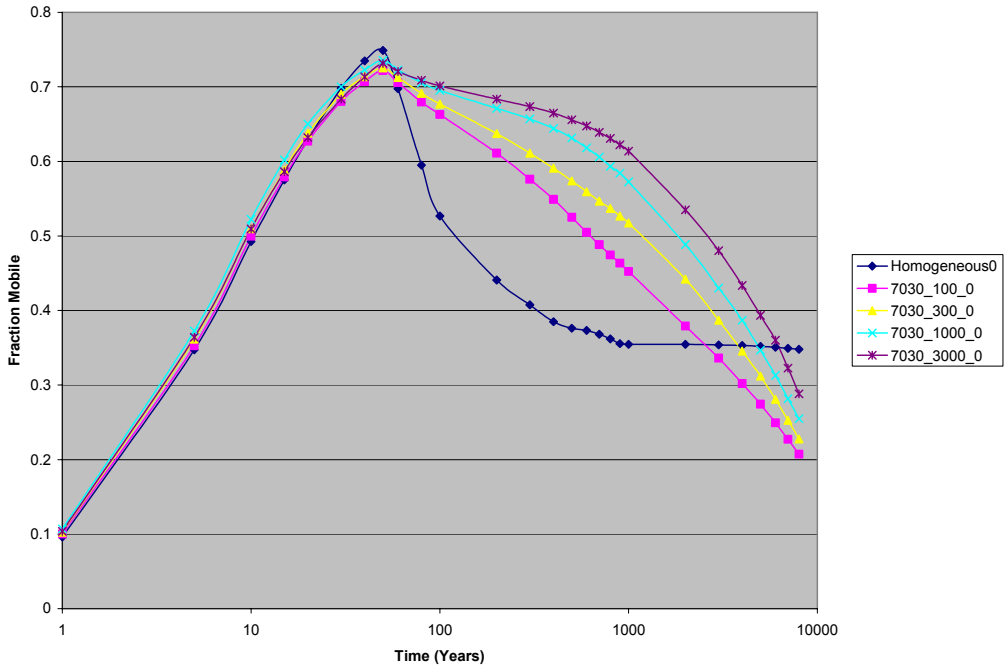

Figure D-150: Fraction of injection CO_2 remaining mobile - comparison of the 70:30 sand to shale models, various shale lengths, 0 degree slope

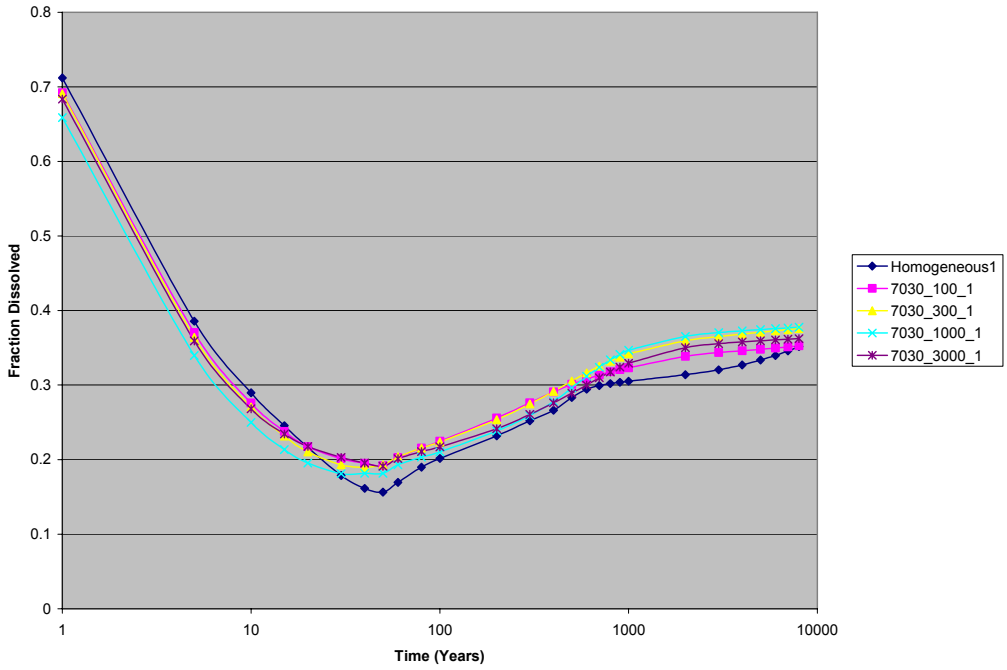

Figure D-151: Fraction of injection CO_2 dissolved - comparison of the 70:30 sand to shale models, various shale lengths, 1 degree slope

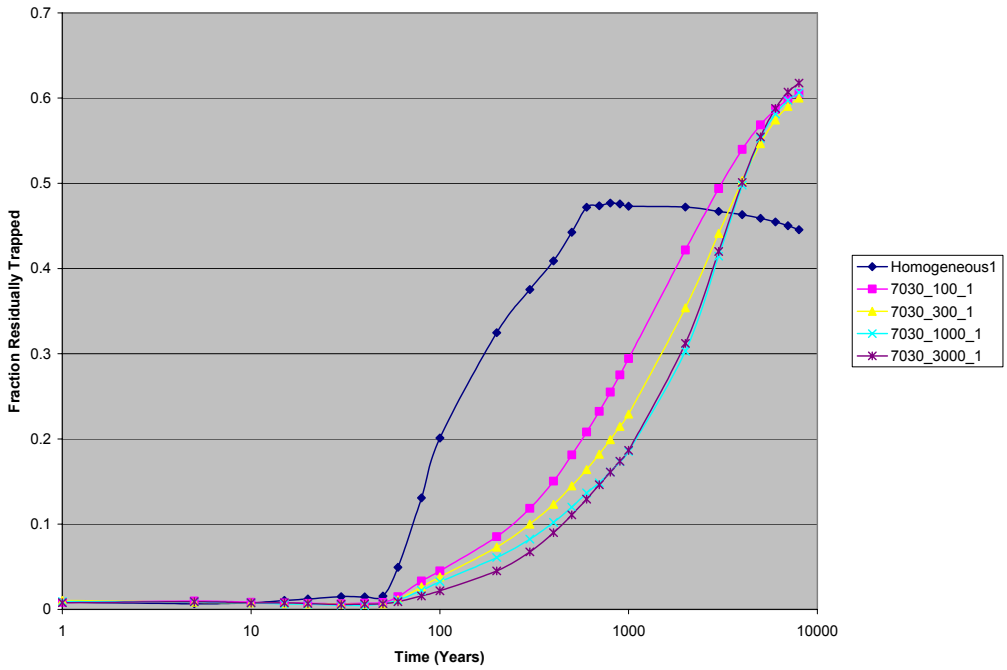

Figure D-152: Fraction of injection CO_2 residually trapped - comparison of the 70:30 sand to shale models, various shale lengths, 1 degree slope

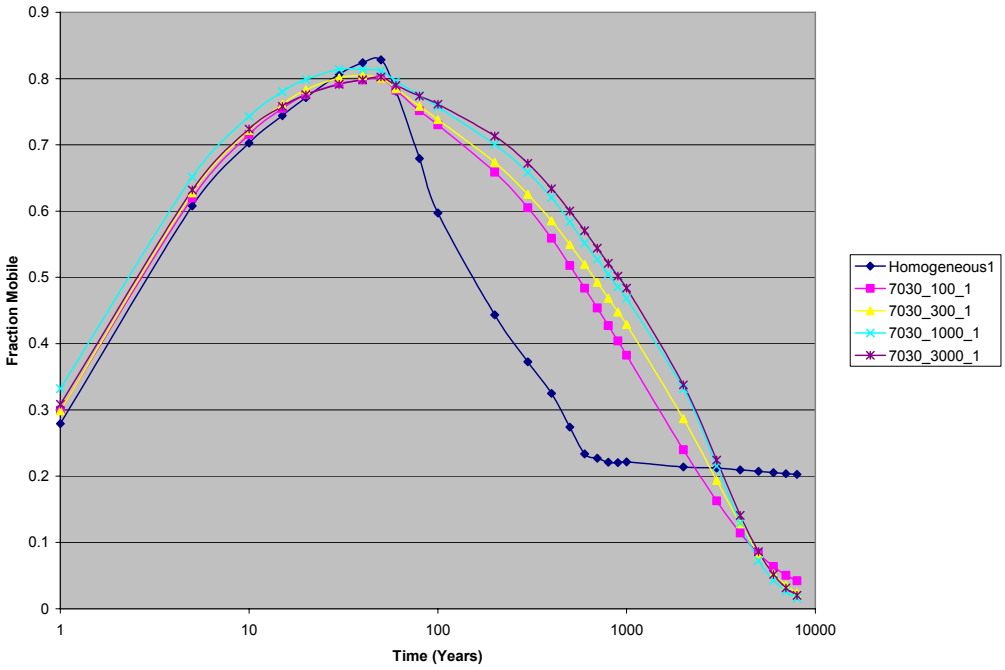

Figure D-153: Fraction of injection CO_2 remaining mobile - comparison of the 70:30 sand to shale models, various shale lengths, 1 degree slope

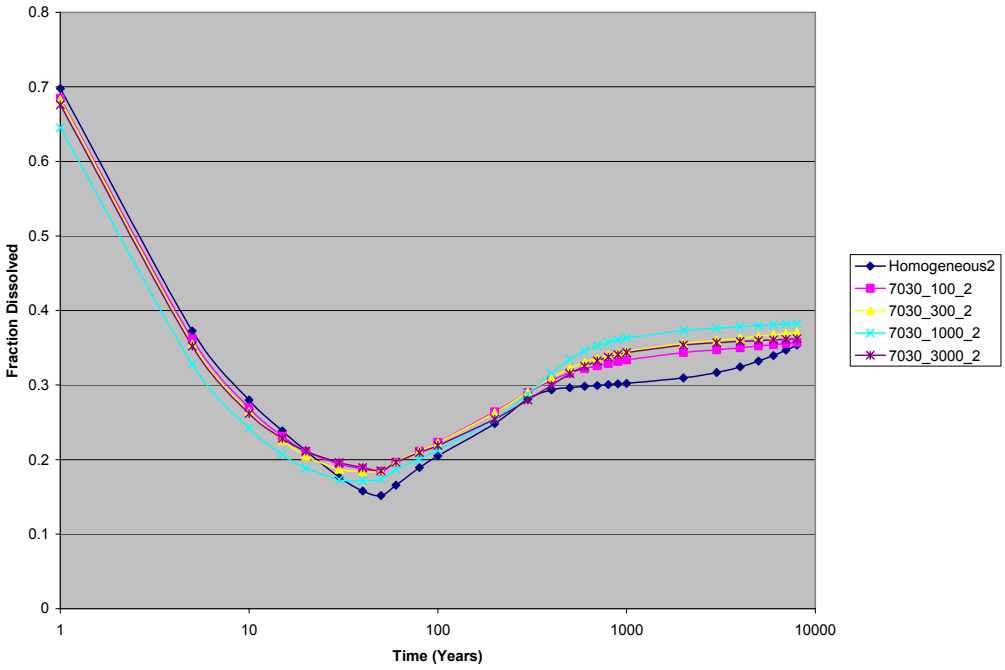

Figure D-154: Fraction of injection CO_2 dissolved - comparison of the 70:30 sand to shale models, various shale lengths, 2 degree slope

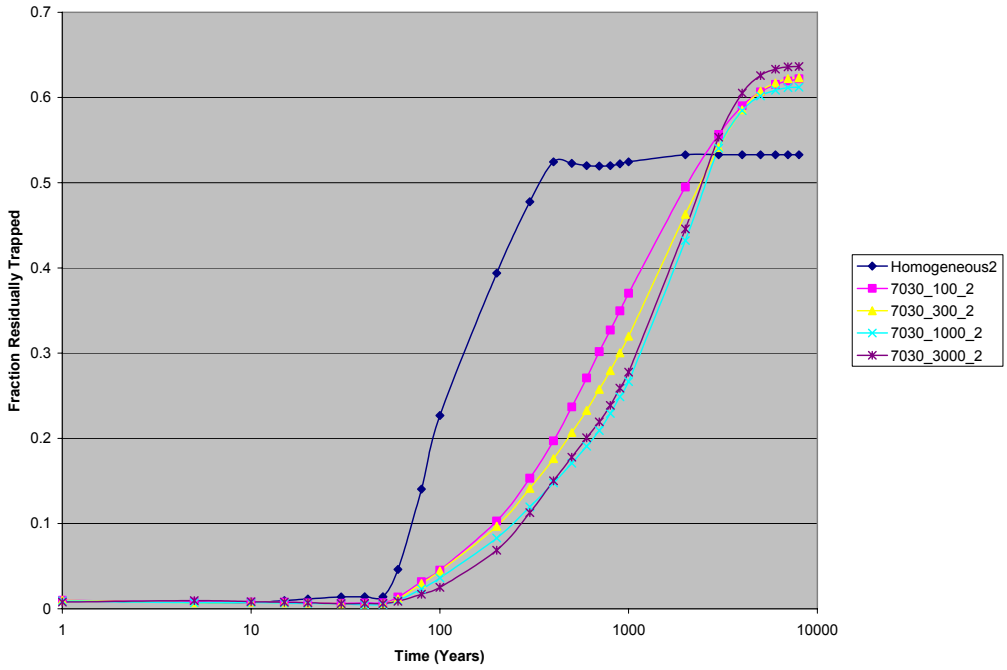

Figure D-155: Fraction of injection CO_2 residually trapped - comparison of the 70:30 sand to shale models, various shale lengths, 2 degree slope

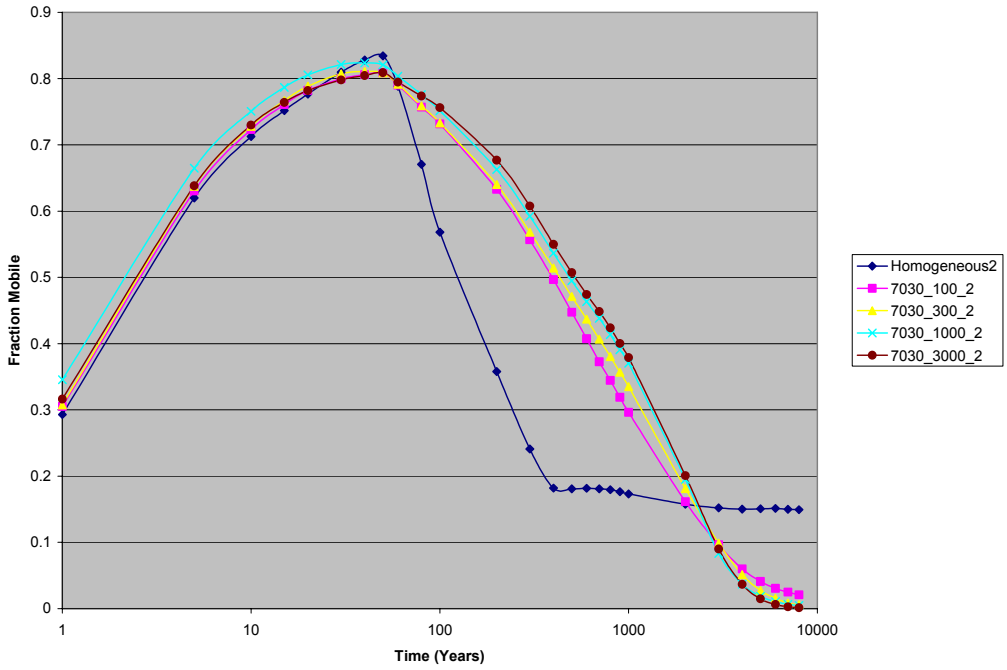

Figure D-156: Fraction of injection CO_2 remaining mobile - comparison of the 70:30 sand to shale models, various shale lengths, 2 degree slope

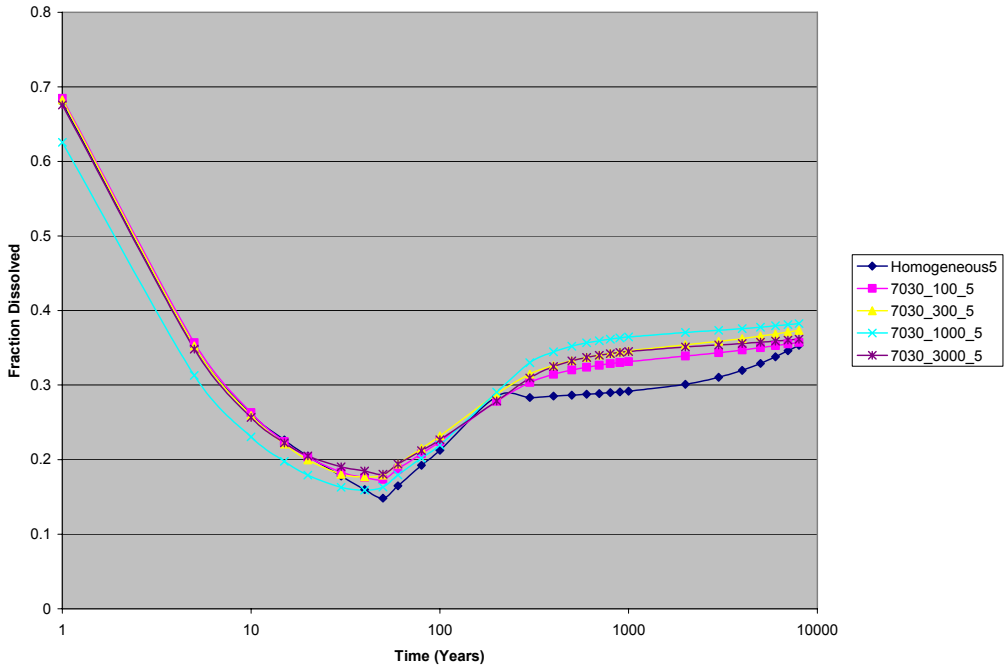

Figure D-157: Fraction of injection CO_2 dissolved - comparison of the 70:30 sand to shale models, various shale lengths, 5 degree slope

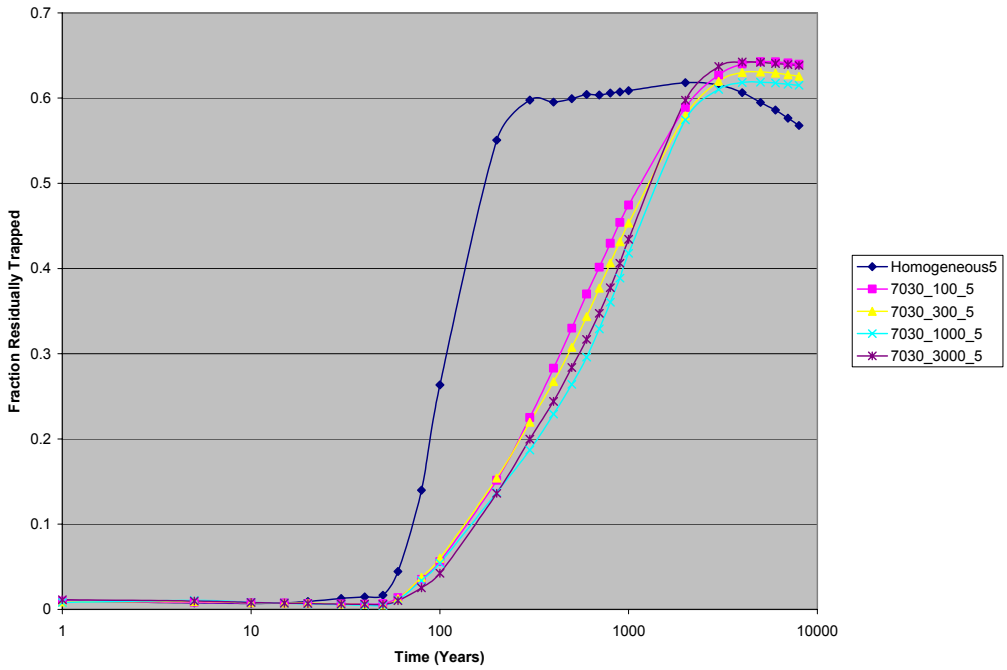

Figure D-158: Fraction of injection CO_2 residually trapped - comparison of the 70:30 sand to shale models, various shale lengths, 5 degree slope

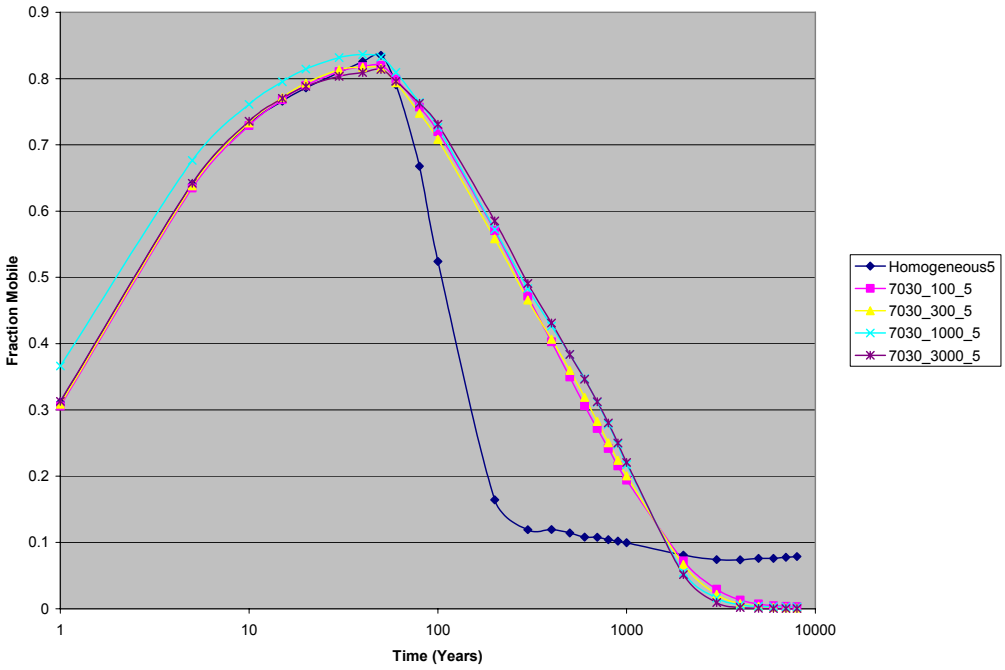

Figure D-159: Fraction of injection CO_2 remaining mobile - comparison of the 70:30 sand to shale models, various shale lengths, 5 degree slope

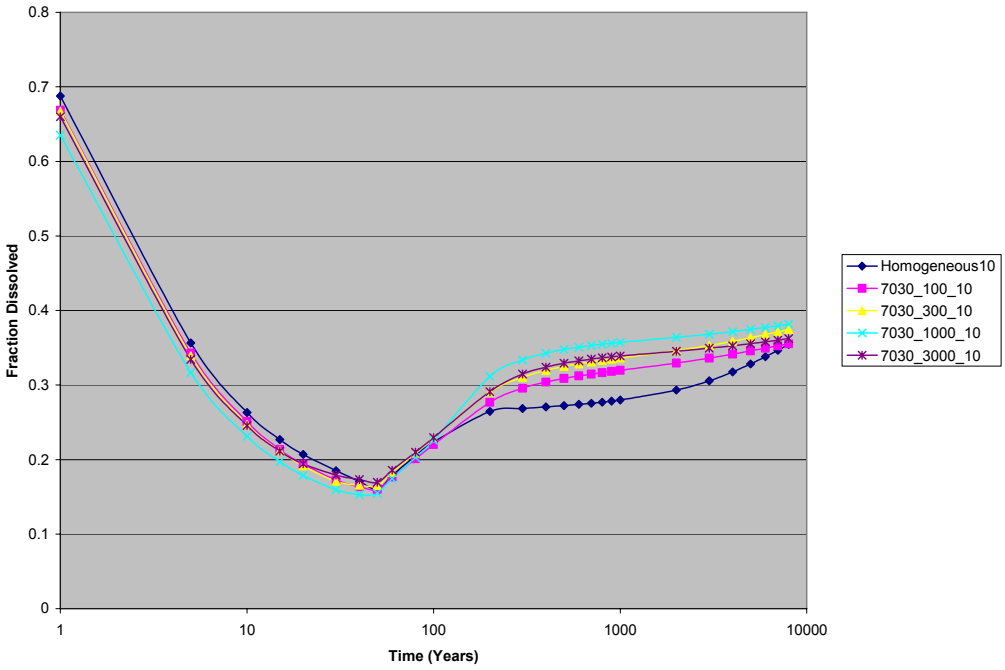

Figure D-160: Fraction of injection CO_2 dissolved - comparison of the 70:30 sand to shale models, various shale lengths, 10 degree slope

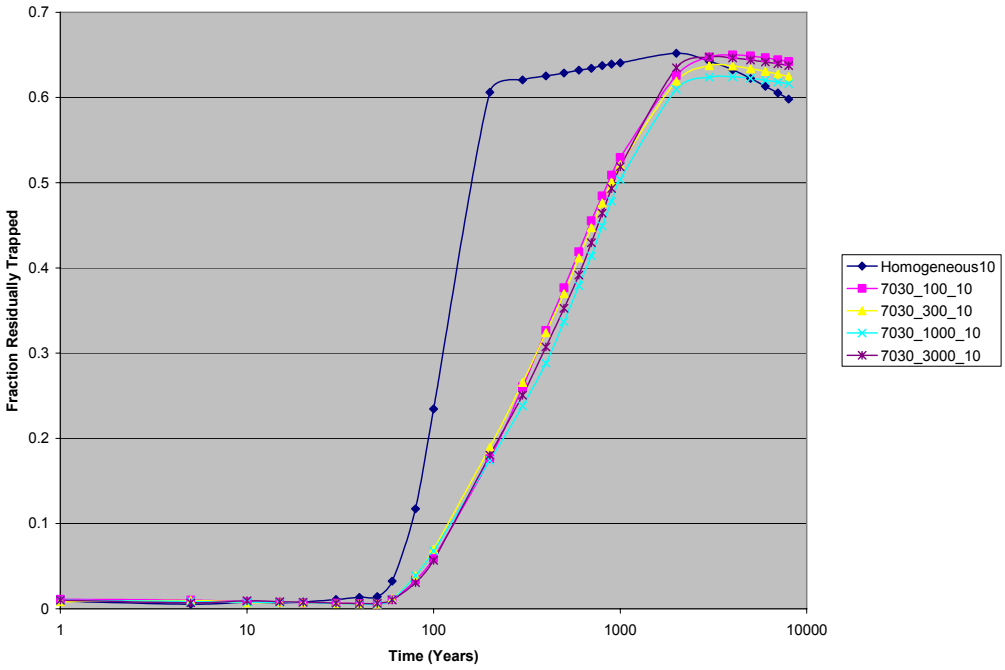

Figure D-161: Fraction of injection CO_2 residually trapped - comparison of the 70:30 sand to shale models, various shale lengths, 10 degree slope

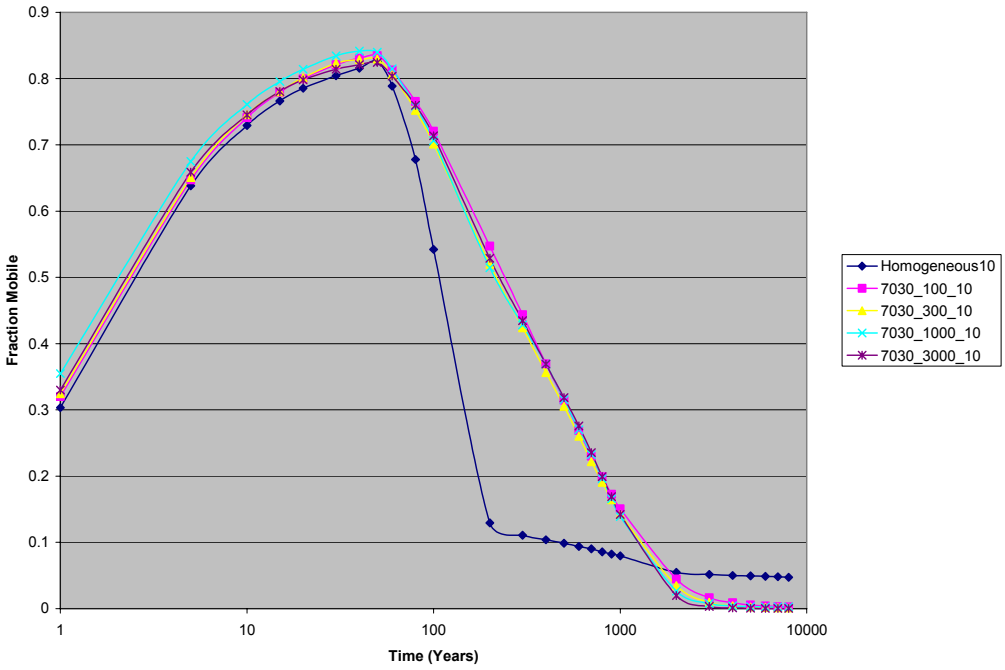

Figure D-162: Fraction of injection CO_2 remaining mobile - comparison of the 70:30 sand to shale models, various shale lengths, 10 degree slope

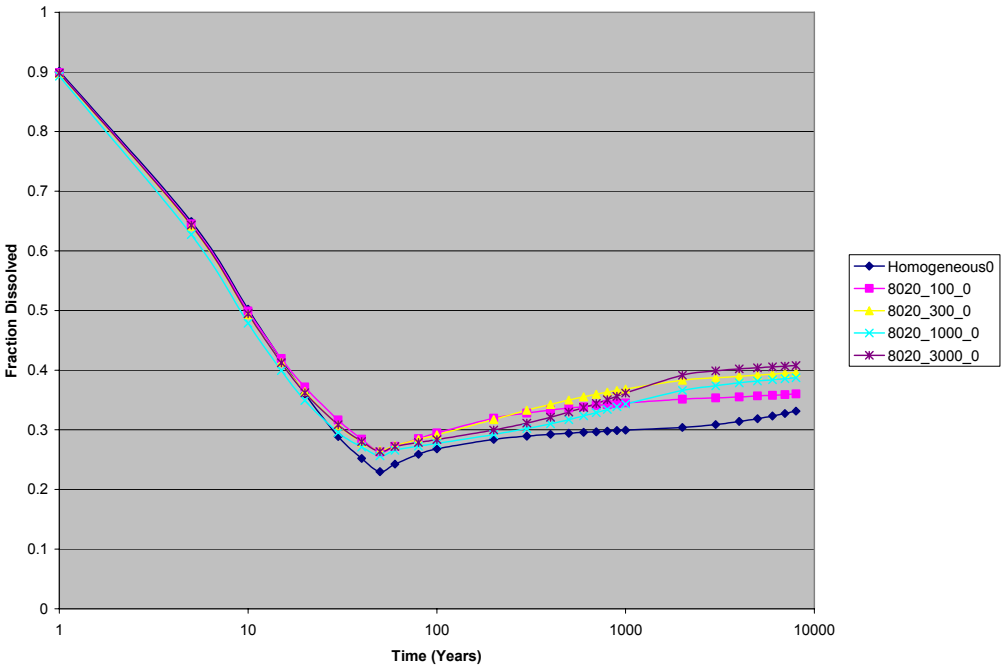

Figure D-163: Fraction of injection CO_2 dissolved - comparison of the 80:20 sand to shale models, various shale lengths, 0 degree slope

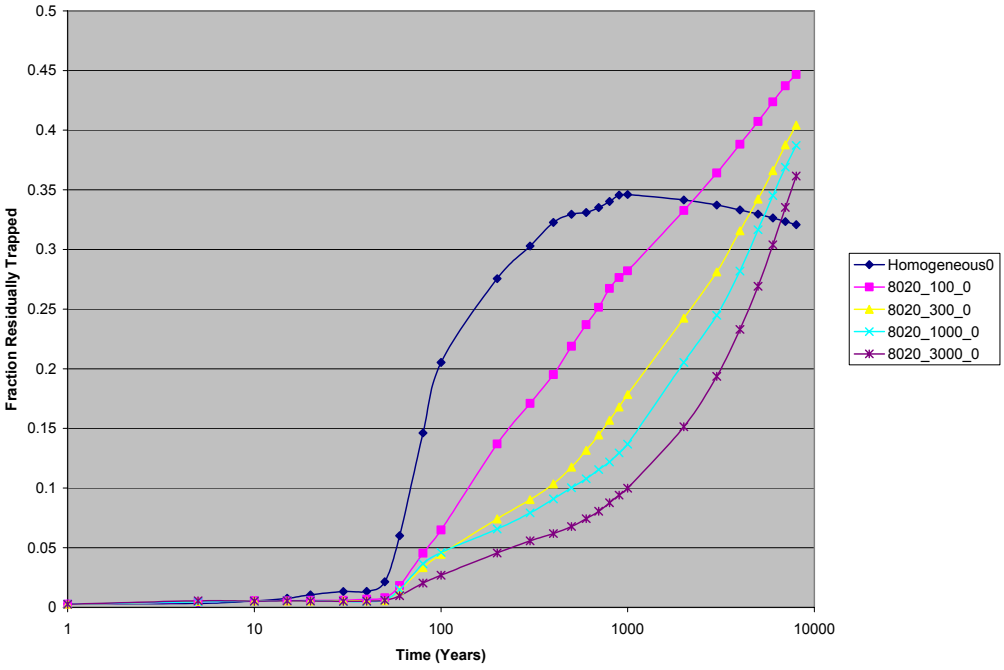

Figure D-164: Fraction of injection CO_2 residually trapped - comparison of the 80:20 sand to shale models, various shale lengths, 0 degree slope

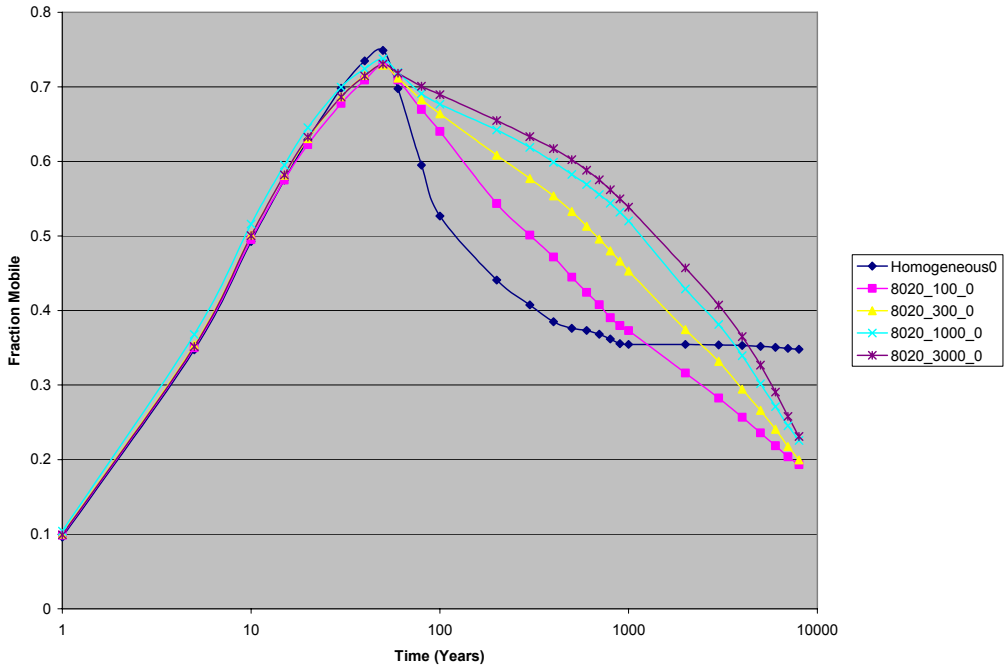

Figure D-165: Fraction of injection CO_2 remaining mobile - comparison of the 80:20 sand to shale models, various shale lengths, 0 degree slope

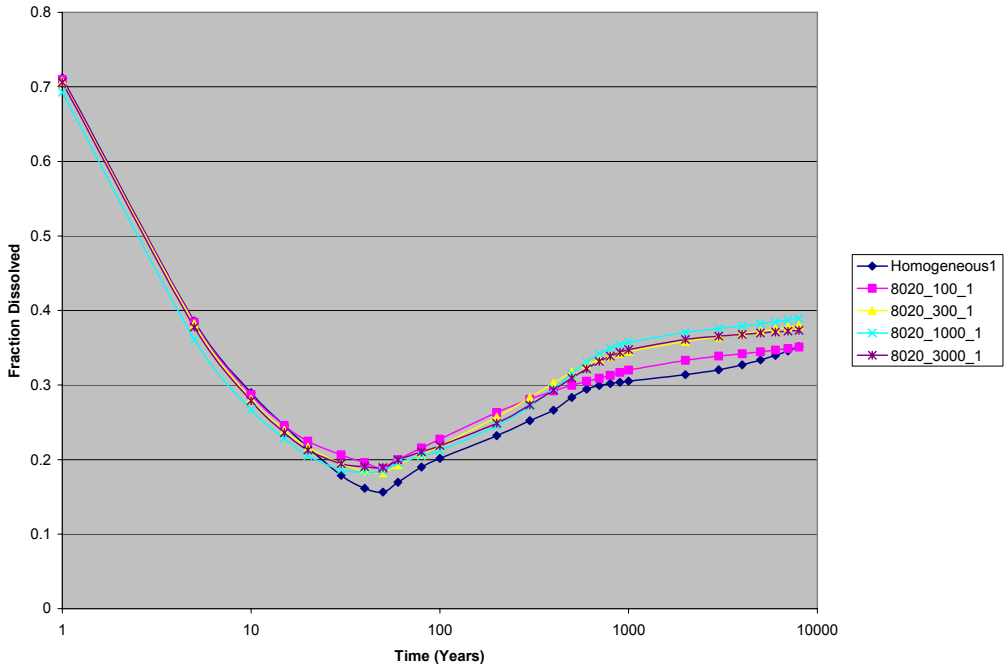

Figure D-166: Fraction of injection CO_2 dissolved - comparison of the 80:20 sand to shale models, various shale lengths, 1 degree slope

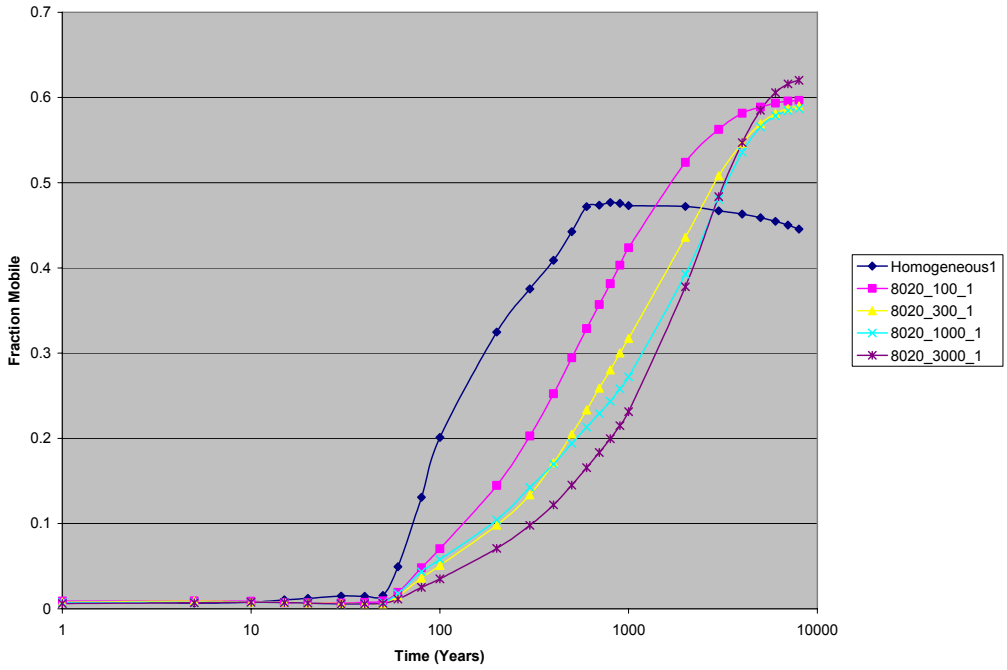

Figure D-167: Fraction of injection CO_2 residually trapped - comparison of the 80:20 sand to shale models, various shale lengths, 1 degree slope

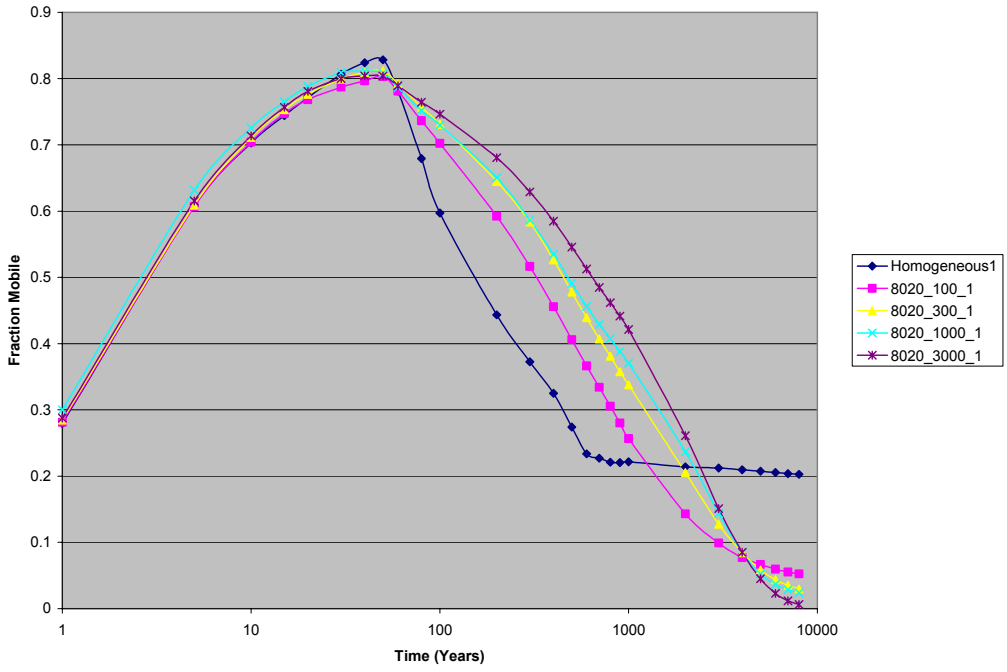

Figure D-168: Fraction of injection CO_2 remaining mobile - comparison of the 80:20 sand to shale models, various shale lengths, 1 degree slope

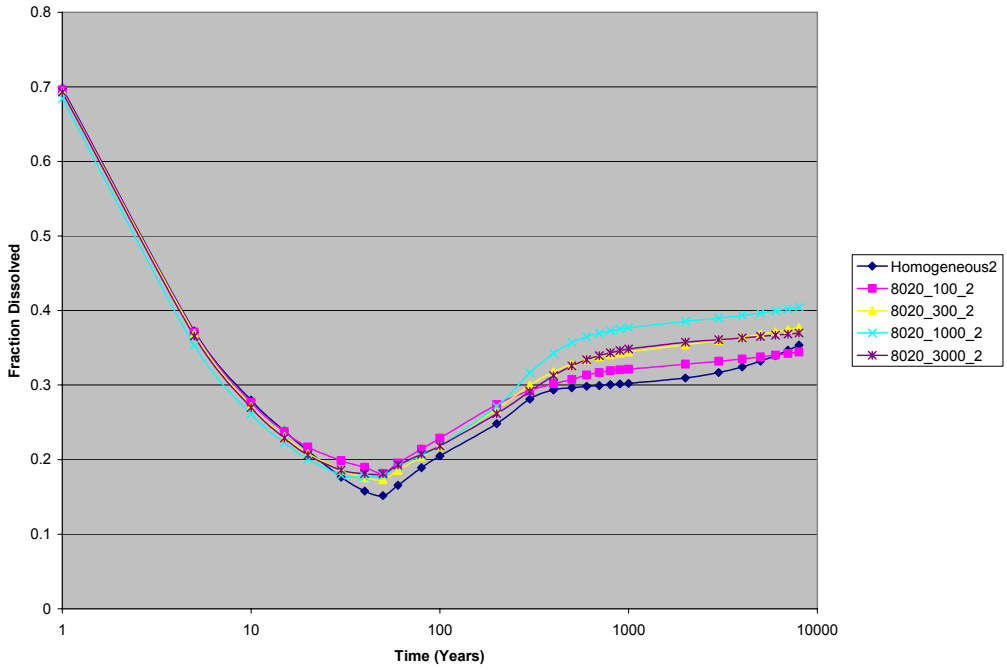

Figure D-169: Fraction of injection CO_2 dissolved - comparison of the 80:20 sand to shale models, various shale lengths, 2 degree slope

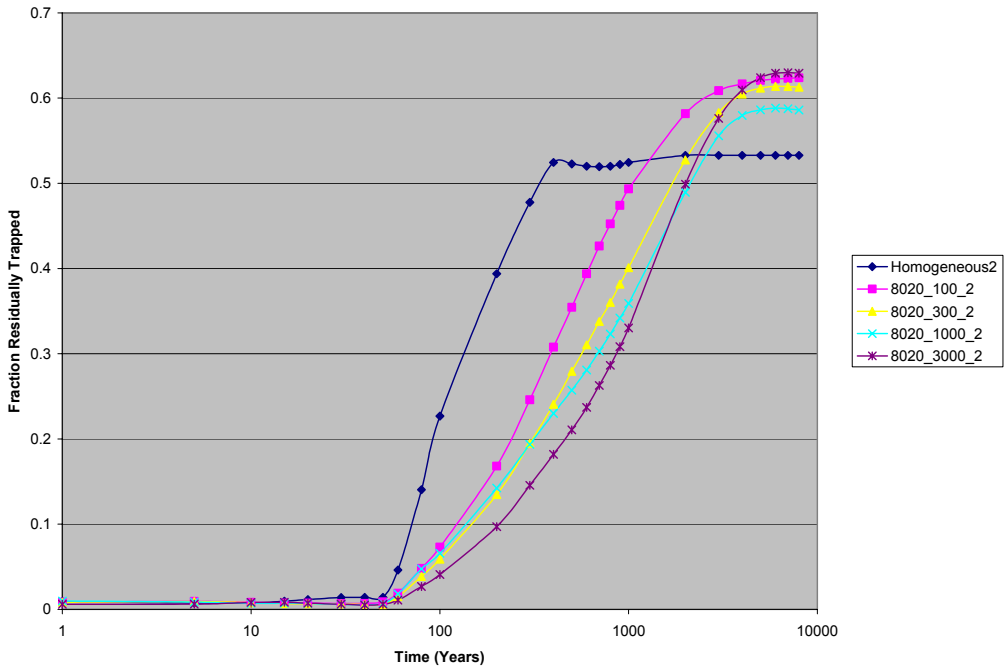

Figure D-170: Fraction of injection CO_2 residually trapped - comparison of the 80:20 sand to shale models, various shale lengths, 2 degree slope

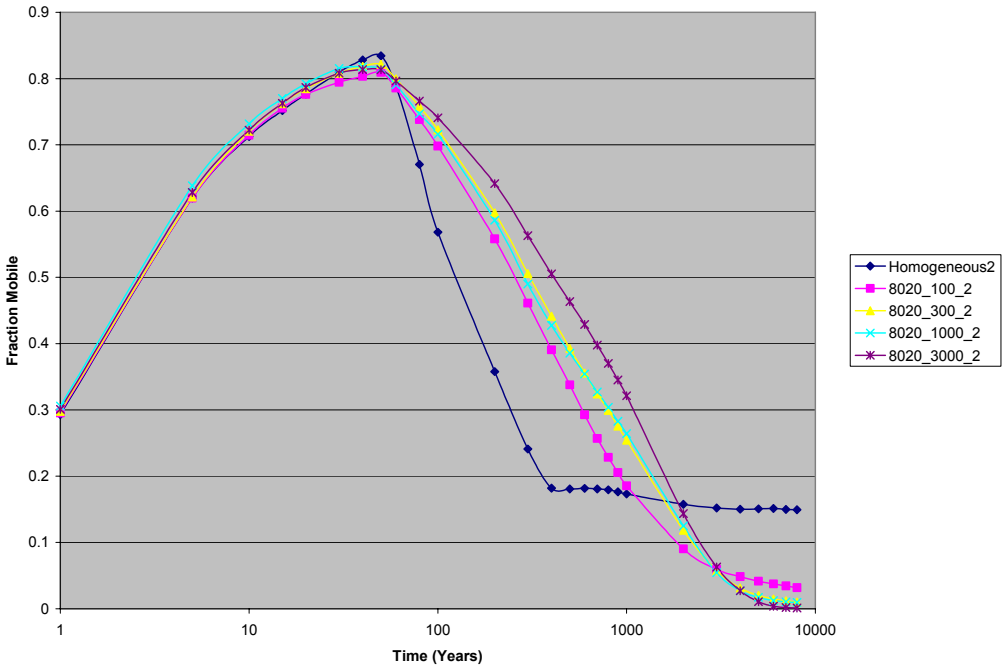

Figure D-171: Fraction of injection CO_2 remaining mobile - comparison of the 80:20 sand to shale models, various shale lengths, 2 degree slope

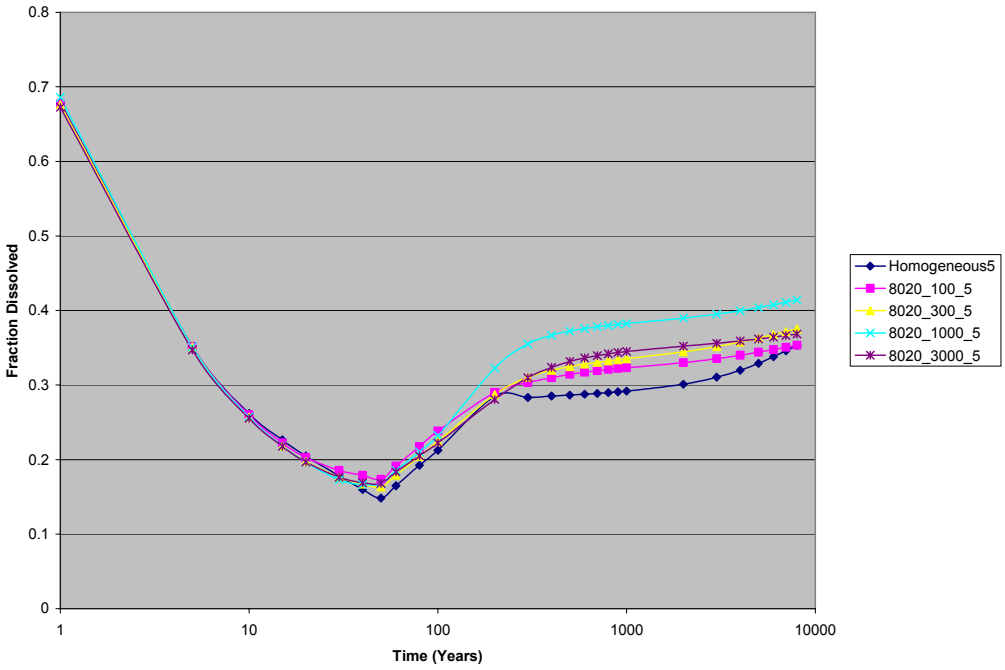

Figure D-172: Fraction of injection CO_2 dissolved - comparison of the 80:20 sand to shale models, various shale lengths, 5 degree slope

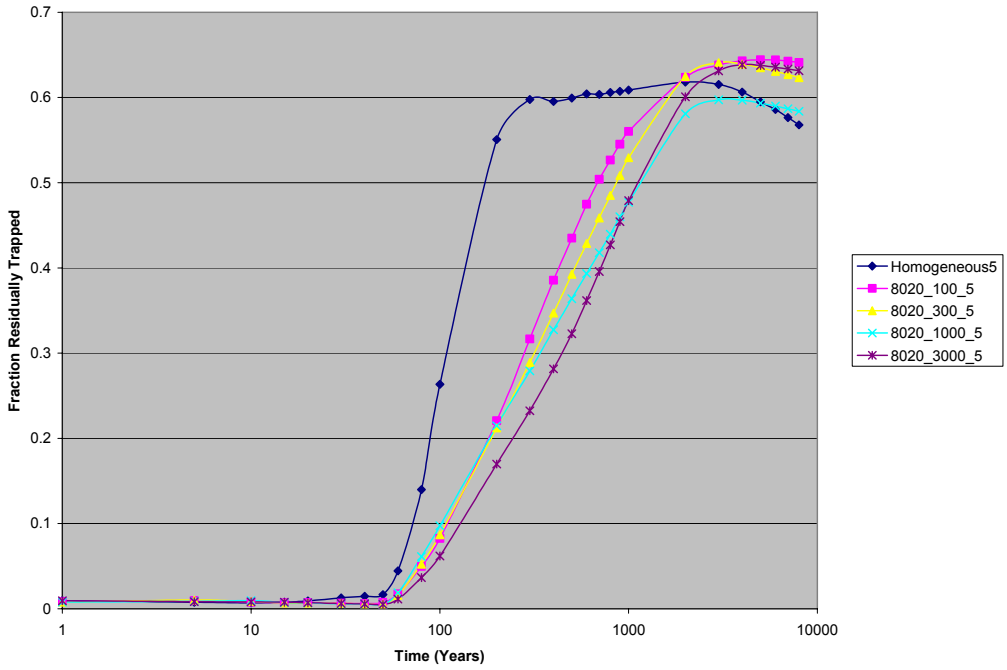

Figure D-173: Fraction of injection CO_2 residually trapped - comparison of the 80:20 sand to shale models, various shale lengths, 5 degree slope

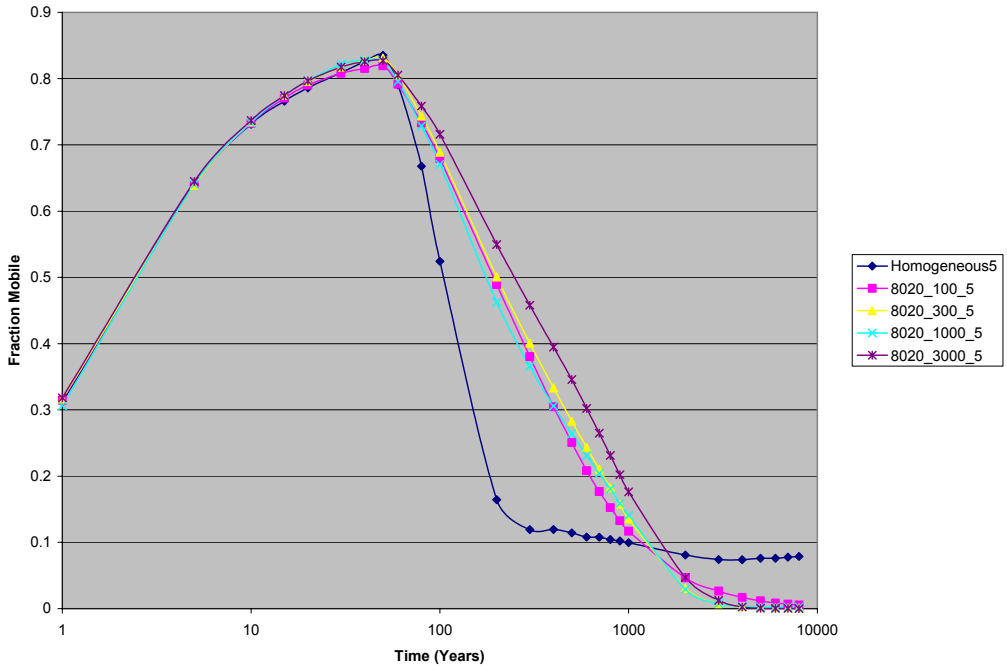

Figure D-174: Fraction of injection CO_2 remaining mobile - comparison of the 80:20 sand to shale models, various shale lengths, 5 degree slope

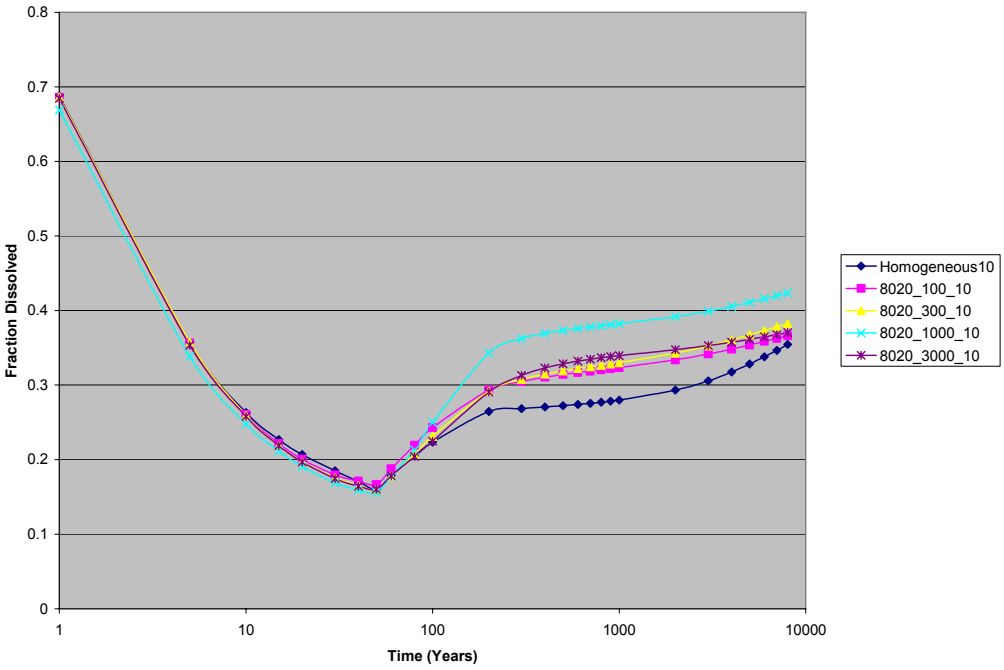

Figure D-175: Fraction of injection CO_2 dissolved - comparison of the 80:20 sand to shale models, various shale lengths, 10 degree slope

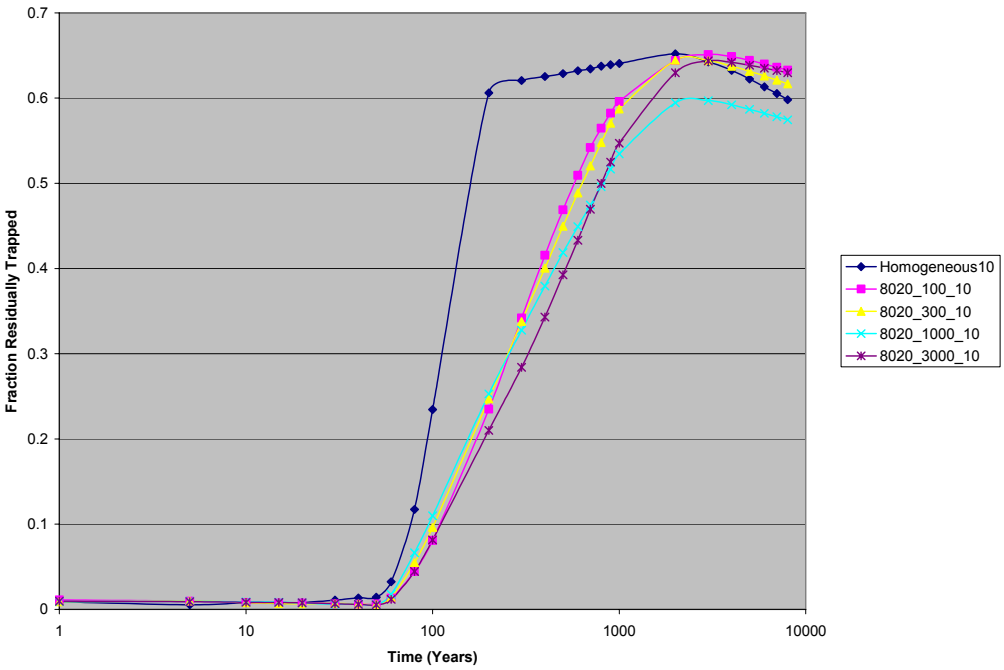

Figure D-176: Fraction of injection CO_2 residually trapped - comparison of the 80:20 sand to shale models, various shale lengths, 10 degree slope

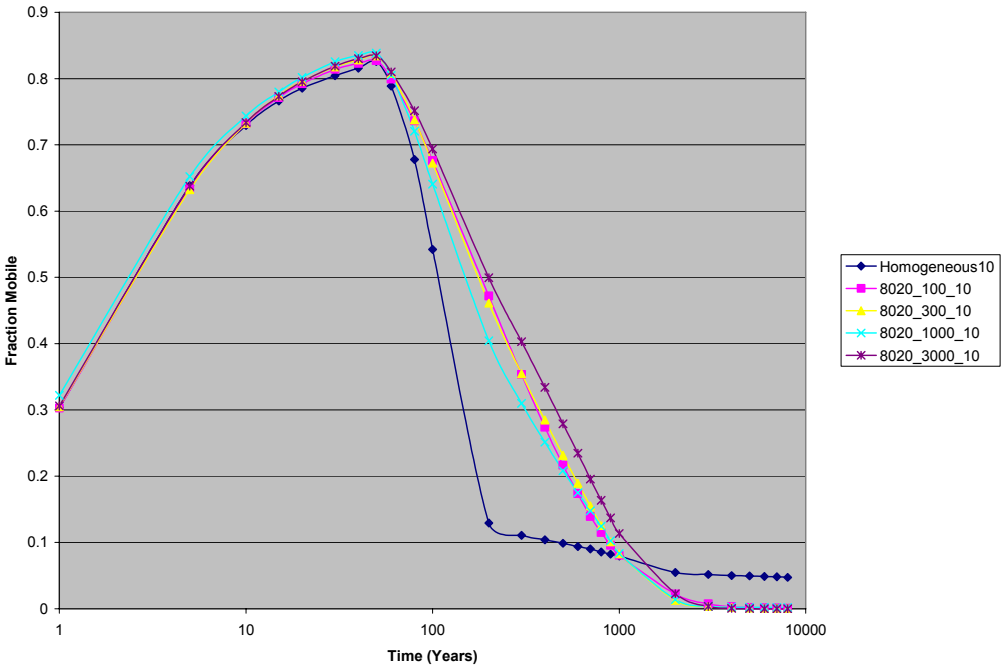

Figure D-177: Fraction of injection CO_2 remaining mobile - comparison of the 80:20 sand to shale models, various shale lengths, 10 degree slope

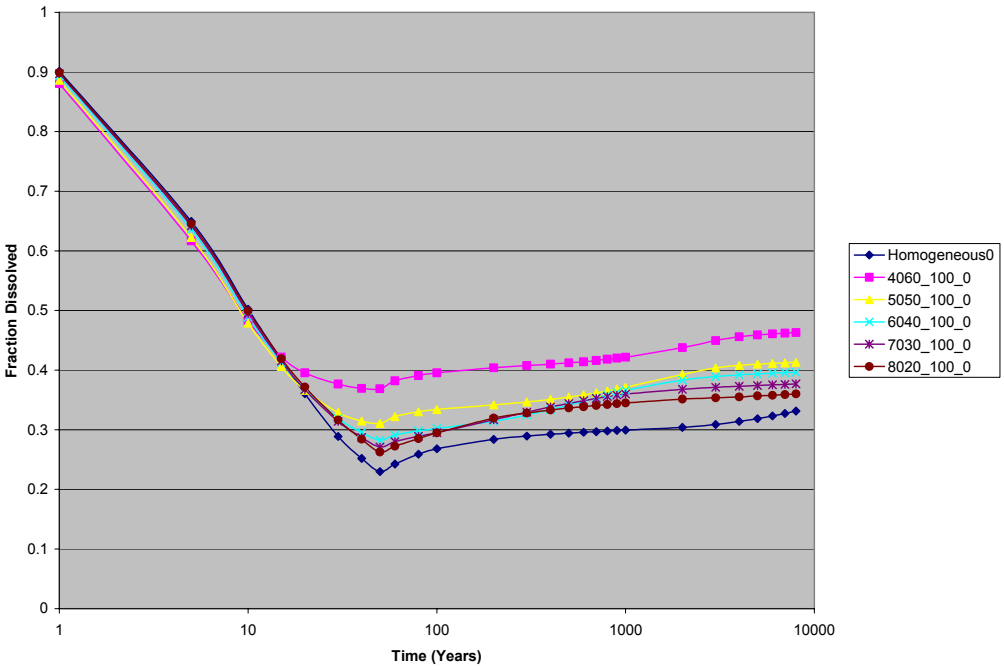

Figure D-178: Fraction of injection CO_2 dissolved - comparison of the 100 m shale length models, various sand:shale ratios, 0 degree slope

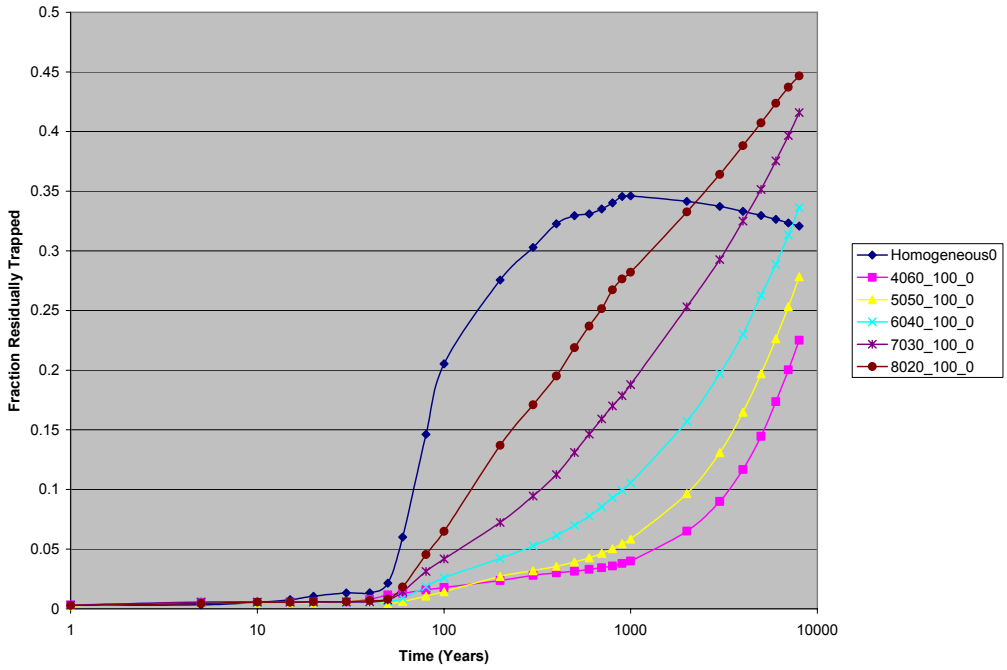

Figure D-179: Fraction of injection CO_2 residually trapped - comparison of the 100 m shale length models, various sand:shale ratios, 0 degree slope

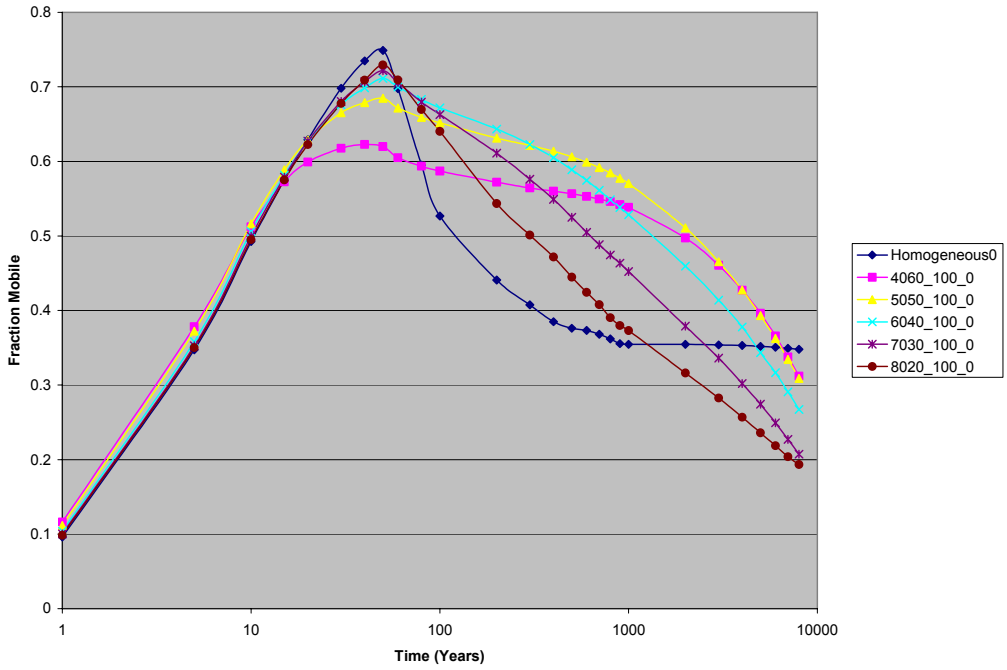

Figure D-180: Fraction of injection CO_2 remaining mobile - comparison of the 100 m shale length models, various sand:shale lengths, 0 degree slope

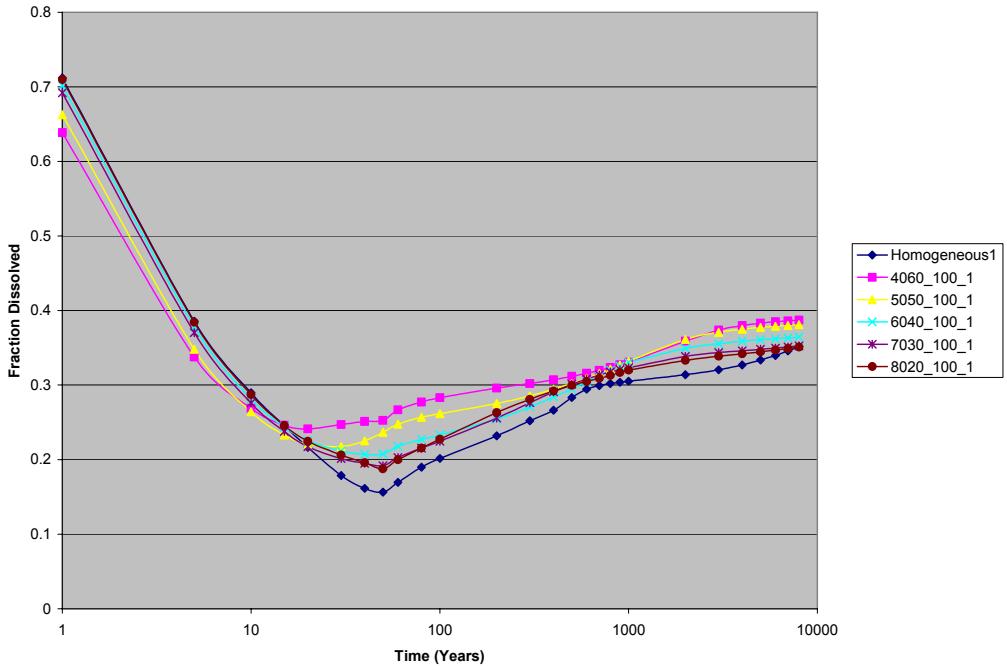

Figure D-181: Fraction of injection CO_2 dissolved - comparison of the 100 m shale length models, various sand:shale ratios, 1 degree slope

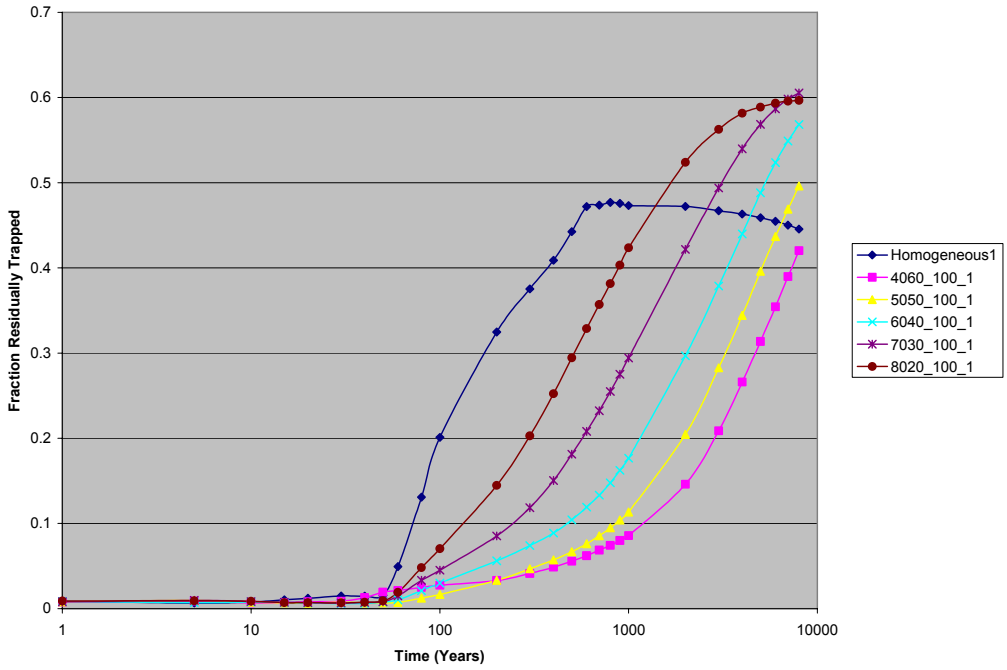

Figure D-182: Fraction of injection CO_2 residually trapped - comparison of the 100 m shale length models, various sand:shale ratios, 1 degree slope

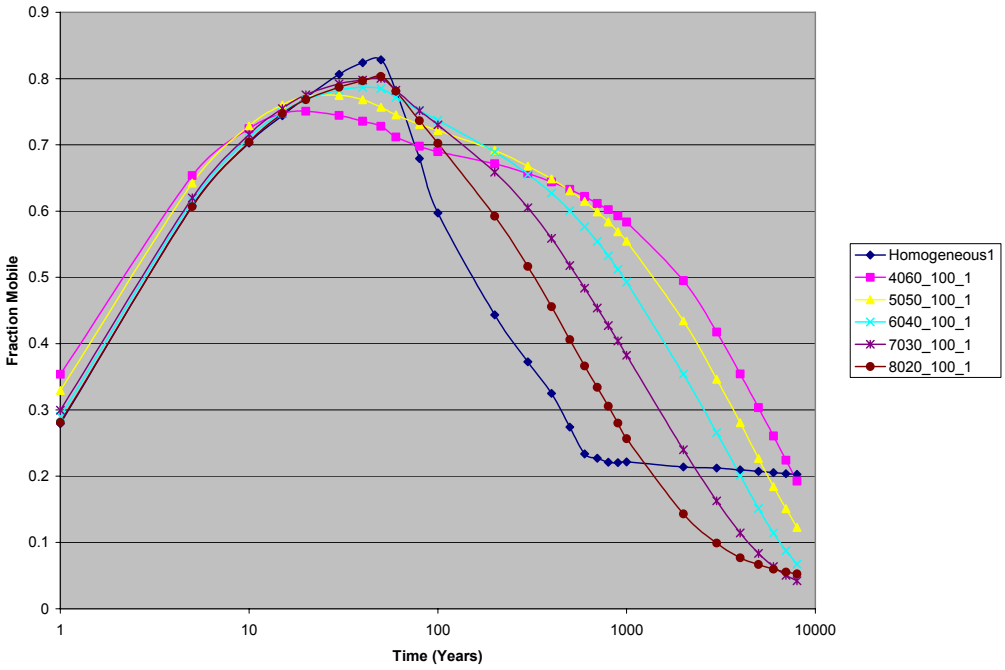

Figure D-183: Fraction of injection CO_2 remaining mobile - comparison of the 100 m shale length models, various sand:shale lengths, 1 degree slope

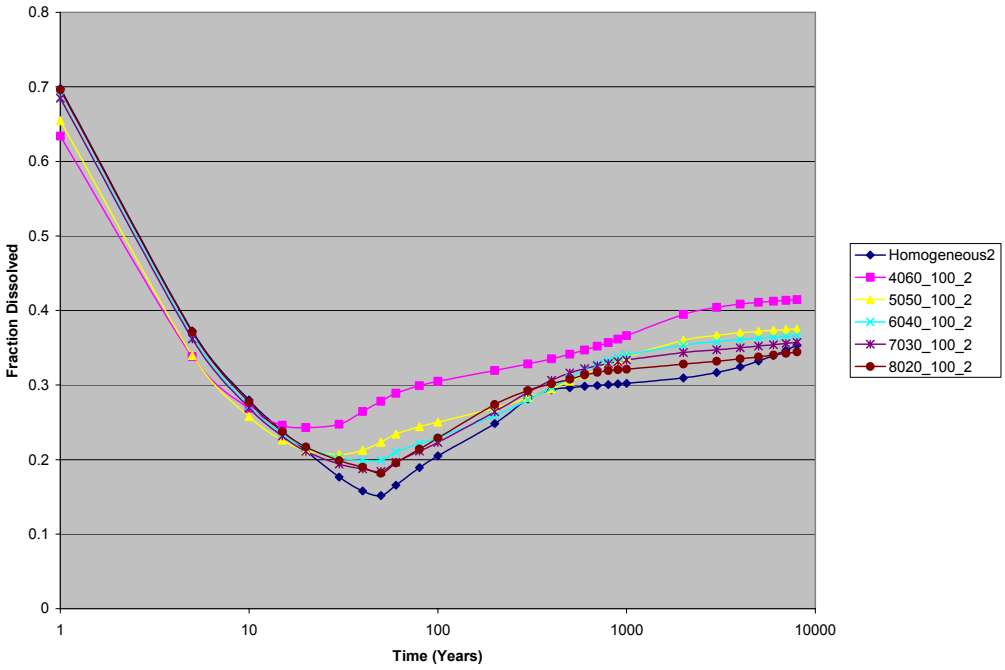

Figure D-184: Fraction of injection CO_2 dissolved - comparison of the 100 m shale length models, various sand:shale ratios, 2 degree slope

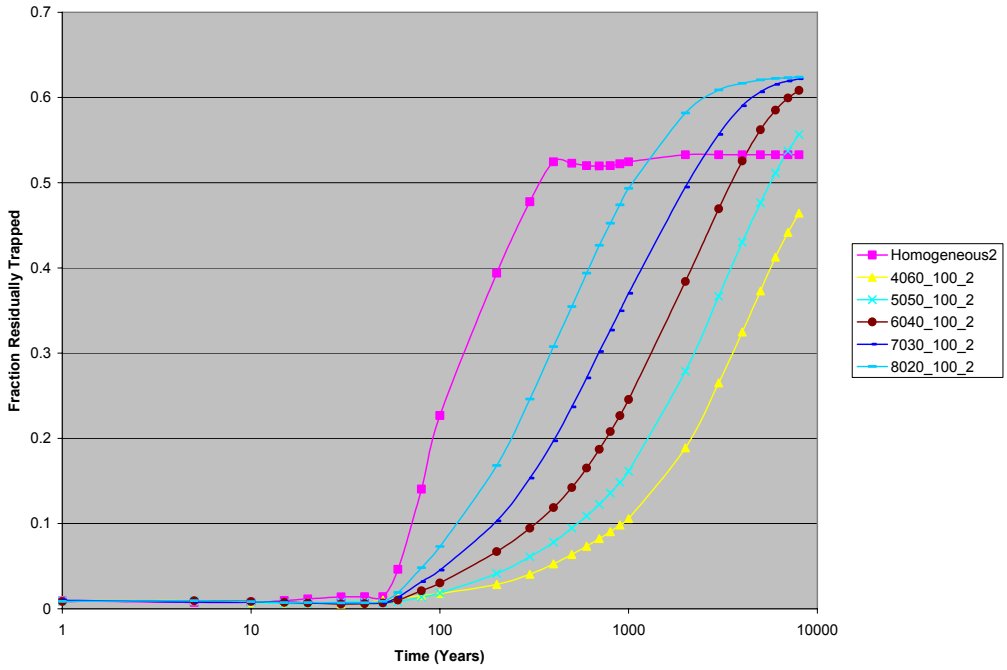

Figure D-185: Fraction of injection CO_2 residually trapped - comparison of the 100 m shale length models, various sand:shale ratios, 2 degree slope

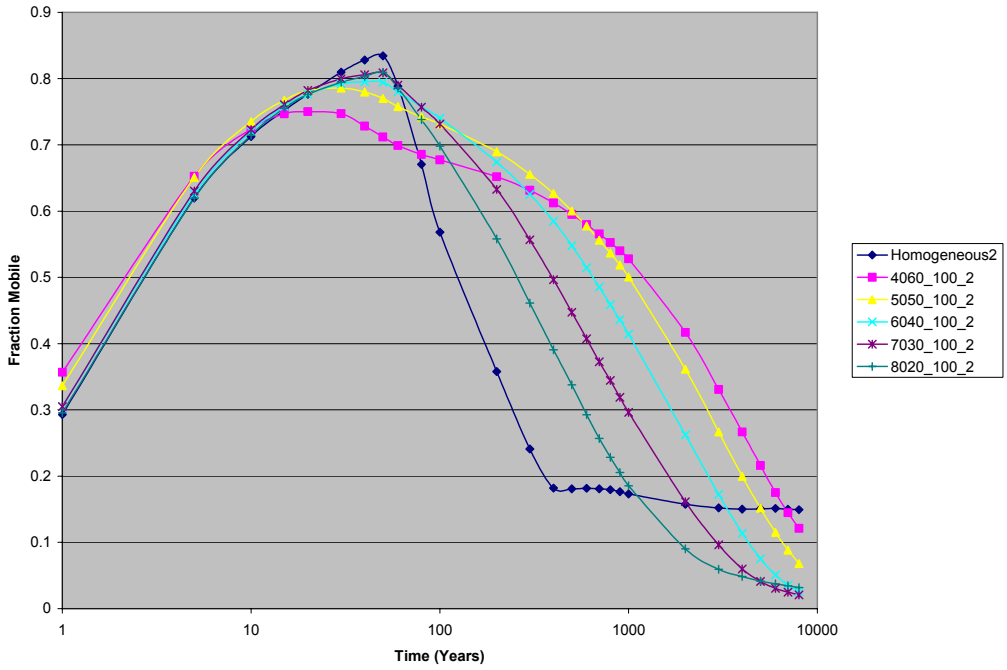

Figure D-186: Fraction of injection CO_2 remaining mobile - comparison of the 100 m shale length models, various sand:shale lengths, 2 degree slope

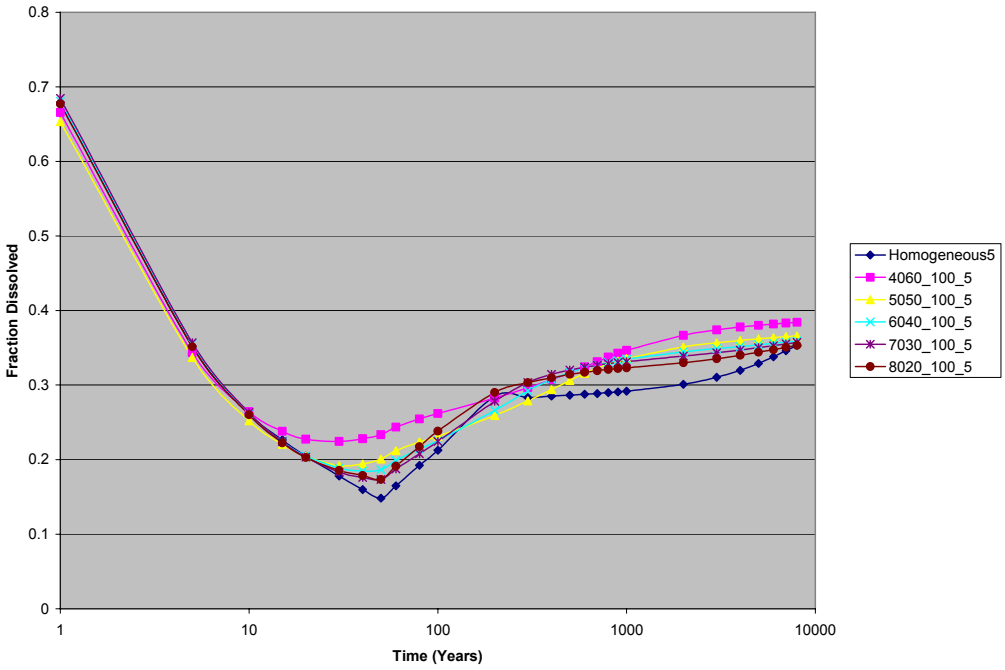

Figure D-187: Fraction of injection CO_2 dissolved - comparison of the 100 m shale length models, various sand:shale ratios, 5 degree slope

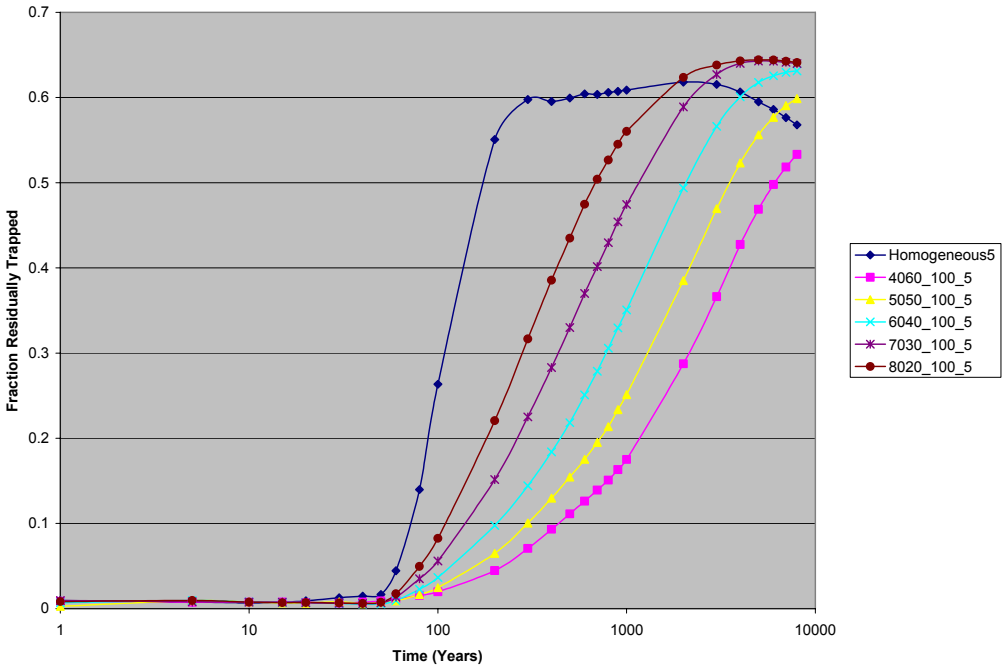

Figure D-188: Fraction of injection CO_2 residually trapped - comparison of the 100 m shale length models, various sand:shale ratios, 5 degree slope

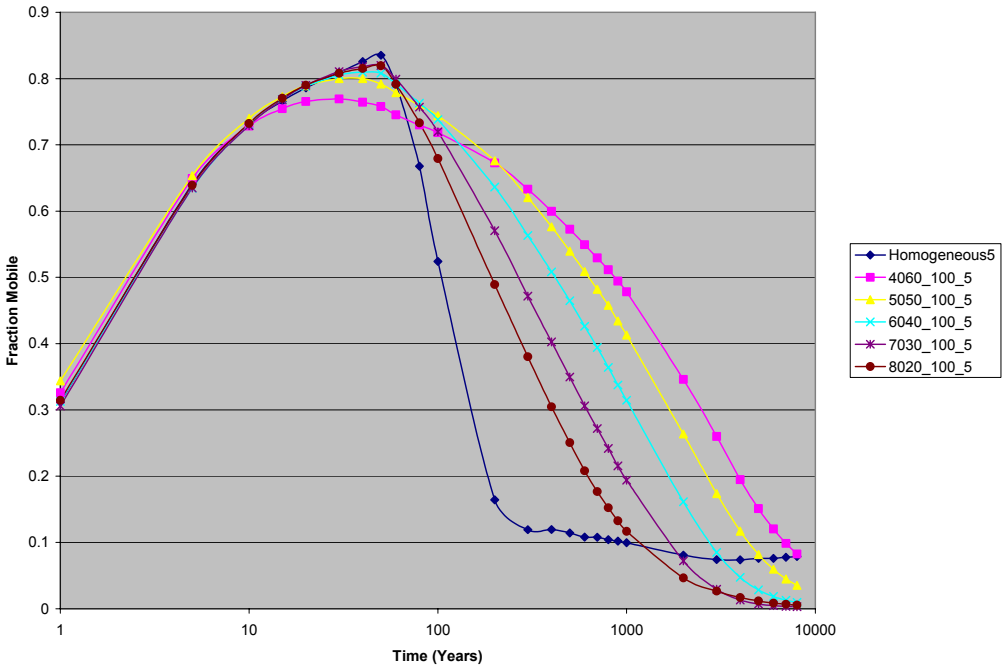

Figure D-189: Fraction of injection CO_2 remaining mobile - comparison of the 100 m shale length models, various sand:shale lengths, 5 degree slope

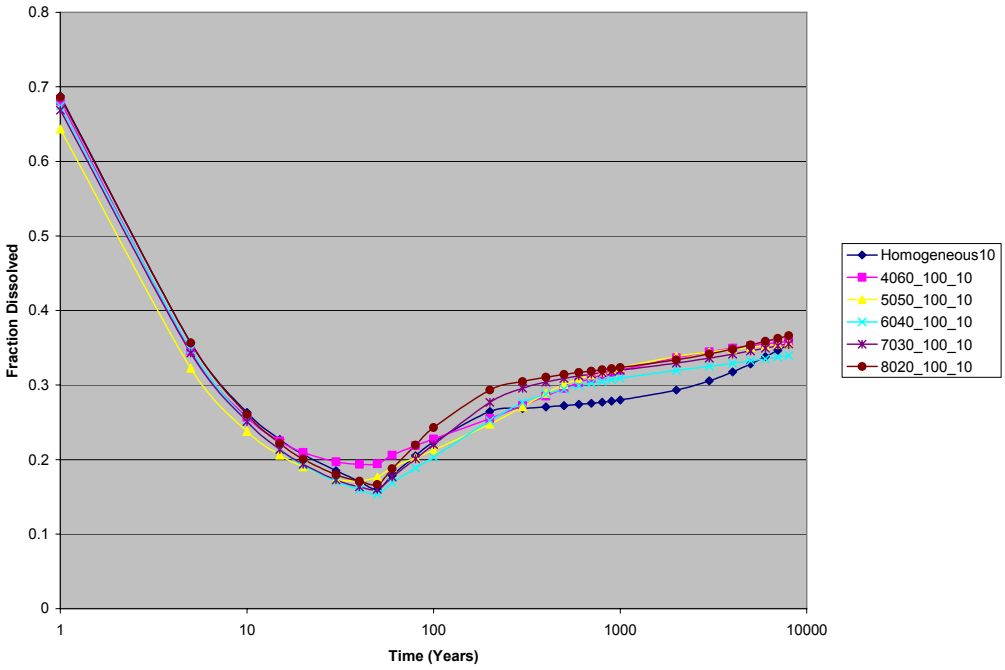

Figure D-190: Fraction of injection CO_2 dissolved - comparison of the 100 m shale length models, various sand:shale ratios, 10 degree slope

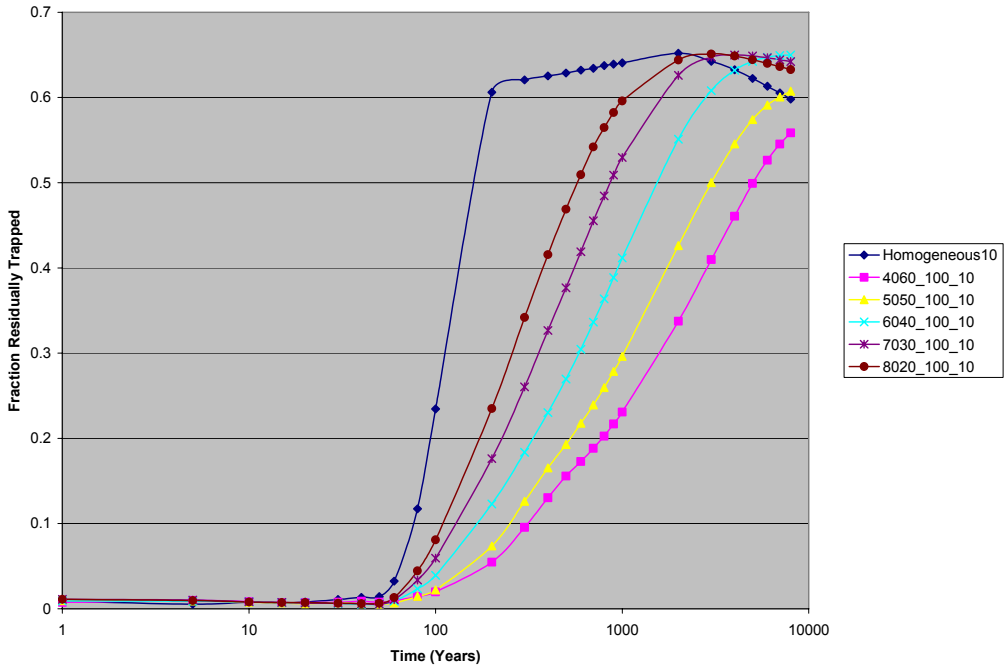

Figure D-191: Fraction of injection CO_2 residually trapped - comparison of the 100 m shale length models, various sand:shale ratios, 10 degree slope

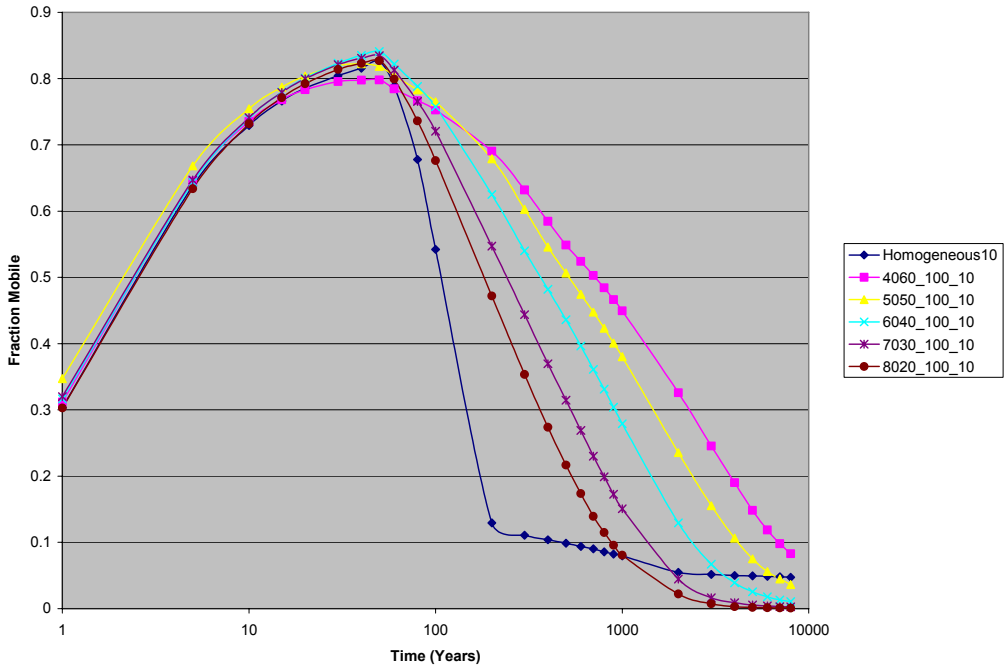

Figure D-192: Fraction of injection CO_2 remaining mobile - comparison of the 100 m shale length models, various sand:shale lengths, 10 degree slope

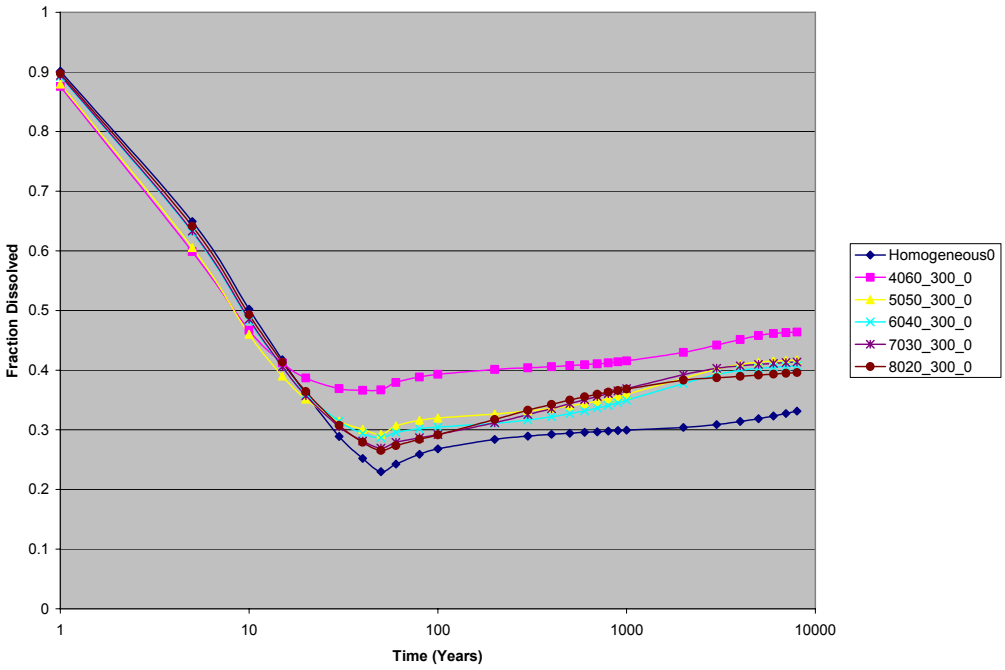

Figure D-193: Fraction of injection CO_2 dissolved - comparison of the 300 m shale length models, various sand:shale ratios, 0 degree slope

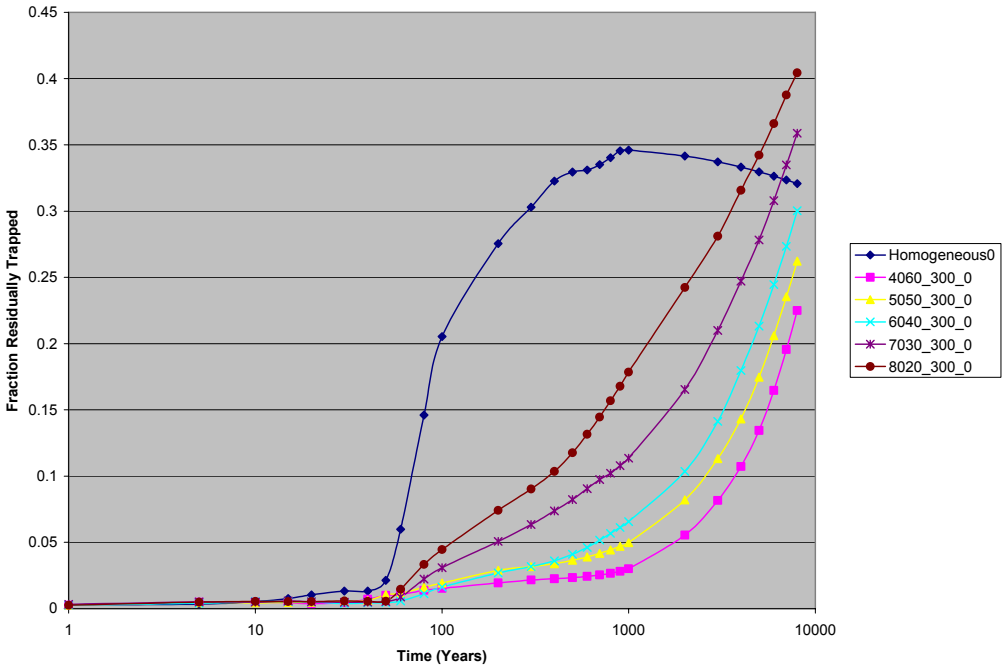

Figure D-194: Fraction of injection CO_2 residually trapped - comparison of the 300 m shale length models, various sand:shale ratios, 0 degree slope

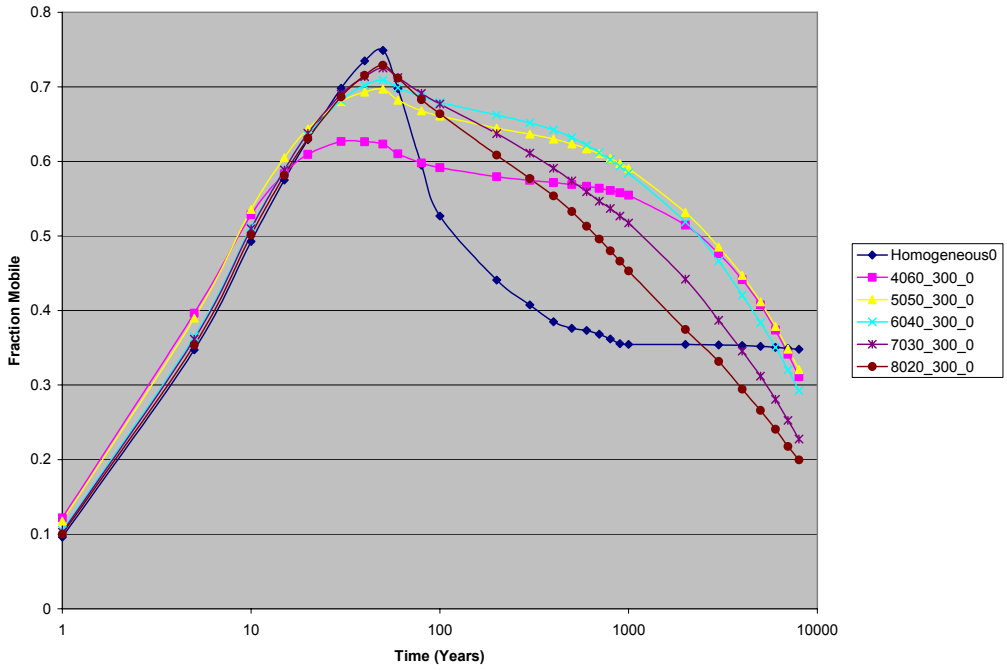

Figure D-195: Fraction of injection CO_2 remaining mobile - comparison of the 300 m shale length models, various sand:shale lengths, 0 degree slope

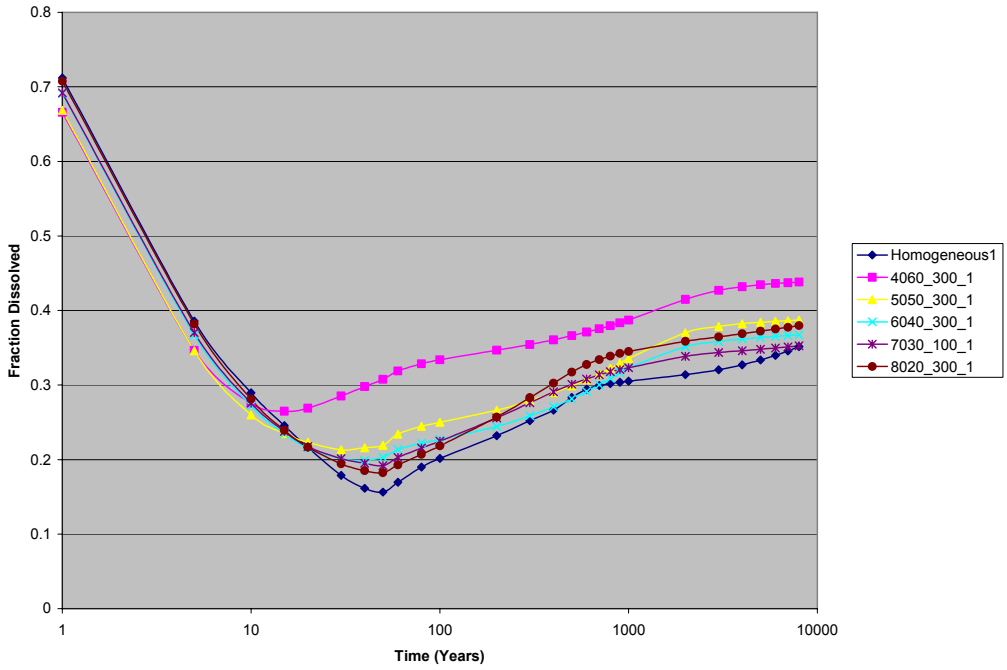

Figure D-196: Fraction of injection CO_2 dissolved - comparison of the 300 m shale length models, various sand:shale ratios, 1 degree slope

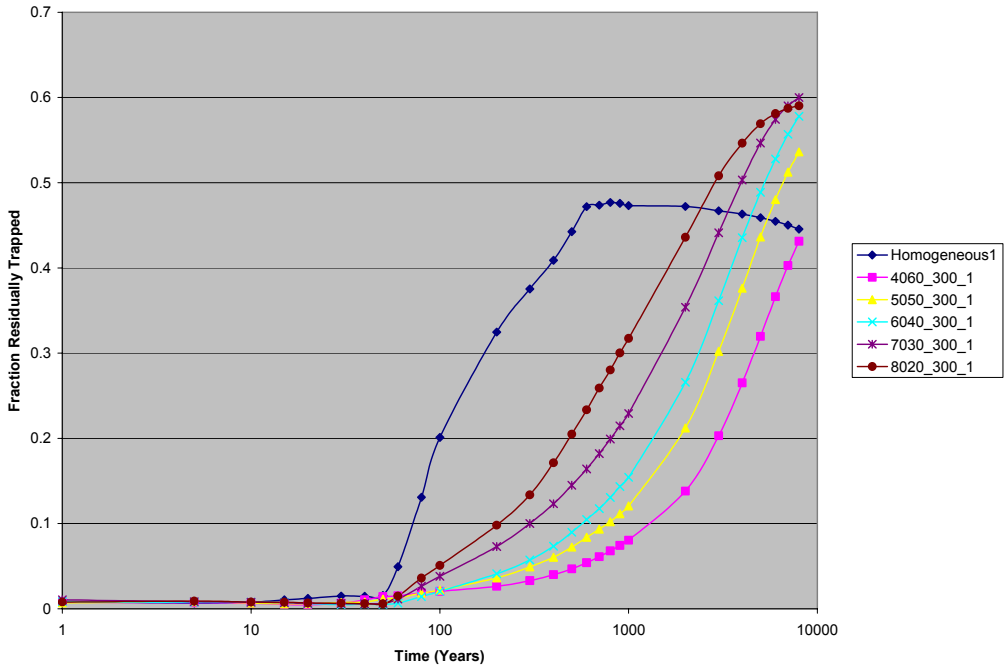

Figure D-197: Fraction of injection CO_2 residually trapped - comparison of the 300 m shale length models, various sand:shale ratios, 1 degree slope

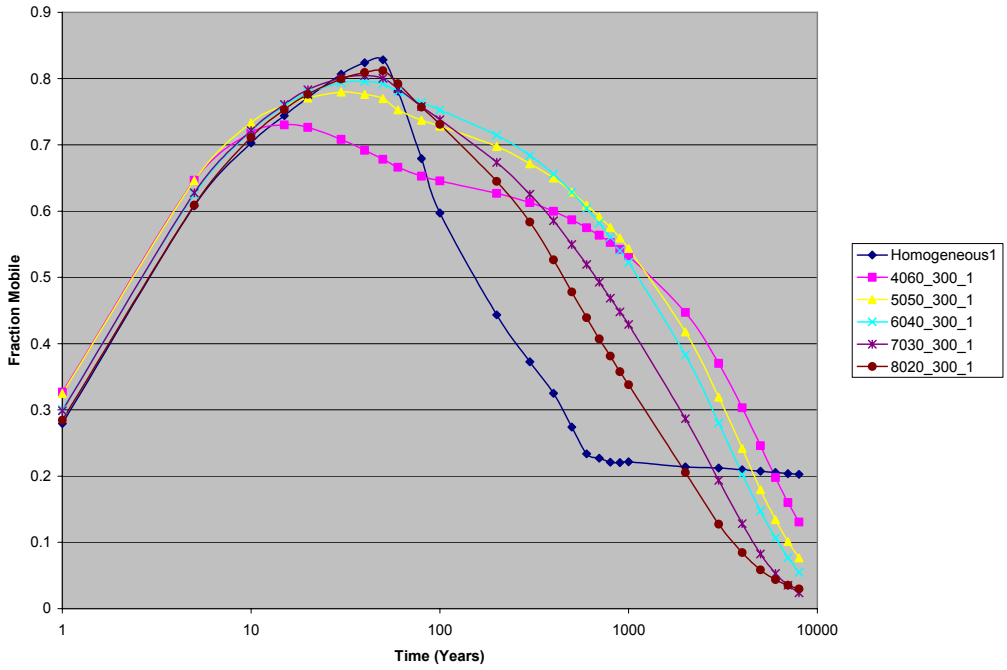

Figure D-198: Fraction of injection CO_2 remaining mobile - comparison of the 300 m shale length models, various sand:shale lengths, 1 degree slope

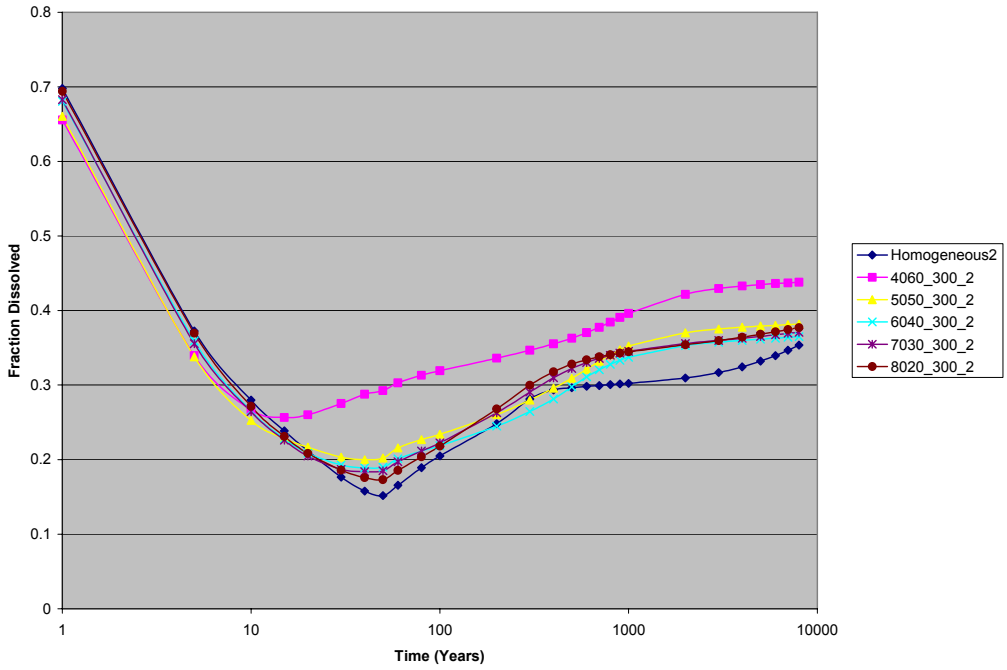

Figure D-199: Fraction of injection CO_2 dissolved - comparison of the 300 m shale length models, various sand:shale ratios, 2 degree slope

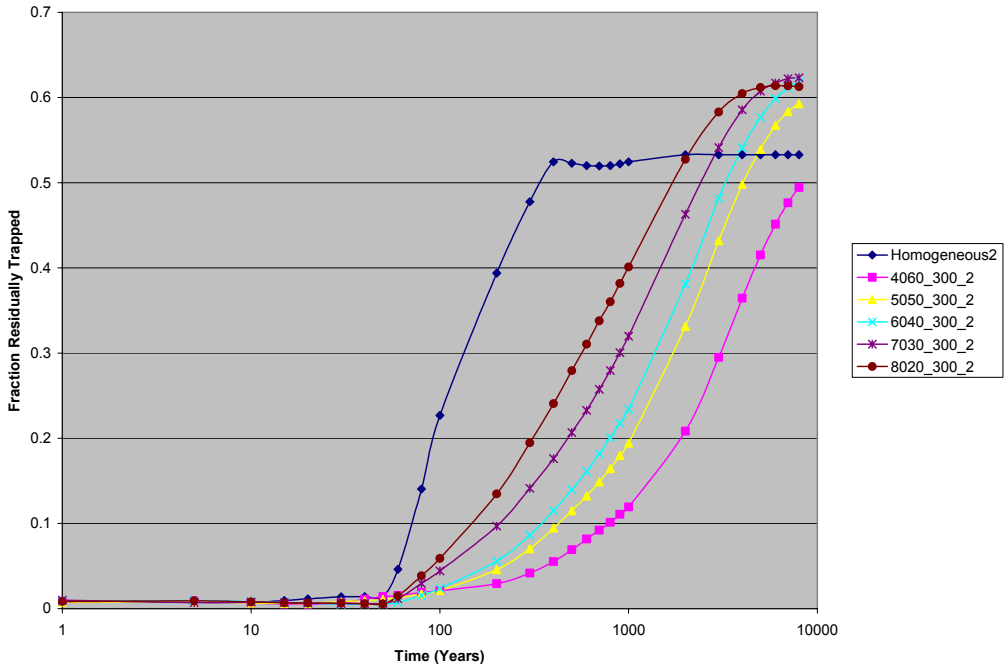

Figure D-200: Fraction of injection CO_2 residually trapped - comparison of the 300 m shale length models, various sand:shale ratios, 2 degree slope

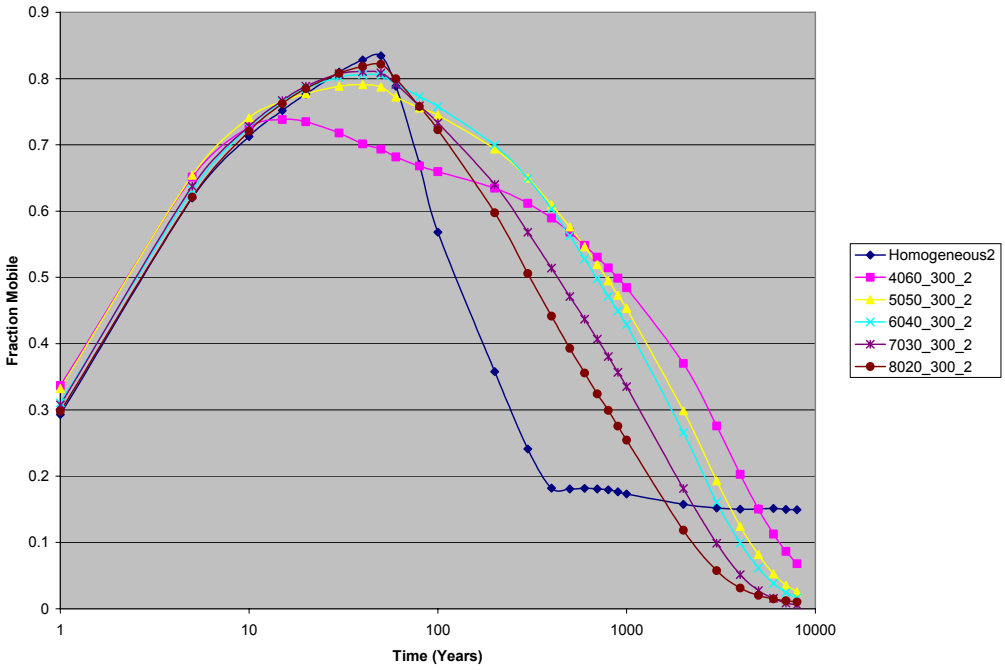

Figure D-201: Fraction of injection CO_2 remaining mobile - comparison of the 300 m shale length models, various sand:shale lengths, 2 degree slope

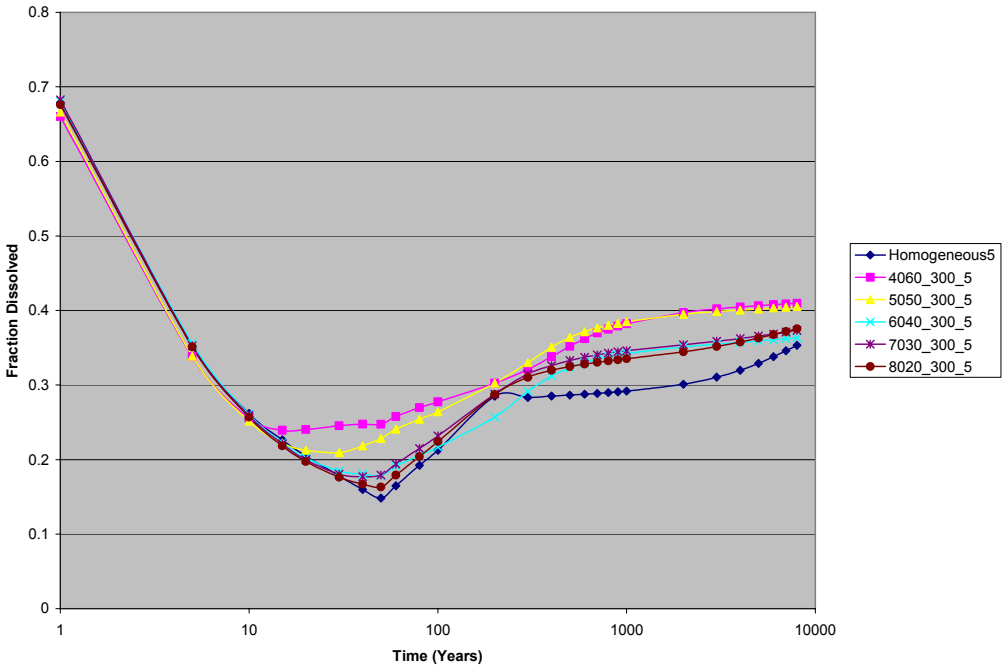

Figure D-202: Fraction of injection CO_2 dissolved - comparison of the 300 m shale length models, various sand:shale ratios, 5 degree slope

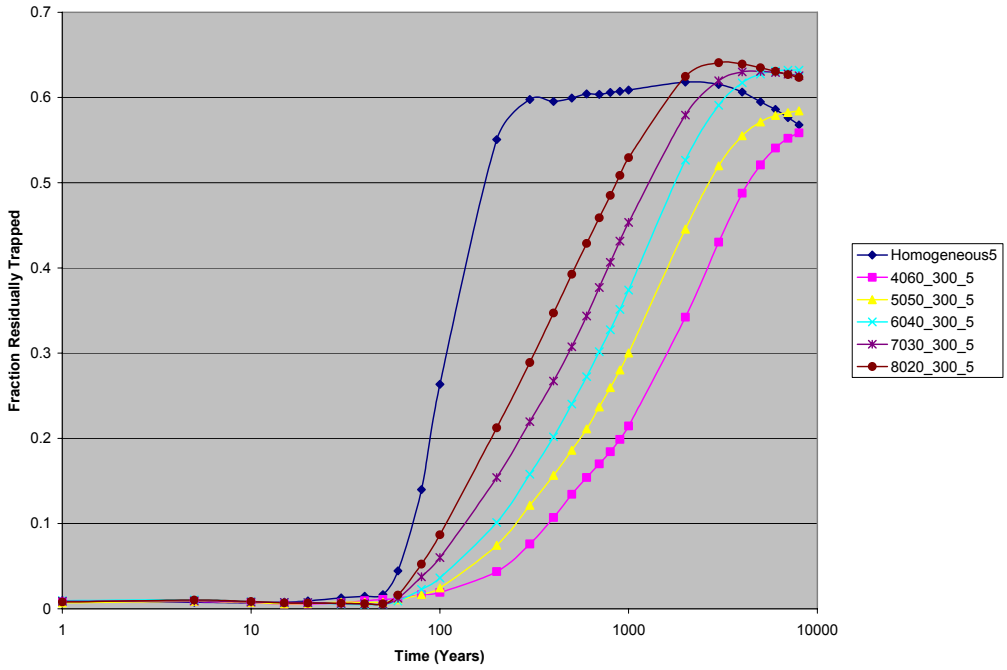

Figure D-203: Fraction of injection CO_2 residually trapped - comparison of the 300 m shale length models, various sand:shale ratios, 5 degree slope

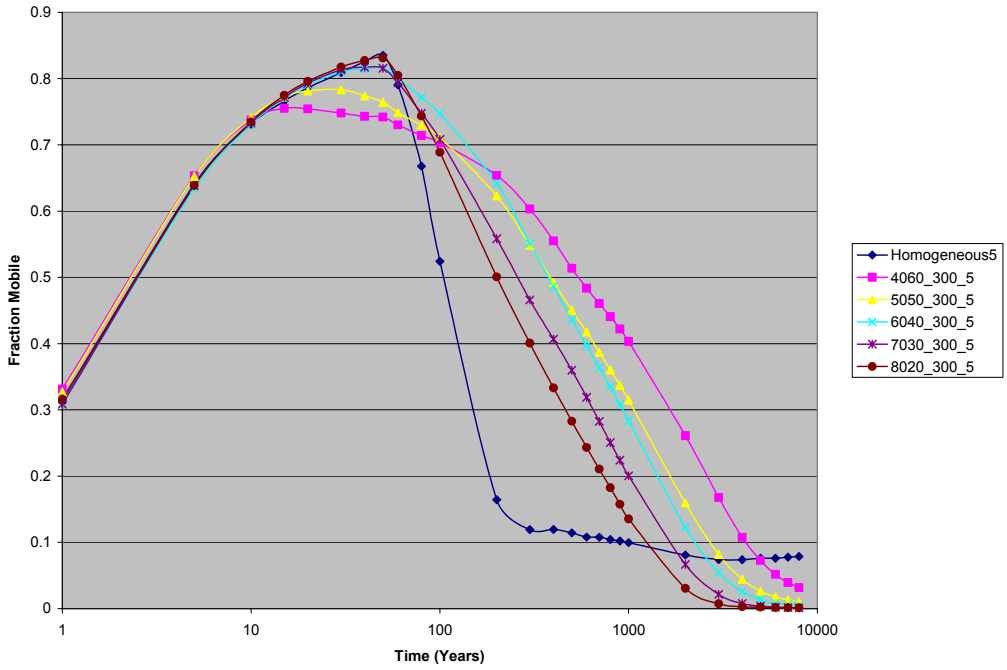

Figure D-204: Fraction of injection CO_2 remaining mobile - comparison of the 300 m shale length models, various sand:shale lengths, 5 degree slope

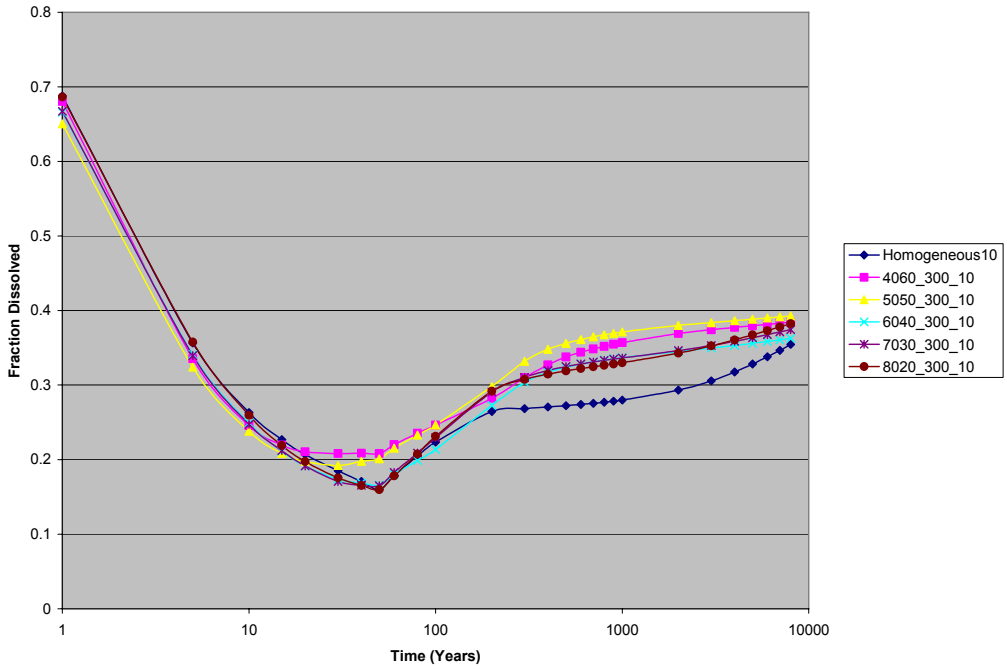

Figure D-205: Fraction of injection CO_2 dissolved - comparison of the 300 m shale length models, various sand:shale ratios, 10 degree slope

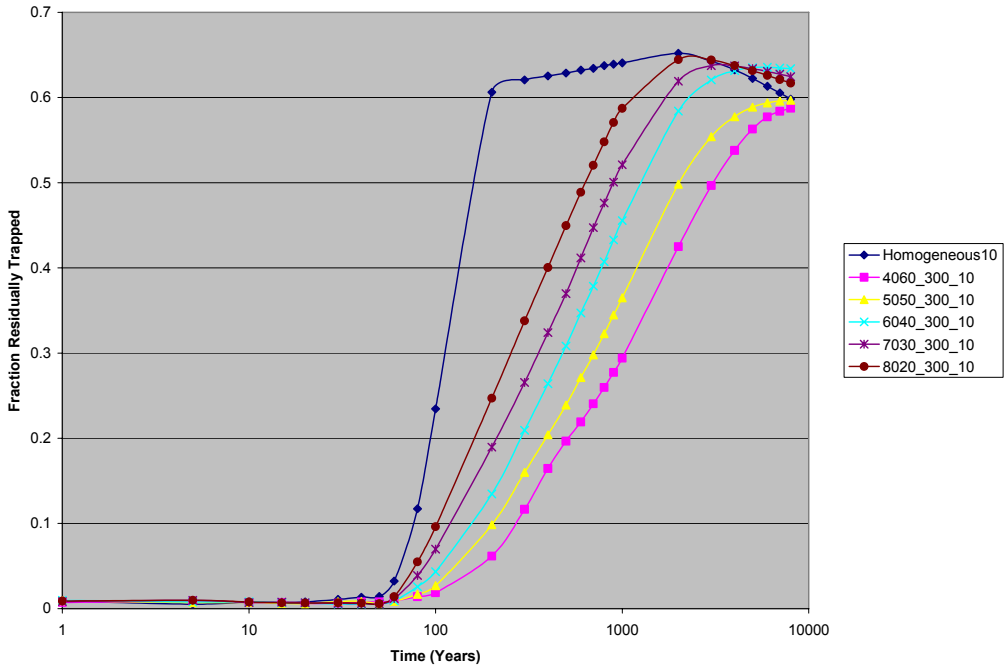

Figure D-206: Fraction of injection CO_2 residually trapped - comparison of the 300 m shale length models, various sand:shale ratios, 10 degree slope

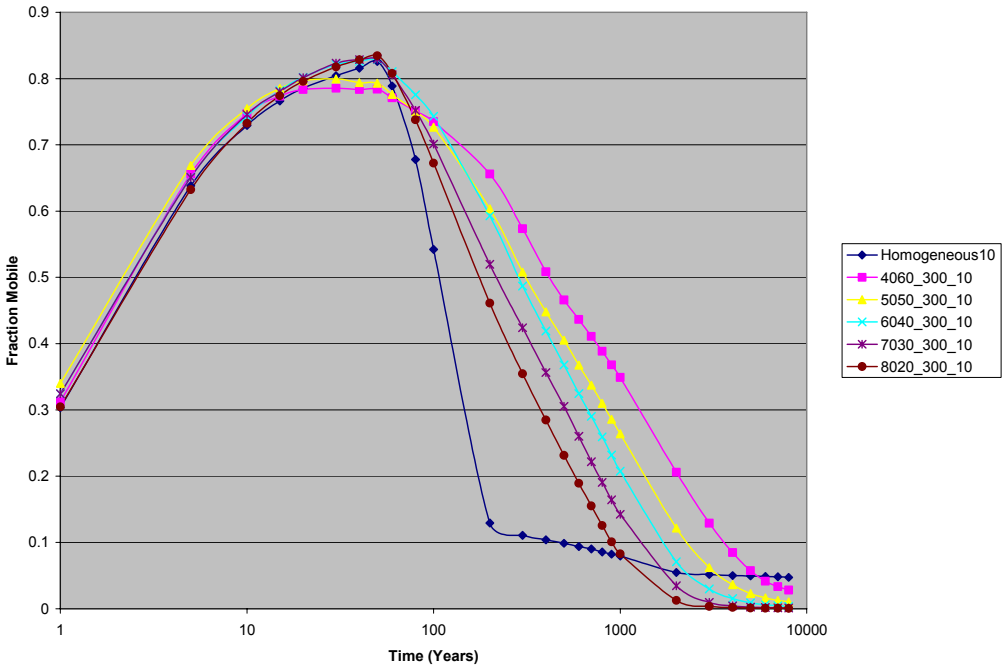

Figure D-207: Fraction of injection CO_2 remaining mobile - comparison of the 300 m shale length models, various sand:shale lengths, 10 degree slope

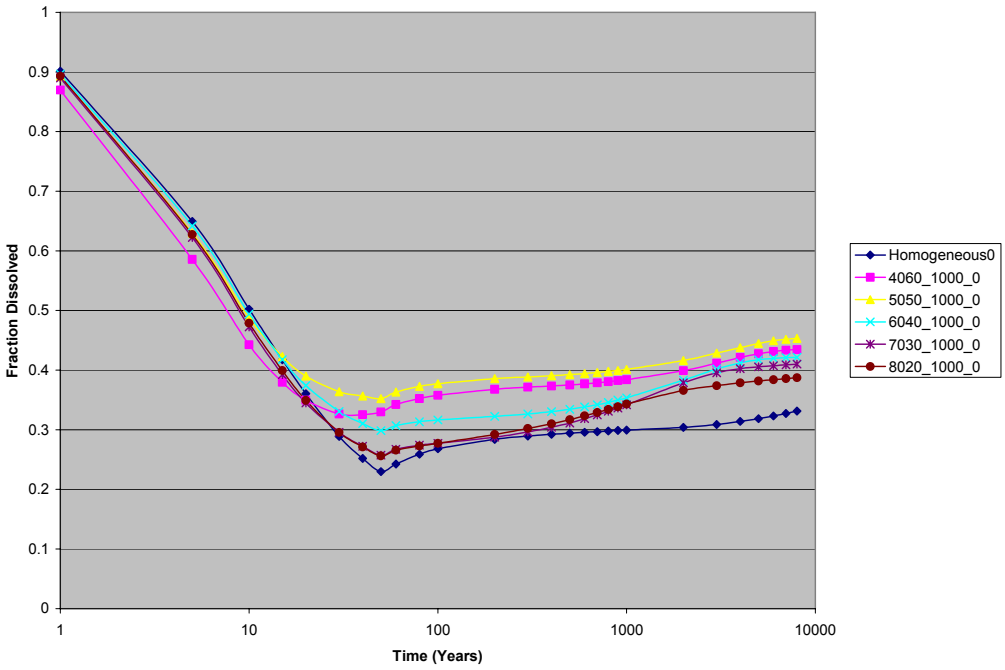

Figure D-208: Fraction of injection CO_2 dissolved - comparison of the 1000 m shale length models, various sand:shale ratios, 0 degree slope

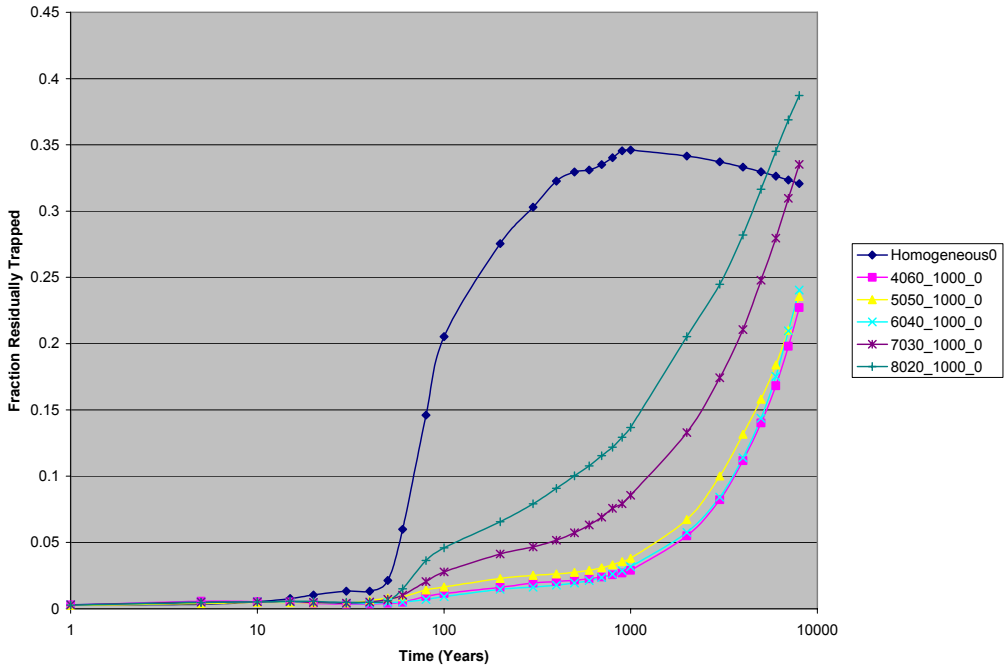

Figure D-209: Fraction of injection CO_2 residually trapped - comparison of the 1000 m shale length models, various sand:shale ratios, 0 degree slope

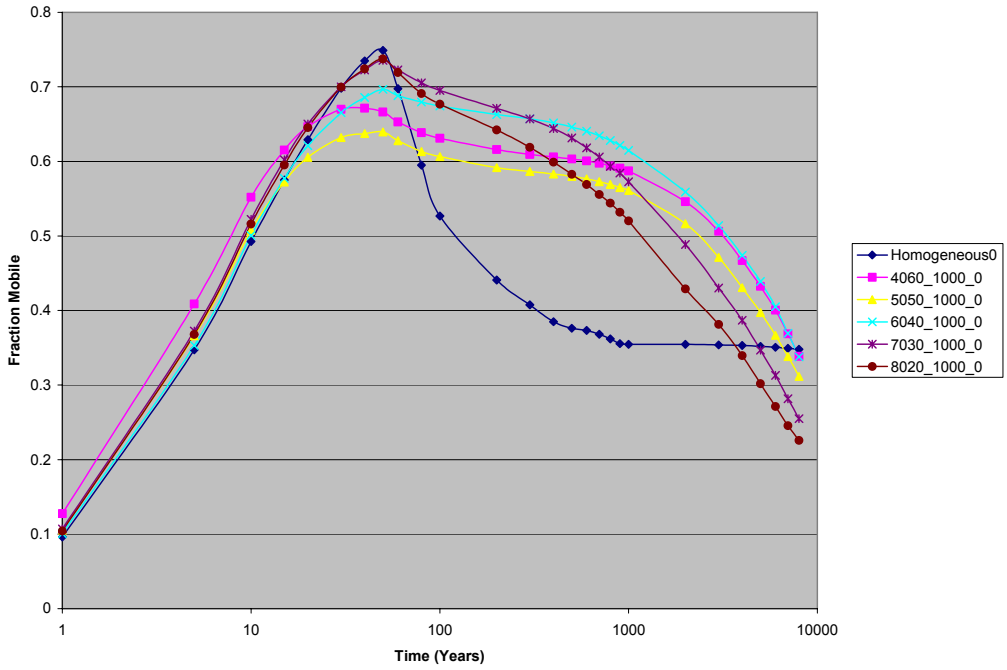

Figure D-210: Fraction of injection CO_2 remaining mobile - comparison of the 1000 m shale length models, various sand:shale lengths, 0 degree slope

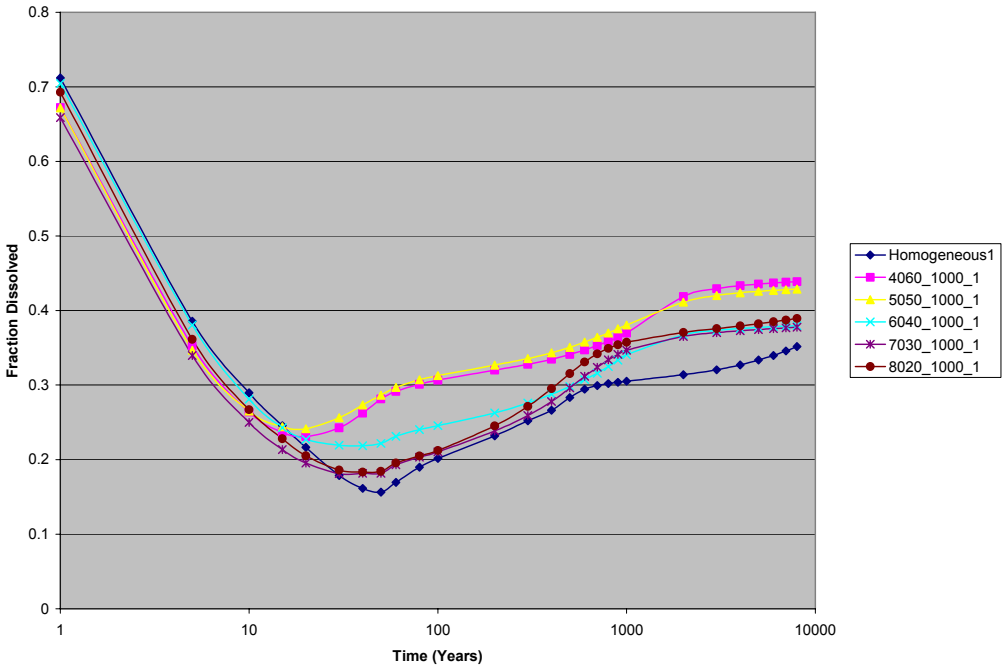

Figure D-211: Fraction of injection CO_2 dissolved - comparison of the 1000 m shale length models, various sand:shale ratios, 1 degree slope

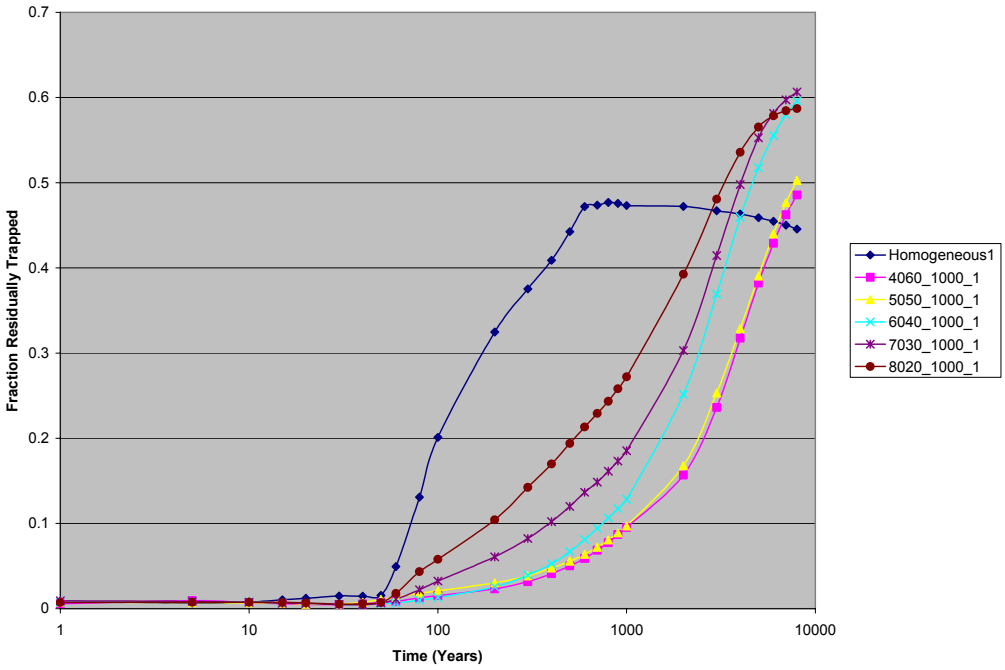

Figure D-212: Fraction of injection CO_2 residually trapped - comparison of the 1000 m shale length models, various sand:shale ratios, 1 degree slope

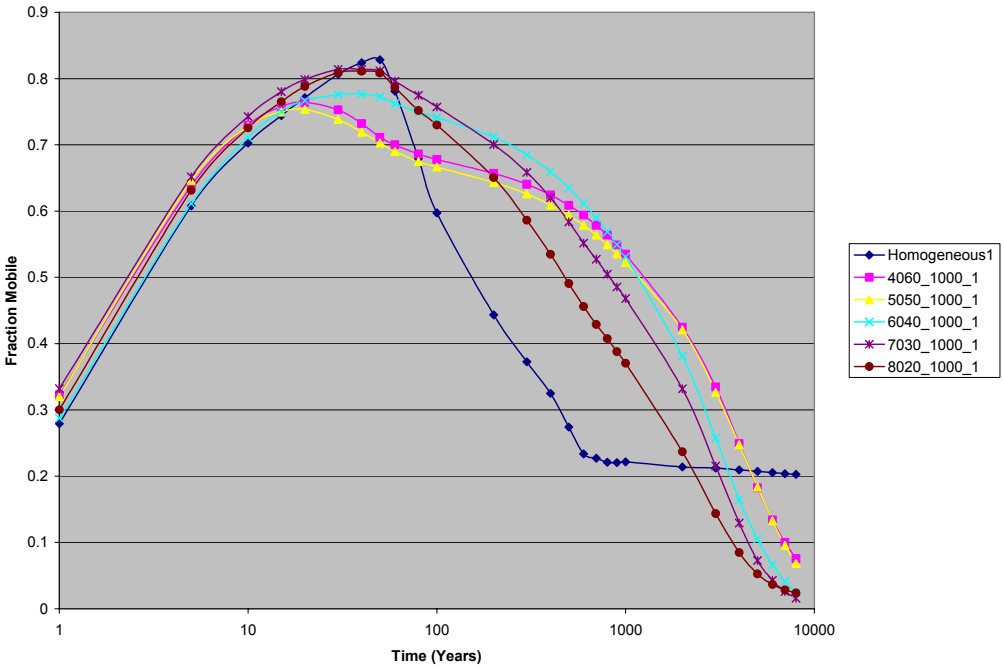

Figure D-213: Fraction of injection CO_2 remaining mobile - comparison of the 1000 m shale length models, various sand:shale lengths, 1 degree slope

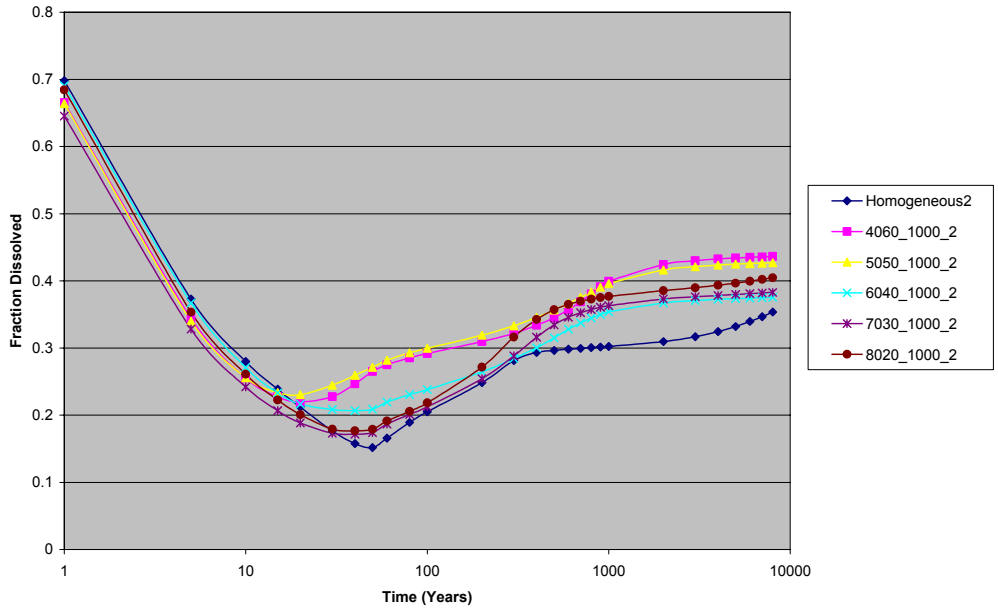

Figure D-214: Fraction of injection CO_2 dissolved - comparison of the 1000 m shale length models, various sand:shale ratios, 2 degree slope

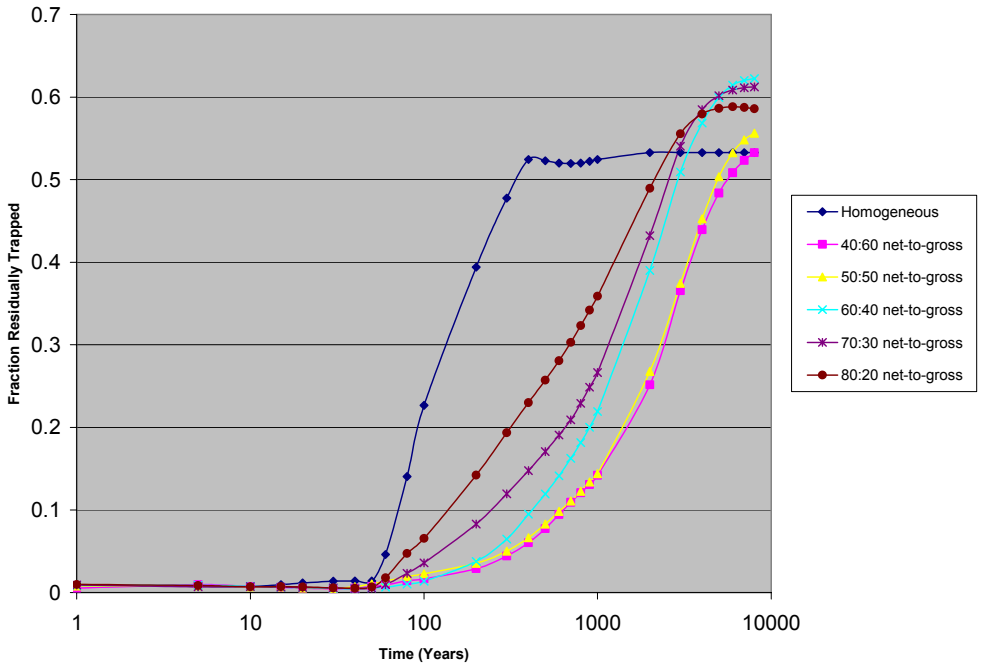

Figure D-215: Fraction of injection CO_2 residually trapped - comparison of the 1000 m shale length models, various sand:shale ratios, 2 degree slope

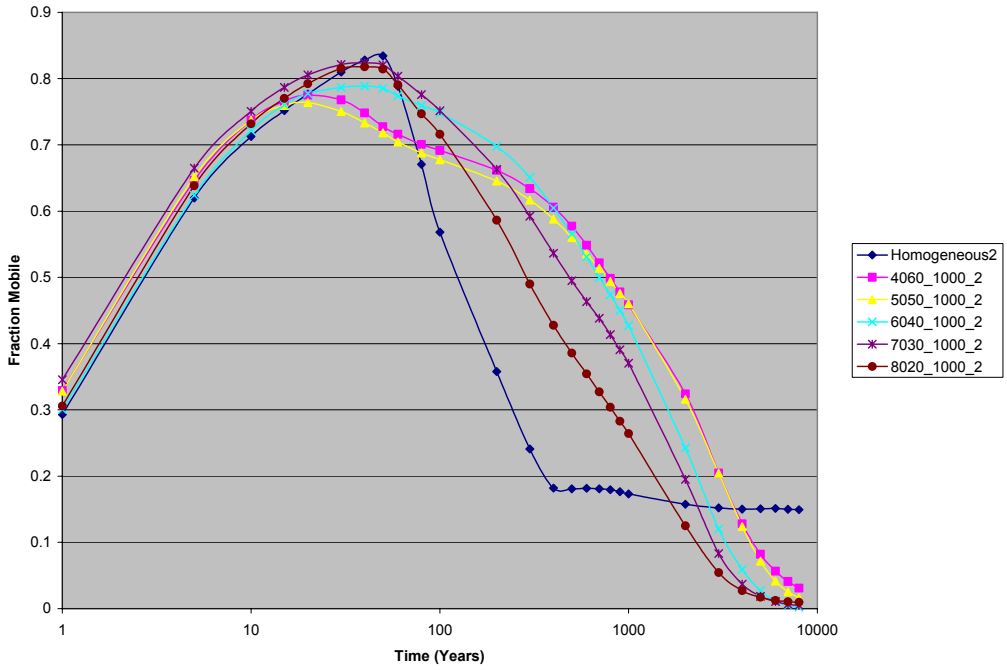

Figure D-216: Fraction of injection CO_2 remaining mobile - comparison of the 1000 m shale length models, various sand:shale lengths, 2 degree slope

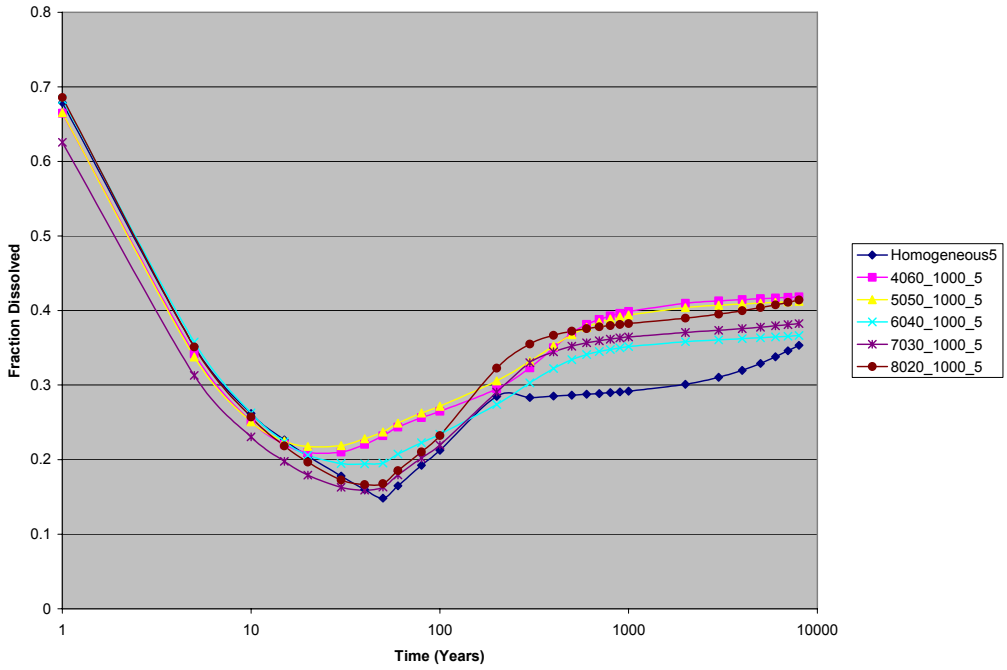

Figure D-217: Fraction of injection CO_2 dissolved - comparison of the 1000 m shale length models, various sand:shale ratios, 5 degree slope

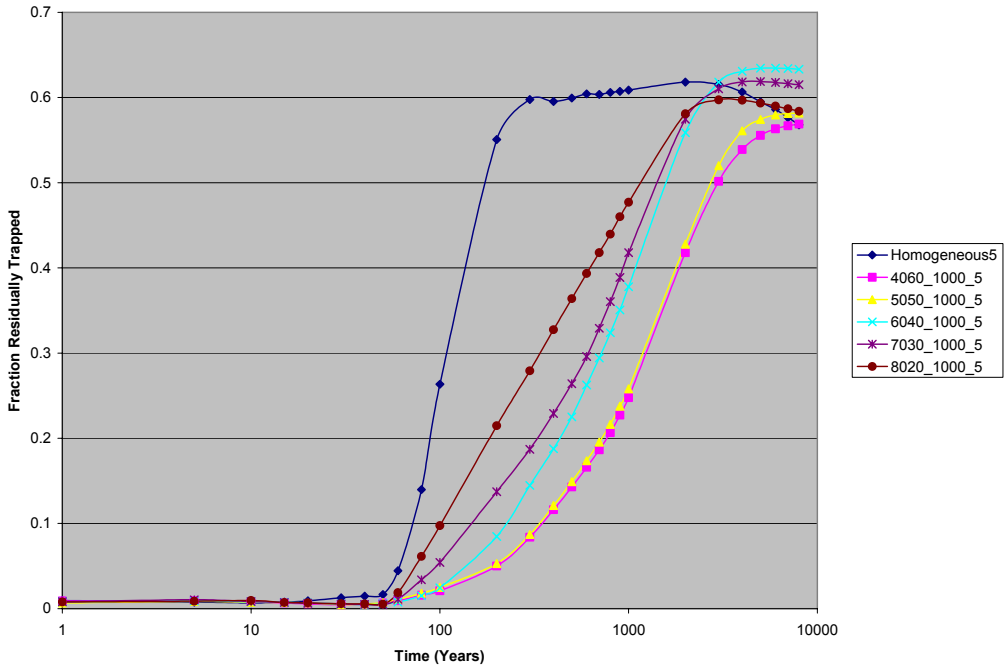

Figure D-218: Fraction of injection CO_2 residually trapped - comparison of the 1000 m shale length models, various sand:shale ratios, 5 degree slope

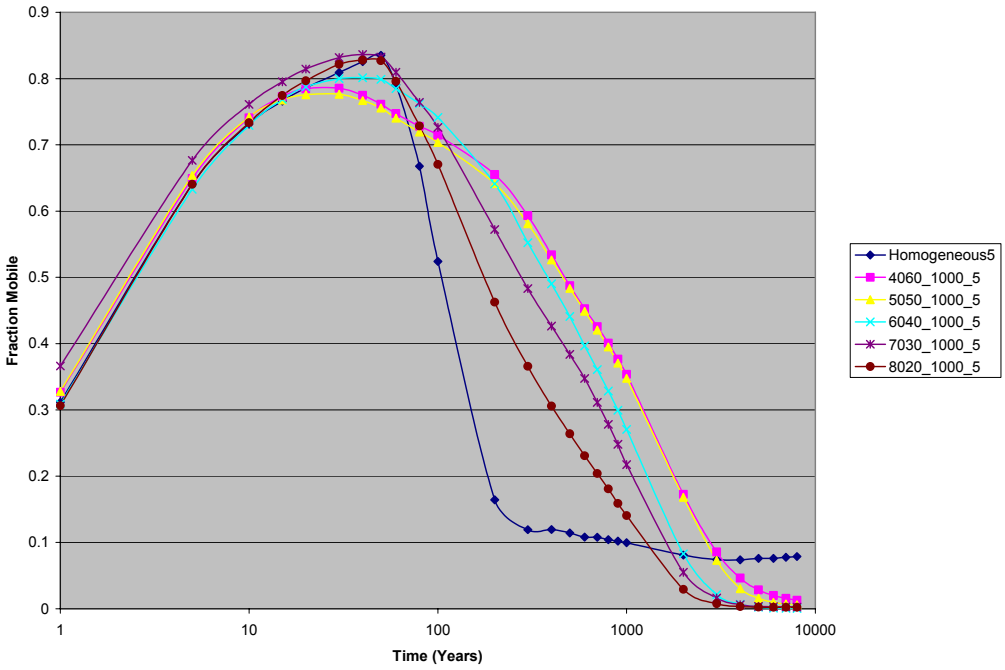

Figure D-219: Fraction of injection CO_2 remaining mobile - comparison of the 1000 m shale length models, various sand:shale lengths, 5 degree slope

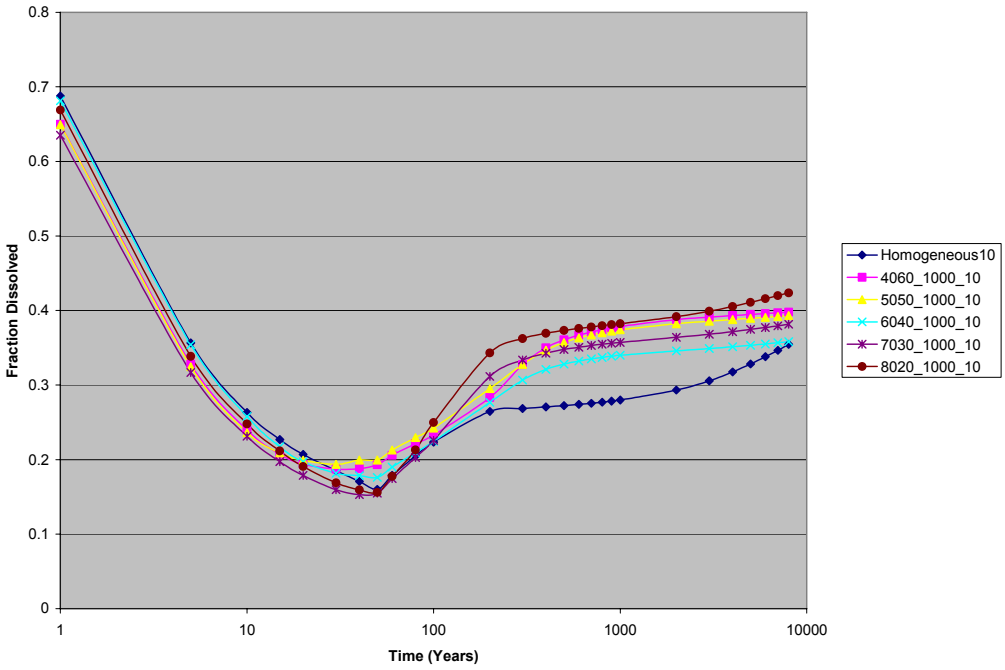

Figure D-220: Fraction of injection CO_2 dissolved - comparison of the 1000 m shale length models, various sand:shale ratios, 10 degree slope

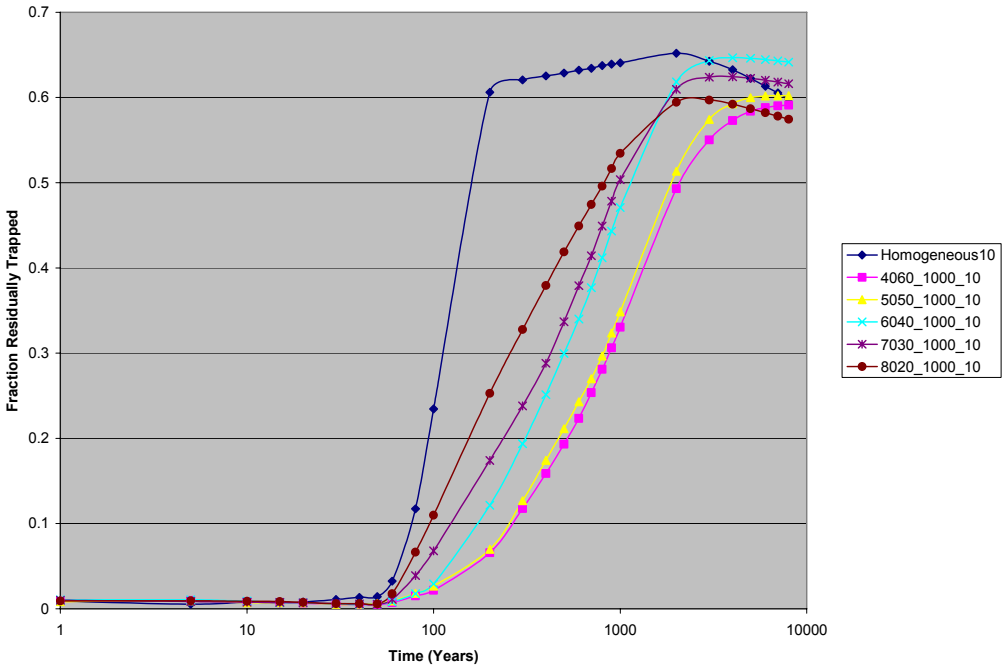

Figure D-221: Fraction of injection CO_2 residually trapped - comparison of the 1000 m shale length models, various sand:shale ratios, 10 degree slope

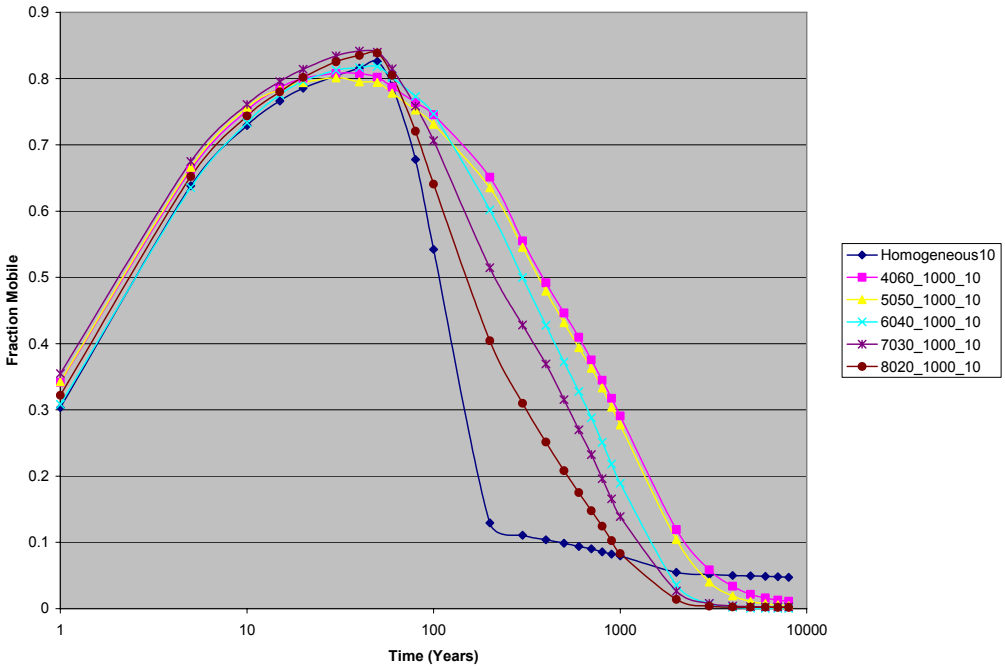

Figure D-222: Fraction of injection CO_2 remaining mobile - comparison of the 1000 m shale length models, various sand:shale lengths, 10 degree slope

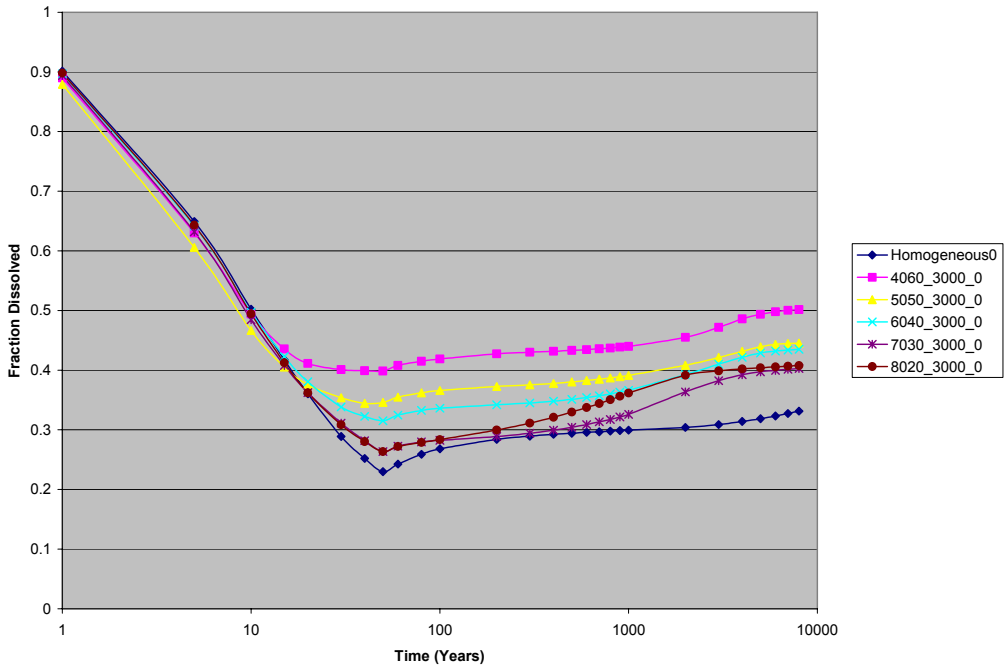

Figure D-223: Fraction of injection CO_2 dissolved - comparison of the 3000 m shale length models, various sand:shale ratios, 0 degree slope

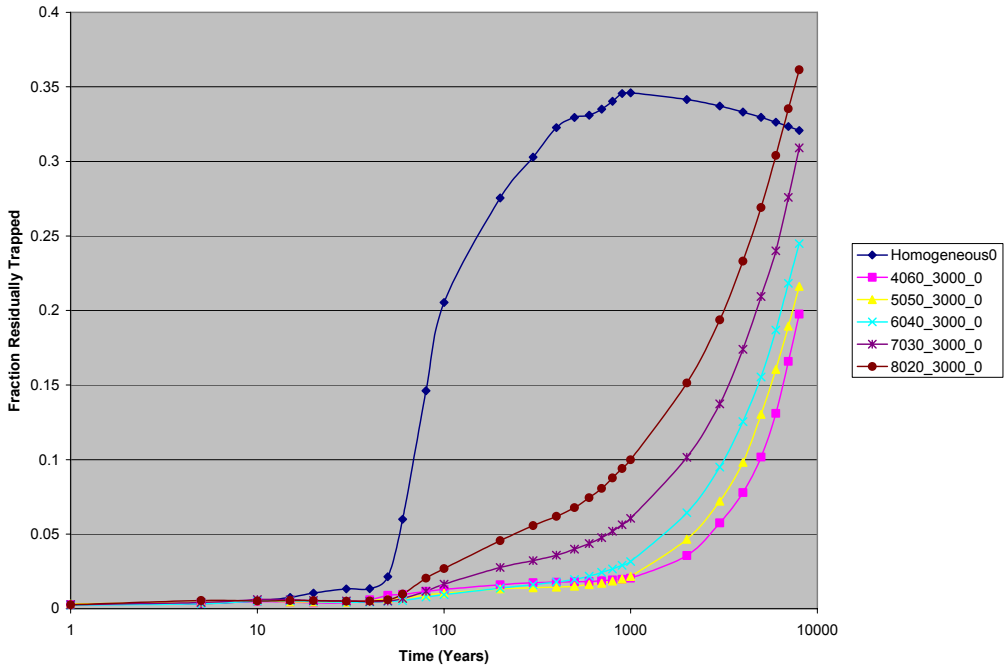

Figure D-224: Fraction of injection CO_2 residually trapped - comparison of the 3000 m shale length models, various sand:shale ratios, 0 degree slope

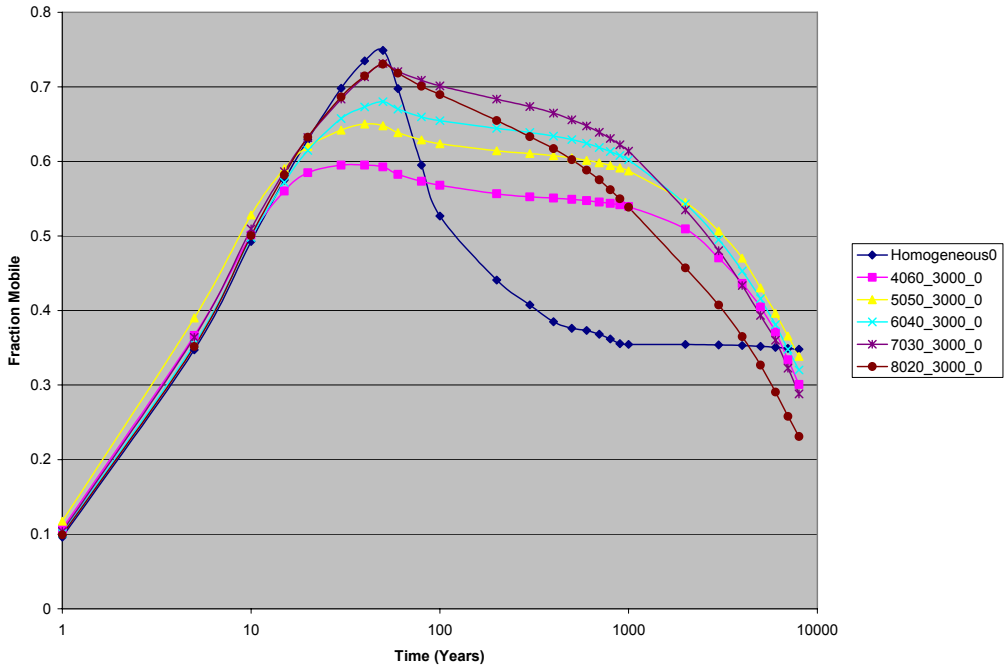

Figure D-225: Fraction of injection CO_2 remaining mobile - comparison of the 3000 m shale length models, various sand:shale lengths, 0 degree slope

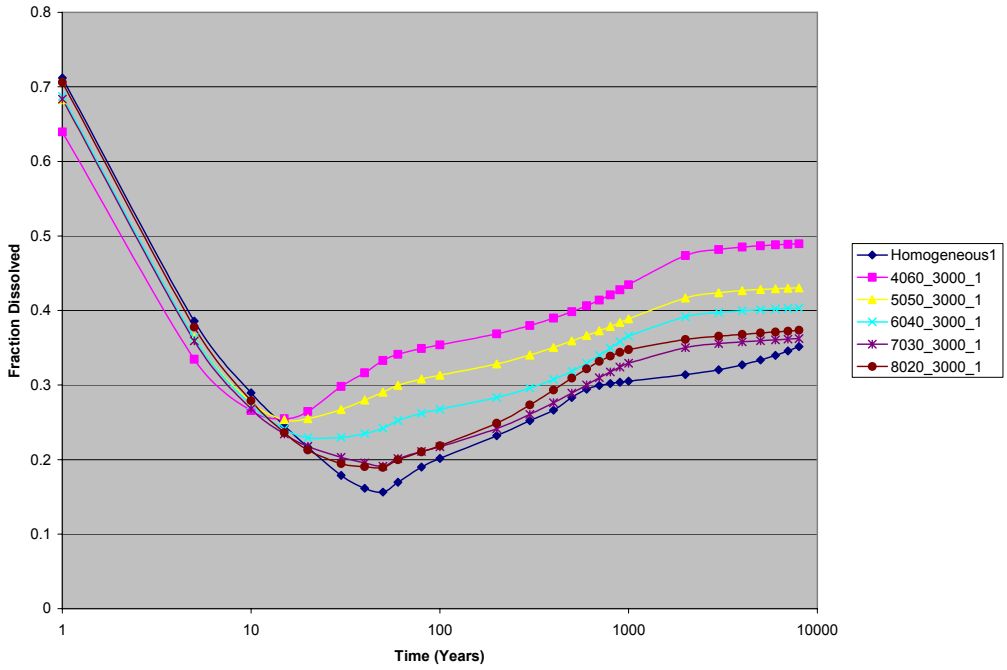

Figure D-226: Fraction of injection CO_2 dissolved - comparison of the 3000 m shale length models, various sand:shale ratios, 1 degree slope

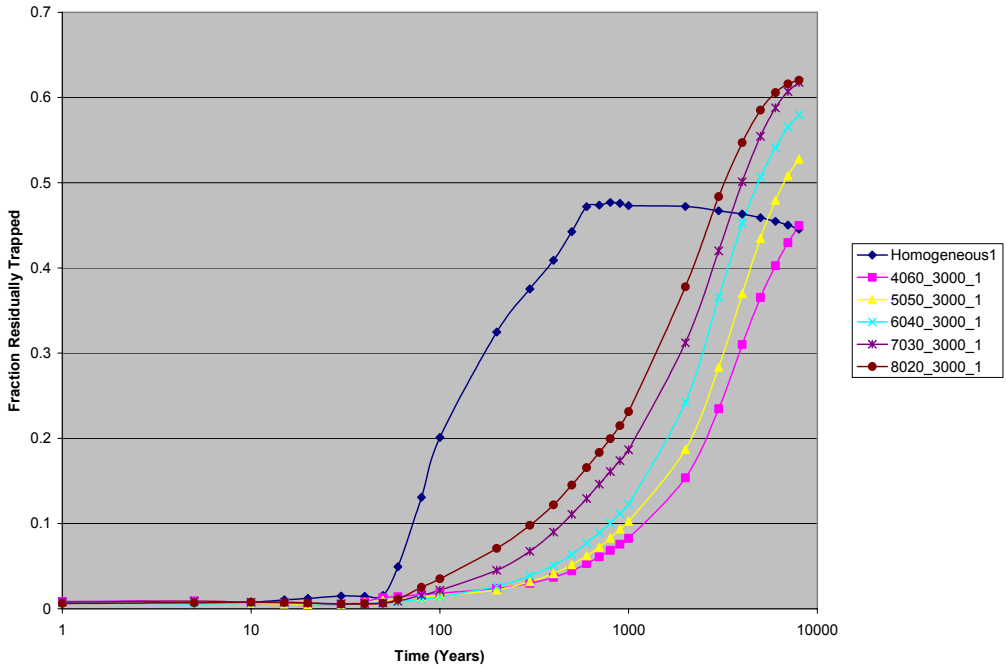

Figure D-227: Fraction of injection CO_2 residually trapped - comparison of the 3000 m shale length models, various sand:shale ratios, 1 degree slope

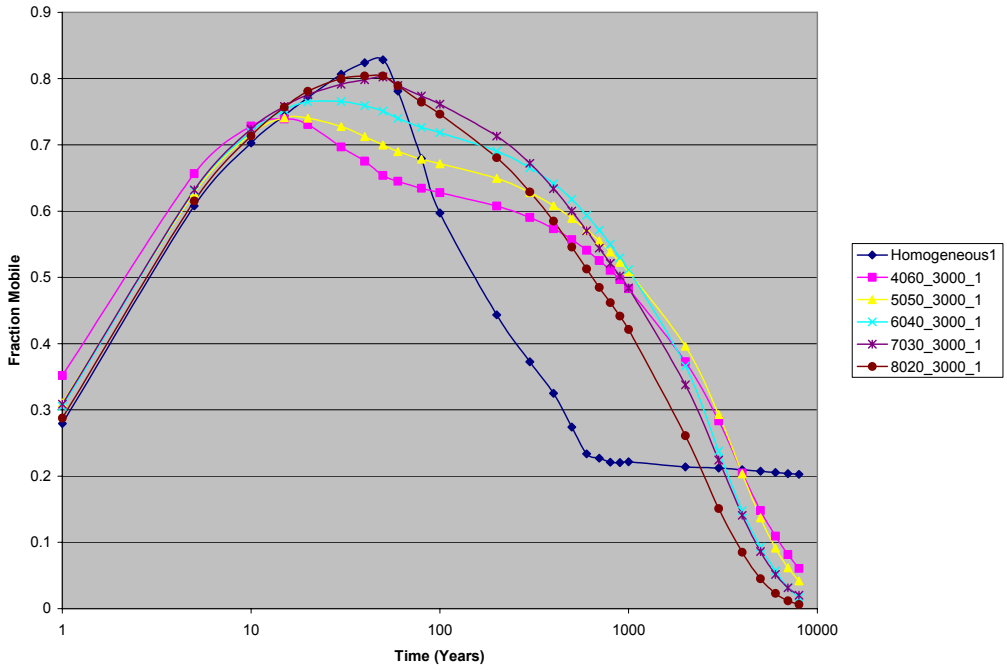

Figure D-228: Fraction of injection CO_2 remaining mobile - comparison of the 3000 m shale length models, various sand:shale lengths, 1 degree slope

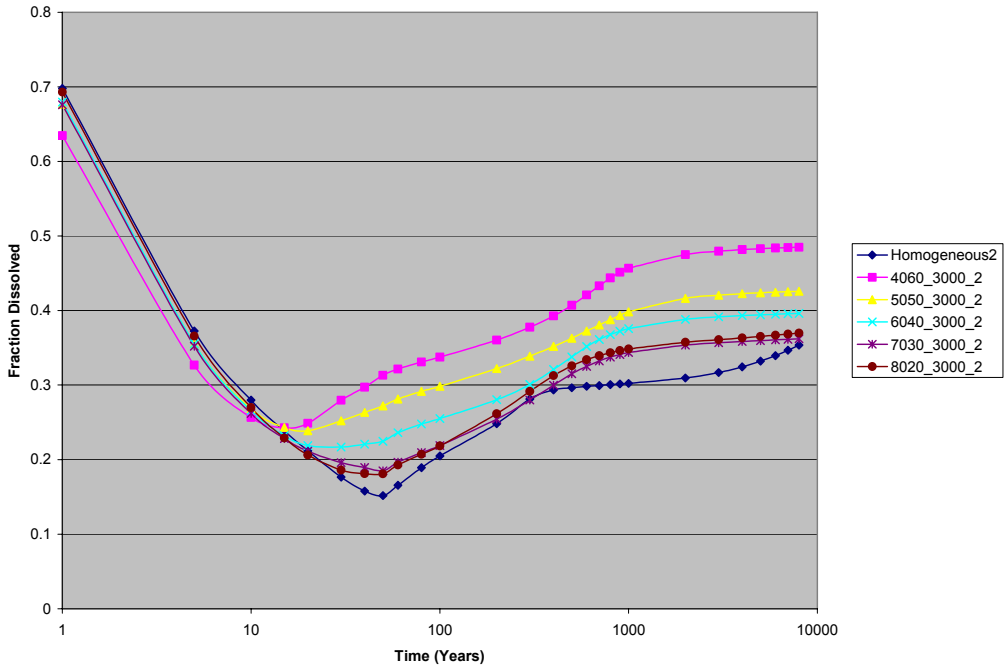

Figure D-229: Fraction of injection CO_2 dissolved - comparison of the 3000 m shale length models, various sand:shale ratios, 2 degree slope

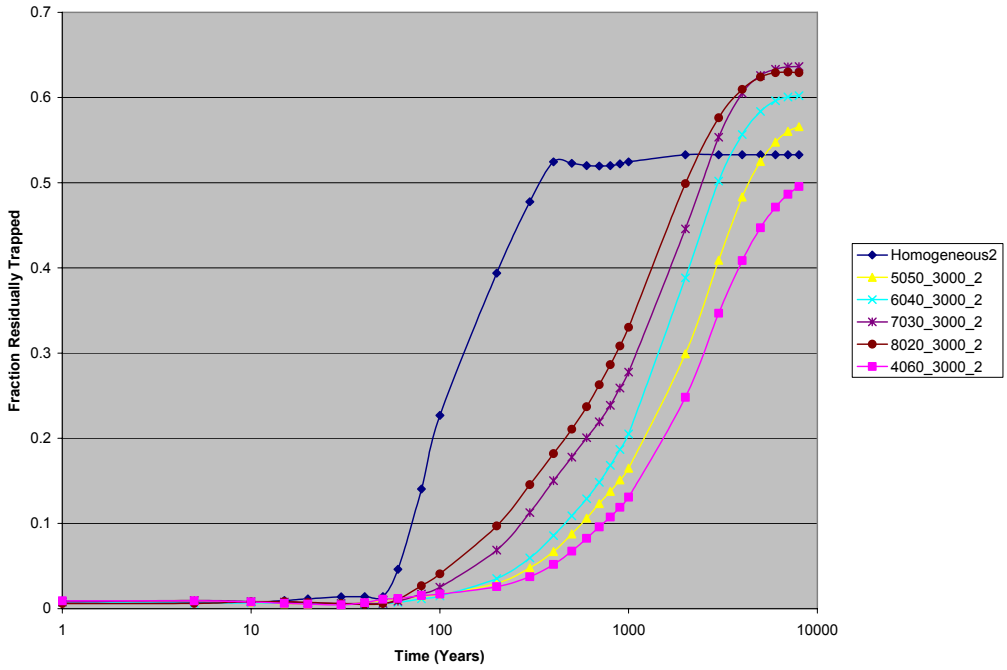

Figure D-230: Fraction of injection CO_2 residually trapped - comparison of the 3000 m shale length models, various sand:shale ratios, 2 degree slope

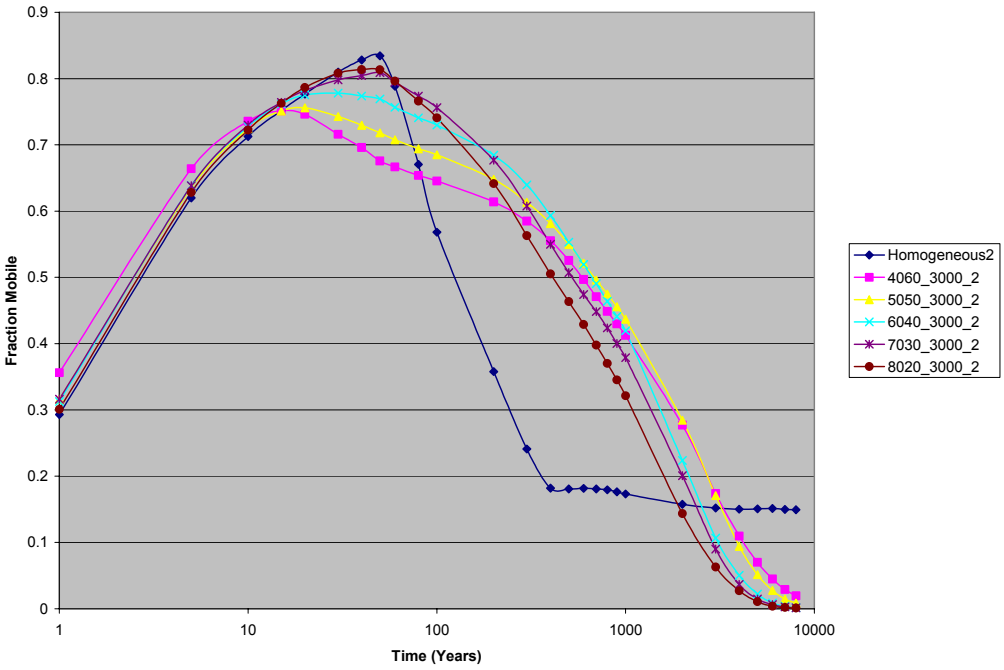

Figure D-231: Fraction of injection CO_2 remaining mobile - comparison of the 3000 m shale length models, various sand:shale lengths, 2 degree slope

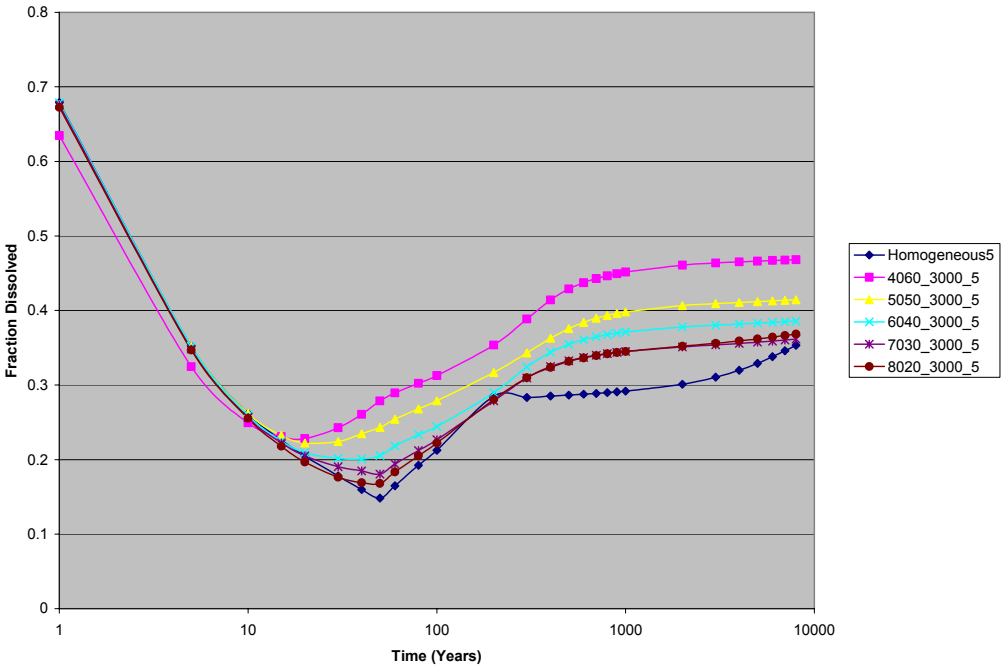

Figure D-232: Fraction of injection CO_2 dissolved - comparison of the 3000 m shale length models, various sand:shale ratios, 5 degree slope

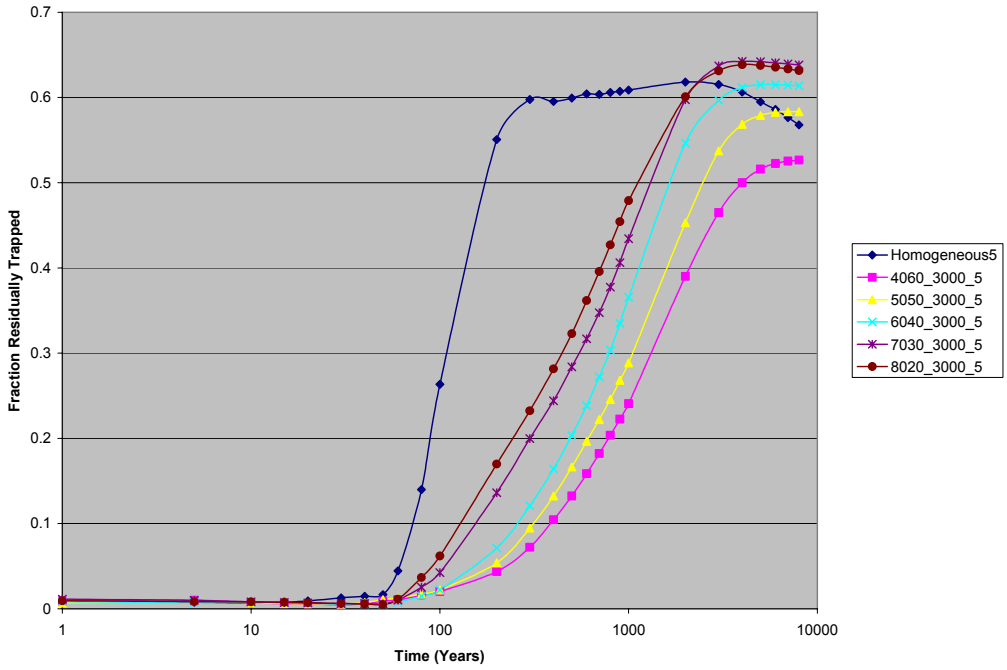

Figure D-233: Fraction of injection CO_2 residually trapped - comparison of the 3000 m shale length models, various sand:shale ratios, 5 degree slope

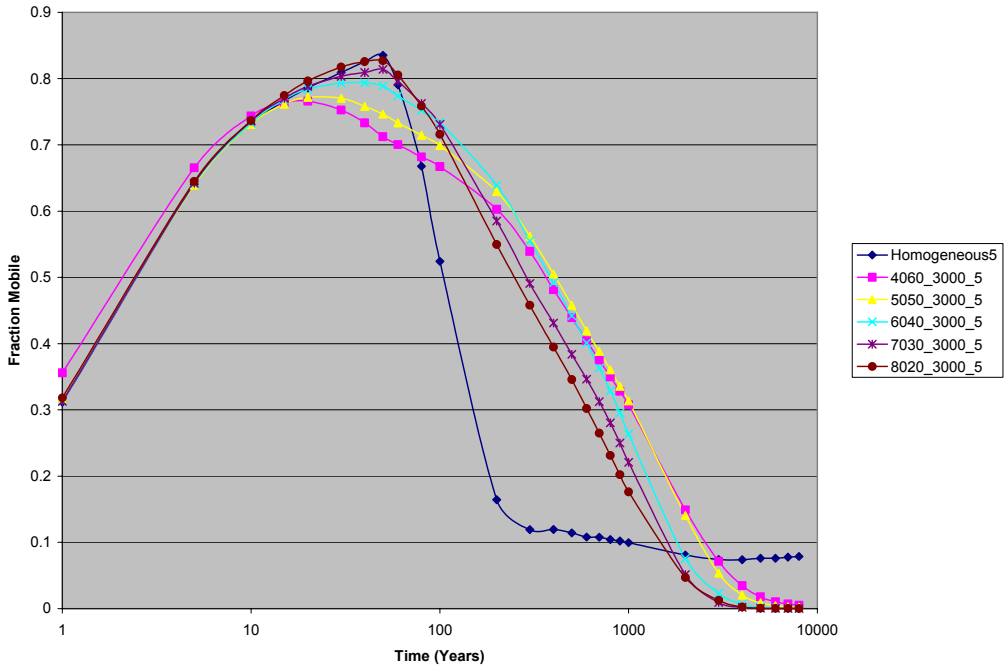

Figure D-234: Fraction of injection CO_2 remaining mobile - comparison of the 3000 m shale length models, various sand:shale lengths, 5 degree slope

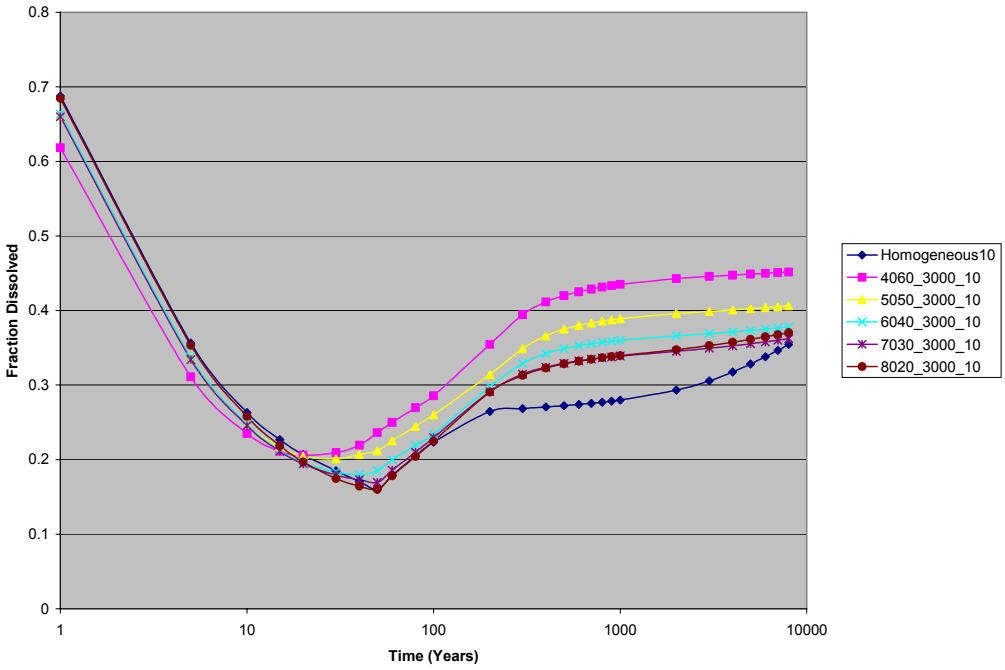

Figure D-235: Fraction of injection CO_2 dissolved - comparison of the 3000 m shale length models, various sand:shale ratios, 10 degree slope

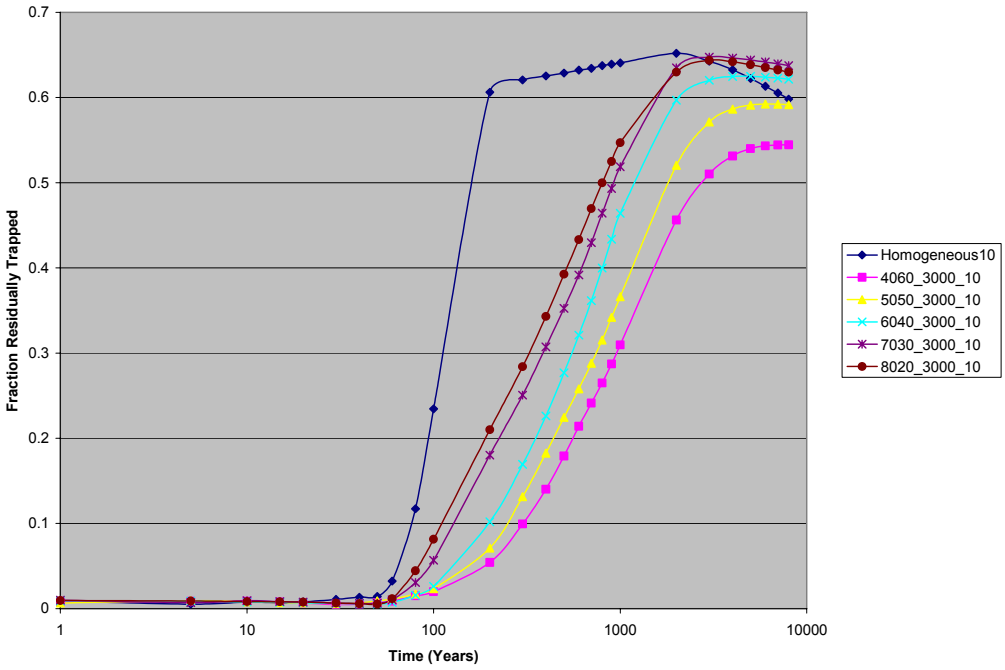

Figure D-236: Fraction of injection CO_2 residually trapped - comparison of the 3000 m shale length models, various sand:shale ratios, 10 degree slope

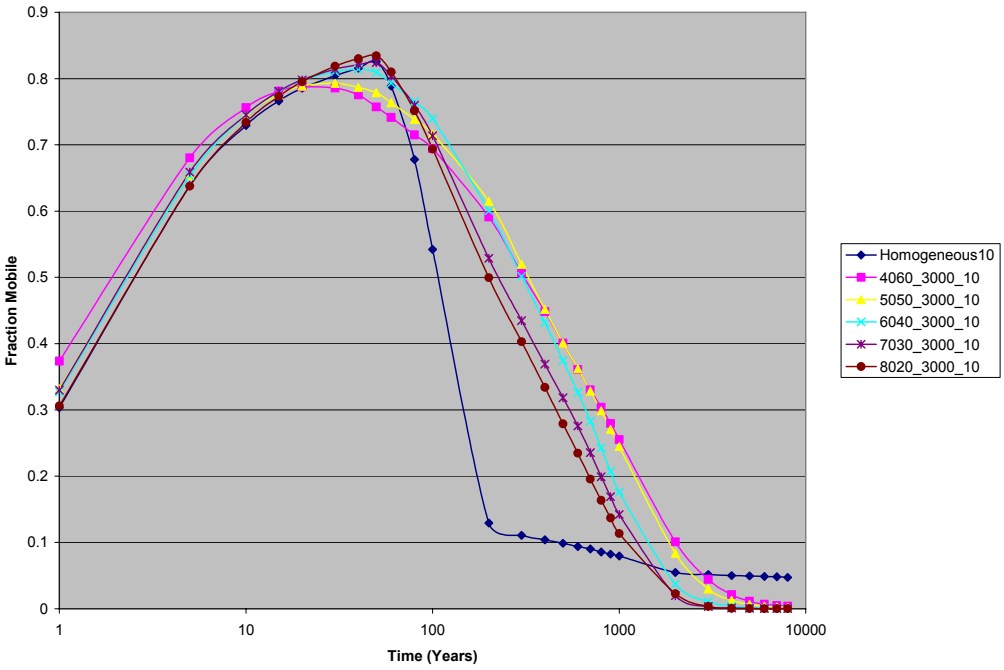

Figure D-237: Fraction of injection CO_2 remaining mobile - comparison of the 3000 m shale length models, various sand:shale lengths, 10 degree slope

APPENDIX E – COPYRIGHT PERMISSIONS

In this Appendix, the necessary permissions for copyright release are recorded from co-authors and publishers of papers included in Appendices A and B. This includes letters from the Society of Petroleum Engineers and co-authors Ian Taggart, Randal Gurton and Geoff Weir.

Society of Petroleum Engineers
Dallas • Dubai • Houston • Kuala Lumpur • London
www.spe.org

28 December 2007

Matthew Flett
Reservoir Engineer
Chevron Australia Pty Ltd
Level 22, 250 St Georges Terrace
Perth, Western Australia 6000
Australia

Emailed Approval

Re: Permission to use SPE Copyrighted Material

Dear Matthew Flett:

Thank you for your request to use material copyrighted to SPE. This is to grant one-time permission to reproduce

SPE paper #88485
"The Function of Gas-Water Relative Permeability Hysteresis in the Sequestration of Carbon Dioxide in Saline Formations"
2004 SPE Asia Pacific Oil and Gas Conference and Exhibition

for use in your doctoral thesis. This permission is granted with the following conditions:
Proper notice of SPE copyright ownership is required on (1) any copy or substantial portion of an SPE paper or other SPE publication and (2) any figure, table, or other portion of any publication to which SPE holds copyright.
SPE requests that each acknowledgment include paper title, authors and either (1) the date of publication of the book or journal in which published or (2) the name, location, and dates of the meeting where first presented.
PLEASE NOTE that SPE does not permit distribution of its papers through an Internet. The policy states further that "no SPE-copyrighted paper may be held in or distributed from an electronic database other than one developed for SPE itself."
The Society's copyright position encourages the broadest possible distribution of technical material to which it holds copyright, as is consistent with our copyright agreements with authors. Thank you for your cooperation in this matter, which is essential to protect the rights of the many authors who make technical material generally available through an SPE Conference.

Sincerely,

Ursula Blum
Copyright Coordinator
SPE Technical Publications

Tel: 972.952.9453
Fax: 972-952-1150
ublum@spe.org

From: Gurton, Randal [RGUR@chevron.com]
Sent: Friday, 29 February 2008 11:30 AM
To: Flett, Matthew
Subject: RE: Copyright release/permission for doctoral thesis

Matt,

No problem. You have my permission to use the papers below, where I was a co-author, for attachment to your thesis. Cheers.

Randy

From: Flett, Matthew
Sent: Thursday, 28 February 2008 3:54 PM
To: 'Ian.Taggart@riscpl.com'; Gurton, Randal; 'weirdoz@bigpond.net.au'
Subject: Copyright release/permission for doctoral thesis

Dear Ian, Randy and Geoff,

Within a few weeks I will be submitting my thesis to Curtin Uni for examination. As I intend to include several papers as appendices to my thesis where you have been co-authors, I formally ask your permission to do so, in order to fulfil copyright provisions of Curtin University.

The papers I intend to include are:

Peer reviewed papers:
1.Flett, M., R. Gurton, and I. Taggart. *Heterogeneous saline formations: long term benefits for geo-sequestration of greenhouse gases*. in *Seventh International Conference on Greenhouse Gas Control Technologies (GHGT-7)*. 2004. Vancouver, Canada.: Elsevier.

2. Flett, M., R. Gurton, and G. Weir, *Heterogeneous saline formations for carbon dioxide disposal: Impact of varying heterogeneity on containment and trapping.* Journal of Petroleum Science and Engineering, 2007. **57**(1-2): p. 106-118

Conference papers:
1. Flett, M., R. Gurton, and G. Weir. *Reservoir performance of disposed carbon dioxide in saline formations: impact of heterogeniety and dip*. in *8th International conference on Greenhouse Gas Control Technologies*. 2006. Trondheim, Norway.

2. Flett, M., R. Gurton, and I. Taggart. *The function of gas-water relative permeability hysteresis in the sequestration of carbon dioxide in saline formations, SPE paper 88485, Presented 2004 SPE Asia-Pacific Oil and Gas Conference and Exhibition, Perth, Australia, 18-20 Oct (2004).* 2004.

In terms of publishers retention of copyright: For the peer-reviewed articles - both have been published by Elsevier, their copyright policy online allows for inclusion of published papers and materials for a paper to be included in a thesis (as long as you are the author). See http://www.elsevier.com/wps/find/authorsview.authors/copyright#whatrights (cited 28/02/2008)

I have received permission from the SPE for paper 88485 and made due acknowledgements through my thesis.

<< File: 88485_Flett, Matthew.doc >>
The GHGT8 paper has not been formally published and thus we have retained copyright.

Could you by return email, please give your permission as co-authors for these papers to be included and state your role in the preparation of these papers.

Thanks for you support,
Regards,

Matt

Matthew Flett
Reservoir Engineer
Gorgon Subsurface Development

Chevron Australia Pty Ltd
250 St Georges Terrace
Perth, Western Australia, 6000
Tel +61 8 9216 4574
Mobile 0421 869 645
Fax +61 8 9216 4860
Email Matthew.Flett@Chevron.com

From: Ian Taggart [Ian.Taggart@riscpl.com]
Sent: Friday, 29 February 2008 3:17 PM
To: Flett, Matthew
Subject: RE: Copyright release/permission for doctoral thesis
Matt

Permission fully granted. My role as named co-author was generally high level technical direction and mentoring as well as structural editing/review of the stated paper/publication.

Dr Ian Taggart
Consulting Reservoir Engineer
RISC Pty Ltd.

From: Flett, Matthew [mailto:Matthew.Flett@chevron.com]
Sent: Thu 28/02/2008 3:54 PM
To: Ian Taggart; Gurton, Randal; weirdoz@bigpond.net.au
Subject: Copyright release/permission for doctoral thesis

Dear Ian, Randy and Geoff,

Within a few weeks I will be submitting my thesis to Curtin Uni for examination. As I intend to include several papers as appendices to my thesis where you have been co-authors, I formally ask your permission to do so, in order to fulfil copyright provisions of Curtin University.

The papers I intend to include are:

Peer reviewed papers:
1.Flett, M., R. Gurton, and I. Taggart. *Heterogeneous saline formations: long term benefits for geo-sequestration of greenhouse gases*. in *Seventh International Conference on Greenhouse Gas Control Technologies (GHGT-7)*. 2004. Vancouver, Canada.: Elsevier.

2. Flett, M., R. Gurton, and G. Weir, *Heterogeneous saline formations for carbon dioxide disposal: Impact of varying heterogeneity on containment and trapping.* Journal of Petroleum Science and Engineering, 2007. **57**(1-2): p. 106-118

Conference papers:
1. Flett, M., R. Gurton, and G. Weir. *Reservoir performance of disposed carbon dioxide in saline formations: impact of heterogeniety and dip*. in *8th International conference on Greenhouse Gas Control Technologies*. 2006. Trondheim, Norway.

2. Flett, M., R. Gurton, and I. Taggart. *The function of gas-water relative permeability hysteresis in the sequestration of carbon dioxide in saline formations, SPE paper 88485, Presented 2004 SPE Asia-Pacific Oil and Gas Conference and Exhibition, Perth, Australia, 18-20 Oct (2004)*. 2004.

In terms of publishers retention of copyright: For the peer-reviewed articles - both have been published by Elsevier, their copyright policy online allows for inclusion of published papers and materials for a paper to be included in a thesis (as long as you are the author). See
http://www.elsevier.com/wps/find/authorsview.authors/copyright#whatrights
(cited 28/02/2008)

I have received permission from the SPE for paper 88485 and made due acknowledgements through my thesis.

<<88485_Flett, Matthew.doc>>
The GHGT8 paper has not been formally published and thus we have retained copyright.

Could you by return email, please give your permission as co-authors for these papers to be included and state your role in the preparation of these papers.

Thanks for you support,
Regards,

Matt

Matthew Flett
Reservoir Engineer
Gorgon Subsurface Development

Chevron Australia Pty Ltd
250 St Georges Terrace
Perth, Western Australia, 6000
Tel +61 8 9216 4574
Mobile 0421 869 645
Fax +61 8 9216 4860
Email Matthew.Flett@Chevron.com

From: Geoff Weir [weirdoz@bigpond.net.au]
Sent: Monday, 17 March 2008 11:34 AM
To: Flett, Matthew
Subject: RE: Copyright release/permission for doctoral thesis

Dear Matt

I have absolutely no objections to you including any papers that I have co-authored with you as appendices to your thesis.

My role in all of this work was as joint supervisor.

Good luck with your submission.

Kind regards

Geoff

Dr G.F.Weir PhD MInstP CPhys

-----Original Message-----
From: Flett, Matthew [mailto:Matthew.Flett@chevron.com]
Sent: Thursday, 28 February 2008 2:54 PM
To: Ian.Taggart@riscpl.com; Gurton, Randal; weirdoz@bigpond.net.au
Subject: Copyright release/permission for doctoral thesis

Dear Ian, Randy and Geoff,

Within a few weeks I will be submitting my thesis to Curtin Uni for examination. As I intend to include several papers as appendices to my thesis where you have been co-authors, I formally ask your permission to do so, in order to fulfil copyright provisions of Curtin University.

The papers I intend to include are:

Peer reviewed papers:
1.Flett, M., R. Gurton, and I. Taggart. *Heterogeneous saline formations: long term benefits for geo-sequestration of greenhouse gases*. in *Seventh International Conference on Greenhouse Gas Control Technologies (GHGT-7)*. 2004. Vancouver, Canada.: Elsevier.

2. Flett, M., R. Gurton, and G. Weir, *Heterogeneous saline formations for carbon dioxide disposal: Impact of varying heterogeneity on containment and trapping.* Journal of Petroleum Science and Engineering, 2007. **57**(1-2): p. 106-118

Conference papers:
1. Flett, M., R. Gurton, and G. Weir. *Reservoir performance of disposed carbon dioxide in saline formations: impact of heterogeniety and dip*. in *8th International conference on Greenhouse Gas Control Technologies*. 2006. Trondheim, Norway.

2. Flett, M., R. Gurton, and I. Taggart. *The function of gas-water relative permeability hysteresis in the sequestration of carbon dioxide in saline formations, SPE paper 88485, Presented 2004 SPE Asia-Pacific Oil and Gas Conference and Exhibition, Perth, Australia, 18-20 Oct (2004).* 2004.

In terms of publishers retention of copyright: For the peer-reviewed articles - both have been published by Elsevier, their copyright policy online allows for inclusion of published papers and materials for a paper to be included in a thesis (as long as you are the author). See

http://www.elsevier.com/wps/find/authorsview.authors/copyright#whatrights
(cited 28/02/2008)

I have received permission from the SPE for paper 88485 and made due acknowledgements through my thesis.
<<88485_Flett, Matthew.doc>>
The GHGT8 paper has not been formally published and thus we have retained copyright.

Could you by return email, please give your permission as co-authors for these papers to be included and state your role in the preparation of these papers.

Thanks for you support,
Regards,

Matt

Matthew Flett
Reservoir Engineer
Gorgon Subsurface Development

Chevron Australia Pty Ltd
250 St Georges Terrace
Perth, Western Australia, 6000
Tel +61 8 9216 4574
Mobile 0421 869 645
Fax +61 8 9216 4860
Email Matthew.Flett@Chevron.com